Proceedings of the 3rd International Conference on Transport, Atmosphere and Climate (TAC-3)

Robert Sausen, Simon Unterstrasser and Anja Blum (eds.)

Deutsches Zentrum
DLR für Luft- und Raumfahrt

Verkehrs-Emissionen, chemische Zusammensetzung der Atmosphäre, Wolken-, Klimaänderung, Vermeidungsstrategien *(Veröffentlicht auf Englisch)*

Robert SAUSEN, Simon UNTERSTRASSER und Anja BLUM
Deutsches Zentrum für Luft- und Raumfahrt (DLR), Institut für Physik der Atmosphäre, Oberpfaffenhofen, Deutschland

Proceedings of the 3rd International Conference on Transport, Atmosphere and Climate (TAC-3)

Dieser Band enthält Beiträge (Vorträge und Poster) der 3. Internationalen Konferenz „Transport, Atmosphere and Climate (TAC-3), die 2012 in Prien am Chiemsee stattfand. Mit dem Ziel, unser Wissen über den Einfluss des Verkehrs auf die Zusammensetzung der Atmosphäre und das Klima auf den neuesten Stand zu bringen, wurden auf der Konferenz alle Aspekte dieses Einflusses aller Verkehrsmoden (Luft-, Straßen-, und Schiffsverkehr) auf die Atmosphärenchemie, Wolkenphysik, Strahlung und Klima behandelt. Diese waren insbesondere: Triebwerksemissionen (gas- und partikelförmig), Emissions-Szenarien und Emissionsdatenbanken für den Verkehrssektor, Prozesse im Nahfeld und der Abgasfahne, effektive Emissionen, Verkehrseinfluss auf die chemische Zusammensetzung der Atmosphäre, Verkehrseinfluss auf das atmosphärische Aerosol, Kondensstreifen, Kondensstreifen-Zirren, „Ship Tracks", indirekte Wolkeneffekte (z.B. Aerosol-Wolken Wechselwirkung), Strahlungsantrieb, Metriken für die quantitative Messung des Klimawandels und daraus folgender Schäden, Vermeidung von Verkehrseinflüssen durch technologische und operationelle Maßnahmen.

Transport emissions, chemical composition of the atmosphere, cloud effects, climate change, mitigation

Robert SAUSEN, Simon UNTERSTRASSER und Anja BLUM
Deutsches Zentrum für Luft- und Raumfahrt (DLR), Institut für Physik der Atmosphäre, Oberpfaffenhofen, Deutschland

Proceedings of the 3rd International Conference on Transport, Atmosphere and Climate (TAC-3)

This volume collects oral and poster contributions to the "3rd International Conference on Transport, Atmosphere and Climate (TAC-3)" held in Prien am Chiemsee, 2012. With the objective of updating our knowledge on the impacts of transport on the composition of the atmosphere and on climate, the TAC-3 conference covered all aspects of the impact of the different modes of transport (aviation, road transport, shipping etc.) on atmospheric chemistry, cloud physics, radiation and climate, in particular: Engine emissions (gaseous and particulate), emission scenarios and emission data bases for transport, near-field and plume processes, effective emissions, transport impact on the chemical composition of the atmosphere, transport impact on aerosols, contrails, contrail cirrus, ship tracks, indirect cloud effects (e.g., aerosol-cloud interaction), radiative forcing, impact on climate, metrics for measuring climate change and damage, mitigation of transport impacts by technological changes in vehicles and engines, mitigation of transport impacts by operational means.

Forschungsbericht 2012-17

Proceedings of the
3rd International Conference
on Transport, Atmosphere and Climate
(TAC-3)

Robert Sausen, Simon Unterstrasser and
Anja Blum (eds.)

Deutsches Zentrum für Luft- und Raumfahrt
Institut für Physik der Atmosphäre
Oberpfaffenhofen

270 Seiten
140 Bilder
 36 Tabellen
506 Literaturstellen

Deutsches Zentrum
DLR für Luft- und Raumfahrt

Proceedings of the
3rd International Conference on Transport, Atmosphere and Climate (TAC-3)

Prien am Chiemsee, Germany,
25 to 28 June 2012

Edited by

Robert Sausen, Simon Unterstrasser and Anja Blum

Bayerisches Staatsministerium
für Wirtschaft, Infrastruktur, Verkehr
und Technologie

http://www.pa.op.dlr.de/tac/proceedings.html

Edited by

Robert Sausen, Simon Unterstrasser and Anja Blum

Oberpfaffenhofen, Oktober 2013

Foreword

The "3rd International Conference on Transport, Atmosphere and Climate (TAC-3)" held in Prien am Chiemsee (Germany), 2012, was organised with the objective of updating our knowledge on the impacts of transport on the composition of the atmosphere and on climate, three years after the TAC-2 conference in Aachen (Germany) and Maastricht (The Netherlands).

The TAC-3 conference covered all aspects of the impact of the different modes of transport (aviation, road transport, shipping etc.) on atmospheric chemistry, microphysics, radiation and climate, in particular:
  – engine emissions (gaseous and particulate),
  – emission scenarios and emission data bases for transport,
  – near-field and plume processes, effective emissions,
  – transport impact on the chemical composition of the atmosphere,
  – transport impact on aerosols,
  – contrails, contrail cirrus, ship tracks,
  – indirect cloud effects (e.g., aerosol-cloud interaction),
  – radiative forcing,
  – impact on climate,
  – metrics for measuring climate change and damage,
  – mitigation of transport impacts by technological changes in vehicles and engines,
  – mitigation of transport impacts by operational means.

The conference benefited from substantial financial support by Bayerisches Staatsministerium für Wirtschaft, Infrastruktur, Verkehr und Technologie[1], to whom the organizers are very grateful.

Prof. Dr. Robert Sausen
DLR, Institut für Physik der Atmosphäre
Oberpfaffenhofen
D-82234 Wessling
Germany

Tel.:   +49-8153-28-2500
Fax.:   +49-8153-28-1841
Email: robert.sausen@dlr.de

---

[1] Bavarian Ministry of Economic Affairs, Infrastructure, Transport and Technology

Scientific Programme Committee

- Prof. Robert Sausen, DLR, Germany (chair)
- Dr. Daniel Cariolle, CERFACS, France
- Prof. Ivar Isaksen, UiO, Norway
- Prof. David S. Lee, MMU, United Kingdom
- Prof. Barbara Lenz, DLR, Germany
- Dr. Patrick Minnis, NASA LaRC, USA
- Dr. Olivier Penanhoat, SNECMA, France
- Prof. Keith Shine, University of Reading, UK
- Dr. Peter van Velthoven, KNMI, The Netherlands
- Dr. Bernhard Vogel, KIT, Germany
- Prof. Christos Zerefos, NKUA, Greece

Table of Contents

EMISSIONS I

EMISSIONS II

AVIATION, CARS AND A BOAT TRIP

EMISSIONS III

IMPACT ON ATMOSPHERIC COMPOSITION

CLOUDS AND CLOUD PROCESSES I

CLOUDS AND CLOUD PROCESSES II

CLOUDS AND CLOUD PROCESSES III

CLOUDS AND CLOUD PROCESSES IV

CLOUDS AND CLOUD PROCESSES V

METRICS AND MITIGATION I

METRICS AND MITIGATION II

POSTERS: A. CLOUDS AND CLOUD PROCESSES

POSTERS: B. EMISSIONS

POSTERS: D. IMPACT ON ATMOSPHERIC COMPOSITION

POSTERS: E. METRICS AND MITIGATION

INDEX OF AUTHORS

TAC-3 AGENDA

1 ORAL PRESENTATIONS

Monday, 25 June 2012	
08:00	Registration
Opening ceremony	
Chair: R. Sausen	
08:40	Ministerialrat D. Schneyer, Bayrisches Staatsministerium für Wirtschaft, Infrastruktur, Verkehr und Technologie: *Opening Address on Behalf of Staatsminister Martin Zeil*
09:00	Prof. Dr.-Ing. U. Wagner, Member of the Executive Board of DLR: *Opening Address*
09:20	Prof. Dr. R. Sausen: *Introduction to Chiemsee and Technical Remarks*
Emissions I	
Chair: A. Petzold	
09:40	B. Anderson, D.L. Bulzan, E. Corporan, M. DeWitt, D. Hagen, S.C. Herndon, R. Howard, C. Klingshirn, W.B. Knighton, X. Li-Jones, J.S. Kinsey, D.S. Liscinsky, P. Lobo, R.C. Miake-Lye, R. Vander Wal, C. Wey, and P. Whitefield: *An Overview of the second NASA Alternative Aviation-Fuel Experiment (AAFEX-II)*
10:20	D. Delhaye, D. Ferry, O. Penanhoat,X. Vancassel, F.-X. Ouf, J. Yon, P. Desgroux, C. Focsa, C. Guin, D. Lottin, N. Harivel, B. Perez, and P. Novelli: *MERMOSE project: Investigation on particulate matter emitted from aircraft engines and contrails formation*
10:40	Poster setup / Coffee
11:20	I. Ježek and G. Mocnik: *Measuring car emission factors in real driving conditions*
11:40	S. Platt, I. El Haddad, A. Zardini, M. Clairotte, C. Astorga, R. Wolf, J. Slowik, B. Temime, N. Marchand, G. Mocnik, L. Drinovek, I. Ježec, U. Baltensperger, and A. Prévôt: *Primary and Secondary Organic Aerosol from Road Vehicles*
Emissions II	
Chair: V. Eyring	
12:00	J. Moldanova, M. Haeger-Eugensson, E. Fridell and T. Lin: *Primary and secondary PM in ship emissions*
12:20	J.-M. Diesch, F. Drewnick, T. Klimach, and S. Borrmann: *Particle and trace gas properties from ship exhaust plumes: Emission characteristics and impact on air quality*
12:40	P. Whitefield, P. Lobo, D. Hagen, Z. Yu, R.C. Miake-Lye, and T. Rindlisbacher: *Experiments to Define and Validate an Aerospace Recommended Practice for measuring Non-volatile PM from Gas Turbine Engines.*
13:00	Lunch / get prepared for boat trip

Aviation, cars and a boat trip	
Chair: R. Sausen	
14:30	U. Schumann, H. Schlager, U. Burkhardt, K. Gierens, V. Grewe, J. Hendricks, B. Kärcher, H. Mannstein, R. Meerkötter, C. Voigt, and H. Ziereis: *Climate-compatible Air Transport System – Results of the DLR CATS project towards reduced uncertainties*
14:50	A. Koch, U. Schumann, K. Dahlmann, V. Grewe, V. Gollnick, F. Linke, M. Kunde, and T. Otten: *Climate-compatible Air Transport System – Results of the DLR CATS project towards the climate impact mitigation potential given by actual and future long-range aircraft*
15:10	J. Borken-Kleefeld, J. Fuglestvedt, and T. Berntsen: *Taking the car, coach, train or plane? Comparing climate impacts from passenger trips*
15:30	Dipl.-Verw.-Wirt J. Seifert, Erster Bürgermeister der Marktgemeinde Prien am Chiemsee: *Welcome Address*
15:50	Coffee
16:30	Departure of the boat
	Visit of Castle Herrenchiemsee
19:45	Arrival at Hotel
20:15	Dinner

Tuesday, 26 June 2012	
08:30	Registration
Emissions III	
Chair: R. Miake-Lye	
09:00	C. Schieberle, U. Kugler, S. Orlikova, M. Uzbasich, J. Theloke and R. Friedrich: *A new European inventory of transport related emissions for the years 2005, 2020 and 2030*
09:20	M. Traut, A. Bows, and R. Wood: *Quantifying Shipping Emissions*
09:40	M. de Ruyter de Wildt, H. Eskes, F. Boersma, and P. van Velthoven: *Remote sensing of ship-emitted NO_2: correlation with economic growth and recession*
Impact on atmospheric composition	
Chair: P. Whitefield	
10:00	A. Petzold, A. Volz-Thomas, J.P. Cammas, and C.A.M. Brenninkmeijer: *IAGOS - In-service Aircraft for a Global Observing System*
10:20	E. G. Olumayede, J. M. Okuo, and C.C. Ojiodu: *Distribution and Temporal Behaviors of Total Volatile Organic Compounds over the Urban Atmosphere of Southwestern Nigeria*
10:40	Posters / Coffee
11:20	S. Barrett, C. Gilmore, J. Koo, and Q. Wang: *Adjoint methods applied to the atmospheric impacts of aviation*
11:40	K. Gottschaldt, C. Voigt, P. Jöckel, M. Righi, and S. Dietmüller: *Global sensitivity of aviation NOx effects to the proposed HO2 + NO -> HNO3 reaction*
12:00	M. Timko, E. Fortner, J. Franklin, Z. Zhu, W.B. Knighton, T. Onasch, R. Miake-Lye and S. Herndon: *Characterizing the Particulate Evolution of Aircraft Exhaust Plumes using Atmospheric Measurements*
12:20	J.E. Williams, O. Hodnebrog, P.F.J. van Velthoven, M. Gauss, V. Grewe, T.K. Berntsen, I.S.A. Isaksen, M.J. Prather,Q. Tang, O. Dessens, D. Olivie and F. Stodal: *The influence of non-mitigated road transport emissions on regional air quality: analysis of the QUANTIFY high-road study*
12:40	Lunch

Clouds and cloud processes I	
Chair: S. Unterstraßer	
14:20	H. Preston and D. Lee: *The inclusion of international aviation within the European Union's Emissions Trading Scheme*
14:40	D. Baumgardner, K. Beswick, M. Gallagher, and R. Newton: *Cloud Microphysical Properties Measured from Commercial Aircraft*
15:00	C. Voigt, K. Graf, A. Schwarzenboeck, U. Schumann, H. Schlager, P. Jeßberger, T. Jurkat, A. Petzold, J.-F. Gayet, M. Krämer, T. Thornberry, D. Fahey, S. Kaufmann, D. Schäuble, A. Minikin, B. Weinzierl, M. Klingebiel, S. Molleker, W. Frey, S. Borrmann, M. Scheibe, F. Dahlkötter, A. Schäfler, and A. Dörnbrack: *Detection of microphysical and optical properties of young contrails and contrail cirrus – selected results from the CONCERT (CONtrail and Cirrus ExpeRimenT) aircraft campaigns 2008 and 2011*
POSTER session	
15:20	Posters on display *Authors in attendance*
16:20	Posters / Coffee
Clouds and cloud processes II	
Chair: A. Heymsfield	
16:50	P. Jeßberger, C. Voigt, A. Petzold, I. Sölch, U. Schumann, J.-F. Gayet, T. Jurkat, and D. Schäuble: *Has the aircraft type an impact on the microphysical parameters of young contrails?*
17:10	J. Picot, R. Paoli, O. Thouron, and D. Cariolle: *Effects of atmospheric turbulence on the structure of a contrail in the vortex phase*
17:30	S. Unterstraßer and I. Sölch: *Numerical Modeling of contrail-cluster formation*
17:50	K. Gierens and S. Unterstraßer: *Formation conditions and simulations of contrails from hybrid engines of a future Blended Wing Body aircraft*
18:10	End of presentations
19:00	Dinner

Wednesday, 27 June 2012	
08:30	Registration
Clouds and cloud processes III	
Chair: M. Krämer	
09:00	D.P. Duda, S.T. Bedka, R.C. Boeke, T.L. Chee, K. Khlopenkov, R. Palikonda, D. Spangenburg, and P. Minnis: *Contrail Detection in the Northern Hemisphere: Methods and Results*
09:20	P. Minnis, D.P. Duda, T. L. Chee, S.K. Bedka, D.A. Spangenberg, R. Palikonda, and K.T. Bedka: *Contrails versus Contrail Cirrus From a Satellite Perspective*
09:40	K. Graf, U. Schumann, H. Mannstein, and B. Mayer: *On the diurnal cycle of cirrus coverage in the North Atlantic flight corridor*
10:00	U. Schumann and K. Graf: *Radiative forcing by contrail cirrus – a combined model and observation analysis method*
10:20	S. Bedka, P. Minnis, D. Duda, and R. Palikonda : *Seasonal and diurnal variability in linear contrail microphysical properties, as derived using MODIS infrared observations*
10:40	Posters / Coffee
Clouds and cloud processes IV	
Chair: R. Paoli	
11:20	K. Eleftheratos, C. Zerefos, and P. Minnis: *Changes in aircraft induced cloudiness during the past three decades*
11:40	J. Hendricks and B. Kärcher: *Do aircraft black carbon emissions affect cirrus clouds on the global scale?*
12:20	A. Gettelman and J. Chen: *The Climate Effect of Anthropogenic and Aviation Aerosol Emissions*
12:40	Lunch
Clouds and cloud processes V	
Chair: P. Minnis	
14:20	Chen, C.-C., A. Gettelman, and C. Craig: *Simulations of contrail and contrail cirrus radiative forcing*
14:40	U. Burkhardt: *Contrail cirrus radiative forcing for increasing air traffic*
POSTER session	
15:00	Posters on display *Authors in attendance*
16:00	Posters / Coffee

Impact on climate	
Chair: P. van Velthoven	
16:30	K. Lundgren, B. Vogel, H. Vogel, and C. Knote: *Regional Scale Impact of Traffic Emission on Radiation over Europe*
16:50	D. Olivié, D. Cariolle, H. Teyssèdre, D. Salas, A. Voldoire, H. Clark, D. Saint-Martin, M. Michou, F. Karcher, Y. Balkanski, M. Gauss, D. Olivier, B. Koffi, and R. Sausen: *Modeling the climate impact of road transport, maritime shipping and aviation over the period 1860-2100 with an AOGCM*
17:10	H. Teyssèdre, P. Huszar, D. Cariolle, A. Voldoire, S. Sénési, M. Michou, D. Saint-Martin, D. Salas Y Melia, P. Ricaud, and F. Karcher: *Impact of aviation on atmospheric chemistry and climate*
17:30	M. Lund, V. Eyring, J. Fuglestvedt, J. Hendricks, A. Lauer, D.S. Lee, and M. Righi: *Global mean temperature change from shipping towards 2050: Improved representation of the indirect aerosol effect in simple climate models*
17:50	End of presentations
18:45	Conference Dinner/ Boat trip on Lake Chiemsee
23:00	End of Conference Dinner

Thursday, 28 June 2012	
08:30	Registration
Metrics and mitigation I	
Chair: U. Schumann	
09:00	M. Eide, S. Dalsøren, Ø. Endresen, B. Samset, G. Myhre, J. Fuglestvedt, and T. Berntsen: *Reducing CO_2 from shipping – Do non-CO_2 effects matter?*
09:20	B. Aamaas, J. Borken-Kleefeld and G.P. Peters: *The climate impact of travel behavior: a German case study*
09:40	S. Seidel, V. Ehrler, and A. Lischke: *Comparability of calculated emissions in freight transport*
10:00	O. Deuber, G. Luderer and O. Edenhofer: *Economic evaluation of climate metrics: A conceptual framework*
10:20	O. A. Søvde, S. Matthes, A. Skowron, L. Lim, D. Iachetti, I. S. A. Isaksen, D. Lee, and G. Pitari: *An updated study of aircraft emission mitigation possibilities*
10:40	Posters / Coffee
11:10	*Technical information concerning your proceedings contribution*
Metrics and mitigation II	
Chair: D. Fahey	
11:20	P. Brok and J. Middel: *Aviation and Emissions Scenario and Policy Analysis Capabilities of AERO-MS*
11:40	R. Singh Chouhan: *Urban Forest and Its Significance in Mitigating Vehicular Pollution*
12:00	S. Meilinger: *Operational Flight Planning using Lido/Flight*
12:20	Matthes, S., M. Duffau, J. Fuglestvedt, V. Grewe, V. P. Hullah, D. Lee, V. Mollwitz, K. Shine, R. Sausen: *REACT4C - Weather-dependent climate-optimized flight trajectories*
12:40	Lunch
14:20	E. Irvine, K. Shine, and B. Hoskins: *The dependence of contrail formation on the weather pattern and altitude in the north Atlantic*
14:40	C. Frömming, V. Grewe, S. Brinkop, S. Dietmüller, J. Fuglestvedt, H. Garny, P. Jöckel, M. Ponater, A. Sovde, E. Tsati, and S. Matthes: *Calculation of climate cost functions for weather dependent, climate optimized flight planning*
15:00	H. Mannstein and U. Schumann: *Smart aircraft routing*
Closing Session	
Chair: R. Sausen	
15:20	Summary, conclusions, awards, ...
16:00	Poster removal / Coffee
16:30	End of meeting

2 POSTERS

A. Clouds and cloud processes	
A.01	L. Bock, U. Burkhardt, and B. Kärcher: *Microphysical and optical properties of contrail cirrus in a global climate model*
A.02	L. Forster, C. Emde, S. Unterstrasser, and B. Mayer: *Effects of three-dimensional photon transport on the radiative forcing of realistic contrails*
A.03	D. Iachetti and G. Pitari: *Study of the impact of altered flight trajectories on soot-cirrus*
A.04	S. Kaufmann, C. Voigt, D. Schäuble, A. Schwarzenboeck, H. Schlager, M. Zöger, T. Thornberry, and D. Fahey: *High resolution measurements of relative humidity in young contrails with the Atmospheric Ionization Mass Spectrometer*
A.05	B. Kärcher, U. Burkhardt, M. Ponater, C. Frömming, P. Minnis, and R. Palikonda : *On the effects of optical depth variability on contrail radiative forcing*
A.06	M. Lainer and S. Unterstrasser : *Numerical simulations of persisting contrails with Lagrangian microphysics*
A.07	L. Lim, J. Carter, D. Lee, B. Owen, and R. Rodríguez De León : *Radiative forcing from present-day and future contrails coverage*
A.08	M. Righi, J. Hendricks, and R. Sausen: *Impact of transportation sector on global aerosol for present-day and future scenarios*
A.09	D. Spangenberg, S. Bedka, D. Duda, R. Palikonda, F. Rose, and P. Minnis: *Contrail Cloud Radiative Forcing over the Northern Hemisphere from Terra and Aqua MODIS Data*
A.10	O. Thouron and R. Paoli: *Large-eddy simulations of kilometer-scale atmospheric turbulence*
A.11	M. Vazquez-Navarro, H. Mannstein, and S. Kox : *Lifetime and physical properties of contrails and contrail cirrus*
A.12	G.M. Whelan, F. Cawkwell, H. Mannstein, and P. Minnis: A 10yr Irish Observational AVHRR and Radiosonde Contrail Climatology
A.13	H.-W. Wong, R. Miake-Lye, R. Moore, S. Crumeyrolle, A. Beyersdorf, L. Ziemba, E. Winstead, B. Anderson, C. Heath, R. Ross, K. Tacina, and D. Bulzan: *Laboratory and Modeling Studies on the Effects of Emissions Performance and Ambient Conditions on the Properties of Contrail Ice Particles in the Jet Regime*

B. Emissions	
B.01	V. Archilla, J. Rodriguez Maroto, M. Pujadas, A. González, E. Rojas, A. Entero, J.M. Fernázndez-Mainez, A. Jimenez, D. Sanz, D. Mercader, and J.C. Bezares *Setting up a turbojet test cell as a platform for environmental impact assessment*
B.02	J. P. Franklin, P. Lobo, P. Whitefield, R. Hoffelt, S. Herndon, W.B. Knighton, E. Fortner, and R. Miake-Lye: *The other emissions from aircraft at a major US airport: auxiliary power unit, tire abrasion, braking*
B.03	D. Heinrichs, V. Ehrler, M. Mehlin, J. Hendricks, M. Righi, R. Sausen, K. Lundgren, B. Vogel, and H. Vogel: *Transport Emission Scenarios and Effects on Regional and Global Air Quality and Climate: The Project 'Transport and the Environment'*
B.04	W.B. Knighton, S. Herndon, E. Wood, R. Miake-Lye, M. Timko, Z. Zhu, J. Franklin, A. Beyersdorf, E. Winstead, B.Anderson, C. Wey, and D. Bulzan: *Near-idle organic gas emissions scaling method for characterizing aircraft engine exhaust emissions: Assessment of the influence of fuel flow, ambient temperature and alternative fuels*
B.05	R. Kurtenbach, P. Wiesen, and Y. Elshorbany: *Adaptation for Sustainable fuel*
B.06	D. Lottin, D. Ferry, J. Yon, F.X. Ouf, and D. Delhaye: *Transmission Electron Tomography : from 2D to 3D microphysical properties of aerosols. Application to aircraft soot emissions*
B.07	S. J. Moon , W. W. Yoon, B. B. Jin, and J. C. Yoo *A Study on University Greenhouse gas Inventory Guideline*
B.08	G. Pitari, D. Iachetti, and N. De Luca: *Perturbations of sulphate and black carbon aerosols due to aviation emissions and impact on ozone photochemistry*
B.09	M. Yahyaoui, E. Joubert, J. Steinwandel, P. Chavrier, and I. Lombaert-Valot: *The Chemical Reactor Network approach for the emission prediction at the exhaust of aircraft gas turbine combustor*
B.10	F. Yin, A. G. Rao, and J. P. van Buijtenen: *Performance Characteristic of a Multi-fuels Hybrid Engine*
B.11	Z. Yu, H.-W. Wang, J. Peck, S. C. Herndon, R. Miake-Lye, M. Jun, I. A. Waitz, D. S. Liscinsky, A. C. Jennings, B.S. True, M. B. Colket, L. D. Ziemba, E. L.Winstead, and B. E. Anderson: *Quantifying the Composition of Volatile Particulate Matter Emissions from Aircraft Engines*
C. Impact on climate	
C.01	S. Matthes, P. Jöckel, A. Sovde, A. Skowron, B. Owen, D. Lee, D. Iachetti, and G. Pitari: *Updated assessment of aviation impact on ozone formation and climate impact - REACT4C multi-model estimate*
C.02	M. Ponater and C. Frömming: *Performance of two GCM borne radiation schemes in calculating contrail radiative forcing*

D. Impact on atmospheric composition	
D.01	A. Barseghyan and A. Amiryan: *Novel Method of Solving Differential Equations for Mathematical Modeling Dynamic Processes in Atmosphere and Climate*
D.02	A. Barseghyan: *Program package for mathematical simulation of complex reaction mechanisms and its illustration on ozone kinetics*
D.03	S. Matthes, P. Brok, D. Raper, T. Tsalvoutas, and P. Wiesen: *ECATS – European networking on Aviation & Environment*
D.04	C. Rojo, X. Vancassel, and J.-L. Ponche: *Modelling alternative fuels for aircraft: influence on the evolution and behaviour of aerosols*
D.05	J. E. Williams and P. van Velthoven: *Future Arctic shipping routes and European air quality in 2025*
E. Metrics and mitigation	
E.01	K. Dahlmann, V. Grewe, and A. Koch *Efficient evaluation of measures for air traffic climate optimization*
E.02	M. Hagström, T. Mårtensson, K. de Cock, and Raj Nangia: *RECREATE - Airworthy cruiser-feeder operations for emission reductions*
E.03	E. Irvine, K. Shine, and B. Hoskins: *Assessing the trade-off in CO2 and contrail climate impacts for an individual flight*
E.04	A. Skowron and D. Lee: *Aviation NOx Global Warming Potential - an insight into its heterogeneity*

Opening Address at the Third International Conference on Transport, Atmosphere and Climate

D. Schneyer on behalf of Staatsminister Martin Zeil
Bayrisches Staatsministerium für Wirtschaft, Infrastruktur, Verkehr und Technologie

Dear Professor Sausen,
Ladies and Gentlemen,

I wish first to convey apologies from State Minister Zeil for not being here in person at today's event. This was due to an urgent political commitment and he has therefore asked me to give this address in his place. In recognition of this conference, however, State Minister Zeil has already willingly agreed to assume the patron ship.

My name is Dietmar Schneyer, and I am head of the Applied Research Unit that focuses on the field of aerospace. Welcome to the 3rd Conference on Transport, Atmosphere and Climate. I hope you are enjoying these delightful surroundings at lake Chiemsee.

I am particularly pleased to see so many international participants. The best brains from all over the world are most welcome here in Bavaria. It's good to see you.

Ladies and Gentlemen!

The theme you have chosen is an extremely topical issue. Growth in national and international transport on land, water and in the air appears to know no limits. When we look at Asia and parts of South America, many places are revealing just the beginnings of a dramatic development.
It is therefore of great interest to study the impacts this trend is having on the atmosphere, and consequently on our climate in the long term. But we do not have to venture so far. In Bavaria we can also identify a development that is not leaving our environment unaffected. Conurbations are having to tackle daily congestion and overloading with all the associated consequences, our trunk roads are being pushed to their outermost limits, among other things due to our geographical position right in the heart of Europe. And air traffic is no exception, as we can see from the development at Munich's Franz Joseph Strauß airport.

As I already mentioned, the focus of my unit is on aeronautics and space and this has numerous points of contact with the topic being addressed today:
Because aviation is a medium that contributes to changes in the atmosphere. And ventures into space can help investigate the various impacts on the atmosphere and the climate.
Let me give you a brief account of the activities we are carrying out in Bavaria in support of optimising the framework conditions for science and research, and also to make sure that the accomplished results are turned into commercially useful products and services as swiftly as possible.
Here are some examples of the activities we have developed over recent years:

1. Networks: in 2006 we organised key sectors of Bavarian industry into 19 innovative clusters. Since the launch of this program five years ago 8,000 companies and research institutes have been involved in over 3,000 events with 180,000 participants. These clusters also include the BavAIRia e.V. that already has some 170 member companies from all subsectors of aeronautics, space and aerospace usage.

The prime goal of BavAIRia is to establish a closer dovetailing between research, industry and state agencies in future proof cross sector technologies, like satellite navigation and geo-information.

2. Direct measures: in order to create local anchors, the State of Bavaria is investing in beacon projects such as, for instance, the Galileo Control Centre in Oberpfaffenhofen, the Centre for Carbon Fibre Composite Materials in Augsburg, a Centre of Excellence for Robotics together with the federal government in Oberpfaffenhofen, or the very latest development of a Centre for Aerospace and Security in Ottobrunn.

3. Similar support is planned for a GMES node, again in Oberpfaffenhofen. In our opinion this should be used to establish an even closer interlinking of competencies in research and in commercial application. This is also an interesting approach in connection with the thematic scope of today's congress.

4. Research funding: Besides several individual measures in support of research, last year a Bavarian aerospace programme was launched with a volume of around 9 million €
To date, a total of 17 specific projects have received funding, primarily in the aerospace usage sector. These include in particular the fields of satellite navigation and earth resources surveying.

5. Idea competition: an abundance of excellent data is, however, of little use if there is no parallel development of applications. For this purpose, the Application Center in Oberpfaffenhofen, AZO, initiated an international idea competition. Originally this competition was restricted to navigation topics, however, as I already pointed out, we aim to interlink Galileo and GMES applications as much as possible. Both of these are addressed by 500 ideas that have already been entered this year from 23 regions across the globe. This I see as a great achievement of the AZO.

6. Incubators: good ideas alone are not sufficient, they also have to be turned into commercial success. In recognition of this, the State of Bavaria launched an initiative within the framework of its High-Tech Offensive back in 2002. In Oberpfaffenhofen we set up an incubator that was aimed to help implement a good idea into a successful start-up company, with the backing of expert support. Based on the great success of this undertaking, the ESA has also participated in the incubator project since 2009. Now 20 companies are founded there every year.

This brief summary is to give you an idea on how, with coordinated measures, we want to help establish an even closer interlinking of excellent research and implementation on a commercial scale, in order to secure the future of Bavaria as a high-tech location.

Ladies and Gentlemen,
After the meteorological start of summer earlier on, the official calendar season began just a few days ago! For many of us this is seen as the most pleasant and most intense time of the year. Take the drive and positive energy associated with this season with you in your discussions at this conference.

I wish the congress much success and all those participating

- new insights,
- fruitful discussions,
- interesting contacts

as well as a very pleasant stay at lake Chiemsee.

Thank you!

Extended Abstracts

Measuring car emission factors in real driving conditions

I. Ježek[*], G. Močnik
Aerosol d.o.o., Slovenia

ABSTRACT: In this study we tested two methods for measuring emission factors (EF) in real driving conditions on three EURO3 diesel cars. The two approaches used were: measuring transient increases of different pollutant concentrations emitted by individual vehicles passing a stationary measuring site; and measuring plumes of individual vehicles by chasing them on the road with a mobile station. Concentrations of back carbon (BC), particle number concentration (PN) and CO2 were measured on an empty safety training track field. The first method was performed with the car driving at two different speeds, and while accelerating. For these three vehicles BC and PN EF vary up to 84 and 87 %, respectively, within the same driving regime. Measuring on the road with a substantial slope did not increase EF. Chasing experiments showed slightly higher average EF values, interpreted as being due to varying speed and acceleration during driving. Time evolution of EF confirms this.

1 INTRODUCTION

Different approaches have been used to describe the contribution of traffic to air pollution. In emission modeling the activity of a source is connected with its intensity, which is presented as an emission factor (EF). For newer vehicles of different types legislation requires emission standards for amount of particulate matter (PM) emitted per kilometre driven on average in a prescribed driving cycle. Newer emission standards for regulating diesel vehicle emissions include also particle number, because newer vehicles produce less particle mass but smaller, more health adverse particles in large numbers. In our study we measured intensity of particle number (PN) and black carbon (BC) emissions of diesel cars. We choose these two particle characteristics because studies have shown higher correlation of health and climate effects for these pollutants, especially BC, than to PM (e.g. Ramanathan et al, 2008; Janssen et al, 2011)

Aerosol BC is a product of incomplete combustion. It is a good indicator of primary emissions as it has no other sources but combustion of carbon fuels. BC particles from different sources have different characteristics that can produce different effects in the atmosphere. Fresh diesel particles are black and absorb light differently than light absorbing particles from other sources. Black carbon is inert and thus not destroyed by in-atmosphere processes; it's removed from the atmosphere only by deposition. It is a good primary emission indicator as it has no other sources but combustion of carbon fuels (Bodhaine et al, 1995; Sciare et al, 2009).

Emission factors (EF) for individual vehicles are usually measured with dynamometers. These studies are good for investigating the influence of fuel type, additives, engine type, temperature, for aging of particles and measuring secondary emissions, but with these tests only emissions of few vehicles supposedly representative for the whole vehicle fleet are measured. Studies have shown that few individual vehicles can contribute significantly to the fleet emissions (Ban-Weis et al, 2009; Wang et al, 2011) much more than the average vehicle in the fleet, and measurements of large number of vehicles are desired.

The amount of pollutants emitted depends on the vehicle engine, its maintenance, quality and consumption of fuel, traffic fluency, driving regime, individual drivers, topography, and weather.

[*] *Corresponding author:* Irena Ježek, Aerosol d.o.o., Kamniška 41, SI-1000 Ljubljana, Slovenia.
Email: irena.jezek@aerosol.si

By measuring EF in real driving conditions we can select a larger random sample of vehicles, we avoid having to simulate dilution or use prescribed driving cycles and can thus obtain EF that are more closely related to real driving situations.

2   METHODOLOGY

For vehicles EF are reported as pollutant per kg fuel used, km driven or per power of engine produced. Measuring random cars we don't know their fuel consumption so we assume complete combustion of fuel, where all carbon turns to CO_2. Measuring CO_2 emissions was thus our measure for fuel consumption (Hansen and Rosen, 1990).

There have been studies performed where emission factors of HDV were measured in real driving conditions. Because there is a significant portion of diesel cars in Europe, we wanted to test two different methods also on diesel cars. One is a stationary method where we measure immediate increase of concentrations caused by vehicles driving by the measuring site (Hansen and Rosen, 1990); the other is a chasing method where a sampling vehicle chases other vehicles on roads as close as possible but within a safe distance (Wang et al, 2011). We also wanted to know, if the two methods are comparable and if they are repeatable. Thus we tested them on a training track.

For the stationary method we set up two measuring sites: one on a slope and one on a flat part of the track. We wanted to see if EFs would be higher or more repeatable on slope where we expected cars would have more constant engine load. We also wanted to see the difference in measuring at two different speeds (50 and 90 km/h) and while accelerating. With each car we repeated both speeds and acceleration by both measuring sites five times. Second method was tested by chasing a car with our mobile station, making 5 rounds on the 1.3 km long circular track that had an up and down slope and two sharp curves.

The stationary station on the flat part of the track was equipped with an ELPI+ for measuring PN, prototype Aethalometer AE33 for BC and a Carbocap 343 for CO_2. The mobile station was equipped with an FMPS for measuring PN, an AE33 and a Carbocap 343. Mobile station was also used for stationary measurements on the slope. With both methods we measured emissions of three diesel cars with different production years (2000, 2002 and 2005) but complying with the same emission standard EURO3.

3   DATA PROCESSING

Outcome of stationary measurements were fast rises of pollutants over the background concentration which we subtracted from our plum increases. For each peak we found an infliction point for the beginning of the plume, we set the background levels by averaging 20s before the beginning of the plume. The end of the plume was not so obvious to set so we calculated EF with two integration times 30 and 40s of the measured parameter and found that there is almost no difference between them (R=0.99 for BC and PN emission factor).

Processing data from chasing method: we set the background concentrations by averaging 20s before the chasing started and subtracted 3%. This correction was applied so we could calculate the changing of the EF in 10s time slots and thus got a time evolving EF.

4   RESULTS

Results show that emission factors measured on the slope varied for both pollutants. Measuring on slope did not increase them significantly, neither did driving at two different speeds, accelerating by the measurement site did result in significantly higher EFs (Figure 1). The distributions on the slope and flat ground were different for both BC and PN. Speed did not affect the distribution in a great manner, but acceleration did.
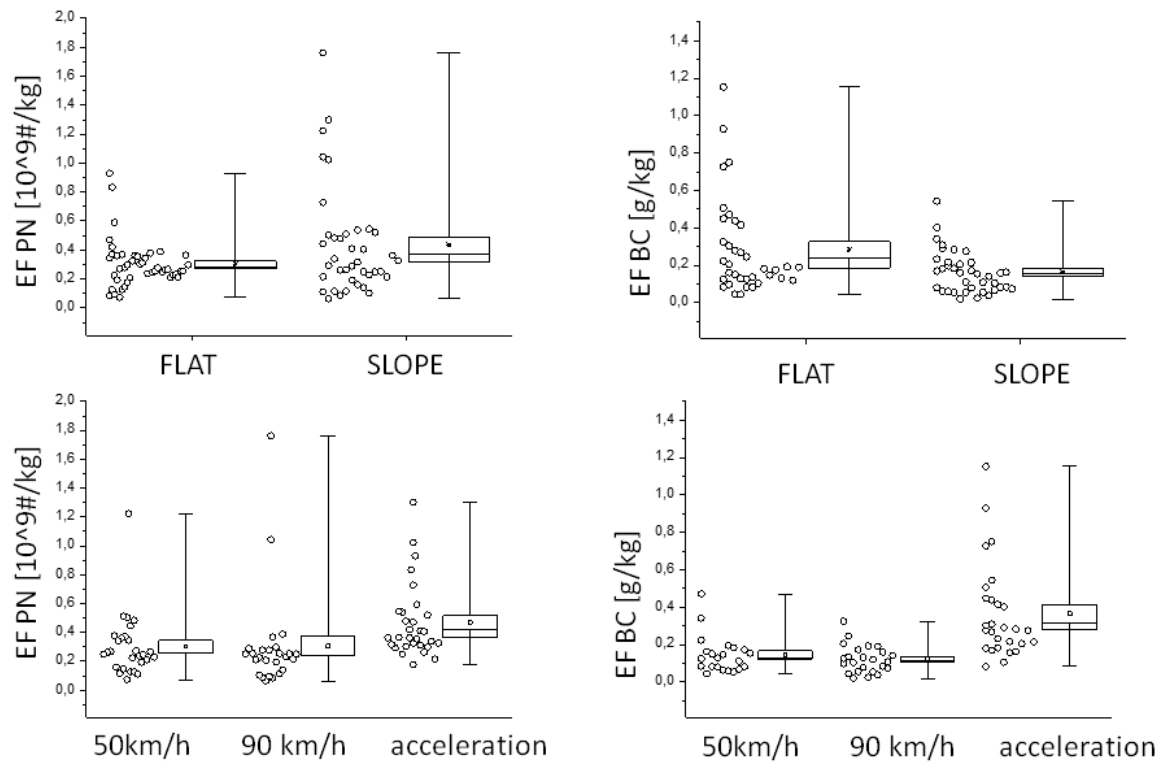
Figure 1: Comparing effects of slope and speed on PN and BC EF.

Comparing different vehicles showed that EF varied for measured individual vehicle. It also showed that the vehicle with higher PN EF had lower BC EF and vice versa (Figure 2). Theory behind the lack of overlap in high emitting PN and BC is that high BC emissions inhibit ultrafine particle formation. Precursors of ultra fine particles condense onto BC particle surfaces instead of nucleating to form new particles when BC is abundant in exhaust (Ban-Weis et al, 2009).
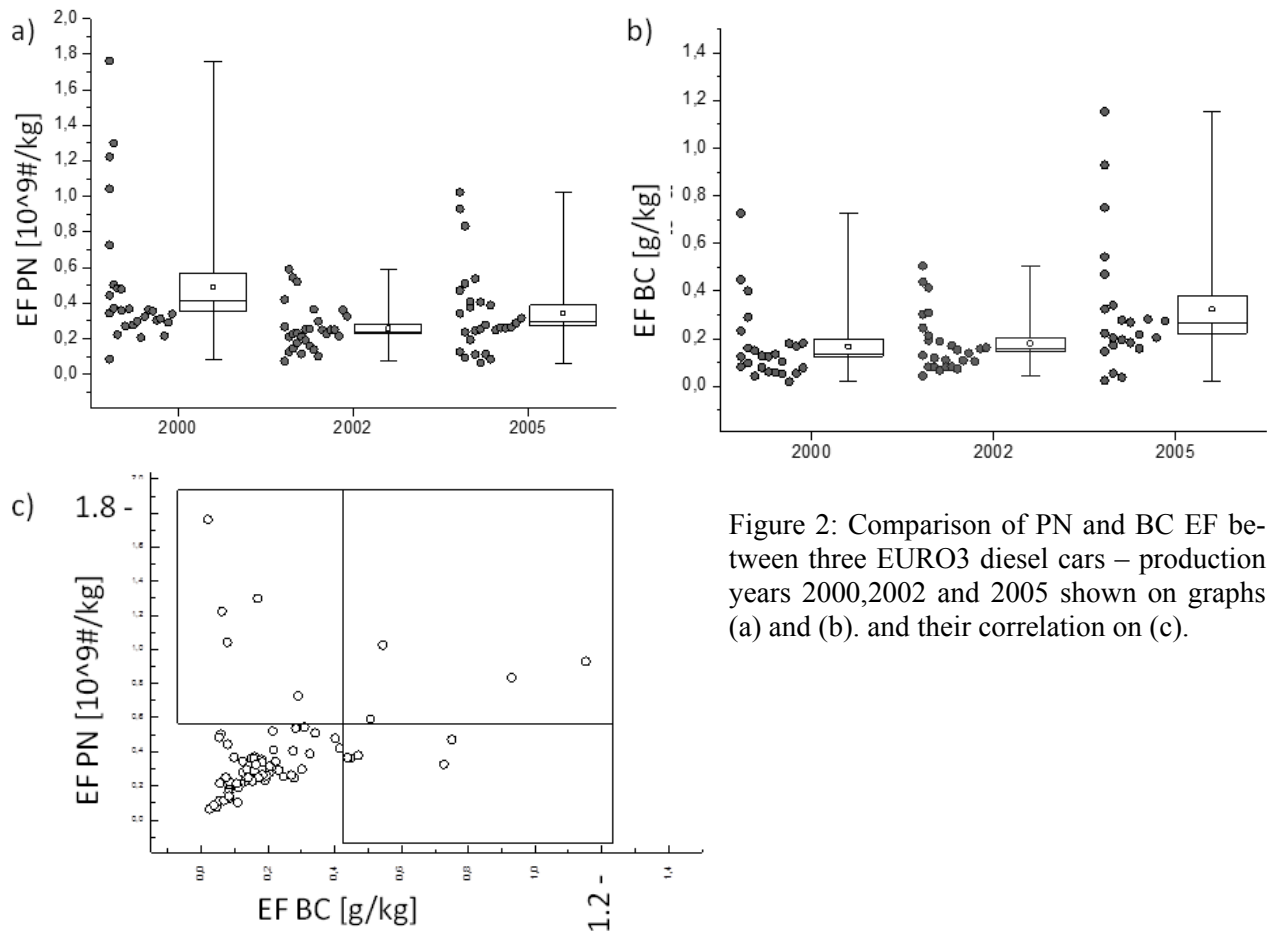
Figure 2: Comparison of PN and BC EF between three EURO3 diesel cars – production years 2000,2002 and 2005 shown on graphs (a) and (b). and their correlation on (c).

EF BC time series plotted one lap over the other show that only one driver's laps were somewhat constant. We can see that consistent driving results in more consistent EF distributions. The distribution of EFs is similar to what we got with the stationary method – majority of EFs is around one value and there is a long tail. Similar picture we got for PN EF, only here the scale for each car is much more different.
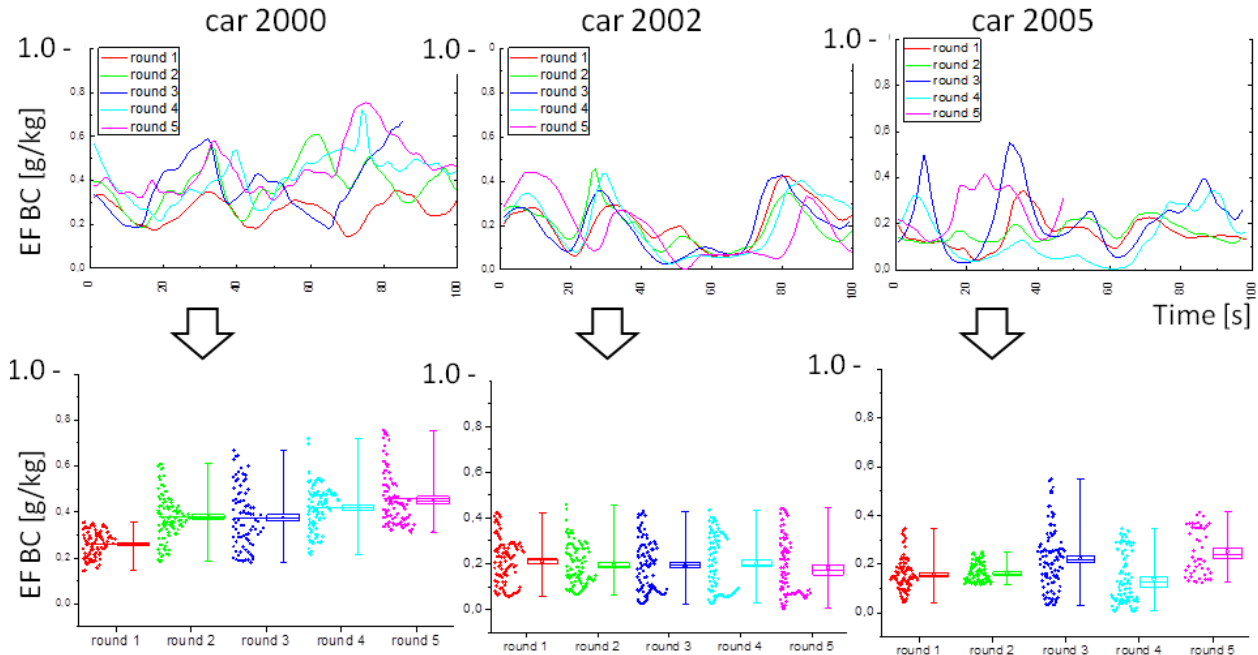
Figure 3: In the first row time evolving BC EF are presented. Each car made five laps on the circular track. Rounds for each car are plotted one over the other (time scale is from 0 to 100s). In the second row distributions for each round are plotted in the same color schemes as time evolved Efs are. Here we can see that consistent driving (car 2002) also results in more consistent EF distribution.
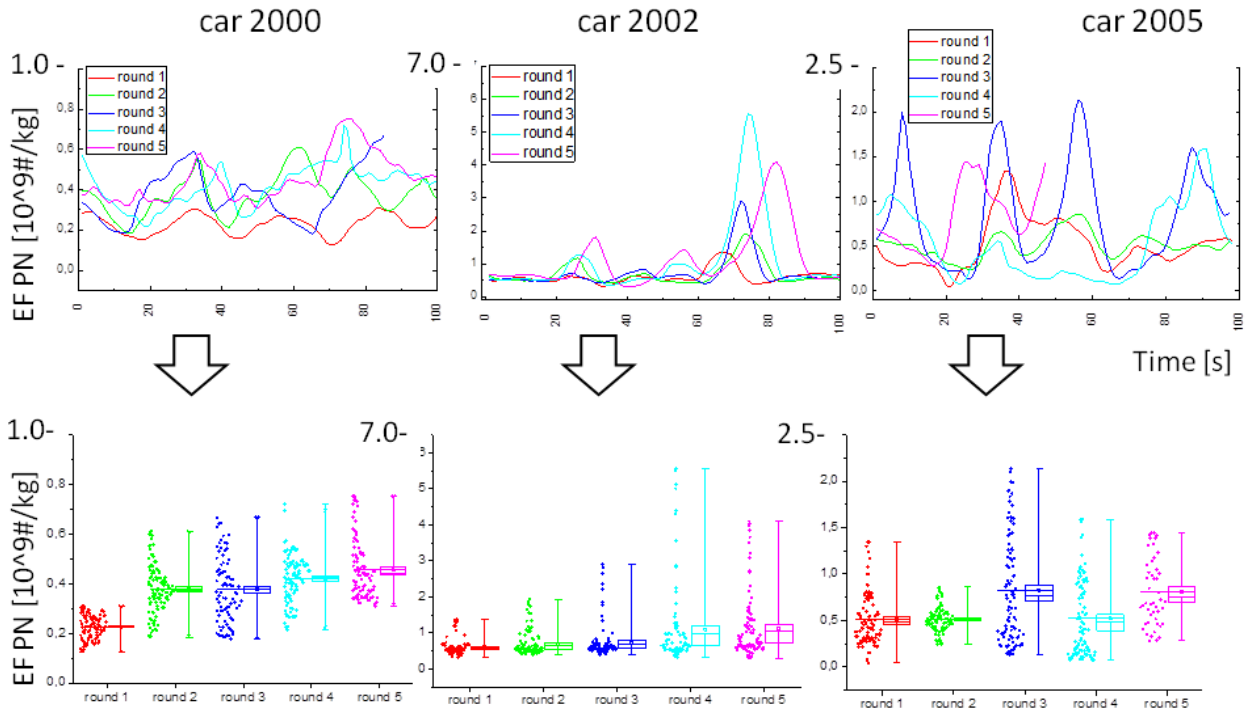
Figure 4: In the first row time evolving PN EF are presented. Color schemes also correspond to 5 rounds of time evolving BC EF on figure 3. As before time scale is from 0 to 100s. In the second row distributions for each round are plotted. PN EF are more versatile than BC EF, note different scales for each car!

5   CONCLUSIONS

Results of both methods are comparable for calculated PN and BC emission factors. Using the stationary method the background affects the PN emission factor on average by 4% (range from 0.4 to 34%) and the BC emission factor by 5% (range 1 to 20%), integration time has little to no effect on the EF size. Changing the background (chasing method) for 10% can change the calculated EF for 50%. Background should thus be measured and set very carefully. Emission factors are variable for the individual vehicle, and a calculated average EF is not representative. EFs for different speeds are similar and significantly increase at acceleration. EF for PN and BC are not the same.

These tests were a methodological introduction to a larger chasing measurement campaign performed on European highways and regional roads where we measured emissions of ~ 250 vehicles and future stationary measurements where EF of larger number of vehicles can be performed in relatively short time. Knowing variability we found in this study, we can apply measured results to fleet contributions or site specific primary emission.

REFERENCES

Ban – Weiss, G. A., Lunden, M. M., Kirchstetter T. W., Harley, R. A., 2009, Measurement of Black Carbon and Particle Number Emission Factors from Individual Heavy-Duty Trucks, Environ. Sci. Technol., 43, 1419–1424

Hansen, A.D.A and Rosen, H., 1990. Individual Measurements of the Emission Factor of Aerosol Black Carbon in Automobile Plumes. Air Waste Manage. Assoc. 40: 1654-1657.

Janssen, N.A.H., Hoek,G., Simic-Lawson, M., Fischer, P., van Bree, L., ten Brink, H., Keuken, M., Atkinson, R.W., Anderson, H.R., Brunekreef, B. and Cassee, F.R., 2011. Black Carbon as an Additional Indicator of the Adverse Health Effects of Airborne Particles Compared with PM10 and PM2.5. Environ Health Perspect 119:1691–1699

Kirchstetter, T.W., Harley, A., Kreisberg, N.M., Stolzenburg, M.R., Hering, S.V., 1999. On-road measurement of fine particle and nitrogen oxide emissions from light- and heavy-duty motor vehicles. Atmospheric Environment 33, 2955–2968.

Ramanathan, V., Carmichael, G., 2008. Global and regional climate changes due to black carbon. Nature Geoscience 1, 221 - 227

Sciare, J., O. Favez, K. Oikonomou, R. Sarda-Estève, H. Cachier, and V. Kazan. 2009. Long-term measurement of fine particle and nitrogen oxide emissions from light- and heavy-duty motor vehicles. Atmospheric Environment 33, 2955–2968.

Wang, X., Westerdahl, D., Wo, Y., Pan, X., Zhang, K. M., 2011, On-road emission factor distributions of individual diesel vehicles in and around Beijing, China; Atmospheric Environment 45, 503-513

Weingartner, E., Keller, C., Stahel, W.A., Burtscher, H., Baltensperger, U., 1997. Aerosol emission in a road tunnel. Atmospheric Environment 31, 451–462.

Primary and secondary PM from shipping

Jana Moldanová [*], Marie Haeger Eugensson, Lin Tang, Erik Fridell
IVL, Swedish Environmental Research Institute, Gothenburg, Sweden

Andreas Petzold
DLR-Institut für Physik der Atmosphäre, Oberpfaffenhofen, Germany

ABSTRACT: Emissions of exhaust gases and particles from seagoing ships contribute significantly to the anthropogenic emissions and thereby affect the chemical composition of the atmosphere and air quality both on the global, regional and on the local scale. Particles emitted by marine engines consist of a volatile and non-volatile fraction. Volatiles are mainly sulphate with associated water and organic compounds. Non-volatiles consist of elemental carbon (soot, char) and of ash and mineral compounds containing Ca, V, Ni and other elements. Within EU-FP7 project TRANSPHORM the available emission factors (EF) of particulate matter mass, chemical composition and number concentration were reviewed and the available information was completed with new data measured during two targeted measurement campaigns on size-resolved EF for OC, EC, metal composition and volatile and non-volatile PM mass fractions.
Relative contribution of primary and secondary PM from shipping to PM concentrations on urban and regional scales were then investigated with a plume model and with a small-scale dispersion model TAPM model in order to elucidate role the often neglected formation of secondary inorganic PM in harbour cities. The secondary sulphate and nitrate from shipping emissions were found to make a significant contribution to the total shipping-related PM. Also in the polluted environment and under low photochemistry this contribution is significant as S can be oxidized in sea-salt particles. The primary PM is, however, an important part of the total and an accurate determination of emissions of PM including the primary particulate sulphate is very important for correct evaluation of the environmental effects of the PM pollution from shipping.

1   INTRODUCTION

Emissions of exhaust gases and particles from seagoing ships contribute significantly to the anthropogenic emissions and thereby affect the chemical composition of the atmosphere and air quality both on the global, regional and on the local scale. On European level shipping in seas surrounding Europe emits 45, 52 and 22% of the EU-27 anthropogenic emission totals for NO_X, SO_2 and particulate matter (PM), respectively (www.emep.int). Uncertainties in emission inventory of PM emission from shipping are, however, large. In harbour cities the PM emissions from shipping can contribute to the total emission as much as the road traffic (excluding the road dust) (Haeger-Eugensson et al., 2010). In addition to the primary emitted PM the gaseous emissions contribute to air pollution with secondary PM after being processed in atmosphere. The environmental effects of PM from shipping include negative impact on human health through increased concentrations of particles in many coastal areas and harbour cities, acidification and eutrophication of waters and ecosystems in coastal areas and the climate impact (Eyring et al., 2010 and references there in).

The reason of the high contribution of navigation to the emission totals is the fact that shipping emissions have been, in difference from the land sources, for a long time unregulated and only in last few years regulation is gradually entering into force through Annex VI of the Marine Pollution Convention (MARPOL) that was adopted by the Marine Environmental Protection Committee (MEPC) of the International Maritime Organisation (IMO). Annex VI which came into force in May 2005 is mainly targeting emissions of sulphur through maximum allowed fuel sulphur content

---
[*] *Corresponding author:* Jana Moldanová, IVL, Swedish Environmental Research Institute, Box 53021, 400 14 Gothenburg, Sweden, Email: janam@ivl.se

and to some extend emissions of NO_X. Emissions of PM are addressed only indirectly through decrease of formation of secondary PM from the reductions in SO_2 and NO_X. The Annex VI measures will also impact emissions of the primary PM due to enforced improvements in fuel quality associated with reduction of the fuel sulphur content and effect of engine improvements and installations of emission cleaning technologies. These effects are, however, very uncertain as only few measurements of PM and PM composition providing this information are available.

The contribution of PM emissions from shipping to the PM emission totals on local/urban scale frequently considers the primary particles only. Majority of the urban air quality studies neglect formation of the secondary PM as this effect is assumed to be small in polluted atmosphere of a city. However, meteorological conditions in harbour cities can often be favourable of more intensive chemistry as a relatively clean marine air enters a city over the harbour. In global and continental-scale studies formation and effects of the secondary inorganic PM is considered and makes a significant contribution to the PM concentration increase caused by shipping. E.g. c.a. 50% of the health effects from shipping-related PM in global study of Corbett et al. (2007) comes from the secondary PM. In this short paper the emission factors of primary PM from shipping and its components are reviewed and role of formation of the secondary PM on small-scale is discussed.

2   EXPERIMENTAL

Emissions from a marine engine will depend on the type of fuel used as well as on characteristics of the engine. The most important fuel parameters are if the fuel is heavy fuel oil (residual fuel, HFO or residual oil, RO) or marine distillates (marine gasoil, MGO or marine diesel, MDO) and the sulphur content (FSC). Emissions have been found to vary significantly between engines. Probably the maintenance and age of the engine are important for certain emission factors. For calculating emissions one usually considers the engine power, the engine speed and the emissions standard. The latter applies to nitrogen oxides only. However, one can suspect that the emissions standard also will influence the emissions of particles and hydrocarbons, although there is, for most cases, not enough data available to draw conclusions about this. Here we present emission factors as emission per kg-fuel consumed meaning that the total emission is obtained from multiplying the emission factor with mass fuel consumed.

Emissions of some species like SO_2, CO_2 and metals are directly proportional to the SFC and fuel composition, regardless the type of engine or its operation regime (abatement techniques not accounted). Others, like NO_X, VOC, CO and PM are dependent on combustion regime and thus on type of engine, its power setting and on physical properties of the fuel. Here we present only the cruise-condition emission factors. More detailed review is given in Moldanová et al. (2012a).

The chemical transformation of ship emissions in plumes was investigated with a plume version of Model Of Chemistry Considering Aerosols (MOCCA) (Moldanová, 2010). The model includes comprehensive gas-phase and condensed phase chemistry including NO_x, SO_x, organics, halogens and reactions on soot. The aerosol is treated with a segmental aerosol module consisting of 7 sea-salt and 7 sulphate bins. Background concentrations and emissions for Göteborg are used from the urban-scale simulations of TAPM (see below). The plume dispersion is simulated by two parallel boxes with the plume box entraining the background air simulated by the second box. The plume mixing is described by Gaussian dispersion, the dispersion parameters were also calculated with help of the TAPM simulations (see below).

While the plume simulations provide qualitative information on formation of the secondary PM, a quantitative assessment needs to be done with a 3-d model. For this purpose the effect of the secondary PM on air pollution from shipping in Göteborg was studied with TAPM model. TAPM is a 3D consisting of two models, one meteorological and one dispersion model (Hurley et al, 2005). TAPM also includes chemistry such as NO/NO_2, ozone formation, SO_2 and particle transformation. The meteorological model was run in 3 nestings, the largest covering Northern Europe, the second south-western past of Sweden and northern Jutland and the smallest for city of Göteborg on resolution 100x100m. Dispersion model with chemistry was run on the smallest scale only and the chemical fields were nested into the chemical fields produced by the EMEP model for gridcells on the border of the city. Emissions for Göteborg including shipping are from the database of Environmental Agency of Göteborg. Three simulations were run: 1. with all shipping emissions, 2. with ship-

ping emissions of primary PM only and 3. without shipping emissions. Difference in PM results 1-2 gives primary PM, difference 1-3 giver primary plus secondary PM from shipping.

3   RESULTS AND DISCUSSION

Particles emitted by marine engines consist of a volatile and non-volatile fraction. Volatiles are mainly sulphate with associated water and organic compounds. Non-volatiles consist of elemental carbon (soot, char) and of ash and mineral compounds containing Ca, V, Ni and other elements. Because of the high content of condensable matter in the exhaust the methodology of sampling impacts the PM mass found. Sampling directly in the hot exhaust captures to a large extend only the non-volatile part of PM while sampling in the diluted and cooled exhaust captures also some of the volatiles.

The PM emissions increase with fuel sulphur content. EFPM for engines using raw oil (RO) vary between 1 and 13 g/kg fuel with the mean around 7, and for engines using marine diesel (MD) between 0.2 and 1 g/kg fuel. Figure 1 shows a plot of the available data on EFPM at cruise conditions (engine load 75-90%) against the fuel-sulphur content (FSC). We can see a clear positive trend in emission factor for PM against the FSC for data measured on engines using RO.
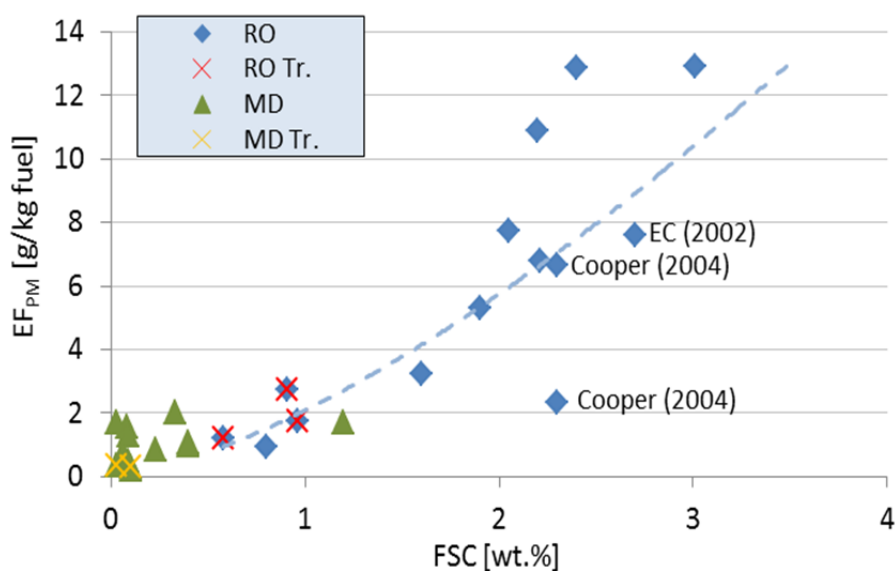
Figure 1. Emission factors for particle mass EFPM as a function of FSC (in wt. %). EFPM for RO is plotted in blue, EFPM for MD is plotted in green. Datapoints with crosses (Tr.) are from the Transphorm measurement campaigns (the dashed line fitted through the RO data has equation EF(PM) = 2.084*FSC1.4633, R2 = 0.75)

PM mass emission factors change with the engine load due to several processes. In the stack typically between 1 and 5% of sulphur is oxidized to SO3 (Moldanová et al., 2009, 2012b; Petzold et al., 2010) and contributes to the exhaust PM. Petzold et al. (2010) showed a positive correlation between the SO$_2$ in-stack oxidation and the engine load for engines using HFO with similar fuel sulphur content (between 2 – 2.5%) (Figure 2a), Transphorm measurements showed an increase in S oxidation from 0.2 to 1.4%. While EF for sulphate is positively correlated to the engine power, i.e. contributes most to the PM emissions at high engine loads, emissions of black or elemental carbon and of organic carbon are higher at low engine loads and have their minima at loads around 50% and increases somewhat at cruise conditions (Figure 2b, Petzold et al., 2010). Emission factors of other elements, mostly metals, are related to the fuel composition (V, Ni), lubricant composition (Ca, Zn and P) or can be associated with engine wear. The data in Moldanová et al., 2012a) show a good agreement between fuel composition and V and Ni found in PM. The ash-related elements make up 3-8% of PM in both HFO and MGO. The variability of the emission factors ter kg-fuel for metals is rather associated with fuel composition and composition and consumption of lubricant rather than with the engine load.

a)

b)
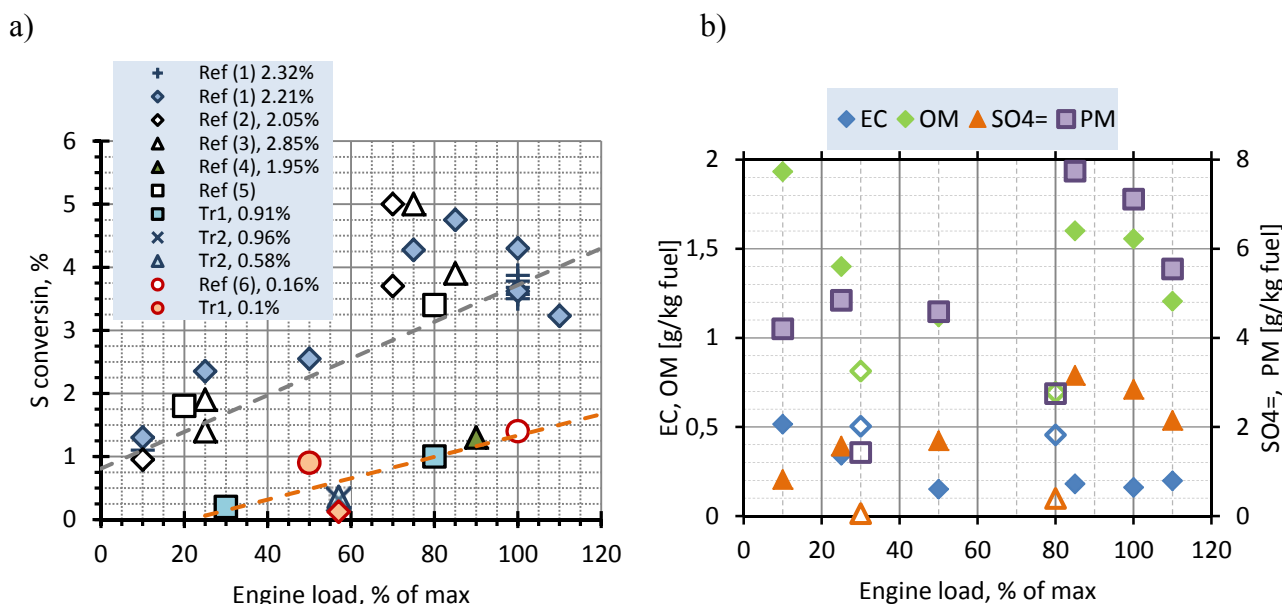
Figure 2. a - Efficiency for converting fuel sulphur to particulate-matter sulphate at various engine loads and for fuels with different sulphur contents given in wt-%; the dashed lines represent linear relationships between part of sulphur in exhaust converted to sulphate and engine load, the grey for HFO, the orange for MGO. (Ref (1): Petzold et al., 2010, Ref (2): Agrawal et al., 2008a; Ref (3): Agrawal et al., 2008b; Ref (4): Moldanová et al., 2009; Ref (5): Kurok, unpublished, Ref (6): Kasper et al., 2007, Tr1, Tr2: Data from Moldanová et al., 2012b, D2.1.4). b - Mass emission factors for carbon-containing compounds, sulphate and PM in the raw exhaust gas, FSC 2.40wt-% (filled symbols) and 0.91% (open symbols) (EC - elemental carbon, OM – organic matter, both analysed by multi-step combustion method) (from Petzold et al. 2010, data in their Table 1 and from Moldanová et al., 2012b).

The resulting dependence of EFPM on engine load thus varies with fuel sulphur content and potentially also with fuel type. One should remember that the fuel consumption varies also with the engine load making the emissions (in g/hour) higher at cruising that at low loads.

In a clean atmosphere the oxidation of the emitted SO_2 proceeds and in ship plumes sulphate becomes the dominant component of the PM (Chen et al., 2005). Our plume model simulations show that in a clean marine atmosphere under summer daytime conditions ca. 30% of the plume SO_2 is lost after 4 h, almost 50% of this loss is SO_x deposition while the other c.a. 50% is SO_2 oxidised to H_2SO_4 and lost to both seasalt and sulphate particles. Also nitrate from NO_X in the ship plume contributes to the PM as long as the sea-salt particles are alkaline enough to keep HNO_3. In our clean atmosphere case c.a. 45% of the plume NO_X was lost in 4 hours with ca. 10% deposited on sea and 35% contributing as nitrate into seasalt particles. Majority of the gas to particle exchange is through $HNO3$ dissolution in seasalt, however, in dark hours significant part goes via heterogeneous reactions of $N2O5$ with particulate water and halogens (e.g. Moldanová et al., 2001). The heterogeneous reactions takes place both on alkaline sea-salt and on acidic sulphate particles, in the second case the nitrate is expelled back to the gas phase as HNO_3. Table 1 summarizes the plume model simulations. It shows that in polluted atmosphere and under dark conditions the contribution of secondary inorganic PM from NO_X and SO_2 in ship plume is much lower, however, still significant when compared with the primary PM from shipping. When 1% of sulphur emitted from combustion of HFO with 1% FSC is oxidised and condenses on particles, it corresponds to emission factor for particulate $H_2SO_4*nH_2O$ of 0.67 g/kg fuel, for NO_X the corresponding EFHNO3 is 0.82 assuming EFNO$_x$ 70 g/kg-fuel. The total EFPM for this fuel is ca. 2 g/kg-fuel. Results in Table 1 show that in polluted situations the sea-salt particles get acidified by nitrate and as sulphate condenses on these acidified sea-salt particles it expels nitrate out.

	CBgnd NOx	SO₂ to PM				NOₓ to PM			
	(ppb)	1h	2h	4h	8h	1h	2h	4h	8h
October-day	1.2	0.15%	0.28%	0.42%	0.49%	0.03%	0.19%	0.60%	4.51%
	5.1	0.12%	0.25%	0.40%	0.48%	-0.05%	0.06%	0.75%	2.46%
	20.7	0.09%	0.15%	0.22%	0.50%	-0.06%	-0.10%	-0.13%	-0.16%
October-night	1.4	0.03%	0.05%	0.05%	0.09%	0.56%	2.96%	7.34%	11.25%
	5.1	0.03%	0.06%	0.11%	0.22%	0.27%	1.51%	3.81%	5.30%
	42.0	0.03%	0.04%	0.10%	0.45%	-0.04%	-0.04%	-0.06%	-0.10%
June-day	0.1	1.71%	6.00%	12.70%	15.30%	3.92%	13.58%	27.83%	35.09%
	0.9	0.85%	2.61%	7.55%	11.77%	1.42%	4.98%	15.72%	27.21%
	12.6	0.43%	0.86%	1.49%	2.03%	-0.21%	-0.52%	-1.10%	-1.69%
June-night	0.2	0.21%	0.43%	0.76%	4.81%	3.98%	11.78%	20.36%	30.82%
	1.5	0.23%	0.48%	0.99%	4.52%	1.76%	5.44%	12.36%	23.76%
	13.5	0.18%	0.36%	0.62%	1.17%	0.24%	0.74%	1.61%	1.54%

Table 1. Contribution of sulphur emitted as SO_2 and nitrogen emitted as NO_X into the PM expressed as part of the total SO_2 and NO_X emission from the ship stack. The 'CBgnd NO_X' is level reached in the model during the first 2 hours outside the plume (city background). The negative values in NO_X to PM contribution are for cases when shipping sulphate expelled HNO_3 originating from background pollution.

The effect of secondary PM from shipping in a more quantitative manner was tested with the TAPM model. The TAPM model does not have an explicit sea-salt chemistry which means that the nitrate contribution from shipping to PM is underestimated. Figure 3 shows PM concentration isolines around a harbour in estuary of Göteborg city simulated for October. A clear shift to higher PM concentrations can be seen when secondary PM is considered. In a 1 km distance the contributin of secondaru PM in almost as high as that of the primary PM.
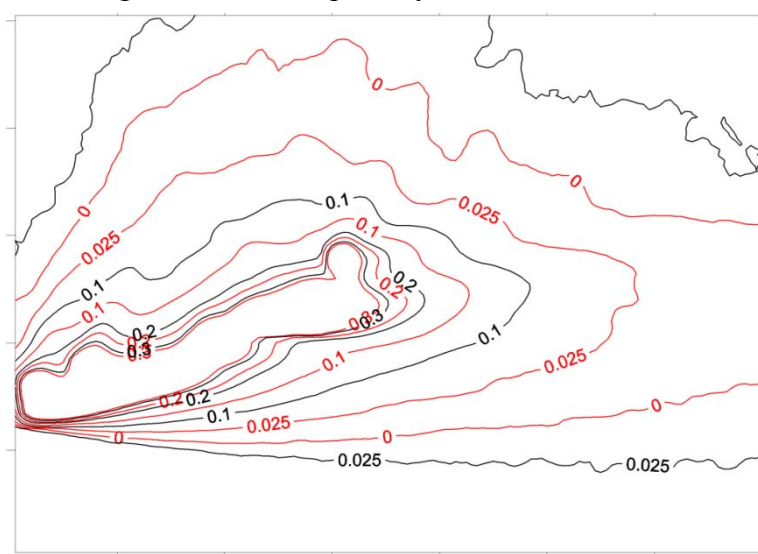
Figure 3. Conntribution of primary PM (red) and primary and secondary PM (black) from shipping emissions to the PM concentrations in Göteborg. The numbers are µg/m3 and the scale on axes is 1 km. The highest shipping PM contributions in the harbour are 10 µg/m3 (not shown).

4 CONCLUSION

The primary PM from shipping main components are non-volatile elemental (or black) carbon and mineral compounds and volatile fractions sulphate, organic carbon and associated water. With exception of mineral compounds, emissions of all other PM compounds were shown to be dependent both of the fuel quality and of the engine operation. The measured volatile part is sensitive to sampling methodology.

The model simulations have shown that secondary sulphate and nitrate from shipping SO_2 and NO_X emissions makes a significant contribution to the shipping related PM. On a regional scale under clean and moderately polluted background conditions this contribution can highly exceed the primary PM emissions. Also in the polluted environment and under low photochemistry this contribution can be in similar order of magnitude as contribution of the primary PM. Contribution of PM from shipping to the high PM concentrations at street level in cities is, however, small regardless if the secondary PM is considered or not. The contribution of shipping to PM levels is rather significant in the urban background and here the secondary PM should be considered. As the primary PM emissions are an important and often dominating part of the total when urban air pollution is concerned an accurate determination of emissions of primary particulate sulphate and OC is very important for correct evaluation of health effects of PM from shipping.

REFERENCES

Agrawal, H., Malloy, Q. G. J., Welch, W. A., Wayne Miller, J., Cocker III., D. R., 2008a. In-use gaseous and particu-late matter emissions from a modern ocean going container vessel. Atmos. Environ., 42, 5504–5510.

Agrawal, H., Welch, W. A., Miller, J. W., Cocker III, D. R., 2008b. Emission measurements from a crude oil tanker at sea. Environ. Sci. Technol., 42, 7098–7103.

Chen, G. et al., 2005: An investigation of the chemistry of ship emission plumes during ITCT 2002. J. Geophys. Res., 110, D10S90, doi:10.1029/2004JD005236.

Corbett, J.J., Winebrake, J.J., Green, E.H., Kasibhatla, P., Eyring, V., Lauer, A., 2007. Mortality from ship emissions: a global assessment. Env. Sci. Technol., 41, 8512–8518.

Eyring, V., Isaksen, I.S.A., Berntsen, T., Collins, W.J., Corbett, J.J., Endresen, Ö., Grainger, R.G., Moldanova, J., Schlager, H., Stevenson, D.S. (2010) Assessment of Transport Impacts on Climate and Ozone: Shipping, Atmos. Env., 44, 3735-3771.

Haeger-Eugensson, M., Moldanova, J., Ferm, M. Jerksjö, M., Fridell, E., 2010. On the increasing levels of NO2 in some cities - The role of primary emissions and shipping. IVL report B1886.

Hurley, P., 2005: The Air Pollution Model (TAPM), User manual. CSIRO Atmospheric Reasearch International Paper No.31, CSIRO Atmospheric Research, Aspendale, Vic.

Kasper, A., Aufdenblatten, S., Forss, A., Mohr, M., Burtscher, H., 2007. Particulate emissions from a low-speed marine diesel engine. Aerosol Sci. Technol., 41, 24–32.

Moldanová, J., Ljungström, E., 2001. Sea salt aerosol chemistry in coastal areas. A model study, J. Geophys. Res., 106, 1271-1296.

Moldanová, J., Fridell, E., Popovicheva, O., Demirdjian, B., Tishkova, V., Faccinetto, A., Focsa, C., 2009: Characterisation of particulate matter and gaseous emissions from a large ship diesel engine. Atmos. Environ. 43, 2632–2641.

Moldanová, J., 2010. Report on ship plume simulations and analysis. IVL report B1920.

Moldanová, J., Fridell, E., Petzold, A., Jalkanen, J.-P., 2012a. Emission factors for shipping – final data for use in Transphorm emission inventories. FP-7 TRANSPHORM report D1.2.3 (www.transphorm.eu)

Moldanová, J., Fridell, E., Winnes, H., Jedynska, H., Peterson, K., 2012b: Physical and chemical PM characterization from the measurement campaigns on shipping emissions. FP-7 TRANSPHORM report D2.1.4 (www.transphorm.eu)

Petzold, A., Weingartner, E., Hasselbach, J., Lauer, P., Kurok, C., Fleischer, F., 2010. Physical properties, chemical composition, and cloud forming potential of particulate emissions from marine diesel engines at various load condi-tions. Environ. Sci. Technol. 44, 3800–3805.

Particle and trace gas properties from ship exhaust plumes: Emission characteristics and impact on air quality

J.-M. Diesch[*], F. Drewnick, T. Klimach
Max-Planck-Institute for Chemistry, Mainz, Germany

S. Borrmann
Max-Planck-Institute for Chemistry, Mainz, Germany

Institute of Atmospheric Physics, Gutenberg University Mainz, Germany

Keywords: ship emissions, ship exhaust plumes, emission factors, vessel types

ABSTRACT: Gaseous and particulate emission plumes from more than 200 individual commercial and marine vessels were sampled in April 2011 on the banks of the Elbe which is passed by numerous ships entering and leaving the port of Hamburg, Germany. The mobile laboratory "MoLa" was located in immediate vicinity (0.3-2 km) of the ship lanes and measured physical and chemical aerosol parameters including particle size distributions and several trace gases. With the help of numerous ship information from the Automatic Identification System (AIS) an extensive study of the emissions from different vessel types was performed. Calculated emission factors indicate that ships either emit high black carbon concentrations or high particle number concentrations. Particle number size distributions have shown nuclei particles in the 10-20 nm size range and two dominant modes at about 35 and 100 nm. The typical immission impact is dominated by container ships, tanker and cargo ships (80-95 %) and amounted on average to 5-20 % of the total pollutant burden dependent on the investigated parameter. While ship emissions have an impact on the ambient aerosol acidification, also a change of the ground level ozone and of the submicron particle composition was found.

1   INTRODUCTION

Exhaust gases and particles emitted from marine vessels contribute to the anthropogenic pollution, affecting the chemical atmospheric composition, local and regional air quality and climate (Moldanova et al., 2009; Petzold et al., 2008). Direct climate effects are caused by positive radiative forcing of CO_2 and black carbon emissions while negative forcing results from particulate sulfate (Endresen et al., 2003; Eyring et al., 2010). Additionally, increased NO_x levels influence the ozone chemistry therefore increase hydroxyl radical concentrations and the oxidation power of the atmosphere (Lawrence and Crutzen, 1999). As particles may act as cloud condensation nuclei, visible as so-called "ship tracks", they indirectly affect global radiative forcing and therefore climate (Dusek et al., 2006). As a large fraction of ship emissions occur next to land a strong impact on air quality in coastal and port regions exists. For this reason, national and international regulations for emissions from commercial marine vessels exist. The North and Baltic Sea comprise an emission control area (ECA) where ships have to switch to low sulfur fuel (max. 1% since July 2010). In this study measurements were performed on the banks of the Elbe in Northern Germany, also belonging to this ECA. Emission factors of chemical and physical aerosol properties and trace gases as well as particle size distributions were determined for the individual vessel plumes. Using ship information data, the vessels were categorized. We also discuss the impact of ship emissions on air quality and chemistry.

---

[*] *Corresponding author:* Jovana-Maria Diesch, Particle Chemistry Department, Max-Planck-Institute for Chemistry, 55128 Mainz, Germany. Email: J.Diesch@mpic.de

2   FIELD EXPERIMENT

Measurements were performed in April, 2011 near the Elbe river mouth, Germany (see Fig. 1a) where numerous private and marine vessels entering and leaving the port of Hamburg, the second largest European freight port. During 5 days of sampling in this ECA more than 200 vessels were probed out of which 111 ship plumes are of sufficient quality to be considered in this study. The remaining ships were measured simultaneously or did not exhibit a significant increase in CO_2 emissions needed to calculate emission factors. The sampling was performed at different sites on the banks of the Elbe, downwind of the river, between Cuxhaven and Hamburg (53°50'N, 9°20'E; Fig. 1b) using the mobile laboratory "MoLa".

A large set of state-of-the-art instruments implemented in "MoLa" measured the ship exhaust plumes with high time resolution at a distance of about 0.3 – 1.5 km to the shipping lanes. This included a Condensation Particle Counter (CPC 3786, TSI, Inc.) and an Environmental Dust Monitor (EDM 180, Grimm) measuring PM_1, $PM_{2.5}$ and PM_{10} for the information on physical aerosol particle properties. Size distributions in the size range from 6 nm until 32 µm were registered using a Fast Mobility Particle Sizer (FMPS 3091, TSI, Inc.), an Aerodynamic Particle Sizer (APS 3321, TSI, Inc.) as well as an Optical Particle Counter (OPC 1.109, Grimm). Chemically classified NR-PM_1 species were detected by the High-Resolution Time-of-Flight Aerosol Mass Spectrometer (HR-ToF-AMS, Aerodyne Res., Inc.). A Multi Angle Absorption Photometer (MAAP, Thermo E.C.) registered black carbon concentrations and polycyclic aromatic hydrocarbons were appointed by a PAH monitor (PAS 2000, EcoChem. Analytics). The Airpointer (Recordum GmbH) monitored SO_2, CO, NO, NO_2 and O_3 and the LICOR 840 gas analyzer (LI-COR, Inc.) measures CO_2. In addition, local meteorology was determined using a WXT510 (Vaisala) weather station.

Specific data of the vessels (ship name, commercial type, length, breath, gauge, speed, position, fuel consumption, gross tonnage, engine power) were gathered via Automated Identification System (AIS) broadcasts.

3   METHODOLOGY AND RESULTS

3.1   *Data processing, plume analysis & vessel classification*

For a more efficient and more objective handling of the comprehensive data set including the numerous ship exhaust plumes, a data analysis tool was programmed. This tool supports the characterization of the ship emissions and the assessment of the emission impact on local air quality. On the one hand it calculates emission factors for each ship and parameter from ratios of excess pollutants (above background) to CO_2 in grams of pollutant emitted per kilogram of fuel burned based on the CO_2 balance method (Hobbs et al., 2000). This method assumes that all of the carbon is emitted as CO_2 and accounts for plume dilution. On the other hand, the emission impact on local air quality was calculated by integration of the complete ship emission peaks for each parameter.

The classification into different ship types using AIS data yielded the following 7 classes with corresponding counts of each type: container ships (57), tankers (20), ferries (7), cargo ships (12), reefer & bulkcarriers (4), riverboats (8), others (3).
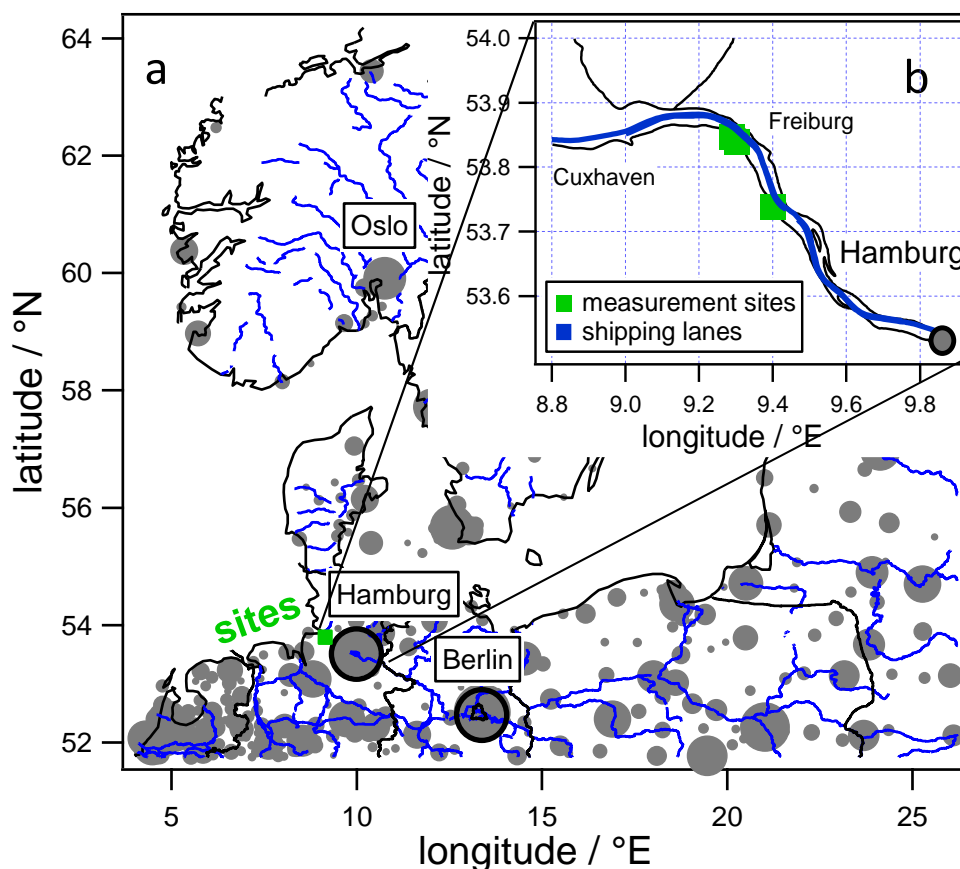
Figure 1. Map showing the measurement sites located between Cuxhaven and Hamburg, Northern Germany on a large scale (a) and in a close-up showing the positions where MoLa was operated (b).

3.2 *Characterization of emissions*

Ship plumes were identified as peaks in the time series that lasted about 2 minutes and are pronounced more or less, dependent on the kind of measured parameter. A sharp increase was observed for the following parameters and used for plume identification: concentrations of total particle number and mass, black carbon, PAH, SO_2, NO_x, CO_2, AMS organic and sulfate. In contrast, O_3 was indirectly affected and decreased within the plume due to reactions with NO. Size-resolved particle number concentrations showed peaks with modes in the 10-120 nm size range (see Fig. 2).

Particle number (PN) emission factors (EF) which amount to $2.55 \cdot 10^{16} \pm 1.19 \cdot 10^{16}$ # kg^{-1}, on average were found to depend on the fuel sulfur content, the engine type and load as higher temperatures and pressures lead to a more complete combustion process. Black carbon emissions (avg. $EF_{BC}=0.15\pm0.17$ g kg^{-1}) instead highly depend on the engine type and apparently have a large impact on the number EFs through suppression of new particle formation by condensation and coagulation. For this reason, a minimal overlap among high PN and high BC emitters was found. NR-PM_1 in the emissions ($EF_{PM1}=2.5\pm2.3$ g kg^{-1}) is mainly composed of organic matter ($EF_{OM}=1.8\pm1.7$ g kg^{-1}), sulfate ($EF_{SO4}=0.54\pm0.46$ g kg^{-1}) and BC and also depends on fuel sulfur content, engine type and load. While OM is the most abundant aerosol fraction (72%) in the emissions, sulfate amounts to 22%, BC to 6% and PAHs to 0.2% ($EF_{PAH}=5.3\pm4.7$ mg kg^{-1}). Like sulfate, SO_2 ($EF_{SO2}=7.7\pm6.7$ g kg^{-1}) is mainly related to the fuel sulfur content. However, both SO_2 and NO_x were found to increase with vessel speed i.e., engine load and therefore combustion temperature. Additionally, also the particle number size distribution mode in the 10-20 nm range depends on the sulfur content in the fuel. In contrast to the smaller vessels (small tankers, riverboats and others) which clearly exhibit this mode, larger vessels have larger engine exhaust systems which lead to increased particle losses by condensation and coagulation of the freshly formed particles. Therefore, the combustion aerosol mode situated at about 30 nm dominates for the larger vessels (container ships, large tankers, ferries & RoRos, cargo ships, reefer & bulkcarriers). Smaller vessels additionally show a mode at about 100 nm which occurred primarily when high BC emitters were sampled.
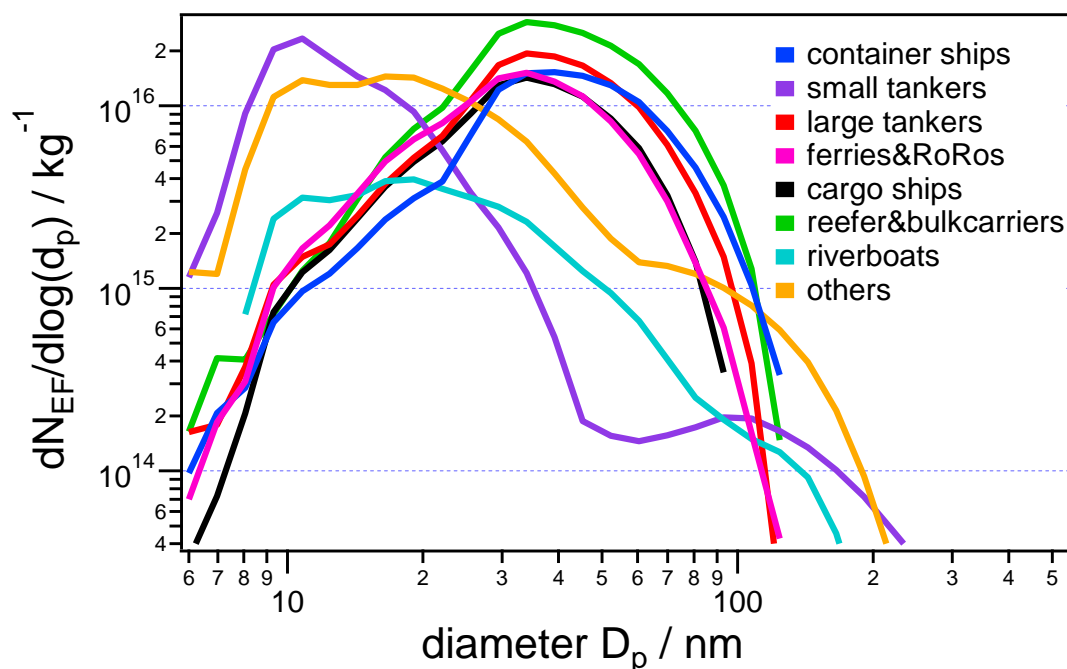
Figure 2. Size-resolved particle number emission factors for the classified vessel types. The size distribution of smaller ships is dominated by a 10-20 nm mode indicating freshly formed particles. A second mode at about 35 nm, the combustion aerosol mode appears predominantly in the plumes of larger ships. A third, weaker mode situated at ~100 nm is again found for the smaller vessels.

3.3 *Air quality impact of emissions*

The contribution of ship emissions to total pollutant immissions on the banks of the Elbe depends on the kind of parameter. For particle mass concentrations (OM, sulfate, BC, PAH) and the trace gas SO_2, the typical immission contribution from ship emissions is 5-10 %, the PN impact even amounts to 20%. When the ship-related immissions were separated into the different vessel types, container ships, tankers and cargos together cover 80-95% (BC, PAH: ~80%; PN, NO_x: ~90%; SO_2, OM, sulfate: ~95%) of the ship-related air quality impact.

Ship emissions influence the ambient submicron aerosol composition as particulate matter from ship engine exhaust is mainly composed of combustion aerosol particles (OM and BC) and sulfate. Therefore, the submicron $NR-PM_1$ in the ship plumes clearly differs from the background aerosol which is additionally composed of nitrate and ammonium.

In a detailed analysis of the sulfate fraction in the measured aerosol we found a strong impact of the ship emissions on aerosol acidification. While the background aerosol is only slightly acidic (green points, Fig. 3), sulfuric acid is suggested to be the most abundant sulfate species present in the expanding plume (blue points, Fig. 3) making the submicron aerosol highly acidic.

Also the ground-level ozone chemistry is indirectly affected by emissions of ships due to reactions of NO with available O_3. This equates to a decrease of ozone by 0.4%, on average on our measurement site. Further downwind, ozone levels will increase formed by sunlight-driven photochemical reactions with precursor species (Lelieveld et al., 2004).
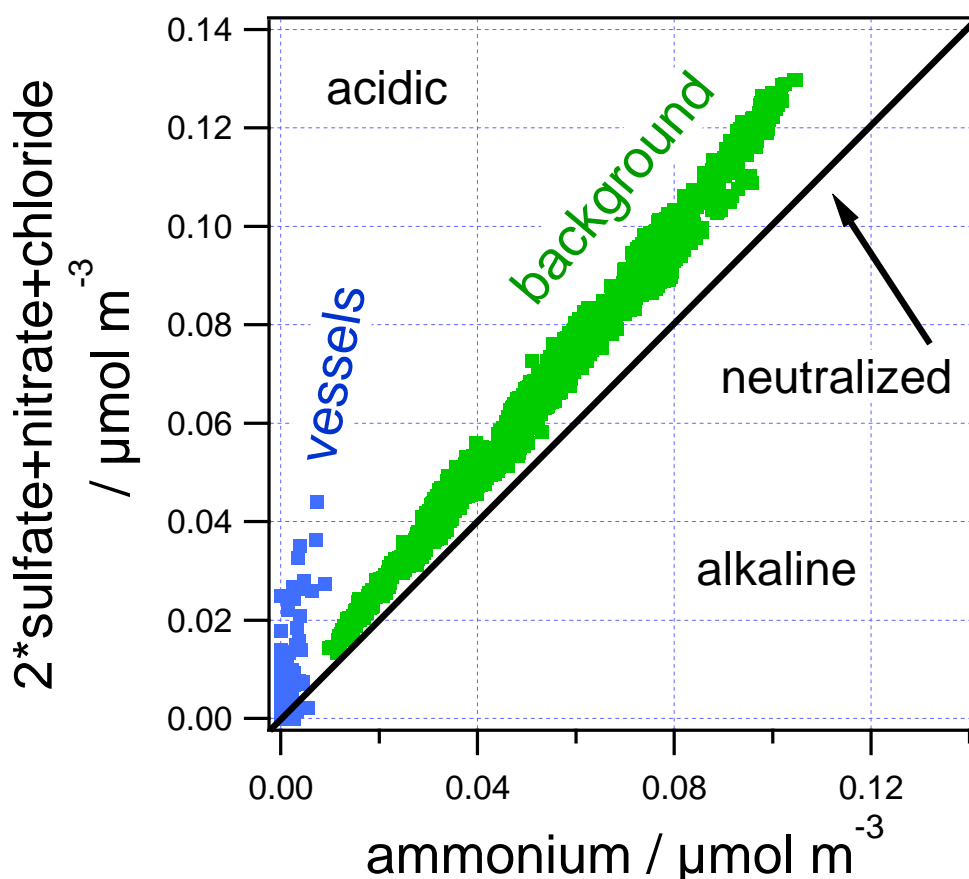
Figure 3. Correlation illustrating the differences of the ion balance between background and ship emission aerosol. Measured anions sulfate (multiplied by 2 due to the stoichiometric ratio, being fully neutralized as ammonium sulfate) nitrate and chloride versus the cation ammonium. While the background aerosol is slightly acidic (green points), due to the formation of sulfuric acid during the combustion process vessels have an impact on aerosol acidification (blue points).

4   CONCLUSIONS

Measurements of ship emissions were performed on the banks of the Elbe which is located in an emission control area using the mobile laboratory MoLa. Emission factors for various pollutants and relations within measured parameters were found. Together with the AIS data we found the particle number and size distributions, the submicron aerosol composition and particulate matter concentrations as well as the trace gas properties largely depend on fuel sulfur content, engine type and load. A detailed analysis of ship emission impact on local air quality and chemistry indicates the typical immission contribution amounts to 5-20% and is dominated by container ships, tankers and cargos, which are the most numerous vessels at the site. Additionally, ship emissions change the submicron aerosol composition and have a strong impact on aerosol acidification and ground-level ozone chemistry. Sulfur regulations affect positively local air quality, climate and health.

REFERENCES

Dusek, U., Frank, G. P., Hildebrandt, L., Curtius, J., Schneider, J., Walter, S., Chand, D., Drewnick, F., Hings,   S., Jung, D., Borrmann, S., and Andreae, M. O.: Size matters more than chemistry for cloud-nucleating ability of aerosol particles, Science, 312, 1375-1378, 2006.

Endresen, O., Sorgard, E., Sundet, J. K., Dalsoren, S. B., Isaksen, I. S. A., Berglen, T. F., and Gravir, G.: Emission from international sea transportation and environmental impact, J. Geophys. Res.-Atmos.,   108, 2003.

Eyring, V., Isaksen, I. S. A., Berntsen, T., Collins, W. J., Corbett, J. J., Endresen, O., Grainger, R. G., Moldanova, J., Schlager, H., and Stevenson, D. S.: Transport impacts on atmosphere and climate: Shipping, Atmos. Environ., 44, 4735-4771, 2010.

Hobbs, P. V., Garrett, T. J., Ferek, R. J., Strader, S. R., Hegg, D. A., Frick, G. M., Hoppel, W. A., Gasparovic, R. F., Russell, L. M., Johnson, D. W., O'Dowd, C., Durkee, P. A., Nielsen, K. E., and Innis, G.: Emissions from ships with respect to their effects on clouds, J Atmos Sci, 57, 2570-2590, 2000.

Lawrence, M. G., and Crutzen, P. J.: Influence of NO_x emissions from ships on tropospheric photochemistry and climate, Nature, 402, 167-170, 1999.

Lelieveld, J., van Aardenne, J., Fischer, H., de Reus, M., Williams, J., and Winkler, P.: Increasing ozone over the Atlantic Ocean, Science, 304, 1483-1487, 2004.

Moldanova, J., Fridell, E., Popovicheva, O., Demirdjian, B., Tishkova, V., Faccinetto, A., and Focsa, C.: Characterisation of particulate matter and gaseous emissions from a large ship diesel engine, Atmos. Environ., 43, 2632-2641, 2009.

Petzold, A., Hasselbach, J., Lauer, P., Baumann, R., Franke, K., Gurk, C., Schlager, H., and Weingartner, E.: Experimental studies on particle emissions from cruising ship, their characteristic properties, transformation and atmospheric lifetime in the marine boundary layer, Atmos. Chem. Phys., 8, 2387-2403, 2008.

Climate-compatible Air Transport System, Climate impact mitigation potential for actual and future aircraft

A. Koch[*], B. Lührs, F. Linke, V. Gollnick
DLR- Air Transportation Systems, Hamburg, Germany

K. Dahlmann, V. Grewe, U. Schumann
DLR- Atmospheric Physics, Oberpfaffenhofen, Germany

T. Otten
DLR – Propulsion Technology, Cologne, Germany

M. Kunde
DLR - Simulation and Software Technology, Cologne, Germany

ABSTRACT: The DLR developed within the project "Climate compatible Air Transport System" (CATS) a comprehensive simulation and assessment approach to quantify the potential to reduce the climate impact of air traffic with operational and technological measures.
Previous studies by the authors have shown the potential to reduce the climate impact of air traffic through global operations of a representative twin engine long-range aircraft at lower cruise altitudes and speeds. The present study analyzes the increased mitigation potential given by the combination of aircraft design and operational changes. Based on the analysis of operational changes, the reference aircraft is optimized for cruise conditions with reduced climate impact. Both aircraft, the reference and the redesigned configuration, are assessed on a global route network with varying cruise conditions relative to typical current flight profiles. Pareto optimum cruise conditions are derived for each route and the global network. The resulting fleet mitigation potential allows a cost benefit analysis, trading climate impact reduction versus increased cash operating costs.

1   CLIMATE IMPACT FROM AVIATION

Air traffic influences the Earth climate by induced cloudiness and concentration changes of atmospheric constituents caused by the emission of carbon dioxides (CO_2), nitrogen oxides (NO_x), sulphur oxides (SO_x), water vapor (H_2O) and aerosols [IPCC 1999]. These atmospheric perturbations change the terrestrial radiation balance and cause a radiative forcing (RF) that drives the earth-atmosphere system to a new state of equilibrium through a resulting temperature change. The global air traffic contributed approx. 3% to the total anthropogenic radiative forcing cumulated until 2005 [Lee et al. 2009]. However, without any countermeasures the projected air traffic growth of approx. 5 % revenue passenger kilometers per year till 2036 [ICAO 2008] will largely surpass the typical annual fuel efficiency improvements of 1-2 % and further increase the climate impact from aviation [IPCC 2007].

   The Advisory Council for Aeronautical Research in Europe (ACARE) states in this sense that a social and climate compatible air transportation system is required for a sustainable development of commercial aviation. To achieve such a climate compatible air transport system, mitigation strategies need to be developed based on comprehensive assessments of the different impacting factors and resulting reduction potentials and costs. Various concepts have been investigated in the past, including trajectory optimization for contrail avoidance [Mannstein et al. 2005; Gierens at al. 2008;

---

   [*] *Corresponding author:* Alexander Koch, German Aerospace Center (DLR) - Air Transportation Systems, Blohmstrasse 18, 21079 Hamburg, Germany, Email Alexander.Koch@dlr.de, Phone +49-40-42878-3634

Campbell et al. 2009; Sridhar et al. 2011; Schumann 2011], general changes in flight altitudes [Fichter 2009; Koch et al. 2011; Dahlmann 2011; Koch et al. 2012; Matthes et al. 2012], and aircraft design changes for reduced climate impact [Egelhofer 2008; Schwartz and Kroo 2011a]

Anyhow, the sound assessment of changes in current flight procedures and aircraft design is a complex task due to many interdependencies between the different areas of the air transport system. Options that appear to provide a benefit in a certain aspect (e.g. climate impact) are likely to bring drawbacks in another aspect (e.g. ATM capacity, flight scheduling, etc.). Further challenge is added to the optimization of air traffic due to the complexity of atmospheric processes and the related effort in climate impact modeling. The evaluation of options to reduce the climate impact from aviation by new technologies and operational changes requires expert knowledge from different disciplines and adequate models that sufficiently incorporate the driving impact factors. Such a comprehensive simulation and analysis approach has been developed in the DLR project *Climate compatible Air Transport System* (CATS) [Koch et al. 2009, 2011, 2012].

2   THE CATS SIMULATION AND ANALYSIS WORKFLOW

The assessment of complex multidisciplinary topics requires a range of experts and models. Commonly the experts from research and/or industry entities are not located at the same location but are regionally distributed. This leads to the need of a distributed design and analysis environment that links the required disciplinary analysis models and provides means for remote triggering, overall process control, convergence and optimization.

The CATS simulation workflow (Figure 1) is based on the integration framework *Remote Component Environment* (RCE)[(viii)] in combination with the *Chameleon Suite*[(viii)] to link the different models models [Seider et al. 2012]. The central data model *Common Parametric Aircraft Configuration Scheme* (CPACS)[(ii)] is used for flexible and efficient data exchange [Nagel et al. 2012]. Both components are developed by DLR and available open source also to external research and industry institutions [DLR 2012]. Different process control scripts are integrated for the variation / optimization of routes or aircraft configurations. The integration framework and analysis models are provided by several DLR institutions and academia as listed at the end of this document (indices *i-viii*). The involved experts ensure in a collaborative way the plausibility of models and simulation results.
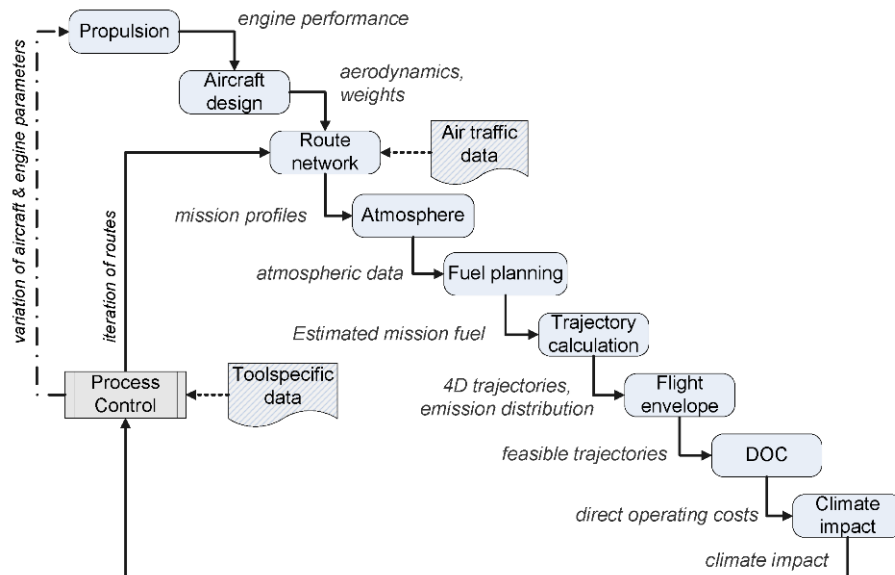
Figure 1: CATS simulation workflow with integrated models and iteration paths for varying routes and/or aircraft design changes.

The multi-disciplinary aircraft design tool *Preliminary Aircraft Design and Optimization*[(viii)] (*PrADO*) is applied to calculate the flight performance and technical characteristics of actual and novel aircraft configurations. *PrADO* comprises physical models with empirical extensions for aerodynamics, structural sizing, weight prediction, flight performance incl. trim calculations and geometry description [Heinze 1994]. *PrADO* can further be applied to determine the influence of aircraft sub-

systems on engine performance through bleed air and shaft power extraction. The surrogate data-base model *TWdat*[(iii)] provides engine performance maps for several current engines and possible future propulsion concepts, which are pre-calculated by the well-established thermodynamic cycle program *Varcycle*[(iii)] [Deidewig 1998] and fitted to real engine data where possible. The performance maps further contain emission indices (i.e. CO, NO_x, soot), thrust and fuel flow characteristics [Döpelheuer and Lecht 1998].

Models for preliminary flight preparation (*RouteGen*[(ii)] and *FuelEstimator*[(ii)]) provide relevant data concerning the route description and mission profile (airports, vertical and lateral flight path, yearly frequencies), estimated mission fuel and resulting payload limitations for all analyzed routes. Annual mean atmospheric data along each route, including temperature, pressure, relative humidity (for NO_x correction), wind vectors are provided by the model *Atmos*[(i)] as function of latitude and altitude. The *Trajectory Calculation Module (TCM)*[(ii)] is applied to calculate the resulting trip fuel and detailed emission inventories with 4D trajectories [Linke 2008]. *TCM* performs a fast-time simulation integrating the relevant flight conditions based on the total energy model. It reads as input the mission parameters, aircraft weight breakdown, engine and aerodynamic performance tables for different high-lift configurations provided by *TWDat* and *PrADO*. This capability enables the flight performance simulation and evaluation of novel aircraft concepts. The model *FlightEnvelope*[(ii)] checks each calculated flight trajectory if aircraft specific operating constraints (stall, buffet and altitude limits) are violated. In such case the concerning trajectories are removed from the dataset.

The climate impact of each flight is assessed with the climate response model *AirClim*[(i)] [Grewe 2008; Fichter 2009; Dahlmann 2011; Grewe and Dahlmann, 2012]. The model comprises response functions derived from 78 steady-state simulations with the DLR climate-chemistry model *E39/CA*, prescribing normalized emissions of nitrogen oxides and water vapor at various atmospheric regions. *AirClim* was specifically developed for aviation studies and considers the altitude and latitude of emission. It further considers the climate agents CO_2, H_2O, CH_4, O_3 and primary mode ozone (latter three resulting from NO_x emissions), line-shaped contrails and contrails cirrus clouds. Combining aircraft emission data with the higher fidelity sensitivities, *AirClim* calculates the temporal evolution of radiative forcing (RF) and resulting global near surface temperature change $\Delta T(t)$. Integrating the temperature change over a specified time horizon provides the average temperature response (ATR, expressed in K), which is a suitable metric to compare the future climate impact of different technologies and air traffic scenarios [Schwartz and Kroo 2011b; Dahlmann 2011].

$$ATR_H = \frac{1}{H} \int_t^{t+H} \Delta T(t) \, dt \tag{1}$$

Applied in comparative studies, *AirClim* further includes a statistical treatment of the uncertainties in climate impact modeling. It provides by means of internal Monte-Carlo simulations the probability distribution of ATR, which allows the definition of the minimum, median and maximum estimated temperature change [Dahlmann 2011].

Depending on the scope and goal of the study, a DOC[(ii)] model calculates the cash operating costs (COC) or direct operating costs (DOC) for each flight [USD/cycle], including the costs for fuel, crew, maintenance, navigation and landing fees (and financing) [Liebeck 1995].

3   EVALUATION METHODOLOGY

The current assessment methodology is split into three sequential evaluation steps. In a first step, the reference traffic scenario is defined for a chosen year. It includes a global route network with route-specific yearly flight frequencies and typical vertical flight profiles as well as the performance model of the reference aircraft.

In a second step, the operational climate impact mitigation potential is assessed for the reference aircraft. This done consecutively for each route in the global network by computing the average temperature response and cash operating costs for numerous flight trajectories with varying cruise altitude and speed. The resulting changes are expressed relative to the route-specific reference tra-

jectory and provide a Pareto front with best combinations of relative ATR and COC changes. The route-specific Pareto fronts are summed for the entire network, allowing a cost-benefit analysis on route level but also on network level.

In a third evaluation step, the frequency distribution of initial cruise altitudes (ICA) and cruise Mach numbers (Ma_{cr}) are assessed for a selected COC change in order to derive new design conditions for future aircraft with reduced climate impact. Based on this, the reference aircraft is optimized for the new cruise conditions while keeping identical payload range capabilities and design constraints. The redesigned configuration is re-assessed like the reference aircraft with the above outlined methodology, showing the mitigation potential resulting from aircraft design changes. Combining operational and technological changes provides an estimate about the mitigation potential and related costs for a climate compatible air transport system.

3.1 *Reference traffic scenario*

The reference traffic scenario includes key aspects of typical current global air traffic. The reference aircraft for the present study is an Airbus A330-200, being a top selling representative in the medium- and long-range market. The configuration equipped with CF6-80E1A3 engines is modeled with *PrADO* and *TWDat*. Therefore the external geometry, cabin configuration and structural layout are modeled according to the real aircraft. The predicted aircraft component weights and drag polar are calibrated on available manufacturer data.

The route network contains all flights operated in the year 2006 by the reference aircraft, resulting in a set of 1178 globally distributed city pair connections with corresponding flight frequencies. Figure 2 depicts the reference aircraft model (a) and analyzed route network (b). The modeled vertical flight profile includes several flight phases based on typical air traffic management (ATM) procedures and respects the common speed and altitude constraints during climb and descend. The cruise phase is modeled as continuous climb cruise with constant lift coefficient. The reference vertical flight profile for each route is derived from real flight plans submitted to Eurocontrol – CFMU, which are analyzed in the present study with respect to the requested initial cruise altitude and speed. The data is kindly provided by Eurocontrol for research purpose and contains 1476 flights that are clustered by mission distance (great circle between origin and destination) into groups of 250 km. For each distance segment the mean cruise conditions are mapped to the corresponding routes in the global network.

(a)   (b)
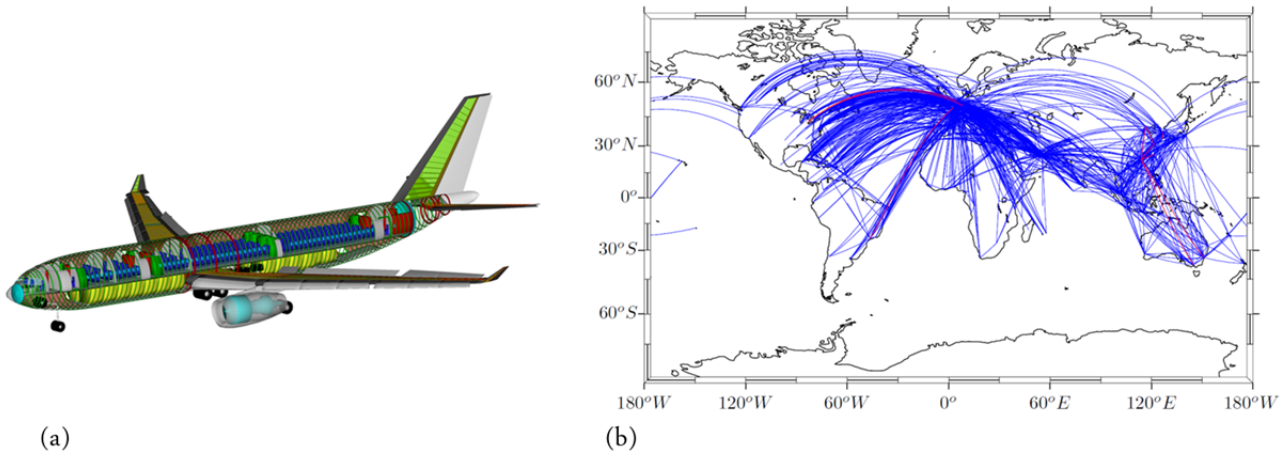
Figure 2: Geometry model of reference A330-200 (subfigure a) and analyzed global route network containing all flights operated by the aircraft in 2006 (subfigure b).

The present assessment focuses on the cash operating costs (COC) per flight with 2006 price levels, assuming a global average fuel price of 0.595 USD/kg. The climate impact is calculated for sustained emissions over 32 years (2006-2038), which corresponds to the average lifetime of the reference aircraft. The average temperature response is integrated for the time frame of H=100 years (ATR_{100}) starting in 2006. Further details concerning the reference traffic scenario and model settings are given in [Koch et al. 2012].

3.2 *Relative change of climate impact and operating costs for varying cruise conditions*

To quantify the mitigation potential given by global operations on lower cruise altitudes and speeds, numerous cruise operating conditions are simulated for each route in the global network. For each route (index i), variations of cruise Mach numbers (Ma_{cr}) and initial cruise altitudes (ICA) are conducted. For each ICA, Ma_{cr} combination and resulting feasible trajectory (index k), the changes of $ATR_{i,k}$ and $COC_{i,k}$ are expressed relative to the route-specific reference trajectory.

$$COC_{rel,i,k} = \frac{COC_{i,k}}{COC_{i,ref}} \tag{2}$$

$$ATR_{rel,i,k} = \frac{ATR_{i,k}}{ATR_{i,ref}} \tag{3}$$

Expressing further the relative changes for all analyzed trajectories (on route i) as cost-benefit ratio $ATR_{rel,i,k}$ vs. $COC_{rel,i,k}$ provides a Pareto front with ICA, Ma_{cr} combinations that maximize the mitigation potential on the given route (Figure 3a). For the following evaluation only the Pareto optimal ICA, Ma_{cr} combinations (elements of the Pareto front) are taken into account (index kp). The relative changes of climate impact and direct operating cost differ for each route due to varying atmospheric sensitivities and cost shares, hence altering the mitigation potential obtained at given cruise condition. To obtain the mitigation potential for the global network with n routes (index *all*) at a given global relative cost change $COC_{rel,all,kp}=x$, every route specific Pareto front is intersected at the specified value of x (Figure 3b). The resulting relative climate impact reductions $ATR_{rel,all,kp}(x)$ are summed for all n routes after being weighted by the route specific flight frequency f_i. The same approach is applied to determine the resulting global change of cash operating costs $COC_{rel,all,kp}(x)$.

$$COC_{rel,all,kp}(x) = \frac{\sum_{i=1}^{n} f_i \cdot COC_{i,kp}(x_i)}{\sum_{i=1}^{n} f_i \cdot COC_{i,ref}} \tag{4}$$

$$ATR_{rel,all,kp}(x) = \frac{\sum_{i=1}^{n} f_i \cdot ATR_{i,kp}(x_i)}{\sum_{i=1}^{n} f_i \cdot ATR_{i,ref}} \tag{5}$$

Applying this process for all cost changes x between the minimum and maximum values of $COC_{rel,i,kp}$ provides the Pareto front for the global route network and world fleet of the analyzed aircraft (Figure 3c). Please note that the mitigation potential is only given at the computed discrete values of relative cost changes, which means that no interpolation between the Pareto elements is possible without loss of the calculated ATR confidence interval.
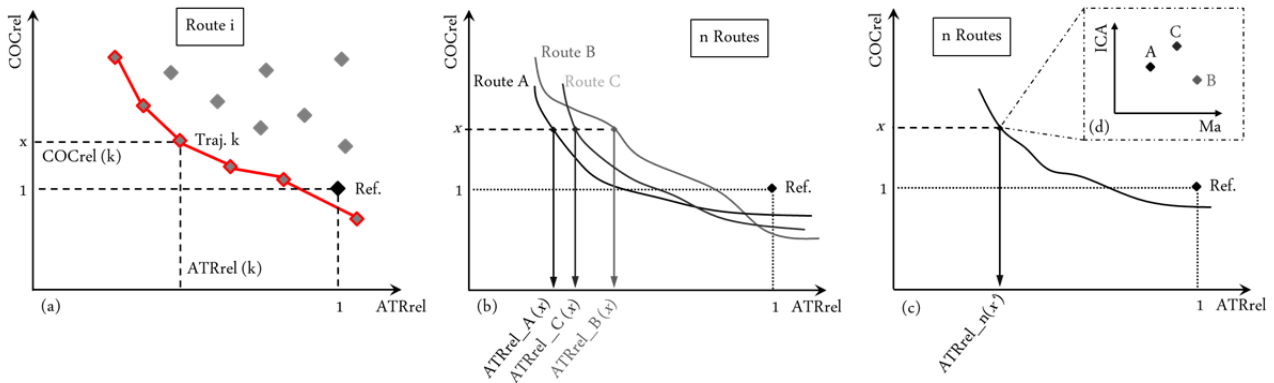

Figure 3: Principle of COC_{rel} vs. ATR_{rel} Pareto front definition for a single route i (subfigure a) and multiple routes at a given costs penalty x (subfigures b-c). Identification of corresponding cruise conditions ICA,Ma_{cr} (inlay in subfigure c).

3.3 *Derivation of new design conditions for aircraft with reduced climate impact*

In aircraft design studies the top level aircraft requirements (TLAR) describe the target performance parameters for new aircraft, including the payload-range capabilities, high and low speed performance, payload arrangement, etc. The TLAR further contain the definition of initial cruise altitude and speed as target condition for the optimization of the aircraft high speed performance.

In order to derive the design conditions of future aircraft that are optimized for cruise conditions with reduced climate impact, the frequency distribution of ICA and Ma_{cr} is evaluated at an accepted global cost change $COC_{rel,all,kp}$. Therefore, following the previously described approach, each route-specific Pareto front is intersected at the defined cost change x, providing the climate impact reduction $ATR_{rel,i,kp}(x_i)$ as well as the corresponding cruise condition $ICA_{i,kp}(x_i)$ and $Ma_{cr,i,kp}(x_i)$. Applying this procedure to all i=1,…,n routes of the global route network provides the normalized frequency distribution $\Phi_x(ICA, Ma_{cr})$ of cruise conditions (Figure 3d inlay), where $\delta_i(ICA, Ma_{cr})$ is an indicator of occurrence (Equation 6-7). Each occurring cruise condition is weighted with the absolute route specific climate mitigation potential $(f_i \cdot (1-ATR_{rel,i,kp}) \cdot ATR_{i,ref})$.

$$\Phi_x(ICA, Ma_{cr}) = \frac{\sum_{i=1}^{n} f_i \cdot \left(1 - ATR_{rel,i,kp}(x_i)\right) \cdot ATR_{i,ref} \cdot \delta_i(ICA, Ma_{cr})}{\sum_{i=1}^{n} f_i \cdot \left(1 - ATR_{rel,i,kp}(x_i)\right) \cdot ATR_{i,ref}} \tag{6}$$

$$\delta_i(ICA, Ma_{cr}) = \begin{cases} 1, & ICA = ICA_{cr,i,kp} \quad \& \quad Ma = Ma_{cr,i,kp} \\ 0, & else \end{cases} \tag{7}$$

From the frequency distribution $\Phi_x(ICA, Ma_{cr})$ that results for an accepted cost change $COC_{rel,all,kp}$, the mean cruise Mach number $\overline{Ma_{cr}(x)}$ and mean initial cruise altitude $\overline{ICA(x)}$ are derived according Equation 8 and 9.

$$\overline{Ma_{cr}(x)} = \sum_{ICA, Ma_{cr}} \Phi_x(ICA, Ma_{cr}) \cdot Ma_{cr} \tag{8}$$

$$\overline{ICA(x)} = \sum_{ICA, Ma_{cr}} \Phi_x(ICA, Ma_{cr}) \cdot ICA \tag{9}$$

Both parameters serve as new design conditions for aircraft configurations optimized at cruise conditions with reduced climate impact.

4   CLIMATE IMPACT MITIGATION POTENTIAL OF THE REFERENCE AIRCRAFT

In order to determine the climate impact mitigation potential given by the operation of the reference aircraft on lower cruise altitudes and speeds, the cruise conditions are varied for each route according Table 1.

	Minimum value	Maximum value	Step width
Initial cruise altitude [ft]	13000	41000	1000
Cruise Mach number	0.4	0.85	0.01

Table 1: Range of ICA, Ma_{cr} variations applied in the present study to derive the operational mitigation potential of the reference aircraft.

To ensure that only feasible flight conditions are considered, each calculated flight trajectory is checked with respect to speed, altitude, buffeting and stall limits taken from available manufacturer data. Please note that the wide ranges of ICA and Ma_{cr} values reflect less current ATM practice but are rather chosen to identify the maximum potential of climate impact reduction over the full range of cruise flight conditions feasible by the aircraft.

Applying the CATS simulation workflow with the above described settings, ICA and Ma_{cr} parameter ranges provides the following climate impact mitigation potential and cost penalty for the world fleet of the reference aircraft. As shown in Figure 4a , there exists a considerable potential to reduce the climate impact of air traffic with small to moderate cost penalty (relative to typical cur-

rent cruise conditions) through reduced flight altitudes and speeds. It also highlights that the mitigation efficiency, which expresses the ratio of achievable ATR reduction for a selected COC increase, is especially favorable for small COC changes. Exemplarily assuming that airlines or the paying passenger would accept a 10% COC penalty, the possible ATR reduction accounts 42%. For this case, the reference aircraft is operated 3170m lower and Mach 0.095 slower compared to typical current A330 average cruise conditions. Due to the fact that the route-specific reference cruise conditions are not necessarily part of the Pareto front it appears possible to reduce the climate impact in small bounds without cost increase by trading fuel costs vs. time related costs. However this effect depends on the applied model characteristics and settings.
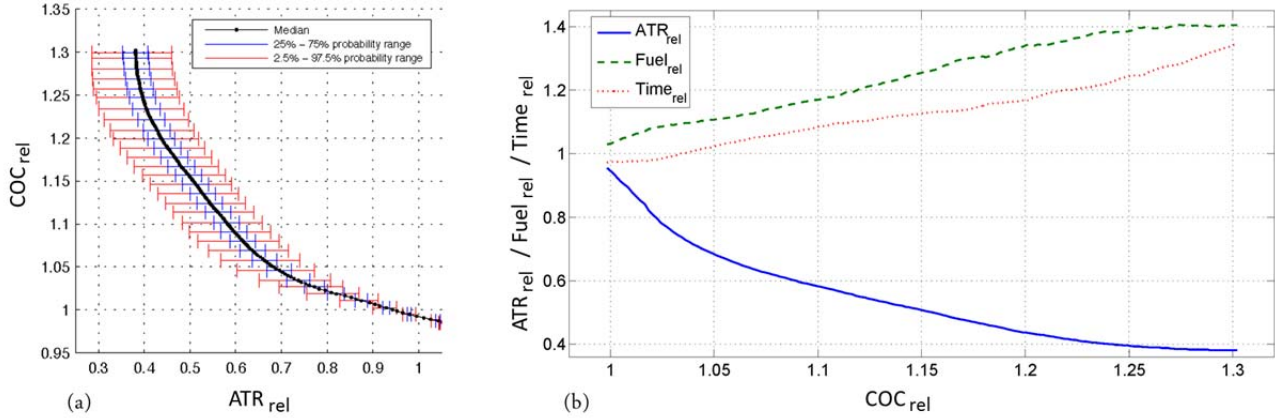
Figure 4 (a): Pareto front of mitigation potentials and costs (ATR$_{rel,all}$ vs. DOC$_{rel,all,k}$) expressed relative to the global reference (ICA$_{ref,all}$ = 11142 m, Ma$_{cr, ref,all}$ = 0.812) for all analyzed routes operated by the reference aircraft A332 in 2006. (b): Evolution of relative mission fuel, mission time and ATR changes (frequency weighted fleet average) for increasing COC$_{rel}$.

The impact of increasing fuel prices on the climate impact mitigation potential of the reference aircraft and design conditions for future aircraft are investigated in the previous study of the authors [Koch et al. 2012]. The analysis showed that the climate impact mitigation potential given by lower cruise altitudes and speeds remains favorable, even for high fuel price scenarios that are expected to materialize in the future. It further outlined that the impact of regional price variations have a negligible impact on the design conditions.

However, to achieve the discussed climate impact reduction current aircraft need to be operated in off design conditions and experience performance losses, which lead to increased fuel burn. Figure 4b depicts the evolution of mean mission fuel and mission time values (frequency weighted fleet average) as function of increasing COC (and related ATR) changes. The cost for fuel compose a considerable fraction of the cash operating costs (especially on long-haul flights) and will gain further importance with increasing fuel prices that are expected to materialize in the future. In order to limit this cost penalty, current aircraft need to be optimized for lower cruise conditions with reduced climate impact.

5 AIRCRAFT DESIGN OPTIMIZATION FOR CRUISE CONDITIONS WITH REDUCED CLIMATE IMPACT

The conducted analysis allows the derivation of new design criteria for aircraft that are specifically optimized for lower altitudes and speeds. The present study exemplarily considers the 10% COC penalty case for aircraft optimization. Analyzing the corresponding cumulated frequency distribution of cruise altitudes and speeds reveals that the reference aircraft is operated in average at ICA = 7974m and Ma$_{cr}$ = 0.717.

The reference configuration is thus optimized for ICA$_{Design}$ = 8000m and Ma$_{cr,Design}$ = 0.72 with *PrADO* and *TWDat*. In order to identify the mitigation potential solely rooting in aircraft desgin changes, the design optimization is conducted with constant technology level, engine performance map and payload-range capabilities. Based on this requirements the fuselage and cabin layout are kept identical to the reference aircraft. Instead the wing sweep, aspect ratio, wing area and spanwise

twist distribution are optimized for the new conditions. Further the leading edge (LE) sweep angle and area of the vertical and horizontal tail planes are adapted according to the wing planform changes with constant tail volume coefficient. Figure 5 depicts the geometrical changes of the redesigned configuration in comparison to the reference aircraft.
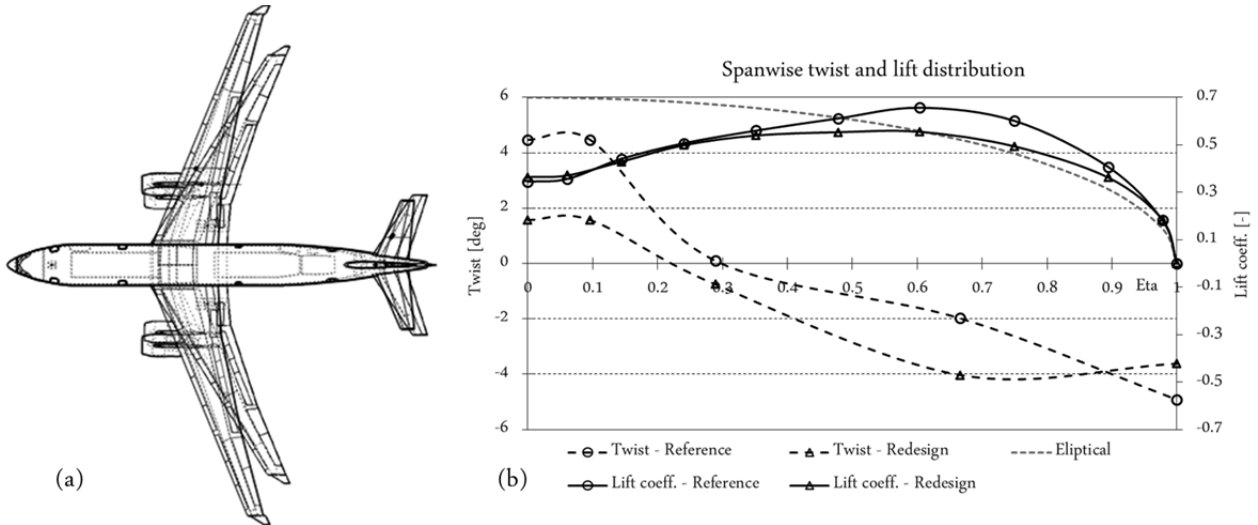
Figure 5: Comparison of reference and redesigned aircraft. (a): Changes in wing and HTP planform. (b): Changes in spanwise twist distribution and local lift coefficient (Cl).

The redesigned configuration shows decreased leading edge sweep of the wing and empennage according the lower Mach number. The wing span increases at nearly constant wing area, which leads to an increased aspect ratio and improved aerodynamic efficiency (L/D) by 15%, but also increased wing weight. The area of the horizontal tail plane (HTP) decreases due to the increased lever arm, whereas the vertical tail plane (VTP) area increases due to the increased wing span. The fuselage weight decreases due to the lower pressure difference at the new design cruise conditions. In total, the operational empty weight (OWE) increases by 4%. Despite the increased OWE, the improved aerodynamic efficiency leads to reduced drag and required thrust during cruise flight. The specific fuel consumption (TSFC) increases slightly by 1.7% due to engine performance losses at the new cruise conditions. In combination both effects lead to a reduction in mission fuel of 11% compared the reference aircraft operated at the new design mission. Table 2 shows key design parameters for the reference and redesigned aircraft operated at ICA 8000m with Mach 0.72 on the design mission.

Geometry	Redesign	Reference	Performance	Redesign	Reference
Wing area [m2]	360	361.6	OWE [t]	120.2	115.7
Wing sweep (LE) [°]	22	32	MTOW [t]	223.6	221.6
Wing aspect ratio [-]	13	9.3	L/D at ICA [-]	23	20
HTP area [m2]	58.9	71.5	CL at ICA [-]	0.463	0.466
HTP sweep (LE) [°]	24	34	TSFC at ICA [kg/N/h]	0.05827	0.05728
VTP area [m2]	64	53	Mission fuel [t]	52.9	59.6
VTP sweep (LE) [°]	31	44			

Table 2: Key design parameters for the reference and redesigned aircraft at initial cruise conditions.

6   CLIMATE IMPACT MITIGATION POTENTIAL OF THE REDESIGNED AIRCRAFT

The climate impact mitigation potential for the redesigned aircraft operated on lower cruise altitudes and speeds is determined in analogy to the reference aircraft. The cruise conditions are varied for each route according Table 3. Please note that the new operational limits of the redesign aircraft are considered in this analysis, limiting thus the operational maximum altitude and speed (compare Table 1).

	Minimum value	Maximum value	Step width
Initial cruise altitude [ft]	13000	35000	1000
Cruise Mach number	0.4	0.78	0.01

Table 3: Range of ICA, Ma_{cr} variations applied in the present study to derive the operational mitigation potential of the redesigned aircraft.

Computing the COC and ATR changes for each trajectory relative to the route-specific reference trajectory shows a considerable improvement in costs and climate impact due to the increased fuel efficiency compared to the reference aircraft. Figure 6 depicts the Pareto fronts for the reference and redesigned aircraft resulting for the route Detroit-Frankfurt (a) and the global route network (b).
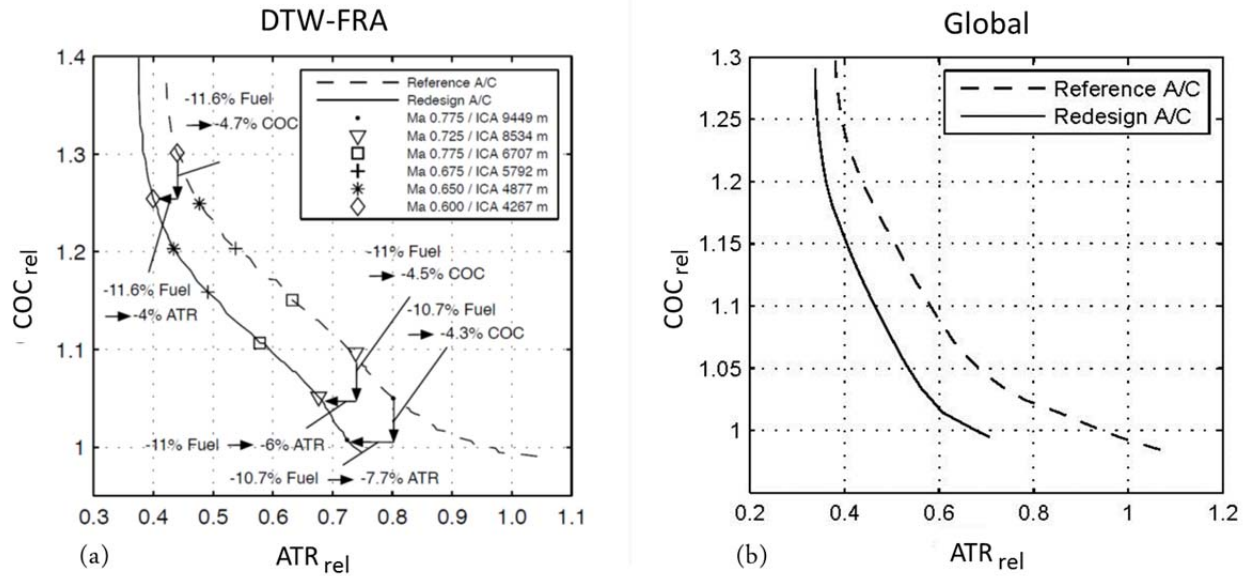
Figure 6: Comparison of Pareto fronts (ATR_{rel} vs. COC_{rel}) for the reference aircraft and the redesigned aircraft operated at lower cruise altitudes and speeds on route DTW-FRA (a) and the global route network (b). For both aircraft the plotted COC and ATR changes are expressed relative to the route-specific reference flight profiles derived from CFMU data.

The comparison of selected cruise conditions for DTW-FRA shows that the fuel burn improvement of 10-11% leads to a 4-5% reduction of COC, which is in good agreement with the average share of fuel costs on total COC. The fuel burn reduction further reduces ATR by 4-8% (depending on altitude) due to less emitted pollutants. The ATR reduction increases towards higher altitudes due to the increased impact of specific components, e,g, NO_x and H_2O. The trends observed for DTW-FRA are also visible in the Pareto front for the global route network (Figure 6b). It shows that for the selected 10% COC penalty, the ATR reduction is increased from 42% to 54%. Considering the importance of economic efficiency for the airlines it is rather interesting to keep the COC penalty as low as possible. In this sense, the redesign of the reference aircraft for lower cruise altitudes and speeds allows the cost-neutral reduction of ATR by 32% relative to typical current cruise operations. To achieve this, the redesigned aircraft is globally operated at ICA = 9930m with Ma_{cr} = 0.774. Table 4 summarizes the resulting $ATR_{rel,all,kp}$ values for selected $COC_{rel,all,kp}$ with corresponding mean ICA and Ma_{cr} values derived from the respective frequency distributions.

DOC increase ($DOC_{rel,all,kp}$ - 1)	ATR reduction (1 - $ATR_{rel,all,kp}$)		Mitigation efficiency (1 - $ATR_{rel,all,kp}$)/($DOC_{rel,all,kp}$ -1)		ICA [m] (mean)		Ma_{cr} (mean)	
	Ref.	RD	Ref.	RD	Ref.	RD	Ref.	RD
neutral	5 %	32 %	-	-	11278	9932	0.814	0.774
1.0 %	12 %	37 %	12	37.4	10188	9637	0.836	0.771
5.0 %	32 %	46 %	6.4	9.3	9065	8562	0.783	0.728
10 %	42 %	54 %	4.2	5.4	7974	7408	0.717	0.682
20 %	56 %	64 %	2.8	3.2	5460	4948	0.649	0.613
30 % (max)	62 %	66 %	2.0	2.3	4221	4333	0.549	4333

Table 4: Climate impact mitigation potentials and efficiencies for the reference and redesigned aircraft (RD) expressed relative to the reference scenario. Related ICA and Ma_{cr} combinations are derived from the frequency distribution resulting at given COC penalty.

7   CONCLUSIONS AND OUTLOOK

DLR developed within the project "*Climate compatible Air Transport System* (CATS)" a comprehensive simulation and assessment approach with detailed models for various aviation disciplines to quantify the potential to reduce the climate impact of air traffic through operational and technological measures.

The present study focuses on the mitigation potential given by the global operation of actual and future aircraft on lower cruise altitudes and speeds. The scope of study therefore includes the world fleet of a representative current twin engine long-range aircraft and a redesigned aircraft that is optimized for cruise conditions with reduced climate impact. Both configurations are operated on a global route network with varying cruise conditions. For each flight trajectory the changes in average temperature response (ATR) and cash operating costs (COC) are expressed relative to a typical current reference traffic scenario and flight profiles derived from Eurocontrol CFMU data. Based on this, Pareto optimum cruise conditions are derived for each route in the network and discussed as cost benefit analysis, allowing the trade-off between climate impact and operating costs. The analysis further identified aircraft design requirements for future aircraft concepts specifically designed for cruise conditions with reduced climate impact.

The conducted study shows considerable potential for current aircraft to mitigate climate impact with small to moderate penalties of cash operating costs, e.g. 42% ATR reduction for 10% COC increase. The distribution of cruise conditions showed for this specific case that the reference aircraft is operated in average at 8000m with Mach 0.72.

In a further step the reference aircraft is optimized exemplarily for the identified cruise conditions. The resulting configuration shows increased fuel efficiency, which leads to a considerable reduction of the COC penalty at lower cruise altitudes and speeds. The increased fuel efficiency further improves the ATR reduction due to the reduced amounts of emitted pollutants. In combination, the redesign of the reference aircraft allows a cost-neutral climate impact reduction of 32%.

The conducted study clearly shows that the reduction of aviation climate impact is feasible by adapting aircraft design and operations in a combined approach. The developed methodology is applicable and extendable to any other operational or technological scenario, providing thus a contribution to a climate compatible air transportation system.

8   ACKNOWLEDGMENTS

REFERENCES

Campbell, S.E., Neogi, N.A., Bragg, N.B., An operational strategy for persistent contrail mitigation, 9th AIAA Aviation Technology, Integration, and Operations Conference (ATIO), (2009)

Dahlmann, K., Eine Methode zur effizienten Bewertung von Maßnahmen zur Klimaoptimierung des Luftverkehrs, PhD Thesis - Ludwig Maximilians University München (2011)

Deidewig, F., Ermittlung der Schadstoffemissionen im Unter- und Überschallflug, PhD-thesis, (1998)

DLR Software: http://software.dlr.de, (2012)

Döpelheuer, A., Lecht, M., Influence of engine performance on emission characteristics, Gas Turbine Engine Combustion, Emissions and Alternative Fuels, RTO MP-14, ISBN 92-837-0009-0, p. 20, 11 (1998)

Egelhofer, R. Aircraft design driven by climate change, Dissertation, PhD Thesis - Technische

Fichter, C.: Climate impact of air traffic emissions in dependency of the emission location and altitude, DLR Forschungsbericht 2009-22, ISSN 1434-84543, Oberpfaffenhofen, (2009)

Gierens, K., Lim, L., Eleftheratos, K., A review of various strategies for contrail avoidance, Open Atmos. Sci. J. 2, 1–7 (2008)

Grewe, V., Stenke, A., AirClim: An efficient tool for climate evaluation of aircraft technology, Atmos. Chem. Phys. 8, 4621–4639 (2008).

Grewe, V. and Dahlmann, K., Evaluating Climate-Chemistry Response and Mitigation Options with Air-Clim, in Atmospheric Physics: Background – Methods - Trends, Ed. U. Schumann, Research Topics in Aerospace, Springer Verlag, 591-608, (2012).

Heinze, W., Ein Beitrag zur quantitativen Analyse der technischen und wirtschaftlichen Auslegungsgrenzen verschiedener Flugzeugkonzepte für den Transport großer Nutzlasten, PhD-thesis TU Braunschweig, ZLR Forschungsbericht 94-01, (1994)

Intergovernmental Panel on Climate Change (IPCC), Aviation and the global atmosphere, Cambridge University Press, Cambridge, UK, 1999

Intergovernmental Panel on Climate Change (IPCC), Climate Change 2007: Synthesis Report, Cambridge University Press, Cambridge, UK, (2007)

International Civil Aviation Organization (ICAO), FESG CAEP-8 Traffic and Fleet Forecasts, Committee on Aviation Environmental Protection, CAEP-SG/20082-IP/02, (2008)

Koch, A., Dahlmann, K., Grewe, V., Kärcher, B., Schumann, U., Gollnick, V., Nagel, B. Integrated analysis and design environment for a climate compatible air transport system, 9th AIAA Aviation Technology, Integration, and Operations Conference (ATIO), Hilton Head, USA (2009)

Koch, A., Lührs, B., Dahlmann, K., Linke, F., Grewe, V., Litz, M., Plohr, M., Schumann, U., Gollnick, V., Nagel, B., Climate impact assessment of varying cruise flight altitudes applying the CATS simulation approach, 3rd International Conference of the European Aerospace Societies (CEAS), Venice, Italy (2011).

Koch, A., Lührs, B., Dahlem, F., Lau, A., Linke, F., Dahlmann, K., Gollnick, V., and Schumann, U., Studies on the Climate Impact Mitigation Potential of Actual and Future Air Traffic, 16th Air Transport Research Society (ATRS) World Conference, Tainan, Taiwan (2012)

Lee, D.S., et al., Aviation and global climate change in the 21st century, Atmospheric Environment, 2009.

Liebeck, R. H., et al., Advances in subsonic airplane design & economic studies, NASA CR 195443, (1995)

Mannstein, H., Spichtinger, P., Gierens, K., How to avoid contrail cirrus, Transp. Res. D 10, 421–426 (2005)

Matthes, et al., Climate Optimized Air Transport, Atmospheric Physics: Background – Methods - Trends, Ed. U. Schumann, Research Topics in Aerospace, Springer Verlag, 591-608, (2012).

Nagel, B., Gollnick, V., Böhnke, D., Zill, T., Alonso, J.J., Rizzi, A., La Rocca, G., Communication in Aircraft Design: Can we establish a Common Language?, 28th Congress of the International Council of the Aeronautical Sciences (ICAS), Brisbane, Australia, (2012)

Schumann, U., Graf, K., Mannstein, H., Potential to reduce the climate impact of aviation by flight level changes, 3rd AIAA Atmospheric and Space Environments Conference No. 1020774, 1020771-1020722, (2011)

Schwartz, E., and Kroo, I. M., Aircraft design for reduced climate impact, 49th AIAA Aerospace Sciences Meeting including the New Horizons Forum and Aerospace Exposition, Orlando, USA AIAA 2011-265, (2011a).

Schwartz, E., Kroo, I. M., Metric for Comparing Lifetime Average Climate Impact of Aircraft, AIAA Journal, Vol. 49-8, 2011b.

Seider, D., Fischer, M. P., Litz, M., Schreiber, A., Gerndt, A., Open Source Software Framework for Applications in Aeronautics and Space, IEEE Aerospace Conference 2012, Big Sky, Montana, USA, (2012)

Sridhar, B., Chen, N.Y., Ng, H.K., Linke, F., Design of aircraft trajectories based on trade-offs between emission sources, 9th USA/Europe Air Traffic Management Research and Development Seminar (ATM2011), http://www.atmseminar.org/, (2011)

A new European inventory of transport related emissions for the years 2005, 2020 and 2030

C. Schieberle [*], U. Kugler, S. Laufer, M. Knecht, J. Theloke, R. Friedrich
Institut für Energiewirtschaft und Rationelle Energieanwendung (IER)

Keywords: Emission inventory, On-road and off-road transport, Particulate matter

ABSTRACT: Emission inventories provide the fundamental input for air quality models. A new emission inventory for Europe covering the whole transport sector was compiled in this study. The focus is on transport activities since they are a major contributing source of pollutants released into the atmosphere. Due to a high level of disaggregation of underlying activity data and due to the application of recent data sets of emission factors an accurate and detailed inventory was generated including NO_x, PM2.5, PM10, EC, OC, BaP, SO_2, NMVOC, CH_4, NH_3, CO and CO_2 as well as the number of total and solid particles. The inventory comprises the EU27 countries, as well as Norway, Island, Switzerland and all neighboring sea regions. It covers the year 2005 and provides projections for 2020 and 2030. After quantifying the shares of all relevant subsectors the emissions were spatially allocated on a mesoscale grid.

1 INTRODUCTION AND MOTIVATION

Backed by numerous epidemiological studies, it is commonly accepted that poor air quality causes severe effects on human health. These studies show a correlation between the exposure to certain concentration levels of pollutants and the probability of suffering from specific diseases. Thus, decline in concentration levels at polluted sites is correlated to positive health response at receptor regions but actually occurs due to the implementation of abatement strategies at emitting sources that might, in general, be located elsewhere. Therefore, policy makers use integrated assessment tools to investigate the impact of different mitigation measures and combine them to efficient environmental protection strategies.

The most severe environmental health risks related to air quality in Europe are caused by particulate matter (measured as PM10, PM2.5, EC (elemental carbon), OC (organic carbon) and PNC (particle number concentration)). During the EU FP7 funded project TRANSPHORM such an integrated assessment is currently undertaken aiming to gain new insight on mitigation potentials to reduce negative health impacts caused by particulate matter.

Existing emission inventories were found to be insufficient due to the lack of detail in terms of disaggregation in both activity data and emission factors. However, a certain level of detail is critical to subsequently determine the effect of measures that tackle only a subset of activities and emission factors. Therefore, as an initial step for the assessment process an emission inventory at European scale needed to be generated for the year 2005 as well as for the reference scenario years 2020 and 2030.

2 METHODOLOGY

The inventory covers all relevant on-road and off-road modes of the transport sector, namely:
- On-road transportation including passenger cars, light and heavy duty vehicles and motorcycles,
- Rail-bound traffic from passenger and freight trains,

---
[*] *Corresponding author:* C. Schieberle, Institut für Energiewirtschaft und Rationelle Energieanwendung (IER), Heßbrühlstraße 49a, 70565 Stuttgart, Germany

- International maritime navigation including in-port activities at coastal harbors,
- Shipping activities on inland rivers, and
- Landings and take-offs from civil aviation including activities from ground support equipment on airports.

Emissions from civil aviation beyond 3000 feet altitude above ground level were excluded within the scope of this work due to the lack of detailed emission factors.

2.1 On-road transportation

For on-road transportation, the inventory covers distinct activity categories for more than 300 different vehicles types in all considered countries characterized by their engine capacity and technology, the weight class of the vehicle and the fuel used from the TREMOVE model (De Ceuster, 2011). The distinction is necessary since emission factors vary largely between vehicle types. Activities are based on the TEMOVE model and are available for different regions and on different road network types (De Ceuster, 2011). The activities were associated to an evenly detailed set of emission factors by (Samaras, 2012). For the reference scenario years 2020 and 2030, current legislation was included such as the Euro 6/VI standards for on-road vehicles and an increase in bio-fuel usage. Emissions are derived by setting

$$E_{p,c,r,n,t,e,f} = a_{c,r,n,t,e,f} ef_{p,c,r,n,t,e,f}$$

where $E_{p,c,r,n,t,e,f}$ is the yearly emission of pollutant p in country c at region r on network n for a vehicle of type t using technology e and is powered by fuel type f. The activity $a_{c,r,n,t,e,f}$ is given in kilometers-driven and the emission factor $ef_{p,c,r,n,t,e,f}$ is given in grams per kilometers-driven or particle number per kilometers-driven, respectively.

2.2 Railways Rail-bound traffic

Rail-mounted passenger and freight transportation is considered based on fuel usage data. Thus, only exhaust emissions are considered. The emission factors vary by locomotive type and fuel type, i.e. line-haul locomotives, shunting locomotives and diesel railcars (Fridell, 2012). The emissions were derived by

$$E_{p,c,t,f} = a_{c,t,f} ef_{p,t,f}$$

where $E_{p,c,t,f}$ corresponds to the yearly emission of pollutant p in country c of train types t powered by fuel f. The activity $a_{c,t,f}$ is the respective energy usage due to combustion.

2.3 Civil aviation

Data on landing and take-off cycles for 2005 are available from Eurostat based on arrivals and departures per aircraft type at European airports (European Commission, 2012). The data were projected for 2020 and 2030 using scaling factors derived from modeled activity data for these years as in TREMOVE (De Ceuster, 2011). Emission factors per LTO of every arrival or departure of an aircraft are modeled by means of the count and type of engines per aircraft and their fuel flow per second in the respective mode. The respective data is yet unpublished and were provided by the German Aerospace Center (DLR). The average time-in-mode per cycle is available from the ICAO database. Thus, yearly emissions below 3000 feet above ground are modeled per airport by

$$E_{p,i} = \sum_j \left(\sum_{m \in \{TA,AP\}} f_{arr,j,i} t_m n_j ef_{p,j,m} + \sum_{m \in \{TD,TO,CO\}} f_{dep,j,i} t_m n_j ef_{p,j,m} + E_{p,GSE}(f_{arr,j,i} + f_{dep,j,i}) \right)$$

where p is a pollutant, i is an airport, j is an aircraft type, n_j is the number of engines of an aircraft type, $f_{arr,j,i}$ and $f_{dep,j,i}$ depict the number of arriving and departing flights of a given aircraft type at a given airport, and t_m is the time-in-mode during an LTO cycle, i.e. during taxi-approach (*TA*), approach (*AP*), taxi-departure (*TD*), take-off (*TO*) and climb out (*CO*). Emissions of ground service equipment, $E_{p,GSE}$, are added on a per-flight basis.

2.4   International maritime navigation and coastal harbors

Emissions at sea from maritime shipping activities particularly for SO2 and secondary particulate matter depend on the sulfur content (FSC) of the amount of fuel necessary to power the engines. The global mean content in mass-% in 2005 was about 2.3 (Cooper and Gustafsson, 2004), whereby marine diesel was at 0.5 and heavy fuel at 2.7 in average (Moldanova, 2012). The IMO global limit is aimed at reaching levels below 0.5 by 2020. Within Emission Control Areas, namely the Baltic Sea, the North Sea and the English Channel, there are tighter limits already in effect: They were at 1.5 mass-% in 2006/2007, at 1 mass-% after mid of 2010 and will be at 0.1 mass-% from 2015 onwards. Compliance to the above regulations is assumed in 2020 and 2030.

The TREMOVE model activities per sea region are categorized by different ship types, respective engine power, average engine-load during cruise and the fuel type used which may be either residual oil (2.7 mass-%), marine distillates (0.5 mass-%) or marine gas oil (0.1 mass-%).

In addition to the above, all ships newly built - or with an installed engine manufactured after 1990 - are bound to comply with emission limits for NO_x. The thresholds have been lowered for engines built after 2011 and will be even further confined after 2016. Due to the lack of detailed fleet data on the compliance to the above, half of the ships are assumed to have installed a pre-1990 engine in 2005 while the rest is estimated to meet Tier-I regulations. For 2020, a shift of the same split was adopted between Tier-I and Tier-II, while in 2030, a complete fulfillment of the latter is expected. Activities in kWh per region s of a ship of type t having an engine of type e powered by fuel f is derived by

$$a_{s,t,e,f} = \frac{d_{s,t}}{v_t} \sum_{u \in \{MAIN,AUX\}} p_{u,t,e,f} l_{u,CRUISE,t,e}$$

where $d_{s,t}$ is the distance traveled per region and ship type, v_t denotes the average speed per ship type, $p_{MAIN,t,e,f}$ and $p_{AUX,t,e,f}$ denote the main and auxiliary engine power of a ship of type t having an engine of type e powered by fuel f, at respective loads $l_{MAIN,CRUISE,t,e}$ and $l_{AUX,CRUISE,t,e}$ during cruise. Emissions per pollutant and sea region are subsequently calculated by

$$E_{p,s} = a_{s,t,e,f} ef_{p,s,e,f}$$

In ports, ships produce emissions due to maneuvering and hoteling. They are mainly using their auxiliary engines, so their loads differ from the loads during cruise at sea (European Environment Agency, 2009). Activity data can be derived by the number of port callings and the dwelling time in respective modes. Thus, the emissions are essentially

$$a_{c,t,e,f} = k_{c,t,e,f} \sum_{m \in \{H,M\}} t_m \sum_{u \in \{MAIN,AUX\}} p_{u,t,e,f} l_{u,m,t,e}$$

$$E_{p,c} = \sum_{t,e,f} a_{c,t,e,f} ef_e$$

where $k_{c,t,e,f}$ is the number of port callings, t_m is the mean time a ship is hoteling (H) or maneuvering (M). The power $p_{u,t,e,f}$ and engine load $l_{u,m,t,e}$ correspond to the description above. Emission factors ef_e are given per engine.

2.5   Inland shipping

Emission factors due to traffic on rivers were available based on the power output of engines times the period at full load in hours, i.e. in kWh. The engines are classified by ship type and loading capacity. Activities in vessel kilometers-driven from TREMOVE were converted in hours driven based on specific average speeds, yielding

$$E_{p,c,t,h} = a_{c,t,h} ef_{p,t}$$

where the emission is calculated per pollutant p, country c, ship type t and capacity h.

3   RESULTS

Due to space limitations, only an exemplary subset of results is discussed in the following. The focus is on NO_x and PM2.5.
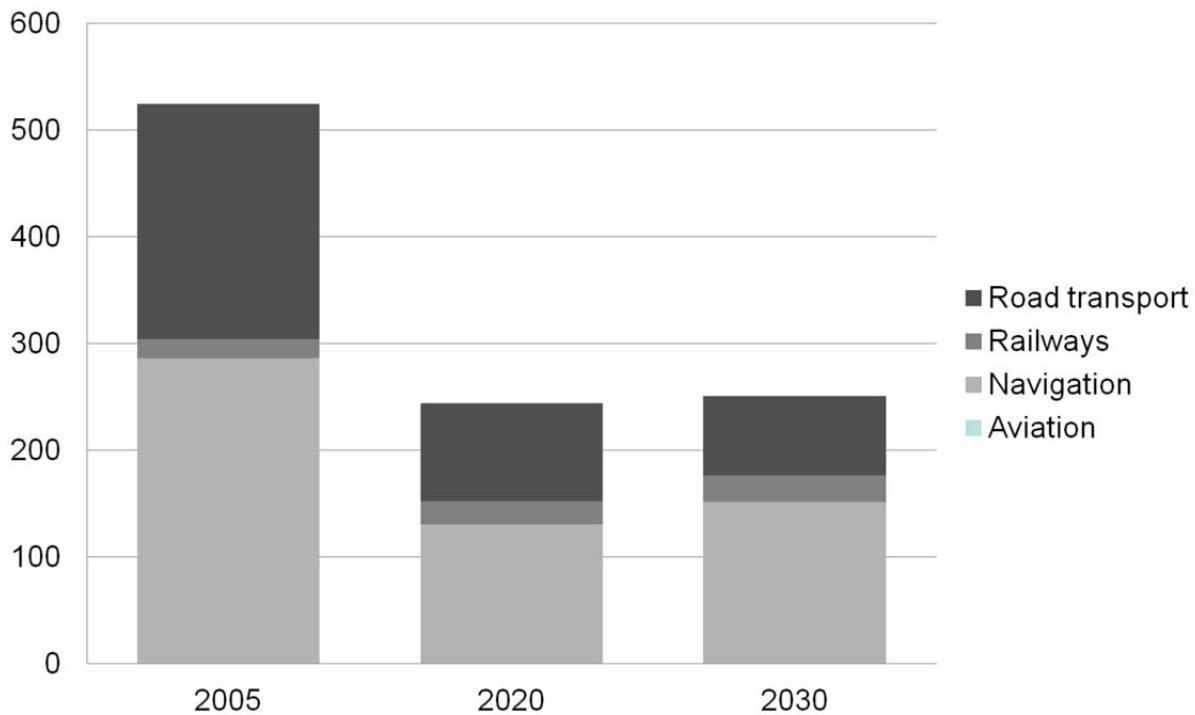
Figure 1: Transport-related PM2.5 emissions [kt].
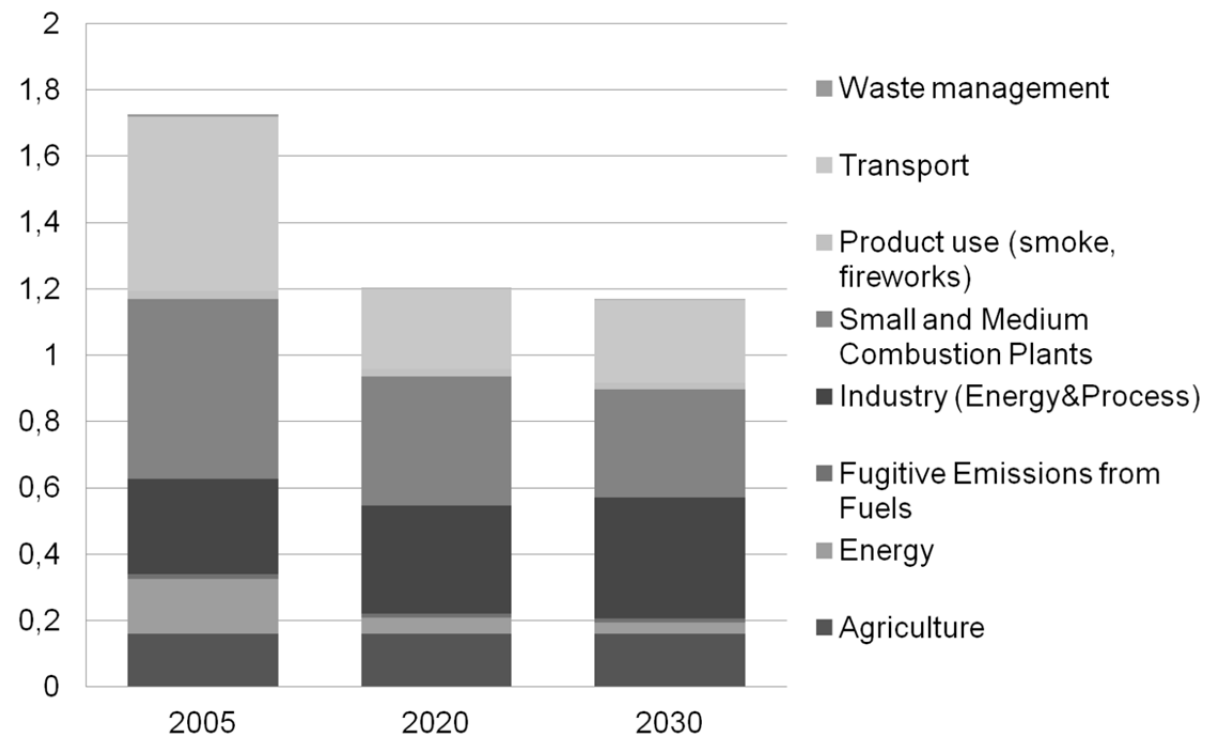
Figure 2: PM2.5 emissions of all sectors [Mt].

As depicted in Figure 1, levels of transport related PM2.5 emissions are projected to decline by more than 50% in 2020 compared to 2005 and will in turn slightly increase until 2030. The former is mostly due to a technology shift in shipping and on-road transportation. The two modes will continue to be the major sources of particulate matter in the considered modes of transportation. The

decrease contributes to the reduction of PM2.5 emissions in all sectors which is at about 30% in 2020 and is only very small in 2030, as is shown in Figure 2. While this shows the projected decline in the reference scenarios, it underlines the importance of the transportation sector which still has potential for mitigating emissions.
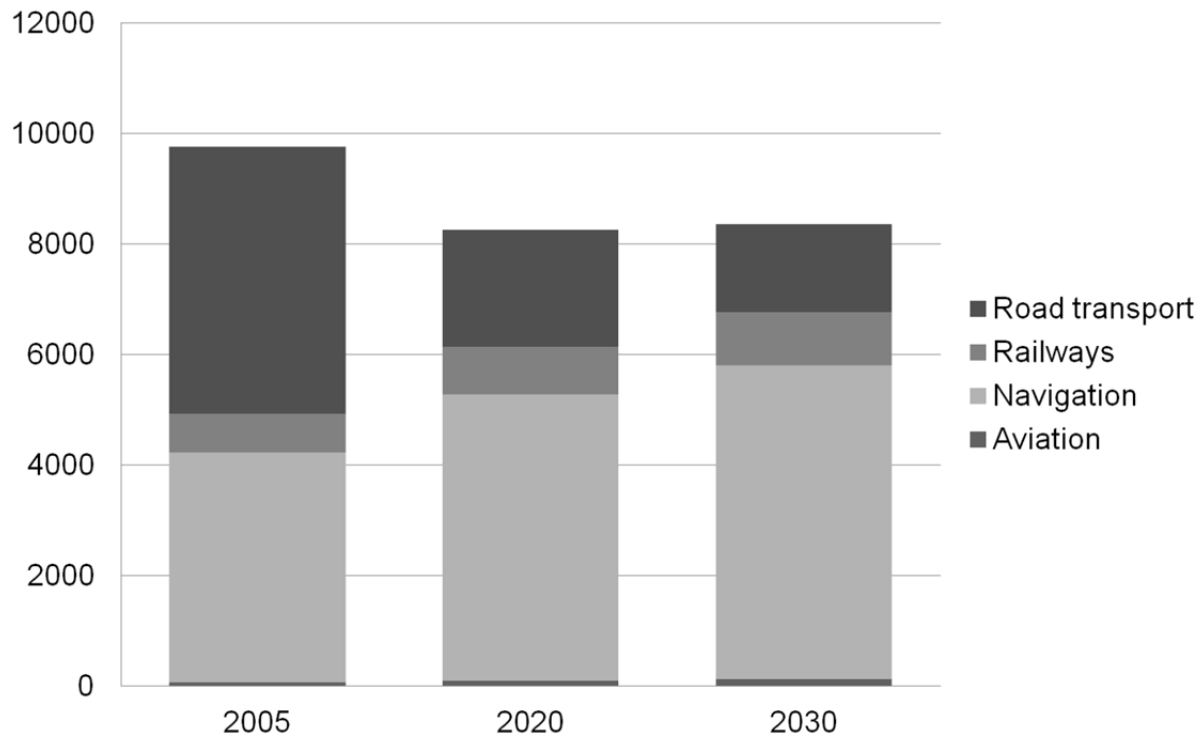
Figure 3: Transport-related NO_x emissions [kt].
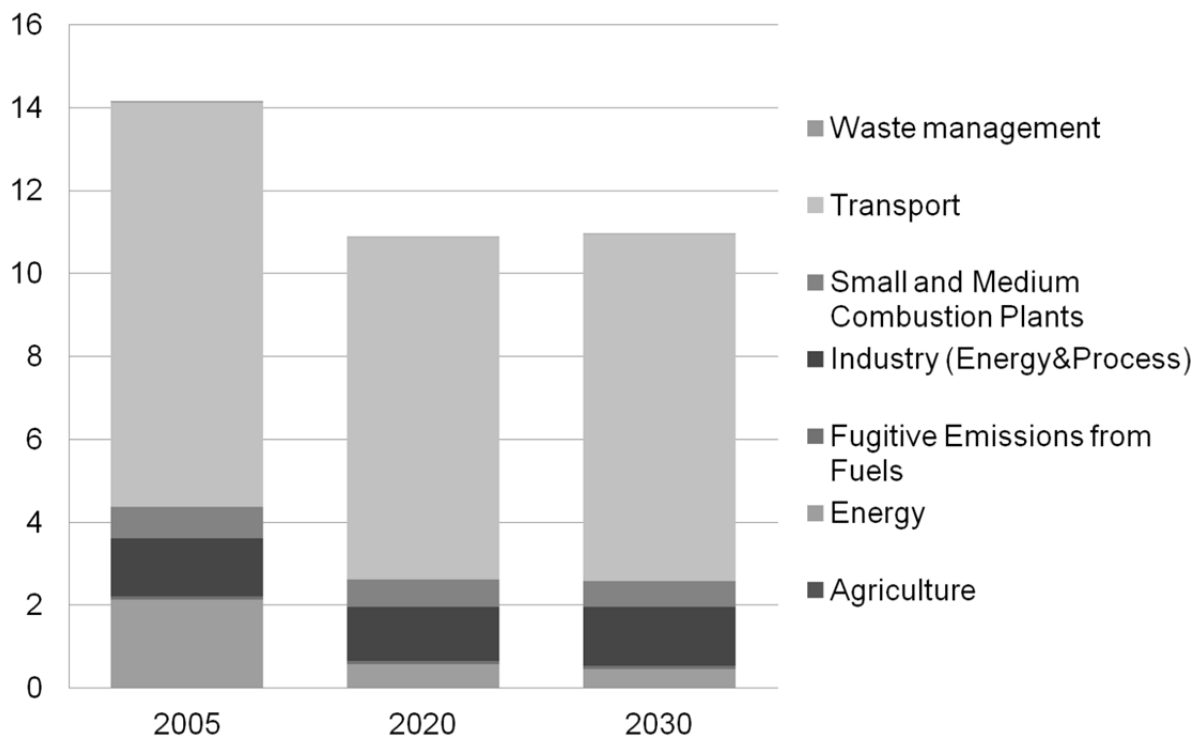
Figure 4: NO_x emissions of all sectors [Mt].

As show in Figure 3, NO_x emissions from transportation activities show a decrease of less than 20% in 2020 and 2030, respectively, compared to 2005. But, the source profiles for the years show large differences: On-road activities contribute half of the NO_x emissions in 2005 while shipping activities is the other major contributor. Projections show that the latter will be responsible for two third

of the emissions in 2030 while on-road transportation will then contribute with less than 25%. Figure 4 shows that mitigation measures for shipping activities could have an overall high effect across sectors since transportation remains the main contributor of NO_x emissions.

4   CONCLUSIONS AND FUTURE WORK

A detailed emission inventory for all modes of the transport sector at a European scale for 2005 and for future years 2020 and 2030 was compiled. The inventory is linked to a broad set of activities and emission factors ensuring that the calculated amounts of pollutant release remain associated to the contributing sources.

The emissions data were spatially allocated on a 1/8 by 1/16 degree grid (about 7 x 7 km) and was subsequently embedded in a previously established cross-sectoral inventory of the remaining activities not related to transport. In a subsequent effort numerous abatement measures will be applied to the inventory to facilitate a detailed assessment of the effects of several mitigation strategies at different scales.

REFERENCES

Cooper, D., and Gustafsson, T., 2004: Methodology for calculating emissions from ships: 1. Update of emission factors. Report series SMED and SMED&SLU Nr.4-2004.

De Ceuster, G., 2011: TRANSPHORM Europe 2005-2020-2030 activity data, report for Work package 1.2 Transport emission baseline. Transport & Mobility Leuven, Belgium.

European Environment Agency, 2009: EMEP/EEA air pollutant emission inventory guidebook. Technical report No 9/2009

European Commission, 2012: Eurostat: Air transport measurement - traffic data by airports, aircrafts and airlines. Available online: http://epp.eurostat.ec.europa.eu/portal/page/portal/ transport/data/database, last accessed on 19 January 2012.

Fridell, E., 2012: Report on railway emission factors. DG ENV, 2010-2014. March 2012

Moldanova, J., 2012: Emission factors for shipping – final dataset for use in Transphorm emission inventories. DG ENV, 2010-2014.

Samaras, Z., 2012: Emission Factors Database for TRANSPHORM (Transport related Air Pollution and Health impacts-Integrated Methodologies for Assessing Particulate Matter. DG ENV, 2010-2014.

Quantifying Shipping Emissions

M. Traut[*]
Tyndall Centre for Climate Change Research. School of Mechanical, Aeronautical and Civil Engineering, University of Manchester

A. Bows, R. Wood
Sustainable Consumption Institute. Tyndall Centre for Climate Change Research. School of Mechanical, Aeronautical and Civil Engineering, University of Manchester

Keywords: Climate Change, Shipping, Emissions

ABSTRACT: Shipping needs to control its annual release of CO_2 emissions. Key is the development of appropriate methods of accounting and monitoring. According to greenhouse gas protocol, if methods are to be of use to policymakers, they should fulfil five essential criteria: relevance, completeness, consistency, transparency, and accuracy. It is demonstrated here that all of the methods currently used fail to fulfil one or more of these criteria and are associated with high levels of uncertainty. As a solution, this paper presents a new method based on AIS (Automatic Identification System) data collected by satellite and land-based receivers. All ships of 300 gross tonnage and above are required to send AIS messages at regular intervals, including the ship's geographical position, course, and speed. Dedicated receivers in Earth orbit, and on the coast, pick up AIS messages from ships in their field of view. Using data from the International Space Station (ISS), complemented with data from land-based receiver stations, and a database of the world cargo shipping fleet, a viable method for calculating fuel consumption – and in turn CO_2 emissions – on the individual ship basis is presented. The method is subsequently assessed in terms of the five criteria. Suggestions on how the method should be calibrated and fine-tuned as it is scaled up to more complete data coverage are made. The paper demonstrates that this new method has the potential to provide a clear picture of international shipping CO_2 emissions, and is well-suited to be incorporated into emissions control policies currently being discussed at the global and the European levels, as well as informing the wider policy debate.

1   INTRODUCTION

Global shipping activity in 2007 emitted around 1 Gt of CO_2 per year (Buhaug et al, 2009) - approximately 3% of the global total. If the widely agreed goal of keeping average global warming under 2°C is not to be rendered meaningless, global greenhouse gas emissions must be drastically reduced (Anderson and Bows, 2011). The International Maritime Organization (IMO) has recognised the responsibility of the shipping sector and has declared that it is "determined to develop a mechanism that will enable the industry to achieve the eventually agreed reduction target" (IMO, 2010). However, recent history suggests it will likely take a radical shift away from 'business as ususal' for shipping to reduce its greenhouse gas emissions, let alone at the rate that would be needed to reconcile even a conservative reading of the language employed with climate science (Anderson et al, 2012). In 1997, the Kyoto protocol mandated Annex I nations to „pursue limitation or reduction of emission of greenhouse gases … from … marine bunker fuels, working through … the International Maritime Organization". According to fuel sales data from the International Energy Agency (IEA), over the twelve years that followed, CO_2 emissions from international shipping rose by more than a third, at a much higher rate than global emissions, as shown in figure 1. Over the twenty-five years between 1984 and 2009 (the year of the most recent IEA data), international shipping CO_2 emissions increased by 118% (IEA, 2011), compared to an increase in global CO_2 emissions of 58% (BP, 2012). While the IEA data provide a useful time series of shipping emissions, it

---

[*] *Corresponding author:* Michael Traut, University of Manchester, Tyndall Centre for Climate Change Research, H Floor, Pariser Building, Manchester, M13 9PL, UK. Email: michael.traut@postgrad.manchester.ac.uk

has been argued that actual emissions are much higher, due to likely under-reporting of fuel sales (Corbett and Koehler, 2003). Perhaps the most authoritative estimate is that from the 2nd IMO greenhouse gas study (Buhaug et al, 2009). For 2007, it estimates that international shipping emitted 870Mt CO_2 into the atmosphere, 139% of the value based on the IEA fuel stats figures, while stating an uncertainty of 20% (figure 1). The value is derived from a fleet activity model, for 2007 only.
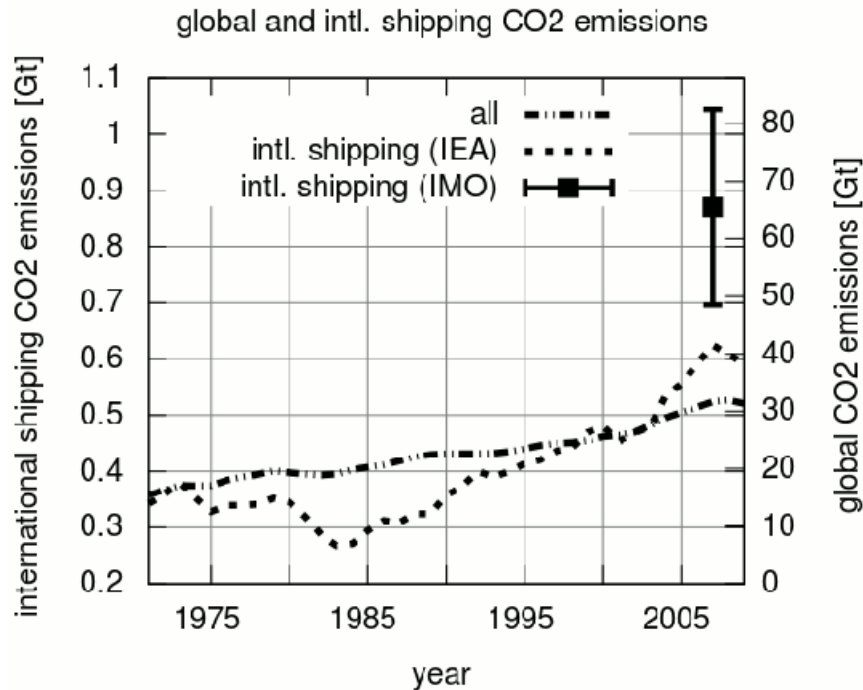
Figure 1: CO_2 emissions from international shipping based on fuel sales data (IEA, 2011) and on a fleet activity model (Buhaug, 2009), and global CO_2 emissions from all sectors (BP, 2012).

So, while shipping faces a huge challenge in drastically reducing its greenhouse gas emissions – following a strong upward trend over past decades – emissions are not accurately known in quantitative terms. Estimates are associated with large uncertainties and many methods are not well-suited to monitor the emissions trajectory over time. An accurate method of estimating greenhouse gas emissions from shipping that is sensitive to fuel saving measures may allow for a better grasp of the problem (Gilbert and Bows, 2012). In terms of its emissions, shipping needs to change course urgently and an exact instrument for determining its position would be useful to policymakers.

This paper explores a method based on AIS (Automatic Identification System) data. All large ships are required to send their position and state of motion at regular intervals and the messages can be picked up by satellite. The underlying idea is to infer a vessel's fuel consumption based on its movements, as represented by the set of its associated AIS messages. Applied to the whole fleet, CO_2 emissions could be estimated over time - and with little time lag. While AIS recorders are already deployed in orbit, the majority are commercial, and the data are expensive. Only a small sample of limited geographical and temporal coverage was available to the authors. The aims of this study are therefore to demonstrate the principle, and conduct a comparative assessment with other methods, with a view to populating the navigational toolkit that shipping may draw upon in steering a low carbon course.

Section 2 gives an overview of the currently used methods for estimating shipping emissions. Section 3 presents the method. Initial results are given in section 4, and discussed in section 5. Section 6 concludes.

2   EXISTING METHODS OF ESTIMATING SHIPPING EMISSIONS

Various ways of estimating greenhouse gas emissions from shipping are found in the literature. They are typically based on: a fleet activity model; a dataset of ship-movements; transport work; or fuel sales. The 2nd IMO greenhouse gas study uses a world fleet register and, according to size and type, the vessels' annual fuel consumption is calculated from assumptions on the installed engine power, engine load factor and specific fuel consumption, and days at sea. Uncertainty in these parameters directly translates into uncertainty in the results, shown in figure 1. Perhaps more importantly, measures aiming to reduce shipping's carbon cost, such as slow-steaming, are only indirectly accounted for, if at all. Paxian et al (2010), on the other hand, developed an algorithm for determining a ship's route and travel speed, based on ship movements in and out of ports. From the ship voyage as determined by the algorithm, the associated fuel consumption is estimated on the basis of ship parameters, such as installed engine power. While such ship movement data exist, they provide no immediate information about the actual route, and speed, travelled. Furthermore, they are usually very expensive and it is not clear how complete a coverage they provide. Paxian et al (2010) scale their results up, by extrapolating from the ship numbers in their data to the ship numbers in the fleet register used in the 2nd IMO greenhouse gas study, to compare results.

   Some other methods focus on the cargo rather than the vessels. Agencies like Eurostat or UNCTAD provide extensive data on traded goods. By making assumptions on the type of ship – fuel consumption and loading condition in particular – that the cargo travels on, a carbon cost can be assigned to the transporting of the good, in gCO_2 per tonne-km. If the origin and destination of the cargo is known, the distance can be looked up, and together with the assumed amount of CO_2 emitted per tonne-km, the CO_2 emissions arising from the transport of the goods is estimated (Schrooten et al, 2009). One major advantage is that it allows for an apportionment of emissions to individual regions or countries. However, the uncertainties in the emission factors are large, and the measures required to reduce uncertainty are not straightforward because there is no direct way of adjusting emissions factors to the uptake of such measures. As mentioned in section 1, fuel sale records provide a good time series, but it has been argued that they significantly under-estimate emissions (Corbett and Koehler, 2003). Beyond the indirect methods detailed here, it is obviously viable for vessels to record their own fuel consumption at a reasonable cost assuming some technical adaptation (Faber et al, 2009). However, there is no regulation in place that would make this mandatory and as these data are commercially sensitive they are not typically disclosed.

3   METHOD FOR ESTIMATING FUEL CONSUMPTION FROM AIS DATA

The IMO's International Convention for the Safety of Life at Sea (SOLAS) requires all ocean-going ships of gross tonnage of 300 or above to radio AIS messages at regular intervals. The messages contain a number of parameters including the ship's location and speed, and allow for its identification. While AIS messages have a horizontal range of the order of 50 miles, they travel much further vertically, meaning they can be received by satellite. A number of AIS receivers have been deployed in space, both by governments and private enterprises. The NORAIS experiment on board the ISS uses such a receiver to record AIS data. The data recorded by the NORAIS experiment between 27 June and 18 July 2010 are used in this study. The receiver's field of view moves with the trajectory of the ISS. Disentangling the messages from the potentially large number of vessels in the field of view is one of the main challenges in the designing of receivers, and in areas of dense ship traffic the detection probability deteriorates significantly (Eriksen et al, 2006). In the same areas, however, one may expect coverage by land-based receiver stations to be highest – because, for obvious reasons, they are likely to be found in locations of high traffic and land-based receivers have a much smaller field of view and disentangling messages is therefore not an issue. To complement the NORAIS data, four sets of land-based AIS data were acquired from a commercial provider, Vesseltracker, covering the Baltic Sea, the North Sea, the Mediterranean and China, over the time period from 18 June to 27 July 2010.

   The fuel consumption of individual vessels is estimated over the two week time period from 1 July to 14 July 2010, based on vessel motion during that time and the installed engine power and inferred loading. Vessel movements are derived from its associated AIS data and vessel parameters

are read from a database of the world cargo fleet, by Clarkson. The core time interval was chosen to lie within the time period covered by both AIS data sets, with time margins before and after so that, ideally, a vessel's location is known before entering and after leaving the time period of analysis.

As the first step, all AIS messages pertaining to the ship under scrutiny are collected and time-ordered. Its IMO number serves as the ship's identifier. The land-based AIS data are delivered in a pre-processed format with all messages in the same format and including the IMO number. The space-based data are delivered in their original format, and there are two differing message types. One (called type 1 here) is sent every 2 to 10 seconds but it does not contain an IMO number. The other (called type 5 here) is sent every 6 minutes and it does contain the IMO number. Messages are associated by way of the MMSI (Maritime Mobile Service Identity). Because the MMSI is not as reliable an identifier as the IMO number, only those vessels and messages were selected for which there is a strict one-to-one correspondence between IMO number and MMSI throughout the data. The sample from the NORAIS dataset contains 119 thousand messages of type 5, and 3 million messages of type 1, with 15,804 distinct IMO numbers.

As the second step, for every pair of consecutive AIS messages the fuel consumption over the time interval between the two messages is calculated, using a version of the basic formula for the fuel consumption fc:

$$fc = 0.8 \cdot P_{ME} \cdot SFOC \cdot \left(\frac{v_{transient}}{v_{service}}\right)^3 \cdot \Delta t$$

Where 0.8 is the assumed engine loading at service speed, P_{ME} is the installed main engine power, $SFOC$ is the specific fuel consumption of the engine, assumed to be 200g kWh^{-1}, v is ship speed, and Δt is the time interval between messages. Ideally, with near-complete coverage, this time interval would be very short, and the actual ship movement over time would be well-resolved. Given the limited scope and coverage of the data used here, this case cannot be expected. In order to be conservative (i.e. rather under-estimate than over-estimate fuel consumption), three cases are distinguished in determining the transient speed, according to the length of the time interval. 1. ($\Delta t <$ 10min.) $v_{transient}$ is the mean v_m of the velocities stated in the AIS messages. 2. (10min. $< \Delta t <$ 3h.) $v_{transient}$ is the geographic distance Δs, between locations stated in the AIS messages divided by the time interval Δt. (3h. $< \Delta t$) $v_{transient} = v_m^{2/3} (\Delta s / \Delta t)^{1/3}$. The reasoning for this is as follows: for very small time intervals, the transient speed transmitted is deemed accurate for the whole interval. For longer intervals, a constant speed is considered a more conservative assumption about the motion of the vessel. For yet longer time intervals, this may lead to gross under-estimation when the ship passes between two locations and then idles.

In the third step, fuel consumption over all time intervals lying in the study period is aggregated, for every ship in the fleet register.

A number of checks are included in the analysis to guard against missing or faulty data. If no main engine power is given it is determined from a fit formula, based on the ship's deadweight and service speed[1]. If no service speed is given in the fleet register, it is assumed to be the value between the 4th and 5th quintile of speed values in the set of AIS messages associated with the ship. If the speed value is considered unreasonable, it is replaced by applying the inverse engine power fit formula. Finally, all outliers in the results are checked and discarded if any parameter appears faulty. It is noted that examples of faulty speed values, faulty position readings, and mis-identifications were found in the land-based data but none in the space-based data, indicating that this does not pose an intrinsic problem to the use of AIS data.

4   RESULTS

Overall, out of 33,380 vessels in the data base, 22,270 vessels, or 2/3, are identified in the AIS data. However, not all of the detected and identified vessels' movements over the core two week time period are resolved well by the data. In order to understand how well ship movements are resolved by

---

[1] The main engine power formula is $P_{ME}[HP] = 0.0561913 \cdot dwt^{0.398105} \cdot v_{service}[knots]^3$, based on data from the fleet register.

the AIS data, two parameters are considered. The coverage for a vessel is here defined as the fraction of the core time interval which is covered by the AIS data associated with the ship i.e. the coverage is the time stamp of the last AIS message (or the end of the core time interval if the last AIS message is later) minus the time stamp of the first message (or the start of the core time period, if the first AIS message dates earlier). So the coverage ranges between 0, if the ship is (a) not detected at all, or (b) only before the core time interval, or (c) only after the core time interval, and 1, if the vessel first appears in the data before the core time interval began and last after it ended.

   The second parameter is the maximum time interval between messages. This is the longest time interval between two consecutive messages in the core time interval (cut at the start or end point if it extends beyond the core time interval), as a fraction of the core time interval. The maximum time interval ranges from very small numbers where AIS messages from the vessel are received continuously, without any long interruptions, to 1 where the vessel is seen before and after the core time interval, but no message is recorded during the core time interval. Coverage and maximum time interval provide a measure for how closely a vessel is tracked by the AIS data. Figure 2 shows the distribution of both parameters for the entire ship register used in this study. In 15,719 cases, the AIS records cover the full core time interval. This means that about one half of all vessels are located by the AIS data sample both before the core time interval begins and after it ends. In the other cases, the vessel is either first detected some time after the beginning of the core time period or it is last seen some time after the end of the core time period, or – in about one third of the cases – is not detected at all.
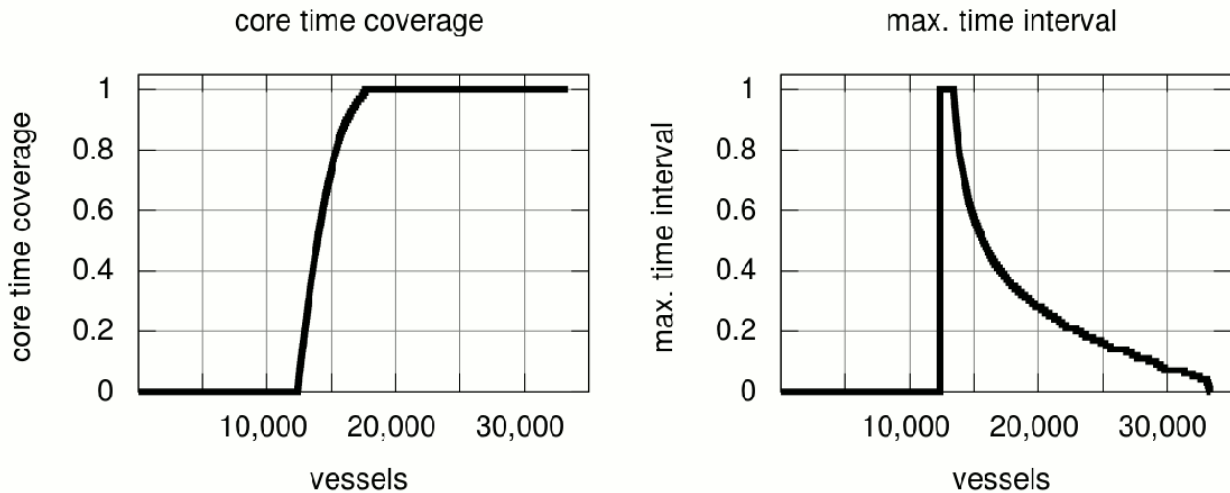
Figure 2: Coverage and core time interval for all vessels in the register of the world cargo fleet used in this study.

For the vessels with a coverage parameter of 1, on average, the maximum time interval is 0.28, or 94 hours, about four days. This provides an estimate of how well the vessel movement during that time period is monitored by the AIS data. In a time interval of four days, a vessel could have undertaken a return voyage, taking up to two days per leg, that would not be reflected in the data, and the ensuing fuel consumption would go unnoticed.

   For vessels that are mainly tracked by the NORAIS data, the ideal value of the maximum time interval is just below 0.04, or about half a day, as a result of the flightpath of the ISS, which equals the trajectory of the field of view of the NORAIS receiver. For deep sea shipping, half a day already appears to provide a reasonable detection frequency. Figure 2, on the right, shows the distribution of maximum time intervals of the vessels in the ship register moving towards that value, with a small tail of vessels that have even smaller values, because they are not covered over the whole time period or because they spent the whole time period in one of the areas covered by land-based receiver stations.

To consider an example, figure 3 shows the track of a vessel on its voyage from Santos (Brazil) to Singapore, as recorded in the AIS data. The 76,784 dwt bulk carrier has the IMO number 9304239, its service speed is 14.5 knots, and the installed main engine power is 12,550 HP. According to the formula given in section 2, its fuel consumption over the two week study period was 366 metric tons. The coverage is 1 and the maximum time interval between two consecutive messages in the two week core time interval is 0.05, or 17 hours. This example represents an almost ideal case. In most cases, the data are not as complete, if the vessel either spent more time outside the field of view of the receivers or was in the field of view of the NORAIS receiver but its messages were not recorded, which is the more probable the denser the ship traffic in the area (cf. Eriksen et al, 2006).
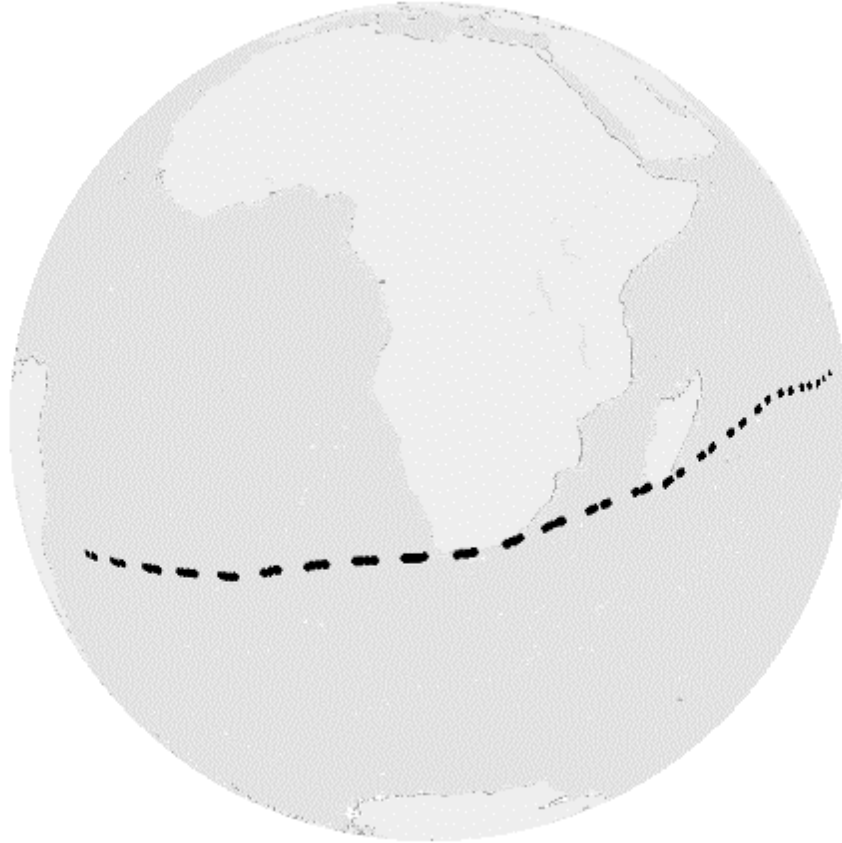
Figure 3: Track of AIS messages from a bulk carrier as recorded by the NORAIS receiver between 27 June and 18 July 2010.

To gain an understanding to what degree fuel consumption may be inferred from even such a severely limited data sample table 1 shows results for six size categories of container vessels: the average coverage parameter per category, together with the number of ships in that category and the average annual fuel consumption per ship, as calculated from the AIS data (multiplying the fuel consumption over the two week core time period by 365/14 to get its annual fuel consumption).

Size	number of ships this study	average GT	average main engine fuel consumption [ktons/year]	coverage
>8,000 TEU	287	101,263	24.39	0.935
5,000-8,000 TEU	523	68,024	16.93	0.843
3,000-4,999 TEU	877	44,066	12.35	0.825
2,000-2,999 TEU	694	28,294	6.77	0.789
1,000-1,999 TEU	1,230	15,501	2.73	0.730
<999 TEU	1,189	6,715	1.04	0.617

Table 1: For size categories of container vessels, the table shows the number of vessels in the used database of the world cargo fleet, average gross tonnage, average annual fuel consumption based on the limited AIS sample, and coverage.

5   DISCUSSION

The sample of AIS data available for this study does not provide full global coverage. Therefore, the results presented in table 1 are clearly expected to under-estimate emissions because of the limitations of the data and a conservative formula for estimating fuel consumption. However, the results indicate that even from such a severely limited data sample, a significant share of vessels is tracked reasonably well, indicating that estimating shipping emissions from recorded AIS data is indeed viable.

There are two obvious steps towards further development and application of the presented method. First, if the method could be applied to AIS data with full global coverage, an accurate resolution of all vessel movements, with respect to inferring their fuel consumption, can be expected, providing an estimate of international shipping emissions. While the data are not readily available, they exist, and the method is feasible. Second, the formula used in deriving fuel consumption is rather simplistic, and it could be modified (for example, by developing a more sophisticated speed dependency), calibrated, and fine-tuned if fuel consumption records from ships, along with the corresponding AIS data were available as a training and test sample.

Having addressed the viability of the method, it is now assessed in comparison to other methods currently in use with respect to its advantages as well as potential barriers and caveats. The greenhouse gas protocol lists five criteria that greenhouse gas accounting and reporting methods should fulfil: relevance, completeness, consistency, transparency, and accuracy (Ranganathan et al, 2004).

5.1   *Relevance:*

Relevance means the method "appropriately reflects the GHG emissions" (Ranganathan et al, 2004). The AIS method directly maps international shipping activity onto fuel consumption and ensuing CO_2 emissions, rather than indirectly inferring the activity from the existing fleet or goods transported. It is also a more direct mapping than bottom-up methods based on ship movements in and out of ports as those need to make assumptions about the actual route and speed. The fuel sales method yields a value directly but it does not account for how and where emissions take place – information that is arguably key to a market based measure (MBM) to control greenhouse gases from shipping (Faber et al, 2009).

5.2   *Completeness:*

The AIS method includes all ships of gross tonnage of 300 or more. With respect to fuel consumption from international shipping, that means it is almost complete. A fleet activity model using a world fleet register is also complete in principle. The completeness of data on ship movements in and out of port, i.e. the relative number of ship movements recorded in the data, is not known, and they do not contain details of the journey between ports (Paxian et al, 2010). Completeness is limited for methods based on transport work and it has been argued that fuel sales under-estimate fuel consumption (Corbett and Koehler, 2003). In practice, the completeness of the AIS method depends on the completeness of coverage, and potentially on the extent to which AIS is switched off, which can be the case when it would compromise security, in piracy areas for example.

5.3   *Consistency:*

One main advantage of the AIS method over others is that it can yield continuous emission estimates over time, with very little time-lag. None of the other methods is as quick or provides the same degree of time-resolution.

5.4   *Transparency:*

The criterion of transparency is met well by all of the methods discussed in this study.

5.5   *Accuracy:*

Accuracy is clearly a criterion that is absolutely key. All of the methods currently in use are associated with large uncertainties. While the proposed AIS-based method has the potential to be accurate to a very high degree, future work will have to prove this. What is crucially important, with respect to any effort to meet the low carbon challenge for shipping, is the method's sensitivity to changes in shipping practices aimed at reducing emissions.

One method that has not been discussed is the recording and reporting of the fuel consumption by the ships. While there are ships that would need to fit additional equipment in order to accurately record their fuel consumption, this could be done at moderate cost (Faber et al, 2009). If such a method were put in place, it would likely be the most ideal one, particularly in relation to accuracy. If a stringent MBM were put in place, this would likely have to include regulation for ships to record and disclose their actual fuel consumption (Faber et al, 2009). In that case, the proposed AIS method could play an important role in monitoring the whole system, including fraud detection. More importantly, however, shipping has not managed to put in place a stringent MBM, despite many and long discussions at the IMO and elsewhere. Establishing a concise and effective instrument for monitoring shipping emissions that provides a clear picture of CO_2 emissions from shipping could constitute an important first step towards meaningful mitigation measures. The notion of providing such a clear picture may meet with opposition, and acquiring the data and producing the information would incur a cost. Nevertheless, if shipping is serious about controlling its greenhouse gas emissions and making its fair contribution to the problem then these barriers must be overcome.

6   CONCLUSIONS

In terms of its greenhouse gas emissions, shipping must urgently change course. However, there is an absence of navigational instruments that may prove useful in executing this manoeuvre. Estimates of shipping emissions are associated with large uncertainties, and methods currently available often lack sensitivity with respect to measures aimed at reducing fuel consumption, and are unable to monitor progress adequately. This paper presents a new method for monitoring the greenhouse gas emissions from shipping using AIS data, collected in space as well as on land, to track ship movements. An analysis of limited samples of AIS data in combination with a register of the world cargo fleet indicates that the method is viable. It is assessed according to a set of criteria for greenhouse gas monitoring and shown to be fit for the task. In particular, yielding near real time results, with accurate spatial and temporal resolution, based on the actual vessel movements, are key properties and advantages of this new method over others. Implementing the method on a complete global scale will need to navigate some obstacles, including the cost of acquiring AIS data guaranteeing sufficient coverage. But the shipping sector must overcome these barriers if it is to reconcile what it says with what it does to address climate change.

7   ACKNOWLEDGEMENTS

REFERENCES

Anderson, K. and A. Bows, 2011: Beyond dangerous climate change: emission scenarios for a new world. Philosophical Transactions of the Royal Society A: Mathematical, Physical and Engineering Sciences, 369.

Anderson, K., P. Gilbert, and A. Bows, 2012: Executing a Scharnow turn: why, when and how the shipping sector can be reconciled with international commitments on climate change. Carbon Management. submitted.

BP, 2012: Statistical Review of World Energy. BP.

Buhaug, Ø., J.J. Corbett, Ø. Endresen, V. Eyring, J. Faber, S. Hanayama, D.S. Lee, D. Lee, H. Lindstad, A.Z. Markowska, et al, 2009: Second IMO GHG study. International Maritime Organization (IMO) London, UK.

Corbett, J.J. and H.W. Koehler, 2003: Updated emissions from ocean shipping. J. Geophys. Res 108,4650-64.

Eriksen, T., G. Høye, B. Narheim and B.J. Meland, 2006: Maritime traffic monitoring using a space-based AIS receiver. Acta Astronautica, 58, 537-549.

Faber, J., A. Markowska, D. Nelissen, M. Davidson, V. Eyring, I. Cionni, E. Selstad, P. Kageson, D. Lee, O. Buhaug, et al, 2009: Technical support for European action to reducing greenhouse gas emissions from international maritime transport. CE Delft, Delft.

Gilbert, P., and A. Bows, 2012: Exploring the scope for complementary sub-global policy to mitigate CO_2 from shipping. Energy Policy, available online.

IEA, 2011: CO_2 emissions from fuel combustion. International Energy Agency (edition: 2011).

IMO, 2010: Control of greenhouse gas emissions from ships engaged in international trade. Position note by the International Maritime Organisation. COP 16. Cancun, Mexico.

Paxian, A., V. Eyring, W. Beer, R. Sausen, and C. Wright, 2010: Present-day and future global bottom-up ship emission inventories including polar routes. Environ. Sci. Technol. 44, 1333-1339.

Ranganathan, J., L. Corbier, P. Bhatia, S. Schmitz, P. Gage, and K. Oren, 2004: The greenhouse gas protocol: a corporate accounting and reporting standard. World Resources Institute and World Business Council for Sustainable Development. Washington, DC, US.

Schrooten, L., I. De Vlieger, L. I. Panis, C. Chiffi, and E. Pastori, 2009: Emissions of maritime transport: A European reference system. Science of The Total Environment, 408, 318-323.

IAGOS - In-service Aircraft for a Global Observing System

A. Petzold[*], A. Volz-Thomas
Forschungszentrum Jülich GmbH (FZJ), Institute of Energy and Climate Research, IEK-8 Troposphere, Jülich, Germany

V. Thouret, J.-P. Cammas
Laboratoire d'Aérologie, CNRS, and Universite Paul Sabatier Toulouse III, Toulouse, France

C.A.M. Brenninkmeijer
Max Planck Institute for Chemistry, Mainz, Germany

Keywords: Global monitoring, atmospheric observation, MOZAIC, CARIBIC

ABSTRACT: IAGOS is a new European research infrastructure which aims at constructing a global observation system for atmospheric composition by deploying autonomous instruments aboard a fleet of passenger aircraft. IAGOS builds on more almost 20 years of scientific and technological expertise gained in the research projects MOZAIC (Measurement of Ozone and Water Vapour on Airbus In-service Aircraft) and CARIBIC (Civil Aircraft for the Regular Investigation of the Atmosphere Based on an Instrument Container). The European consortium behind IAGOS includes research centres, universities, national weather services, airline operators and aviation industry. The two elements IAGOS-CORE and IAGOS-CARIBIC are complementary building blocks of one unique global atmospheric observation system. IAGOS-CORE deploys newly developed high-tech instrumentation for regular in-situ measurements of atmospheric chemical species (O_3, CO, CO_2, CH_4, NO_x, NO_y, H_2O), aerosols and cloud particles. Involved airlines ensure global operation of the network. In IAGOS-CARIBIC an extensively instrumented cargo container is operated as a flying laboratory aboard one aircraft. IAGOS provides data for users in science and policy including air quality forecasting, verification of CO2 emissions and Kyoto monitoring, numerical weather prediction, and validation of satellite products. It is considered a major contributor to the in-situ component of GMES Atmospheric Services. In combination with its predecessor programs MOZAIC and CARIBIC, IAGOS allocates long-term observation data of atmospheric chemical composition in the upper troposphere and lowermost stratosphere since 1994, while the most recent IAGOS-CORE aircraft went into service in 2011 and 2012.

1 RATIONALE

The largest uncertainties in our current knowledge on climate change are associated with the complex feedback mechanisms in the climate system, for example the amplification of the CO2-induced greenhouse effect by water vapour (Lacis et al. 2010), the effect of aerosol on cloud formation and cloud microphysics (Clarke; Kapustin 2010; Schwartz et al. 2010), the role of deep convection for transport of gases and aerosol particles into the UTLS, in particular over South-East Asia (Monsoon), and its behaviour within a changing climate (Randel et al. 2010), or the modification of biological cycles by climate change (Mahowald 2011) including feedbacks through biogeochemical and bio-geophysical processes which alter the sources and sinks of the greenhouse gases CH_4 and CO_2 (Friedlingstein et al. 2006). These uncertainties, in turn, imply large unknowns in predicting the future climate, especially at regional scales (Lenton 2011).

The atmospheric greenhouse effect is not confined to the lower atmosphere, but is largely driven by changes in the upper troposphere and the lower stratosphere (UTLS) (Riese et al. 2012). For instance, the small increase of water vapour in the stratosphere (by only ~0.8 ppm between 1980 and 2010) is likely responsible for 25% of the total anthropogenic greenhouse effect of ~0.5°C during

[*] *Corresponding author:* PD Dr. Andreas Petzold, Forschungszentrum Jülich GmbH, Institut für Energie- und Klimaforschung, IEK-8: Troposphäre, 52425 Jülich, Phon +49 (0) 2461-615795, Email: a.petzold@fz-juelich.de

this time (Solomon et al. 2010). Climate change also influences air quality by modifying atmospheric transport and weather patterns (Min et al. 2011) with impacts on air quality in Europe and other regions of the world due to long range transport of pollutants, ozone, and aerosol from growing economies (Monks et al. 2009).

In order to reduce the uncertainty of climate predictions, the models require input from measurements, both as boundary conditions and for the evaluation and improvement of parameterizations. Indeed, observational capacity is essential for all aspects of atmospheric research, including the assessment of causes for past changes as well as the prediction of further future changes and the economic and social consequences (e.g., IGACO 2004; IGCO 2004; Solomon et al. 2007). Also, pressing scientific issues require detailed long-term observations of atmospheric chemical composition on a global scale. Of highest scientific interest are data on greenhouse gases like CO_2, CH_4, and water vapour, reactive trace gases like ozone (being also a short-lived greenhouse gas) and nitrogen oxides, aerosol particles, and clouds.

2   IAGOS OBJECTIVES AND SCIENTIFIC VALUE

The European Research Infrastructure IAGOS (In-service Aircraft for a Global Observing System; www.iagos.org) responds to the increasing requests for long-term, routine in-situ observational data by using commercial passenger aircraft as measurement platforms. Table 1 summarises the objectives of IAGOS and the expected scientific value. Thus IAGOS closes the gap between space borne and ground based observations:

1. In the Tropopause Region: Most important for climate change, and dynamical processes (stratosphere-troposphere-exchange); hardly observable from space or from ground.
2. Vertical profiles in the troposphere: Essential for carbon cycle research, air quality, climate change, and weather prediction.

Table 1. Objectives and Scientific Value of IAGOS

Objectives	Scientific Value
IAGOS-CORE	**Changes in the Tropopause Region**
Routine atmospheric observation by 20 long-haul aircraft equipped with scientific instruments for:	- high spatial and temporal resolution of in-situ observations
- atmospheric chemical composition (H_2O, O_3, CO, NO_x, NO_y, CO_2, CH_4)	- ozone background and trend
	- water vapour background and trend
- aerosol number concentration and size	**Validation of Atmospheric Models and Satellite Retrievals**
- cloud particle number concentration	
Long-term deployment (20 yrs)	- tropospheric profiles of H_2O, O_3, CO, NO_x, aerosol, CO_2, CH_4, cloud particles
Global coverage	
Open data policy (GMES/GEO/GEOSS)	- UTLS data of H_2O, O_3, CO, NO_x, aerosol, CO_2, CH_4, cloud particles
Near real time data provision	
	Global Air Quality
	- influence of developing regions
	- long-range transport of air pollutants
IAGOS-CARIBIC	- vertical transport of air pollutants by deep convection
Monthly deployment of the instrumented CARIBIC Container:	**International Transfer Standards**
- Large number of species ($\cong$ 100), inclu- ding those of IAGOS-CORE and VOCs, CFCs, aerosol chemical composition, H_2O isotopologues, and SO_2	- use of proven measurement technology
	- global deployment of same instruments
	- regular Quality Assurance including calibration against reference instruments, based on GAW standard procedures

Utilizing global aviation for routine atmospheric observation is cost efficient and makes optimum use of the existing infrastructure. By deploying a set of autonomous instruments aboard a fleet of passenger aircraft of internationally operating airlines, global data of atmospheric chemical composition in the upper troposphere and lower stratosphere are collected. In addition, vertical profiles of trace species are gained during each single landing of instrumented passenger aircraft. IAGOS is designed for global coverage and a lifetime of at least 20 years and will thus provide long-term, fre-

quent, regular, accurate, and spatially resolved in-situ atmospheric observation data to the global scientific community.

3 HISTORY

The use of commercial aircraft for in situ observation of the atmosphere has a long history beginning in the 1970s when NASA implemented the Global Atmospheric Sampling Programme (GASP) during the period of March 1975 to July 1979. Parameters measured by the aircraft included various meteorological variables, ozone, carbon monoxide and particle densities, and flight information; for more information visit http://gcmd.nasa.gov/records/GCMD_NCAR_DS368.0.html. The historical evolution of this research area is described in detail in the IGAC Newsletter No. 37 (issued November 2007; www.igacproject.org).

IAGOS builds on almost 20 years of scientific and technological expertise gained in the research projects MOZAIC (Measurement of Ozone and Water Vapour on Airbus In-service Aircraft) and CARIBIC (Civil Aircraft for the Regular Investigation of the Atmosphere Based on an Instrument Container). The history of IAGOS and its predecessor programmes MOZAIC (www.iagos.org) and CARIBIC (www.caribic-atmospheric.com) is illustrated with more detail in Figure 1. In 1993, the idea of using commercial aircraft for atmospheric observation was revived with the European MOZAIC project in which airborne systems for ozone and water vapour were installed on five A340 aircraft (Marenco et al. 1998), with CO and NO_y added in 2001. More than 35,000 flights have been completed since 1994 and three of the aircraft are still in service. CARIBIC started independently, using a measurement container aboard one Boeing 767 aircraft in 1997. To date, more than 230 ISI referenced publications have emerged from the programmes MOZAIC and CARIBIC.
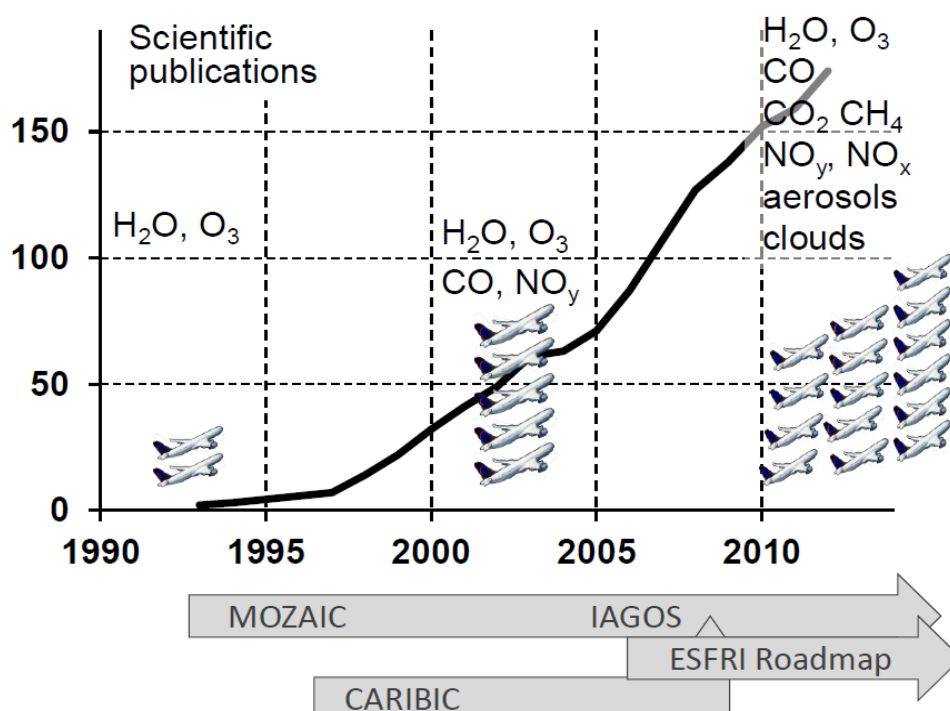
Figure 1. Evolution of airborne observations using instrumented passenger aircraft from programmes MOZAIC and CARIBIC to IAGOS; the graph shows the number of scientific publications from the MOZAIC data set whereas the aircraft represent the number of equipped units in operation. Observation parameters are indicated for the various evolution stages of the programme.

As part of the transformation process from MOZAIC to IAGOS which started in 2005, the set of observation parameters was significantly extended. Formerly separated programmes MOZAIC and CARIBIC have been merged into IAGOS which serves now as a single infrastructure designed for sustainable long-term and global operation (Volz-Thomas; IAGOS-team 2007; Volz-Thomas et al. 2009). The resulting infrastructure is built from two complementary approaches: The CORE component comprises the implementation and operation of autonomous instruments installed on up to

20 long-range aircraft of international airlines for continuous measurements of important reactive gases and greenhouse gases (e.g. carbon dioxide ,and methane and water vapour), as well as aerosol particles, dust and cloud particles. The fully automated instruments are designed for operation aboard the aircraft in unattended mode for several weeks and the data are transmitted automatically.

The complementary CARIBIC component consists of the monthly deployment of a cargo container equipped with instrumentation for a larger suite of components (Brenninkmeijer; CARIBIC-team 2007; Brenninkmeijer et al. 2007). It includes instruments that cannot yet be implemented in full routine operation for measuring, e.g., organic compounds or water vapour isotopologues. The installation combines instrumentation for in-situ measurements and remote sensing and the collection of air and aerosol samples (Andersson et al. 2013) for post-flight analysis in the laboratory. This dual setup of IAGOS should aims at providing global coverage of key observables on a day-to-day basis with a more complex set of observations with lesser reduced coverage. With its partners from leading research institutions in Germany, France, and the UK, IAGOS was successfully established on the roadmap of the "European Strategy Forum on Research Infrastructures" (ESFRI); and is listed among the ESFRI success stories; see ec.europa.eu/research/infrastructures.

4   IAGOS INSTRUMENTATION

The suite of instruments operated on board of IAGOS-CORE aircraft consists of one unit (Package 1), which measures ozone, water vapour, carbon monoxide and cloud particle number concentration, and is deployed on every aircraft. In addition, one option of a second unit (Package 2, option a-d), which targets specific species and properties such as nitrogen-containing compounds, greenhouse gases or aerosol particle properties, will be installed. The atmospheric trace species and properties measured by the IAGOS-CORE instrumentation and applied measurement techniques are compiled in Table 2. The fully equipped IAGOS-CORE instrument rack weighs approx. 120 kg and is mounted in the avionic bay of Airbus A340/A330 aircraft. Figure 2 shows a photograph of the first IAGOS-CORE aircraft operated by Lufthansa. Details on the extensive measurement techniques of CARIBIC are given by Brenninkmeijer et al. (2007) and the CARIBIC team (2007).

Figure 2.   IAGOS-CORE installation position aboard the Lufthansa A340-300 "Viersen" (photograph by courtesy of A. Karmazin); the insert shows details of the IAGOS Inlet Plate which carries the inlet probes for trace gas sampling (photograph by courtesy of Lufthansa).

Table 2. IAGOS-CORE Instrumentation

		Parameter	Method	TR*	Precision	Responsibility/ Reference
Package 1	All aircraft	O_3	UV absorption	4s	± 2ppb	CNRS (Thouret et al. 1998)
		CO	IR Absorption	15s	± 5ppb	CNRS (Nédélec et al. 2003)
		H_2O	Humicap	4-10s	± 5% RH	FZJ (Helten et al. 1998)
		Cloud Particles	Backscatter Probe	4s		Univ. Manchester, UK
Package 2 (1 option)	Opt. a	NO_y	Chemiluminescence Gold converter	4s	± 50 ppt	FZJ (Volz-Thomas et al. 2005)
	Opt. b	NO_x	Chemiluminescence Photolytic conversion	4s	± 50 ppt	FZJ
	Opt. c	Aerosol Particles	Condensation Particle Counter (0.01– 3μm) Optical Particle Counter (0.25 – 3μm)	4s	± 10 cm^{-3} ± 5 cm^{-3}	FZJ/DLR
	Opt. d	CO_2 CH_4 H_2O CO	Cavity Ring-Down Spectroscopy	4s	± 0.1 ppm ± 2 ppb ± 6-15 ppm ± 10 ppb	Max Planck Institute for Biogeo-chemistry, Jena, Germany

*TR: Time resolution or data rate, whatever is longer

Table 3. IAGOS data set provided to GEOSS

Parameter	MOZAIC	IAGOS CORE	CARIBIC Phase II
Ozone	1994	2011	2004
Water Vapour	1994	2011	2004
Carbon Monoxide	2002	2011	2004
Odd Nitrogen (NO_y)	2001	2011	2004
Nitrogen Oxides(NO_x)		2011	2004
Carbon dioxide		2013	2004
Methane		2013	2004
Aerosol number concentration and size		2013/2014	2004
Cloud particle number concentration		2011	
~100 trace species			2004

   The data set which has emerged so far from the IAGOS project and its predecessor programmes is listed in Table 3. These data sets are freely accessible for the global scientific community on request via the IAGOS data base hosted by the French joint venture ETHER at www.iagos.fr/web. As an example for today's use, Figure 3 shows a statistical analysis of vertical profiles of CO over Frankfurt/Main, Germany, for February 2013. In-situ data are used for near-real-time validation of model results from the EU FP7 programme MACC (Monitoring Atmospheric Composition and Climate). Details on the applied models are given at www.iagos.fr/macc/nrt_day_profiles.php and links listed on this website.
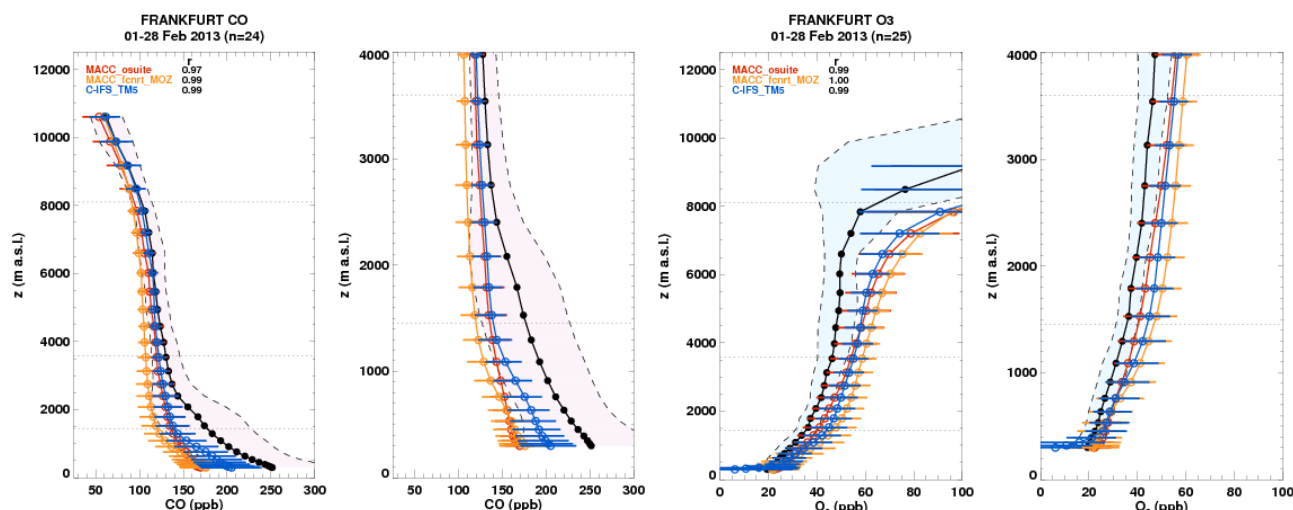
Figure 3. Average vertical profiles of CO and O_3 for Frankfurt/Main, Germany (black circles); coloured lines and symbols represent results from model analyses performed in the EU FP7 project MACC (Monitoring Atmospheric Composition and Climate). For details visit www.iagos.fr/macc/nrt_day_profiles.php.

5   THE IAGOS GLOBAL NETWORK

The IAGOS Global Network is built from components of the various contributing programmes. In 2010, the CARIBIC container was fully revised and recertified and returned into operation aboard Lufthansa A340-600 with a deployment of four flights per month. Destinations covered by CARIBIC are globally distributed with the majority of flights heading to North America and the Far East, and few directions to South Africa and South America. A map of recent destinations is accessible at www.caribic-atmospheric.com.

Also in 2010, instruments on the remaining three MOZAIC Airbus A340 aircraft went back into service. These aircraft are operated by Air Namibia (one aircraft) and Lufthansa (two aircraft).

IAGOS-CORE has started its operation with Lufthansa A340-300 "Viersen" in July 2011 out of Frankfurt Airport. The second Airbus A340 went into service in July 2012 and is operated by China Airlines from its home base Taipei, Taiwan. In 2013 instrument installations are scheduled for Air France and Iberia, and for an Airbus A330 operated by Cathay Pacific. Thus, by end of 2013 five aircraft will be equipped with IAGOS-CORE instruments. In addition, the CARIBIC aircraft, and three MOZAIC aircraft will be in operation. The emerging global network is illustrated in Figure 4.
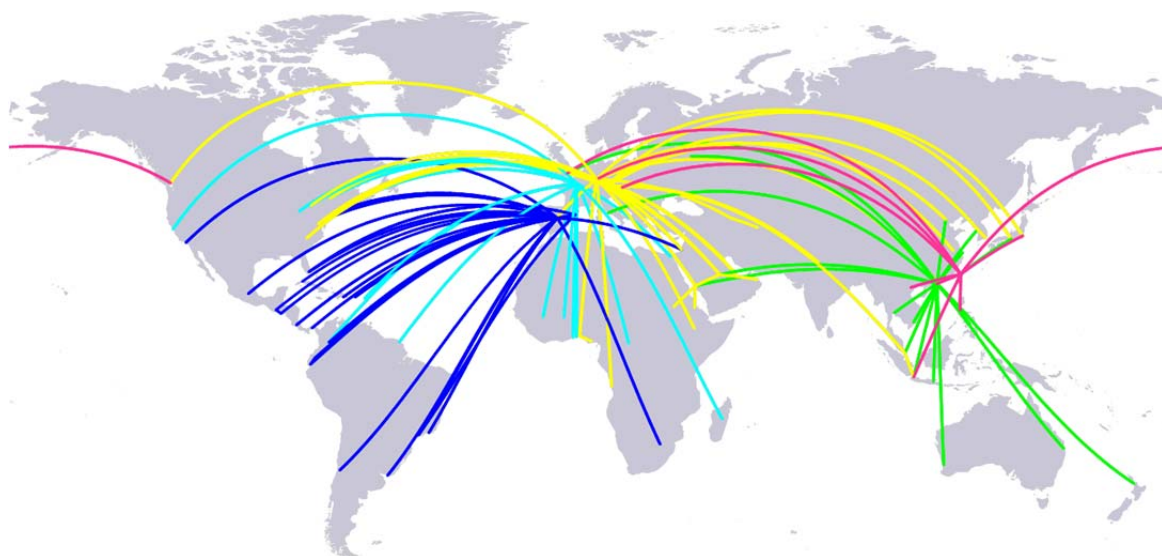

Figure 4. IAGOS-CORE Global Network 2013; coloured lines represent participating airlines Lufthansa (yellow), Air France (cyan), Iberia (blue), Cathay Pacific (green) and China Airlines Taiwan (magenta).

6   SUMMARY AND OUTLOK

Routine aircraft observations are providing valuable information on atmospheric composition that improve the understanding of global and regional air quality, as well as the potential impact of greenhouse gases on climate change. The comparability of measurements from an airborne monitoring network that collects data on a global scale by few identical systems with identical QA procedures, is inherently better than that from many stations operated by different institutions and using different instrumentation. . In that respect, routine aircraft observation could even provide useful information for harmonisation of different global networks.

IAGOS builds on previous European initiatives with novel technological developments and a strong emphasis to expand the network to the Pacific, North America and into the Southern Hemisphere. The success relies heavily on the willingness of airlines to support the operation. Besides contributing airlines Lufthansa, Air France, China Airlines, Cathay Pacific, and Iberia, South African Airlines has already expressed its interest in participating in the new IAGOS infrastructure. Discussions are also underway with US scientists to enable a partnership with IAGOS in the USA, in addition to expanding the NOAA network of small aircraft.

Sustainable operation of IAGOS has been addressed by securing a sustainable funding stream in the frame of international observing strategies such as GEOSS and its European component GMES, and from national funding institutions. Furthermore, a sustainable governance structure, which is currently in preparation, will be implemented by the end of year 2013 in order to ensure long term operation and continuous data provision from IAGOS.

7   ACKNOWLEDGMENTS

REFERENCES

Andersson, S. M., and Coauthors, 2013: Composition and evolution of volcanic aerosol from eruptions of Kasatochi, Sarychev and Eyjafjallajökull in 2008–2010 based on CARIBIC observations. *Atmos. Chem. Phys.*, **13,** 1781–1796.

Brenninkmeijer, C., and CARIBIC-team, 2007: The CARIBIC aircraft system for detailed, long-term, global-scale measurement of trace gases and aerosol in a changing atmosphere. *IGAC Newsletter*, **37,** 2-9.

Brenninkmeijer, C. A. M., and Coauthors, 2007: Civil Aircraft for the regular investigation of the atmosphere based on an instrumented container: The new CARIBIC system. *Atmos. Chem. Phys.*, **7,** 4953-4976.

Clarke, A., and V. Kapustin, 2010: Hemispheric Aerosol Vertical Profiles: Anthropogenic Impacts on Optical Depth and Cloud Nuclei. *Science*, **329,** 1488-1492.

Friedlingstein, P., and Coauthors, 2006: Climate-carbon cycle feedback analysis: Results from the (CMIP)-M-4 model intercomparison. *J. Climate*, **19,** 3337-3353.

Helten, M., H. G. J. Smit, W. Strater, D. Kley, P. Nedelec, M. Zoger, and R. Busen, 1998: Calibration and performance of automatic compact instrumentation for the measurement of relative humidity from passenger aircraft. *J. Geophys. Res.*, **103,** 25643-25652.

IGACO, 2004: Integrated Global Observing Strategy for the Monitoring of our Environment from Space and from Earth, 54 pp.

IGCO, 2004: Integrated Global Carbon Observation Theme - Executive Summary.

Lacis, A. A., G. A. Schmidt, D. Rind, and R. A. Ruedy, 2010: Atmospheric CO2: Principal Control Knob Governing Earth's Temperature. *Science*, **330,** 356-359.

Lenton, T., 2011: 2 degrees C or not 2 degrees C? That is the climate question. *Nature*, **473,** 7-7.

Mahowald, N., 2011: Aerosol Indirect Effect on Biogeochemical Cycles and Climate. *Science*, **334,** 794-796.

Marenco, A., and Coauthors, 1998: Measurement of ozone and water vapor by Airbus in-service aircraft: The MOZAIC airborne program, An overview. *J. Geophys. Res.*, **103,** 25631-25642.

Min, S. K., X. B. Zhang, F. W. Zwiers, and G. C. Hegerl, 2011: Human contribution to more-intense precipitation extremes. *Nature*, **470,** 378-381.

Monks, P. S., and Coauthors, 2009: Atmospheric composition change - global and regional air quality. *Atmos. Environ.*, **43,** 5268-5350.

Nédélec, P., and Coauthors, 2003: An improved infra-red carbon monoxide analyser for routine measurements aboard commercial Airbus aircraft: Technical validation and first scientific results of the MOZAIC program. *Atmos. Chem. Phys.*, **3,** 1551–1564.

Randel, W. J., and Coauthors, 2010: Asian Monsoon Transport of Pollution to the Stratosphere. *Science*, **328,** 611-613.

Riese, M., F. Ploeger, A. Rap, B. Vogel, P. Konopka, M. Dameris, and P. Forster, 2012: Impact of uncertainties in atmospheric mixing on simulated UTLS composition and related radiative effects. *J. Geophys. Res.*, **117**.

Schwartz, S. E., R. J. Charlson, R. A. Kahn, J. A. Ogren, and H. Rodhe, 2010: Why Hasn't Earth Warmed as Much as Expected? *J. Climate*, **23,** 2453-2464.

Solomon, S., K. H. Rosenlof, R. W. Portmann, J. S. Daniel, S. M. Davis, T. J. Sanford, and G. K. Plattner, 2010: Contributions of Stratospheric Water Vapor to Decadal Changes in the Rate of Global Warming. *Science*, **327,** 1219-1223.

Solomon, S., and Coauthors, 2007: *IPCC, 2007: Climate Change 2007: The Physical Science Basis. Contribution of Working Group I to the Fourth Assessment Report of IPCC.* Cambridge University Press, 996 pp.

Thouret, V., A. Marenco, J. A. Logan, P. Nédélec, and C. Grouhel, 1998: Comparisons of ozone measurements from the MOZAIC airborne program and the ozone sounding network at eight locations. *J. Geophys. Res.*, **103,** 25695–25720.

Volz-Thomas, A., and IAGOS-team, 2007: In-service Aircraft for Global Observations – the future. *IGAC Newsletter*, **37,** 18-22.

Volz-Thomas, A., J.-P. Cammas, C. A. M. Brenninkmeijer, T. Machida, O. Cooper, C. Sweeney, and A. Waibel, 2009: Civil Aviation Monitors Air Quality and Climate. *EM Magazine, Air & Waste Manage. Assoc.,* 16-19 (Oct. 2009).

Volz-Thomas, A., and Coauthors, 2005: Measurements of total odd nitrogen (NOy) aboard MOZAIC in-service aircraft: instrument design, operation and performance. *Atmos. Chem. Phys.*, **5,** 583-595.

Global sensitivity of aviation NO$_x$ effects to the HO$_2$ + NO → HNO$_3$ reaction

K. Gottschaldt [*], C. Voigt, P. Jöckel, M. Righi, S. Dietmüller
DLR-Institut für Physik der Atmosphäre Oberpfaffenhofen, Germany

Keywords: atmospheric chemistry, methane lifetime, aviation, NOx, radiative forcing

ABSTRACT: The impact of a recently proposed HNO$_3$-forming channel of the HO$_2$ + NO reaction (Butkovskaya et al., 2005, 2007) on atmospheric mixing ratios of ozone, methane and their precursors is assessed with a global stratosphere-troposphere chemistry-climate model. Previous modelling studies applied a rate coefficient that depends only on pressure and temperature. We additionally considered a possible enhancement of the reaction by humidity, as found by a laboratory study (Butkovskaya et al., 2009). This particularly reduces the oxidation capacity of the atmosphere, increasing methane lifetime significantly.

The effects of aircraft NO$_x$ emissions on atmospheric chemistry are altered when considering the above reaction, resulting in a negative net radiative forcing relative to an atmosphere without aviation NO$_x$. Uncertainties associated with the inclusion of the HO$_2$ + NO → HNO$_3$ reaction and with its corresponding rate coefficient propagate a considerable additional uncertainty on estimates of the climate impact of aviation and on NO$_x$-related mitigation strategies.

This contribution is based on Gottschaldt et al. (2013).

1   INTRODUCTION

Aircraft emissions of reactive nitrogen oxides (NO$_x$ = NO + NO$_2$) peak in the upper troposphere and lower stratosphere (UTLS), and the resulting NO$_x$ increase impacts on the radiatively active trace gases ozone (O$_3$), methane (CH$_4$) and stratospheric water vapour. The level of scientific understanding of this contribution to anthropogenic climate forcing has been judged as moderate to poor (Lee et al., 2010, Holmes et al., 2011). This judgement did not include the possible effects of the proposed HO$_2$ + NO → HNO$_3$ reaction (Butkovskaya et al., 2005, 2007, 2009, Chen et al., 2009).

The concentration of ozone in the UTLS is determined by transport, mixing and by chemical processes, mainly the ozone destroying, catalytic peroxy radical (HO$_x$ = HO$_2$ + OH) and halogen radical cycles in concert with reactions involving reactive nitrogen oxides (Wennberg et al., 1998). Adding (aviation) NO$_x$ to the chemical system and considering gas phase chemistry only, the effect on ozone changes sign in the altitude range of 12 to 25 km (e.g. Søvde et al., 2007). Above that altitude region of zero net effect, aircraft NO$_x$ emissions intensify the NO$_x$ cycle, enhancing catalytic ozone destruction. This cycle operates more efficiently higher up in the stratosphere, because peroxy radicals (sequestering NO$_x$ into reservoir species such as nitric acid, HNO$_3$) and NO$_2$ photolysis are less important at higher altitudes. Below that region, the ozone destroying NO$_x$ cycle is bypassed via peroxy radicals, and direct emissions of NO$_x$ by aircraft can lead to increased ozone production by reducing the abundance of HO$_x$ molecules.

Furthermore, the rates of the major net loss reactions of peroxy radicals, as well as ozone production, all depend nonlinearly and even non-monotonically on NO$_x$ levels (Ehhalt and Rohrer, 1994). However, such chemical nonlinearities are expected to be small for the atmospheric response to aircraft emissions (Holmes et al, 2011).

Methane is emitted from the Earth's surface and lost in the troposphere mainly by the reaction with OH. Thus NO$_x$ emissions affect methane life time via OH. Methane perturbations in turn have

---
[*] *Corresponding author:* Klaus Gottschaldt, DLR-Institut für Physik der Atmosphäre, Oberpfaffenhofen, D-82205 Wessling, Germany. Email: klaus-dirk.gottschaldt@dlr.de

an effect on ozone (Ehhalt et al., 2001). Methane oxidation is also a major source of stratospheric water vapour.

Beyond these well-known reactions, the effects of NO_x emissions may be further affected by the recently discovered HNO_3-forming channel of the $HO_2 + NO$ reaction (Butkovskaya et al., 2005, 2007, Chen et al., 2009):

$$HO_2 + NO \rightarrow NO_2 + OH \tag{R1a}$$

$$HO_2 + NO\ (+\ M) \rightarrow HNO_3\ (+\ M) \tag{R2a}$$

with the rate coefficients k_{1a} and k_{2a}, respectively. Butkovskaya et al. (2009) supposed that $HO_2 + NO$ forms the HOONO intermediate complex that mostly decomposes into $OH + NO_2$. A small fraction forms nitric acid, possibly involving another molecule (M). We note that reaction R2 is not generally accepted yet (IUPAC, 2008, Sander et al., 2011).

The effects of reaction R2a on atmospheric composition have been studied before (Brühl et al., 2007, Cariolle et al., 2008, Søvde et al., 2011), accounting for pressure and temperature dependence of k_{2a}. We additionally considered that both reaction channels may be modified in the presence of water vapour (Butkovskaya et al., 2009), which will be introduced as reactions R1b and R2b. Unger (2011) reported a negligible impact of R2a on short-lived ozone perturbations due to aviation NO_x. In the following we demonstrate the potential importance of R2 for assessing the climate impact of aviation NO_x, when considering radiative forcing (RF) from perturbations in ozone and methane. The results emphasize the need for further experimental data on the rate coefficient for reaction R2 that are valid in the entire range of atmospheric temperatures, pressures, and water vapour concentrations.

2   METHODOLOGY

2.1   *Model setup*

This study is based on the global ECHAM/MESSy Atmospheric Chemistry (EMAC) model (Jöckel et al., 2006). The core atmospheric model is the 5th generation European Centre Hamburg general circulation model (ECHAM5, Roeckner et al., 2003). For the present study EMAC was applied (ECHAM5: version 5.3.01, MESSy: modified version 1.10) with a spherical truncation of T42, and 90 vertical hybrid pressure levels up to 0.01 hPa. All simulations cover two years and were nudged in the free troposphere (up to about 200 hPa) to the synoptic meteorological conditions (ECMWF) of the years 2000 and 2001.

Emissions from natural and anthropogenic sources were provided to the model as monthly mean offline fields, representing conditions of the simulated period around the year 2000. Aircraft emissions for the year 2000 were taken from the QUANTIFY project (Lee et al. 2005), and included NO_x only, emitted as 1.815 Tg NO per year. Online emissions of soil NO and isoprene were simulated as a function of specific meteorological conditions.

Gas phase chemistry was calculated with the MECCA1 chemistry submodel (Sander et al., 2005), consistently from the surface to the stratosphere. The applied chemical mechanism included full stratospheric complexity, but neglected the sulphur and halogen families in the troposphere.

Further details about the model setup can be found in Gottschaldt et al. (2013).

2.2   *Modifications to the chemical mechanism*

A temperature-dependent rate coefficient (Sander et al., 2003),

$$k_0 = k_1 + k_2 \tag{1}$$

was assumed for the $HO_2 + NO$ conversion via both reaction pathways (R1 and R2). The base simulation had $k_1 = k_0$ for reaction R1. Reaction R2 was switched off, i.e. $k_2 = 0$.

Sensitivity simulations with HNO$_3$ forming channel and no humidity modification differ from the base simulation in the definition of k_1 and k_2:

$$k_{2a} = \frac{k_0 \cdot \beta}{1 + \beta} \tag{2}$$

$$k_{1a} = k_0 - k_{2a} \tag{3}$$

The factor β has been derived by Butkovskaya et al. (2007) and depends on pressure p and temperature T.

An enhancement of HNO$_3$ formation in the presence of water has been measured in the laboratory (Butkovskaya et al., 2009), suggesting the following chemical mechanism instead of reactions R1a and R2a:

$$H_2O \cdot HO_2 + NO \rightarrow OH + NO_2 + H_2O \tag{R1b}$$

$$H_2O \cdot HO_2 + NO \rightarrow HNO_3 + H_2O \tag{R2b}$$
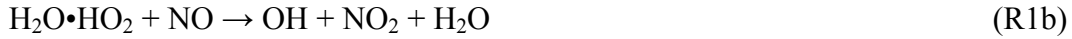
Humidity effects were considered as a modification of Equations 2 and 3:

$$k_{2b} = \frac{k_0 \cdot \beta \cdot (1 + \gamma \cdot \alpha)}{(1 + \beta) \cdot (1 + \alpha)} \quad \text{and} \quad k_{1b} = k_0 - k_{2b} \tag{4}$$

The term $\alpha = c_{H2O} \cdot K_{eq}$ depends on the equilibrium coefficient K_{eq} (in cm^3) of reaction R3 and on the molecular concentration of water, c_{H2O} in cm^{-3}, and $\gamma = 42$ is a constant factor (Butkovskaya et al., 2009).

2.3 *Simulations*

Six simulations were performed for this study that all share the same meteorology, but differ in their atmospheric chemistry. The <u>B</u>ase simulation without R2, and with <u>A</u>ircraft emissions (BA) serves as reference for the comparison to simulations DA (<u>D</u>ry = rate coefficient for reaction R2a according to Eq. 2, with Aircraft emissions) and WA (<u>W</u>et = rate coefficient for R2b with humidity modification according to Eq. 4, with <u>A</u>ircraft emissions). Any pair of a reference and a sensitivity simulation is denoted as "sensitivity block". The sensitivity blocks (BA versus DA) and (BA versus WA) serve to isolate the effects of R2 on atmospheric HNO$_3$, HO$_x$, NO$_x$ and O$_3$ background mixing ratios.

Each of the above simulations represents a different chemical atmospheric chemical regime, but all three have identical emissions. Thus three more reference simulations are needed to isolate aviation NO$_x$ effects by pairs. B0 (<u>B</u>ase simulation, <u>0</u> = zero aircraft emissions) is compared to BA. D0 and W0 serve as reference cases for the sensitivities DA and WA, respectively. The corresponding sensitivity blocks are denoted ΔB, ΔD and ΔW.

This study focuses on chemical effects, but small chemical differences cause a divergence of model dynamics in a coupled system. In order to avoid such dynamically induced "noise", EMAC was operated in Quasi Chemistry Transport Model (QCTM) mode (Deckert et al., 2011) for all simulations, switching off any feedback from chemical perturbations to the dynamical state (meteorology) of the atmosphere. In turn, the meteorological parameters (e.g. temperature, pressure, flow field, radiation, humidity) entering atmospheric chemistry calculations are also identical throughout the suite of simulations. The sensitivity simulations contain only the chemical effects of the applied perturbations.

3   RESULTS

3.1   *Effects of the $HO_2 + NO \rightarrow HNO_3$ reaction on atmospheric background chemistry*

While the relative effects of the HNO_3 forming channel of the $HO_2 + NO$ reaction are pronounced in the UTLS, the absolute effects on $[HNO_3]$[1], $[NO_x]$, $[OH]$ and $[O_3]$ have their maximum at about 10 hPa. HNO_3 mixing ratios mostly increase compared to an atmosphere without reaction R2. NO_y mixing ratios decrease in the troposphere and increase in the stratosphere. NO_x generally decreases from the ground up to 1 hPa. This leads to less ozone in the troposphere, but enhances it in the altitude range of highest atmospheric ozone mixing ratios. The global annual mean ozone column in the simulation with $k_{2a}(p,T)$ decreases by 0.5 % compared to the simulation without the HNO_3-forming channel. Reaction R2 decreases the oxidizing capacity of the atmosphere, leading to a 10.5 % longer methane lifetime in DA. Our results with $k_{2a}(p,T)$ generally confirm the findings of Cariolle et al. (2008) and Søvde et al. (2011). Humidity enhances the effects of R2, particularly in the lower troposphere with its high water mixing ratios. The ozone burden decreases by 1.8 % and methane lifetime increases by 50 % when comparing the simulation with $k_{2b}(p,T,c_{H2O})$ to the simulation without R2.

In an attempt to check if any of the chemical regimes yields unrealistic results, HNO_3, NO_x, CO and O_3 profiles from simulations BA, DA and WA were compared to observational profiles of Emmons et al. (2000). However, all simulations match the observed trace gas mixing ratios well and none could be ruled out according to this analysis. Global concentrations of the hydroxyl radical (determining atmospheric oxidizing capacity) were compared to the measurement based values of Spivakovsky et al. (2000). A new modification to NMHC oxidation (Taraborrelli et al., 2012) was not yet included in the chemical mechanism used for this study. It would likely bring the regime with R2 with humidity modification into best agreement with observations, concerning the oxidizing capacity of the atmosphere.

3.2   *Chemical and Radiative Forcing effects of aviation NO_x*

Aviation NO_x primarily leads to more ozone and more hydroxyl radicals in the altitude-latitude region, where most emissions occur. More tropospheric ozone translates into a positive radiative forcing (RF_{O3}^{short}), i.e. warms the Earth. More hydroxyl radicals destroy more methane, resulting in a negative radiative forcing (RF_{CH4}^{long}). Less methane means less stratospheric water vapour from methane oxidation (RF_{H2O}^{long}). A chemical feedback leads to an ozone decrease in response to less methane, and thus to an additional negative forcing (RF_{O3}^{long}). Correcting for different emissions, all forcing terms from the sensitivity block without reaction R2 agree very well with the results from a recent multi-model aviation study (Holmes et al., 2011), which did not include R2. Positive and negative forcings nearly compensate each other for sustained aircraft NO_x emissions of the year 2000, leaving a positive net RF of about +0.2 mW/m^2 in our study.

Considering $HO_2 + NO \rightarrow HNO_3$ increases the effects of aircraft NO_x emissions on $[O_3]$ and $[OH]$. RF_{O3}^{short} is primarily determined by the absolute ozone perturbation due to aviation NO_x. Essentially the same absolute $[NO_x]$ perturbation increases $[O_3]$ more in the regimes with R2 than in the one without. The long lived methane-related forcings RF_{CH4}^{long}, RF_{O3}^{long} and RF_{H2O}^{long} are determined by relative methane lifetime changes, and thus by the relative perturbations of OH concentrations. Lower background $[OH]$ due to R2 directly results in enhanced radiative forcing, even for the same absolute $[OH]$ perturbation. However, $[OH]$ increases more in response to aircraft $[NO_x]$ emissions, when the HNO_3 forming channel is considered, thus additionally pronouncing RF_{CH4}^{long}, RF_{O3}^{long} and RF_{H2O}^{long} in sensitivity blocks with R2. All in all the negative forcings are more sensitive to the intro-

---

[1] [] is used as an abbreviation for „mixing ratio" of the compound in brackets

duction of HO$_2$ + NO $\rightarrow$ HNO$_3$ than the positive short-lived ozone forcing (Figure 1). The net forcing from aviation NO$_x$ effects decreases to -1.6 mW/m^2 in the regime with $k_2(p,T)$, and to -12.1 mW/m^2 in the one with $k_2(p,T,c_{H_2O})$.
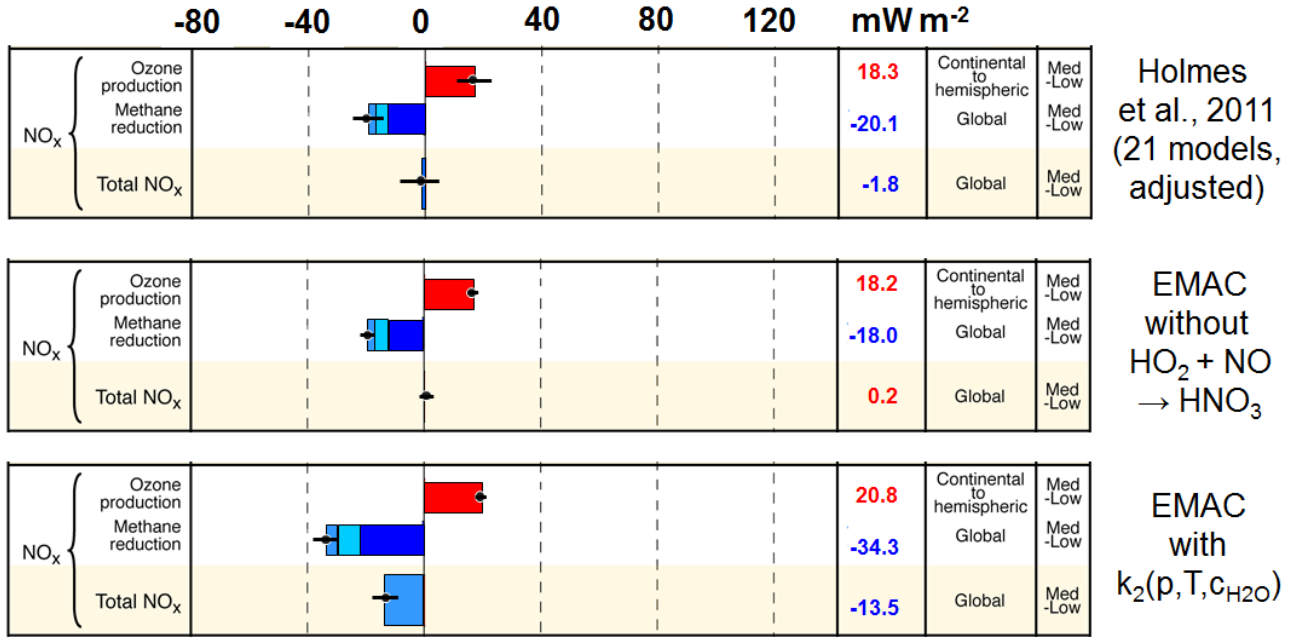

Figure 1: Radiative forcing contributions from aviation NO$_x$ in a recent multi-model study (top), in a pair of EMAC simulations without the HNO$_3$ forming channel of HO$_2$ + NO (middle), and when considering that reaction (bottom). Colors mark the different forcing components: RF$_{O3}^{short}$ (red), RF$_{CH4}^{long}$ (dark blue), RF$_{H2O}^{long}$ (medium blue), RF$_{O3}^{long}$ (light blue). Stratospheric adjusted RF$_{O3}^{short}$ was calculated directly from the perturbations of the ozone field due to aviation NO$_x$. The forcings related to methane reduction were derived from perturbations of hydroxyl radical, assuming sustained aviation NO$_x$ emissions of the year 2000. The blue bar at the bottom of each panel illustrates the net radiative forcing from all components. The values of Holmes et al. (2011) were linearly scaled to aircraft NO$_x$ emissions of 0.85 Tg(N)/year, and RF$_{H2O}^{long}$ (not considered by Holmes et al., 2011) was calculated from their RF$_{CH4}^{long}$. Details of the calculations and the error bars are discussed in Gottschaldt et al. (2013).

4   CONCLUSIONS

Considering the regime with $k_2(p,T,c_{H_2O})$ to be the most likely one, according to this study, aircraft NO$_x$ emissions are likely to cool the Earth. This tentative conclusion has potentially important implications for strategies, which aim to mitigate aviation RF by NO$_x$ reduction or even trade less NO$_x$ against more CO$_2$ emissions. We note three effects that might be interesting for strategies, which aim to mitigate aviation RF by changing the emission location: (i) Most aircraft NO$_x$ emissions occur in the UTLS of NH mid-latitudes, while R2 impacts most in the tropical UTLS. Emitting more NO$_x$ in latitude-altitude regions where R2 is more/less important would likely increase/decrease the effects on [O$_3$] and [OH], thereby changing the net forcing. (ii) The current aircraft fleet flies close to the altitude where the [OH] response to NO$_x$ emissions changes sign. Flying only a little bit higher might drastically reduce OH-induced cooling RF effects. (iii) RF$_{O3}^{short}$ is concentrated in NH mid-latitudes and perturbations take full effect within weeks, while the methane related forcings act globally on a decadal time scale. The time lag between RF$_{O3}^{short}$ and methane effects also implies that the short-lived positive forcing becomes more important for increasing air-

craft NO$_x$ emissions, while the long-lived negative forcings would dominate for decreasing emissions.

However, further research is necessary before any recommendation regarding aircraft NO$_x$ emission reduction can be made. Considering the NMHC oxidation mechanism recently introduced by Taraborrelli et al. (2012) might increase the [OH] background, consequently reducing aviation induced relative [OH] perturbations. This would imply smaller (less negative) methane related RF components in all regimes. Some NO$_x$ related effects are neglected in this study, e.g. formation of nitrate aerosols (Forster et al., 2007), direct RF from NO$_2$ (Kvalevåg and Myhre, 2007), interaction of O$_3$ and OH perturbations with the sulphate burden (Unger et al., 2006). We also did not consider plume effects in this study, which might reduce the ozone response to aviation NO$_x$ by 10 to 25 % (Cariolle et al., 2009). Furthermore the robustness of our results should be tested with different models and methodologies. Above all, further experimental work is urgently needed to consolidate parameterizations of the rate coefficient. This need includes stratospheric conditions, and measurements of the effects of humidity on reaction R2 at more than a single configuration of pressure and temperature. Currently, uncertainties associated with the HNO$_3$-forming channel of the HO$_2$ + NO reaction just propagate a considerable additional uncertainty on estimates of the radiative forcing due to aircraft NO$_x$ emissions.

5   ACKNOWLEDGEMENTS

REFERENCES

Brühl, C., Steil, B., Stiller, G., Funke, B., and Jöckel, P., 2007: Nitrogen compounds and ozone in the stratosphere: comparison of MIPAS satellite data with the chemistry climate model ECHAM5/MESSy1, *Atmos. Chem. Phys., 7*, 5585–5598.

Butkovskaya, N., Kukui, A., Pouvesle, N., and Le Bras, G., 2005: Formation of Nitric Acid in the Gas-Phase HO$_2$ + NO Reaction: Effects of Temperature and Water Vapor*, J. Phys. Chem. A*, 109, 6509–6520, doi:10.1021/jp051534v.

Butkovskaya, N., Kukui, A., and Le Bras, G., 2007: HNO$_3$ Forming Channel of the HO$_2$ + NO Reaction as a Function of Pressure and Temperature in the Ranges of 72–600 Torr and 223–323 K, *J. Phys. Chem. A*, 111, 9047–9053, doi:10.1021/jp074117m.

Butkovskaya, N., Rayez, M.-T., Kukui, A., and Le Bras, G., 2009: Water Vapor Effect on the HNO$_3$ Yield in the HO$_2$ + NO Reaction: Experimental and Theoretical Evidence, *J. Phys. Chem. A*, 113, 11327–11342, doi:10.1021/jp811428p.

Cariolle, D., Evans, M. J., Chipperfield, M. P., Butkovskaya, N., Kukui, A., and Le Bras, G., 2008: Impact of the new HNO$_3$- forming channel of the HO$_2$+NO reaction on tropospheric HNO$_3$, NO$_x$, HO$_x$ and ozone, *Atmos. Chem. Phys., 8*, 4061– 4068, doi:10.5194/acp-8-4061-2008.

Cariolle, D., Caro, D., Paoli, R., Hauglustaine, D. A., Cuénot, B., Cozic, A., and Paugam, R., 2009: Parameterization of plume chemistry into large-scale atmospheric models: Application to aircraft NO$_x$ emissions. *J. Geophys. Res., 114*, D19302, doi:10.1029/2009JD011873.

Chen, C., Shepler, B. C., Braams, B. J., and Bowman, J. M., 2009: Quasiclassical trajectory calculations of the HO$_2$ + NO reaction on a global potential energy surface, *Phys. Chem. Chem. Phys., 11*, 4722–4727, doi:10.1039/b823031e.

Deckert, R., Jöckel, P., Grewe, V., Steil, B., Gottschaldt, K., and Hoor, P., 2011: A quasi chemistry-transport mode for chemistry-climate modelling with EMAC, *Geosci. Model Dev., 4*, 195-206, doi:10.5194/gmd-4-195-2011.

Ehhalt, D., and Rohrer, F., 1994: The impact of commercial aircraft on tropospheric ozone, *Proceedings of the 7th BOC Priestly conference*, Lewisburg, Pennsylvania, USA.

Ehhalt, D., Prather, M., Dentener, F., Derwent, R., Dlugokencky, E., Holland, E., Isaksen, I., Katima, J., Kirchhoff, V., Matson, P., Midgley, P., and Wang, M., 2001: Atmospheric Chemistry and Greenhouse Gases, in: *Climate Change 2001: The Scientific Basis. Contribution of Working Group I to the Third Assessment Report of the Intergovernmental Panel on Climate Change*, Houghton, J. T., Ding, Y., Griggs, D. J., Noguer, M., van der Linden, P. J., Dai, X., Maskell, K., and Johnson, C. A. (eds.), Cambridge University Press, Cambridge, United Kingdom and New York, NY, USA, 239-287.

Emmons, L. K., Hauglustaine, D. A., Müller, J.-F., Carroll, M. A., Brasseur, G. P., Brunner, D., Staehelin, J., Thouret, V., and Marenco, A., 2011: Data composites of airborne observation of tropospheric ozone and its precursor, *J. Geophys. Res., 105*, 20 497–20 538, 2000. Data downloaded from http://acd.ucar.edu/~emmons/DATACOMP/camp_table.htm.

Forster, P., Ramaswamy, V., Artaxo, P., Berntsen, T., Betts, R., Fahey, D. W., Haywood, J., Lean, J., Lowe, D. C., Myhre, G., Nganga, J., Prinn, R., Raga, G., Schulz, M., and Van Dorland, R., 2007: Changes in Atmospheric Constituents and in Radiative Forcing, in: *Climate Change 2007: The Physical Science Basis. Contribution of Working Group I to the Fourth Assessment Report of the Intergovernmental Panel on Climate Change*, Solomon, S., Qin, D., Manning, M., Chen, Z., Marquis, M., Averyt, K. B., Tignor, M., and Miller, H. L. (eds.), Cambridge University Press, Cambridge, United Kingdom and New York, NY, USA.

Gottschaldt, K., Voigt, C., Jöckel, P., Righi, M., Deckert, R., and Dietmüller, S.: Global sensitivity of aviation NOx effects to the HNO3-forming channel of the HO2 + NO reaction, Atmos. Chem. Phys., 13, 3003-3025, doi:10.5194/acp-13-3003-2013, 2013.

Holmes, C. D., Tang, Q., and Prather, M. J., 2011: Uncertainties in climate assessment for the case of aviation NO, *P. Natl. Acad. Sci. USA, 108*, 10997-11002, www.pnas.org/cgi/doi/10.1073/pnas.1101458108.

Jöckel, P., Tost, H., Pozzer, A., Brühl, C., Buchholz, J., Ganzeveld, L., Hoor, P., Kerkweg, A., Lawrence, M. G., Sander, R., Steil, B., Stiller, G., Tanarhte, M., Taraborrelli, D., van Aardenne, J., and Lelieveld, J., 2006: The atmospheric chemistry general circulation model ECHAM5/MESSy1: consistent simulation of ozone from the surface to the mesosphere, *Atmos. Chem. Phys., 6*, 5067-5104, doi:10.5194/acp-6-5067-2006.

Kvalevåg, M. M., and Myhre, G., 2007: Human impact on direct and diffuse solar radiation during the industrial era, *J. Climate 20 (19),* 4874-4883.

Lee, D. S., Owen, B., Graham, A., Fichter, C., Lim, L. L., and Dimitriu, D., 2005: Allocation of International Aviation Emissions from Scheduled Air Traffic - Present Day and Historical, *Final Report to DEFRA Global Atmosphere Division*, Manchester Metropolitan University, Centre for Air Transport and the Environment, Manchester, UK.

Lee D. S., Pitari, G., Grewe, V., Gierens, K., Penner, J. E., Petzold, A., Prather, M. J., Schumann, U., Bais, A., Berntsen, T., Iachetti, D., Lim, L. L., and Sausen, R., 2010: Transport impacts on atmosphere and climate: Aviation, *Atmos. Environ., 44*, 4678–4734.

Roeckner, E., Bäuml, G., Bonaventura, L., Brokopf, R., Esch, M., Giorgetta, M., Hagemann, S., Kirchner, I., Kornblueh, L., Manzini, E., Rhodin, A., Schlese, U., Schulzweida, U., and Tompkins, A., 2003: The atmospheric general circulation model ECHAM5. PART I: Model description, Technical report, Max Planck Institute for Meteorology, *MPI-Report 349*,
 http://www.mpimet.mpg.de/fileadmin/publikationen/Reports/max scirep 349.pdf.

Sander, R., Kerkweg, A., Jöckel, P., and Lelieveld, J., 2005: Technical note: The new comprehensive atmospheric chemistry module MECCA, *Atmos. Chem. Phys., 5*, 445–450.

Sander, S. P., Finlayson-Pitts, B. J., Friedl, R. R., Golden, D. M., Huie, R. E., Kolb, C. E., Kurylo, M. J., Molina, M. J., Moortgat, G. K., Orkin, V. L., and Ravishankara, A. R., 2003: Chemical Kinetics and Photochemical Data for Use in Atmospheric Studies, *Evaluation Number 14, JPL Publication 02-25*, Jet Propulsion Laboratory, Pasadena, CA.

Søvde, O.A., Gauss, M., Isaksen, I. S. A., Pitari, G. and Marizy, C., 2007: Aircraft pollution – a futuristic view, *Atmos. Chem. Phys., 7*, 3621-3632.

Søvde, O. A., Hoyle, C. R., Myhre, G., and Isaksen, I. S. A., 2011: The HNO$_3$ forming branch of the HO$_2$ + NO reaction: pre-industrial-to-present trends in atmospheric species and radiative forcings, *Atmos. Chem. Phys., 11*, 8929-8943, doi:10.5194/acp-11-8929-2011.

Spivakovsky, C. M., Logan, J. A., Montzka, S. A., Balkanski, Y. J., Foreman-Fowler, M., Jones, D. B. A., Horowitz, L. W., Fusco, A. C., Brenninkmeijer, C. A. M., Prather, M. J.,Wofsy, S. C., and McElroy, M. B., 2000: Three-dimensional climatological distribution of tropospheric OH: Update and evaluation, *J. Geophys. Res., 105*, 8931–8980.

Taraborrelli, D., Lawrence, M. G., Crowley, J. N., Dillon, T. J., Gromov, S., Groß, C. B. M., Vereecken, L., and Lelieveld, J., 2012: Hydroxyl radical buffered by isoprene oxidation over tropical forests, *Nat. Geosc., 5*, 190–193, doi:10.1038/ngeo1405.

Unger, N., Shindell, D. T., Koch, D. M., and Streets, D. G., 2006: Cross influences of ozone and sulfate precursor emissions changes on air quality and climate, *P. Natl. Acad. Sci. USA, 103(12)*, 4377–4380, doi:10.1073/pnas.0508769103.

Unger, N., 2011: Global climate impact of civil aviation for standard and desulfurized jet fuel, *Geophys. Res. Lett. 38*, L20803, doi:10.1029/2011GL049289.

Wennberg, P. O., Hanisco, T. F., Jaegle, L., Jacob, D. J., Hintsa, E. J., Lanzendorf, E. J., Anderson, J. G., Gao, R.-S., Keim, E. R., Donnelly, S. G., Del Negro, L. A., Fahey, D. W., McKeen, S. A., Salawitch, R. J., Webster, C. R., May, R. D., Herman, R. L., Proffitt, M. H., Margitan, J. J., Atlas, E. L., Schauffler, S. M., Flocke, F., McElroy, C. T., and Bui, T. P., 1998: Hydrogen Radicals, Nitrogen Radicals, and the Production of O$_3$ in the Upper Troposphere, *Science 279*, 49-53.

Evolution of Aircraft Engine Emissions in the Atmosphere

S.C. Herndon [*], E.C. Wood, M.T. Timko, Z. Yu, and R.C. Miake-Lye
Aerodyne Research, Inc., Billerica, MA, USA

W.B. Knighton
Montana State University, Bozeman, MT USA

Keywords: aircraft emissions, Fischer-Tropsch synthesis fuel, particles, composition, alternative fuel, atmospheric processing

ABSTRACT: Aircraft gas-turbine engines are different from most other combustion sources of emissions in that they use their exhaust in the atmosphere to provide the thrust, i.e. the work performed by the engine. As a consequence, the mixing, dilution, and chemistry in a gas-turbine engine exhaust is different from most other emissions sources. Recent work has examined how the gaseous and particulate emissions from gas-turbine engines evolve in the atmosphere by making measurements at the engine exit plane and downstream locations ranging from some tens of meters (30-50m) through over one hundred meters (145m) to approaching 1 kilometer and more. The chemical evolution of hydrocarbons and NO_x provides insight into oxidative chemistry and its dependence on background ambient air composition. Data on the evolution of particles emitted demonstrate that on-going microphysical evolution significantly affects particle properties for the first few hundred meters in the exhaust plume, with contributions from sulfate, products of incomplete combustion of the jet fuel, and engine lubrication oil. The impact of alternative fuels on the emissions and their evolution will also be described.

1 INTRODUCTION

Aircraft emissions have been characterized using primarily three different experimental methods: 1) engine exit plane measurements, (Bulzan et al., 2010b; Corporan et al., 2008; Kinsey et al., 2010; Kinsey et al., 2011; Lobo et al., 2011; Lobo et al., 2007; Miracolo et al., 2011; Onasch et al., 2009; Presto et al., 2011; Timko et al., 2011; Timko et al., 2010a; Timko et al., 2010b; Timko et al., 2010c; Wey et al., 2007) 2) advected plume studies, (Herndon et al., 2008; Herndon et al., 2005; Herndon et al., 2006; Herndon et al., 2004; Johnson et al., 2008; Mazaheri et al., 2009; Wood et al., 2008; Yu et al., 2010) 3) airport studies. (Adamkiewicz et al., 2010; Arunachalam et al., 2011; Dodson et al., 2009; Hsu et al., 2011; Zhu et al., 2011) Of these, engine exit plane measurements have been far and away the most common. However, aircraft particle emissions contain components that evolve as they dilute and cool due to mixing with atmospheric gases. Both physical and chemical mechanisms, each with their own sets of time scales, have been implicated. In theory, advected plume studies performed down wind of an active runway afford a cost effective means of studying atmospheric processing of particle emissions from in-use aircraft. Advected plume studies suffer from a lack of knowledge of the aircraft engine power condition and fuel composition. Careful monitoring of trace gas components (specifically CO, NO_X, and SO_2) can reduce – but not eliminate – these uncertainties. (Herndon et al., 2008; Herndon et al., 2006) Airport studies, performed "beyond the airport fenceline", are necessary to quantify potential exposures to aircraft emissions. But like advected plume studies, plume attribution is nearly impossible for individual airport study measurements due to interference with other ambient sources and mixing of aircraft plumes with one another. Modeling efforts (Vancassel et al., 2004; Wong et al., 2008; Wong et al., 2011) and extraction probe development (Blanco et al., 2011) have been performed to address these deficiencies,

---

[*] *Corresponding author:* Scott Herndon, Aerodyne Research, Inc., 45 Manning Road, Billerica, MA 01821-3976, USA. Email: herndon@aerodyne.com
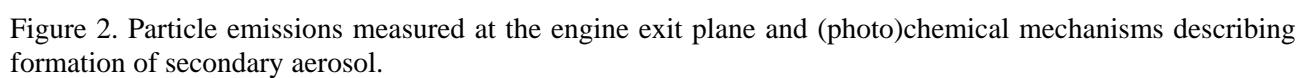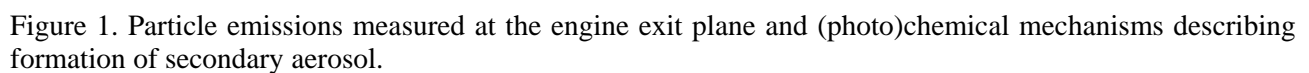
but no consensus exists on the importance of the relevant physical and chemical transformations that occur during atmospheric processing of aircraft exhaust particles.

To address this deficiency in our understanding, we have performed a series of unique measurements as part of the AAFEX-1 and AAFEX-2 (Alternative Aviation Fuels Experiment) field campaigns. Exhaust plume samples were characterized at various locations downwind of an operating CFM56-2C1 aircraft engine (Bulzan et al., 2010a; Lobo et al., 2007; Wey et al., 2007; Yelvington et al., 2007) running on a series of well characterized fuels, including: high sulfur JP-8 (1148 ppm_w), low sulfur JP-8 (121 ppm_w), ultralow sulfur and aromatic alternatives, Fischer-Tropsch jet fuel (FTJF) and hydro-renewable jet fuel (HRJF), an FTJF spiked with an organosulfur compound to bring its sulfur content to 1,083 ppm_w, and an HRJF/JP-8 blend (containing 276 ppm_w of sulfur). This paper summarizes particle number, size distribution, mass, and composition of aircraft emissions – and how physical and chemical processes lead to their evolution on the time scales of seconds to minutes. The measurements and data analysis fill a gap between engine exit plane measurements and regional and global emissions burdens.

2   FRAMEWORK

Figure 1 is a schematic representation of aircraft particle emissions, as measured in close vicinity to the engine exit plane (30 m) during the AAFEX-1 field campaign. The purpose of Figure 1 is to place particle evolution measurements in context. Figure 1 shows that aircraft particle emissions consist of an inorganic carbon (soot) component, an organic carbon component (particulate organic material, POM), and a sulfate component (particulate sulfate material) that we suspect is dominated by sulfuric acid. Nitrates make a negligible contribution on a particle mass basis. The overall particle emission index is greater at take-off than at idle, though individual components exhibit distinct trends. Specifically, increasing engine thrust from idle to take-off: increases soot emissions by a factor of nearly 10; decreases POM emissions by about a factor of 20; PSM emissions are relatively stable and may increase slightly. Soot particles range in size from 50 to 100 nm (on a volume basis) and soot particle diameter increases with increasing power. Initially, the POM and PSM are present as soot coatings and may inhabit nucleation and growth particles with characteristic diameters much less than 30 nm. The distribution of POM and PSM depends on a number of factors that influence physical evolution, including the relative quantities of POM and PSM to soot, aging time, mixing history, etc. Figure 2 summarizes the primary physical mechanisms of particle aging, including particle nucleation, growth, soot activation, coagulation, and condensation. Wong et al. (2008) have developed a model framework that describes all of these parallel processes. The first sub-objective of this work was to obtain data to validate the Wong et al. (2008) framework.

Figure 1 provides potential mechanisms for chemical and photochemical evolution of the volatile organic compounds (VOCs), SO_2, and NO_2 (and NO) present in aircraft exhaust to form "secondary particulate matter". Specifically, co-emission of OH radicals and VOCs can lead to VOC oxidation and formation of secondary POM. OH radical can oxidize: NO to nitric acid, which then undergoes neutralization reactions with ambient NH_3 to form ammonium nitrate particulate matter; and SO_2 to SO_3 that forms ammonium sulfate particulate matter after reaction with ambient ammonia. The Figure 1 mechanisms are active under atmospheric conditions; however, the presence of elevated OH radical concentrations in the aircraft exhaust plume should accelerate the atmospheric processes and lead to higher formation rates of POM in the exhaust plume than would be calculated under typical atmospheric conditions. Recent smog chamber measurements reported by Allan Robinson's research team at CMU (Miracolo et al., 2011; Presto et al., 2011) indicate that secondary particle formation can dominate point-of-emission particle masses. The second sub-objective of this work was to look for evidence of OH promoted formation of secondary POM (or PSM) in aircraft exhaust plumes undergoing atmospheric processing.

Figure 1. Particle emissions measured at the engine exit plane and (photo)chemical mechanisms describing formation of secondary aerosol.

Figure 2. Particle emissions measured at the engine exit plane and (photo)chemical mechanisms describing formation of secondary aerosol.

3 RESULTS

Figures 3 and 4 provides measurements of the POM and PSM in the expanding plume, plotted as emission indices (EI) against ΔCO_2 – that is the difference between the exhaust plume CO_2 and the ambient CO_2 levels. Because POM and PSM dominate the overall particle mass budget at idle conditions (see Figure 1), we restricted our analysis in Figures 3 and 4 to plumes attributed to engine idle conditions. We choose to plot EIs to account for the first order effects of plume dilution. And, we chose ΔCO_2 as the horizontal axis because: 1) CO_2 is a tracer for the exhaust plume; 2) CO_2 is one of our primary measurements and we have a steady stream of CO_2 data available for all time periods with 1 sec resolution and 1 ppm precision, 3) because dilution is tied to aging, ΔCO_2 is a good proxy for plume aging time. As plume age increases, ΔCO_2 monotonically decreases. Corroboration of engine activity with concurrent observations of the local wind field indicate that $\Delta CO_2 >$ 200 ppm corresponds to roughly 5 sec of aging whereas $\Delta CO_2 < 10$ ppm corresponds to aging times between 2 and 3 min. Qualitatively, the main points from Figures 3 and 4 are similar: 1) POM and PSM increase monotonically with increasing age (decreasing ΔCO_2) and 2) fuel composition (both aromatic and sulfur) influence the rate of change. More specifically, "standard" aviation jet fuel (JP-8), with typical aromatic and sulfur contents, shows increases in EI-POM from about 5-10 mg kg^{-1} for the freshest captured plumes to 30-50 mg kg^{-1} for the oldest plumes. For standard JP-8, EI-PSM increases from approximately 0.5 mg kg^{-1} to nearly 4 mg kg^{-1} over the same range of plume aging conditions. Removing both aromatics and sulfur from the fuel (as was done for the HRJ tests) results in plumes with EI-POM and EI-PSM less than instrument detection limits (about 0.5 and 0.2 mg kg^{-1}, respectively) that show no evidence of change during the process of dilution. Removing aromatic but not sulfur (as was done for the FTF spiked with additional sulfur), delays the increase observed in EI-POM and accelerates the increase observed for EI-PSM.
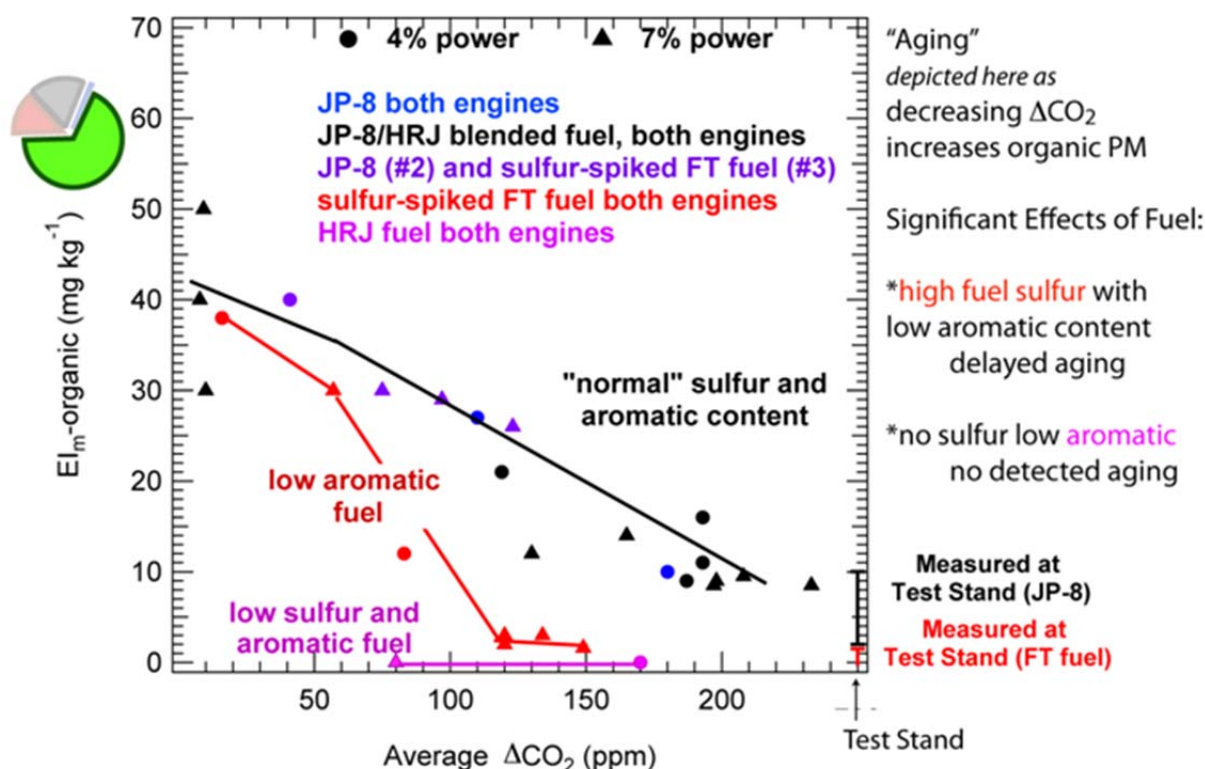

Figure 3. Evolution of EI-POM measured in idle engine aircraft exhaust plumes. Decreasing ΔCO_2 corresponds to increasing plume aging times.
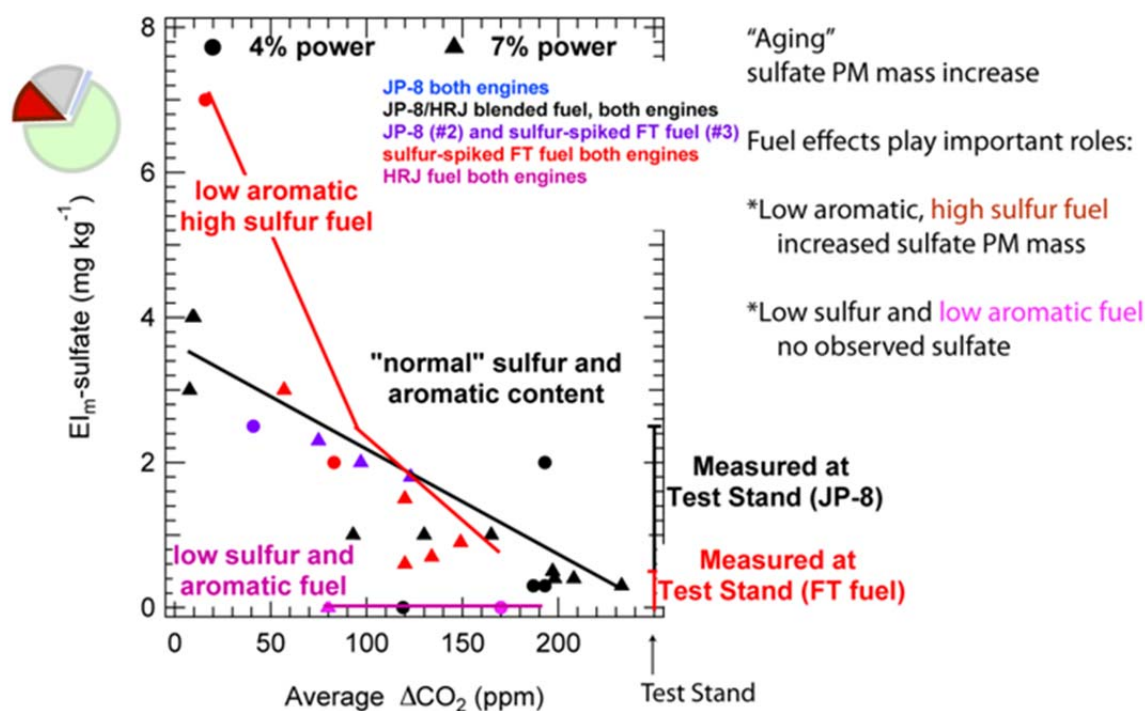
Figure 4. Evolution of EI-PSM measured in idle engine aircraft exhaust plumes. Decreasing ΔCO_2 corresponds to increasing plume aging times.

EI-POM and EI-PSM measured at the engine exit plane tests stand are plotted in Figures 3 and 4 for comparison with the aircraft plume data. Figures 3 and 4 clearly establish that EI-POM and EI-PSM measured at the test stand are a fraction of that reached after only minutes of atmospheric processing. From an emissions budget and potential exposure standpoint, local and regional models should account for the difference between the test stand and plume EIs. Validating the Wong et al. (2008) particle microphysics framework is the subject of future work in this area.

Having established that physical evolution of aircraft exhaust particles is an important effect, we interrogated our data for evidence of chemical composition changes. To do so, we used a mass spectrometer method (specifically the aerosol mass spectrometer, AMS) to obtain chemical signatures for the "freshest" and "oldest" plumes shown in Figure 3. Figure 5 is the result of subtracting the mass spectrum of the "oldest" plume from that obtained for the "freshest" plume – after accounting for first order differences in the spectra due to dilution. To aid interpretation, individual species (as assigned using high resolution mass defect methods to differentiate between hydrocarbon and oxygenate species of equal unit masses) are colored either green (for hydrocarbons) or blue (for oxygenates). Consistent with oxidation aging of the plume VOCs, the aged plume is enriched in many key oxygenates, including C_2H_3O, C_2H_2O, C_3H_3O, and C_3H_6O. The fresh plume is enriched strictly in hydrocarbons, including C_3H_7, C_4H_9, C_4H_7. Interestingly, the aged plume is enriched in several hydrocarbon species, notably CH_2, CH_3 and C_2H_3, suggesting that that both the oxygenate and hydrocarbon composition changes during aging from 5 sec to 2-3 min. Finally, "stable" species that contain aromatic fragments (e.g., C_6H_5) are in enriched in neither the fresh nor the aged plume. This observation is consistent with a chemical mechanism to explain the enriched oxygenate content found in the aged plume. The objective of future work on this topic will be to analyze additional plumes and perform complementary field studies to provide data to validate a comprehensive chemical aging model.
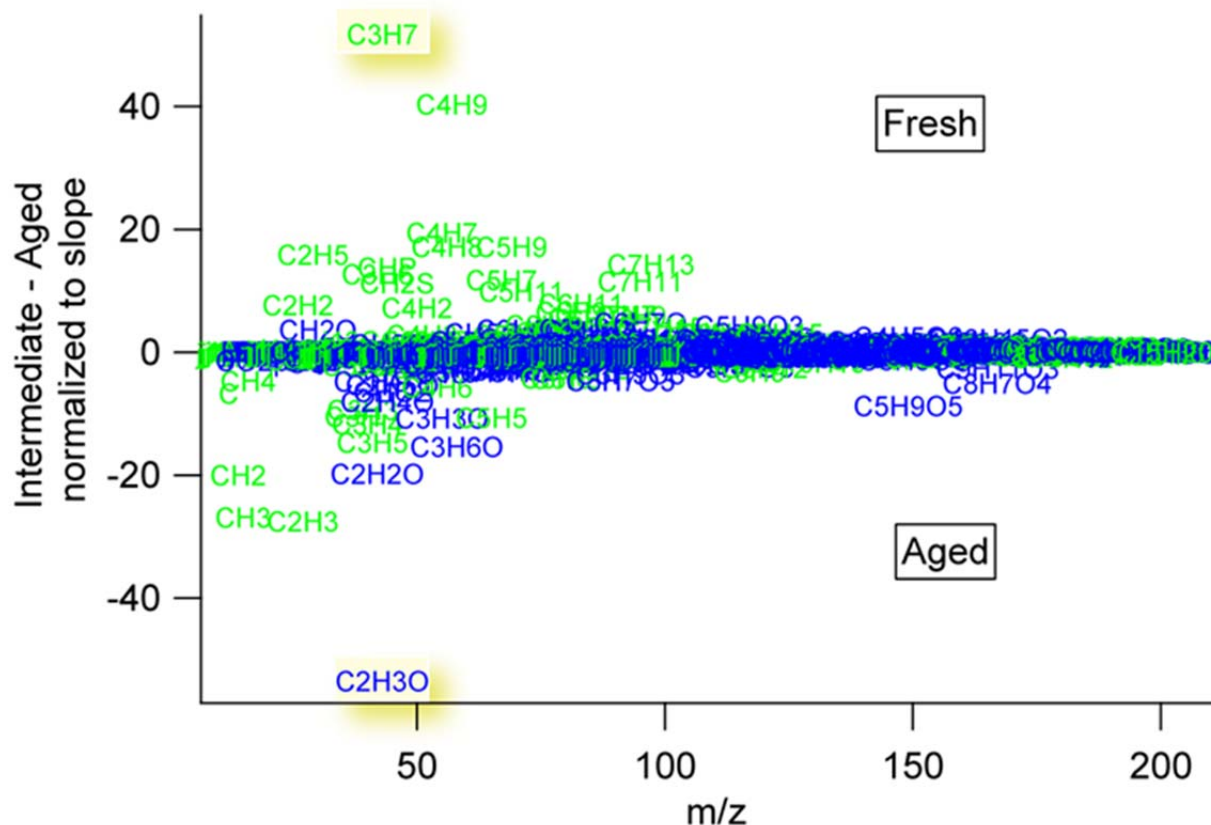
Figure 5. Difference mass spectrum of an aged idle aircraft exhaust plume relative to a mass spectrum of a fresh aircraft exhaust plume. Hydrocarbon species are plotted green whereas oxygenated species are blue.

4   CONCLUSIONS

We have performed aircraft plume measurements for a CFM56-2C1 engine running a range of petroleum and synthetic fuels. Our data support evolution of the organic and sulfate components of the particle budget due to physical evolution that occurs on the time scales of tens of seconds. Evidence for chemical evolution is present when the "oldest" plumes (corresponding to aging times on the order of 2-3 min) are compared to the "freshest" plumes (corresponding to aging times on the order of 5 sec). These measurements suggest that aircraft emissions budgets be re-evaluated.

REFERENCES

Adamkiewicz, G. Hsu, H.-H. Vallarino, J. Melly, S. J. Spengler, J. D. Levy, J. I. 2010. Nitrogen dioxide concentrations in neighborhoods adjacent to a commercial airport: a land use regression modeling study. Environmental Health 9.

Arunachalam, S. Wang, B. Davis, N. Baek, B. H. Levy, J. I. 2011. Effect of chemistry-transport model scale and resolution on population exposure to PM(2.5) from aircraft emissions during landing and takeoff. Atmospheric Environment 45, 3294-3300.

Blanco, E. d. l. R. Peck, J. Miake-Lye, R. C. Hills, F. B. Wood, E. C. Herndon, S. C. Annen, K. D. Yelvington, P. E. Leach, T. 2011. Minimizing Sampling Loss in Trace Gas Emission Measurements for Aircraft Engines by Using a Chemical Quick-Quench Probe. Journal of Engineering for Gas Turbines and Power-Transactions of the Asme 133.

Bulzan, D. Anderson, B. Wey, C. Howard, R. Winstead, E. Beyersdorf, A. Corporan, E. DeWitt, M. J. Klingshirn, C. Herndon, S. Miake-Lye, R. Timko, M. Wood, E. Tacina, K. M. Liscinsky, D. Hagen, D. Lobo, P. Whitefield, P. Asme (2010a) Gaseous and particulate emissions results of the NASA Alternative Aviation Fuel Experiment (AAFEX). 1195-1207 p.

Bulzan, D. Anderson, B. E. Wey, C. Howard, R. Winstead, E. L. Beyersdorf, A. J. Corporan, E. DeWitt, M. J. Klingshirn, C. D. Herndon, S. C. Miake-Lye, R. C. Timko, M. T. Wood, E. C. Tacina, K. Liscinsky, D.

S. Hagen, D. E. Lobo, P. Whitefield, P. D. Gaseous and Particulate Emissions Results of the NASA Alternative Aviation Fuel Experiment (AAFEX); 2010b; Glasgow, Scotland.

Corporan, E. Quick, A. DeWift, M. J. 2008. Characterization of particulate matter and gaseous emissions of a C-130H aircraft. Journal of the Air & Waste Management Association 58, 474-483.

Dodson, R. E. Houseman, E. A. Morin, B. Levy, J. I. 2009. An analysis of continuous black carbon concentrations in proximity to an airport and major roadways. Atmospheric Environment 43, 3764-3773.

Herndon, S. C. Jayne, J. T. Lobo, P. Onasch, T. B. Fleming, G. Hagen, D. E. Whitefield, P. D. Miake-Lye, R. C. 2008. Commercial aircraft engine emissions characterization of in-use aircraft at Hartsfield-Jackson Atlanta International Airport. Environmental Science & Technology 42, 1877-1883.

Herndon, S. C. Onasch, T. B. Frank, B. P. Marr, L. C. Jayne, J. T. Canagaratna, M. R. Grygas, J. Lanni, T. Anderson, B. E. Worsnop, D. Miake-Lye, R. C. 2005. Particulate emissions from in-use commercial aircraft. Aerosol Science and Technology 39, 799-809.

Herndon, S. C. Rogers, T. Dunlea, E. J. Jayne, J. T. Miake-Lye, R. Knighton, B. 2006. Hydrocarbon emissions from in-use commercial aircraft during airport operations. Environmental Science & Technology 40, 4406-4413.

Herndon, S. C. Shorter, J. H. Zahniser, M. S. Nelson, D. D. Jayne, J. Brown, R. C. Miake-Lye, R. C. Waitz, I. Silva, P. Lanni, T. Demerjian, K. Kolb, C. E. 2004. NO and NO2 emission ratios measured from in-use commercial aircraft during taxi and takeoff. Environmental Science & Technology 38, 6078-6084.

Hsu, H.-H. Adamkiewicz, G. Houseman, A. Vallarino, J. Melly, S. Wayson, R. Spengler, J. Levy, J. 2011. Spatiotemporal Patterns of Ultrafine Particle Counts and Fine Particle Mass in Neighborhoods Surrounding an Airport. Epidemiology 22, S208-S208.

Johnson, G. R. Mazaheri, M. Ristovski, Z. D. Morawska, L. 2008. A plume capture technique for the remote characterization of aircraft engine emissions. Environmental Science & Technology 42, 4850-4856.

Kinsey, J. S. Dong, Y. Williams, D. C. Logan, R. 2010. Physical characterization of the fine particle emissions from commercial aircraft engines during the Aircraft Particle Emissions eXperiment (APEX) 1-3. Atmospheric Environment 44, 2147-2156.

Kinsey, J. S. Hays, M. D. Dong, Y. Williams, D. C. Logan, R. 2011. Chemical Characterization of the Fine Particle Emissions from Commercial Aircraft Engines during the Aircraft Particle Emissions eXperiment (APEX) 1 to 3. Environmental Science & Technology 45, 3415-3421.

Lobo, P. Hagen, D. E. Whitefield, P. D. 2011. Comparison of PM Emissions from a Commercial Jet Engine Burning Conventional, Biomass, and Fischer-Tropsch Fuels. Environmental Science & Technology 45, 10744-10749.

Lobo, P. Hagen, D. E. Whitefield, P. D. Alofs, D. J. 2007. Physical characterization of aerosol emissions from a commercial gas turbine engine. Journal of Propulsion and Power 23, 919-929.

Mazaheri, M. Johnson, G. R. Morawska, L. 2009. Particle and Gaseous Emissions from Commercial Aircraft at Each Stage of the Landing and Takeoff Cycle. Environmental Science & Technology 43, 441-446.

Miracolo, M. A. Hennigan, C. J. Ranjan, M. Nguyen, N. T. Gordon, T. D. Lipsky, E. M. Presto, A. A. Donahue, N. M. Robinson, A. L. 2011. Secondary aerosol formation from photochemical aging of aircraft exhaust in a smog chamber. Atmospheric Chemistry and Physics 11, 4135-4147.

Onasch, T. B. Jayne, J. T. Herndon, S. Worsnop, D. R. Miake-Lye, R. C. Mortimer, I. P. Anderson, B. E. 2009. Chemical Properties of Aircraft Engine Particulate Exhaust Emissions. Journal of Propulsion and Power 25, 1121-1137.

Presto, A. A. Nguyen, N. T. Ranjan, M. Reeder, A. J. Lipsky, E. M. Hennigan, C. J. Miracolo, M. A. Riemer, D. D. Robinson, A. L. 2011. Fine particle and organic vapor emissions from staged tests of an in-use aircraft engine. Atmospheric Environment 45, 3603-3612.

Timko, M. T. Herndon, S. C. Blanco, E. D. Wood, E. C. Yu, Z. H. Miake-Lye, R. C. Knighton, W. B. Shafer, L. DeWitt, M. J. Corporan, E. 2011. Combustion Products of Petroleum Jet Fuel, a Fischer-Tropsch Synthetic Fuel, and a Biomass Fatty Acid Methyl Ester Fuel for a Gas Turbine Engine. Combustion Science and Technology 183, 1039-1068.

Timko, M. T. Herndon, S. C. Wood, E. C. Onasch, T. B. Northway, M. J. Jayne, J. T. Canagaratna, M., R. Miake-Lye, R. C. Knighton, W. B. 2010a. Gas Turbine Enginer Emissions - Part I: Volatile Organic Compounds and Nitrogen Oxides. Journal of Engineering for Gas Turbines and Power-Transactions of the ASME 132.

Timko, M. T. Onasch, T. B. Northway, M. J. Jayne, J. T. Canagaratna, M., R. Herndon, S. C. Wood, E. C. Miake-Lye, R. C. Knighton, W. B. 2010b. Gas Turbine Engine Emissions - Part II: Chemical Properties of Particulate Matter. Journal of Engineering for Gas Turbines and Power-Transactions of the ASME 132.

Timko, M. T. Yu, Z. Onasch, T. B. Wong, H. W. Miake-Lye, R. C. Beyersdorf, A. J. Anderson, B. E. Thornhill, K. L. Winstead, E. L. Corporan, E. DeWitt, M. J. Klingshirn, C. D. Wey, C. Tacina, K. Liscinsky, D. S. Howard, R. Bhargava, A. 2010c. Particulate Emissions of Gas Turbine Engine Combustion of a Fischer-Tropsch Synthetic Fuel. Energy & Fuels 24, 5883-5896.

Vancassel, X. Sorokin, A. Mirabel, P. Petzold, A. Wilson, C. 2004. Volatile particles formation during PartEmis: a modelling study. Atmospheric Chemistry and Physics 4, 439-447.

Wey, C. C. Anderson, B. E. Wey, C. Miake-Lye, R. C. Whitefield, P. Howard, R. 2007. Overview on the aircraft particle emissions experiment. Journal of Propulsion and Power 23, 898-905.

Wong, H. W. Yelvington, P. E. Timko, M. T. Onasch, T. B. Miake-Lye, R. C. Zhang, J. Y. Waitz, I. A. 2008. Microphysical modeling of ground-level aircraft-emitted aerosol formation: Roles of sulfur-containing species. Journal of Propulsion and Power 24, 590-602.

Wong, H. W. Yu, Z. H. Timko, M. T. Herndon, S. C. Blanco, E. D. Miake-Lye, R. C. Howard, R. P. 2011. Design Parameters for an Aircraft Engine Exit Plane Particle Sampling System. Journal of Engineering for Gas Turbines and Power-Transactions of the Asme 133.

Wood, E. C. Herndon, S. C. Timko, M. T. Yelvington, P. E. Miake-Lye, R. C. 2008. Speciation and chemical evolution of nitrogen oxides in aircraft exhaust near airports. Environmental Science & Technology 42, 1884-1891.

Yelvington, P. E. Herndon, S. C. Wormhoudt, J. C. Jayne, J. T. Miake-Lye, R. C. Knighton, W. B. Wey, C. 2007. Chemical speciation of hydrocarbon emissions from a commercial aircraft engine. Journal of Propulsion and Power 23, 912-918.

Yu, Z. H. Liscinsky, D. S. Winstead, E. L. True, B. S. Timko, M. T. Bhargava, A. Herndon, S. C. Miake-Lye, R. C. Anderson, B. E. 2010. Characterization of Lubrication Oil Emissions from Aircraft Engines. Environmental Science & Technology 44, 9530-9534.

Zhu, Y. Fanning, E. Yu, R. C. Zhang, Q. Froines, J. R. 2011. Aircraft emissions and local air quality impacts from takeoff activities at a large International Airport. Atmospheric Environment 45, 6526-6533.

The influence of non-mitigated road transport emissions on regional air quality: analysis of the QUANTIFY high-road study

J. E. Williams [*], P. F. J. van Velthoven
Koninklijk Nederlands Meteorologisch Institute, De Bilt, The Netherlands

Ø. Hodnebrog[1], M. Gauss[2], T. K. Berntsen, I. S. A. Isaksen, F. Stodal
Department of Geosciences, University of Oslo, Norway

V. Grewe
DLR-Institut für Physik der Atmosphäre Oberpfaffenhofen, Germany

O. Dessens[3]
Centre for Atmospheric Science, Department of Chemistry, Cambridge, UK

D.Olivié[4]
Centre National de Recherches Météorologiques GAME/CNRM (Météo-France), Toulouse, France

Q. Tang[5] and M. J. Prather
Department of Earth System Science, University of California, Irvine, USA

    1 now at CICERO, Oslo, Norway
    2 now at Norwegian Meteorological Institute, Oslo, Norway
    3 now at UCL Energy Institute, University College London, London, UK
    4 now at Department of Geosciences, University of Oslo, Norway and CICERO
    5 now at Department of Biological and Environmental Engineering, Cornell University, New York, USA

ABSTRACT: Road Transport emissions (RTE) act as a significant global NO_x source and are responsible for enhancing the chemical production of tropospheric ozone (O_3) in the lower troposphere. In this study we analyse a multi-model ensemble which adopts the SRES A1B emission scenario and a pessimistic "policy-failure" scenario for RTE (A1B_HIGH) for the years 2025 and 2050. Analysing the regional trends between RTE NO_x estimates shows that differences of between 0.2-0.3 Tg N yr^{-1} occur for most world regions in 2025, apart from Asia where there is a larger difference of 1.4 Tg N yr^{-1}. For 2050 these differences fall significantly to ~0.1 Tg N yr^{-1}. By normalizing the seasonal ensemble means of near-surface (0-500m) O_3 with the recommended EC exposure limit of 60 ppb in order to derive an exceedence ratio (ER), we show that ER values greater than 1.0 occur across a wide area for boreal summer during the simulation year of 2003 when adopting the QUANTIFY emission estimates for the year 2000. When adopting the future A1B_HIGH estimates the Middle East is the region which exhibits the worst air quality, followed by Asia. For these regions the area of exceedence (ER > 1.0) is ~40% and ~25% of the total area of each region, respectively. Comparing simulations employing the various scenarios shows that in the instance of a policy failure for RTE the area of exceedences of the EC air quality standards increases by ~6% and ~2% for the Middle East and Asia regions, respectively. This implies that a policy failure related to RTE would have a detrimental effect on health of the population in these world regions. The cumulative mitigation of anthropogenic emissions from both transport and non-transport sources in Europe and the USA results in cleaner surface air meaning that slower mitigation of RTE is not crucial in achieving air quality targets for these regions.

---

[*] *Corresponding author:* Jason Williams, Chemistry and Climate division, Royal Netherlands Meteorological Institute, De Bilt, The Netherlands. Email: williams@knmi.nl

1   INTRODUCTION

Emissions of nitrogen oxides (NO_X) from road transport have been shown to have important impacts on tropospheric ozone (O_3) in the lower troposphere at the turn of this century (Hoor et al, 2009). Estimates in the future SRES A1B emission scenarios (Nakicenovic et al., 2000) predict a reduction in global NO_X Road Transport Emissions (RTE) from 9 Tg N yr^{-1} in 2000 to ~7 Tg N yr^{-1} in 2025 (~2 Tg N yr^{-1} in 2050), where the regional emission trends in RTE exhibit significant inhomogeneities. It is thought that the A1B scenario is the most realistic scenario to date concerning CO_2 emissions, where global anthropogenic emissions are thought to have exceeded the SRES estimates upto 2008 (Garnaut et al, 2008), after which there was a decline associated with the recent economic crisis. Although there is no corresponding analysis related to NO_X emissions satellite observations have observed a decrease in regional NO_X over the last few years related to anthropogenic emissions (e.g. Castellanos and Boersma, 2012). This global reduction in RTE in future decades means that the influence of RTE on atmospheric composition will diminish as a result (Koffi et al, 2010). However, there is of course the possibility that the estimated reductions in RTE will not be attained, resulting in a so-called 'policy-failure' scenario (Uherek et al, 2010), which could influence the ability to achieve certain air quality targets in future decades.

A common tool for investigating the effects of future emission scenarios on air-quality and tropospheric composition are large-scale global 3D Chemistry Transport (CTM) and Chemistry Climate (CCM) models (e.g. Hodnebrug et al, 2011). By fixing the meteorology used to drive such models whilst changing the anthropogenic emissions towards future estimates, the direct influence of changes in each of the transport sectors can be determined. By using a host of different CTMs and CCMs model biases due to choice of particular chemical mechanisms and parameterizations used to describe physical processes such as convective transport can be largely eliminated. This leads to a robust assessment of the potential changes in future air quality induced by specific emission scenarios.

Here we analyse the results of a multi-model ensemble performed as part of the EU-QUANTIFY project to investigate the consequences that a "policy-failure" regarding RTE (hereafter referred to as A1B_HIGH) would have on regional air quality for a number of important world regions in the near-future. By using recommendations provided by the European Commission (EC) regarding safe air-quality standards we determine the world regions which exhibit the highest sensitivity towards unmitigated RTE and assess the extent to which exceedences above this safe threshold increase.

2   TRENDS IN REGIONAL TRANSPORT EMISSIONS

By examining the global trends in NO_X emissions from different transport sectors defined in the SRES A1 and B1 scenarios (Nakicenovic et al., 2000) it has been show by Hodnebrog et al. (2011) that the A1B_HIGH scenario results in the sector having the highest global NO_X emissions across all transport sectors by 2025 (~9.5 Tg N yr^{-1}), becoming the second most important by 2050 (~3 Tg N yr^{-1}).
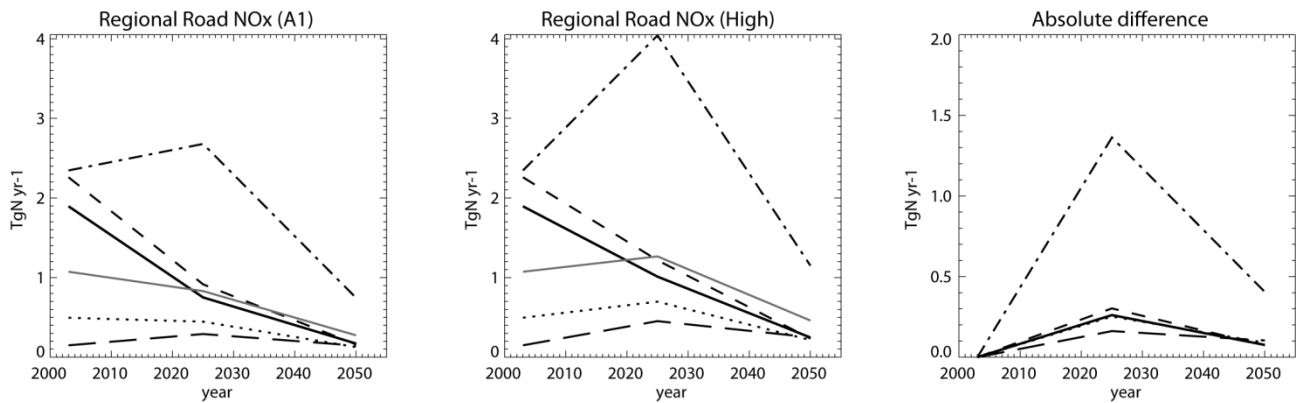
Figure 1: Regional changes in NO$_x$ RTE in Tg N yr^{-1} between 2000 and 2050 as defined in the SRES A1B (left panel) and A1B_HIGH (middle panel) emission scenarios. The difference between the 2 scenarios is given in the right panel. Key to regions: Europe (----), the USA (___), Asia (-.-.-), the Middle East (grey line), South America (……) and Africa (_ _).

Figure 1 shows the regional trends for RTE of NO$_X$ for both the A1B and A1B_HIGH emission scenarios integrated in six pre-defined world regions containing large urban centres, these being: Europe (20°W-35°E, 40-80°N), the USA (70-140°W, 30-60°N), Asia (60-140°E, 10°S-60°N), South America (40-100°W, 40°S-10°N), Africa (30°W-50°E) and the Middle East (16-60°E, 14-50°N). For clarity the absolute differences between the scenarios in Tg N yr^{-1} are show in the third panel. The Asian region has the largest RTE of NO$_X$ across the entire timeline, with RTE being approximately double those of Europe and the USA in future decades. The A1B_HIGH scenario results in an extra 1.4 Tg N yr^{-1} to be emitted from the Asia region by 2025. For other regions such as South America and Africa, the A1B_HIGH scenario results in the trend changing from a modest decrease towards a modest increase by 2025 (equating to differences of ~0.2-0.3 Tg N yr^{-1}). For the Middle East (ME) the A1B_HIGH scenario results in this region becoming the second-most important region for RTE.

3 DESCRIPTION OF THE MULTI-MODEL ENSEMBLE

The multi-model ensemble used in this study is similar to that used before to assess the present-day impact of transport emissions on tropospheric composition (Hoor et al, 2009) and contains five members, these being: TM4, OSLO CTM2, p-TOMCAT, MOCAGE and the UCI CTM. All are CTMs except MOCAGE which is a CCM. There is some homogeneity between the different models in that all are driven by or nudged towards the ECMWF operational data for the year 2003. It has previously been shown that the impact of a changing climate does not introduce a significant perturbation towards the effects on tropospheric ozone production (Koffi et al, 2010). Some models include only tropospheric chemistry (TM4 and p-TOMCAT) whilst the others include both stratospheric and tropospheric chemistry. For brevity, the details concerning the number of reactions and chemical species included, along with the vertical and horizontal resolution employed by each of the ensemble members, are listed in Hodnebrog et al (2011). All results are re-binned on 40 levels and at T42 resolution for the analysis.

The biogenic emissions estimates in the ensemble are taken from the climatology calculated by the EMAC model averaged over the period 2000-2003 (Jöckel et al, 2006). The lightning NO$_X$ emissions are constrained to ~5 Tg N yr^{-1} across the ensemble. For biomass burning the GFEDv1 estimates for 2000 are adopted (van der Werf et al, 2006) with burning activity described by using a multi-year average (1997-2002) using emission factors from Andrea and Merlet (2001).

The global distribution of tropospheric ozone in the model ensemble has been validated in Hodnebrog et al (2011) against a climatology assembled from ozonesonde measurements (Logan, 1999).

4   GLOBAL AIR QUALITY IN THE ENSEMBLE

To assess whether the present day distribution of near-surface (0-500m) O_3 simulated by the model ensemble results in regional exceedences of air quality safety limits, we normalize the seasonal mean calculated for June-July-August (JJA) by the recommendation provided by the EC of 60 ppb exposure for a period of 25 days in any one year. This recommendation is higher than that of 51 ppb provided by the World Health Organization and lower than that of 75 ppb provided by the Environmental Protection Agency in the USA, where the exposure times for these other recommendations are given in hours of exceedence per day and thus are not as suitable for application to the ensemble seasonal means.
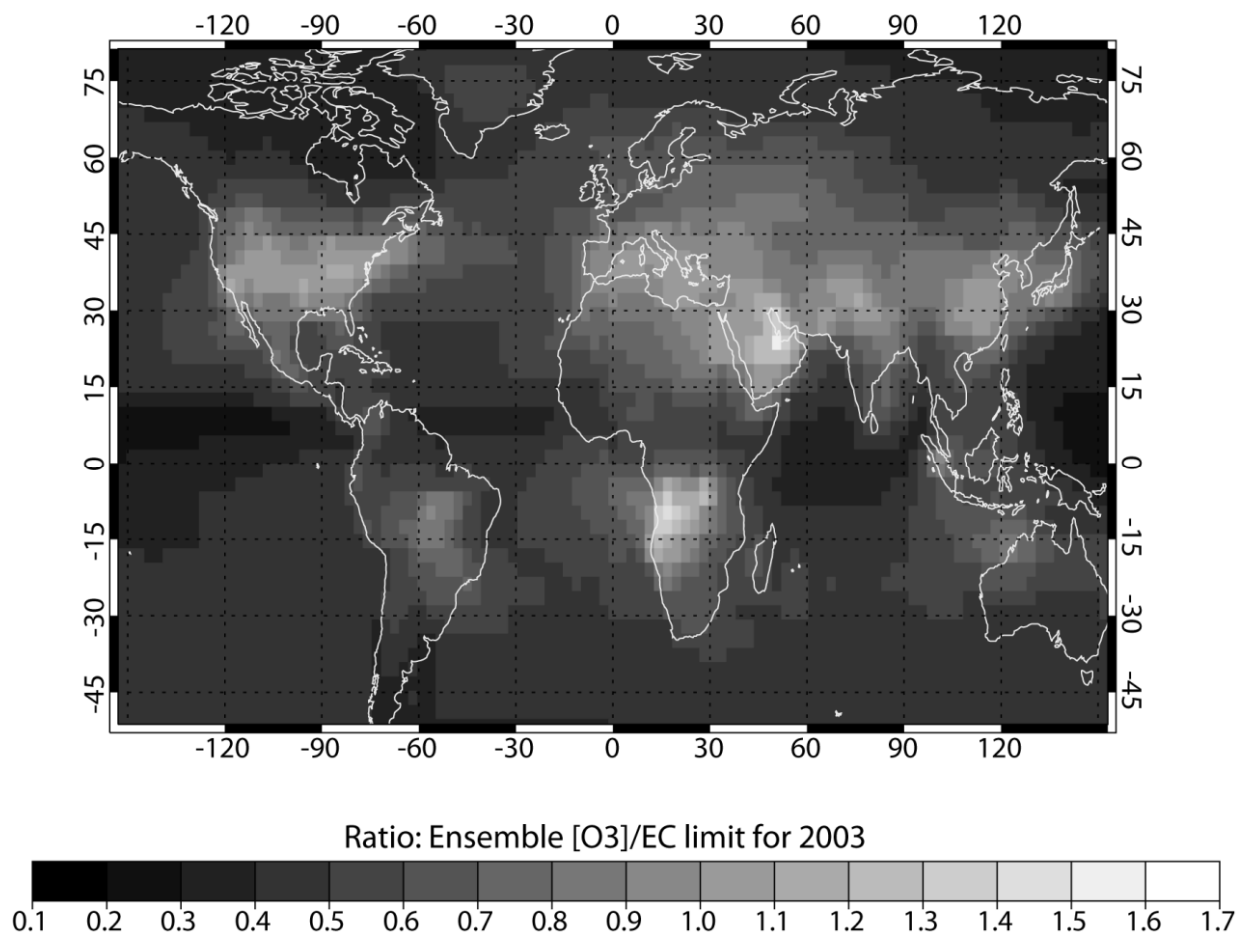

Figure 2: The global distribution of the Exceedence Ratio (ER) for near-surface O_3 for JJA during 2003 calculated using the seasonal ensemble mean.

Figure 2 shows the distribution of the Exceedence Ratio (ER) for 2003 during JJA. The lighter areas of the map represent regions where the highest exceedences occur for the season. It can be seen that the ensemble predicts significant exceedences over wide areas of Europe, the USA, Asia and the Middle East. These high near-surface O_3 values occur as a result of the combined effects of mainly biogenic, transport and non-transport emissions. For the future the strong mitigation practices associated with anthropogenic emissions that are expected to occur for both Europe and the USA means that, even for the A1B_HIGH scenario, the near-surface O_3 values will fall below the EC limit resulting in ER values of between 0.6-0.8 (not shown). Therefore any failure in mitigating RTE will not be critical for reaching air quality targets in these developed regions. For other developing regions such as South America, the RTE is rather small considering the large area over which they are integrated. The fact that the highest RTE occur in the Asian region and that the ME has notoriously high surface O_3 values during JJA (Lelieveld et al, 2009) provided us with a strong motivation to select these two regions to investigate the impact of the A1B_HIGH emission scenario.
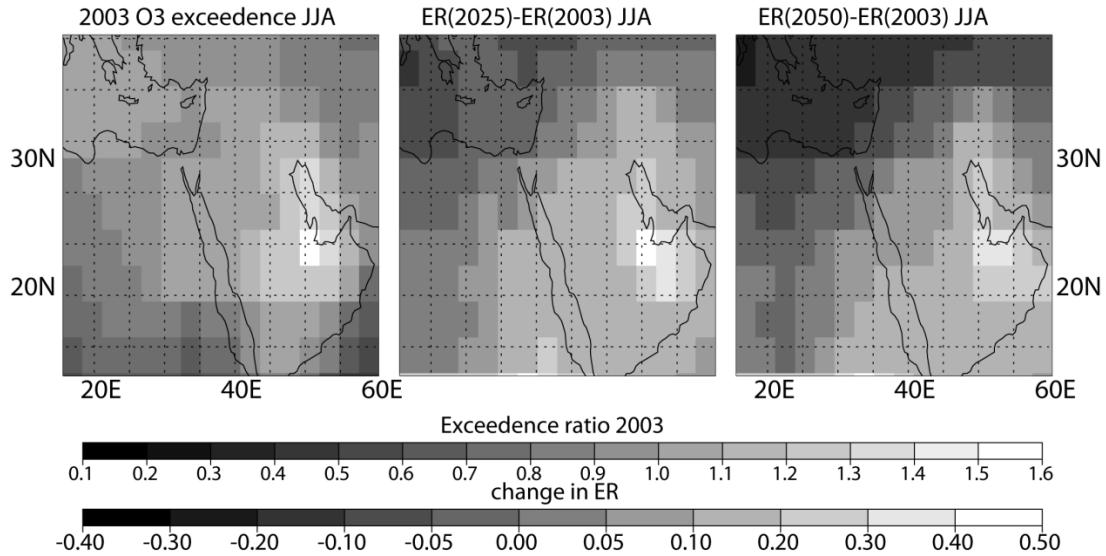
5 REGIONAL DEGREDATIONS IN AIR QUALITY

Figure 3: The regional distribution of ER for the Middle East during JJA 2003 (left panel) and the differences in the regional ER for 2025 (middle panel) and 2050 (right panel) when using the A1HIGH emission scenario.

Figure 3 shows the ER for 2003 across the ME, including parts of the Mediterranean basin. The differences in the ER between 2003 and both the 2025 and 2050 A1B_HIGH scenario are also shown. For 2003 there are exceedences over a wide area including Greece, Egypt, Iraq and Israel, with the maximum exceedences (above 1.5) occurring around Qatar, Bahrain and the Gulf of Oman. When integrating exceedences for the entire region ~40% of the total area exhibits ER values higher than 1.0. When comparing the differences in the ER for 2025 and 2050 it can be seen that the mitigation of European emissions improves air quality over the Mediterranean and Turkey as the timeline progresses. However, for the Persian Gulf region the exceedences increase in magnitude. Therefore there is a latitudinal shift southwards in areas exhibiting bad air-quality away from Europe and towards the ME. When comparing the number of exceedences which occur in the ME for the 2025 A1B_HIGH simulation there is little change compared to 2003. For the 2050 A1B_HIGH simulation the number of exceedences falls to ~33% of the total area of the ME region. Taking the differences in the ER ratios between the A1B and A1B_HIGH simulations reveals that for 2025 the "policy-failure" for RTE increases the area for which air quality limits are exceeded by ~6% of the total regional area in the ME. For 2050 the differences become much smaller with the "policy failure" for RTE only increasing the exceedences of the total regional area by ~1%.
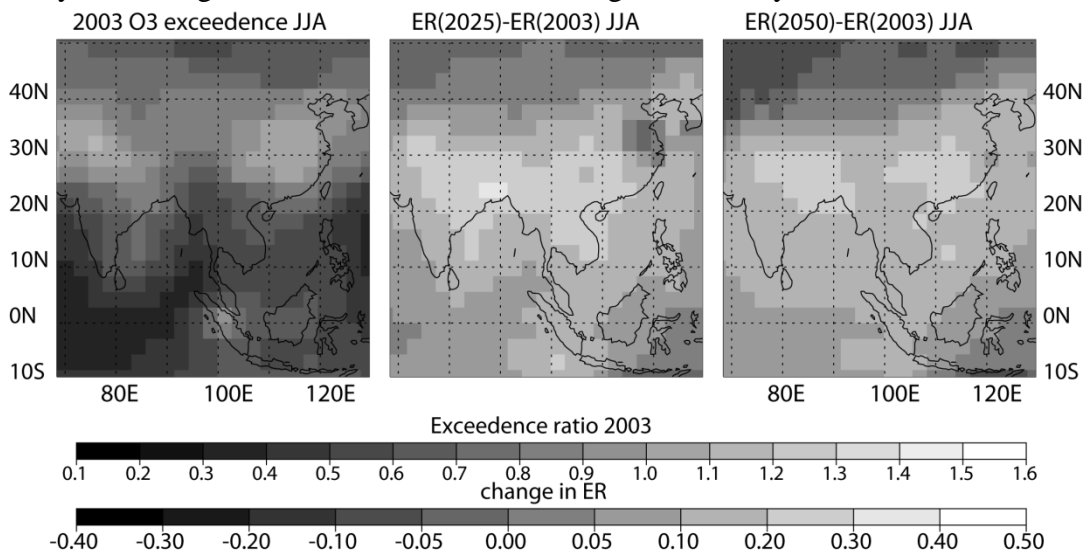

Figure 4: As Fig. 3 except for the Asian region.

Figure 4 shows the corresponding distribution in the ER for 2003 for the Asian region. The most polluted regions are around the Ganges valley in Northern India and Eastern China. The other regions are relatively clean, especially over the oceans, with the integrated exceedences only covering ~8% of the region shown. Moreover the maximum exceedences in the region of 1.3-1.4 are somewhat lower than those simulated for the ME. For the future A1B_HIGH simulations there is a substantial increase in the area of exceedences of up to ~25% for 2025. This is due to the large increases in e.g. energy production and shipping activity, as well as the increases in RTE. For 2050 the area of exceedences remains approximately the same. Again, taking differences in the ER ratios between the A1B and A1B_HIGH simulations reveals that there is an increase in the exceedence area of ~2%, although this equates to a larger area than that for the ME due to the size of each of the regions shown.

6   SUMMARY

We have shown that although road transport NO_X emissions are typically decreasing in the 21st Century for many world regions, a "policy-failure" concerning mitigation would offset such a decline to around 2035, with emissions from Asia increasing significantly. By analyzing a set of multi-model ensemble simulations we have shown that during 2003 regional near surface (0-500m) tropospheric O_3 can exceed EC air quality targets at continental scale for regions such as Europe, the USA, the Middle East and Asia during boreal summertime. Comparing distributions from simulations adopting the SRES A1B and the A1B_HIGH "policy-failure" emission scenario we conclude that the region in which the most significant degradation of air quality would occur is the Middle East, with the number of exceedences increasing significantly. The impact of a "policy-failure" concerning road transport emissions would make a marked contribution (~6% of the total area of the region) in the Middle East. For the Asian region there is also a significant decrease in air quality, although mainly due to increasing emissions due to energy production, industry and shipping. Here, although a "policy failure" concerning road transport emissions does contribute it only increase the area of exceedence by ~2% of the total regional area.

REFERENCES

Andreae, M. O. and P. Merlet, 2001: Emissions of trace gases and aerosols from biomass burning, Global Biogeochem. Cy., 15, 955-966.

Castellanos, P. and K. F. Boersma, Reductions in nitrogen oxides over Europe driven by environmental policy and economic recession, 2012: Sci, Reports, 2, doi:10.1038/srep00265, 265-273.

Garnaut, R., S. Howes, F. Jotzo and P. Sheehan, 2008: Emissions in the Platinum Age: the implications of rapid development for climate-change mitigation, Oxf. Rev. Econ. Policy, 24(2), 377-401.

Hodnebrog, Ø., T. K. Berntsen, O. Dessens, M. Gauss, V. Grewe, I. S. A. Isaksen, B. Koffi, G. Myrhe, D. Olivié, M. J. Prather, J. A. Pyle, F. Stordal, S. Szopa, Q. Tang, P. van Velthoven, J. E. Williams, and K. Ødemark, 2011: Future impact of non-land based traffic emissions on atmospheric ozone and OH – an optimistic scenario and a possible mitigation strategy. Atms. Chem. Phys., 11, doi:10.5194/acp-11-11293-2011, 11293-11317.

Hoor, P., J. Borken-Kleefeld, D. Caro, O. Dessens, O. Endresen, M. Gauss, V. Grewe, D. Hauglustaine, I. S. A. Isaksen, P. Jöckel, J. Lelieveld, G. Myrhe, E. Meijer, D. Olivié, M. J. Prather, C. Schnadt Poberaj, K. P. Shine, J. Staehelin, Q. Tang, J van Aardenne, P. van Velthoven, and R. Sausen, 2009: The impact of traffic emissions on atmospheric ozone and OH: results from QUANTIFY. Atms. Chem. Phys., 9, doi;10.5194/acp-9-3113-2009, 3113-3136.

Jöckel, P., H. Tost, A. Pozzer, C. Brühl, J. Buchholz, L. Ganzeveld, P. Hoor, A. Kerkweg, M. G. Lawrence, R. Sander, B. Steil, G. Stiller, M. Tanarhte, D. Taraborrelli, J. van Aardenne and J. Lelieveld, 2006: The atmospheric chemistry genrela circulation model ECHAM5/MESSy1: consistent simulation of ozone for surface to the mesosphere, Atms. Phys. Chem., 6, doi:10.5194/acp-6-5067-2006, 5067-5104.

Lelieveld, J., P. Hoor, P. Jöckel, A. Pozzer, P Hadjinicolaou, J.-P. Cammas and S. Beirle, 2009: Severe ozone air pollution in the Persian Gulf region, Atms. Chem. Phys., 9, 1393-1406.

Logan, J., 1999: An analysis of ozonesondes data for the troposphere: Recommendations for testing 3-D models and development of a gridded climatology for tropospheric ozozne, J. Geophys. Res., 104, doi:10.1029/1998jd100096,16115-16149.

Koffi, B., S. Szopa, A. Cozic, D. Hauglustaine, and P, van Velthoven, 2010: Present and future impact of aircraft, road and shipping emissions on global tropospheric ozone, Atms. Phys. Chem., 10, doi:10.5194/acp-10-11681-2010, 11681-11705.

Nakicenovic, N., O. Davidson, G. Davis, A. Grübler, T. Kram, E. L. La Rovere, B. Metz, T. Morita, W. Pepper, H. Pitcher, A. Sankovski, P. Shukla, R. Swart, R. Watson and Z. Dadi, 2000: Special Report on Emissions Scenraios, Cambridge University Press, Cambridge, 599pp.

Uherek, E., T. Halenka, J. Borden-Kleefeld, Y. Balkanski, T. Berntsen, C. Borrego, M. Gauss, P. Hoor, K. Juda-Rezler, J. Lelieveld, D. Melas, K. Rypdal and S. Schmid, 2010: Transport impacts on atmosphere and climate: Land transport, Atms. Environ. 44(37), 4772-4816.

Van der Werf, G. R., J. T. Randerson, L. Giglio, G. J. Collatz, P. S. Kasibhatla and A. F. Arellano Jr., 2006: Interannual variability in global biomass burning emission from 1997 to 2004, Atms. Phys. Chem., 6, doi:10.5194/acp-6-3423-2006, 3423-3441.

The inclusion of international aviation within the European Union's Emissions Trading Scheme

H. Preston[*], D.S. Lee, L.L. Lim
Dalton Research Institute, Manchester Metropolitan University, Manchester, United Kingdom

ABSTRACT: In response to limited action on an international level, in January 2012 international aviation emissions were included within the European Union's Emissions Trading Scheme, requiring all flights departing from and arriving to EU Member State airports to participate purchasing and surrendering carbon credits within the market. As part of a project to investigate the potential effectiveness of the EU's policy, a suite of future aviation emission scenarios under a variety of technology outlooks, were compared alongside three EU ETS emission cap scenarios. A global aviation emissions inventory model (FAST) was used with flight movement data from ICAO's ninth CAEP cycle, to produce distance (km), fuel use (kg), and CO_2 emissions (kg), for international and domestic flight movements both globally and for EU-27 Member States (plus Norway, Iceland, and Liechtenstein) for the years 2006, 2016, 2026 and 2036 under five technology outlooks. Preliminary results demonstrated a projected steady increase in aviation emissions to 2036, compared with a slow downward trend in the emissions available under the three cap scenarios. The results raised issues regarding the limited scope of emission reductions under the technology outlooks (between a low technology improvements outlook and an optimistic outlook), compared with a gradual reduction of emissions under the EU ETS policy. However, the potential future of the policy comes into question with the considerable opposition that it has already received in its infancy. Nonetheless, aviation emissions under EU ETS do have the potential to be mitigated and at the very least, the policy has acted as a stimulant for more concerted international action.

1   INTRODUCTION

International aviation emissions were not included within the legally binding targets of the United Nations Framework Convention on Climate Change's Kyoto Protocol, and since the Protocol's adoption and implementation in 1997 and 2005 respectively, the sector has been subjected to limited significant international action to curb its CO_2 emissions. Emissions from the sector, however, have continued to rise and are projected to do so into the future; a report by the Group on International Aviation and Climate Change (GIACC – a group within the International Civil Aviation Organization, ICAO) concluded from a number of emissions projections, that global CO_2 emissions (not accounting for any impacts that may arise from the use of alternative fuels) are forecast to increase from 632 Mt in 2006, to a range of 890 to 2,800 Mt in 2050 (ICAO, 2009: 1). Without action to reduce emissions from the sector, the likelihood of achieving climate mitigation goals, for example, limiting global temperature increases to no more than 2° C, as outlined in the text for the Copenhagen Accord (UNFCCC, 2009: 5), becomes unrealistic as such climate stabilization goals often work on the assumption of reduction efforts from all regions of the globe and all sectors (Edmonds *et al*, 2008: 356). To achieve the 2°C target, global emissions would have to peak before 2020 and then steeply decline thereon after, eventually meeting negative emissions in the longer term future[1] (UNEP, 2011: 9). Efforts are being made by other sectors to curb greenhouse gas emissions, and the aviation industry must follow suit to mitigate its international emissions to ensure that such policies are achievable. Furthermore, not only is there the issue of a lack of significant mitigation effort fo-

---

[*] *Corresponding author:* Holly Preston, Dalton Research Institute, Manchester Metropolitan University, E0.04, John Dalton Building, Chester Street, Manchester, M1 5GD. Email: h.preston@mmu.ac.uk

[1] This would be the emissions pathway consistent with a 'likely' chance of meeting the 2°C goal (UNEP, 2011: 9).

cused toward reducing international aviation CO_2 emissions, the sector is also responsible for a suite of non-CO_2 impacts, some of which have the potential to warm the Earth's climate. In response to the limited regulatory action to mitigate aviation emissions at an international level, in 2008 the European Commission proposed an extension to the European Union's Emissions Trading Scheme (EU ETS) to cover emissions from EU Member State airports; and in January 2012, all international flights departing from and arriving at EU-27 airports (plus Norway, Iceland and Liechtenstein) were included within the European Union's Emissions Trading Scheme (EU ETS). Under the policy, airlines must purchase and surrender emissions credits for every tonne of CO_2 emissions that they emit for the part of the flight that is connected to the EU country.

2   RESEARCH PROJECT

2.1   *Research aims*

The research aim of this project is to investigate the potential effectiveness of the inclusion of international aviation emissions within the EU ETS. This paper represents the first step within the overall project, comparing a suite of future international aviation emissions scenarios with a variety of ETS caps.

2.2   *Methodology*

The model used in this project is FAST, a global aviation emissions inventory model which uses data on flight movements and data on fuel flow to produce fuel use, distance travelled, carbon dioxide, NOx, black carbon and particle number (Owen *et al*, 2010: 2255). The input flight movement data is derived from the Committee on Aviation Environmental Protection's ninth cycle (CAEP/9). This paper looks at future international aviation emissions (from 2012 to 2036; 2012 being the date of introduction of aviation into the EU ETS and 2036 the date at which the CAEP/9 data is extended to), for a number of technology scenarios (technology freeze, low technology, moderate technology, advanced technology and optimistic technology) on a central demand forecast (ICAO, 2009). The technology scenarios used by CAEP/9 are based on a variety of assumptions including operational improvements and efficiencies, technology improvements, and fuel burn improvements (ICAO, 2009). For example, the assumptions under the low technology scenario include "fuel burn improvements at 0.95% per annum for all aircraft entering the fleet after 2006 and prior to 2015, and 0.57% per annum for all aircraft entering the fleet beginning in 2015 and out to 2036"; as well as operational improvements in the fleet of "0.5, 1.4, and 2.3% in 2016, 2026 and 2036 respectively" (ICAO, 2009).

   The CAEP/9 data is inputted into FAST[2] for the variety of years and technology scenarios. FAST then outputs the various data (as mentioned above); for this project the output of interest is distance (km), fuel use (kg), and CO_2 emissions (kg). The model was run for all global flights (international, intra-national, and domestic flights) for 2006, 2016, 2026, 2036. A secondary run was undertaken to determine the flight movements for the EU-27 countries which are covered under the EU ETS (all international, domestic and intra-EU flights to and from EU-27 Member State airports). The emissions were interpolated from 2006 to 2036 to give an annual emissions figure, and then the data from 2012 to 2036 were selected for analysis. Three future emissions caps were used within the analysis: (a) Emissions Cap Scenario 1: the EU ETS Aviation Cap, which is based on the current rate of reduction for the aviation emissions cap (a 2% reduction in the cap for each trading period); (b) Emissions Cap Scenario 2: IATA Goal, based on the IATA goal of reducing aviation emissions by 50% by 2050[3] (an annual reduction in the cap post-2020 of 1.22%); (c) Emissions Cap Scenario 3: Main EU ETS Cap, based on the main EU ETS cap reduction (an annual reduction in the cap post-20120 of 1.74%). Table 1 outlines the cap reductions for the three scenarios. For all three of the scenarios, for the period 2012, 2013 to 2020, the cap follows the pathway set out by the

---

   [2] FAST has been used in a number of impact studies, as well as used "under the aegis" of ICAO's CAEP (Owen *et al*, 2010).

   [3] The IATA goal is based on a basket of measures to reduce aviation emissions, including investment in technology, effective operations, efficient infrastructure, and positive economic instruments. Here, however, we assume that emission trading is the measure being used to produce emission reductions (IATA, 2009).

EU ETS of 97% of historical emissions for 2012, then 95% of historical emissions[4] for the period of 2013 to 2020 (European Parliament, 2008: 8). After this time, the cap is subject to review and it is from this point onwards where the scenarios will differ according to the annual cap reductions.

Table 1: Emission Cap Scenarios

Year	Emissions Cap Scenario 1	Emissions Cap Scenario 2	Emissions Cap Scenario 3
	Percentage of historical emissions		
2012	97%	97%	97%
2013-2020	95%	95%	95%
2026	93%	87.68%	84.56%
2036	91%	75.48%	67.16%

2.3 *Preliminary results*

Figure 1 presents the aviation emissions (international and domestic) in Mt of CO_2, for all global emissions on a central demand forecast for a variety of technology scenarios (the top 5 set of lines) to 2036; aviation emissions for those flights included under the EU ETS policy (the middle 5 lines – the EU-27 lines), again for various technology scenarios under a central demand forecast; and the three future emissions caps (the lower three dotted lines). Under the 5 technology scenarios there is a steady increase in aviation emissions up to 2036. Alongside this projected growth in emissions, is plotted the 3 emissions cap scenarios which show a downward trend in the emissions available under the caps to 2036.
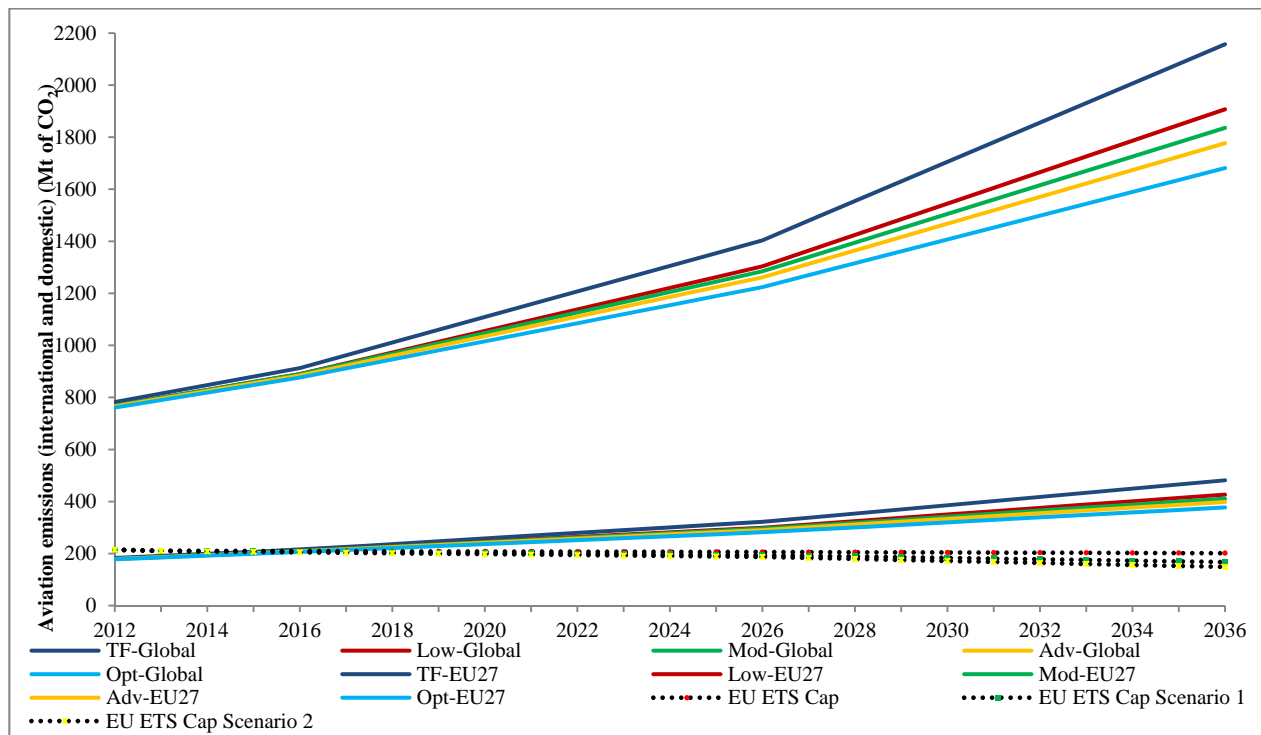

Figure 1: (a) International and domestic emissions for global flights from 2012 to 2036 under five technology scenarios (top five lines); (b) International and domestic emissions for flights from EU-27 Member States covered under the EU ETS from 2012 to 2036 under five technology scenarios (middle five lines); (c) Emissions caps for three cap reduction scenarios (the bottom three lines).

---

[4] The EU ETS aviation emissions cap is based upon a percentage of historical aviation emissions, which are defined as "the mean average of the annual emissions in the calendar years 2004, 2005 and 2006 from aircraft performing an aviation activity listed in Annex I to Directive 2003/87/EC" (European Commission, 2011: 42).

3 SUMMARY AND DISCUSSION

The increase in international aviation emissions to 2036 and beyond has been widely projected (see IPCC, 1999; Lee *et al*, 2010), and therefore the results from the FAST runs using the CAEP/9 data are as expected. However, it is interesting to note that under the five technology scenarios, ranging from a low to advanced technology outlook, the projected emissions (on the global projections) are not significantly different with a variation of just 130 Mt of CO_2 between the low and advanced outlook. This suggests that there is limited scope for emissions reductions through technological, operational, and fuel burn improvements in the future (though this is not to say that such improvements will not be important). If we look at the emissions cap scenarios, the gradual reduction of emission allowances provides the industry with a gradual reduction in its emissions over time (for the EU-27 countries), with potential savings of 246[5] Mt of CO_2 for just those EU-27 countries covered by the EU ETS. It is important to note, however, that this is a theoretical analysis that assumes that the cap accommodates all emissions generated by the flights covered by the EU ETS. In reality, however, it is much more likely that the actual emissions generated will exceed the cap and therefore emissions credits will have to be purchased from other areas of the market. The findings do demonstrate, nonetheless, that the EU ETS has the potential to make reductions in aviation emissions, and therefore should be considered a valuable mitigation measure to be used in a basket of measures. However, the introduction of aviation within the EU ETS has not been met with resounding praise. Whilst it is fairly common for environmental policies to provoke strong reactions, particularly policies mitigating climate change impacts; the policy has triggered extreme opposition. The inclusion of international aviation emissions within the EU ETS, represents a unilateral policy – a unilateral "action or decision" which is "performed by or affecting […] one group or country" (Oxford Dictionaries, 2010) compared with a bilateral policy which is "between two parties or countries" or a multilateral policy, which is "between more than two parties" (Collin, 1997). Whilst in theory the policy is unilateral, it does however have wider reaching impacts; the policy has implications of those non-EU countries and airlines which have flights to and from EU Member State airports. Consequently, the policy has resulted in considerable opposition from countries, airlines and trade associations.

Retaliation against the policy has included arguments that it infringes international trade laws, that it raises the issue of sovereignty, and that it is impeding the efforts of ICAO (the organization which many opponents to the policy feel is the most appropriate to tackle the issue) to address international aviation emissions. Even before the policy entered into force in January 2012, the Air Transport Association of America (ATA, now known as Airlines for America (A4A)) and others, filed a law suit against the EU in response to aviation's inclusion within the EU ETS, pleading that the "directive was unlawful in the light of international treaty law and customary international law" (ECJ, 2011). The case was sent to the European Court of Justice, and the judgement ruled in favour of the EU stating that "examination of Directive 2008/101 has disclosed no factor of such a kind as to affect its validity" (ECJ, 2011). Further opposition to the policy has come from the US, with the European Union Emissions Trading Prohibition Act, the aim of which is to prevent US airlines from participating in the scheme. At point of publication, the Prohibition Act has passed through the House of Representatives and the Senate (US Congress, 2012). Nonetheless, as stated by Preston *et al* (2012: 55) "the true value of the policy may lie in its capacity to act as a precursor for concerted international action", and the policy has certainly put the subject of mitigating international aviation emissions firmly on the agenda, as well as having the potential to make emissions reductions.

4 NEXT STEPS

The next steps in this research will be to investigate a further suite of emissions cap scenarios, with a variety of stringencies from soft to hard; and to undertake an investigation of the comparative emission savings that can be generated from technology efficiencies and ETS.

---

[5] This is an average of five technology scenarios for the EU-27 member state aviation emissions, compared with an average of the three cap scenarios.

REFERENCES

Collin, P.H. (1997) Dictionary of Government and Politics, Second Edition, Peter Collin Publishing

Edmonds, J., Clarke, L., Lurz, J. & Wise, M. (2008) "Stabilizing CO_2 concentrations with incomplete international cooperation", Climate Policy, **8**: 355 - 376

European Commission (2011) Commission Decision of 7 March 2011 on historical aviation emissions pursuant to Article 3c(4) of Directive 2003/87/EC of the European Parliament and of the Council establishing a scheme for greenhouse gas emission allowance trading within the Community (notified under document   C(2011) 1328)(Text with EEA relevance) (2011/149/EU), Available from: http://eur-lex.europa.eu/LexUriServ/LexUriServ.do?
uri=OJ:L:2011:061:0042:0043:EN:PDF

European Court of Justice (ECJ) (2011) Judgement of the Court (Grand Chamber) of 21 December 2011. Air Transport Association of America and Others v Secretary of the State for Energy and Climate Change. Case C-366/10, Available from: http://curia.europa.eu/juris/liste.jsf?pro=&lgrec=fr&nat=&oqp=&dates
=&lg=&language=en&jur=C%2CT%2CF&cit=none%252CC%252CCJ%252CR%252C2008E%252C%2
52C%252C%252C%252C%252C%252C%252C%252Ctrue%252Cfalse%252Cfalse&num=C-
366%252F10&td=ALL&pcs=O&avg=&page=1&mat=or&jge=&for=&cid=4027287

European Parliament (2008) Directive 2008/101/EC of the European Parliament and of the Council of 19 November 2008 amending Directive 2003/87/EC so as to include aviation activities in the scheme for greenhouse gas emission allowance trading within the Community (Text with EEA relevance), Available from: http://eur-lex.europa.eu/LexUriServ/LexUriServ.do?uri=CELEX:32008L0101:EN:NOT

Intergovernmental Panel on Climate Change (IPCC) (1999) Aviation and the global atmosphere, In: Penner, J., Liste, D.H., Griggs, D.J., Noguer, M., van der Linden, P.J., McFarland, M. (Eds.), Intergovernmental Panel on Climate Change, Cambridge University Press, Cambridge, UK

International Air Transport Association (IATA) (2009) A global approach to reducing aviation emissions. First stop: carbon neutral growth from 2020, Available from: http://www.iata.org/
SiteCollection Documents/Documents/Global_Approach_Reducing_Emissions_251109web.pdf

International Civil Aviation Organization (ICAO) (2009) "Group on International Aviation and Climate Change (GIACC) Fourth Meeting, Montreal, 25 to 27 May 2009. Agenda Item 2: Review of aviation emissions-related activities within ICAO and internationally. Global Aviation CO_2 Emissions Projections to 2050"

Owen, B., Lee, D.S. & Lim, L. (2010) "Flying into the Future: Aviation Emissions Scenarios to 2050", Environmental Science and Technology, **44** (7): 2255 – 2260

Oxford Dictionaries (2010) Oxford Dictionaries April 2010, Oxford University Press, Available from: http://oxforddictionaries.com/definition/english/unilateral

Preston, H., Lee, D.S. & Hooper, P.D. (2012) "The inclusion of the aviation sector within the European Union's Emissions Trading Scheme: What are the prospects for a more sustainable aviation industry?", Environmental Development, **2**: 48 – 56

UNEP (2011) Bridging the Emissions Gap. United Nations Environment Programme

United Nations Framework Convention on Climate Change (UNFCCC) (2009) Report of the Conference of the Parties on its fifteenth session, held in Copenhagen from 7 to 19 December 2009. Part Two: Action taken by the Conference of the Parties at its fifteenth session, Available from: http://unfccc.int/resource/docs/2009/cop15/eng/11a01.pdf

United States Congress (2012) European Union Emissions Trading Scheme Prohibition Act of 2011 (Engrossed in Senate [Passed Senate] – ES), Available from: http://thomas.loc.gov/cgi-bin/query/z?c112:S.1956:

ACKNOWLEDGEMENTS

Cloud Microphysical Properties Measured from Commercial Aircraft

D. Baumgardner[*], R. Newton
Droplet Measurement Technologies, Boulder, CO., USA

K. Beswick, M. Gallagher
University of Manchester, Manchester United KingdomAuthor(s)

Keywords: cloud properties, commercial aircraft, optical particle spectrometer

ABSTRACT: In an ambitious program, funded by the European Union, commercial aircraft are being outfitted with instruments for measuring water vapor, ozone, carbon monoxide, nitrogen oxides and cloud particles. The Jülich Research Centre is working with 15 European partners on the project, named IAGOS (In-service Aircraft for a Global Observing System), that uses civil aviation aircraft to collect much larger quantities of data, over longer time spans and larger spatial scales than would have been possible using flights with special, instrumented aircraft. One the instruments, the backscatter cloud probe (BCP), measures the size distribution of cloud particles between 5 and 60 um from which cloud liquid/ice water is also derived. The first instrument package was fitted to Lufthansa's Airbus A340-300 "Viersen", with the initial flight taking place on July 7, 2011. Routine measurements began September 14, 2011 and are being routinely made on flights based in Frankfort and traveling to North and South America, Europe and Asia. The preliminary analysis of the BCP measurements from these flights show that moderately high concentrations of cloud particles, over the entire size range of the instrument, are frequently encountered over the South Atlantic, as well as during descents and ascents into North American Destinations. These measurements will contribute to the data base of cloud climatology that is needed to validate microphysical properties of clouds derived from satellite measurements and improve climate model parameterizations.

1 BACKGROUND

Clouds are one of the principal components of the atmosphere that moderate climate through the cooling effect when they reflect solar radiation and their warming effect when they trap terrestrial infrared radiation. Their impact on climate is also one of the most uncertain factors in global climate change models due to the complexity of cloud structures and the underlying microphysics that govern their formation and evolution. Satellite measurements provide important information about cloud evolution and their structure, information that is used to improve the climate model forecasts. This information, however, is derived from algorithms that must be validated with in situ measurements made in many types of clouds, in many regions and under many environmental conditions. Numerous aircraft campaigns for cloud studies have been conducted over the years, yielding invaluable data that has helped us better understand cloud processes; however, such campaigns are expensive to run and only cover relatively short time periods and limited areas.

In order to complement and augment the measurements made during airborne research campaigns, and to provide a much more extensive set of data in time and space, a program, funded by the European Union is underway to outfit commercial aircraft with instruments for measuring water vapor, ozone, carbon monoxide, nitrogen oxides and cloud particles (*www.iagos.org/*). The Jülich Research Centre, along with 15 European partners, are working on the In-service Aircraft for a Global Observing System (IAGOS), that uses civil aviation aircraft to collect large quantities of data. The instrument that measures cloud particle size distributions is called the Backscatter Cloud Probe (BCP), whose operations and some preliminary results are described below.

---

[*] *Corresponding author:* Darrel Baumgardner, Droplet Measurement Technologies, Boulder, CO, 80301, USA. Email: darrel.baumgardner@gmail.com

2   BCP MEASUREMENT TECHNIQUE

Initially conceived as a simple cloud detector for quality control of the trace gas measurements from IAGOS instrument packages it is also capable of delivering scientifically useful cloud microphysical information. The BCP measures light that is scattered by individual particles that pass through a focused laser beam, as shown in the left panel of Fig. 1. The geometry of the optics is designed to collect the fraction of the light that is scattered backward over a solid angle of 144-156° and focuses it on a photo-detector that converts the photons to an electrical signal. The maximum amplitude is digitized and, through calibration, is converted to an optical diameter. The size range of the BCP is nominally 2-80 μm. A complete description of the BCP operating principles is found in Beswick et al. (2012).

The BCP is designed to mount inside the aircraft, needing only a very small window through which the laser beam projects and scattered light is collected (Fig. 1, right panel). The sensor itself is quite small, 10 cm in length, weighing only 0.5 Kg with a very small volume.
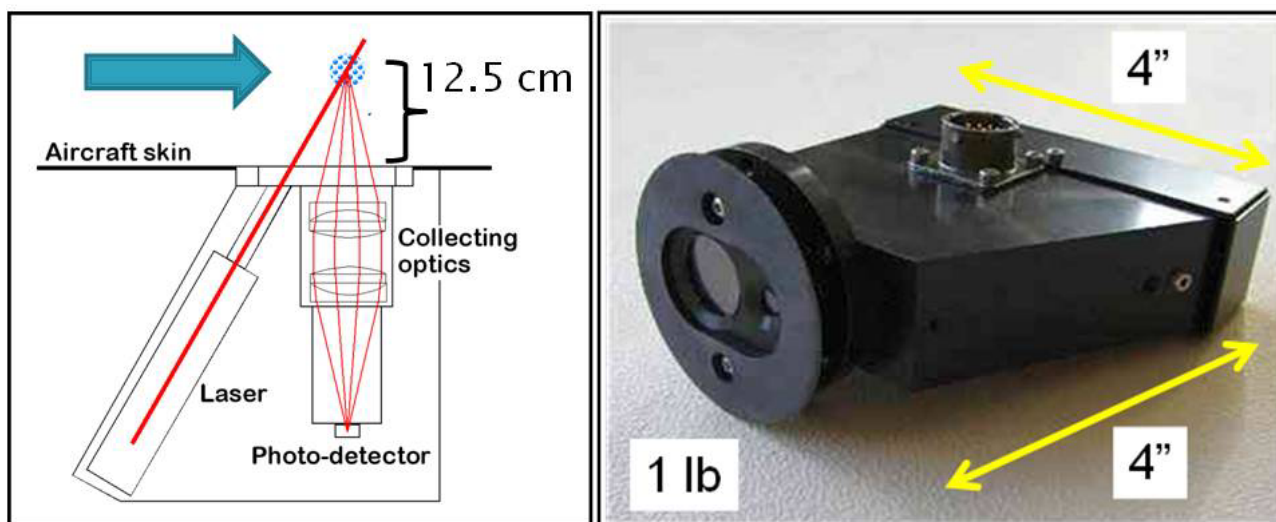

Figure 1

3   RESULTS

The BCP has been flown on a number of research aircraft carrying other cloud particle sensors. One of these aircraft is the North Dakota Citation (photograph in Fig. 2) that carries a suite of such sensors, including a Droplet Measurement Technologies Cloud Droplet Probe (CDP), shown in an insert of the photograph in Fig. 2, that measures in the size range as the BCP (Lance et al., 2010). Also identified and shown in another insert is the window of the BCP.
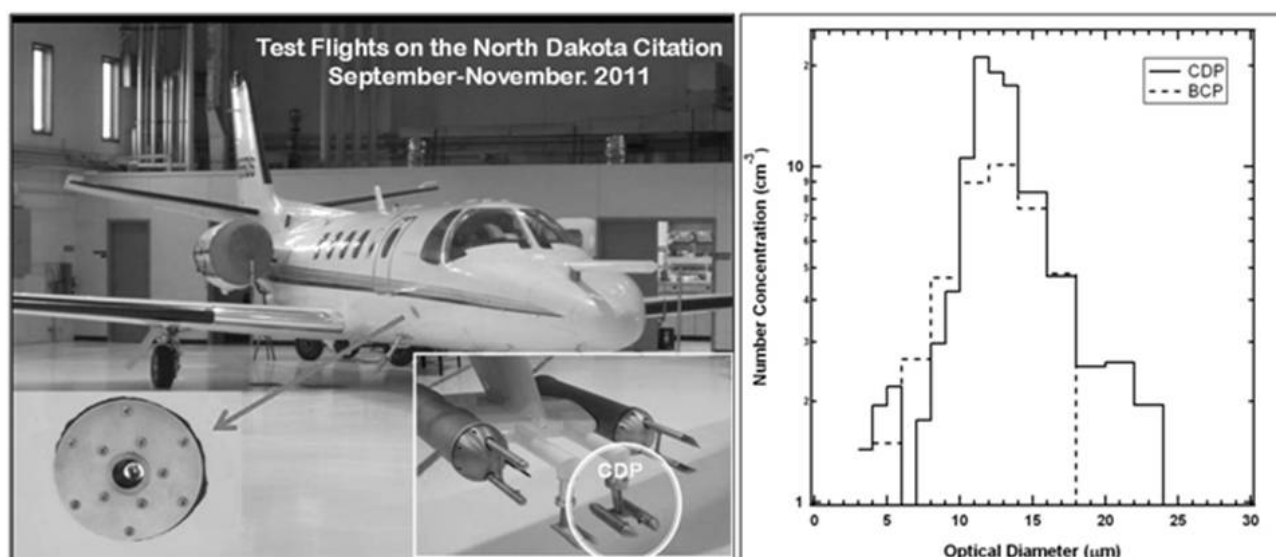

Figure 2

A number of flights were made in the fall of 2011 in all water and mixed phase clouds. The total number concentrations were in excellent agreement and, as shown in the right panel of Fig. 2, for a representative time period in an all liquid water cloud, the size distributions were also in very good agreement.

The first IAGOS instrument system including the BCP was installed on Lufthansa airlines' A340-300 'Viersen'. The maiden test flight was launched from Frankfurt in July 2011 which began making routine, international flights in September of that same year. Since that time the BCP has logged more than 2400 hours of data during 319 flights up to May, 2012. Figure 3 illustrates the flight trajectories of the aircraft demonstrating that measurements have been made over the Atlantic Ocean to and from North and South America, over Europe to Africa, the Middle East and Asia. The filled circles indicate where clouds (including dust I arid cloud free regions) were encountered and the coloring shows the cloud particle number concentrations within its measured size range, on a logarithmic scale.
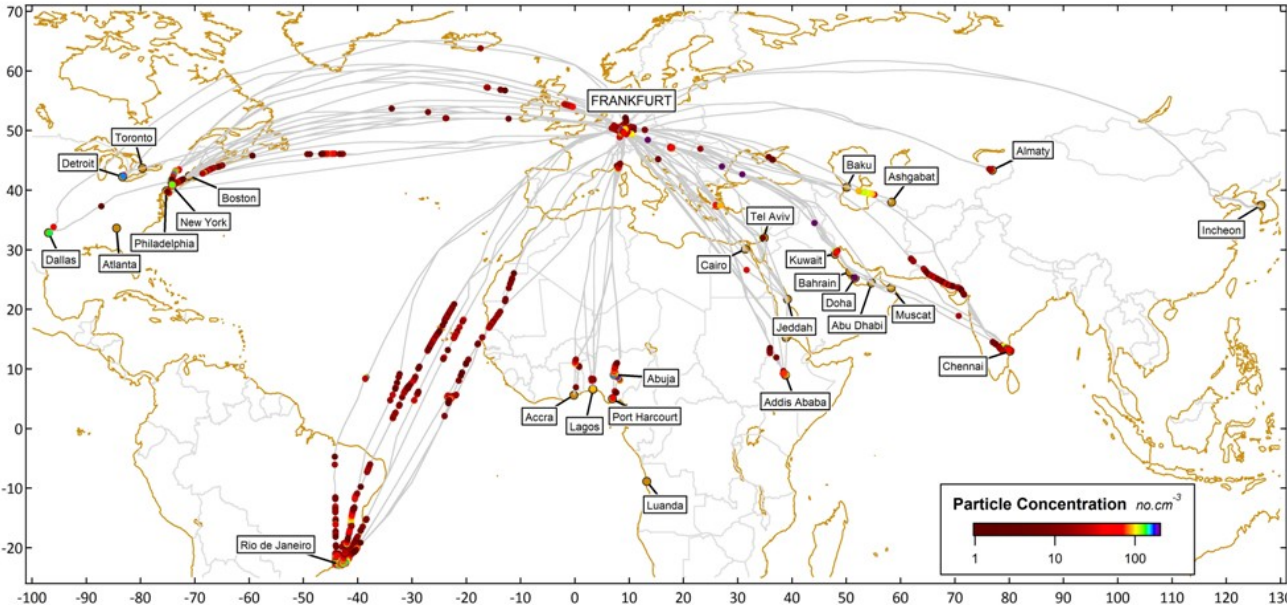

Figure 3

Table I lists the fraction of the 319 flights where clouds were encountered at cruise altitude and during the takeoff and landing phases. On 66% of the flights, the aircraft made vertical profiles of cloud as it took off or landed and in more than 50% of the flights, clouds were encountered at high altitude. The table also shows what fraction of the clouds had concentrations less or greater than $100 \ \mathrm{l}^{-1}$.

Table 1

Particle Characteristics	Take Offs/ Landings	Mid-Flight
Total Cloud Events	66%	54%
Low Concentration ($<100 \ \mathrm{L}^{-1}$)	11%	28%
High Concentration ($>100 \ \mathrm{L}^{-1}$)	50%	26%
Dust	14%	1%

The clouds that were encountered on takeoff and landings were a combination of all liquid water or mixed phase cloud, based on the recorded ambient temperature and those encountered at cruise altitude would have to be (most likely) all ice since temperatures were always lower than the required homogeneous freezing limit for water droplets. Most of the ice clouds were most likely thin cirrus, based on the measured number concentration; however, on at least one occasion the number concentrations were remarkably large, suggesting an encounter with deep convection. An example of this is shown in Figs. 4 and 5 for a cloud encounter over Nigeria when the aircraft was at an altitude of 11 km and the ambient temperature was -50°C, maximum number concentrations were more than $100{,}000 \ \mathrm{l}^{-1}$ and ice water content more than $1.0 \ \mathrm{gm}^{-3}$.
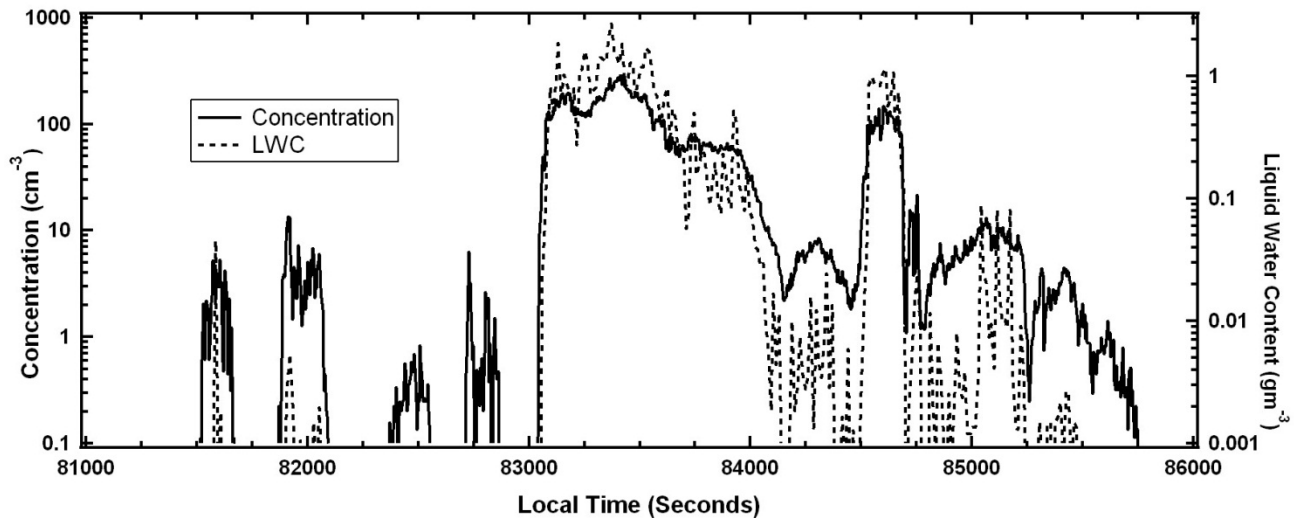
Figure 4

Figure 5 is a distribution of number and liquid water concentrations highlighted as a function of the optical diameter, where the liquid (ice) water content is derived assuming the particles are spherical with a density of 0.9 g cm^{-3}. This is an overestimate of the ice water content; however, the BCP is unable to provide information on the particle shapes, i.e. habit, when they are ice crystals. We see that the majority of the particles are less than 10 μm in size; however, there is a second mode in the number concentration spectra at around 70 μm. The particles in this size range contribute the most to the ice water mass.

Figure 5

4   OUTLOOK
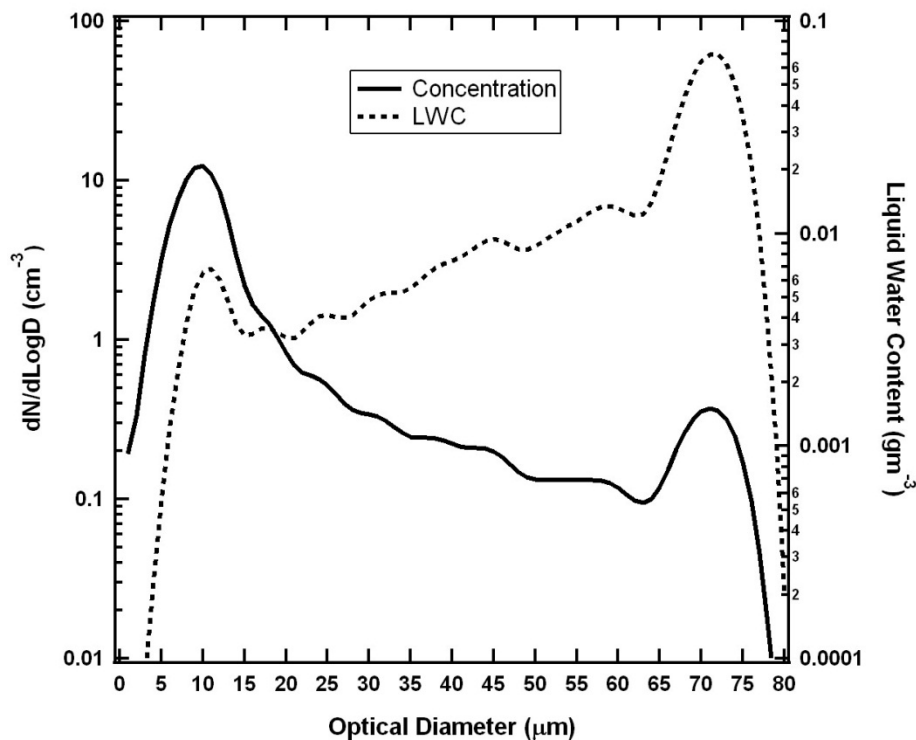
A number of BCPs, as part of the IAGOS instrument package, will be installed on other commercial airliners operated by Air France, Iberia Airlines and Cathay Pacific. IAGOS are consulting with several other airlines including Air China to incorporate these packages in the future. A total of 20 BCPs are expected to be flying within the next five years, providing extensive temporal and spatial

coverage worldwide that will be an invaluable resource for validating and complementing satellite measurements and climate model forecasts.

5 ACKNOWLEDGEMENTS

REFERENCES

Beswick, K., Baumgardner, D., Gallagher, M., and Newton, R.: The Backscatter Cloud Probe – a compact low-profile autonomous optical spectrometer, Atmos. Meas. Tech. Discuss., 6, 7379-7424, doi:10.5194/amtd-6-7379-2013, 2013.

Lance, S., C.A. Brock, D. Rogers and J.A. Gordon, 2010: Water droplet calibration of the Cloud Droplet Probe (CDP) and in-flight performance in liquid, ice and mixed-phase clouds during ARCPAC, Atmos. Meas. Tech., 3, 1683-1706, doi:10.5194/amt-3-1683-2010.

Effects of atmospheric turbulence and humidity on the structure of a contrail in the vortex phase

J. Picot[*], R. Paoli, O. Thouron, D. Cariolle
CERFACS, Toulouse, France

Keywords: contrail, turbulence, large-eddy simulations

ABSTRACT: The effects of atmospheric turbulence and humidity on the vortex phase of a contrail are analyzed using Eulerian-Lagrangian large-eddy simulations where turbulence is sustained via a stochastic forcing method. Humidity controls the fraction of surviving ice particles and ice growth rate, whereas turbulence controls the vortex breakup time when ice growth is enhanced by the mixing with supersaturated ambient air. On other hand, in supersaturated atmosphere, the maximum optical depth remains approximately constant over the simulation time.

1   INTRODUCTION

It is known that contrails form a line line-shaped ice clouds, but they can spread under favorable atmospheric conditions to form cirrus clouds that persist for hours and extend over areas of several square kilometers, becoming almost indistinguishable from natural cirrus. These "contrail cirrus" artificially increase cloudiness and are among the most uncertain contributors to the anthropogenic radiative forcing (Sausen et al, 2005, Lee et al, 2009). The modeling and simulation of contrail cirrus in the diffusion phase requires suitable initial conditions that have to be deduced form detailed large-eddy simulations resolving the fine scale features of the wake during the vortex phase. This problem has been addressed in the past by various authors with the focus on different aspects of the problem, often in the optic of a sensitivity analysis (Unterstrasser and Gierens, 2010a, Unterstrasser and Gierens, 2010b). In this work the focus is laid on the effect of background turbulence and humidity in determining the characteristics of the contrail in the vortex phase. In particular atmospheric turbulence is sustained via a stochastic forcing approach (Paoli and Shariff, 2009), which is useful for insuring consistency with future studies covering wake ages beyond the vortex phase.

2   COMPUTATIONAL MODEL

The numerical code is NTMIX, a compressible Navier-Stokes solver coupled to a Lagrangian particle-tracking module for the ice phase. The code has been used in previous studies of wake vortex simulations including contrails (Paoli et al, 2004). The initial conditions are obtained from separate large-eddy simulations of the jet phase. The computational domain is a box of $L_x \times L_y \times L_z = 1$ km $\times$ 1 km $\times$ 400 m with $N_x \times N_y \times N_z = 519 \times 619 \times 100$, and $N_p = 2 \times 10^6$ clusters are transported each one representing $N_{pc} = 2 \times 10^8$ physical particles. The initial vortex profile is a Lamb-Oseen vortex pair with parameters chosen to match those of a B747. Two levels of atmospheric turbulence (case B: strong and D: weak) and two values of background humidity ($RH_i = 130$ and 95) were selected.

3   RESULTS

The contrail structure in the vortex phase is best observed in Fig. 2, which shows the particle spatial distribution colored with their radius at different wake ages and for different background turbulence. Fig. 1 shows that for the present 4 engines configuration, particles exhausted from the out-

---
[*] *Corresponding author:* Joris Picot, CERFACS, 42, Avenue Gaspard Coriolis, 31057 Toulouse Cedex 01, France. Email: joris.picot@cerfacs.fr

board jets are partially trapped inside the vortex cores ($t = 30$ s). Afterwards, although the effects of baroclinc torque and turbulence fluctuations (especially in the case of strong turbulence) tend to redistribute them in the vertical direction, most of the particles still reside in the primary wake at $t = 2$ min. As a consequence the largest ice crystals are found in the secondary wake because the same amount of the available supersaturation has to be shared among less particles.
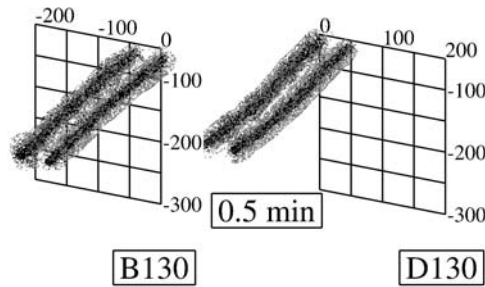

Fig. 1: Location of ice particles at $t = 30$ s. Particles emitted from the outboard jets are represented in black and particles emitted from the inboard jets are in grey.
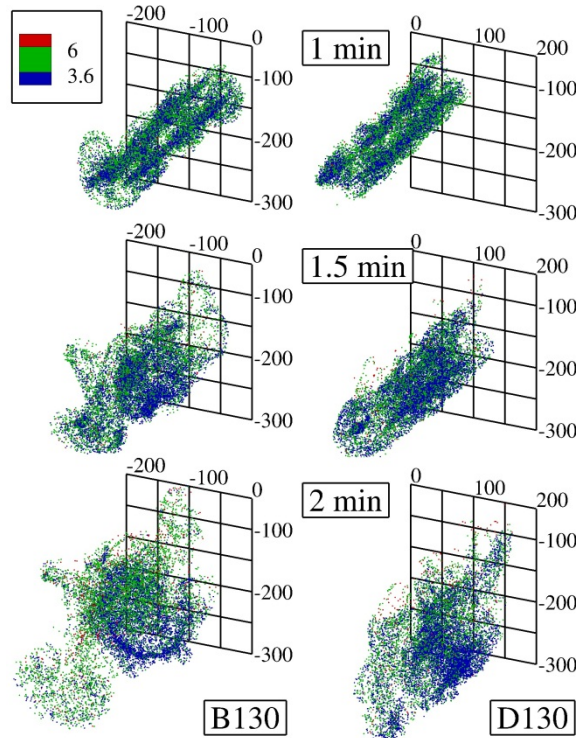

Fig. 2: Location of ice particles at different times. Particles are colored according to their diameter.

The effects of ambient conditions (turbulence and saturation) are shown in Fig. 3 (mean diameter of ice crystals) and Fig. 4 (number of surviving crystals). In the supersaturated cases, the mean radius initially grows due to the entrainment of external humid air (a process that starts already in the jet phase) and quickly reaches a plateau corresponding to a thermodynamic equilibrium with a saturation of 100 %. Afterwards, the saturation pressure in the interior of the contrail increases as the vortices descend into a warmer environment. In order to maintain thermodynamic equilibrium vapor pressure also increases, which leads to a slight ice sublimation (adiabatic compression, see Sussmann, 1999). When the vortices break up following Crow instability, ice crystals initially trapped inside the vortex pair are exposed to high ambient superaturation, which leads again to a quick growth of the mean radius. Depending on the ambient turbulence, break up time varies between 1.5 and 2 minutes. In the subsaturated case, ice starts to evaporate immediately (already at the end of the jet phase/beginning of the vortex phase) so the mean radius decreases monotonically. Background humidity controls the fractions of surviving ice crystals that is reported in Fig. 4. It can be observed that in the subsaturated case ice starts to sublimate completely (crystal loss) at a wake age of 1 min and about 90 % of ice crystal are lost at 3 min, while in the high supersaturated case less than 1 % of particles is lost overall. Fig. 5 finally shows the evolution of cross-sectional distribution of optical depth for the different cases analyzed. As expected, it attains the largest values in the su-

persaturated case. Furthermore, a double-peak structure identifying the two vortex cores appears at $t = 1$ min which later smoothes out as the contrail mixes with the ambient air. However, despite the decrease of concentration by dilution, the maximum value of optical depth is rather well maintained to around 0.3 up to 2.5 min, which in agreement with previous numerical studies (Paugam et al, 2010).
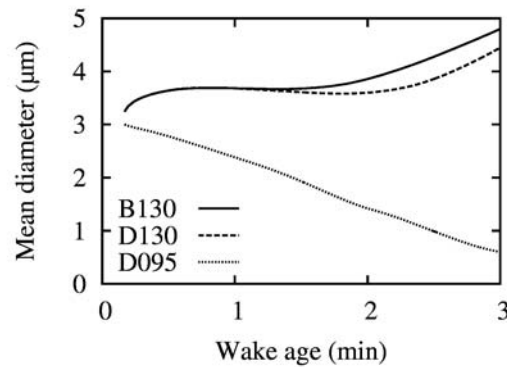

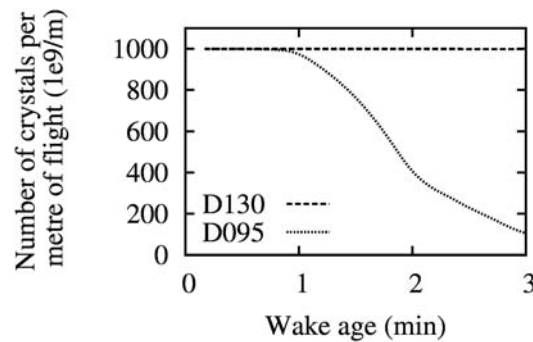Fig. 3: Mean diameter of ice crystals versus wake age.

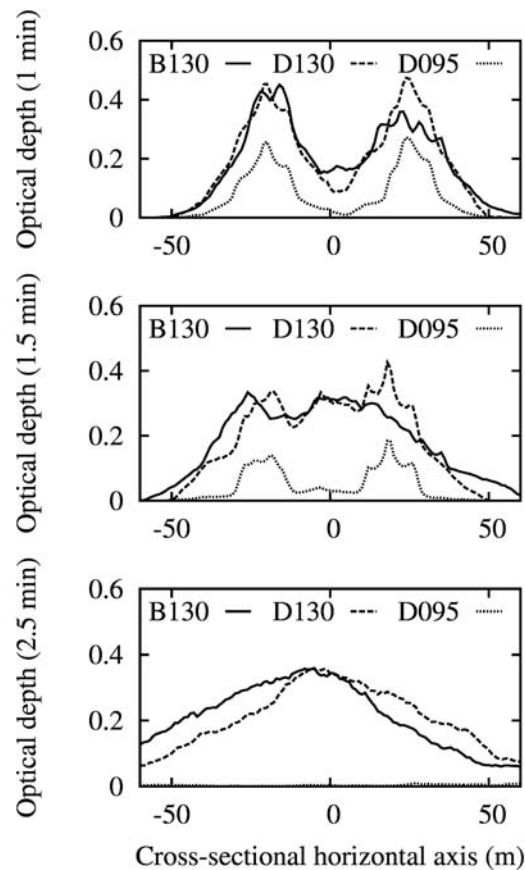Fig. 4: Number of surviving ice crystals per meter of flight versus wake age.

Fig. 5: Cross-sectional distribution of optical depth at different times.

4   CONCLUSIONS

The contrail evolution was simulated over the first three minutes for different background turbulence levels. The results showed that the growth of ice crystals is mainly controlled by humidity. Furthermore, in a subsaturated atmosphere, 90 % of ice crystals evaporate within 2 min. The optical depth is maintained at a value of 0.3 up to 2.5 min.

In the future we will extend the numerical simulations up to 30 min to 1 hour of contrail age to understand how and to which extent the ice growth and the microphysical parameters like optical depth are affected by atmospheric turbulence in the long term.

REFERENCES

Lee, D.S., Fahey, D.W., Forster, P.M., Newton, P.J., Wit, R.C.N., Lim, L.L., Owen, B., Sausen, R., 2009. Aviation and global climate change in the 21st century. *Atmos. Environ. 43*, 3520–3537.

Paoli, R., Hélie, J., Poinsot, T., 2004. Contrail formation in aircraft wakes. *J. Fluid Mech. 502*, 361–373.

Paoli, R., Shariff, K., 2009. Turbulent Condensation of Droplets: Direct Simulation and a Stochastic Model. *J. Atmos. Sci. 66*, 723–740.

Paugam, R., Paoli, R., Cariolle, D., 2010. Influence of vortex dynamics and atmospheric turbulence on the early evolution of a contrail. *Atmos. Chem. Phys. 10*, 3933–3952.

Sausen, R., Isaksen, I., Grewe, V., Hauglustaine, D., Lee, D.S., Myhre, G., Köhler, M.O., Pitari, G., Schumann, U., Stordal, F., Zerefos, C., 2005. Aviation radiative forcing in 2000: An update on IPCC (1999). *Meteorol. Z. 14*, 555–561.

Sussmann, R., Gierens, K.M., 1999. Lidar and numerical studies on the different evolution of vortex pair and secondary wake in young contrails. *J. Geophys. Res. 104*, 2131–2142.

Unterstrasser, S., Gierens, K., 2010a. Numerical simulations of contrail-to-cirrus transition – Part 1: An extensive parametric study. *Atmos. Chem. Phys. 10*, 2017–2036.

Unterstrasser, S., Gierens, K., 2010b. Numerical simulations of contrail-to-cirrus transition – Part 2: Impact of initial ice crystal number, radiation, stratification, secondary nucleation and layer depth. *Atmos. Chem. Phys. 10*, 2037–2051.

Numerical Modeling of contrail cluster formation

S. Unterstrasser [*], I. Sölch
DLR Oberpfaffenhofen, Institute of Atmospheric Physics, Germany

Keywords: Cloud resolving modelling, contrail, contrail-cirrus, contrail cluster, saturation effects

ABSTRACT: For the first time numerical simulations of contrail clusters were performed. Contrail clusters emerge when several contrails overlap. They may then interact with each other and compete for the available water vapour. Depending on the separation distance of the initial contrails and the prevailing wind shear conditions, the spreading of individual contrail can be strongly inhibited in contrail clusters. This implies that saturation effects occur and the climate impact of contrail, therefore, does not scale linearly with total fuel consumption or fleet kilometres of air traffic.

1 MOTIVATION

Aviation contributes to climate change via several pathways. The largest contribution is probably due to the formation of contrails which increases upper tropospheric cloudiness as they evolve into long-living contrail-cirrus (Burkhardt and Kärcher, 2011). Aged irregularly shaped contrail-cirrus can hardly be discriminated from natural cirrus in observations. Thus cloud resolving modelling is an appropriate tool to study contrail-cirrus evolution.

2 MODEL

The numerical simulations have been carried out with the non-hydrostatic anelastic model EULAG (Smolarkiewicz and Margolin, 1997) which employs the positive definite advection scheme MPDATA (Smolarkiewicz and Margolin, 1998) in its Eulerian operation mode. The subgrid turbulence model uses the TKE-approach. A microphysical module using Lagrangian tracking of ice crystals (Sölch and Kärcher, 2010) is fully coupled to EULAG and forms the version EULAG-LCM. With this model version the aggregation process in a mid-latitude cirrus cloud system (Sölch and Kärcher, 2011) or the contrail evolution during the vortex phase (Unterstrasser and Sölch, 2010) were studied recently, both in 2D and 3D. The microphysical module LCM uses an explicit representation of size-resolved non-equilibrium aerosol and ice microphysical processes. Within this study homogeneous/heterogeneous nucleation of ice and aggregation was switched off. Furthermore radiation effects are not considered here, although this can strongly alter the evolution of contrail-cirrus (Unterstrasser and Gierens, 2010), especially in a weakly stratified atmosphere. Synoptic scale updraft is prescribed via an external forcing term in the temperature equation in order to accommodate for the adiabatic temperature change. Details of the implementation can be found in Spichtinger and Gierens (2009).

3 SETUP

The 2D domain consists of nx = 4096 and nz = 301 grid points in horizontal and vertical direction, respectively. In both directions grid increments of $\Delta x = \Delta z = 10$ m are used and the domain size is correspondingly $L_x = 40.96$ km times $L_z = 3$ km. We use periodic boundary conditions in horizontal direction.

---

[*] *Corresponding author:* Simon Unterstrasser, DLR Oberpfaffenhofen, Institute of Atmospheric Physics, Münchner Straße 20, 82234 Weßling, Germany

The total simulated time is Tsim = 21600 s (= 6 hours). The time step is constant over one simulation and ranges between 0.75 s and 2.0 s depending on the vertical wind shear value.

The ambient relative humidity RHi* is uniformly 120% in the middle part of the domain (a 1 km deep layer). Above and below RHi* drops as shown in Fig.1 left. Turbulence induces fluctuations on the order of 5% around the mean state.
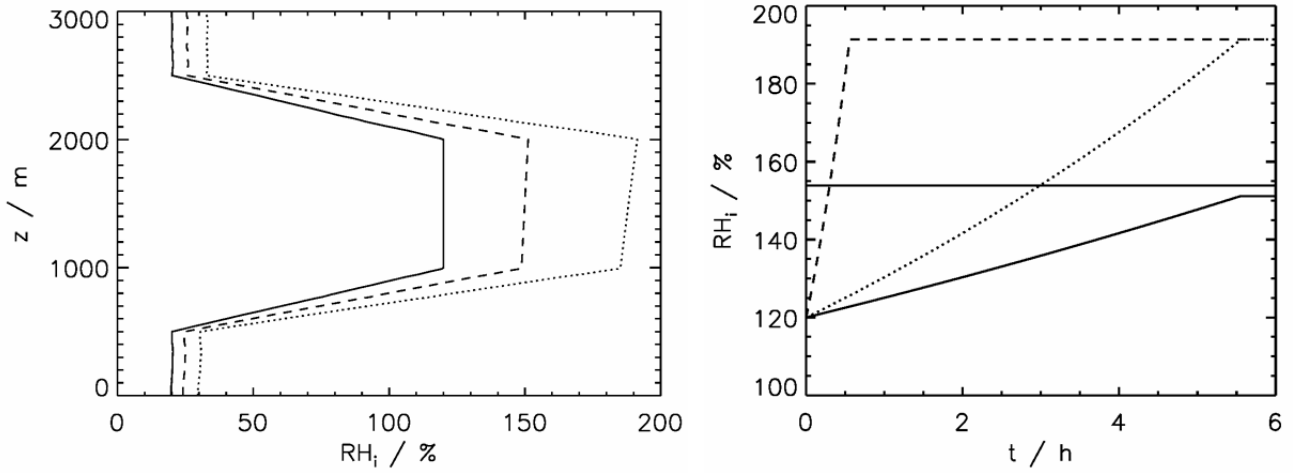

Figure 1, left. Vertical profile of background relative humidity RHi*in the beginning (solid) and after an adiabatic temperature reduction by 2K (dashed, w_{syn}=1 cm/s) or 4K (dotted, w_{syn}=2 and 20 cm/s). Right. Temporal evolution of relative humidity for updraft speeds w_{syn}=1 (solid), 2 (dotted) and 20 cm/s (dashed).

Synoptic scale updrafts of w_{syn} = 1, 2 and 20 cm/s are prescribed for various time spans of T_{updr} = 20000, 20000 and 2000 s, respectively. This results in an adiabatic cooling of 4 K or 2 K. Without ice the relative humidity with respect to ice would then reach 150% or 190% at an initial temperature of T* = 217 K. Subsequently the updraft comes to a halt and the background relative RHi* remains constant. The temporal evolution of relative humidity RHi*(t) is shown in Fig.1 right.

The turbulent velocity field was generated a-priori and the turbulent fluctuations have an rms-value of 0.12 m/s. The atmosphere is stably stratified with a Brunt-Väisälä frequency $N_{BV} = 10^{-2}$ s^{-1}. The impact of vertical wind shear is investigated and we perform simulations with shear rate s = 0.002, 0.004 and 0.006 s^{-1}.
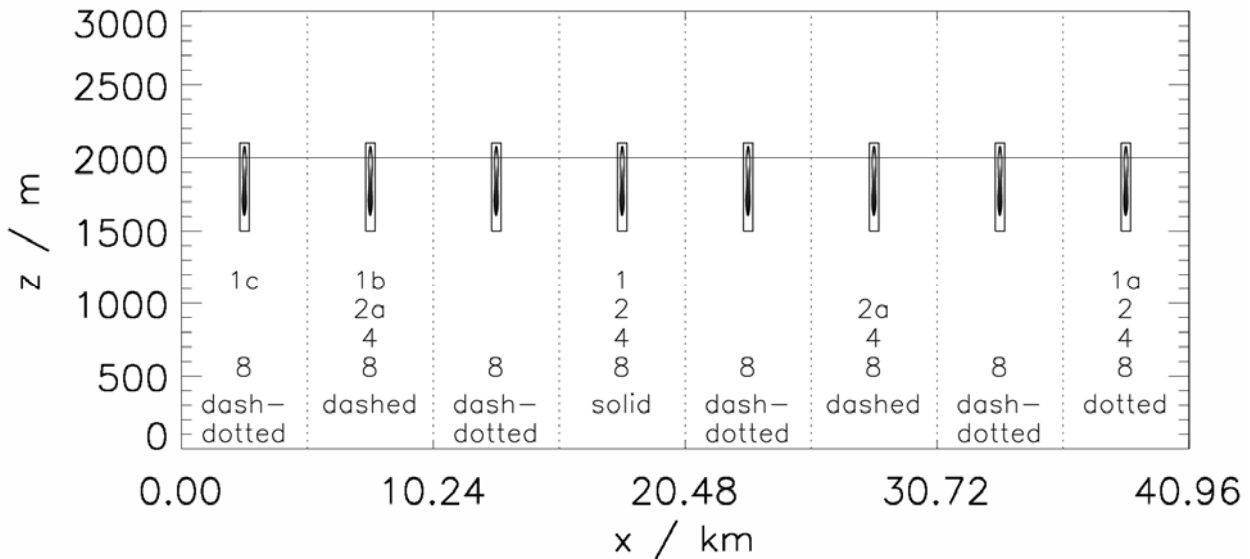
Figure 2. Contrail-cluster initialization with 5 minute old contrails is sketched. The black rectangles indicate the simulation domain of 3D vortex phase simulation. The cruise altitude is at z = 2000 m. Various scenarios with 1, 2, 4 or 8 contrails are used and the labels mark the selection of the contrail location(s) for different scenarios. We use several instances of 1-contrail (label 1, 1a, 1b and 1c) and 2-contrail (label 2 and 2a) simulations where the initial locations are horizontally shifted. Note the different scales on the x- and y-axis.

To initialise a set of contrails the domain is divided in 8 equal cells along the horizontal direction and in each cell a contrail may be present initially (depending on the setup). The contrails are centred within the 5.12 km broad cells. The simulations start with 1, 2, 4 or 8 contrails whose locations are shown in Fig. 2. In the contrail cluster scenario (cases with more than one contrail) the contrails have equal distances of 20.48, 10.24 or 5.12 km. For the single contrail case, the domain width had to be increased to 81.92 km in simulations with high wind shear in order to avoid a spurious interference via the periodic boundaries.

Although each individual contrail in the cluster faces the same ambient conditions and is equally separated to neighbouring ones, turbulent fluctuations trigger slight differences in growth histories for the members in the cluster. To guarantee more robust results, we repeated the simulations with one or two contrails where we shifted their initial horizontal position. In Fig. 2 the various initial positions are marked with 1, 1a, 1b and 1c as well as 2 and 2a, respectively. Overall, a set of 8 simulations is used to study saturation effects for one meteorological ambient state: one simulation with 8 contrails, one with 4 contrails, two with 2 contrails and four with 1 contrail.

The data for contrail initialization stems from a detailed 3D vortex phase simulation with EULAG-LCM. These results were averaged along flight direction for the 2D approach. The contrail was initially generated at the cruise altitude $z = z_{CA} = 2000$ m (labelled by a solid line in Fig. 2). The initial contrail is about 500 m deep and 100-300 m broad.

The geometrical configuration mimics an idealized contrail cluster in several aspects. First, the contrails are generated at the same time, i.e. only contrails of the same age interact. Second, the flight tracks of the contrail-producing aircraft are all parallel, i.e. perpendicular to the simulation domain cross-section. Third, the contrails are all generated at the same height.

The time $t = 0$ s corresponds to the beginning of the dispersion phase.

4   EXEMPLARY SIMULATION

We first discuss the contrail cluster evolution in an environment with $w_{syn} = 2$ cm/s and vertical wind shear $s = 0.004$ s^{-1} and compare configurations with one, two, four and eight contrails.
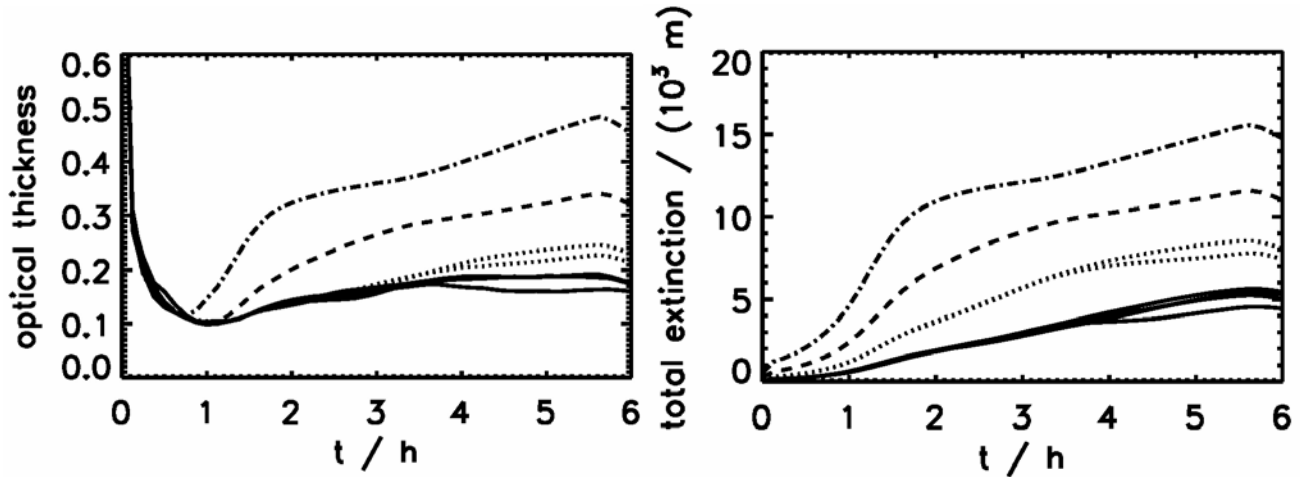
Figure 3. Temporal evolution of mean optical thickness and total extinction of a contrail cluster consisting of 8 (dash-dotted), 4 (dashed), 2 (dotted) or 1(solid) individual contrail(s) is shown. The ambient parameters are updraft speed w_{syn}=2 cm/s and vertical wind shear s=0.004 s^{-1}

During the first 30 minutes the mean optical depth of the contrail cluster (which still consists of well separated contrails at that stage) drops strongly as the young narrow contrails spread (Figure 3 left). After this initial dilution, depositional uptake of the ambient water vapour can compensate for the shear induced horizontal spreading and the optical depth starts to rise.

Contrails start to overlap as illustrated in Figure 4 left which shows the extinction of the 8-contrail case after 1 hour. The first overlap occurs after 40 min in the 8-contrail case and 80 min in the 4-contrail case. Concurrently, the optical depth increases more strongly than in the single contrail case.

Figure 4. The extinction of a contrail cluster consisting initially of 8 individual contrails is displayed. The snapshot shows a 1h (left) and 2h (right) old cluster. Ambient conditions as in Figure 3.

The quantity total extinction E is defined as the horizontal integral of extinction 1 - exp(-τ(x)):

$$E = \int (1 - e^{-\tau})dx \approx \tilde{\tau} \times \tilde{B}$$

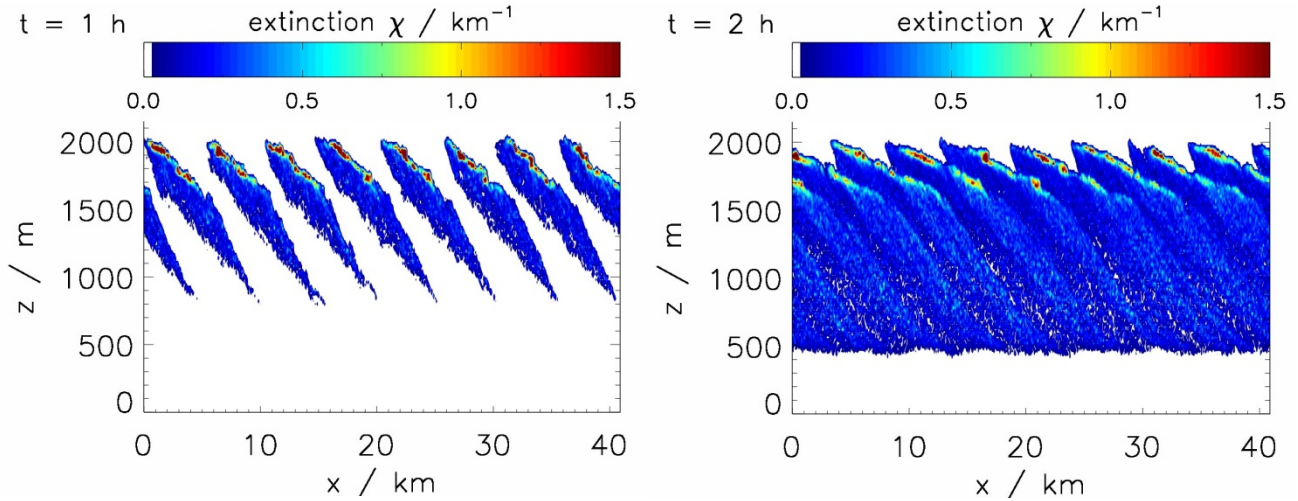Total extinction measures the disturbance of the shortwave flux. For small τ-values the approximation holds and E can be interpreted as product of a characteristic optical depth $\tilde{\tau}$ and width $\tilde{B}$ and thus comprises information on optical and geometrical properties of a contrail (cluster). Figure 3 right shows the temporal evolution of E. It increases over time as the contrails spread. Whereas in the single contrail case the rate of change is similar over 6 hours, the increase is decelerated in multi-contrail cases. This happens once the contrails start to intersect (as shown in Figure 4 right) and compete for the same available water vapour. We want to point out that for tilted contrails overlapping does not imply their immediate intersection as evinced in Figure 4. After 6 hours, the total extinction of the 8-contrail cluster is only 3 times larger than that of the single contrail. This means that each individual contrail is on average less than half as "strong" as a single isolated contrail.

5   SATURATION EFFECTS

To study saturation effects we first define the mean contrail impact $\bar{C}$ of an individual contrail in a cluster with n contrails as

$$\bar{C}(n) = \frac{1}{n} \int_0^{6h} E(t)\, dt$$

The above quantities E and $\bar{C}$ solely describe the properties of a contrail and cannot be related to contrail radiative forcing or a related energy metric in a straightforward way since the latter quantities additionally depend on many external parameters like surface albedo/temperature, solar zenith angle or the surrounding cloudiness. Ideally, $\bar{C}$ measures the "strength" of a contrail over its entire lifetime. Note that the simulation time of 6 hours may be too short to capture the whole lifecycle (depends primarily on the synoptic scenario).

Finally, $\bar{C}$ is normalized by the single contrail case

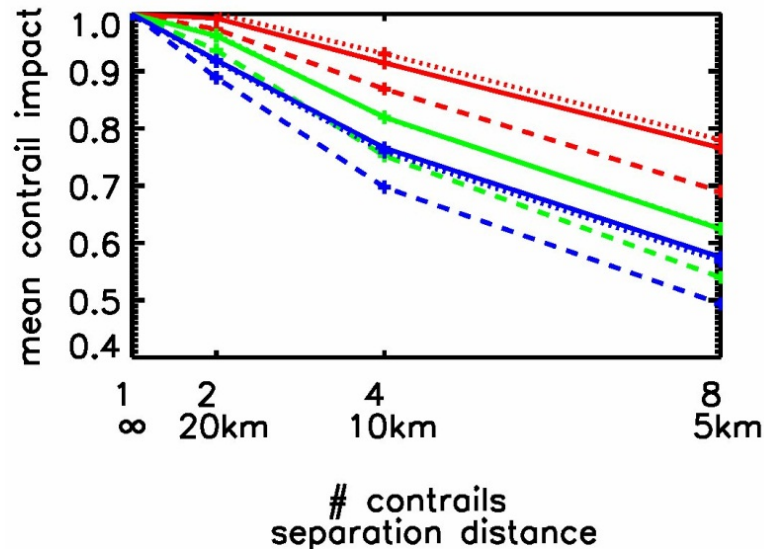$$\hat{C}(n) = \frac{\bar{C}(n)}{\bar{C}(1)}$$

Figure 5. Mean normalized contrail impact as a function of contrail number (i.e. contrail separation distance). Various vertical wind shear values s (0.002 s^{-1} red; 0.004 s^{-1} green; 0.006 s^{-1} blue) and synoptic scenarios w_{syn} (1 cm/s solid; 2 cm/s dotted; 20 cm/s dashed) are displayed. Note that the green dotted curve is hidden by the green solid line.

Figure 5 shows $\hat{C}(n)$ for the various synoptic scenarios and vertical wind shear values and gives a hint on how to improve estimates relying on some linear relationship between climate impact and air traffic measure. By definition all curves start at (1,1) and decrease as expected with increasing n. The saturation is stronger for higher wind shear. Although the synoptic scenarios are remarkably different, $\hat{C}(n)$ is not affected too much by this variation.

6   SUMMARY AND CONCLUSIONS

For the first time numerical simulations of contrail-clusters are performed. In this first step, idealized geometrical configurations are used, such that all contrails were produced at the same altitude, same time and in regular horizontal separations. We found that the spreading of contrails is inhibited, the smaller their initial separation and the higher the vertical wind shear is. The initial contrail separations reflect different levels of air traffic density. The simulations results suggest that in analytical climate estimates contrail properties should not be scaled linearly with air traffic density.

REFERENCES

Burkhardt, U. and B. Kärcher, 2011: Global radiative forcing from contrail cirrus. *Nature Clim. Change* 1 (1), 54–58.
Smolarkiewicz, P. and L. Margolin, 1997: On Forward-in-Time Differencing for Fluids: an Eulerian/Semi-Lagrangian Non-Hydrostatic Model for Stratified Flows. *Numerical Methods in Atmospheric and Oceanic Modelling: The Andre J. Robert Memorial Volume, edited by Lin, C., Laprise, R., and Ritchie, H., Canadian Meteorological and Oceanographical Society, Ottawa, Canada* 35, 127–152.
Smolarkiewicz, P. and L. Margolin, 1998: MPDATA: A Finite-Difference Solver for Geophysical Flows. *Journal of Computational Physics* 140, 459–480.
Sölch, I. and B. Kärcher, 2010: A large-eddy model for cirrus clouds with explicit aerosol and ice microphysics and Lagrangian ice particle tracking. *Quarterly Journal of the Royal Meteorological Society* 136, 2074–2093.
Sölch, I. and B. Kärcher, 2011: Process-oriented large-eddy simulations of a midlatitude cirrus cloud system based on observations. *Quarterly Journal of the Royal Meteorological Society* 137, 374–393.
Spichtinger, P. and K. M. Gierens, 2009: Modelling of cirrus clouds – Part 1b: Structuring cirrus clouds by dynamics. *Atmospheric Chemistry and Physics* 9, 707–719.

Unterstrasser, S. and K. Gierens, 2010: Numerical simulations of contrail-to-cirrus transition - Part 2: Impact of initial ice crystal number, radiation, stratification, secondary nucleation and layer depth. *Atmospheric Chemistry and Physics* 10, 2037–2051.

Unterstrasser, S. and I. Sölch, 2010: Study of contrail microphysics in the vortex phase with a Lagrangian particle tracking model. *Atmospheric Chemistry and Physics* 10, 10003–10015.

Formation conditions and simulations of contrails from hybrid engines of a future Blended Wing Body aircraft

K. Gierens [*], S. Unterstrasser
DLR-Institut für Physik der Atmosphäre Oberpfaffenhofen, Germany

ABSTRACT: A novel propulsion system using in particular two combustion chambers in series, the first one burning liquid hydrogen or liquid natural gas and the second one burning biofuel under flameless conditions, is proposed by the AHEAD (Advanced Hybrid Engines for Aircraft Development) project under EC Framework Program 7. The goal is to provide a breakthrough technology that is needed to achieve the challenging targets laid out in Vision 2020 and Flight Path 2050. Environmental aspects as potential climate impacts have been considered right from the beginning of the project. In this contribution we describe the consequences of the new engine concept for contrail formation. It is shown that because of the increased emission of water vapour compared to a conventional combustion system, contrails would form in a much deeper layer beneath the tropopause. As the new hybrid engine is designed for a blended wing-body (BWB) aircraft, we additionally perform numerical simulations of contrail formation and vortex phase from a BWB with three centrally installed hybrid engines.

1 INTRODUCTION

Recent ACARE studies indicate that the targets laid out in Vision 2020 (i.e. CO_2 and noise reduction by 50%, NO_x reduction by 80%) and in Flight Path 2050 (CO_2 −75%, noise −65%, NO_x −90% relative to year 2000) cannot be achieved using current incremental technological improvements. There is an urgent need for breakthrough technologies.

The hybrid engine proposed in the European Commission's Framework Program 7 project AHEAD (Advanced Hybrid Engines for Aircraft Development) is a novel propulsion system with a different architecture as compared to the conventional turbofan engine. The hybrid engine uses in particular a dual hybrid combustion system (using hydrogen and biofuel under flameless conditions to reduce CO_2 and NO_x emission respectively). The hybrid engine proposed in AHEAD will constitute a leap forward in terms of environmental friendliness, and will enable the design of fuel-efficient Blended Wing Body (BWB) aircraft configurations. The project aims to establish the feasibility of proposed hybrid engine configuration and will demonstrate that the concept will substantially lower the engine emissions, installation drag and noise. The BWB configuration along with the proposed hybrid engine concept will bring in the much required breakthrough in civil aviation. Special attention will be directed to evaluate the effect of H_2O emission and contrail formation on the environment.

Here we report on the modification of the Schmidt-Appleman criterion required for the hybrid engine. Both a LH2 (liquid hydrogen fuel) version and a LNG (liquid natural gas, i.e. methane) version have been considered. Consequences for the expected climate effects are discussed. Numerical simulations of contrails from the proposed BWB aircraft with three hybrid engines have been performed. They will be compared with contrails from conventional engines.

---

[*] *Corresponding author:* Klaus Gierens, DLR-Institut für Physik der Atmosphäre, Oberpfaffenhofen, D-82205 Wessling, Germany. Email: klaus.gierens@dlr.de

2 CONTRAIL FORMATION

2.1 *The Schmidt-Appleman criterion*

The Schmidt-Appleman criterion has been explained several times in the series of AAC and TAC conferences, it is not necessary to repeat this here. For understanding the rest of the paper it suffices to state that the essence of the criterion is captured in one quantity, *G*, that is the ratio of the rates of change of water vapour partial pressure change and temperature in the expanding jet exhaust plume. *G* is given as

$$G = (\varepsilon^{-1} c_p \, p \, EI_{H2O}) / [Q(1-\eta)].$$

G depends on ambient pressure *p*, fuel properties (emission of water vapour per kilogram fuel burnt, EI_{H2O}, and heat energy per kilogram fuel burnt, *Q*), and on the overall propulsion efficiency, η (Schumann, 1996). c_p is the specific heat of air at constant pressure, and ε is the ratio of the molar masses of water and air. Using different fuels, the fuel specific values in this quantity become different, and a different propulsion system will also have a different overall propulsion efficiency. Thus these quantities have to be determined for the hybrid engines before statements on their contrail formation can be made.

2.2 *Contrail formation conditions for the LH2 and LNG versions of the AHEAD aircraft*

In the following table 1 we present the water vapour emission index EI_{H2O}, the heat value *Q*, the overall propulsion efficiency η, and the factor *g* (which is the factor *G*, taken in Pa/K, divided by the ambient pressure *p*, taken in hPa, so that *g* consists only of aircraft and fuel specific quantities), i.e.

$$g:=(G_{AHEAD}/p)/[(Pa/K)/hPa].$$

Using engine design specifications from the TU Delft (Rao, personal communication) these quantities have been computed for both versions of the AHEAD designs.

Table 1: Characteristic figures determining the slope of the mixing trajectory, *G*, in the Schmidt-Appleman criterion for the LH2 and LNG versions of the AHEAD engine designs.

version	EI_{H2O} (kg/kg)	*Q* (MJ/kg)	η	*g*
LH2	7.21	101.2	0.396	1.91×10^{-2}
LNG	2.15	49.3	0.389	1.17×10^{-2}

For comparison: for conventional kerosene aircraft, assuming similar η as for the AHEAD ones, $g=7.74\times10^{-3}$. Thus the mixing trajectory for an AHEAD engine is at least 2.45 (LH2) or 1.52 (LNG) times as steep as that of a present day conventional aircraft, that is, the propensity for contrail formation is much larger.

2.3 *Consequences*

The following figure 1 shows the Schmidt–Appleman criterion for a conventional aircraft (assuming $\eta = 0.333$) and for both the LH2 and LNG versions of AHEAD. Contrails are possible if the atmospheric properties (temperature and water vapour pressure) are left of the respective threshold mixing trajectory (thick straight lines). Evidently, both AHEAD versions allow contrail formation in a much wider area of the parameter space than the conventional aircraft. The trajectories have been computed for an ambient pressure of 200 hPa.
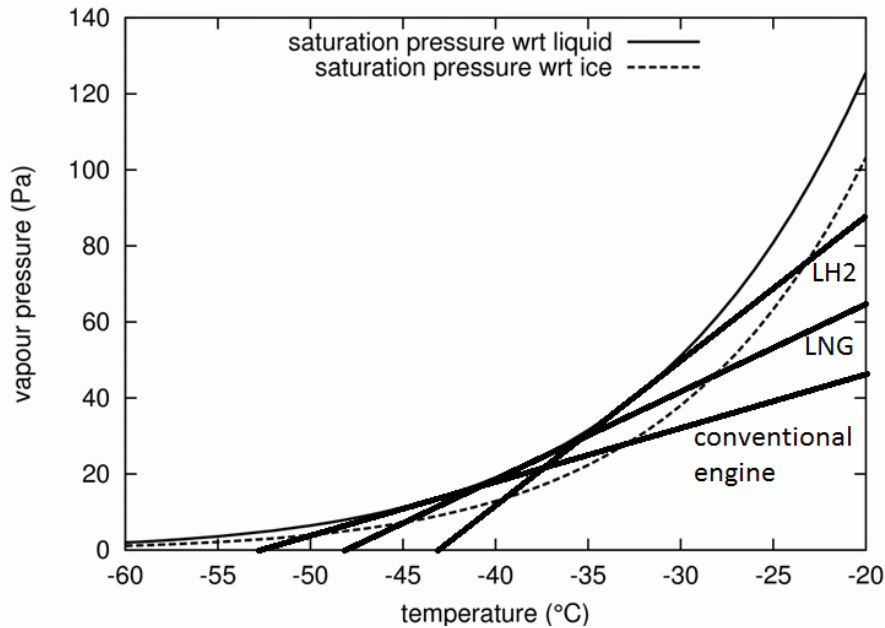
Figure 1: *(T, e)*–phase diagram showing the Schmidt–Appleman threshold trajectories (thick straight lines) for a conventional aircraft together with two versions of AHEAD aircraft. The respective threshold temperature for contrail formation is given by the tangent point of the trajectories with the liquid saturation curve (thin solid curve).

The steeper mixing trajectories of AHEAD imply not only higher contrail formation temperature thresholds than for conventional engine but also a much larger altitude range in the troposphere where contrails can form, because the temperature typically decreases by about 6 to 10 K per km with altitude. Contrail formation would start for the LNG version roughly 1 km lower (7 to 8 km) than for a conventional engine and even 2 km lower (6.5 to 7 km in a mean, e.g. US Std., atmosphere) with the LH2 version.

2.4 *Considering design cruise altitudes*

The optimum flight altitudes for the AHEAD blended wing body aircraft are much higher than for conventional aircraft, 11.9 km (initial cruise), 13.2 km (mid cruise), and 14.4 km (end cruise). These altitudes correspond to the following pressures in the US Standard and tropical Standard Atmospheres (in hPa): 196/216, 160/177, 132/146. These altitudes are mostly in the stratosphere north of 45°N (see Hoinka, 1998, figure 10 and Hoinka, 1999, figure 1). As the stratosphere is very dry, only very short contrails can usually be formed there. Thus AHEAD BWBs will cause contrails mainly when flying south of 45°N and more often when flying south of 30°N, i.e. in the tropics. From Hoinka (1999, figure 5) we find that the mean water vapour mixing ratio in these regions of the atmosphere is of the order 10 ppmv. In spite of this low value, ice supersaturation is quite frequent (Spichtinger et al., 2003). Thus we must expect that BWBs will produce contrails frequently when flying in the tropics. However, the contrails will generally be optically thin because the amount of condensable water vapour is low. To see this, let us assume the temperature of the 1976 US Std. Atm., which is 216.65 K for all three cruise levels. The ice saturation pressure is 1.7 Pa at this temperature. At a ten degree higher temperature typical for midlatitude cruise levels the ice saturation pressure is 6.0 Pa, i.e. more than a factor of three higher. Thus one may estimate that a BWB contrail in the tropics will on average contain smaller ice mass than a contrail produced in mid-latitudes cruise levels by a normal aircraft.

However, this does not imply a small or even negligible climate impact. The problem is probably not the direct effect of the contrails but rather that it will potentially consist of very small ice crystals (depending on the so far unknown soot emission). These small ice crystals have very weak tendency to sediment or coagulate, thus they can stay very long time in the TTL and thus have a relatively large impact integrated over their life time. Fortunately, the maximum cruise altitude of the BWBs is below 15 ± 0.5 km, i.e. still in levels where radiation is cooling the air which leads to subsidence (Gettelman et al., 2004) and finally to sublimation of the ice crystals.

3 NUMERICAL SIMULATIONS OF BWB CONTRAILS

3.1 *Setup*

3D numerical simulations of contrails from BWB aircraft have been performed using the EuLag code (Prusa et al., 2008) together with a Lagrangian ice microphysics code (Sölch and Kärcher, 2010). Recent contrail simulations with this code have been performed by Unterstrasser and Sölch (2010); their paper should be consulted for more details. The AHEAD simulations are peculiar for the special geometry of the three engines, which are located close to the centre of the aircraft, and for the ice and water content of the exhaust plume.

We use a domain of $200 \times 384 \times 600$ m^3 in the three dimensions flight direction × span × height. The grid boxes are $2 \times 1 \times 1$ m^3 in these dimensions and the time step is 0.03 s initially up to 50 s simulation time, then 0.05 s up to 190 s and finally 0.08 s until the simulation ends at 310 s. The simulation starts at an assumed plume age of about 2–3 s, that is, 5 to 10 spans behind the aircraft, when the microphysical process of ice formation is already terminated and the roll–up process of the wing–tip vortices is in an advanced state.

For the initial exhaust distribution we assume that a rectangle of 20×8 m^2 is filled homogeneously with the emitted water vapour and the ice crystals that have formed almost immediately (within a fraction of a second after exhaust, about one wingspan after engine exit). The number concentration of the ice crystals depends on the soot emission and we simply assume here that the Kerosene burning produces soot at a rate typical for conventional engines. The mass concentration of the ice crystals is assumed to equal the water vapour emission, which is completely transformed into ice. Using these assumptions we have an initial ice concentration of 3×10^{-2} kg m^{-1} and 0.51×10^{12} m^{-1} (per metre of flight path).

For the flowfield behind the BWB aircraft we used a pair of vortices in analogy to conventional aircraft (after private communication with Dr. Martin Hepperle from the DLR Institute of Aerodynamics and Flow Technology). The simplification of assuming a pair of counterrotating vortices centred at about 90% span is considered justified in the farfield, i.e. 5 to 10 spans behind the aircraft. Thus the plume is modelled as a pair of Lamb–Oseen vortices 500 m above the bottom of the model domain, with core radius of 4 m. From weight, speed and span of the BWB we then computed the initial vortex strength (550 m^2 s^{-1}).

For the atmospheric conditions we chose a tropical atmosphere at about 13 km altitude, an ambient temperature of 217 K, a Brunt-Väisällä frequency of 1.184×10^{-2} s^{-1} and a relative humidity with respect to ice of 120%. The latter is a moderate supersaturation value that guarantees that the contrail would be persistent, but natural cirrus formation via homogeneous freezing of ambient liquid aerosol droplets would not yet commence.

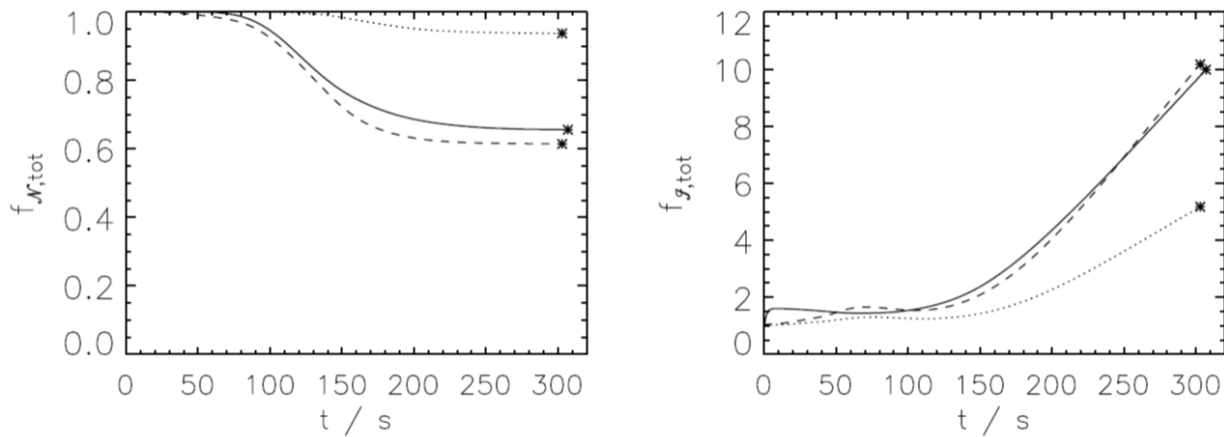### 3.2 *Results of simulations*

Figure 2: Temporal evolution of the total ice number (left) and mass (right) normalised with their initial values for three different cases: The BWB contrail (dotted), a standard aircraft (solid), and a hypothetical BWB contrail but with standard kerosene fuel (dashed).
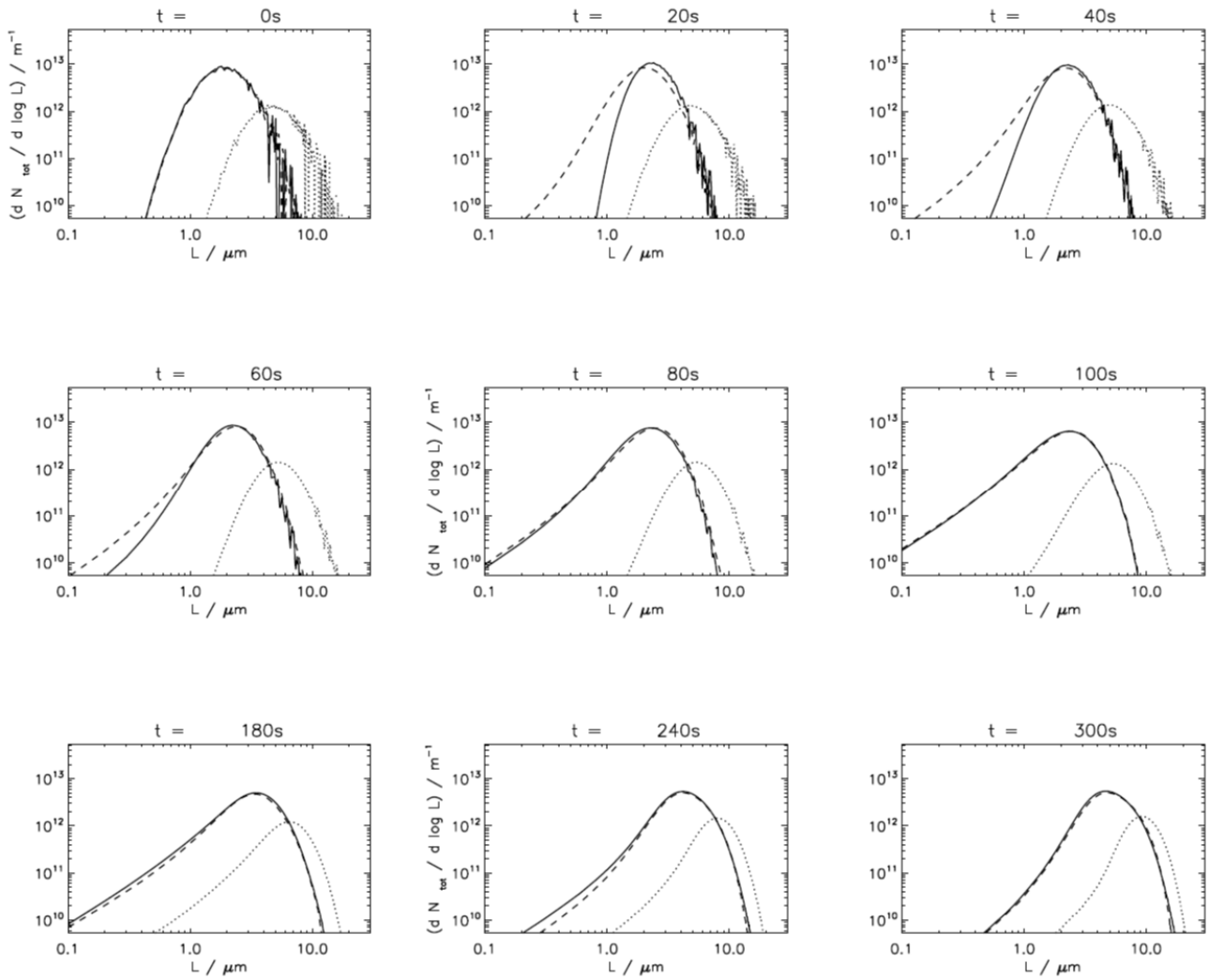
Figure 3: Temporal evolution of the ice crystal size distribution (expressed as the maximum dimension in μm) for three different cases: The BWB contrail (dotted), a conventional aircraft (solid), and a hypothetical BWB contrail but with standard kerosene fuel (dashed). The contrail ages are indicated in each panel and increase from top left to bottom right.

Here we only show the evolution of the crystal size spectra, other results will be presented elsewhere. Figures 2 and 3 show the temporal evolution of the total ice crystal number and ice mass and their size distribution. Three cases are compared to allow a better justification of the environmental benefit of the BWB in terms of contrail formation and their probable climate impact. These are (1) the BWB itself with the hybrid engines (dotted lines), (2) a standard aircraft (A340 of B747 type, solid lines), and (3) a hypothetical aircraft with BWB geometry but with standard kerosene combustion (dashed). Ice crystal number and mass in figure 2 are normalised by their initial values. First we note both in figures 2 and 3 that the difference between the solid and the dashed lines are much smaller than the difference of these with the dotted lines. This shows that the contrail properties depend stronger on the composition of the exhaust (water and soot particles) than on the aircraft geometry (wing shape and position of the engines), as long as the wing span and aircraft weight and speed are similar. In all cases there is some crystal loss due to sublimation in the downward travelling vortex pair, but the fraction of crystals that get lost is larger for the conventional and pure kerosene aircraft than for the BWB (figure 2 left), obviously because the smaller crystals of the conventional and kerosene aircraft can be sublimated more easily than the bigger crystals of the BWB contrail. However, the BWB contrail consists of much less ice crystals than a contrail of conventional aircraft. The shrinking and eventual sublimation of ice crystals is signified in figure 3 by the growing left tails of the distribution curves (indication of a growing fraction of very small crystals). In spite of this sublimation the total ice mass increases eventually. This occurs in the secondary wake where ambient air is not disclosed from the contrail ice as it is in the quickly rotating primary vortex pair. Since the BWB contrail contains less ice crystals than the other considered contrails,

the mass growth rate is smaller in this case. However, the total ice mass in a contrail is sooner or later determined by the ambient humidity such that differences after 5 minutes evolution are more or less insignificant (Unterstrasser and Gierens, 2010). It is the size and the number of ice crystals that become important for the contrails climate impact. Larger and less ice crystals as in the BWB case imply (1) smaller optical thickness of the contrail and (2) larger crystal fall speeds and thus (3) shorter lifetime than in the cases with conventional aircraft or pure kerosene combustion. If these results are correct (depending on the actual number emission index of soot particles, which was only estimated here, see above) the contrail climate impact of BWB aircraft is expected to be smaller than that of conventional aircraft.

4   SUMMARY AND CONCLUSIONS

Revised Schmidt-Appleman criteria have been obtained for dual combustion engine designs in the framework of the AHEAD project and numerical simulations of early contrail evolution for blended wing body aircraft equipped with such engines have been performed as an effort to estimate the environmental impact of such novel aircraft design. The following results have been obtained:
- The threshold altitude for contrail formation of AHEAD BWB is about 1 to 2 km lower than for conventional aircraft.
- However, design cruise altitude of AHEAD BWB is significantly higher than that of conventional aircraft. Thus:
  - mid and high latitudes: contrail formation mainly during ascent and descent; cruise altitudes in stratosphere.
  - tropics: frequent contrail formation, but fortunately below the average level of zero radiation flux divergence (i.e. subsiding air, thus constrained survival times of ice crystals).
- If soot emission index is as for conventional aircraft, then ice crystals in BWB contrail are on average larger and of smaller number than in conventional aircraft contrails. This would imply lower optical thickness and shorter life time.
- Water vapour emission in the stratosphere can be a problem.

REFERENCES

Gettelman, A., P.M. de F. Forster, M. Fujiwara, Q. Fu, H. Vömel, L.K. Gohar, C. Johanson, and M. Ammerman, 2004: Radiation balance of the tropical tropopause layer. J. Geophys. Res., 109, D07103, doi:10.1029/2003JD004190.
Hoinka, K.P., 1998: Statistics of the global tropopause pressure. Monthly Weather Rev., 126, 3303–3325.
Hoinka, K.P., 1999: Temperature, humidity, and wind at the global tropopause. Monthly Weather Rev., 127, 2248–2265.
Prusa, J., P. Smolarkiewicz, and A. Wyszogrodzki, 2008: EULAG, a computational model for multiscale flows. Computers and Fluids, 37, 1193–1207.
Schumann, U., 1996: On conditions for contrail formation from aircraft exhausts. Meteorol. Z., 5, 4–24.
Sölch, I., and B. Kärcher, 2010: A large–eddy model for cirrus clouds with explicit aerosol and ice microphysics and Lagrangian ice particle tracking. Q. J. R. Meteorol. Soc., 136, 2074–2093, doi:10.1002/qj.689.
Spichtinger, P., K. Gierens, and W. Read, 2003: The global distribution of ice–supersaturated regions as seen by the Microwave Limb Sounder. Q. J. R. Meteorol. Soc., 129, 3391–3410.
Unterstrasser, S., and K. Gierens, 2010: Numerical simulations of contrail-to-cirrus transition - Part 2: Impact of initial ice crystal number, radiation, stratification, secondary nucleation and layer depth. Atmos. Chem. Phys., 10, 2037–2051.
Unterstrasser, S., and I. Sölch, 2010: Study of contrail microphysics in the vortex phase with a lagrangian particle tracking model. Atmos. Chem. Phys., 10, 10003–10015, doi:10.5194/acp-10-10003-2010.

Contrail Detection in the Northern Hemisphere: Methods and Results

David P. Duda[*], Sarah Bedka, Robyn Boeke, Thad Chee, Konstantin Khlopenkov, Rabindra Palikonda, Doug Spangenburg
Science Systems and Applications, Inc., Hampton, VA

Patrick Minnis
Science Directorate, NASA Langley Research Center, Hampton, VA

Keywords: Contrail, optical properties, radiative forcing

ABSTRACT: Previous estimates of linear contrail coverage and contrail optical properties have been produced only regionally with a variety of satellite platforms and observation methods, and large uncertainties in global contrail properties remain. A consistent global observational dataset of linear contrail coverage and optical properties using a single satellite with the same methodology is needed to reduce our uncertainties. Here, we develop a Northern Hemisphere contrail climatology to provide a consistent empirical estimate of contrail coverage, radiative forcing and optical properties. The automated contrail detection algorithm (CDA) of Mannstein et al. is modified to use additional thermal infrared channels available from the Moderate Resolution Imaging Spectrometer (MODIS) onboard the *Aqua* satellite, and commercial aircraft flight data from the AEDT (Aviation Environment Design Tool) database to screen out false detections in the CDA and to compute linear contrail coverage over the Northern Hemisphere from *Aqua* MODIS imagery during 2006. The Northern Hemisphere estimates of annual mean linear contrail coverage range from 0.067 to 0.37 percent. The contrail coverage data are then used to compute several other contrail-related parameters including contrail cirrus coverage, contrail optical properties, and contrail radiative forcing. The contrail climatology is under development, and is expected to produce a contrail property dataset from two years of *Aqua* and Terra MODIS data.

1   INTRODUCTION

Clouds are an important part of the atmospheric radiation system. Changes in cloud cover can alter the radiation budget and may ultimately influence climate. Because cirrus clouds form at high altitudes and are often optically thin, they tend to cause a warming of the Earth-atmosphere system. Persistent contrails are aircraft-generated cirrus clouds that form in regions of ice-supersaturation at temperatures less than -39°C. Thus, they add to the naturally occurring cloud cover and may also be important to climate.

Several studies have attempted to estimate linear contrail coverage and contrail optical properties over high air-traffic regions. An early study by Bakan et al. (1994) visually analyzed AVHRR IR imagery to estimate linear contrail coverage over the eastern North Atlantic Ocean and northwestern Europe. The Bakan et al. regional estimate was extrapolated with air traffic data to obtain a global linear contrail coverage estimate of 0.087%. This result has been used in several studies to estimate global contrail radiative forcing (e.g., Penner et al., 1999). Mannstein et al. (1999) developed an objective linear contrail detection algorithm (CDA) and applied it to AVHRR data over central Europe, and determined a regional annual coverage of approximately 0.2%. Meyer et al. (2002) re-estimated coverage over Europe with the CDA and computed a mean contrail optical depth of 0.11. Several researchers have applied the CDA and cloud retrieval algorithms over different regions of the globe (Meyer et al. (2007), Southeast Asia; Palikonda et al (2005), contiguous

---

[*] *Corresponding author:* David P. Duda, Science Systems and Applications, Inc., 1 Enterprise Parkway, Suite 200, Hampton, VA 23666; email:david.p.duda@nasa.gov

United States; Minnis et al. (2005), north Pacific) to determine contrail coverage and optical properties, but the studies have used data from different AVHRR sensors, each with a different sensitivity to contrails. No satellite-based global estimate of linear contrail coverage and optical properties has been completed.

Another obstacle in assessing the possible impacts of contrail coverage on climate is determining the total contrail cirrus coverage from the observed linear coverage. Minnis et al. (1998) used GOES data to track contrails and found substantial cirrus formation within linear contrails, leading to the conclusion that the overall effect of contrail cirrus must be greater than from linear contrails. Duda et al. (2004) and Minnis et al. (2004) concluded that contrail cirrus increases the contrail coverage by a factor of two, while Mannstein and Schumann (2005) estimated that contrail cirrus coverage might be as large as ten times the detectable linear coverage. Mannstein et al. (2010) determined from comparisons with surface-based camera imagery that the CDA might be underestimating contrail coverage by a factor of 1.5 to 6. Although it appears likely that linear contrail coverage has been underestimated, contrail cirrus coverage is also very uncertain. To address these concerns a consistent global observational dataset of linear contrail coverage and optical properties using a single satellite with the same methodology is needed to reduce our uncertainties. Here, we develop a Northern Hemisphere contrail climatology to provide a consistent empirical estimate of contrail coverage, radiative forcing and optical properties. Several research programs including ACCRI (Aviation-Climate Change Research Initiative) have recognized that such a database would be a valuable first step towards a more realistic representation of contrails and cirrus within climate models for model improvement and validation. As the Northern Hemisphere accounts for over 90% of the global air traffic, this climatology would attempt to measure nearly all of the global linear contrail coverage.

The next section describes the refinements made to the original Mannstein et al. CDA used in this study. Section 3 discusses how waypoint data from the AEDT database (Wilkerson et al., 2010) are used to improve estimates of contrail coverage by screening out false detections. Section 4 shows samples of the screened contrail coverage results and methods to extend the contrail detection method to contrail cirrus, and the final section briefly describes related studies that use the contrail coverage data to compute contrail optical properties and contrail radiative forcing.

2 METHODOLOGY

The contrail detection algorithm (CDA) used in this study is a modified version of the technique described by Mannstein et al. (1999), which detects linear contrails in multi-spectral thermal infrared (IR) satellite imagery using only two channels (11 and 12 μm) from the Advanced Very High Resolution Radiometer (AVHRR) onboard polar-orbiting NOAA satellites. This method requires only the brightness temperatures (BT) from the IR channels, with no other ancillary data, and can be applied to both day and night scenes. It uses a scene-invariant threshold to detect cloud edges produced by contrails, and 3 binary masks to determine if the detected linear features are truly contrails. However, these masks are not always sufficient to remove all non-edge features. To reduce the number of false positive detections due to lower cloud streets and surface features, we add observations from other IR radiance channels (8.6 and 13.3 μm) available on the MODerate-resolution Imaging Spectroradiometer (MODIS) on the *Aqua* satellite. The modified method uses additional masks derived from the added thermal infrared channels to screen out linear cloud features that appear as contrails in the original method. The additional channels were used in part because of differences in sensitivity of the MODIS imagery, resulting in more false positives for a scene than a similar AVHRR image, even when the original algorithm was modified to account for the higher sensitivity of the MODIS images.

During the development and testing of the CDA, three sets of binary check masks were created to produce three contrail masks with varying sensitivities. The first mask, mask A, had the lowest sensitivity and thus the detected the fewest number of contrails, but minimized the number of false detections. The second mask, mask B, was more sensitive and could detect more linear contrail coverage (and also wider contrails) than mask A, but contains more false detections. The third mask, mask C, was the most sensitive and provided an upper bound on linear contrail cirrus detection.

To determine the overall accuracy of the contrail masks, a subjective error analysis was performed using an updated version of the interactive program developed by Minnis et al. (2005). The analysis was first applied to sets of 44 MODIS images over the contiguous United States and the North Atlantic flight corridor. Four different human analysts interactively evaluated the images to estimate the number of false detections, missed contrails, and positive contrail detections for Mask A. A composite mask for each image was determined from the four results.

While it is assumed that the analysts' subjective assessments constitute the "truth" set for the CDA selection, it is apparent in viewing many of the images that defining a linear contrail is not always straightforward. This difficulty arises primarily from the presence of older contrails that have spread significantly. This evolution is common (Minnis et al., 1998), especially in contrail outbreaks (Carleton et al., 2008). Such outbreaks may be responsible for much of the excess cloudiness due to contrails, but are difficult to quantify with automated methods. The ambiguity resulting from the older and overlapping contrails in such outbreaks should be considered when defining the extent of linear contrails. Thus, it is likely that the truth set from the analysts is an underestimate and the corresponding CDA results will also underestimate the true contrail coverage.

3   FLIGHT TRACK SCREENING

Global aircraft emissions waypoint data provided by FAA (Wilkerson et al., 2010) allowed comparison of detected contrails with commercial aircraft flight tracks. A pixel-level product based on the advected flight tracks defined by the waypoint data and the three dimensional wind component profiles from the NASA GMAO GEOS-4 reanalyses was developed to assign a confidence of contrail detection (CCD) for the contrail mask pixels. The product computes a flight track "strength" value for each pixel in a MODIS granule determined from the relative age of the advected flight tracks passing over the pixel. Flight tracks as old as 4 hours before image time were considered. To compute the confidence of contrail detection parameter, the CDA results were compared to a second set of subjective visual error analyses of 22 MODIS granules over the North Atlantic Ocean. The visual analyses served as "ground truth" observations within a logistic regression model to compute the likelihood that a pixel determined from the CDA was actually a contrail. The logistic regression model used several flight track parameters including the total number, relative ages, and bearing of the advected flight tracks passing over each pixel to determine the CCD of each contrail mask pixel. The CCD thus acts as a validation/screening mask in the contrail detection algorithm to reduce the number of false detections in all three masks. The flight track screening is especially useful in the tropical regions where thin cirrus streaks from tropical convection are often misinterpreted by the CDA as contrail cirrus.

4   CONTRAIL COVERAGE RESULTS

Figure 1 shows the screened contrail coverage for mask B computed for each the seasonal months (January, April, July, October) of 2006 *Aqua* MODIS data. The results are shown for the daytime and nighttime pixels combined. The daytime pixels are defined as those pixels with a computed solar zenith angle of 87.5 degrees or less at the time of the overpass. Although the location of the contrail coverage in each month generally follows the general global pattern of air traffic, the seasonal results show the regional differences due to the overall changes in temperature and humidity resulting from the variability in the general circulation of the NH atmosphere throughout the year. The most noticeable differences include the variability in coverage over the North Atlantic flight corridor, with a peak in April and a relative minimum in October, the minimum in coverage over the Sahara Desert and surrounding regions in July, and the maximum in coverage over the Northern Pacific flight corridor during April and especially July.

Jan   2006 Aqua screened CT fraction B (day+night)

0.00   0.01   0.05   0.15   0.25   0.35   0.5   1.0   2.0   8.0   16.0

Apr   2006 Aqua screened CT fraction B (day+night)

0.00   0.01   0.05   0.15   0.25   0.35   0.5   1.0   2.0   8.0   16.0

Jul (-8 days)   2006 Aqua screened CT fraction B (day+night)

0.00   0.01   0.05   0.15   0.25   0.35   0.5   1.0   2.0   8.0   16.0

Oct   2006 Aqua screened CT fraction B (day+night)

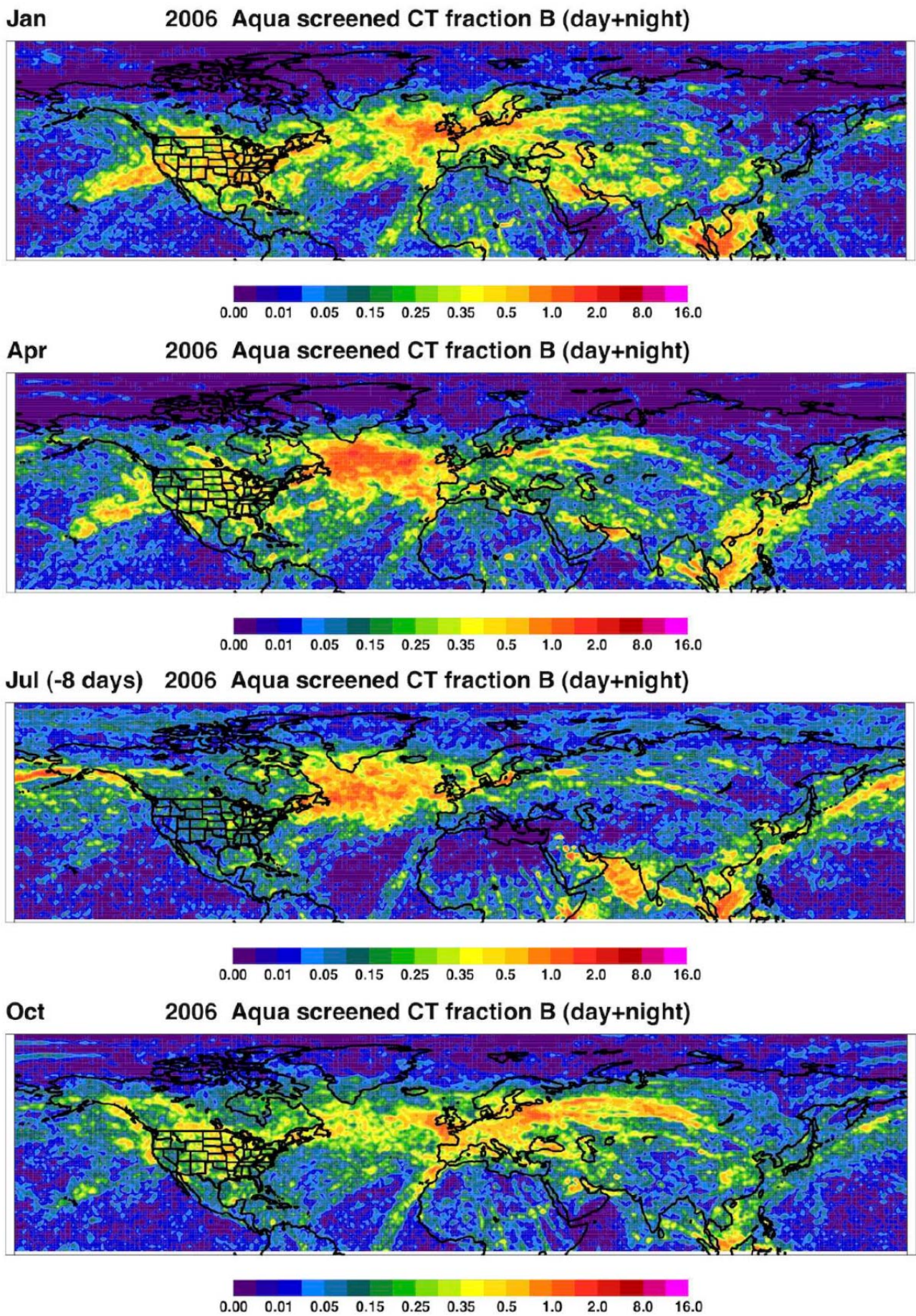0.00   0.01   0.05   0.15   0.25   0.35   0.5   1.0   2.0   8.0   16.0

Figure 1: Flight track screened contrail coverage fractions computed using Mask B from *Aqua* MODIS data for each seasonal month (Jan, Apr, Jul and Oct) of 2006.

Figure 2 presents the mean screened contrail coverage for mask B computed from the summation of all four seasonal months of 2006 *Aqua* MODIS data. The plot of the daytime and nighttime coverage for the four-month period reflects the overall pattern in commercial air traffic over the Northern Hemisphere, and most of the main flight track corridors are prominently visible in the image. The second and third images in Figure 2 show the breakdown of the coverage computed for the daytime and nighttime pixels respectively. Many of the differences between day and night coverage can be traced to differences in air traffic coverage around the time of the satellite overpasses each day and night. For example, more air traffic in the corridor between Europe and South America occurs during the nighttime *Aqua* overpasses than during the daytime. Conversely, more air traffic is evident between the western United States and Hawaii during the daytime *Aqua* overpasses than during the nighttime.
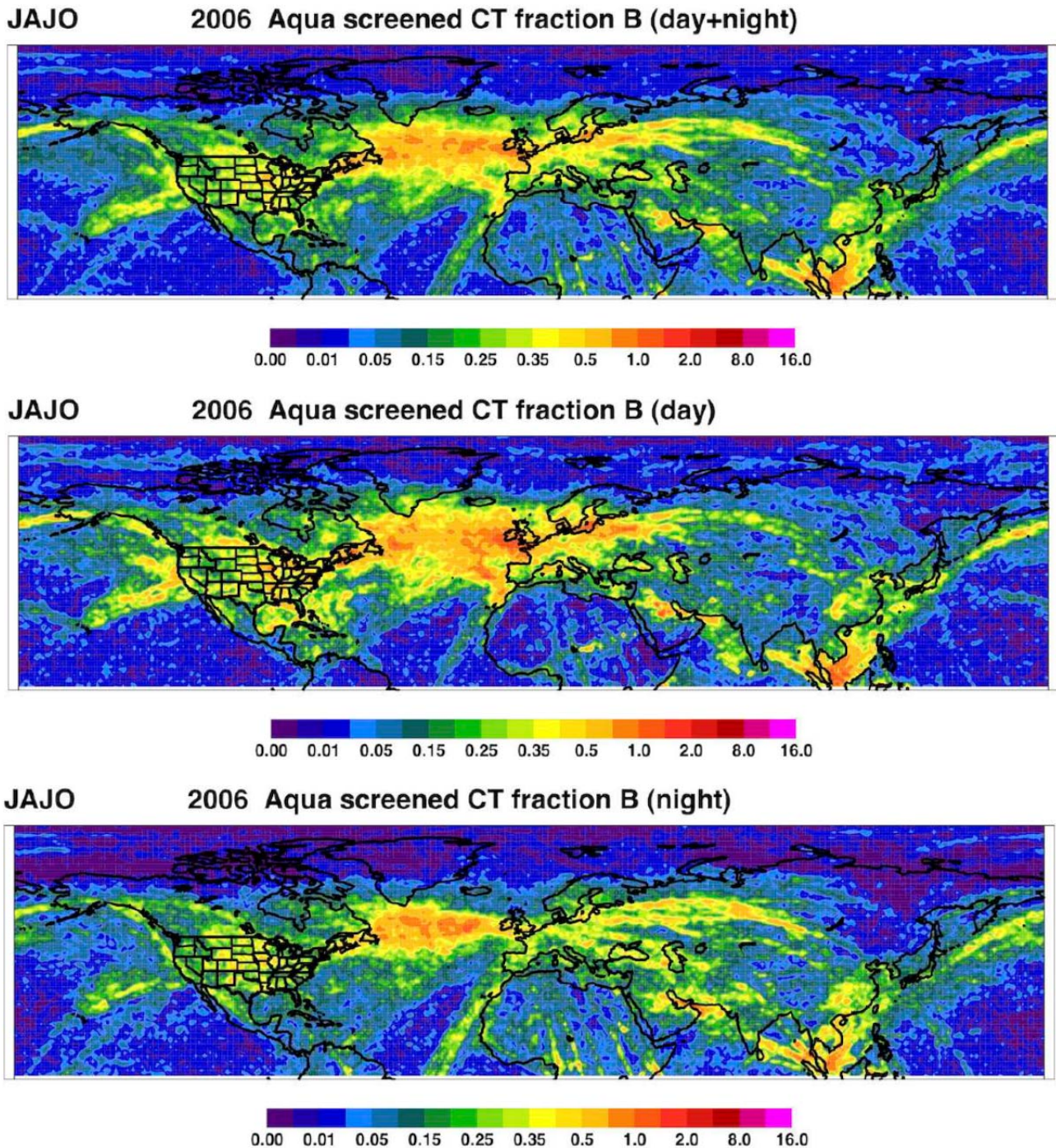

Figure 2: Mean flight track screened contrail coverage fractions computed using Mask B from *Aqua* MODIS data for the combined seasonal months of 2006.

Table 1 shows the overall contrail coverage computed by each of the three CDA masks for the 4-month period. Mask B detected approximately twice as many contrail pixels as Mask A, while Mask C detected 5.5 times as many contrail pixels as Mask A. When averaged over the four months, the daytime to nighttime ratio of contrail coverage was approximately 1.2 for all three masks, with the largest day to night ratios during January and the smallest ratios during July. The contrail coverage presented here have not been corrected for the effects of the variability in the background thermal infrared brightness temperatures on the sensitivity of the CDA (as discussed in Mannstein et al. (1999) and Meyer et al. (2002)) and thus need further processing to correct for this bias.

Table 1: Flight track screened contrail coverage fractions (in percent) over Northern Hemisphere from *Aqua* MODIS data.

	Mask A			Mask B			Mask C		
	Total	Day	Night	Total	Day	Night	Total	Day	Night
Jan	0.066	0.10	0.045	0.13	0.19	0.096	0.38	0.54	0.29
Apr	0.071	0.067	0.075	0.13	0.12	0.14	0.37	0.33	0.42
Jul	0.066	0.060	0.076	0.12	0.11	0.15	0.35	0.30	0.44
Oct	0.063	0.076	0.052	0.12	0.14	0.10	0.36	0.42	0.31
JAJO	0.067	0.075	0.059	0.13	0.14	0.12	0.37	0.39	0.35

To address the problem of estimating contrail cirrus from linear contrail cirrus coverage determined from the CDA, the following approach was used. To look for spreading contrails (i.e., contrail cirrus) we compared pixels near detected linear contrail pixels, and added those with similar radiative properties (specifically, thermal infrared brightness temperatures) to the linear contrail cirrus. For example, in this study we determined a series of thermal infrared brightness temperature (BT) and brightness temperature difference (BTD) thresholds from a simple radiative transfer model that would correspond to a contrail cirrus optical depth between 0 and 1.5. The neighboring satellite pixels with measured BT and BTD values that fell within the prescribed thresholds were considered to be contrail cirrus. A preliminary run of the contrail cirrus model run based on Mask A results produced an increase in the NH contrail cirrus fraction from 0.067% to 1.12%, a 17-fold increase in coverage. We emphasize that these results are preliminary and require more research and testing, but provide a reasonable upper bound on contrail cirrus coverage measured by satellite. In a related study, Minnis et al. (2012) compare linear contrail coverage determined by AVHRR and MODIS during large outbreaks of contrail cirrus with numerical model estimates of contrail cirrus coverage to determine how much of the total contrail cirrus the CDA can measure.

5   CONTRAIL CIRRUS PROPERTIES AND RADIATIVE FORCING

To complete the contrail climatology, contrail optical properties and radiative forcing were computed based on the contrail coverage determined from the CDA. Bedka et al. (2012) describe in detail the radiative transfer model used to compute contrail optical depth and effective diameter from the MODIS measurements. Bedka et al. use the method of Inoue (1985) to determine the contrail properties simultaneously by minimizing the difference between the observed and calculated BTD for 11 and 12 μm radiances. Nine hexagonal ice column models are used to estimate the contrail optical properties, and the AEDT waypoint data is used to estimate the contrail temperature. The contrail optical properties presented in Bedka et al. (2012) were then used as input to the contrail radiative forcing (CRF) calculations described by Spangenburg et al. (2012). Spangenburg et al. applied the Fu-Liou (1993) radiative transfer model to the *Aqua* MODIS pixels to compute upwelling solar (SW) and longwave (LW) fluxes and CRF computed at the top of the atmosphere. Three atmospheric conditions (clear sky, ice cloud below contrail, and water cloud below contrail) were considered, and surface albedo was estimated from snow/ice maps and CERES monthly albedo maps. Although the CRF calculations were done at the 1-km MODIS pixel level, the mean CRF were averaged over a 1x1 deg NH grid. For this preliminary study, only a simple first-order flight track screen based on air traffic density only was used. Spangenburg et al. determined the net NH CRF for the four seasonal months to be 16 mW m^{-2}. Future efforts to expand the contrail climatology (including contrail

coverage, contrail optical properties, and 24-hr contrail radiative forcing) for two years of *Aqua* and *Terra* MODIS data are currently underway.

6   ACKNOWLEDGMENTS

REFERENCES

Bakan, S., Betancour, M., Gayler, V., and Grassl, H., 1994: Contrail frequency over Europe from NOAA-satellite images. Ann. Geophysicae, 12, 962–968.

Bedka, S., P. Minnis, D. Duda, and R. Palikonda, 2012: Seasonal and diurnal variability in linear contrail microphysical properties as derived using MODIS infrared observations. 3rd International Conference on Transport, Atmosphere and Climate. Prien am Chiemsee, Germany, June 25-28.

Carleton, A., Travis, D. J., Master, K., and Vezhapparambu, S., 2008: Composite atmospheric environments of jet contrail outbreaks for the United States, J. Appl. Meteorol Climatol., Vol. 47, 641-667.

Duda, D., P. Minnis, L. Nguyen, and R. Palikonda 2004: A case study of the development of contrail clusters over the Great Lakes. J. Atmos. Sci., 61, 1132-1146.

Duda, D. P., R. Palikonda, K. Khlopenkov, T. Chee, and P. Minnis, 2011: A MODIS-based contrail climatology of coverage and cloud properties. AMS 15th Conf. on Aviation, Range, and Aerospace Meteor., Los Angeles, CA, August 1-4, 9.4, 14 pp.

Fu, Q., and K. –N. Liou, 1993: Parameterization of the radiative properties of cirrus clouds. J. Atmos. Sci., 50, 2008-2025.

Inoue, T., 1985: On the temperature and effective emissivity determination of semitransparent cirrus clouds by bispectral measurements in the 10 μm window region. J. Meteor. Soc. Japan, 63, 88-98.

Mannstein, H., R. Meyer, and P Wendling, 1999: Operational detection of contrails from NOAA-AVHRR data. Int. J. Remote Sensing, 20, 1641-1660.

Mannstein, H, and U. Schumann, 2005: Aircraft induced contrail cirrus over Europe. Meteorol. Z., 14, 549-554.

Mannstein, H., A. Brömser, and Bugliaro, L., 2010: Ground-based observations for the validation of contrails and cirrus detection in satellite imagery. Atmos. Meas. Tech., Vol. 3, 655-669.

Meyer, R., Mannstein, H., Meerkötter, R., Schumann, U., and Wendling, P., 2002: Regional radiative forcing by line-shaped contrails derived from satellite data. J. Geophys. Res., 107, DOI: 10.1029/2001JD000426.

Meyer, R., Büll, R., C. Leiter, C., Mannstein, H., S. Pechtl, S., T. Oki, T., and P. Wendling, P., 2007: Contrail observations over southern and eastern Asia in NOAA/AVHRR data and comparisons to contrail simulations in a GCM. Intl. J. Remote Sens., Vol. 28, 2049–2069.

Minnis, P., Young, D. F., Nguyen, L., Garber, D. P., Smith, W. L., Jr., and Palikonda, R., 1998: Transformation of contrails into cirrus during SUCCESS. Geophys. Res. Lett., 25, 1157-1160.

Minnis, P., J. K. Ayers, R. Palikonda, and D. N. Phan, 2004: Contrails, cirrus trends, and climate. J. Climate, 17, 1671-1685.

Minnis, P., Palikonda, R., Walter, B. J., Ayers, J. K., and Mannstein, H., 2005: Contrail properties over the eastern North Pacific from AVHRR data. Meteorol. Z., 14, 515-523.

Minnis, P., D. P. Duda, T. L. Chee, S. K. Bedka, D. A. Spangenburg, R. Palikonda, and K. T. Bedka, 2012: Contrails versus contrail cirrus from a satellite perspective. 3rd International Conference on Transport, Atmosphere and Climate. Prien am Chiemsee, Germany, June 25-28.

Palikonda, R., Minnis, P., Duda, D. P., and Mannstein, H., 2005: Contrail coverage derived from 2001 AVHRR data over the continental United States of America and surrounding areas. Meteorol. Z., 14, 525-536.

Penner, J. E., D. H. Lister, D. J. Griggs, D. J. Dokken, and M. McFarland, 1999: Aviation and the Global Atmosphere. Cambridge University Press, 373 pp.

Spangenberg, D., S. Bedka, D.Duda, R. Palikonda, F. Rose, and P. Minnis, 2012: Contrail cloud radiative forcing over the Northern Hemisphere from Terra and *Aqua* MODIS data. 3rd International Conference on Transport, Atmosphere and Climate. Prien am Chiemsee, Germany, June 25-28.

Wilkerson, J. T., M. Z. Jacobson, A. Malwitz, S. Naiman, and S. K. Lele, 2010: Analysis of emission data from global commercial aviation: 2004 and 2006. Atmos. Chem. Phys., 10, 6391-6408.

On comparison between ISCCP and PATMOS-x high cloud variability over air traffic corridors

K. Eleftheratos[*]

Faculty of Geology & Geoenvironment, University of Athens, Greece

ABSTRACT: A comparison of high cloud variability between ISCCP and PATMOS-x cloud data sets is presented in this study. The comparison was performed over selected areas with high air traffic density in the northern hemisphere and covers the period from January 1984 to December 2009. The geographical areas of interest are the US, Europe, North Atlantic, North Pacific, China and SE Asia high air traffic corridors. High cloud variability from ISCCP was found to be highly correlated with high cloud variability from PATMOS-x over all areas under study. By subtracting the zonal mean from the regional cloud data, the correlation coefficients increased approximately by 10%, thus improving the agreement between ISCCP and PATMOS-x high cloud anomalies over the studied areas. High cloud trends from the two independently produced data sets are also compared.

1   INTRODUCTION

Observations of cloudiness by satellites from space cover more than 25 years in length. This might be considered long enough to investigate local, regional and larger scale variations in high, middle and low level cloudiness in the long run. In this study, we analyze high cloud amounts from two independently produced cloud data sets, ISCCP (International Satellite Cloud Climatology Project) and PATMOS-x (AVHRR Pathfinder Atmospheres-Extended), and examine the long-term variability of high level cloudiness over selected areas in the northern hemisphere with high air traffic. Here, we do not relate any changes in high level clouds with aviation activities or natural parameters. We just focus on the investigation of the consistency of the variability of the two data sets as a first step before analyzing any relations with natural or manmade parameters.

Table 1 defines the regions in which high cloud data from ISCCP have been compared with those from PATMOS-x.

Table 1: Definition of high air traffic regions analyzed in this study. USA: Unites States of America, EUR: Europe, NA: North Atlantic, NP: North Pacific, CHN: China, SE Asia: Southeast Asia.

Region	Coordinates
east USA	30°-45° N, 65°-100° W
west USA	30°-45° N, 105°-130° W
east EUR	40°-55° N, 10°-30° E
west EUR	40°-55° N, 10° W-10° E
east NA	40°-55° N, 15°-35° W
west NA	40°-55° N, 40°-60° W
east NP	42.5^o-55° N, 130°-180° W
west NP	42.5^o-55° N, 145°-180° E
CHN	25°-40° N, 110°-140° E
SE Asia	0°-25° N, 90°-120° E

---

[*] *Corresponding author:* Kostas Eleftheratos, Lab. of Climatology & Atmospheric Environment, Faculty of Geology & Geoenvironment, National & Kapodistrian University of Athens, Greece, 15784 Athens, Greece. Email: kelef@geol.uoa.gr

2   DATA SOURCES

Cloud data analyzed in this study are monthly high cloud amounts for the period 1984-2009 from two independantly produced cloud data sets.

The first cloud data set was produced by the International Satellite Cloud Climatology Project (ISCCP; Rossow and Schiffer, 1999). The data are based on observations from a suite of operational geostationary and polar orbiting satellites. Visible radiances are used to retrieve the optical thickness of clouds and infrared radiances to retrieve cloud top temperature and pressure. The D2 dataset used in this study has a spatial resolution of 280 km (2.5o at the equator) and provides monthly averages of cloud properties of fifteen different cloud types. The cloud types are derived based on radiometric definitions that rely on cloud optical thickness and cloud top pressure. The high cloud amounts analysed in this study were calculated by adding the cirrus, cirrostratus and deep convective cloud amounts (Ci+Cs+Cb), i.e., by adding all type of clouds with cloud top pressure above 440 hPa as described in the ISCCP cloud clasification scheme. The data were downloaded from the ftp site ftp://isccp.giss.nasa.gov/pub/data/D2Tars/.

The second satellite cloud data set is the AVHRR Pathfinder Atmospheres-Extended data set (PATMOS-x; Heidinger and Pavolonis, 2009). PATMOS-x cloud data were downloaded from the webpage http://cimss.ssec.wisc.edu/patmosx/ under the data directory v5_Level 3 (GEWEX format). More specifically, we downloaded the global, 1.0 degree resolution high cloud amount data which contributed to the Global Energy and Water Exchanges (GEWEX) Cloud Climatology Assessment (ftp://ftp.ssec.wisc.edu/pub/awalther/GEWEX/PATMOSX/). We analyzed the data files provided at 0130pm. PATMOS-x defines high cloud as cloud with cloud-tops above 440 hPa.

3   ANALYSIS AND DISCUSSION

The comparison of ISCCP with PATMOS-x high clouds was performed after removing variations related to the seasonal cycle of the data based on the following regression model:

$$Clouds\ (i,j) = S\ (i,j) + residuals \tag{1}$$

Where i denotes the month and j is the year of high cloudiness and its seasonal (S) component, as described by Eleftheratos et al. (2007). The deseasonalized time series of cloudiness at each region was calculated by subtracting from each individual monthly value the overall mean monthly value for the whole period 1984–2009. The residuals from Eq. (1) were used as input for the correlation analysis between the deseasonalized cloud anomalies from ISCCP and PATMOS-x. Deseasonalized cloud anomalies from ISCCP were correlated with deseasonalized cloud anomalies from PATMOS-x based on a simple regression statistical model:

$$ISCCP\ (i,j) = a\ x\ PATMOS\text{-}x\ (i,j) + b \tag{2}$$

Where i denotes the month and j is the year of the examined variables, a is the slope and b is the intercept of the regression model. The correlation analysis between the examined parameters was performed for the regions of Table 1 from January 1984 to December 2009 (data points, N=300) and the statistical significance (p-value) of the correlation coefficients was determined. The correlation coefficients between high cloud deseasonalized anomalies from the two independantly produced data sets are presented in Table 2 (second column).

Table 2: Correlation coefficients (R_1) between high cloud anomalies from ISCCP and PATMOS-x over high air traffic regions (second column). Respective correlation coefficients (R_2) with the zonal mean anomalies removed (third column). Number of data used in the correlation analysis and statistical significance of the R (fourth and fifth columns). USA: Unites States of America, EUR: Europe, NA: North Atlantic, NP: North Pacific, CHN: China, SE Asia: Southeast Asia.

Region	Correlation coefficient (R_1)	Correlation coefficient (R_2)	Number of data (N)	Statistical significance (p-value)
east USA	+0.54	+0.59	300	<0.0001
west USA	+0.65	+0.72	300	<0.0001
east EUR	+0.67	+0.73	300	<0.0001
west EUR	+0.75	+0.80	300	<0.0001
east NA	+0.54	+0.60	300	<0.0001
west NA	+0.62	+0.70	300	<0.0001
east NP	+0.54	+0.61	300	<0.0001
west NP	+0.72	+0.80	300	<0.0001
CHN	+0.66	+0.75	300	<0.0001
SE Asia	+0.82	+0.89	300	<0.0001

Next, we have performed the correlation analysis again, after subtracting the zonal mean from the regional time series, i.e., the difference between the regional and zonal mean cloudiness. For SE Asia we subtracted the tropical mean (0°–25° N) deseasonalized anomalies, whereas in all other regions we subtracted the zonal mean deseazonalized anomalies of the northern mid-latitudes (25°–55° N). As can be seen from Table 2 (third column), the correlation coefficients between ISCCP and PATMOS-x anomalies are improved in all regions approximately by 10%. This could be explained by the fact that the regional cloud data with the zonal means removed are not influenced by large-scale cloudiness changes, thus reflecting better the real changes in cloudiness on smaller space scales. The removal of zonal/global means from local or regional data has been used in several studies examining changes in climatic parameters including regional cloudiness changes (Deser and Phillips, 2006; Biasutti et al, 2009; Deser et al, 2010; Solomon and Newman, 2011; Meyssignac et al, 2012; Tokinaga et al, 2012; Young et al, 2012).

Figure 1 shows the time series of high cloud anomalies from ISCCP and PATMOS-x over the areas under study.
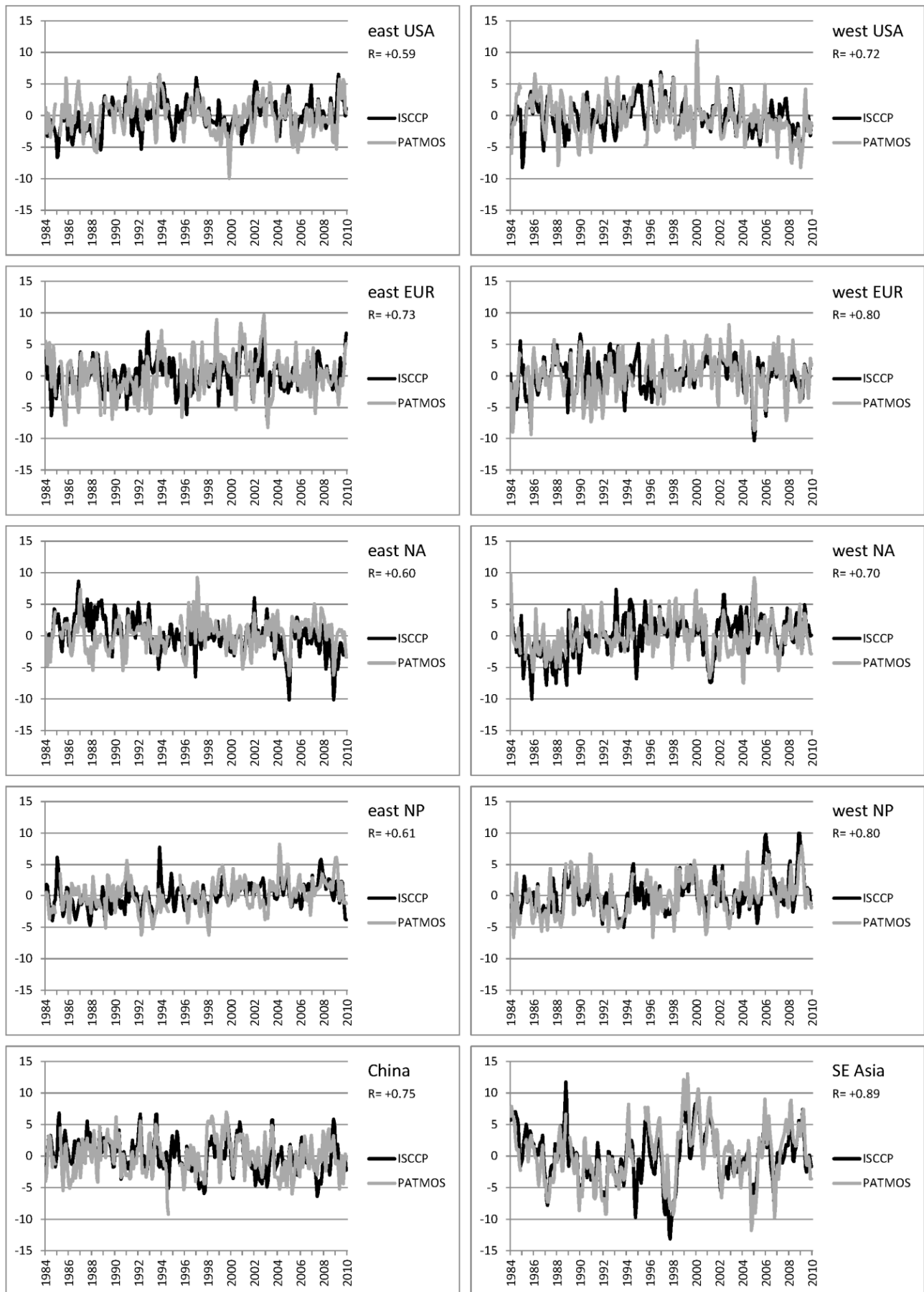
Figure 1: Comparison of high cloud anomalies from ISCCP and PATMOS-x over high air traffic regions in the USA, Europe, North Atlantic, North Pacific, China and SE Asia.

In view of the better agreement of ISCCP and PATMOS-x cloud anomalies after removing the zonal averages, we have calculated linear trends at the selected regions by applying linear fits to the data with the zonal means removed. The results are presented in Table 3 which shows for comparison the trends for the period 1984-2009 before and after the removal of the zonal means.

Table 3: Comparison of long-term trends in high cloud cover (% per decade) from ISCCP and PATMOS-x over high air traffic regions in the USA, Europe, North Atlantic, North Pacific, China and SE Asia before and after removing the zonal means. Bold: significant at the 99% confidence level based on Student's t-test. Italics: significant at the 95% confidence level.

Region	ISCCP high clouds	PATMOS-x high clouds	ISCCP high clouds minus zonal mean	PATMOS-x high clouds minus zonal mean
east USA	**+1.2**	+0.2	**+1.0**	-0.3
west USA	-0.2	-0.5	*-0.5*	**-1.0**
east EUR	**+0.8**	**+1.2**	**+0.6**	+0.6
west EUR	+0.5	**+1.3**	+0.3	*+0.8*
east NA	**-1.4**	**+1.0**	**-1.6**	+0.4
west NA	**+1.7**	**+1.1**	**+1.5**	+0.5
east NP	**+1.2**	**+1.5**	**+1.0**	**+0.9**
west NP	**+1.3**	**+1.6**	**+1.1**	**+1.0**
CHN	**-0.8**	+0.4	**-1.0**	-0.1
SE Asia	+0.4	+2.0	0.0	*+0.9*

Over the eastern and western US air traffic regions, high cloud trends from ISCCP were estimated to be +1.0% and -0.5% per decade, and -0.3% and -1.0% per decade from PATMOS-x respectively. The trends agree better over the eastern and western parts of Europe while the best consistency was found for the eastern and western North Pacific selected regions (Table 3). The largest discrepancies were found over the eastern North Atlantic where ISCCP data showed negative trends of 1.6% per decade, contrasting the positive trends seen by PATMOS-x (+0.4% per decade). Over China, linear trends were estimated to be -1.0% per decade from ISCCP, and -0.1% per decade from PATMOS-x accordingly. Over SE Asia, ISCCP showed no trend, while PATMOS-x showed a change of +0.9% per decade.

4   CONCLUSIONS

High cloud amounts from ISCCP have been compared with high cloud amounts from PATMOS-x over selected areas with high air traffic. By removing the average seasonal cycle from the monthly cloud data, we found strong consistency between the ISCCP and PATMOS-x high cloud deseasonalized data over all areas under study. By further subtracting the zonal mean deseasonalized data from the regional deseasonalized data we found stronger coherence between the ISCCP and PATMOS-x cloud anomalies, with the correlation coefficients being improved by 10% in all areas. Linear trends in high cloud cover from ISCCP have been compared with those from PATMOS-x. The trends from the two data sets were found to be consistent over the western US, western North Atlantic, eastern/western Europe, and eastern/western North Pacific areas, while less consistency was found over the eastern US, eastern North Atlantic, China and SE Asia.

REFERENCES

Eleftheratos, K., C.S. Zerefos, P. Zanis, D.S. Balis, G. Tselioudis, K. Gierens, and R. Sausen, 2007: A study on natural and manmade global interannual fluctuations of cirrus cloud cover for the period 1984-2004. Atmos. Chem. Phys. 7, 2631–2642.

Heidinger, A.K. and M.J. Pavolonis, 2009: Gazing at Cirrus Clouds for 25 Years through a Split Window. Part I: Methodology. Journal of Applied Meteorology and Climatology 48, 1100– 1116, DOI: 10.1175/2008JAMC1882.1.

Rossow, W. B. and R. A. Schiffer, 1999: Advances in understanding clouds from ISCCP. Bull. Amer. Meteor. Soc. 80, 2261–2288.

Deser, C. and A. Phillips, 2006: Simulation of the 1976/77 Climate Transition over the North Pacific: Sensitivity to Tropical Forcing. J. Climate 19, 6170–6180.

Biasutti, M., A.H. Sobel, and S.J. Camargo, 2009: The Role of the Sahara Low in Summertime Sahel Rainfall Variability and Change in the CMIP3 Models. J. Climate 22, 5755–5771, DOI: 10.1175/2009JCLI2969.1.

Deser, C., A.S. Phillips, and M.A. Alexander, 2010: Twentieth century tropical sea surface temperature trends revisited. Geophys. Res. Lett., 37, L10701, doi:10.1029/2010GL043321.

Solomon, A. and M. Newman, 2011: Decadal predictability of tropical Indo-Pacific Ocean temperature trends due to anthropogenic forcing in a coupled climate model. Geophys. Res. Lett., 38, L02703, doi:10.1029/2010GL045978.

Meyssignac, B., D. Salas y Melia, M. Becker, W. Llovel, and A. Cazenave, 2012: Tropical Pacific spatial trend patterns in observed sea level: internal variability and/or anthropogenic signature? Clim. Past, 8, 787–802, doi:10.5194/cp-8-787-2012.

Tokinaga, H., S.-P. Xie, A. Timmermann, S. McGregor, T. Ogata, H. Kubota, and Y.M. Okumura, 2012: Regional Patterns of Tropical Indo-Pacific Climate Change: Evidence of the Walker Circulation Weakening. J. Climate 25, 1689–1710, DOI: 10.1175/JCLI-D-11-00263.1.

Young, P.J., K.H. Rosenlof, S. Solomon, S.C. Sherwood, Q. Fu, and J.-F. Lamarque, 2012: Changes in Stratospheric Temperatures and Their Implications for Changes in the Brewer–Dobson Circulation, 1979–2005. J. Climate 25, 1759–1772, DOI: 10.1175/2011JCLI4048.1.

Regional Scale Impact of Traffic Emission on Radiation over Europe

K. Lundgren[*], B. Vogel, and H. Vogel
Institute for Meteorology and Climate Research, Karlsruhe Institute of Technology, Karlsruhe, Germany

C. Knote
Laboratory for Air Pollution/Environmental Technology, EMPA, Switzerland

*) now at Atmospheric Chemistry Division, NCAR, Boulder (CO), USA

ABSTRACT: This study focuses on the role on-road transport may play for the atmospheric chemical composition, the aerosol particle mass and number densities, and on the subsequent effect on atmospheric radiation. Current studies mainly focus on the impact of transport emissions on the chemical composition of the atmosphere and the climate impacts. Detailed high-resolution studies on the regional scale are, however, still rare. Our investigation is based on detailed online-coupled simulations for Europe with the regional scale model system COSMO-ART. This is a pilot study with COSMO-ART, with respect to the effect of transport on aerosols and their radiative effects in the framework of the DLR research project 'Transport and the Environment'. Here, simulations with EMAC boundary data and TNO-emission data are performed with a horizontal resolution of 0.125° (~14 km). These first simulations with respect to the effect of on-road transport emissions show that a reduction in the emissions from on-road transport lead to a general decrease in gas and particle concentrations over Europe. For particles, the change in PM_{10} was in the order of approx. ~15% and the corresponding change for particle number was in the order of approx. ~5-15% over central Europe. However, also enhancements of particle concentrations were found due to local new particle formation as a result of the reduced emissions. In the concentrations of gaseous species such as NO_2 and ozone, local to regional increases in the concentrations are found. Thus, a reduction of emissions most certainly can lead to non-linear responses in the concentrations of species in the atmosphere. A comparison between the simulations with and without on-road transport emissions reveals a net direct radiative effect of -0.02 W m^{-2} at the surface and +0.26 W m^{-2} at the TOA due to the emissions of on-road transport emissions. Any significant temperature effect was not seen in these first simulations.

1 INTRODUCTION

The impact of road transport on aerosols is yet connected to large uncertainties. Transport emissions affect the atmosphere both directly and indirectly, and the response of the atmospheric characteristics is therefore complex and non-linear. The main mechanisms include the emissions of greenhouse gases, e.g. CO_2, and emissions of greenhouse gas precursors. Moreover, gases such as NO_x, CO, and VOC (volatile organic compounds) that affect the oxidation capacity of the atmosphere are emitted. Further mechanisms are the radiative effects of transport emissions on the features of the atmosphere. Transport emissions can influence the atmospheric radiative fluxes both directly and indirectly. The direct radiative effects are due to scattering and absorption of radiation by particles, e.g. black carbon (BC), organic carbon (OC), and sulfur. Through e.g., changed particle sizes, chemical compositions etc., the transport emissions can lead to modified cloud optical properties and a subsequent altering of the atmospheric radiative fluxes via the clouds. These effects are the indirect radiative effects. Transport emissions may cause both cooling and warming effects. The cooling is connected to a reduced life time of methane and to the reflection by OC and SO_4. Green-

---

[*] *Corresponding author:* Kristina Lundgren, Institute for Meteorology and Climate Research, Karlsruhe Institute of Technology, Karlsruhe, 76344 Eggenstein-Leopoldshafen, Germany.

house gases cause a warming and in addition the absorbing characteristics of BC can cause a warming of the atmosphere. All these mechanisms together result in a complex system with processes that overlap and depend on each other.

Current studies focus on the impact of transport emissions on the chemical composition of the atmosphere and the climate impacts. Detailed high-resolution studies on the regional scale are, however, still rare. Here, we provide a comprehensive study with the focus on the role road transport may play for the aerosol particle chemical composition and the particle mass and number densities in the atmosphere. We also consider the subsequent effect the transport emissions may have for the particle scattering and absorption of radiation. We base our investigation on detailed online-coupled simulations for Europe with the regional scale model system COSMO-ART (Vogel et al., 2009). This is a pilot study with COSMO-ART, with respect to the effect of transport on aerosols and their radiative effects in the framework of the DLR research project 'Transport and the Environment'. Within this project COSMO-ART is coupled to the global model EMAC and applied for the investigation transport emissions on the regional scale for different scenarios. The model system is summarized in the following section.

2   THE MODEL SYSTEM

COSMO-ART (Vogel et al., 2009) is an online coupled model system designed for regional scale applications. COSMO is the meteorological driver of the model and ART stands for Aerosols and reactive Trace gases. That the model system is online coupled means that the feedback between the aerosols and the atmosphere is taken into account. This means that any change in e.g., temperature is directly considered in the calculations for the chemistry and aerosols and so on. Such a feedback is neglected in most other investigations connected to this topic but may play in important role when investigating the impact on the atmosphere, which is a chaotic system.

In COSMO-ART we treat complex gas phase chemistry that is coupled directly to the particle phase. The size distribution of the particles is described by overlapping log-normal functions, so called modes, which represent particle sizes from a few nanometers to tenth of micrometers. Five modes describe the size distribution of the aged soot particles, pure soot particles, and internally mixed particles without soot. Except for the pure soot particles, which are directly emitted, these particles are formed through homogeneous nucleation, coagulation, and condensation processes. The aged soot particles consist of internal mixtures of SO_4^{2-}, NO_3^-, NH_4^+, secondary organic aerosol (SOA) soot, and water. The soot-free particles contain SO_4^{2-}, NO_3^-, NH_4^+, secondary organic aerosol (SOA), and water internally mixed. Natural aerosol particles are additionally considered. Sea salt particles and mineral dust particles are described by three modes each. Volcanic ash and pollen are represented by several mono-disperse particle classes.

COSMO-ART is applied to investigate the impact of road transport emissions on the atmosphere on the regional scale. The setup of the model for this purpose is described in the following.

3   MODEL SETUP

The simulations with COSMO-ART are performed with a horizontal resolution of 0.125° (~14 km) in both directions and a time step of 40 s. The vertical resolution is 40 terrain following model levels up to approx. 20 km, with increased resolution close to the surface. The meteorological initial- and boundary data were achieved from the global GME model and applied every 6 hours. Chemical boundary data was taken from simulations with the EMAC-MADE model. Chemical input from the global model was applied every 3-hours. Both gaseous (17 gaseous species) and particle concentrations were considered.

3-D hourly emission data of TNO (Visschedijk et al., 2006, Kuenen et al., 2011) for a "typical" weekday, Saturday, and Sunday were utilized. This means that we account for both a daily and a weekly cycle in the emissions. One data set with all emission sectors was applied, and one additional data set in which the on-road transport emissions were removed was utilized to investigate the impacts of on-road transport emission.

To investigate the impact of road transport emissions over Europe, three simulations were performed. Run B refers to the base run, in which all emissions are considered but. In this run no aerosol-radiation interaction is taken into account. In run R the aerosol-radiation interaction is accounted for and in run NT the aerosol radiation interaction is still taken into account, but the on-road transport emissions are excluded. First simulations were performed for 1-5 May, 2008, and the main results are summarized in the following section.

4   RESULTS BASED ON NUMERICAL SIMULATIONS WITH COSMO-ART

When comparing the base run R to the run NT, the impact of reducing the emissions from on-road transport by 100% is achieved. A period of 5 days in May 2008 was simulated and the last two days (4-5th May) were chosen for the evaluation of these simulations. This means that three days are left to the model for spin-up.

The simulated NO_2 and ozone concentrations and the corresponding differences (NT-R) are illustrated in Fig 1.
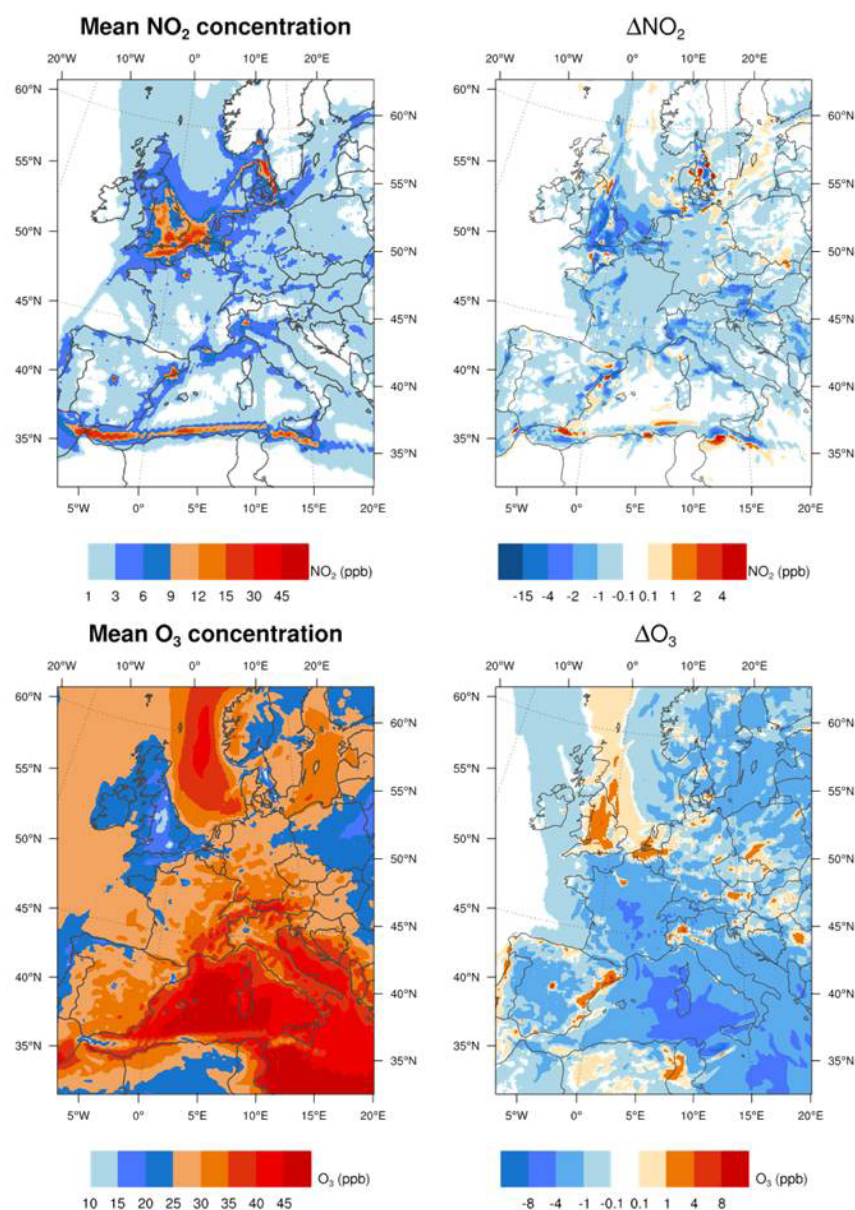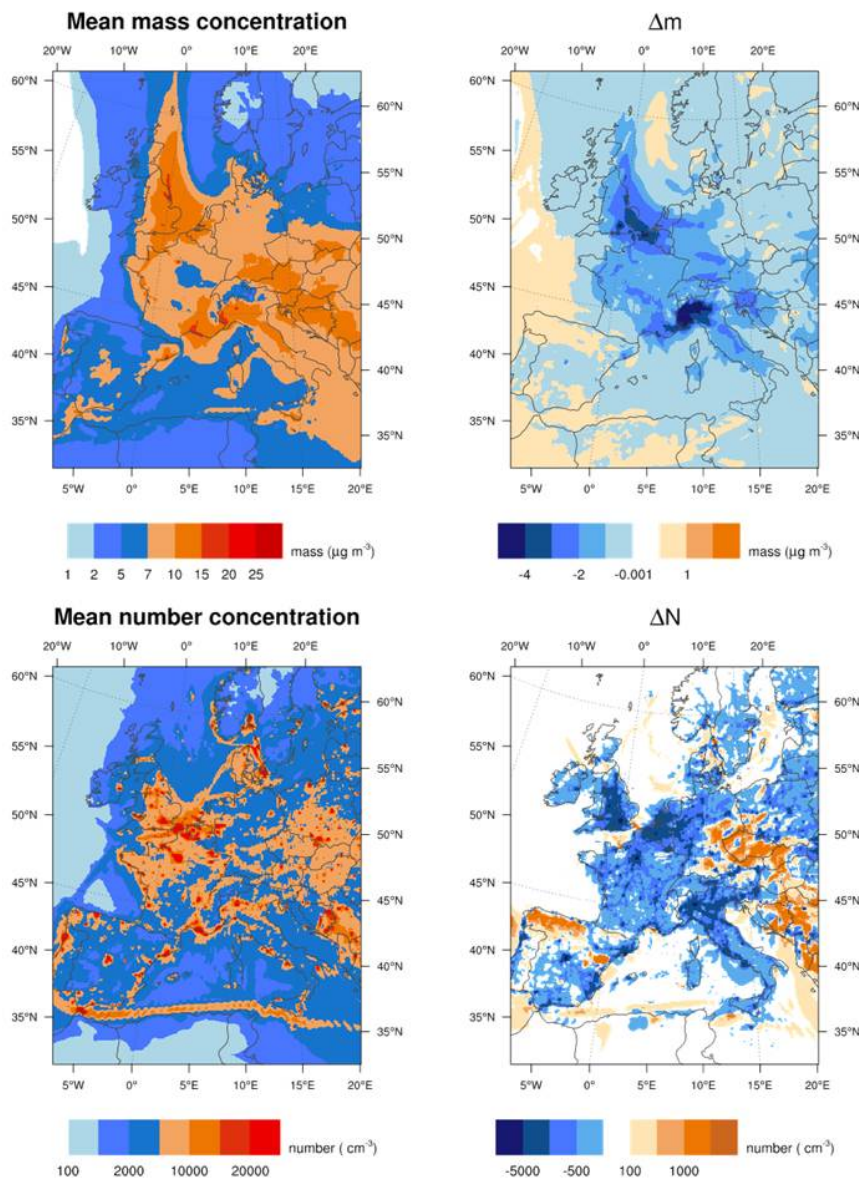

Figure 1. Simulated concentrations for the 4-5 May and the corresponding concentration differences when reducing the emissions (run NT-R).

The simulations without on-road transport emissions show a general decrease of e.g., NO_2 and O_3 over the European continent (Fig. 1). However, there are also local effects that indicate an increase

in the gaseous concentrations when reducing the emissions. For Ozone an increase is found over parts of Germany and the Benelux countries. For NO_2 local non-linear effects in the concentrations are found especially near the shipping routes in e.g., the Mediterranean. These effects are indications of the non-linear response when reducing transport emissions. When reducing the emissions of a specific component such as NO_2, a straight forward decrease in the atmospheric concentration of the same component cannot be assured due to the chain of complex chemical reactions that take place in the atmosphere and the modified oxidation capacity of the atmosphere.

The simulated mass and number densities and the corresponding differences (NT-R) are illustrated in Fig 2.

Figure 2. Simulated mass and number concentrations of particles for the 4-5 May, and the corresponding concentration differences when reducing the emissions (run NT-R).

The change in mass concentration and the number concentration of aerosol particles is illustrated in Fig. 2. The mass concentration, approx. corresponding to PM_{10}, shows a strong decrease over the continent. The general reduction close to the ground (lowest model level, approx. 20 m depth) is in the order of 15% of the total dry aerosol mass. Maximum decreases are found in areas as the Po Valley, and the region of East England and the Benelux countries. One explanation for the strong decrease of total aerosol mass in these areas is the change in the nitrate content of the aerosol particles. The strongest effect of reduced on-road transport emissions on aerosol mass was seen on aged soot-particles in the accumulation size range.

As for the mass concentration, also the number concentration of particles is generally reduced over the European continent when reducing the emissions. The decrease over most of the domain is

in the order of 5-15 % relative to the total particle number concentration. In contrast to the mass concentration, the number concentration also increases in some areas. These areas are connected to strong sulfur emissions from different sources. As the strongest increase in particle number concentration is found for Aitken mode particles, this increase indicates enhanced new particle formation. This is probably a result of changed oxidation capacity of the atmosphere in these regions. Thus, reduced on-road transport emissions may lead to increased numbers of small particles.

The simulated impact of the reduced emissions on the radiation is achieved by comparing the run R and the run NT. The aerosol-radiation interaction is taken into account in both runs. Run R considers all the emission sources and in run NT no on-road transport emissions were accounted for. For investigating the radiative impact of the aerosols, clear sky conditions were chosen. The difference R-NT corresponds to the contribution of on-road transport emissions to the total radiative effect of particles. A net radiative effect of -0.02 W m^{-2} was found at the surface. Thus, the on-road transport emissions are in this case connected to a net cooling effect at the surface. At the top of the atmosphere TOA, the net radiative effect was +0.26 W m^{-2}. The radiative effect of all aerosols when considering all emission sources is achieved when comparing the runs R and B. In run B the aerosol-radiation interaction is not accounted for. The net radiative effect of all aerosols was -4.23 W m^{-2} at the surface and -2.47 W m^{-2} at the TOA. Thus, the overall direct radiative effect of aerosols was a cooling for this region during the two last days. The contribution from transport emissions to the aerosol radiative effect was a slight cooling at the surface and a warming at the TOA. For this time period, no significant temperature effect was simulated.

5   SUMMARY AND OUTLOOK

The effect of reduced on-road transport emissions on gaseous species, particulate matter, and radiation over Europe is investigated based on simulations with the regional scale model system COSMO-ART. COSMO-ART is a comprehensive model system that treats complex chemistry and aerosol dynamics online coupled to the dynamical core of the model. Here, we perform sensitivity studies, by excluding the on-road transport emissions, to investigate the impact on-road transport emissions may have. These simulations show that reduced on-road transport emissions may lead to non-linear responses in gas and particle concentrations. A general reduction was found in particle mass densities (PM$_{10}$) of approx. 15% over central Europe. For the number densities a overall decrease in the order of approx. 5-15% over central Europe was simulated. Local and regional enhancement of new particle formation was seen, which probably is a result of the modified oxidation capacity of the atmosphere when reducing the emissions. The impact on radiation of on-road transport emissions was a net cooling on the surface and a net warming at the TOA. The temperature effect at the surface was however not significant. This was a pilot study for the VEU project. Further simulations will be performed for longer time scales and with cloud-microphysics interactions included.

REFERENCES:

Vogel, B., H. Vogel, D. Bäumer, M. Bangert, K. Lundgren, R. Rinke, and T. Stanelle, 2009: The comprehensive model system COSMO-ART – Radiative impact of aerosol on the state of the atmosphere on the regional scale, *Atmos. Chem. Phys. 9*, 8661–8680.

Visschedijk, A., Zandveld, P., and Denier van der Gon, H., 2007: A high resolution gridded European emission database for the EU integrated project GEMS, TNO report 2007-A-R0233/B, Apeldoorn.

Kuenen, J., Denier van der Gon, H., Visschedijk, A., van der Brugh, H., 2011: High resolution European emission inventory for the years 2003 – 2007, TNO report TNO-060-UT-2011-00588, Utrecht.

Modelling the climate impact of road transport, maritime shipping and aviation over the period 1860-2100 with an AOGCM

D. Olivié[*]
University of Oslo and CICERO, Oslo, Norway

D. Cariolle
CERFACS and CNRM, Toulouse, France

H. Teyssèdre (†), D. Salas, A. Voldoire, H. Clark, D. Saint-Martin, M. Michou, F. Karcher
CNRM, Météo-France, Toulouse, France

Y. Balkanski, B. Koffi
LSCE, Paris, France

M. Gauss
Norwegian Meteorological Institute, Oslo, Norway

O. Dessens
University College London, London, UK

R. Sausen
Deutsches Zentrum für Luft- und Raumfahrt (DLR), Institut für Physik der Atmosphäre, Oberpfaffenhofen, Germany

ABSTRACT: For the period 1860-2100 (SRES scenario A1B for 2000-2100), the impact of road transport, maritime shipping and aviation on climate is studied using an Atmosphere Ocean General Circulation Model (AOGCM). In addition to carbon dioxide (CO_2) emissions from these transport sectors, most of their non-CO_2 emissions are also taken into account, i.e. the forcing from ozone, methane, black carbon, organic carbon, sulfate, CFC-12 and HFC-134a from air conditioning systems in cars, and contrails. For the year 2000, the CO_2 emissions from all sectors together induce a global annual-mean surface air temperature increase of around 0.1 K. In 2100, the CO_2 emissions from road transport induce a global mean warming of 0.3 K, while shipping and aviation each contribute 0.1 K. For road transport, the non-CO_2 impact is largest between 2000 and 2050 (of the order of 0.1 K) becoming smaller at the end of the 21st century. The non-CO_2 impact from shipping is negative, reaching -0.1 K between 2050 and 2100, while for aviation it is positive and its estimate varies between 0 and 0.15 K in 2100. When focusing on the geographical distribution, the non-CO_2 impact from road transport and shipping is only slightly stronger in northern than in southern mid-latitudes, while the impact from aviation can be a factor of 5 stronger in the northern than in the southern hemisphere. Further it is observed that most of the impacts are more pronounced at high latitudes.

1   INTRODUCTION

In recent years, the evidence for anthropogenic impacts on climate has increased (Solomon et al., 2007). Where observational studies have shown that the global mean surface air temperature has risen by around 0.8 K over the 20th century, modelling studies have demonstrated that this increase, in particular since the mid-20th century, can be attributed mainly to anthropogenic influences. It is

---

[*] *Corresponding author:* Dirk Olivié, Department of Geosciences, University of Oslo, PO Box 1022 Blindern, 0315 Oslo, Norway. Email: dirk.olivie@geo.uio.no

important to quantify the contribution from individual sectors such as road transport, shipping, or aviation to climate change, because this allows more informed assessments of the potential effects of mitigation of emissions from these sectors, given the high growth rate of transport emissions in comparison to other anthropogenic sources. From the transport sector, an important contribution to climate change is from carbon dioxide CO_2 emissions, but the emissions of other species, including short lived ones, are also important.

Here we present a study where an AOGCM is used to assess the impact of the transport sectors on climate. Using an AOGCM allows the study of geographical distributions of changes in surface air temperature, precipitation and cloud cover, and to quantify impacts on typical ocean parameters such as ocean 3-dimensional (3D) temperature, sea-level rise, and the meridional overturning circulation (MOC). We study the period 1860-2100 and perform full 240-year long integrations. We focus on the impact of road transport, maritime shipping and aviation, and distinguish between the impact from CO_2 emissions and the impact from all other emissions (which we call, collectively, non-CO_2).

Here we will only report on the impacts on surface air temperature – for the other impacts we would like to refer to Olivié et al. (2012).

2   DESCRIPTION OF MODEL, FORCINGS, AND EXPERIMENTS

2.1   *The CNRM-CM3.3 AOGCM*

The Centre National de Recherches Météorologiques (CNRM) Coupled Model version 3.3 (CNRM-CM3.3) consists of the atmosphere component ARPEGE-Climat4.6, the ocean component OPA8.0 and the sea-ice component GELATO2. The atmosphere component ARPEGE-Climat4.6 is a spectral model with a T42 horizontal resolution (equivalent to about 2.8°x2.8°) and 31 hybrid sigma levels (model top at 10 hPa). Both the ocean model OPA8.0 and the sea-ice model GELATO2 are grid point models and share the same mesh of 182x152 points. OPA8.0 has 31 levels, including 10 levels in the upper 100 m of the ocean.

2.2   *Forcings*

From the transport sectors, we take into account 6 different forcings. This includes for all sectors, the forcing from CO_2, methane (CH_4), ozone (O_3), and aerosols. In addition we take into account the emissions of CFC-12 and HFC-134a from road transport (from air conditioning systems in cars), and contrails and aviation-induced cirrus. The perturbations from CO_2, CH_4, CFC-12 and HFC-134a are assumed to be homogeneous perturbations (both horizontally and vertically), while the other perturbations have a geographical and vertical distribution.
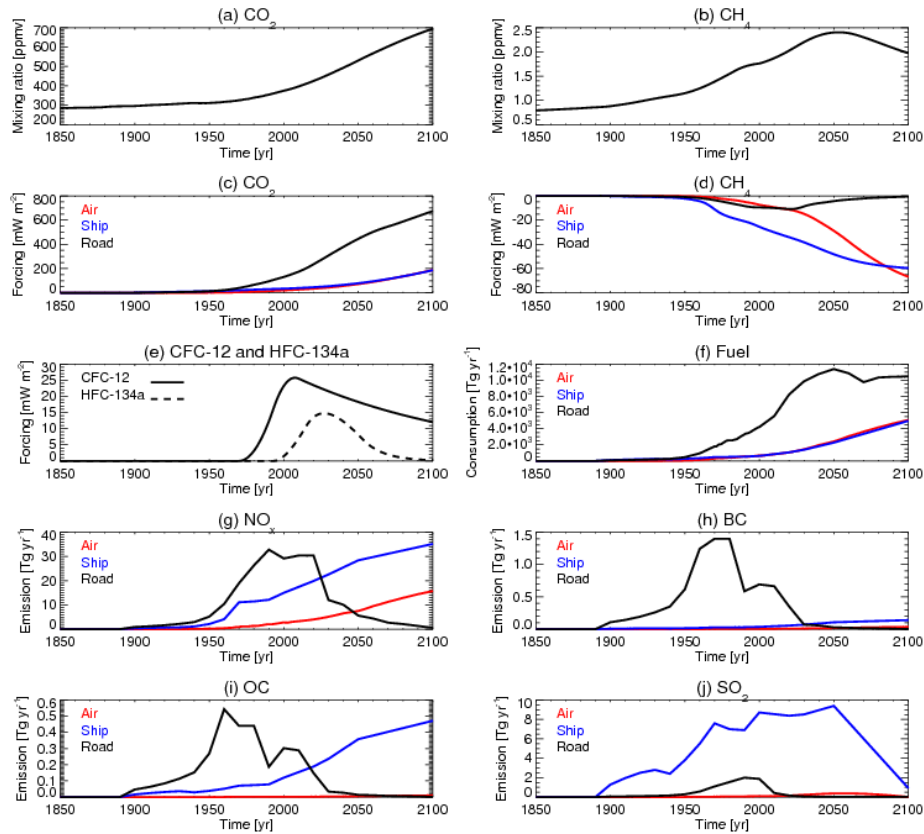
Figure 1 Time series of the forcings taken into account in the model integrations over the period 1860-2100. The first row shows the evolution of (a) CO_2 and (b) CH_4 mixing ratios in the reference simulation. Row 2 until 5 show forcings and emissions from the transport sectors: (c) radiative forcing from CO_2, (d) radiative forcing from CH_4, (e) radiative forcing from CFC-12 and HFC-134a from road transport, (f) global annual fuel consumption, and emissions from (g) NO_x, (h) BC, (i) OC and (j) SO_2.

As a reference show Figs. 1.a and 1.b the evolution of the atmospheric CO_2 and CH_4 concentration due to all anthropogenic activities from 1860 until 2100 assuming the A1B emission scenario. Figures 1.c to 1.j give an overview of the perturbations by the transport sectors taken into account (except contrail and aviation-induced cirrus). Figure 1.c shows the radiative forcing from CO_2, Fig. 1.d the reduction of radiative forcing due to CH_4 (caused by emission of nitrogen oxides (NO_x)), and Fig. 1.e the radiative forcing by CFC-12 and HFC-134a.

For O_3 and aerosol perturbations caused by the transport sectors, we use 3D distributions derived by chemistry transport models (see Balkanski et al. (2010) and Hoor et al. (2009)), combined with the time evolution of the global emission amount of the specific species or their principal precursor. For the perturbation in O_3 we use two approaches: the first one (dynamical O_3 approach) uses the time evolution and 3D distribution of the NO_x precursor combined with an extended linearized O_3 chemistry scheme based on Cariolle and Teyssèdre (2007). The second one (fixed O_3 approach) directly imposes the 3D O_3 perturbations.

The impact of contrails and aviation-induced cirrus is taken into account by a parameterization which is calibrated to give a radiative forcing of 0.024 W m^{-2} in the year 2000 (more details can be found in Olivié et al. (2012)).

2.3 *Experiments*

We perform several simulations with the CNRM-CM3.3 model over the period 1860-2100. The reference simulation uses the standard forcings to model the evolution of the Earth's climate over the period 1860-2100 (scenario A1B from 2000 onwards). The CO_2 and CH_4 evolutions are the ones shown in Figs. 1.a and 1.b, but also N_2O, CFC-11, CFC-12, the surface properties, and the sulfate aerosol evolve with time. Comparing this simulation with a simulation under pre-industrial conditions allows the derivation of the "total anthropogenic impact".

To study the impact of the different transport sectors, we perform a number of sensitivity simulations, making separate simulations to quantify the CO_2 and non-CO_2 impact. The non-CO_2 impact includes the effects from O_3, CH_4, CFC-12 and HFC-134a, aerosols, and contrails. To study the

CO_2 impact, we do two types of simulations: a first one without the CO_2 contribution from a certain sector, and a second one with five times the CO_2 contribution from that sector. To study the non-CO_2 impact, we perform simulations where we add five times the non-CO_2 forcing from a certain sector w.r.t. the reference simulation. We perform simulations using the dynamical O_3 approach (which we will call non-CO_2), and simulations using the fixed O_3 approach (which we call non-CO_2*).

Each simulation is repeated three times, using different initial conditions for the ocean, sea-ice and atmosphere, resulting in small ensembles of three members. Because shipping and aviation have almost the same temporal evolution for their CO_2 contribution in scenario A1B (see Fig. 1.c), we perform only one simulation that represents the CO_2 impact for both sectors.

3 RESULTS

In this section, we describe the impact of the three transport sectors on the surface air temperature over the period 1860-2100. For the impact on other key aspects of the atmosphere (O_3, TOA forcing, atmospheric temperature profiles, precipitation, cloud cover, and NAO index) or the ocean (3D temperature, sea-level rise, and MOC), we refer to Olivié et al. (2012). We show the separate impact of the transport sectors and distinguish between the CO_2 and non-CO_2 impacts, and, as a reference, we also show the total anthropogenic impact. We show time averages over four different periods, i.e., 1980-1999, 2011-2030, 2046-2065 and 2080-2099, which also have been studied in Solomon et al. (2007).
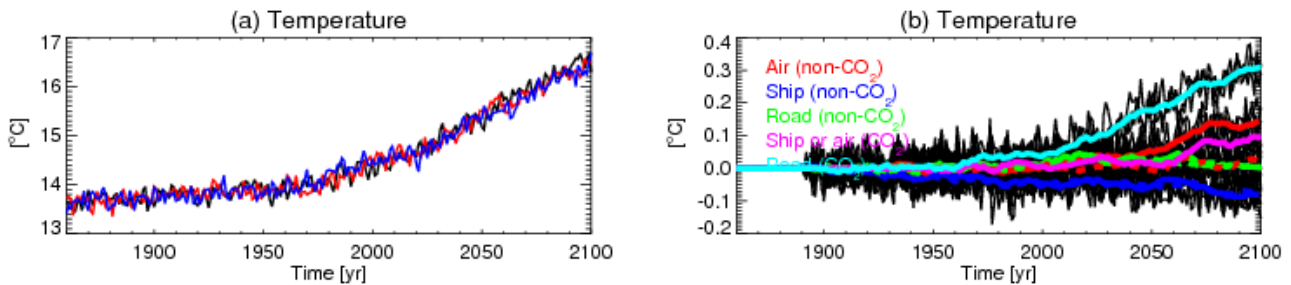

Figure 2 Left: time series of annual global mean surface air temperature over the period 1860-2100 taking into account the total anthropogenic forcing. The three different lines (black, red and blue) represent the three different members of the ensemble. Right: time series of impact on surface air temperature by road transport, shipping and aviation, separately for their CO_2, non-CO_2 and non-CO_2* impact (the non-CO_2* impact is indicated by the dashed lines). The thin black lines indicate the individual impact from each of the three members of the simulation, and the thick lines indicate the 11-year running average of the ensemble mean.

Figure 2.a shows time series of the global annual-mean of the surface air temperature for the three members of the reference simulation. Around the year 2000, the temperature increase is around 0.8 K w.r.t. 1860, increasing by almost 3.0 K in 2100. One notices that the three members of the ensemble show a very similar behavior. Figure 2.b shows time series of the impact of the transport sectors on the evolution of the global annual-mean surface air temperature. For CO_2 the impact of road transport is strongest, showing a temperature increase of around 0.05 K in 2000, reaching 0.3 K in 2100. For aviation and shipping, the temperature impact until 2050 is small, reaching 0.1 K in 2100. The non-CO_2 impact from road is strongest between 2000 and 2050 (around 0.05 K), and reduces thereafter. This is mainly caused by a strong reduction in the road transport emissions of NO_x in the second half of the 21st century and of the earlier reductions in the emission of CFC-12 and HFC-134a. Taking into account a stronger impact of BC (which is possibly underestimated in our simulations) would probably strengthen this behaviour. The non-CO_2 emissions from shipping show a negative impact on the temperature of around -0.05 to -0.1 K over the period 2000-2100. This is caused by significant SO_2 emissions leading to the formation of sulfate aerosols, together with a strong impact of OH on CH_4 by, on the one hand, significant NO_x emissions, and on the other hand, a characteristic strong impact of NO_x shipping emissions on the CH_4 lifetime (Hoor et al., 2009). For the non-CO_2 impact from aviation we see a strong difference between the non-CO_2 and non-CO_2* approaches, caused by the rather different O_3 perturbations. The non-CO_2 approach shows a positive impact reaching 0.15 K in 2100. This is caused by the strong increase in the NO_x

aviation emissions that are more than 2.5 times more efficient than the other transport emissions at producing O_3 (Hoor et al., 2009), and by the impact from the linear contrails and aviation-induced cirrus. However, in the extended linear O_3 scheme the O_3 production in the upper troposphere seems to be overestimated (not shown). Using the non-CO_2* approach leads to almost no temperature signal, except for a very small increase in the last part of the 21st century. Both approaches probably are affected by a possibly too strong negative forcing from sulfate aerosols. Taking this into consideration together with the fact that the model is not very sensitive to O_3 perturbations (not shown), we assume that the actual impact from aviation will be somewhere in between the results for both approaches.
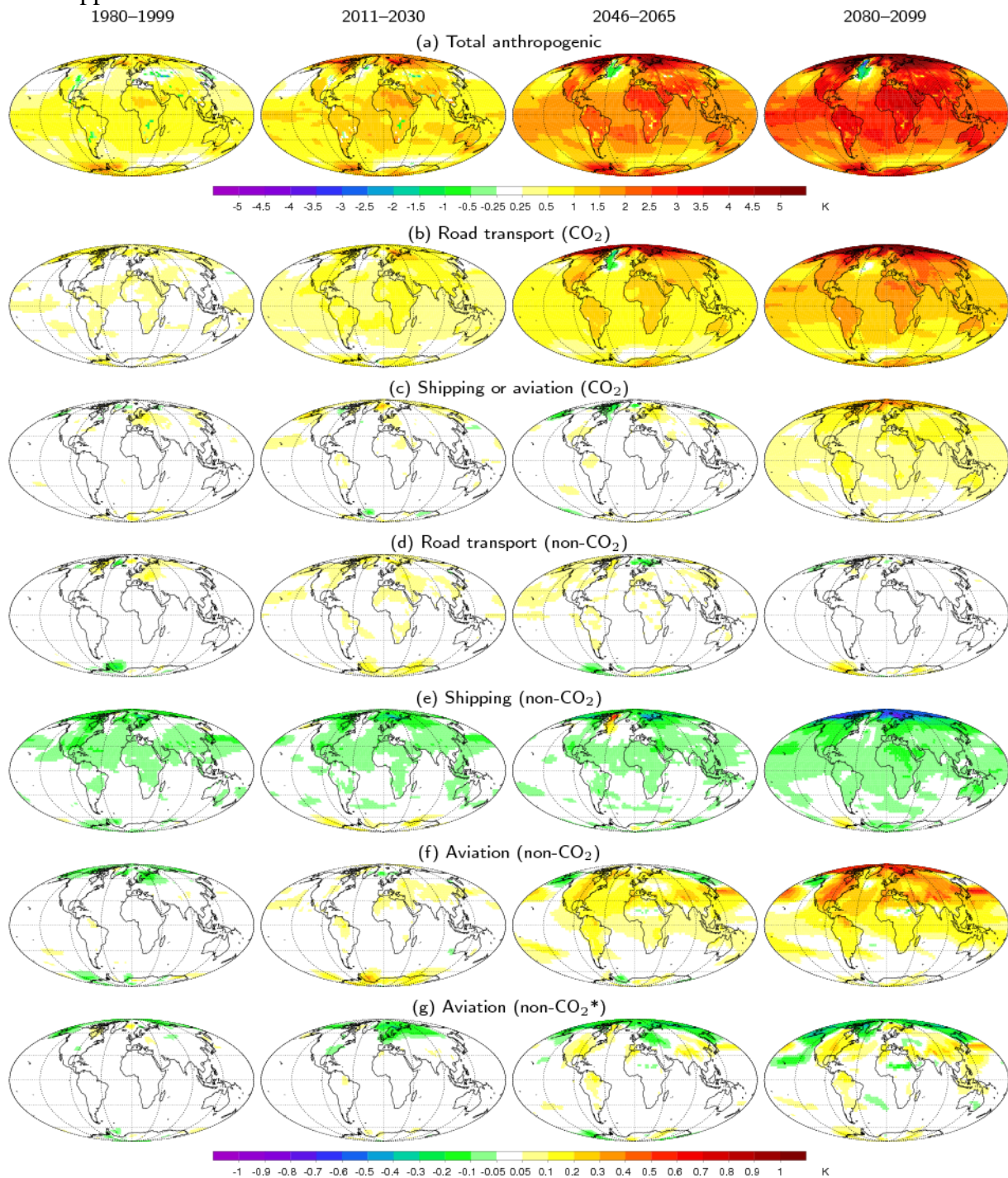
Figure 3 Global maps of the annual mean surface air temperature impact in the periods 1980-1999, 2011-2030, 2046-2065 and 2080-2099 caused by (a) the total anthropogenic forcing, the CO_2 forcing from (b) road transport and (c) shipping or aviation, by the non-CO_2 forcing from (d) road transport, (e) shipping and (f) aviation where we use the dynamical O_3 approach to take into account the effect of O_3, and (h) by the non-CO_2* impact from aviation (using the fixed O_3 approach). Notice that the contour intervals are 5 times larger for the total anthropogenic perturbation (a).

We now focus on the geographical distribution of the surface air temperature impact. In Fig. 3 we present the annual mean changes averaged over the periods 1980-1999, 2011-2030, 2046-2065 and 2080-2099 from the total anthropogenic impact (row a) and from the separate transport impacts (rows b-g). Note the difference in the contour intervals between the first row and the other rows. For the total anthropogenic impact, a clear signal can already be seen in 1980-1999, which increases gradually until 2080-2099. Continents show a considerably stronger impact than oceans, and the temperature over the Labrador Sea shows an even stronger negative temperature response in 2046-2065 and 2080-2099. In the Southern Ocean, we also find a weak warming. A strong impact is also noticeable poleward of 65°N. These results compare well with results shown in Solomon et al. (2007).

For the road sector, we find a significant CO_2 impact of 0.2 K over continents for 2011-2030, with some regions showing increases of more than 0.4 K in 2080-2099. Large similarities with the total anthropogenic impact exist, e.g., the stronger impact at high northern latitudes and the stronger impact over continents. For the CO_2 impact from shipping and aviation, increases of 0.2 K over continents are seen in 2080-2099. The non-CO_2 impact for road transport is slightly positive in 2011-2030 and 2046-2065, whereas that from shipping is clearly negative and rather constant over the 21st century, with some extremes over the continents and over the northern high latitude regions. Using the non-CO_2 approach, the impact from aviation is clearly positive by 2011-2030, and a steady increase is seen for the periods 2046-2065 and 2080-2099 especially in the northern hemisphere. However, using the non-CO_2* approach, we observe a clearly positive signal over the northern mid-latitudes only in 2080-2099.

4   CONCLUSIONS

For the period 1860-2100 (SRES scenario A1B for 2000-2100), we have studied the impact of road transport, maritime shipping and aviation on climate with the atmosphere ocean general circulation model CNRM-CM3.3. In the reference simulation, we found an increase in global annual-mean surface air temperature of around 0.8 K in 2000, reaching 3.0 K in 2100. In 2000, the CO_2 impact from all transport sectors together is of the order of 0.1 K. The emission of CO_2 from road transport contributes to a global mean warming of 0.3 K in 2100, while shipping and aviation each contribute to 0.1 K in 2100. The contribution of CO_2 from the transport sectors to the total anthropogenic temperature change increases from 12.5% in 2000 to 16.7% in 2100. The non-CO_2 impact differs strongly among the different sectors. For road, this impact is largest between 2000 and 2050 (order of 0.1 K) becoming smaller at the end of the 21st century. The non-CO_2 impact from shipping is clearly negative reaching -0.1 K between 2050 and 2100, while from aviation it is positive but depends strongly on the treatment of the O_3 perturbations, reaching possibly 0.15 K in 2100. This indicates that during the period 1900-2100, the net impact of road transport on climate is positive and dominated by its CO_2 impact, the net impact of maritime shipping is mainly negative only becoming neutral at the end of the 21st century, while for aviation it is clearly positive and presumably dominated by its non-CO_2 emissions, even in 2100.

REFERENCES

Balkanski, Y., G. Myhre, M. Gauss, G. Rädel, E. J. Highwood, and K. P. Shine, 2010: Direct radiative effect of aerosols emitted by transport: from road, shipping and aviation. Atmos. Chem. Phys., 10, 4477–4489, doi:10.5194/acp-10-4477-2010.

Cariolle, D. and H. Teyssèdre, 2007: A revised linear ozone photochemistry parameterization for use in transport and general circulation models: multi-annual simulations. Atmos. Chem. Phys., 7, 2183–2196, doi:10.5194/acp-7-2183-2007.

Hoor, P., J. Borken-Kleefeld, D. Caro, O. Dessens, O. Endresen, M. Gauss, V. Grewe, D. Hauglustaine, I. S. A. Isaksen, P. Jöckel, J. Lelieveld, G. Myhre, E. Meijer, D. Olivie, M. Prather, C. Schnadt Poberaj, K. P. Shine, J. Staehelin, Q. Tang, J. van Aardenne, P. van Velthoven, and R. Sausen, 2009: The impact of traffic emissions on atmospheric ozone and OH: results from QUANTIFY. Atmos. Chem. Phys., 9, 3113–3136, doi:10.5194/acp-9-3113-2009.

Nakicenovic, N., J. Alcamo, G. Davis, B. de Vries, J. Fenhann, S. Gaffin, K. Gregory, A. Grübler, T. Y. Jung, T. Kram, E. L. L. Rovere, L. Michaelis, S. Mori, T. Morita, W. Pepper, H. Pitcher, L. Price, K. Riahi, A. Roehrl, H.-H. Rogner, A. Sankovski, M. Schlesinger, P. Shukla, S. Smith, R. Swart, S. van Rooijen, N. Victor, and Z. Dadi, 2000: Emissions scenarios. Cambridge University Press, 599 pp.

Olivié, D. J. L., D. Cariolle, H. Teyssèdre, D. Salas, A. Voldoire, H. Clark, D. Saint-Martin, M. Michou, F. Karcher, Y. Balkanski, M. Gauss, O. Dessens, B. Koffi, and R. Sausen, 2012: Modeling the climate impact of road transport, maritime shipping and aviation over the period 1860–2100 with an AOGCM. Atmos. Chem. Phys., 12, 1449–1480.

Solomon, S., D. Qin, M. Manning, M. Marquis, K. Averyt, M. M. B. Tignor, H. L. Miller Jr., and Z. Chen (eds.), 2007: Climate Change 2007: The Physical Science Basis. Cambridge University Press, 996 pp.

Impact of Aviation on Atmospheric Chemistry and Climate

H. Teyssèdre (†), P. Huszár[*], S. Sénési, A. Voldoire, D. Olivié, M. Michou, D. Saint-Martin, A. Alias, F. Karcher, P. Ricaud, D. Salas Y Melia
GAME/CNRM, METEO-FRANCE, CNRS, France

D. Cariolle
CERFACS, France

Keywords: aviation, climate, chemistry, simulations

ABSTRACT: We applied the CNRM-AOCCM model, which is an extension of CRNM-CM5 with online chemistry in the upper troposphere and stratosphere, i.e. the altitudes where the majority of aviation emissions occur. We examined the impact of aviation on atmospheric chemistry and climate over the period 1940-2100 under the A1B scenario. The emissions from air traffic follow the corresponding A1i scenario: "A1 GDP driven moderate to good fuel efficiency, without NO_x improvements". In our simulations we considered emissions of CO_2, NO_x, CO and H_2O, a plume chemistry parameterization for the NO_x-chemistry, and an empirical contrail induced cirrus (CIC) treatment. For the period 1940-2100 we ran the model with all the forcings all together, and with each one of the forcings excluded. We also performed a simulation with no aviation forcings at all. The results suggest a considerable signal of the aviation emissions on the atmospheric composition for both present-day and future conditions, but the signal on the climate is non-detectable for present day conditions. The strongest signal is modelled towards the end of the 21st century. The CO_2 induced effect represents a statistically significant surface warming of up to 0.1-0.2 K over many regions of the globe, not uniform though, while for the stratosphere, cooling is of up to -0.4 K by a zonal mean. The aviation NO_x has a weak effect throughout the whole period, however the combined effects of CO_2 and NO_x are stronger than that of CO_2 alone. The impact on precipitation is negligible even towards the end of the 21st century. The global averaged SST is due to rise by up to 0.2 K due to aviation CO_2 while NO_x emissions do not cause a significant change. The evaluation of the CIC impact is not fully available yet, but the results for the 2000-2049 period suggest a statistically significant heating due to additional cloudiness and this effect is expected to increase by the end of the 21st century, causing potential SST increase as well.

1   INTRODUCTION

Global aviation represents a considerable environmental issue due to their emissions of green-house gases, and other pollutants perturbing the atmospheric chemistry and the Earth's radiative balance, as well as causing health and respiration effects. The global emissions from aircraft are increasing, therefore their impact is expected to be even higher in the future. Therefore, to assess their impact, it is necessary to use a climate model that simulates both chemical and radiative processes. For this purpose, we used the climate model CNRM-CM5 that is a global general circulation climate model, where we included online stratospheric chemistry, coupled with an ocean and a sea ice model. This study is one of the first attempts to evaluate the impact of aviation emissions using such kind of model, and follows Olivié et al. (2012) who used the former version of the model with simplified chemistry.

In section 2, we detail the model and its setup. Temperature and radiative forcing are presented in section 3 and conclusions in section 4.

---

[*] *Corresponding author:* Peter Huszar, Department of Meteorology and Environment Protection, Faculty of Mathematics and Physics, Charles University, Prague, V Holesovickach 2, Czech Republic. Email: peter.huszar@mff.cuni.cz

2   THE MODEL SETUP AND EXPERIMENTS

2.1   *General description of the model*

The model used in this study to assess the climate impact of aviation is based on the fully coupled ocean/atmosphere CNRM-CM5 model, that has been used for the IPCC/CMIP5 simulations, is described in Voldoire et al. (2013). This climate model is composed by the atmospheric general circulation model (GCM) ARPEGE-Climat that solves prognostic Navier-Stokes equations and several parameterizations of different physical processes (convection, clouds, …). Note that the radiative transfer of the atmosphere follows the RRTM code of Morcrette et al. (2001). Biosphere/atmosphere interactions are described throughout the SURFEX module. The TRIP river model is implemented to drive continental runoffs to the ocean. The atmospheric GCM is coupled to the NEMO ocean model and to the GELATO sea-ice model on a daily basis, through the OASIS coupler.

2.2   *Specific developments for the aviation impact*

This climate modelling system was modified by introducing stratospheric 'on-line' chemistry in the atmospheric GCM, which has been evaluated in Michou et al. (2011). This allows to take into account the main chemical reactions involving ozone, nitrogen oxides and carbon monoxide and dioxide that interact with the climatic system throughout the radiative scheme. Three-dimensional emissions of aviation from the QUANTIFY project were added to the atmospheric model. We also used the ANCAT climatology (Schumann et Huntrieser, 2007) as an additional source of NO_x, produced by lightning. This source is comparable in magnitude to the one from aircraft and was prescribed to the model. An additional tracer with a given lifetime ranging from 2 hours at the ground up to 15 hours at cruise altitudes, has been added to the atmospheric model. It represents aircraft plumes within the mesh of the model, and takes into account the non-linear chemistry occurring between the exhaust from the engine and the diluted plume 'entering' the scales resolved by the model, using effective reaction rates (Cariolle et al, 2009). This technique reduces the ozone perturbation due to aircraft emissions that becomes more realistic. This tracer is also used to parametrise the radiative impact of contrails and contrail induced cirrus (CIC). Following the approach of Olivié et al. (2012), CIC is expected to occur where the atmospheric temperature is below –40°C and relative humidity greater than 80% as no supersaturation with respect to ice is computed within the model. The model large scale cloud ice mixing ratio is perturbed by the amount of the tracer tuned to obtain a value of 31 mWm^{-2} for the top of the atmosphere radiative forcing in 2005, according to Burkhardt and Kärcher (2011).

The standard version of the atmospheric model of CNRM-CM5 was set at T127 (i.e.; 1.4° horizontal resolution) with 31 layers . As the stratospheric chemistry needs to increase the number of stratospheric levels, the number of vertical layers has been increased to 60. As the chemistry is also computationally expensive in itself (50 three dimensional species added), it has been necessary to reduce the horizontal resolution of the atmospheric model to 2.8° so as to limit the computational cost of CNRM-CCM. This introduces a discrepancy between the atmospheric (at 2.8°x2.8°) and the ocean models (at 1°x1°) that leads to a cold bias for the atmospheric surface temperature, especially over the polar regions. We then tuned our CNRM-CM5 version to reduce this bias in order to get a reasonable atmospheric circulation, by reducing the gravity wave drag in the stratosphere.

2.3   *Experiments*

Before starting simulations, it was necessary to rerun CNRM-CM5 over a century to get an equilibrium between the atmosphere, the ocean and the sea-ice components as the atmospheric resolution changed from its initial version (see Voldoire et al., 2013). Then, we initialized the model for pre-industrial conditions and ran it following an historical emission scenario, until 1920. At that date, the stratospheric chemistry was switched on in the model that ran until 1940 as spin-up for the chemistry. Aviation emissions become significant after this date. Then, several simulations were performed to distinguish the effects of the non-CO_2 emissions, the non-NO_x emissions, the non-CIC parameterization effect, the all gathered aviation emissions and the non aviation emissions. All these simulations were performed from 1940 (the beginning of significant air traffic) until 2100 fol-

lowing the A1B emission scenario. Each simulation was performed 3 times for the 2000-2100 period by changing the initial conditions of 2000 so as to enhance the signal to noise ratio.

3 RESULTS

Including the stratospheric chemistry leads to similar evolutions of the atmosphere, ocean and sea-ice to CNRM-CM5 simulations (Voldoire et al., 2013). Therefore, only the aviation impact is detailed hereafter.

3.1 *Atmospheric temperature*

The impact of aviation studied with CNRM-CM5 reproduces the well-known general pattern: a warming in the troposphere and a cooling in the stratosphere (see Figure 1).
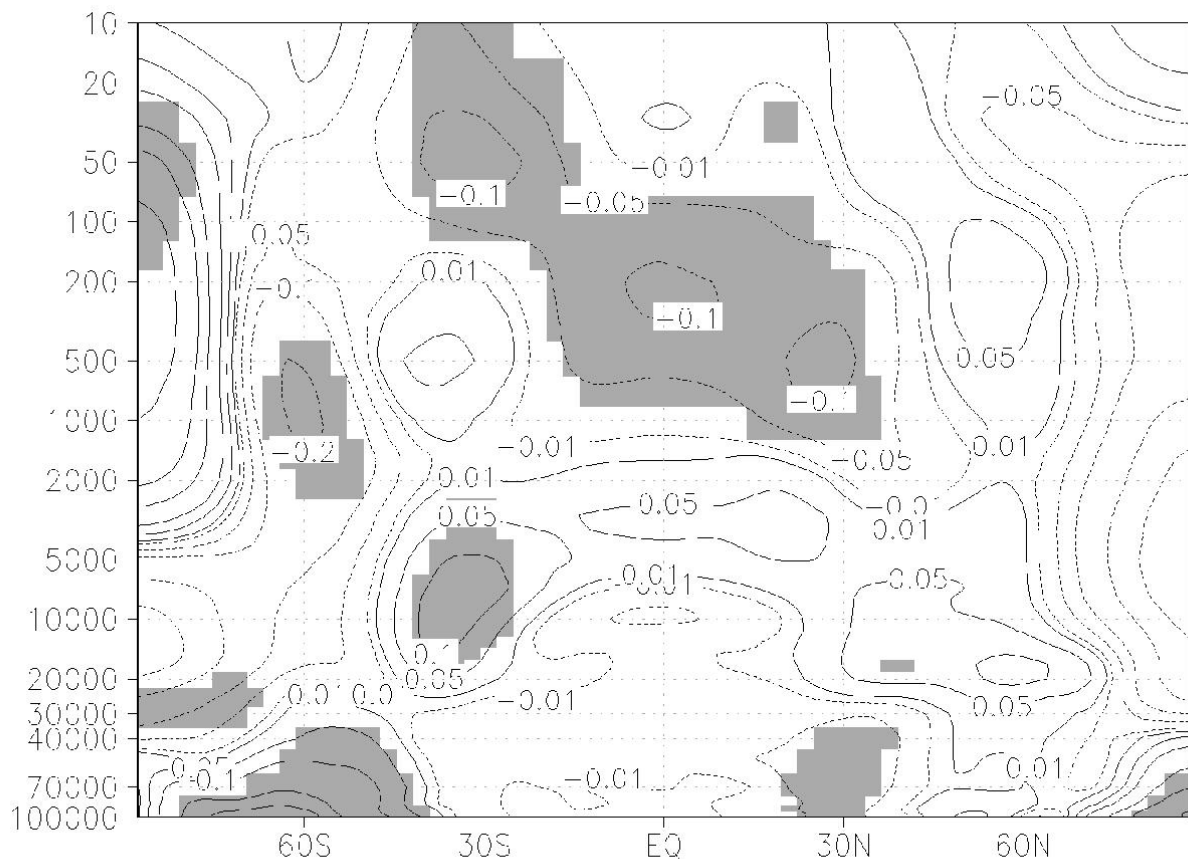
GrADS: COLA/IGES

Figure 1: Latitude/pressure (Pa) zonal cross section of the temperature anomaly (K) due to aviation emissions, for the period 1991-2010. Positive values are indicated by solid lines, negative by dashed lines and grey shaded areas indicate 90% statistical significance.

For present day conditions (1991-2010), the aviation impact is almost negligible for individual forcings: the largest effect is found for CIC with a significant warming of 0.05-0.1 K over the tropical upper troposphere / lower stratosphere, especially in August and September. The NO_x plus CIC signal is similar (indicating a small NO_x signal), but the maximum warming occurs earlier in the summer. For the "total" impact, some considerable warming is found (0.15 K) in the troposphere, while there is a cooling in the stratosphere (-0.2 K), significant every month (not shown).
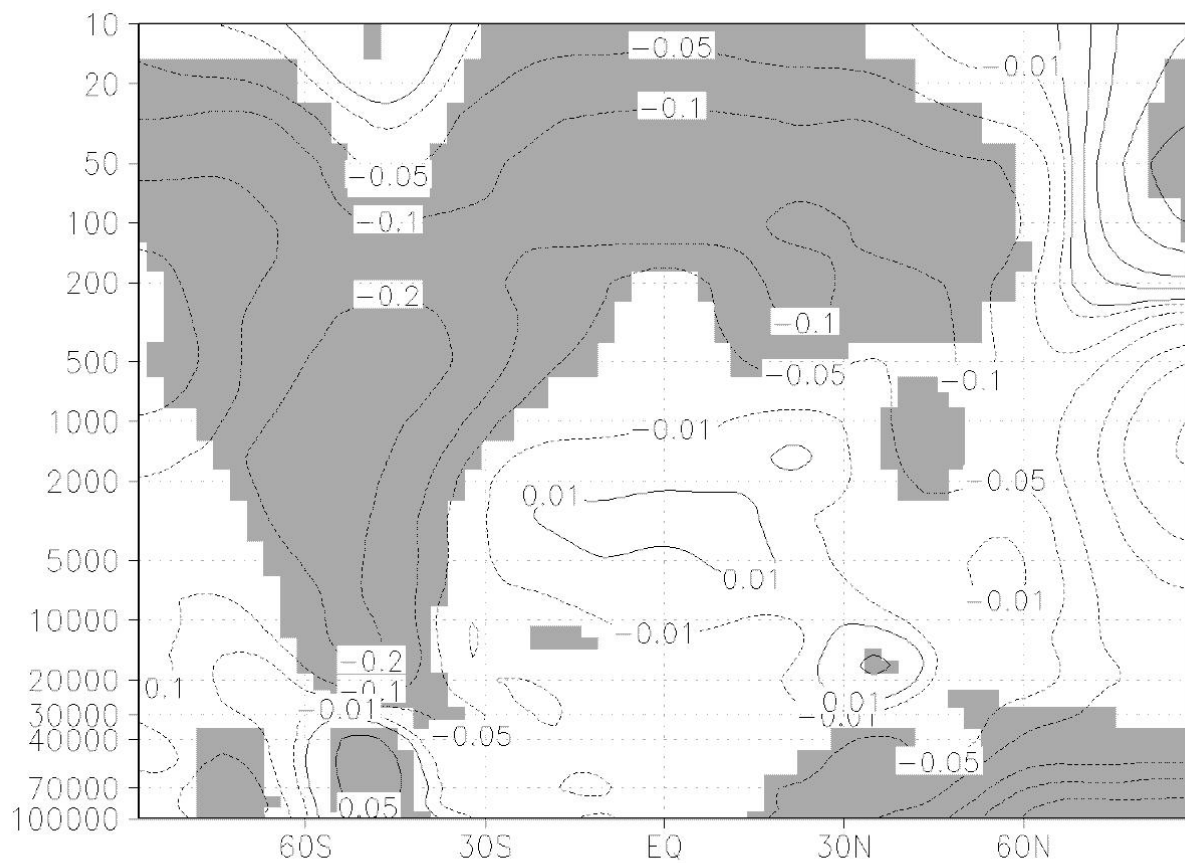
Figure 2: same as figure 1 for the period 2031-2050.
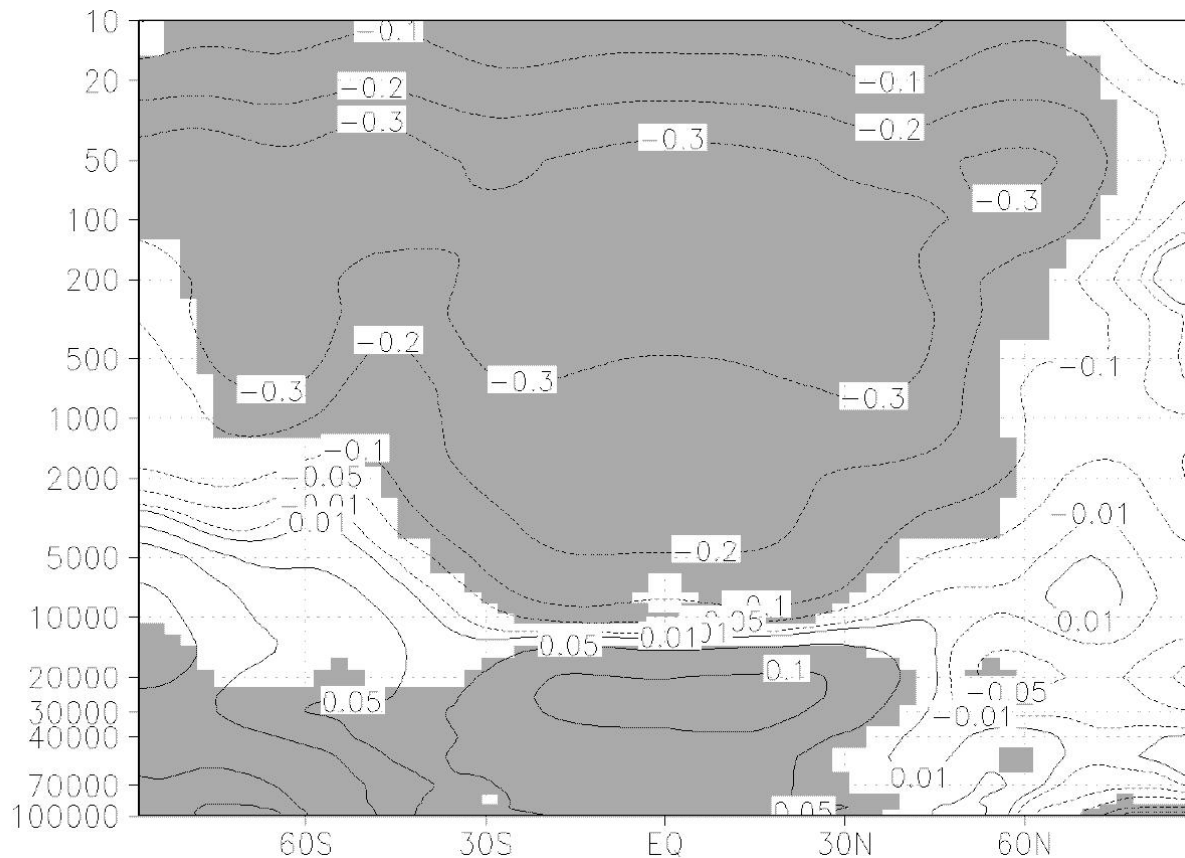
Figure 3: same as figure 1 for the period 2080-2099.

For the mid of the century (2031-2050), the model shows a cooling over the Artic, a small warming over the Antarctic, due to CO_2 and a cooling in the stratosphere (figure 2). The NO_x impact exhibits a strong warming over the Arctic (+0.4 K), a cooling over the Antarctic and a warming in the upper stratosphere (0.04 K), while the CIC impact leads to a warming in the troposphere up to 0.15 K, largest in June and July (not shown).

In the end, the total impact has a significant warming over 0.1 K in the entire troposphere, up to 0.2 K, and a significant cooling in the stratosphere (-0.2 K), all year round (not shown).

At the end of the century (2080-2099), the CO_2 effect generates a warming up to 0.2 K in the troposphere, that is the largest in September, and a warming of 0.1 K as global average for the 2m temperature; meanwhile a cooling is obtained in the stratosphere (-0.3 K).

We modelled overall small NO_x effects (even for the end of the 21st century). This is possibly due to a very limited impact on the ozone formation while a large imposed CH_4 concentration decrease in the troposphere, that produce a negative radiative forcing, and counterbalance the positive radiative forcing attributable to additional ozone.

The combined effect of CO_2 and NO_x is however larger than that of CO_2.

The CIC impact assessment is not yet finalised, but for the first half of the 21st century the impact is larger than that of CO_2 for the same period so we expect even larger CIC induced warming towards the end of the 21st century.

3.2 *Radiative forcing*

The resulting distributions of the 'fuel' tracer lead to radiative perturbations associated to aircraft, in the main corridors, but also in the neighbouring areas. The evolution during the 21st century shows a spreading impact over the entire Northern Hemisphere and the continents of the Southern Hemisphere, except Antarctica. The values of the Top Of Atmosphere (TOA) radiative forcing strongly increase by about a factor of 10 between the beginning and the end of the 21st century. A similar radiative impact was also found by Olivié et al. (2012) who used a former version of CNRM-CM with somewhat lower values (see Table 1).

Table 1:

TOA radiative forcing (mW/m^2)	2005	2050	2100
Olivié et al, ACP, 2012	24	101	211
This study	31 (*)	131	290

(*) corresponding to the tuning year according to (Burkhardt and Kärcher, 2011)

3.3 *Some other results*

The impact of the aviation CO_2 emissions on the SST is evident only at the end of the 21st century with a warming by 0.1 K, while that of the NO_x emissions, is not significant throughout the examined period.

We expect that the CIC impact on SST towards the end of the 21st century will be of similar magnitude than that of the CO_2 emissions.

No clear signal associated to aircraft was found neither on sea-ice nor on precipitations.

4   CONCLUSIONS

A version of CNRM-CM5, a global climate model coupled with ocean and sea-ice models, with online stratospheric chemistry in the atmosphere, has been successfully used to study the impact of aviation on the atmospheric chemistry and climate over the period 1940-2100. Several forcing agents were considered, such as emissions of CO_2, NO_x, CO, contrails and contrail induced cirrus. The model was run for a century as spinup, and revealed deficiencies in modelling the Arctic sea-ice, probably due to large differences between the resolutions of the atmosphere and of the ocean used (respectively 2.8° x 2.8° and 1° x 1°), resulting in erroneous energy fluxes at the sea-ice edges.

The impact of aviation studied with CNRM-CM5 reproduces the well-known pattern: a warming in the troposphere and a cooling of the stratosphere. However, the impact is generally smaller for both present day and future conditions than previous studies suggest – possibly due to higher de-

grees of freedom in the model, e.g. higher model variability (online coupled stratospheric chemistry).

For present-day conditions, the aviation impact is almost negligible for individual forcing and the largest effect is found for CIC.

At the end of 21st century, the CO_2 effect generates a warming of up to 0.2 K in the troposphere and a warming of 0.1 K (global average) for the near surface temperature, while a cooling is obtained in the stratosphere (-0.3 K). The NO_x effects are generally very weak.

The results on temperature are in agreement with those reported in Olivié et al. (2012) that used a similar AOGCM but with a simplified stratospheric chemistry, although the impacts are sometimes smaller.

As a perspective to this work, the problem of discrepancy between the oceanic and the atmospheric grids should be addressed. The chemistry developments should account for tropospheric chemistry in general, and include a more sophisticated CIC parameterization to better assess the aviation impact.

REFERENCES

Burkhardt, U. and Kärcher, B., 2011: Global radiative forcing from contrail cirrus, *Nature Climate Change*, 1, 54–58, doi:10.1038/NCLIMATE1086.

D. Cariolle, D. Caro, R. Paoli, D.A. Hauglustaine, B. Cuénot, A. Cozic, and R. Paugam, 2009: Parameterization of plume chemistry into large-scale atmospheric models: Application to aircraft NO emissions. *J. Geophys. Res.*, 114, D19302, doi:10.1029/2009JD011873.

Michou, M., D. Saint-Martin, H. Teyssèdre, A. Alias, F. Karcher, D. Olivié, A. Voldoire, V.-H. Peuch, H. Clark, J.N. Lee and F. Chéroux, 2011: A new version of the CNRM Chemistry-Climate Model, CNRM-CCM: description and improvements from the CCMVal2 simulations, *Geosci. Model Dev.*, 4, 873-900, 2011, www.geosci-model-dev.net/4/1/2011, doi:10.5194/gmd-4-873-2011.

Morcrette J.-J, Mlawer, E..J., Iacono, M.J., and Clough, S. A., 2001: Impact of the radiation-transfer scheme RRTM in the ECMWF forecasting system, *ECMWF Newsletter* No. 91.

Olivié, D.J.L., D. Cariolle, H. Teyssèdre, D. Salas, A. Voldoire, H. Clark, D. Saint-Martin, M. Michou, F. Karcher, Y. Balkanski, M. Gauss, O. Dessens, B. Koffi, and R. Sausen, 2012: Modeling the climate impact of road transport, maritime shipping and aviation over the period 1860–2100 with an AOGCM. *Atmos. Chem. Phys.*, 12, 1449-1480.

Schumann, U. and H. Huntrieser, 2007: The global lightning-induced nitrogen oxides source , *Atmos. Chem. Phys.*, 7, 3823-3907.

Voldoire A., E. Sanchez-Gomez, D. Salas y Mélia, B. Decharme, C. Cassou, S.Sénési, S. Valcke, I. Beau, A. Alias, M. Chevallier, M. Déqué, J. Deshayes, H. Douville, E. Fernandez, G. Madec, E. Maisonnave , M.-P. Moine, S. Planton, D.Saint-Martin, S. Szopa, S. Tyteca, R. Alkama, S. Belamari, A. Braun, L. Coquart, F. Chauvin, 2013 : The CNRM-CM5.1 global climate model: description and basic evaluation. *Climate Dynamics*, 40, 2091-2121, DOI:10.1007/s00382-011-1259-y.

Global mean temperature change from shipping towards 2050: Improved representation of the indirect aerosol effect in simple climate models

M.T. Lund[*], J. Fuglestvedt
CICERO - Center for International Climate and Environmental Research Oslo, Oslo, Norway

V. Eyring, J. Hendricks, M. Righi
Deutsches Zentrum für Luft- und Raumfahrt (DLR), Institut für Physik der Atmosphäre, Oberpfaffenhofen, Germany.

A. Lauer
International Pacific Research Center, University of Hawaii at Manoa, Hawaii, USA.

Now at Institute for Advanced Sustainability Studies e.V. (IASS) Potsdam,

D.S. Lee
Dalton Research Institute, Department of Environmental and Geographical Sciences, Manchester Metropolitan University, United Kingdom.

The shipping sector is a significant source of CO_2 and other pollutants, and has a complex impact on climate through mechanisms that results in both warming and cooling effects and that operate on very different temporal scales. The net temperature change depends on the mix of emissions. We utilize a range of emission scenarios for shipping as input to a simple climate model (SCM) to determine the induced present-day and anticipated future global mean radiative forcing (RF) and surface temperature change.(published as Lund et al. 2012 in Environ. Sci. Technol.) Ship emission scenarios consistent with the new regulations on nitrogen oxides (NO_x) and sulfur dioxide (SO_2) from the International Maritime Organization (IMO) (Buhaug et al., 2009) and the Representative Concentration Pathways (RCPs) 4.5 and 8.5 (Clarke et al., 2007; Riahi et al., 2007; Smith & Wigley, 2006; Wise et al., 2009) are used (Figure 1).
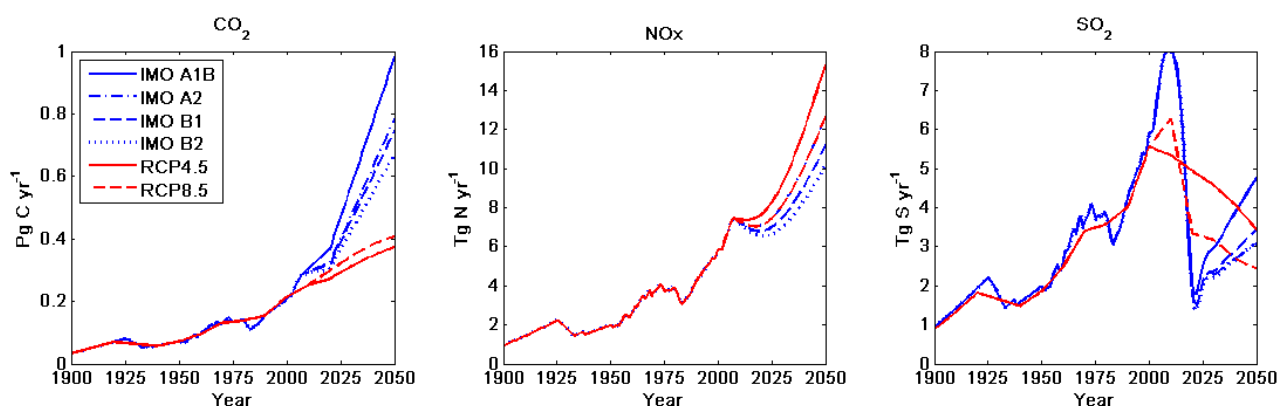
Figure 1: Historical emissions of CO2, NOx and SO2 from shipping and future emission developments to year 2050 from IMO (blue: A1B (solid), A2 (dash-dot), B1 (dashed), B2 (dotted)) and RCP (red: 4.5 (solid) and 8.5 (dashed)). Units: Pg C yr-1, Tg N yr-1, Tg S yr-1. From Lund et al. (2012).

[*] *Corresponding author:* Marianne T. Lund, CICERO - Center for International Climate and Environmental Research Oslo, Oslo, Norway, m.t.lund@cicero.uio.no

We focus particularly on the indirect aerosol effect (IAE), which gives an important contribution to the cooling impact from shipping. However, the magnitude of the IAE, as well as its dependence on SO_2 emissions, is uncertain (Eyring et al., 2010). We explore the relationship between the IAE and SO_2 emissions using results from the global aerosol-climate model EMAC-MADE (Lauer et al., 2009; Lauer et al., 2007; Righi et al., 2011) in order to improve the parameterization of IAE in the SCM. We develop and test new parameterizations that accounts for non-linearities in the RF of ship-induced IAE. The global mean ship-induced RF and total net surface temperature change are first calculated using the standard linear parameterization and reference RF value for IAE in the SCM. Next the standard linear parameterization of IAE is replaced with linear and logarithmic fits to data from EMAC-MADE simulations. These simulations cover various totals and geographical distributions of emissions from shipping, as well as different assumptions on the initial aerosol size distribution.

We find that shipping causes a net global cooling impact throughout the period 1900-2050 across all parameterizations and scenarios. Because of the expected reductions in SO_2 and NO_x emissions reflected in the scenarios, the cooling impact of shipping is initially reduced after 2010. However, in the IMO scenarios the increase in activity outweighs emission reductions from more stringent regulations. The emissions of NO_x and SO_2 increase again and the cooling effect strengthens again despite increases in CO_2. In the RCPs, reductions in SO_2 and NO_x continue up to 2050 and beyond, and result in a continued weakening of the cooling. There is a wide range in the calculated total net global mean temperature change due to shipping in 2050 depending on parameterization of IAE; from -0.03[-0.07,-0.002]°C to -0.3[-0.6,-0.2]°C in the A1B scenario (Figure 2). The uncertainties in the ship-induced temperature change resulting from uncertainties in RF and climate sensitivity, and the differences between calculations with different parameterizations of IAE, are much larger than the differences across the scenarios. This emphasizes the importance of properly representing the IAE in simple climate models and to reflect the uncertainties from complex global models.
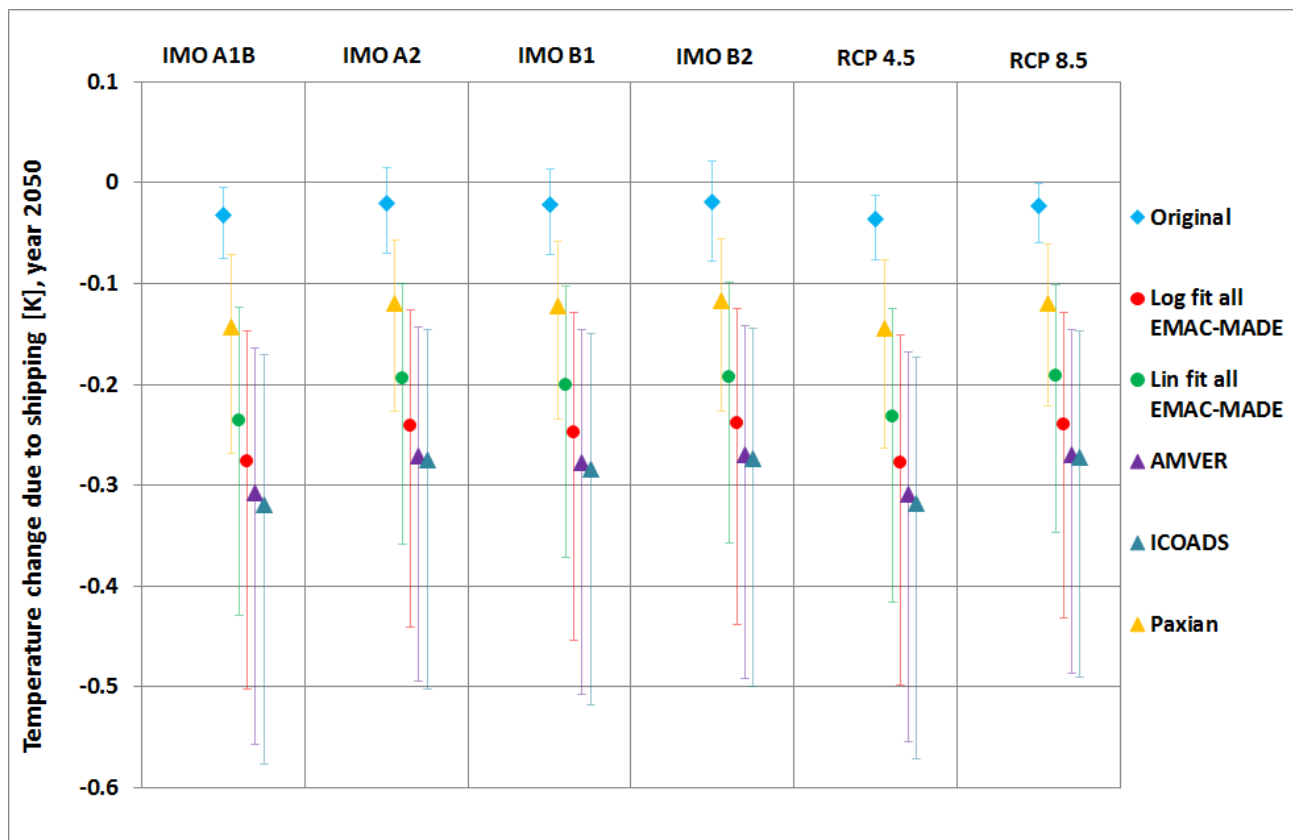

Figure 2: Total net global mean temperature change [K] in 2050 due to shipping in each scenario/pathway (IMO A1B, IMO A2, IMO B1, IMO B2, RCP4.5 and RCP8.5) obtained with different parameterizations of the indirect aerosol effect in the SCM. Error bars show uncertainty (±1 standard deviation) in radiative forcing and climate sensitivity. Uncertainties are calculated using existing literature estimates and a Monte Carlo approach. From Lund et al. (2012).

Our calculations show that the future ship-induced temperature response is likely a continued cooling if SO_2 and NO_x emissions continue to increase due to a strong increase in activity, despite current regulations. This will also exacerbate the significant additional negative impacts of shipping, such as acidification and health-related problems (e.g. Ashmore (2005); Corbett et al. (2007); Winebrake et al. (2009)). As has been emphasized in several previous studies, a continued cooling response does not negate the necessity for reductions in CO_2 emissions, which are crucial to limiting the global climate impact of the sector since the warming effect of CO_2 is long-lived.

REFERENCES:

Ashmore M. R. 2005. Assessing the future global impacts of ozone on vegetation. Plant Cell and Environment. 28(8), 949-964.

Buhaug Ø., Corbett J. J., Endresen Ø., Eyring V., Faber J., Hanayama S., Lee D. S., Lee D., Lindstadt H., Mjelde A., Pålsson C., Wanquing W., Winebrake J. J. & Yoshida K. 2009. Second Study on Greenhouse Gas Emissions from Ships, International Maritime Organization (IMO) London, UK.

Clarke L., Edmonds J., Jacoby H., Pitcher H., Reilly J. & Richels R. 2007. Scenarios of greenhouse gas emissions and atmospheric concentrations. Sub-report 2.1A of Synthesis and Assessment Product 2.1 by the U.S. Climate Change Science Program and the Subcommittee on Global Change Research. Department of Energy, Office of Biological & Environmental Research, Washington, 7 DC., USA, 154pp.

Corbett J. J., Winebrake J. J., Green E. H., Kasibhatla P., Eyring V. & Lauer A. 2007. Mortality from ship emissions: A global assessment. Environmental Science & Technology. 41(24), 8512-8518, DOI: 10.1021/es071686z.

Eyring V., Isaksen I. S. A., Berntsen T., Collins W. J., Corbett J. J., Endresen O., Grainger R. G., Moldanova J., Schlager H. & Stevenson D. S. 2010. Transport impacts on atmosphere and climate: Shipping. Atmospheric Environment. 44(37), 4735-4771, DOI: 10.1016/j.atmosenv.2009.04.059.

Lauer A., Eyring V., Hendricks J., Jockel P. & Lohmann U. 2007. Global model simulations of the impact of ocean-going ships on aerosols, clouds, and the radiation budget. Atmospheric Chemistry and Physics. 7, 5061-5079.

Lauer A., Eyring V., Corbett J. J., Wang C. F. & Winebrake J. J. 2009. Assessment of Near-Future Policy Instruments for Oceangoing Shipping: Impact on Atmospheric Aerosol Burdens and the Earth's Radiation Budget. Environmental Science & Technology. 43(15), 5592-5598, DOI: 10.1021/es900922h.

Lund et al. (2012). Global-mean temperature change from shipping towards 2050: Improved representation of the indirect aerosol effect in simple climate models. *Environ. Sci. Technol.,* 46 (16), pp 8868–8877, DOI: 10.1021/es301166e

Lund M. T., Eyring V., Fuglestvedt J., Hendricks J., Lauer A., Lee D. & Righi M. 2012. Global-mean temperature change from shipping toward 2050: Improved representation of the indirect aerosol effect in simple climate models. Environmental Science & Technology. 46(16), 8868-8877, DOI: 10.1021/es301166e.

Riahi K., Grubler A. & Nakicenovic N. 2007. Scenarios of long-term socio-economic and environmental development under climate stabilization. Technological Forecasting and Social Change. 74, 887-935, DOI: 10.1016/j.techfore.2006.05.026.

Righi M., Klinger C., Eyring V., Hendricks J., Lauer A. & Petzold A. 2011. Climate Impact of Biofuels in Shipping: Global Model Studies of the Aerosol Indirect Effect. Environmental Science & Technology. 45(8), 3519-3525, DOI: 10.1021/es1036157.

Smith S. J. & Wigley T. M. L. 2006. Multi-gas forcing stabilization with the MiniCAM. Energy Journal (Special Issue #3), 373-391.

Winebrake J. J., Corbett J. J., Green E. H., Lauer A. & Eyring V. 2009. Mitigating the Health Impacts of Pollution from Oceangoing Shipping: An Assessment of Low-Sulfur Fuel Mandates. Environmental Science & Technology. 43(13), 4776-4782, DOI: 10.1021/es803224q.

Wise M., Calvin K., Thomson A., Clarke L., Bond-Lamberty B., Sands R., Smith S. J., Janetos A. & Edmonds J. 2009. Implications of Limiting CO2 Concentrations for Land Use and Energy. Science. 324(5931), 1183-1186, DOI: 10.1126/science.1168475.

The climate impact of travel behaviour: a case study for Germany

B. Aamaas[*]
Center for International Climate and Environmental Research – Oslo, CICERO, Norway

J. Borken-Kleefeld
International Institute for Applied Systems Analysis, IIASA, Austria

G. P. Peters
Center for International Climate and Environmental Research – Oslo, CICERO, Norway

ABSTRACT: To help understand the mitigation potential of changing travel behavior requires disaggregating the climate impacts of transportation by transport mode, distance, and socio-economic factors. Here we use disaggregated data on travel behavior to calculate the climate impact of Germans traveling nationally and internationally in 2008. We include all relevant long-lived greenhouse gases and short-lived climate forcers and use global temperature change for 50 years of sustained emissions as the climate metric. We find that the total climate impact is determined almost entirely by car (~50%) and air travel (~43%), with smaller contributions from public transportation. The climate impact from the highest income group is 250% larger than from the lowest income group. However, mitigation must address the middle classes which account for more than two thirds of the total impact. The relatively few trips beyond 100 km contribute more than half of the total impact because of the trip distance and use of aircraft. Individual behavioral changes, like shifting transport modes or reducing distance and frequency, can lead to useful emission reductions.

1 INTRODUCTION

The climate impact for transport modes have typically been investigated for global or regional average conditions. However, neither trips nor their climate impact are evenly distributed among the population. Further, some trips give a much larger impact than other trips (e.g., air travel versus public transport). We analyze these differences for German conditions in 2008 (Follmer et al., 2010).

The emissions from the different transport modes consist of a mix of CO_2 and a few other long-lived greenhouse gases (LLGHGs in the Kyoto Protocol: CO_2, CH_4, N_2O, SF_6, HFCs, and PFCs) and air pollutants that influence the radiative balance of the atmosphere. The air pollutants, often called short lived climate forcers (SLCFs: BC, OC, SO_2, NO_x, VOC, CO, contrail, and aircraft induced cirrus), affect climate either directly (e.g., BC) or indirectly through chemical reactions (e.g., NO_x). Due to different radiative efficiencies and lifetimes, emissions need to be weighted with suitable metrics to compare for their climate impact (Fuglestvedt et al., 2010). The selection of a specific metric is not purely scientific, but involves value judgments (Fuglestvedt et al., 2010;Fuglestvedt et al., 2003).

2 METHODS

The total climate impact from travel *CI* for a group of people *g* is calculated as the product of the distance traveled (*TV*) with a transport mode *m* times an average emission factor *EF* for species s

---
[*] *Corresponding author:* Borgar Aamaas, Center for International Climate and Environmental Research – Oslo (CICERO), PB 1129 Blindern, 0318 Oslo, Norway. Email: borgar.aamaas@cicero.uio.no

times a suitable emission metric (*AM*) for this species, summed over all species emitted and all transport modes used in the period:

$$CI_g = \sum_m \sum_s TV_{m,g} \times EF_{m,s} \times AM_s \tag{1}$$

2.1 *Travel behavior data*

We analyze travel behavior of Germans because it is one of the largest countries of Europe for which comprehensive and detailed information from travel surveys are available. To estimate the transport volume (*TV*), we use the latest national survey of travel behavior (Follmer et al., 2010). The survey data include distance travelled, number of trips, mode choice and trip purpose. Business trips are included, as well as travel within and outside of Germany.

The travel data is differentiated into five classes of the "household economic status", which allows us to investigate how economic wealth affects travelling. The economic status is defined as the household's net income divided by the weighted number of household members, giving an equivalent income relative to the mean domestic household income. We have also calculated the income elasticities of trips, travel, and climate impact, which is a measure of how sensitive a dependent variable is to an increase in income

$$\varepsilon = \left(\frac{dT}{dI}\right)\left(\frac{I}{T}\right) \tag{2}$$

where *I* is net income and *T* is the dependent variable.

We separate trips that are shorter than 25km, between 25 and 100 km, and above 100 km. We term these distances as 'urban', 'inter-urban', and 'long-distance' travel. In order to include all long-distance travel, we combine survey data for regular daily trips and overnight travel.

2.2 *Emission factors*

The emission factors cover the species CO_2, CH_4, N_2O, NO_x, VOC, CO, BC, OC, SO_2, contrail, and aircraft induced cirrus (AIC) for different vehicles and relate to average real-world driving condition for Germany in the year 2005. For most vehicles, the numbers are extracted from the emission factor data base HBEFA3.1 (2010). For aircrafts, the emissions are based on the actual fuel use reported by Lufthansa (2009). We assume that short flights spend less time in the critical zone for contrail and AIC formation. The very limited ferry transport use emissions factors from Makela (2009). Upstream emissions for the provision of fuels and electricity are included, but not emissions from production of vehicles or infrastructure.

2.3 *Emission metrics*

To convert the emissions into the climate impact, we use an emission metric. There are a variety of value choices when selecting an emission metric. The main ones are whether to choose end-point or integrated view (forcing or temperature), what type of emission profile (pulse, sustained, scenario), and what time horizon (e.g. 20, 100, 500 years) (Fuglestvedt et al., 2003). It is also possible to apply metrics in absolute form or to normalize them to a reference gas, usually taken as CO_2. The two most common metrics are integrated radiative forcing (Absolute Global Warming Potential, AGWP) and temperature (Absolute Global Temperature change Potential, AGTP). Since metrics are choice dependent, there is not a single metric with a specific time horizon that is more correct to use than others. As much attention is to avoid a 2°C global temperature increase, we select AGTP. This threshold is likely reached in half a century (Joshi et al., 2011); hence, a time horizon of 50 years is selected. Here, we use sustained emissions to account for the continued transport activity into the future and to include the importance of SLCF when activities continue beyond one year.

The metric values are based on the parameterization of the species' radiative efficiency and lifetime, which comes from these studies: For the long-lived greenhouse gases from IPCC (2007), for BC, OC, SO_2, contrail, and aircraft induced cirrus from Fuglestvedt et al. (2010), for aircraft NO_x from Stevenson et al. (2004), for surface NO_x the mid-lat run from Wild et al. (2001), for CO from Derwent et al. (2001), and for VOC from Collins et al. (2002). The parameterization of the climate system is based on the Hadley model (Boucher and Reddy, 2008). Since the uncertainty of the indirect effect of SO_2 emissions from shipping is large, this indirect effect has not been included. With the emission factors and emission metric parameterizations presented here, the CO_2-equivalent emissions per passenger km for the different transport modes are given in Table 1.

Table 1: The CO_2-equivalent emissions per passenger km. The numbers are based on average German driving conditions in 2005 and the metric GTP for sustained emissions over 50 years.

Transport mode	g CO_2-equivalent per passenger km
Air (<800 km)	416
Air (>800 km)	371
Ferry	205
Car	144
Local bus	105
Local train	90
Coach	59
Long distance train	43

3 RESULTS

3.1 *By household economic status*

Table 1 shows the transport modes used for the average German in terms of number of trips, travel volume, and climate impact. In terms of number of trips per year, the spread in observed mobility is relatively small, with the higher income groups travelling slightly more frequent than the lower income groups. The average is 1250 trips per year. The difference increases when looking at the travel volume, since the highest income groups fly much more frequent and also drive more frequently than the lowest income groups. The average is 22400 km/yr. With the selected emission metric (AGTP, sustained for 50 years), the difference in climate impact widens even more. That is because the high income groups fly the most and aircraft has a much larger specific climate impact per unit of transport than car and even more so for public transport. One main finding is that the climate impact of personal travel is governed by two transport modes, car and air transport, with a 50% and 43% share of the total, respectively. This finding is robust across a range of emission metrics and time horizons. While the top 10% of the population stand for 20% of the climate impact, the middle income classes are much larger (two-thirds) and, thus, also more important for the total climate impact (two-thirds). Thus, if significant reductions in climate impact is wanted, large segments of the society has to be involved, not just the rich.

Table 2: The average behavior of Germans in terms of share of trips, travel volume, and the calculated climate impact for the different transport modes. The metric used is AGTP for sustained emissions over 50 years.

Transport mode	No. trips (%)	Travel volume (%)	Climate impact (%) [$AGTP^{Sus, 50yrs}$]
Car travel (as driver or passenger)	58	59	50
Aircraft (domestic and international)	<1	23	43
Public transport (bus & coach, tram, metro and rail)	8	15	5
Walking	24	2	0
Bicycle	10	2	0
Other, e.g. ferry	<1	1	2
Average totals	1250 trips	22400 km	1.3E-10 K

The income elasticity increases strongly when going from number of trips (0.13) to travel volume (0.56) and to climate impact (0.75). The elasticities are close to 0 for all transport modes except for car transport (0.56) and air transport (1.17), making public transport close to an "inferior good", car transport a "normal good" and air travel a "luxury good" (Gravelle and Rees, 2004).

3.2 *By trip length*

In Figure 1, we present average German travel for number of trips, travel volume, and climate impact separated by trip distance. The majority of trips (90%) are urban, while only 2% are long-distance travel. Car travel is important since its share is more than 50% of all trips in all length categories. In terms of travel volume, the travel is more evenly distributed between the groups. 48% of the travel volume comes from long-distance travel, which is most driven by the few, but very long air travels. On average, Germans fly twice a year covering about 2600 km on each trip. The climate

impact is governed by the long-distance trips, as that category takes 59% of the total. The two other categories have a share of about 20% each.
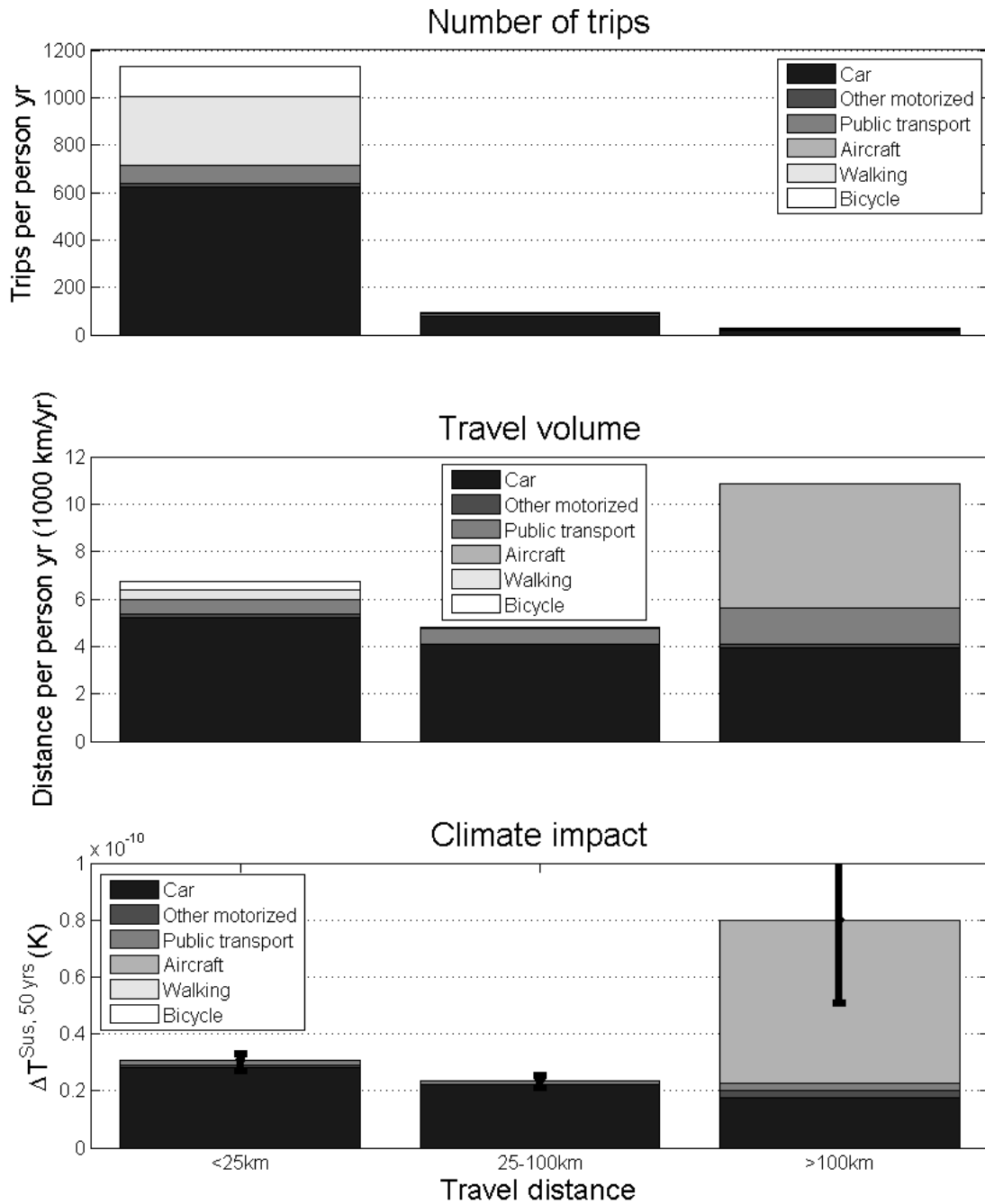

Figure 1: What an average German travels in a year in regards to number of trips, travel volume, and climate impact for urban, inter-urban, and long-distance travel. The bars represent the ±1 SD uncertainty due to the climate impact calculation of AGTP$^{Sus, 50yrs}$. For the long distance group, the bar goes up to 1.7E-10 K.

4 CONCLUSIONS

We have here demonstrated the analysis of the climate impacts of travel behavior for the case of Germany. The methodology presented is more generally applicable to other countries and scenarios where the data exists; however, our results are more widely applicable only to countries that are similar to Germany in wealth and characteristics. The methodology shown here could be used to investigate the climate impact of travel behavior for other countries or with emphasis on other parameters, socio-economic or technological.

The climate impact of personal travel is governed by two modes, car (50%) and air travel (43%). This conclusion is robust whether we look at all relevant climate effects or only CO_2. In terms of travel per person kilometer, air travel has the highest climate impact. We found that people in high income groups travel much more (elasticity of 0.56) and have a much higher climate impact (elasticity of 0.75) than people in low income groups. For air travel, the elasticity is 1.17, indicating that the use of air travel increases faster than income. In a mitigation perspective of the transportation sector, the large middle income classes need to be addressed since those groups are responsible for more than two thirds of the total impact. The relatively few long-distance trips account for more than half of the total impact since the trip distances are long and the use of aircraft. Any change in these trips will have a measureable impact on the total.

5   ACKNOWLEDGEMENT

REFERENCES

Boucher, O., and Reddy, M. S.: Climate trade-off between black carbon and carbon dioxide emissions, Energy Policy, 36, 193-200, 2008.

Collins, W. J., Derwent, R. G., Johnson, C. E., and Stevenson, D. S.: The oxidation of organic compounds in the troposphere and their global warming potentials, Climatic Change, 52, 453-479, 10.1023/a:1014221225434, 2002.

Derwent, R. G., Collins, W. J., Johnson, C. E., and Stevenson, D. S.: Transient behaviour of tropospheric ozone precursors in a global 3-d ctm and their indirect greenhouse effects, Climatic Change, 49, 463-487, 10.1023/a:1010648913655, 2001.

Follmer, R., Gruschwitz, D., Jesske, B., Quandt, S., Lenz, B., Nobis, C., Köhler, K., and Mehlin, M.: Mobility in germany 2008 (mobilität in deutschland 2008), INFAS & DLR, 214, 2010.

Fuglestvedt, J. S., Berntsen, T. K., Godal, O., Sausen, R., Shine, K. P., and Skodvin, T.: Metrics of climate change: Assessing radiative forcing and emission indices, Climatic Change, 58, 267-331, 2003.

Fuglestvedt, J. S., Shine, K. P., Berntsen, T., Cook, J., Lee, D. S., Stenke, A., Skeie, R. B., Velders, G. J. M., and Waitz, I. A.: Transport impacts on atmosphere and climate: Metrics, Atmospheric Environment, 44, 4648-4677, 2010.

Gravelle, H., and Rees, R.: Microeconomics, 3rd ed., Financial Times/ Prentice Hall, Essex, England, 2004.

HBEFA3.1: Handbook emission factors for road transport, in, http://www.hbefa.net/e/index.html, 2010.

IPCC: Climate change 2007: The physical science basis. Contribution of working group i to the fourth assessment report of the intergovernmental panel on climate change, edited by: Solomon, S., Qin, D., Manning, M., Chen, Z., Marquis, M., Averyt, K. B., Tignor, M., and Miller, H. L., Cambridge University Press, Cambridge, United Kingdom and New York, NY, USA, 2007.

Joshi, M., Hawkins, E., Sutton, R., Lowe, J., and Frame, D.: Projections of when temperature change will exceed 2 [deg]c above pre-industrial levels, Nature Clim. Change, 1, 407-412, 2011.

Lufthansa: Umweltkennzahlen 2009, 2009.

Average emissions and energy consumption of passenger waterborne traffic per assenger kilometre in 2007, finland: http://www.lipasto.vtt.fi/yksikkopaastot/henkiloliikennee/vesiliikennee/kaikki_matkustajae.htm, access: 09.28.2011, 2009.

Stevenson, D. S., Doherty, R. M., Sanderson, M. G., Collins, W. J., Johnson, C. E., and Derwent, R. G.: Radiative forcing from aircraft nox emissions: Mechanisms and seasonal dependence, J. Geophys. Res., 109, D17307, 10.1029/2004jd004759, 2004.

Wild, O., Prather, M. J., and Akimoto, H.: Indirect long-term global radiative cooling from nox emissions, Geophys. Res. Lett., 28, 1719-1722, 10.1029/2000gl012573, 2001.

Comparability of calculated emissions in freight transport

S. Seidel[*], V. Ehrler, A. Lischke
Deutsches Zentrum für Luft- und Raumfahrt e.V., Institute of Transport Research Berlin, Germany

Keywords: Carbon Footprint, Calculating CO_2 emissions, Freight transport, Supply chain

ABSTRACT: In 2007 freight transport had a transport volume of 650 billion tkm in Germany. According to forecasts (Prognos AG) it will increase up to 1200 billion tkm by 2050 (BMU 2009). Without significant changes to working practices it is to be assumed that this will result in an increase of related energy consumption, CO_2, and CO_{2e}. At the same time, the EU has stated, that CO_2 emissions should be reduced by 20% by 2020, compared to the levels of 1990.

In this context so-called green logistics become an important topic for producers, shippers and logistics service providers. Several companies in Europe follow a green strategy and calculate their CO_2 emissions already in order to identify the emissions' sources and to reduce energy consumption.

Currently a wide range of different methodologies and tools for CO_2 emission calculation are in use by the various actors. For being able to compare and combine emissions along various supply chains and their elements, a common methodology and standard is needed.

COFRET, the EU part-funded project for the Carbon Footprint of Freight Transport, will develop a methodology and a framework for a standard procedure for the calculation of carbon emissions, considering all modes of transport in the supply chain. First common indicators of already existing and used tools, databases and methodologies have been identified and current gaps have been analysed. Once the COFRET methodology has been drafted it will be tested through real-case scenarios by key stakeholders.

It is the aim of this paper to present an overview on the current initiatives for the development of a pan-European CO_{2e} emission calculation standard and to present the first findings of the COFRET project with a focus on identified needs and requirements of users and stakeholders towards a usable, viable standardised emission calculation methodology for supply chains.

1 INTRODUCTION

The European Union (EU) has stated that global temperatures should not exceed pre-industrial levels by more than 2°C in order to keep impacts of climate change at a manageable level. To achieve this target, European countries are expected to reduce their total annual Greenhouse Gas (GHG) emissions by at least 20% by 2020 and by 60-80% by 2050, compared to 1990 emission levels (Council of the European Union 2007). The current transport system, which currently relies on petroleum products for 95% of its energy, contributes about 23% of global anthropogenic CO_2 emissions and has thereby a significant contribution to the warming of the global climate (Rodrigue et al 2009; ITF 2010). Therefore, the reduction of $CO_{2(e)}$ emissions from transport has an important role to play; and for measuring and achieving such a reduction a basic calculation procedure is a needed instrument in order to effectively control $CO_{2(e)}$ emissions.

As a consequence green logistics is becoming a vital topic for more and more companies and many producers, shippers and logistics service providers already follow a green strategy and calculate their $CO_{2(e)}$ emissions in order to identify the emissions' sources and to reduce their energy consumption.

As there have been no regulations in the past for carbon footprint reporting in the sector of transport and logistics, several tools and methods were developed on the basis of individual initia-

---

[*] *Corresponding author:* Saskia Seidel, Deutsches Zentrum für Luft- und Raumfahrt e.V. (DLR), German Aerospace Center, Institute of Transport Research, Berlin, Germany, saskia.seidel@dlr.de

tives. They were set up by different organisations that had different approaches and intentions in their development. As a result, currently used tools have valuable starting points but different approaches. They differ for example in the:

- – greenhouse gases they take into account (e.g. some focus on energy consumption others focus on total CO_{2e}),
- – number of supply chain elements (SCE) they take into account,
- – approaches regarding the transport modes they consider,
- – databases used to calculate emissions (some calculations are based on data measured by individual companies and organisations, whereas sometimes default data are used that is provided by public sources (e.g. HBEFA, Ex-Tremis).

The use of different tools and methodologies in different companies leads to incomparable and incompatible results and subsequently to a lack of transparency. Furthermore, several transport and logistics service providers are often required to work together to realise a supply chain on national, European or global level. Hence, a harmonised calculation methodology is required to add the CO_{2e} emissions of every supply chain element and finally to contribute to a calculation of the carbon footprint on a product level.

From a regulatory point of view, France has become the first European country to require companies to calculate and publish the carbon footprint of transport services on bids, contract negotiations and invoices to customers and contract parties (Cordes 2012). This is enforced by a national decree which becomes into force in October 2013.

Initial attempts to address the problem of incomparability have been taken through standardisation initiatives such as CEN/TC 320/WG 10, which has produced a draft European norm (EN 16258) for calculation of the carbon footprint of transport services, and the ISO 14064-1:2006 which considers transport and logistics operations. EN 16258:2012 will be the first standard for the transport sector and will be announced at the end of 2012.

These standards do not consistently align the currently used tools and methods however, and e.g. EN 16258:2012 will only consider the transport and neither full logistics operations nor all transport elements of a supply chain. The lack of one Europe-wide or, more significantly, a globally applicable standard therefore remains.

COFRET (Carbon Footprint of Freight Transport) is a collaborative research and demonstration project funded by the European Commission which aims at contributing to the closure of this. The objective of the project COFRET is to develop and test a harmonised methodology and give a framework for the accurate calculation of the carbon footprint of transport and logistics along the full supply chain (Johansen et al 2012). Thereby COFRET encourages consideration of all transport modes and all logistics operations. A close cooperation with stakeholders as well as with initiatives that deal with the calculation of CO_{2e} emissions is an integral part of COFRET.

This paper provides an overview of the COFRET project. First, in section two the methodology applied within the project will be described. Secondly, section three deals with the terminology. In section four the results of the analysis of currently existing and used tools and methodologies is presented, whereas section five discusses the progress to date and six provides a conclusion.

2   METHODOLOGY DEVELOPMENT

The COFRET methodology will build on already existing tools and methodologies. It is used to compute CO_2 emissions of transport and logistics in the context of supply chains. This will be achieved by combining state-of-the-art elements of CO_2 and CO_{2e} emission calculations tools. Any gaps identified along the supply chain will be closed subsequently. In the following sections the identification process of the state-of-the-art calculation tools is described.

The first step was to get an overview of the currently available items on the market that deal with the calculation of greenhouse gas emissions. On the basis of an extensive literature survey, reports and papers etc. dealing with the calculation of greenhouse gas emissions in the sector of transport and logistics, were collected and reviewed. Moreover, methodologies, tools and data that are on the market available were also gathered.

For the analysis of the collected existing carbon footprint calculation methods, tools and data (collectively referred to as items) a template covering more than 70 aspects was used. This analysis

included basic information like a description of the item, whether it is publicly available and whether it is accessible for free or in return for a fee. The item's coverage and potential implications for later stages of the COFRET project were evaluated (Auvinen 2012). Furthermore, strengths and weaknesses of the items as well as their relevance for the COFRET project were recorded.

In addition to the literature survey, during spring 2012 interviews were conducted to identify the users' requirements, gaps of currently used tools as experienced by the users and to learn from their experience. Two kinds of interviews were conducted: in-depth telephone interviews and interviews via an online questionnaire. The online questionnaire was focused on a limited number of questions and served the purpose of gaining an overall impression of the strengths and weaknesses as well as user experiences of current calculations tools. It was sent out to around 400 organisations and companies. The in-depth questionnaire aimed at a very detailed insight into these aspects and they were held with organisations representing the various user fields, therefore shedding light on the different user groups and their needs.

Both questionnaires were divided into three sections, covering:
- who are the main users of emission data?
- why do stakeholders feel that there is a need for a CO_{2e} emission calculation tool?
- what are the technical specifications and accuracy requirements in a desired tool (Johansen et al 2012)?

In addition, two workshops were held - early in 2012 - during which an intensive analysis of the interviews' findings took place by reflecting and discussing them with users and developers of existing CO_{2e} calculation tools.

3   TERMINOLOGY

As specified in the draft for ISO 14067, the carbon footprint of a product (covering goods and services) can be defined as the "sum of greenhouse gas emissions and greenhouse gas removals of a product system, expressed in CO_2 equivalents". The life cycle approach is the basis for this definition and requires the inclusion of the entire life cycle of a transport service as a product system (de Ree et al 2012).

The COFRET methodology considers the greenhouse gases of carbon dioxide (CO_2), methane (CH_4) and nitrous oxide (N_2O) as they are the most important GHG compounds emitted due to combustion of fossil-fuels.
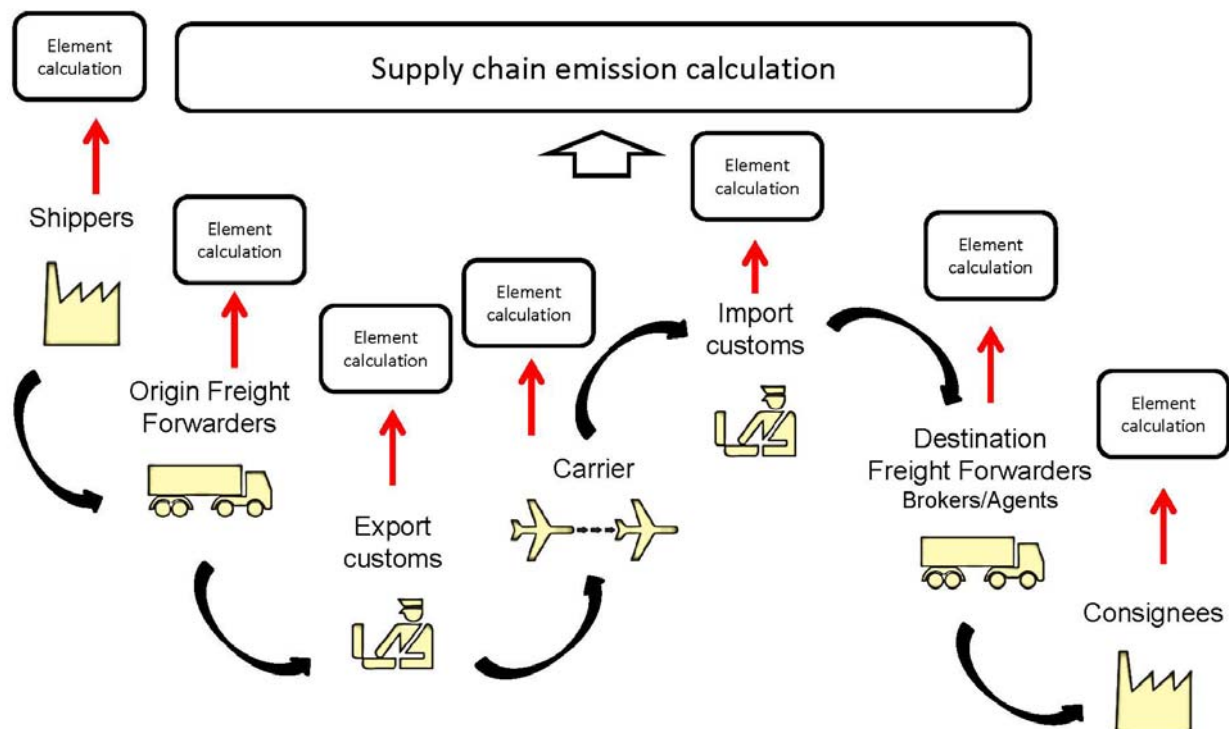
Figure 1 Example of a supply chain

A supply chain can be defined as "a system of entities being involved in producing, transforming and/or moving a product or service from suppliers to customers" (Leukel 2007). Consequently a supply chain can be divided into different elements. These supply chain elements can vary in their order, number, complexity etc., and can be combined into various configurations thus they are able to build different supply chains. The elements can be assigned to logistics and transport operations. Within the road transport mode we can, for example, distinguish between the basic supply chain elements full truck load shipment (FTL), less than full truck load shipment (LTL) and empty truck load (ETL) (de Ree et al 2012). Logistics operations within the COFRET's scope are loading and unloading, transport (transport by any mode, shunting, taxiing, idling, empty driving, transhipment), handling other than loading, special cargo handling (e.g. refrigerated cargo) and warehousing (storage between transports).

4 RESULTS

4.1 *Overview and main findings of user requirements and practices*

4.1.1 *Interview findings*

As described previously, about 400 questionnaires were sent out and over 40 in-depth-interviews were held for the identification of the users' needs.

As a result the following requirements could be recorded in the interviews:

The questionnaire replies demonstrated that there is a wide range of interests in green logistics among stakeholders (Figure 2). Some will only take the measures forced upon them, while others are either concerned about the sustainability of the logistics sector. Moreover, a few are prepared to exploit the marketing potential green logistics involves. Overall, the responses showed a real need for a common methodology, standardized emission factors and transparency over the calculations (Auvinen et al 2012). The calculation of emissions after transport has occurred is, for about 80 per cent of all respondents, of great importance and for 60 per cent of them calculation of the emissions prior to the transport occurring are highly important.
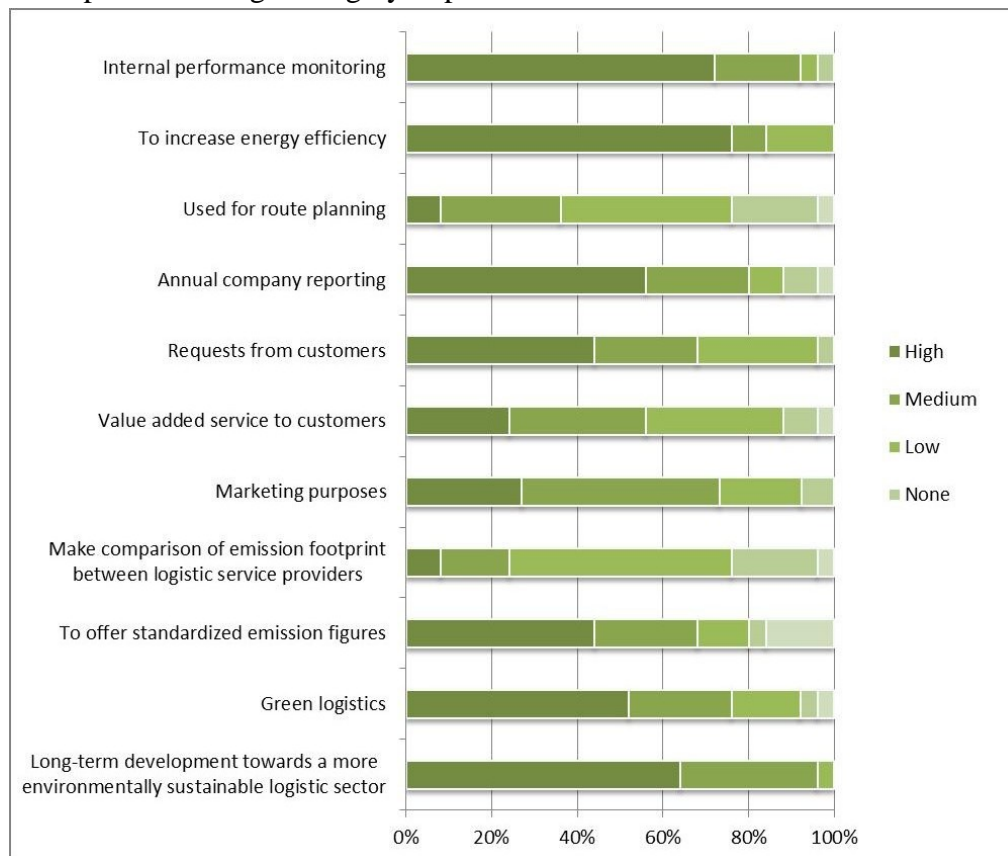
Figure 2 In-depth interviews: Motivations for the use of an emission calculation tool. (source: Johansen 2012, p.12)

The interviews showed that very often in-house tools are developed and used, so that a wide variety of different calculation methods and data sources is used for the emissions calculations by different companies. Due to the variety of these methods and data sources, and considering that most companies prefer an internally developed tool that meets their own specific requirements, a lot of effort needs to be put into creating a common framework for calculations to coincide as much as possible with current practices (Auvinen et al 2012).

4.1.2 *Workshop findings*

During the two workshops users and developers were addressed directly. Here reasons of calculating emissions, currently experienced weaknesses and the requirements and expectations toward future tools and the COFRET methodology were identified.

The two workshops showed that due to the growing ecological awareness of consumers the demand for comparable carbon footprint information for products is increasing. In addition, rising energy costs result in further pressure on companies to optimise their use of energy, especially for their logistics. Another circumstance that makes companies aware of the future significance of emissions calculation is the political discussion about the reduction of emissions.

Four main reasons were identified why companies calculate their emissions:

1) to increase energy efficiency and to be able to capture and improve the carbon efficiency of transport operations,
2) for internal control,
3) for their customers on different levels (e.g. product, shipment or company level) and
4) to see the effect of different company initiatives regarding the carbon footprint.

Besides these motivations, users mentioned the following weaknesses of current tools. Firstly, very often existing tools focus only one transport mode. Secondly, the differences in calculation methods lead to incomparable results and missing interfaces to the tools used by subcontractors, in other companies within the overall supply chain, or in other countries; taken together these factors make it impossible to combine results. Beside these they criticize that companies often have a lack of primary data and there are no standards to be found about which default data should be used in these circumstances. Lastly, currently available tools do not allow the calculation of emissions along full global supply chains.

As the forthcoming CEN standard could be established as an international ISO standard, another finding of the workshop is to build the COFRET methodology on EN 16258-2012 guidelines (Johansen 2012).

4.2 *Overview and main findings of existing methods, tools and data*

As a result of the initial screening phase 102 items were identified and classified in the following four categories by project partners, advisory board members and stakeholders, so building a comprehensive list of emission calculation items (Table 1):

1) Carbon footprint methodologies. These include actual standards, standard-like guidelines, guidebooks and schemes that provide the framework calculation and reporting of the carbon footprint.
2) Carbon footprint calculation tools. Contains all tools, instruments, software, algorithms and other applications that are used to carry out and facilitate the calculations of carbon footprint of transport and logistics along the supply chain or some part of it.
3) Emission factor databases. Comprised collections of GHG emission data that are needed in order to calculate carbon footprint of transport and logistics along the supply chain or some part of it.
4) Other activities like research projects, awareness raising initiatives and different types of communication forums and channels.

All in all the reviewing process covered 18 methodologies, 38 calculation tools, 12 databases and 34 other resources. It revealed that the number of carbon footprint calculation tools and data sources is vast, with wide differences in quality, coverage and originality. Nevertheless, it can be argued that among the existing methods, tools and databases suitable elements for calculation of carbon footprint of transport and logistics along supply chains already exist, even though a harmonised framework is currently missing (Auvinen et al 2012).

Categories	examples
Methodologies	EN 16258:2012 by CEN/T C3 20/WG10,
	2006 IPCC Guidelines,
	PAS 2060
Tools	Eco TransIT World,
	Map & Guide,
	Tremove
Data bases	Ex-Tremis,
	HBEFA,
	Lipasto
Other activities and initiatives	Smartway US,
	Greencart,
	World Ports Climate Initiative (WPCI)

Table 1 Example of emission calculation items and their classification

As the importance of the items was assessed by their relevance for the scope, 21 items were ranked as very important and 14 as relevant to COFRET in the first review (de Ree et al 2012). These 35 items were reviewed more extensively, partly involving the tools' developers. The vision of a harmonised methodology was the main criterion for the decision process on the items' inclusion in the COFRET methodology development.

Once the items were analysed and evaluated to identify best practice solutions and to find elements that could be used in a COFRET methodology, two consortium partners independently reassessed the importance with regard to the COFRET methodology. A ranking took place based on the COFRET objectives and the most important items were identified. As a result of this 15 of these 35 items will form a part of the foundation of further COFRET methodology developments and 14 will be used for additional contributions and for background information. The remaining six items were eventually classified as not relevant.

5   DISCUSSION

The work shows that a variety of different tools and databases exist. It also became evident that companies have a need to calculate emissions on different levels whilst at the same time they need a common methodology in order to calculate and report transport emissions.

Strengths and weaknesses of different items that deal with the calculation of emission within transport and logistics operations were assessed and first steps toward a development of a methodology that harmonises the current available methods and tools were taken. With regard to future use it is important that the COFRET methodology meets the expectations and needs of the individual organisations applying it, whilst at the same time providing a tool that is understood and accepted in the market in general. The challenge is that a balance must be struck between the user requirements for high flexibility and the accuracy of the methodology.

The aim is to have a common methodology for carriers and shippers and to collect and report validated data to enable reliable benchmarking of shippers and carriers. As the different end-users will have different supply chains and therefore different requirements it is important that the COFRET methodology offers the necessary flexibility to calculate these different supply chains emissions. By using a modular approach of supply chain elements a framework and methodology will be provided that offers this combination of flexibility, compatibility and comparability.

The CEN standard EN 16258 to be published by the end of 2012 is expected to have a major impact towards harmonisation, and as our analysis showed many tools and methods already consider CEN as of utmost importance. Also the COFRET methodology will fully comply with the CEN standard. In addition, COFRET will also cover non-transport elements such as handling processes. A close exchange with the CEN is integral part of COFRET.

6 CONCLUSIONS

This paper gives an overview of the first findings of the COFRET project. The next step for COFRET will be the development of the provisional version of the methodology. Based on this provisional version, a prototype will be developed to test the COFRET methodology in real-life supply chain situations. This will allow validation of the COFRET methodology and identification of any weaknesses and necessary improvements. Subsequently the feedback will be incorporated to adjust the COFRET methodology. A final COFRET methodology will be published at the end of 2013.

7 ACKNOWLEDGMENT

REFERENCES

Auvinen, Heidi; Mäkelä, Kari; Lischke, Andreas; Burmeister, Antje; de Ree, Diederik; Ton, Jaurieke, 2011: COFRET Deliverable D2.1 Existing methods and tools for calculation of carbon footprint of transport and logistics.

Auvinen, Heidi; Mäkelä, Kari; Gjerde Johansen, Bjørn; Ruesch, Martin, 2012: COFRET Deliverable D2.4 Methodologies for emission calculations – Best practices, implications and future needs.

Auvinen, Heidi, 2012: Calculating carbon footprint of freight transport and logistics: state of the art. April 4, 2012, not published.

[BMU] Bundesministerium für Umwelt, Naturschutz, und Reaktorsicherheit, 2009: Güterverkehr. Online http://www.bmu.de/verkehr/gueterverkehr/doc/39420.php retrieved April 2012.

Cordes, Michael, 2012: An CO2 Erfassung führt kein Weg vorbei. In: Verkehrs Rundschau 23/2012. p. 24.

Council of the European Union. 2007. Presidency Conclusions – Brussels, 8/9 March 2007. 7224/1/07 REV1. p.12. Online http://register.consilium.europa.eu/pdf/en/07/st07/st07224-re01.en07.pdf retrieved 08.08.2012

[ISO] International Organisation for Standardisation , 2011: ISO/CD 14067.3 Carbon footprint of products. Requirements and guidelines for quantification and communication. Working Draft.

[ITF] International Transport Forum, 2012: Greenhouse Gas Emissions: Country Data 2010. Online accessible: http://www.internationaltransportforum.org/Pub/pdf/10GHGcountry.pdf 27.07.2012

Rodrigue, Jean-Paul; Comtois, Claude; Slack, Brian, 2009: The Georaphy of Transport Systems. New York: Routledge, 352 pages, chapter 8, p.279 ff.)

Johansen, Björn; Eidhammer, Olav; Platz, Tilmann; Ruesch, Martin; Lischke, Andreas; Lewis, Alan, 2012: COFRET Deliverable D2.2: User Needs, Practices and Experiences in the Context of Carbon Footprint Calculations in Supply Chain Configurations. Published: 31. March 2012.

Leukel, J. (Ed.), 2007: BREIN Deliverable D3.3.1: BREIN Value Chain and Scenario-specific Supply Chain Definition.

Ree, Diederik de; Ton, Jaurieke; Davydenko, Igor; Chen, Ming; Kiel, Jan; Auvinen, Heidi; Mäkelä, Kari, 2012: D 3.1 Assessment and typology of existing CO2 calculation tools and methodologies

A conceptual framework for climate metrics

O. Deuber[*], G. Luderer, O. Edenhofer
Potsdam Institute for Climate Impact Research, Potsdam

ABSTRACT: The design of multi-gas mitigation policies requires methods for comparing the climate impact of different forcing agents, so-called metrics. A multitude of climate metrics has been presented in the literature. Key characteristics of any metric are (a) its impact function, i.e. its functional relationship to physical climate parameters, and (b) the weighting of impacts over time. In view of these characteristics we present a physico-economic framework which allows classifying climate metrics in a straight forward manner. From the economics perspective, the Global Damage Potential can be considered as a first-best benchmark metric since it ensures that the trade-off between different forcing agents is efficient. Our conceptual framework shows that virtually all climate metrics including Global Warming Potential and Global Cost Potential can be constructed as variants of this benchmark. The framework facilitates a structured discussion on climate metrics since it reveals normative assumptions and simplifications that are implicit to the choice of a climate metric. Further, the choice of metric is largely coined by trade-offs between different kinds of uncertainties, explicit ones which are directly linked to operational feasibility and implicit structural ones which reflect the degree of policy relevance. Based on our findings we suggest as an alternative option for policy applications to base metric approaches on an explicit analysis of the value-based, scientific and scenario uncertainties in the context of a physico-economic metric, rather than an elimination of relevant uncertainties by the choice of a physical metric.

1 INTRODUCTION

Methods for quantitatively comparing the potential climate impact of different radiatively active substances, so called metrics, are needed to establish an exchange ratio between different greenhouse gases in the context of a multi-gas emissions trading system (e.g. Fuglestvedt et al. 2010). The design of climate metrics, involves explicit or implicit assumptions on the functional relationship between climate impacts and physical climate change, and the weighting of impacts occurring at different points in time.

Here we provide a conceptual framework based on economic rationales, which allows classifying prevalent climate metrics from the literature. It highlights how scientific, economic and normative aspects of climate metrics interrelate, and aims to provide a valuable basis for trans-disciplinary discussions.

2 METHODOLOGICAL APPROACH

The starting point of the conceptual framework is a generalized formulation of an emission metric as previously introduced by Kandlikar (1996) and Forster et al. (2007). It is grounded in the cost-benefit analysis, building on marginal climate change impacts and marginal costs of emission reductions, and can be formalized as the integral over time of the incremental impact incurred by a pulse emission of gas i

---

$$AM_i = \int_0^\infty \frac{I(\vec{C}_{(ref+\Delta E_i)}(t)) - I(\vec{C}_{ref}(t))}{\Delta E_i} \cdot W(t) \ dt \qquad (1),$$

where the *impact function I* describes the emission-induced climate impact as a function of physical climate change along a reference concentration pathway *ref*. *W* specifies the *temporal weighting function*. The corresponding metric value M_i ($M_i = AM_i / AM_{CO_2}$) refers to the impact of 1 kg of emission *i* (ΔE_i) normalised to the one of 1 kg reference gas, usually CO_2 (ΔE_{CO2}).

The impact function relates the metric to a climate impact proxy, such as the change in global mean radiative forcing (RF), global mean temperature (ΔT), or economic damage. In some cases, also the rate of change of a climate impact parameter is used as proxy. An ideal metric would consider the entire causal chain of impacts, ranging from emission via concentration changes to physical climate impacts and economic damages. Since, however, the last step, quantifying damages as a function of physical impact parameters, is subject to large scientific and value-based uncertainties (e.g. Forster et al., 2007; Wuebbles, 2010; Stern, 2007; Hannemann, 2010) it is common to take simplifying implicit assumptions on the interrelation between economic damage and physical impact and apply physical climate parameters as an impact proxy. The choice of impact proxy is most pivotal and therefore used as key criterion for the classification in our conceptual framework.

The weighting function describes the weighting of impacts along the temporal axis. There are three variants commonly used in climate metric design:

    a) the exponential weighing function ($W(t) = r \cdot e^{-rt}$), corresponding to the discount function commonly used in economics for aggregating monetary values over time with a discount rate r, given in % per year;

    b) the unit step function $W(t) = 1/H \ \theta(H-t) = \{1 \ for \ t \leq H \ and \ 0 \ for \ t > H$ (θ-function) which assigns equal weight to all impacts occurring over a finite time horizon H (physical average mean weighting); and

    c) the Dirac Delta function $W(t) = \delta(t_x - t) = 0 \ for \ t \neq t_x \ with \ \int_{-\infty}^{\infty} F(t)\delta(t_x - t)dt = F(t_x)$

(δ-function) which only evaluates the impacts at one discrete time step t_x in time (end point weighting).

For each of these weighting functions free time frame parameters exist that determine the time scale of evaluation: the discount rate *r* (discounting), the time horizon *H* (θ-function) and the end point t_x (δ-function).

3   CATEGORISATION OF CLIMATE METRICS

In the following, we distinguish three categories according to the underlying assumptions on the impact proxy.

3.1 *the Global Damage Potential*

The Global Damage Potential (e.g. Kandlikar, 1996) or Economic Damage Index (Hammitt et al., 1996) refers to the future stream of discounted economic damages caused by different greenhouse gases. The interrelation between physical impact parameter and economic damage including its large uncertainty range is explicitly taken into account, often as convex economic damage function based on the change in global mean temperature ($D=\alpha \cdot \Delta T^n$) (e.g. Nordhaus, 1991; Kandlikar, 1995; Stern, 2007). Typically, assumptions on future atmospheric concentration pathways are taken exogenously.

3.2 *Physical climate metrics*

Physical metrics avoid the perils of economic evaluation by choosing an impact parameter that is located further upstream in the chain of impacts. They are derived from the GDP by assuming linear relationship between economic damage (D) and the physical impact proxy ($D=\alpha \cdot \Delta T$; $D=\gamma \cdot \Delta T$). To avoid the complexities of climate modelling the impact proxy often calculated under the assumption

of a constant atmospheric state, either the one at the time of emission release ($\vec{C}_{ref} = \vec{C}_{ref}(t_0)$) or an average value over possible future ranges in concentration ($\vec{C}_{ref} = \vec{C}_{ref}(\emptyset\,future)$). Other metrics use the historical greenhouse gas concentration pathway.

In contrast to physico-economic metrics, physical metrics apply alternative weighting functions to discounting (θ-function, δ-function). In most metric approaches the time frame parameter is defined as constant. Some physical metrics exist, however, in which this parameter is replaced by the distance between the point in time of emission release and a specific target year (e.g. Berntsen et al., 2010; Shine et al., 2007; Tanaka et al., 2009).

3.3 *the Global Cost Potential*

In view of the large uncertainty associated with economic evaluation of climate impacts, the cost-effectiveness framework is proposed as an alternative to the cost-benefit approach (Markandya et al. 2001): "guardrails" or "tolerable windows" for one or several climate variables such as ΔT or the rate of ΔT are adopted as boundary condition for climate mitigation strategies. Analytically, they can be treated as a special case of the cost-benefit analysis in which the damage cost curve is implicitly assumed to be zero within the "tolerable window" and to diverge to infinity at a physical impact threshold PI_{thres} (θ_∞-function):

$$D(PI) = \theta_\infty(PI - PI_{thres}) = \begin{cases} 0 & for\ PI < PI_{thres} \\ \infty & for\ PI \geq PI_{thres} \end{cases}$$

While the cost effectiveness approach is primarily designed for the derivation of global emission targets, it has peculiar implications for the derivation of metrics, which are an inherently marginal concept. Marginal damages are implicitly assumed to be zero below the climate target and infinitely large at the threshold. Taking advantage of the conditions for cost-optimal climate policy the metric also has to be equal to the ratio of marginal abatement costs (MAC) ($M_i^{CE} = MAC_i^{PI_{thres}} / MAC_{CO_2}^{PI_{thres}}$). This gives rise to the Global Cost Potential (Kandlikar, 1996, Tol et al., 2008), also referred to as "price ratios" (Manne and Richels, 2001), which is given by the ratio of two gases' MACs least cost emission trajectory maintaining a prescribed climate target.

Concluding, the impact proxy makes apparent the assumed interrelation between economic damage and physical impact parameter in each metric approach (schematic overview: Fig. 1).
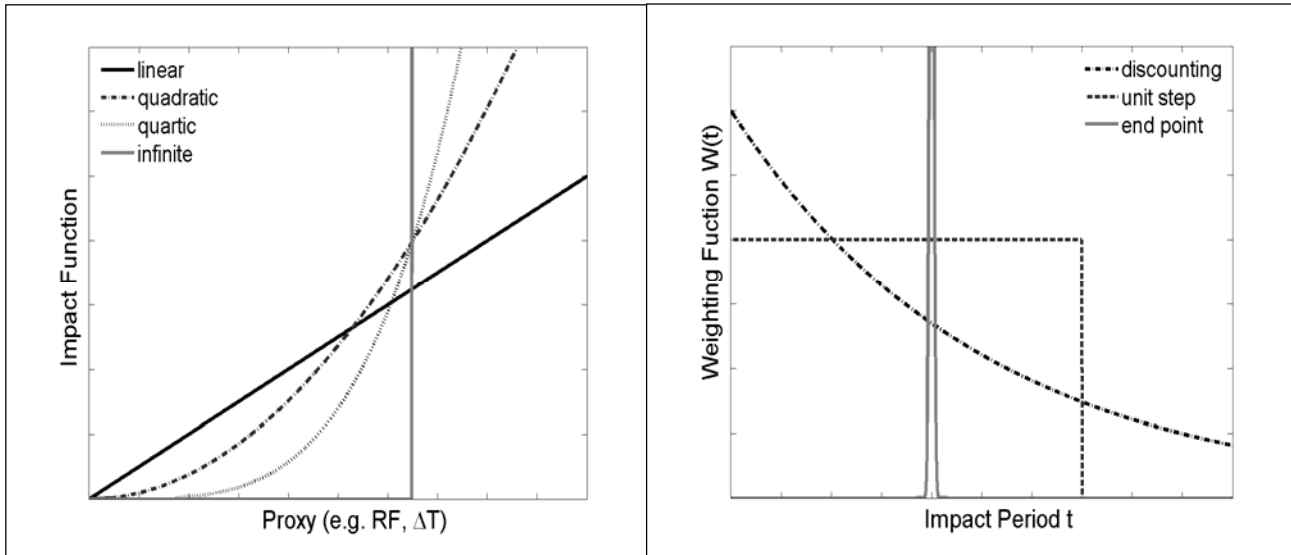
Figure 1: Schematic representation of commonly used (a) impact functions and (b) temporal weighting functions.

4 METRIC CLASSIFICATION AND INTERRELATIONS BETWEEN THE CATEGORIES

The conceptual framework based on impact and weighting function allows classifying the most prevalent climate metric approaches. Table 1 provides an overview on the classification of the GDP, the GCP with a physical impact threshold PI_{thres} expressed in terms of ΔT (e.g. Manne and Richels, 2001) or RF (e.g. Van Vuuren et al., 2006) and a series of physical climate metrics such as the Global Warming Potential GWP(H) (IPCC 1990), GWP(r)) (Lashof and Ahuja, 1990) and EGWP (Wallis, 1994), the Global Temperature Change Potential GTP_p (Shine et al., 2005) and $GTP_p(t)$ (Shine et al., 2007), the Mean Global Temperature Potential MGTP(H) (Gillet and Matthew, 2010), The Temperature Proxy Index TEMP (Tanaka et al., 2009) and the Forcing Equivalent Index FEI (Manning and Reisinger, 2011; Wigley, 1998). The framework visualizes the interrelations between different metrics (Fig. 2).
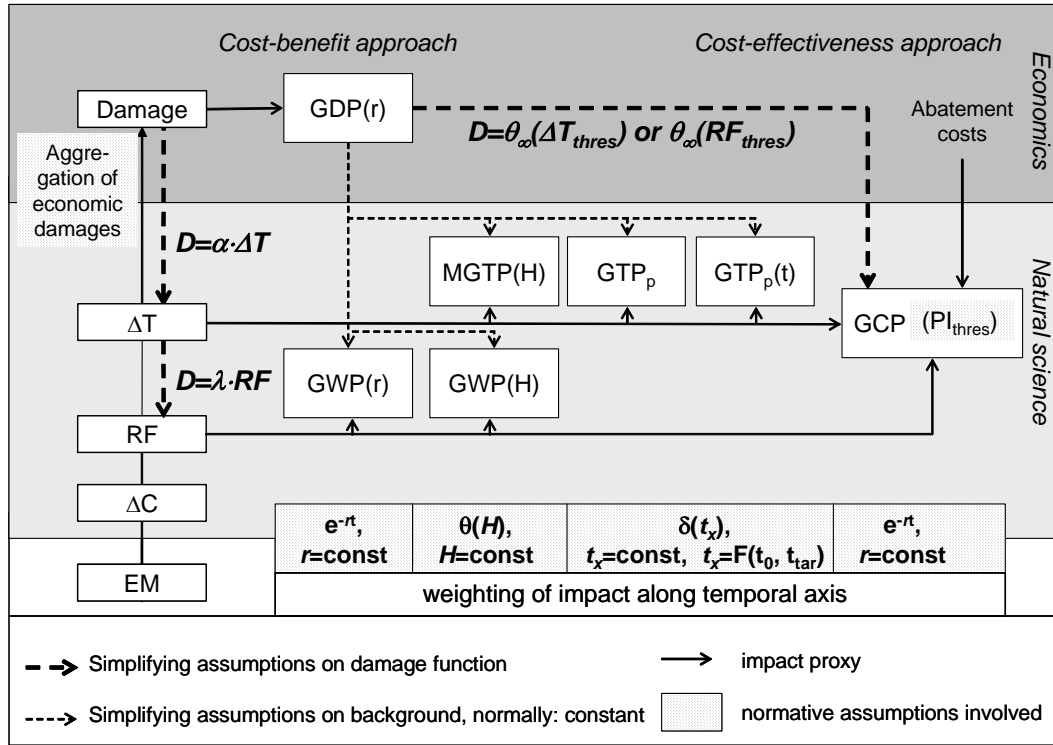
Figure 2: Interrelation between the GDP and selected physical and physico-economic metric approaches (GWP, MGT_p, GTP_p, $GTP_p(t)$ and GCP) highlighting the underlying policy objective, impact proxy, weighting function and respective scientific discipline

Impact function *I*		Weighting function *W*		
Implicit Damage function	Atmospheric background $(\vec{C}_{ref}, specification)$	Discounting *dicount rate r*	constant $(\theta - function)$ *time horizon H*	End point $(\delta - function)$ *end point t_x*
$D \quad D = f(\Delta T)$	scen, *exogenous*	**GDP**		
$\Delta T \quad D = \theta_\infty (\Delta T - \Delta T_{thres})$	scen, *endogenous*	**GCP(T)**		
$D \propto \Delta T$	const, *ref(t_0)*		**MGTP**	
$D \propto \Delta T$	const, *ref(t_0)*			**GTP**
$D \propto \Delta T$	scen, *historical*		**TEMP**	
$\Delta RF \quad D = \theta_\infty (RF - RF_{thres})$	scen, *endogenous*	**GCP(RF)**		
$D \propto RF$	scen, *ref(Øfuture)*	**GWP(r)**		
$D \propto RF$	const, *ref(t_0)*		**GWP(H)**	
$D = \gamma \cdot RF + \omega \cdot \partial RF / \partial t$	const, *ref(t_0)*	**EGWP**		
$D \propto RF$	scen, *historical*			**FEI**

Table 1: Classification of climate metrics. *I* specifies the selected climate impact proxy including the underlying damage function and scenario (scen), constant (const), specifications see text. *W* is characterised by the type of weighting function and the relevant time frame parameter r, H or t_x, respectively (specification see text).

5   METRIC CHOICE AND UNCERTAINTIES

The paramount challenge in the design of metrics is to deal with uncertainty. Following Dorbian et al. (2011), we distinguish between the following types of uncertainties:

 − structural uncertainty: degree to which the metric represents the real world trade-off,
 − value-based uncertainty: degree to which normative judgments are involved,
 − scientific uncertainty: uncertainty in the knowledge about the underlying processes in the causal chain between emissions and impact function, and
 − scenario uncertainty: degree to which the metric depends on the future states of the world, e.g. atmospheric background conditions

The choice of metric is largely coined by trade-offs between different kinds of uncertainties. This can be illustrated by comparing the GWP and GDP metrics. The key advantage of the GWP lies in the fact that (a) the value-based uncertainty is reduced to the choice of time horizon, (b) the scientific uncertainty is kept to a manageable level by only considering the causal chain between emissions and RF, and (c) the scenario uncertainty is eliminated by assuming constant background conditions. On the other hand, the GWP is characterized by rather high structural uncertainty, since there is no direct link between RF and climate damages, and likewise, future atmospheric background conditions will not remain constant. The GDP, by contrast, ensures economic efficiency, thus it accurately represents real-world trade-offs and features low structural uncertainty. This comes, however, at the expense of (a) high value based uncertainty as in addition to the choice of discount rate normative judgments are involved in the valuation and aggregation of damages, (b) higher scientific uncertainty as the entire causal chain from emissions to damages is represented, and (c) scenario uncertainty as we are unsure about future atmospheric conditions. Generally speaking, physico-economic metrics are characterized by lower structural uncertainty (which in principle makes them most policy relevant), but higher scientific, value-based and scientific uncertainties (which make them more difficult to operationalize), while physical metrics have high structural but lower value-based, scientific and scenario uncertainties.

So far, the GWP, easy to operationalize, has been the metric of choice for policy applications. In this metric, many of the relevant uncertainties are concealed by simplifying structural assumptions. While physico-economic metrics such as the GDP are much more difficult to operationalize, it can be seen as their advantage that they make the relevant uncertainties explicit. As an alternative approach to the use of simplifying physical metrics, policymakers could consider a GDP-based approach, in which the relevant value judgments and assumptions are considered in a direct and transparent manner.

REFERENCES

Berntsen, T.M., K. Tanaka, and J.S. Fuglestvedt, 2010: Does black carbon abatement hamper CO_2 abatement? *Clim. Change Lett.* 103, 627-633.

Dorbian, C.S., P.J. Wolfe, and I.A. Waitz, 2011: Estimating the climate and air quality benefits of aviation fuel and emission reductions. *Atmos. Environ.* 45, 2750-2759.

Forster, P., V. Ramaswamy, P. Artaxo, T. Berntsen, R. Betts, D.W. Fahey, J. Haywood, J. Lean, D.C. Lowe, G. Myhre et al., 2007: Changes in Atmospheric Constituents and in Radiative Forcing. In: *Climate Change 2007: The Physical Science Basis*. Contribution of Working Group I to the Fourth Assessment Report of the IPCC [Solomon S, D. Qin, M. Manning et al. (eds.)]. Cambridge University Press, Cambridge, United Kingdom and New York, NY, USA. 129 – 234.

Fuglestvedt, J.S., K.P. Shine, T. Berntsen, J. Cook, D.S. Lee, A. Stenke, R.B. Skeie, G.J.M. Velders, and I.A. Waitz, 2010: Transport impacts on atmosphere and climate: Metrics. *Atmos. Environ.* 44, 4648 – 4677.

Gillet, N.P. and H.D. Matthews, 2010: Accounting for carbon cycle feedbacks in a comparison of the global warming effects of greenhouse gases. *Environ. Res. Lett.* 5, 034011, 1-6.

Hammitt, J.K.H., A.K. Jain, J.L. Adams and D.J. Wuebbles, 1996: A welfare-based index for assessing environmental effects of greenhouse-gas emissions. *Nature* 381, 301–303.

Hannemann, M., 2010: The Impact of Climate Change: An Economic Perspective. In: *Climate Change Policies: Global Challenges and Future Prospects*. [Cerdá E. and X. Labandeira (eds)]. Edward Elgar, Cheltenham UK, Northhampton, MA, USA, 9-28.

Kandlikar, M., 1995: The relative role of trade gas emissions in greenhouse abatement policies. *Energy Policy* 23, 879-883.

Kandlikar, M., 1996: Indices for comparing greenhouse gas emissions: integrating science and economics. *Energy Econ.* 18, 265-281.

Lashof, D.A. and D.R. Ahuja, 1990: Relative contributions of greenhouse gas emissions to global warming. *Nature* 344, 529-531.

Manne, A.S. and R.G. Richels, 2001: An alternative approach to establishing trade-offs among greenhouse gases. *Nature* 410, 675-677.

Manning, M. and A. Reisinger, 2011: Broader perspective for comparing different greenhouse gases. *Phil. Trans. R. Soc. A*. 369, 1891-1905.

Markandya, A., K. Halsnæs, A. Lanza, Y. Matsuoka, S. Maya, J. Pan, J. Shogren, R.S. de Motta and T. Zhang, 2001: Costing methodologies. In: Metz, B., O. Davidson, R. Swart, J. Pan (eds.): *Climate change 2001: Mitigation.* Contribution of Working Group III to the Third Assessment Report of the Intergovernmental Panel on Climate Change. Cambridge University Press, Cambridge, 451-498

Nordhaus, W.D., 1991: To slow or not to slow: the economics of the greenhouse effect. *Econ. J.* 101, 920-937.

Shine, K.P., J.S. Fuglestvedt, K. Hailermariam and N. Stuber, 2005: Alternatives to the global warming potential for comparing climate impacts of emissions of greenhouse gases. *Clim. Change* 68, 281-302.

Shine, K.P., T.K. Berntsen, J.S. Fuglestvedt, R.B. Skeie and N. Stuber, 2007: Comparing the climate effect of emissions of short- and long-lived climate agents. *Philos. Trans. R. Soc. London A* 365, 1903-1914.

Stern, N., 2007: *The Economics of Climate Change*. The Stern Review. Cambridge University Press, New York. 692 pp.

Tanaka, K., B.C. O'Neill, D. Rokityanskiy, M. Obersteiner and R.S.J Tol, 2009: Evaluating Global Warming Potentials with historical temperature. *Clim. Change* 96, 443-466.

Tol, R.S.J., T.K. Berntsen, B.C. O'Neill, J.S. Fuglestvedt, K.P. Shine, Y. Balkanski and L. Makra, 2008: Metrics for Aggregating the Climate Effect of Different Emissions: A Unifying Framework. *The Economic and Social Research Institute Working Paper* No. 257, 1-16.

Van Vuuren, D.P., Weyant, J. and de la Chesnaye F., 2006: Multi-gas scenarios to stabilize radiative forcing. *Energy Econ.* 28, 102-120.

Wallis, M.K. and N.J.D. Lucas, 1994: Economic Global Warming Potentials. *Intern. J. Energy Res.* 18, 57-62.

Wigley T.M.L., 1998: The Kyoto Protocol: CO_2, CH_4 and climate implications. *Geophys. Res. Lett.* 25, 2285-2288.

Wuebbles, D., P. Forster, H. Rogers, and R. Herman, 2010: Issues and uncertainties affecting metrics for aviation impacts on climate. *Bull. Am. Meteorol. Soc.* 91, 461-463.

Aviation and Emissions Scenario and Policy Analysis Capabilities of AERO-MS

P. Brok[*]
National Aerospace Laboratory (NLR), The Netherlands

I. de Lépinay
European Aviation Safety Agency (EASA), Germany

Keywords: Aviation, environment, emissions, policy, modelling, AERO-MS, SAVE, TEAM_Play, EASA

ABSTRACT: One of the key systems for future policy assessment studies in Europe is a Responsive Modelling System: this involves the existing Aviation Emissions and evaluation of Reduction Options Modelling System (AERO-MS). It is a policy analysis tool with the capability to assess economic and environmental impacts of measures to reduce global aviation emissions. Over the last 15 years, AERO-MS has been frequently used for ICAO-CAEP, the European Commission and other organisations such as UNFCCC and IATA.

In the AERO-MS, policy measures are evaluated in the context of alternative future "business-as-usual" economic and technological scenarios for the aviation sector. The AERO-MS comprehensively integrates the relevant economic, commercial and technological responses of alternative policy options within the scenario context considered. In this respect, the AERO-MS distinguishes between three different modelling situations:

1) Base situation, representing the best possible knowledge of the air transport system in today's world;
2) Projections of future scenarios containing alternative, autonomous economic and technological developments without policy options;
3) Projections of alternative (sets of) policy options within a specified scenario context.

In 2010, the EASA-commissioned project called SAVE (Study on Aviation Economic Modelling) updated the AERO-MS primary input data on world-wide aircraft movements, air-service demand and aircraft technology characteristics from the original Base Year 1992 to the new Base Year 2006. In 2011 and beyond, further AERO-MS enhancements are covered in the framework of the part EC-funded TEAM_Play project; e.g., creating structural linkages from the AERO-MS outputs to other models for detailed computation of noise, emissions and environmental impacts; for instance to climate models for full environmental impact assessment capabilities.

All these AERO-MS enhancements will further improve the quality of impact assessments and fulfil the broadening needs of policy-makers in the aviation & environment field.

1   INTRODUCTION

Models are playing an increasing role in the assessment of aviation's environmental impact, as well as how this impact may evolve in the future according to different scenarios and the potential implementation of new environmental policy options. Being able to anticipate the impact of such policies is indeed crucial given the long duration of R&D cycles and the lifetime of aircraft. The Aviation Emissions and evaluation of Reduction Options Modelling System (AERO-MS) was developed with this objective. AERO-MS is an advanced tool capable of analysing and assessing the impacts of different policies, including technological and operational measures and market-based options, aimed at the reduction of international and domestic aviation greenhouse gas emissions.

---

[*] *Corresponding author:* Ivan de Lépinay, European Aviation Safety Agency (EASA), Postfach 10 12 53, D-50452 Köln, Germany. Email: ivan.de-lepinay@easa.europa.eu

The development of AERO-MS was initiated by the Dutch Civil Aviation Authority in the early 1990s and went through several phases in the period 1992 to 2001. EASA took over ownership of AERO-MS in 2009 and initiated a study on aviation economic modelling (SAVE) which involved an extensive update to the tool and its underlying databases from the original base year of 1992 to 2006 (MVA, 2010). Since its creation, AERO-MS has formed a key part of over 25 international studies where the results have provided a quantified basis for policy judgement related to environmental protection, among which an analysis of Market-Based Options (MBO) for the reduction of global air transport related CO_2 emissions for CAEP's Forecast and Economic Support Group (Pulles et al, 2000). More examples of AERO-MS applications can be found on the EASA website (see the reference section for the link).

The following sections provide an overview of the key features and capabilities of AERO-MS and explain the major developments the tool has gone through as part of the FP7 TEAM_Play project.

2   OVERVIEW OF AERO-MS

2.1 *A system of interacting models*

The economic and technical modelling of air transport within the AERO-MS consists of five interacting core models, namely: the aircraft technology model (ATEC) to determine aircraft technology characteristics based on fleet development; the air transport demand model (ADEM) to forecast demand for air services and aircraft flights; the aviation cost model (ACOS) to estimate the overall aircraft operating costs; the flights and emissions model (FLEM) to calculate aircraft fuel use and engine emissions; the direct economic impacts model (DECI) to provide a comprehensive overview of the cost and revenues of air transport and a number of other economic impacts.
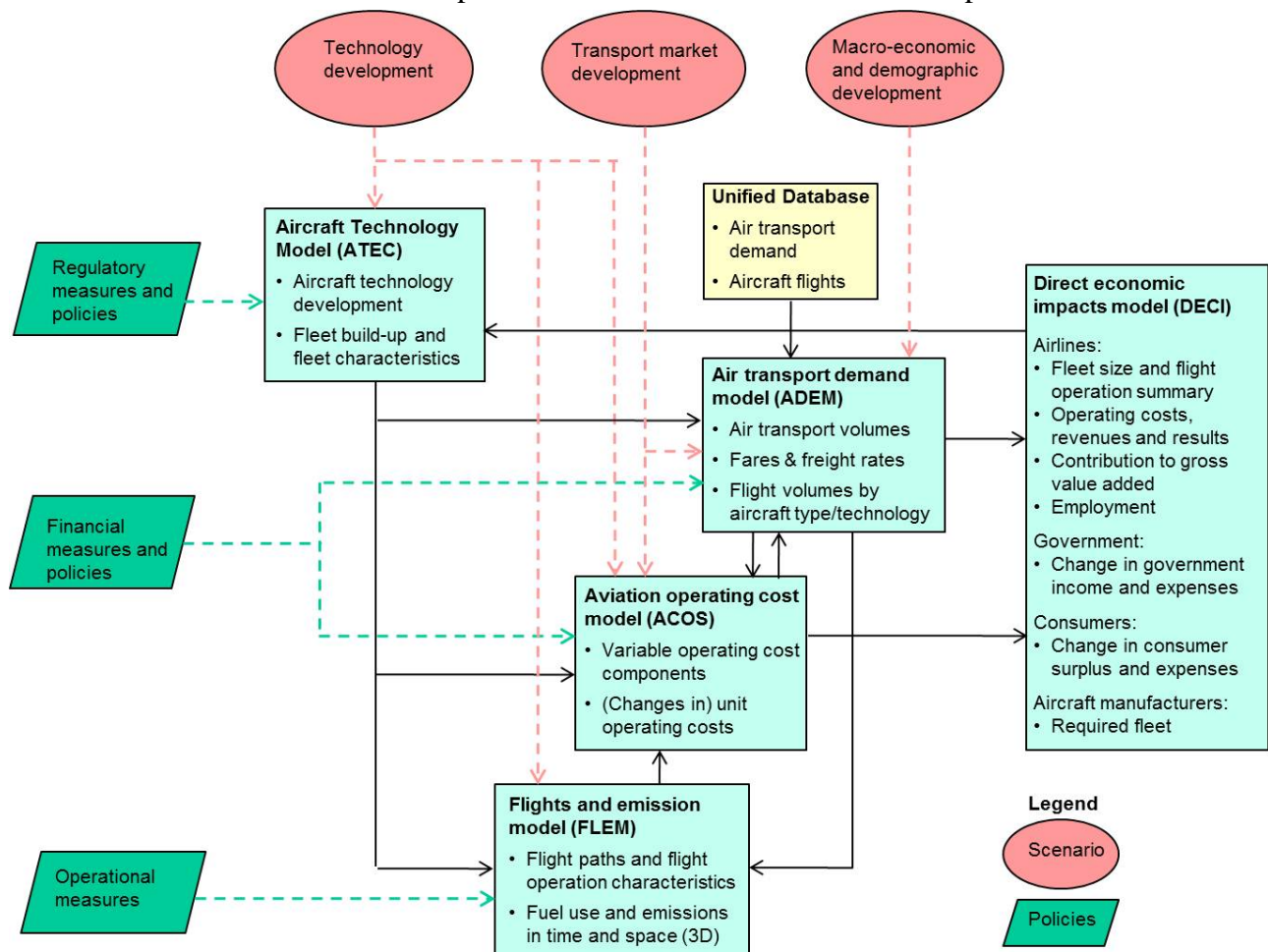
Figure 1. The AERO-MS core models and interactions

The key strength of AERO-MS relies in the interaction between the above models: e.g. the information on fuel-burn resulting from FLEM computations is used in ACOS to allow for the computation of fuel cost. Policy measures can indeed affect the supply side costs of the industry, which may lead to air operators increasing the prices for their customers. Through the multiple interactions between the core models, AERO-MS can assess the effect of price variations on air travel demand, as well as the changes in the global fleet with respect to fuel efficient technology.

2.2 *Underlying data*

The starting point for the modelling of air transport demand and aircraft flights is provided by the Unified Database, which is a computerised description of the volume and pattern of global air transport activity in the base year (presently 2006). The current Unified Database was compiled using a number of input data sources, including: EUROCONTROL's 2006 WISDOM Operations Database of aircraft movement data; the 2006 ICAO Traffic by Flight Stage (TFS) scheduled air movement and demand data; the 2006 U.S. Department of Transport (DOT) T-100 scheduled air movement and demand data; and the 2006 IATA Route Tracker passenger class split data.

For 2006, the Unified Database records 123,025 airport-pairs, 33.1 million civil flights, 2.6 billion passenger trips, 4,658 billion passenger-km, 44.8 million tonnes of cargo transported and 158 billion cargo tonne-km.

Lastly, the FLEM module uses EUROCONTROL's Base of Aircraft Data (BADA) combined with the ICAO Aircraft Engine Emissions Databank to generate fuel burn and emissions.

2.3 *AERO-MS outputs*

The AERO-MS outputs are presented in the form of a standard *scorecard* which allows the comparison of model runs reflecting different scenario and/or policy situations. The main categories of outputs in the scorecard representation are:

- Air transport and aircraft operations: passenger and cargo demand by type; revenue ton-km; number of flights; aircraft-km.
- Effects on airlines: operating costs, revenues and results; contribution to gross value added; airlines related employment.
- Economic effects on other actors: (change in) government income/expenses; consumer surplus and expenses; required fleet.
- Fuel consumption and emissions (CO_2, NO_x, SO_2, C_xH_y, CO and H_2O). Emissions can be computed using either the Boeing Fuel Flow Method 2 (BFFM2) or the P_3T_3 method, and presented in the form of 3D grids potentially reusable in a climate model.

Policy options are evaluated in the context of alternative future "business-as-usual" economic and technological scenarios for the aviation sector. In this respect, the AERO-MS distinguishes between three different modelling situations: the *Base* situation representing the best possible knowledge of the air transport system in today's world; projections of future scenario's containing alternative, autonomous economic and technological developments without policy options (referred to as the *Datum* situation); projections of alternative (sets of) policy options within a specified scenario context (referred to as the *Forecast* situation). The effects of alternative policy options are quantified in relation to a common benchmark represented by the selected *Datum* situation. This produces a snapshot of each policy option against the same scenario in the same year, allowing a comparative evaluation of policy options on a consistent basis.

3   TEAM_PLAY ENHANCEMENTS

The earlier-mentioned SAVE study (MVA, 2010) also identified and proposed further improvements to the AERO-MS. Selections from these proposals are currently addressed in the EU FP7 project TEAM_Play – Tool Suite for Environmental and Economic Aviation Modelling for Policy Analysis. TEAM_Play (www.teamplay-project.eu) is a collaborative project co-funded by the European Commission. It is aimed at setting up an effective and efficiently working Tool Suite to provide powerful tools to conduct policy assessment studies within ICAO-CAEP and on European, national and local levels.

The enhancements made to the AERO-MS in the framework of TEAM_Play are:
- Software-technical, data structure and user interface enhancements, which resulted in a completely renewed and modernised AERO-MS framework. The revised system is referred to as "AERO-MS vNext". As part of the development of AERO-MS vNext, changes have been made to programs, data manager and models.
- Improvements in representation of aircraft types and enhancements in flight, emissions and noise modelling, all with the aim to improve the modelling of the aviation environmental system and to enhance interdependency modelling and analysis. The specific enhancements of AERO-MS (elements) are:
  - Update of the Unified Database (air traffic in Base Year 2006)
  - Revision of utilisation rates and further specification of retirement curves
  - Modifications to the aircraft demand model (ADEM) and aircraft technology model (ATEC)
  - Definition and implementation of a technology restriction measure
  - Floating Attributes Tool introducing the (cap)ability to investigate and analyse a range of aircraft and engine technology characteristics in a finer detail
  - Improved representation of aircraft technology and performance using BADA
  - New features in the Flight and Emissions Model (FLEM), including aircraft noise indicators for enhanced interdependency modelling and policy analysis.
- Integration and interfaces with higher-precision, pre-processing ("up-stream") and post-processing ("down-stream") models; for instance, creating structural linkages from the AERO-MS outputs to a range of downstream environmental models for detailed computation of noise, emissions and environmental impacts (the AERO-MS is now linked to climate response models for environmental impact assessment and policy analysis concerning the reduction of NOx emissions and or the reduction of contrails and cirrus). Other linkages involve those with technology response, energy, macro-economic, interdependency metrics and impact monetisation tools.

The calibration, validation and testing of the enhanced AERO-MS will be finished and reported in the final quarter of 2012.

4 FUTURE DEVELOPMENTS

Further enhancement of the AERO-MS is needed, for instance, to address remaining SAVE-proposed improvements, but also to be able in the future to fulfil the broadening needs of policy-makers in the aviation & environment field. For the time being, there is no program, project or study planned to further develop the AERO-MS. Opportunities will however come up when considering, for instance, a TEAM_Play follow-up project in the EU research framework programme and or other relevant European programmes like Clean Sky and SESAR which involve evaluation, assessment and interdependency modelling activities.

5 ACKNOWLEDGEMENTS

REFERENCES

MVA, NLR, TAKS, QinetiQ, DLR, 2010: Study on Aviation and Economic Modelling (SAVE) – Final Report. Research Project EASA.2009.OP.15, 243 pp.

Pulles J.W., A. van Velzen, R. Hancox et al, 2000: Analysis of Market-Based Options (MBO) for the reduction of global air transport related CO2 emissions. Study for CAEP/4's Forecast and Economic Support Group (FESG).

EU FP7 TEAM_Play project website: www.teamplay-project.eu

Further information on AERO-MS, including applications of the modelling system in policy assessments for EC/ICAO/UNFCCC/IATA, can be found at the following website: http://www.easa.europa.eu/environment/aero-ms.php

Study of the impact of altered flight trajectories on soot-cirrus: a EC-REACT4C study

D. Iachetti[*], G. Pitari
Dipartimento di Scienze Fisiche e Chimiche, Università degli Studi de L'Aquila, Italy

ABSTRACT: The emission, dispersion and transport of aviation black carbon particles in the atmosphere may trigger additional cirrus clouds ('soot-cirrus') or change the background distribution of upper tropospheric ice particles. These effects and the sensitivity of aerosol and ice accumulation to changes in flight altitude have been studied with the University of L'Aquila climate-chemistry model (ULAQ-CCM), using emission inventories from the collaborative European project EC-REACT4C. Formation of background upper tropospheric ice particles is included by means of homogeneous and heterogeneous freezing of super-cooled aerosols: this scheme considers the basic physical processes that eventually determine the number of ice crystals N_i forming during an adiabatic ascent of air, including the link of N_i on temperature and updraft speed. Background ice particle formation is dominated by the homogeneous freezing process, producing the largest population in the tropical upper troposphere. Ice changes from aviation are dominated by the heterogeneous freezing mechanism, with the ice particle number density increasing with increasing BC particles from aircraft emissions. RF changes produced by flight vertical displacement are negative/positive for upward/downward displacement. A 2000 ft upward shift of aircraft routes, in fact, brings more emissions into the stratosphere, where lower amounts of condensable water vapour are present and less amounts are transported from below due to a rapid decrease of sub-grid updraft velocities above the tropopause.

1   INTRODUCTION

The climate impact of current and potential future aviation is, by convention, quantified using the metric 'radiative forcing of climate', since many climate experiments have found an approximately linear relationship between a change in global mean radiative forcing (RF) and a change in global mean surface temperature. The IPCC (1999) report pointed out that the potential contribution from subsonic aviation for a range of 2050 scenarios could be between 3 and 7% of total radiative forcing, excluding cirrus cloud enhancement. Aviation RFs have recently been updated and quantified for 2005 over those for 2000 (Sausen et al., 2005) and reflect the strong growth in traffic since 2000 (Lee et al., 2009). Aviation traffic grew in terms of RPK by 22.5% over the period 2000–2005, with an increase in fuel usage of 8%, resulting in an increase in aviation RF of 14%. Lee et al. (2009) estimated that total aviation RF (excluding induced cirrus) in 2005 was 55 mW/m^2 (23–87 mW/m^2, 90% likelihood range), which is an average 3.5% of total anthropogenic forcing. Including estimates for aviation-induced cirrus, the total aviation RF increased in 2005 to 78 mW/m^2 (38–139 mW/m^2, 90% likelihood range), which represents an average 4.9% of total anthropogenic forcing. The above numbers point out to the potential significant role of the aviation-induced cirrus cloudiness.

According to the current consensus state of knowledge, emissions from aviation directly affects atmospheric chemistry and climate in the following ways, in terms of radiative forcing: positive RF (warming) from emissions of CO_2, H_2O and black carbon soot particles (BC); negative RF (cooling) from emissions of sulphate particles arising from sulphur in the fuel. The formation of persistent

---

[*] *Corresponding author:* Daniela Iachetti, Dipartimento di Scienze Fisiche e Chimiche, Università degli Studi de L'Aquila, Italy. Email: daniela.iachetti@aquila.infn.it

linear contrails that may form (depending upon atmospheric conditions) in the wake of an aircraft, as well as the formation of contrail-cirrus cloud from spreading contrails similarly to line shaped-contrails both result in positive and negative RF effects but overall they are considered to cause a positive RF effect (warming). In addition, aviation emissions indirectly affects atmospheric chemistry and climate in several ways; the one that will be addressed in this paper is a sub-component of aviation-induced cirrus, through a mechanism whereby BC soot particles seed cirrus clouds (or 'soot-cirrus').

Soot may either increase or decrease the number of ice particles and impact upon both the albedo and the emissivity of cirrus clouds. This effect may result in either positive or negative RF effects (warming/cooling), but is rather uncertain over the sign (Penner et al., 2009). In other words, 'soot cirrus' is defined here as cirrus clouds induced by (or perhaps altered by) the addition of heterogeneous ice nuclei from aviation (BC particles). The sensitivity of 'soot cirrus' ice particles has been studied here by means of subsonic aircraft emission changes in altitude.

2   MODEL DESCRIPTION AND NUMERICAL EXPERIMENTS

ULAQ-CCM is a coupled climate-chemistry model, including on-line an aerosol module with microphysical processes for aerosol production, growth and removal, so that the aerosol size distribution and its perturbations to several external parameters can be predicted, as for example aviation emissions of SO_2 and black carbon aerosols (BC). Aerosol predictions from the ULAQ model have been validated using ground-based, satellite and aircraft measurements (see, in this same volume, Pitari et al., 2012). The ULAQ-CCM uses a T21 horizontal resolution and 126 log-pressure levels from the ground to about 0.04 hPa, with an approximate resolution of 570 m, including troposphere and stratosphere. The cirrus ice parameterization used is that for homogeneous freezing of supercooled aerosols (Kärcher and Lohmann, 2002a; Kärcher and Lohmann, 2002b): this scheme considers the basic physical processes that eventually determine the number of ice crystals N_i forming during an adiabatic ascent, including the link of N_i on temperature and updraft speed. In order to improve the model simulation of ice nucleation mechanisms, a first-order parameterization for heterogeneous freezing has been introduced. In the parameterization used for the formation of aviation soot-cirrus particles in a model grid-box, the change of ice crystals number concentration $\Delta N_{i\text{-}HET}$ is calculated as a function of ΔN_{BC} and P_{HET}, where ΔN_{BC} is the change of soot particles due to aviation emissions, assuming a 10% non-hydrophobic fraction of the particles that may act as ice nuclei. $P_{HET,}$ in turn, is the probability that heterogeneous freezing may occur at given grid-box in the model, calculated as the probability to have ice super-saturation for a given temperature (RH_{ICE} ›100%) and taking into account water vapour transport due to sub-grid vertical updraft velocity (Lohmann and Kärcher, 2002).

Five numerical experiments were performed with the ULAQ-CCM over a period of 15 years (1996-2010) after a 5 years spin-up (1991-1995). Emission inventories are those for year 2006 provided in the collaborative EC-REACT4C project. The numerical experiments are listed here: no aircraft emissions (EXP1); pure gas emissions by the aircraft (EXP2); gas and particle aircraft emissions: EXP3 (BASE scenario), EXP3$^+$ (PLUS scenario), EXP3$^-$ (MINUS scenario).

3   RESULTS

The calculated number, surface area and mass densities of cirrus ice particles are presented in Fig. 1 for EXP3. Ice particle number density maximum values reach 0.25 cm^{-3} at about 13 km altitude in the equatorial latitude and their formation is generally dominated by the homogeneous freezing process: in the paper of Kärcher and Lohmann (2002b) the number density maximum reaches higher values, probably because of higher values used for the updraft vertical velocity. In fact higher values of vertical velocity form more particles of smaller size.
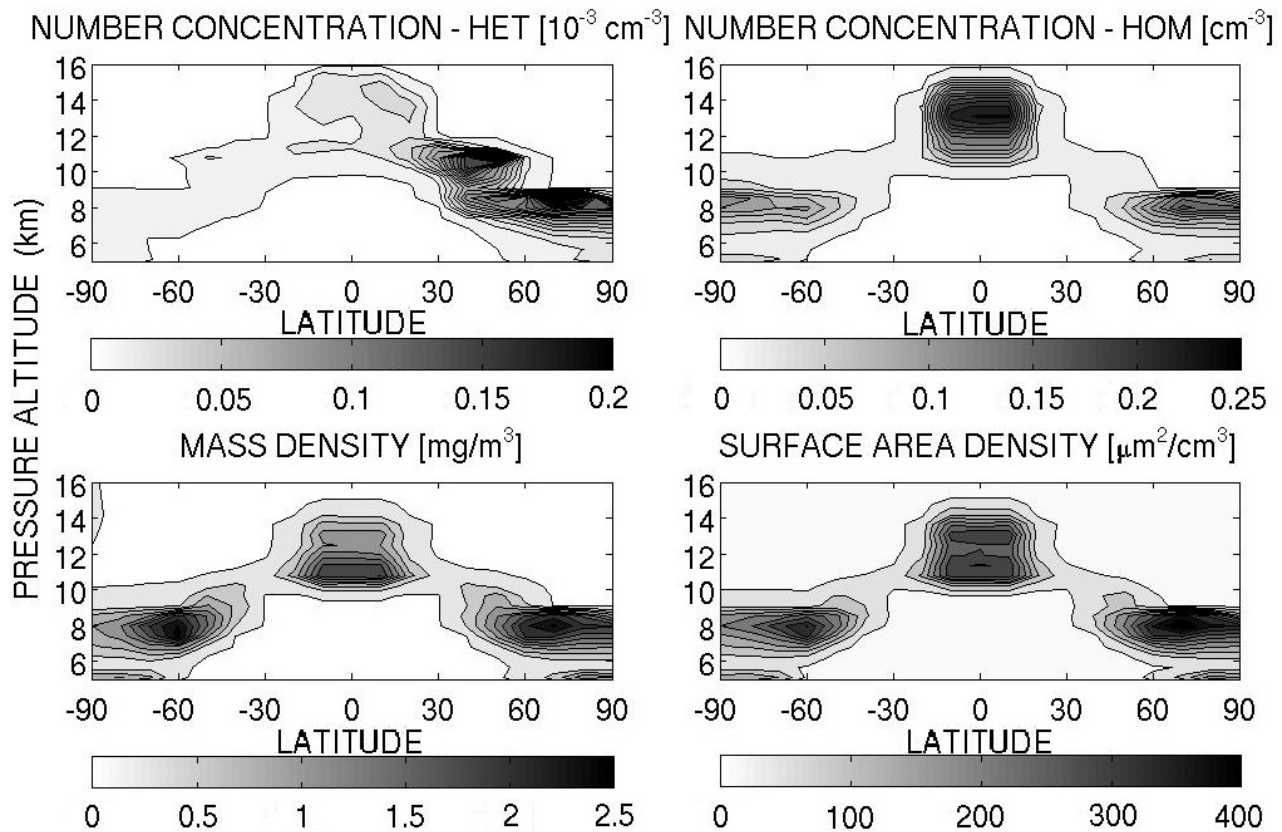
NUMBER CONCENTRATION - HET [10^{-3} cm^{-3}] NUMBER CONCENTRATION - HOM [cm^{-3}]

MASS DENSITY [mg/m^3]   SURFACE AREA DENSITY [μm^2/cm^3]

Fig.1: Zonally and annually averaged values over the entire 15 years period for ice number density (cm^{-3}) (divided into heterogeneous and homogeneous freezing production, cm^{-3} and 10^{-3} cm^{-3}, respectively), surface area (μm^2/cm^3) and mass densities (mg/cm^3) (from top left to bottom right panels). Note that the grey scale on the top left panel is for 10^{-3} cm^{-3}.

For the same years above, the zonal mean changes due to aviation BC emissions are shown in Fig. 2, in terms of soot and ice particle number. Differences are calculated between results from two simulations: EXP3 (gas and particle aircraft emissions, BASE scenario) and EXP1 (no aircraft emissions). Ice changes are dominated by the heterogeneous freezing mechanism (the ice number density increases with increasing number of black carbon nuclei emitted by the aircraft), whereas a smaller decrease is observed from homogeneous freezing, since less water vapor is available for condensation after a fraction of water has been subtracted in ice particles formed via heterogeneous freezing (which occurs at lower super-saturation values). The latter effect can be deduced when comparing the top left panel in Fig. 1 with the right panel in Fig.2.

NUMBER DENSITY CHANGES

SOOT [cm^{-3}]   SOOT CIRRUS [10^{-3} cm^{-3}]
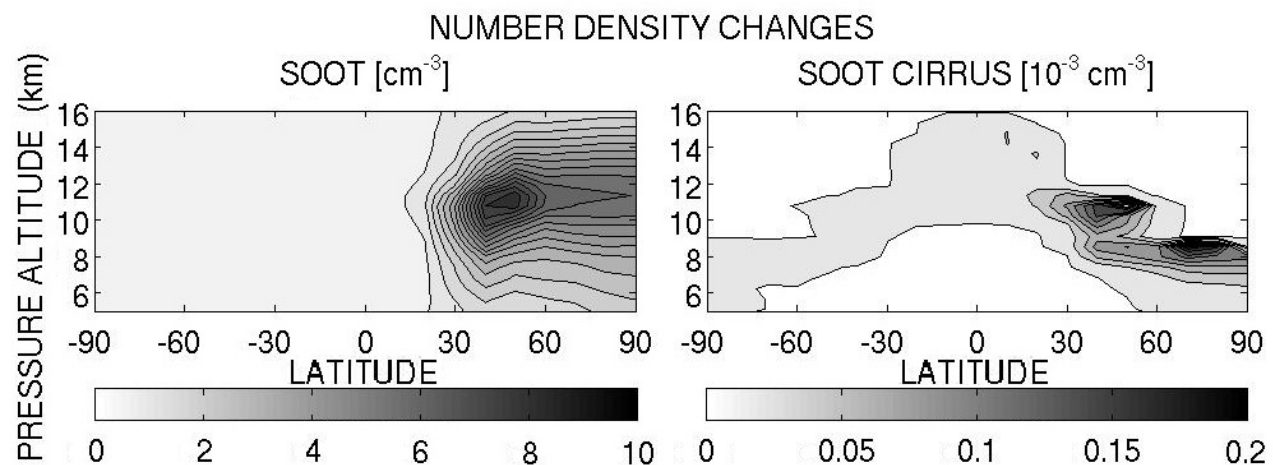
Fig.2: Zonally and annually averaged changes due to aviation soot emissions, in terms of soot and ice particle number densities (cm-3 and 10-3 cm-3, respectively). Note that the grey scale on the right panel is for 10-3 cm-3.

The particle optical depth is shown in Fig. 3 (at 0.55 μm wavelength), with a comparison of aviation BC and calculated soot-cirrus values. Soot and soot-cirrus optical depth changes follow geographical pattern of aviation emissions, with some significant ice optical depth increase also in the Northern Hemisphere high latitudes, because of the transport of aircraft emitted ICN towards the high latitudes, where more frequent conditions of ice super-saturation are found. The calculated horizontally averaged values for soot and soot-cirrus ice optical depth changes are found to be 4.1×10^{-6} and 3.3×10^{-4}, respectively.

OPTICAL DEPTH CHANGES
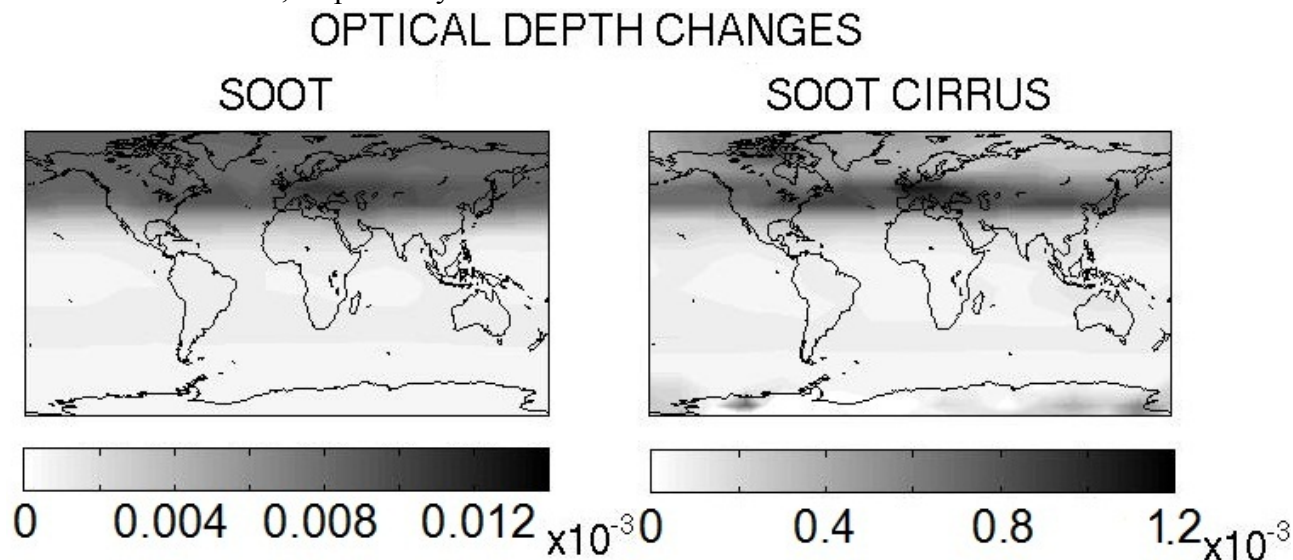
Fig.3: Annually averaged values of BC and ice optical depths at 0.55 μm, as 15-yrs averaged changes due to aviation emissions.

The sensitivity of soot-cirrus formation to the emission altitude is shown in Fig. 4, where we calculate the changes between PLUS and MINUS scenarios with respect to the BASE case. The ice particle behaviour is driven by the soot nuclei perturbation, with the largest impact produced by heterogeneous freezing. As discussed above (see EXP3-EXP1), this last change is partially compensated by an opposite tendency produced by homogeneous freezing. Aviation soot-cirrus RF results from the ULAQ-CCM are summarized in Table 1, along with RF sensitivity moving up or down the cruise altitude (Table 2); short wave and infrared components of RF are shown separately. The calculated cirrus ice net RF due to aviation emissions is 19.0 mW/m^2, in the range of independent model estimates, on the lower limit (see introduction). RF changes produced by flight vertical displacement are negative/positive for upward/downward displacement, respectively. This is a meaningful finding, since a 2000 ft upward vertical shift of aircraft routes brings more emissions into the stratosphere, where much lower amounts of condensable water vapour are present and less amounts are transported from below due to a rapid decrease of sub-grid updraft velocities above the tropopause.
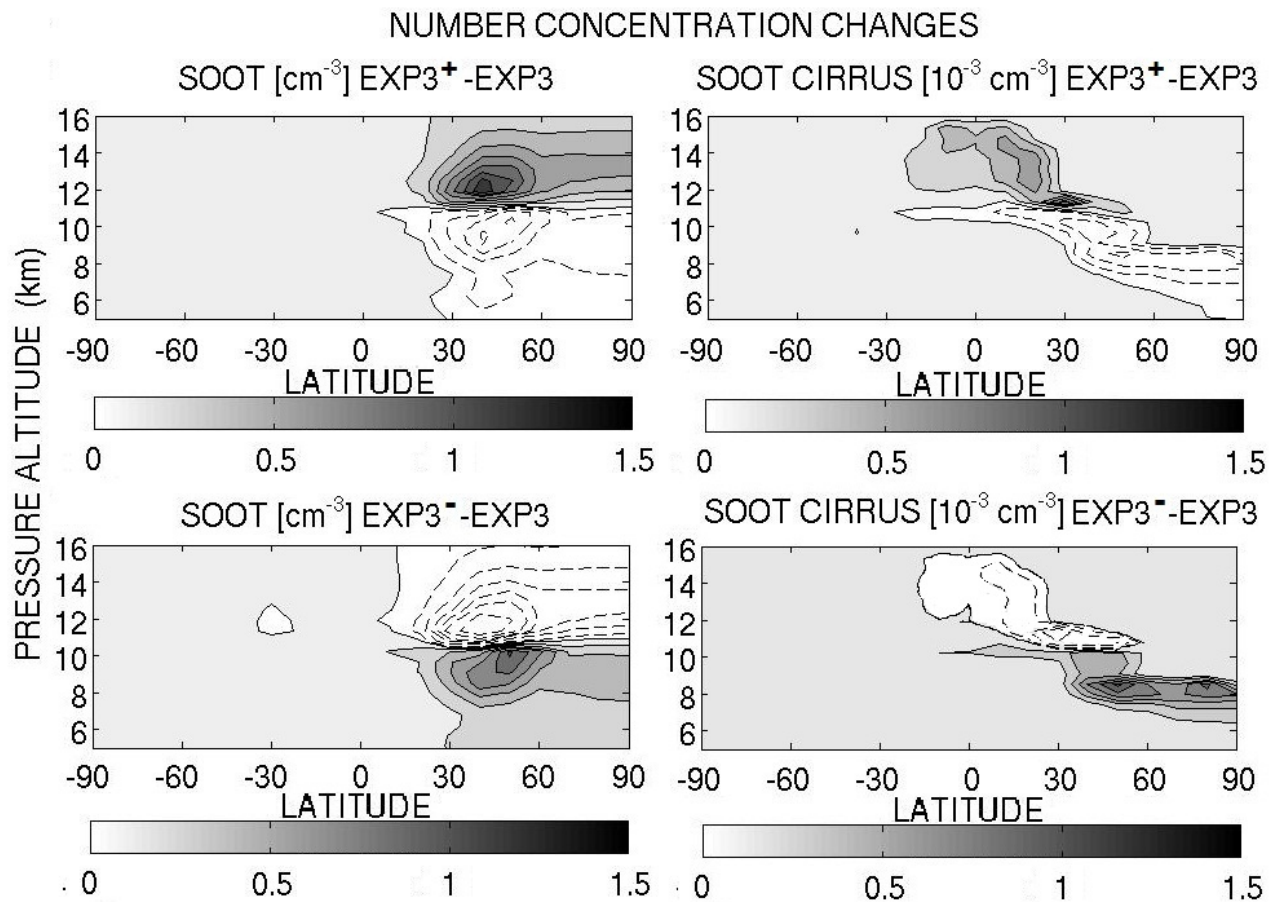
Fig.4: Zonally and annually averaged BC and ice number density changes (cm^{-3} and 10^{-3} cm^{-3}, respectively), in order to study the soot-cirrus sensitivity to route altitudes: EXP3$^+$ - EXP3 (upper panels), EXP3$^-$ - EXP3 (bottom panels). Note that the grey scale on the right panels is for 10^{-3} cm^{-3}. Contour lines are spaced by 0.15 cm^{-3} (BC) and 0.15 x 10^{-3} cm^{-3} (ice).

	RF [mW/m^2] (EXP3$^+$-EXP1)	RF [mW/m^2] (EXP3-EXP1)	RF [mW/m^2] (EXP3$^-$-EXP1)
ICE-SW	-12.6	-12.9	-13.3
ICE-IR	30.9	31.9	32.7
ICE-NET	18.3	19.0	19.4
SOOT-NET	2.30	2.22	2.14

Table 1. Summary of ice Radiative Forcing mean values for year 2006, calculated using aircraft emission scenarios for 2006, along with BC direct RF.

	RF [mW/m^2] (EXP3$^+$-EXP3)	RF [mW/m^2] (EXP3$^-$-EXP3)
ICE-SW	0.3	-0.4
ICE-IR	-1.0	0.8
ICE-NET	-0.7	0.4
SOOT-NET	0.07	-0.08

Table 2. As in Table 1, but for RF changes due to 2000 ft vertical displacement of aircraft routes (PLUS-BASE on the left, MINUS-BASE on the right).

4 CONCLUSIONS

This study on 'soot-cirrus' formation and its sensitivity to aircraft route altitudes shows that the net global RF associated to both BC soot particles and 'soot-cirrus' ice particles decreases by 0.7 mW/m^2 for a 2000 ft upward shift of aircraft routes, whereas it increases by 0.4 mW/m^2 for a corre-

sponding downward shift. A different latitudinal distribution of aircraft routes with more emissions in the tropical regions would most likely change this finding, since more favourable ice supersaturation conditions would be found at higher altitudes in the tropical upper troposphere.

5   ACKNOWLEDGMENTS

REFERENCES

Eyring, V., et al.: Assessment of temperature, trace species, and ozone in chemistry-climate model simulation of the recent past, J. Geophys. Res., 111, D22308, doi:10.1029/2006JD007327, 2006.

JPL: Chemical Kinetics and Photochemical Data for Use in Atmospheric Studies, Evaluation Number 17, JPL Publication 10-6, 2011.

Kärcher, B., and U. Lohmann: A parameterization of cirrus cloud formation: homogeneous freezing of supercooled aerosols, J. Geophys. Res., 107, 4010, 10.1029/2001JD000470, 2002.

Lee, D., et al.: Transport Impacts on Atmosphere and Climate: Aviation, Atmos. Env., 44, 4678-4734, 2010.

Minschwaner, K., R. J. Salawitch, and M. B. McElroy: Absorption of Solar Radiation by O2: Implications for O3 and Lifetimes of N2O, CFCl3, and CF2Cl2, J. Geophys. Res., 98, 10,543–10,561, doi:10.1029/93JD00223, 1993.

Morgenstern, O., et al.: A review of CCMVal-2 models and simulations, J. Geophys. Res., 115, D00M02, doi:10.1029/2009JD013728, 2010.

Penner, J.E., Y. Chen, M. Wang, X. Liu: Possible influence of anthropogenic aerosols on cirrus clouds and anthropogenic forcing, Atmos. Chem. Phys. 9, 879–896, 2009.

Pitari G., E. Mancini, V. Rizi and D. T. Shindell: Impact of Future Climate and Emission Changes on Stratospheric Aerosols and Ozone, J. Atmos. Sci., 59, 2002a.

Pitari, G., E. Mancini, and A. Bregman: Climate forcing of subsonic aviation: indirect role of sulfate particles via heterogeneous chemistry. Geophys. Res. Lett. 29 (22), 2057. doi:10.1029/2002GL015705, 2002b.

Randles, C.A., et al.: Intercomparison of shortwave radiative transfer schemes in global aerosol modeling: Results from the AeroCom Radiative Transfer Code Experiment, submitted to ACPD, 2012.

Schwarz, J.P.: Single-Particle measurements of midlatitude black carbon and light-scattering aerosols from the boundary layer to the lower stratosphere, J. Geophys. Res., 110 , D16207, 2006.

Schwarz, J.P., et al: Coatings and their enhancement of black-carbon light absorption in the tropical atmosphere, J. Geophys. Res., doi:10.1029/2007JD009042, 2008.

Spackman, J.R: Aircraft observations of enhancement and depletion of black carbon mass in the springtime Arctic, ACP, 2010.

Spackman, J.R. , R.S. Gao, J.P. Schwarz, L.A. Watts, D.W. Fahey, L. Pfister, and T.P. Bui: Seasonal variability of black carbon mass in the tropical tropopause layer, Geophys. Res. Lett., 38, L09803, doi:10.1029/2010GL046343, 2011.

Toon, O. B., C. P. McKay, T. P. Ackerman, and K. Santhanam: Rapid Calculation of Radiative Heating Rates and Photodissociation Rates in Inhomogeneous Multiple Scattering Atmospheres, J. Geophys. Res., 94, 16,287–16,301, doi:10.1029/JD094iD13p16287, 1989.

Contrail coverage from future air traffic

L.L. Lim[*], R. Rodríguez De León, B. Owen, D.S. Lee, J.K. Carter
Dalton Research Institute, School of Science & the Environment, Manchester Metropolitan University, United Kingdom

ABSTRACT: The Schmidt-Appleman criterion defines the critical temperature for contrail formation. Offline contrail coverage simulations, similar to those described in Sausen et al. (1998), were conducted using ERA-Interim reanalysis data from 2001 to 2011. These updated climatological data were coupled with the distance travelled calculated by the FAST emissions inventory model. The aircraft movements for the year 2006 were provided by the CAEP/8 Modelling and Database Group (MDG), and their projections were used to estimate the global contrail coverage for 2016, assuming present-day meteorology. The results showed that significant projected growth in air traffic between 2006 and 2016 produced an increase in global contrail coverage by a factor of 1.6. The radiative forcing (RF) impacts based on these coverages and updated temperature-dependent contrail properties, will be calculated with an offline Radiative Transfer Model in the next phase of the study.

1   INTRODUCTION

Contrails form and persist in ice-supersaturated regions of the upper troposphere. They reduce the amount of short-wave (SW) solar radiation reaching the Earth's surface as well as the long-wave (LW) radiation emitted into space. The net radiative forcing (RF) is the residual of the LW and SW opposing effects. The 2005 global contrails net RF is estimated to be 11.8 mWm^{-2}, and by 2050 this is expected to increase to 37.2–55.4 mWm^{-2} (Lee et al., 2009). These RF estimates were linearly scaled from fuel burnt and RF reference values based on older inventories and methods. In this study, distance travelled from a recent 3D aircraft emissions inventory were used in an offline global contrail coverage model. This forms the first phase of the study of providing an updated estimate of the RF impacts from future air traffic.

2   DISTANCE TRAVELLED

The 2006 distance travelled was calculated with the global model of aircraft movements and emissions, 'FAST' (Owen et al., 2010) using the CAEP8/MDG movements (ICAO/CAEP, 2009). This baseline inventory is similar to the one used for the EU 7th Framework project, REACT4C. The total distance travelled in 2006 for all altitudes was 39 billion km, with approximately 86% of it occurring above 500 hPa (approximately 5 km), where ambient conditions tend to meet the contrail formation criterion. The spatial distribution for these distances is presented in Figure 1 (a), showing the greatest amount of traffic over North America, Western Europe, the Far East and the North Atlantic Flight Corridor (NAFC). In these regions, the distance travelled was more than 10 million km.

---

[*] *Corresponding author:* Ling L. Lim, CATE-E0.04, Manchester Metropolitan University, School of Science & the Environment, John Dalton East Building, Chester Street, Manchester M1 5GD, United Kingdom. Email: l.lim@mmu.ac.uk
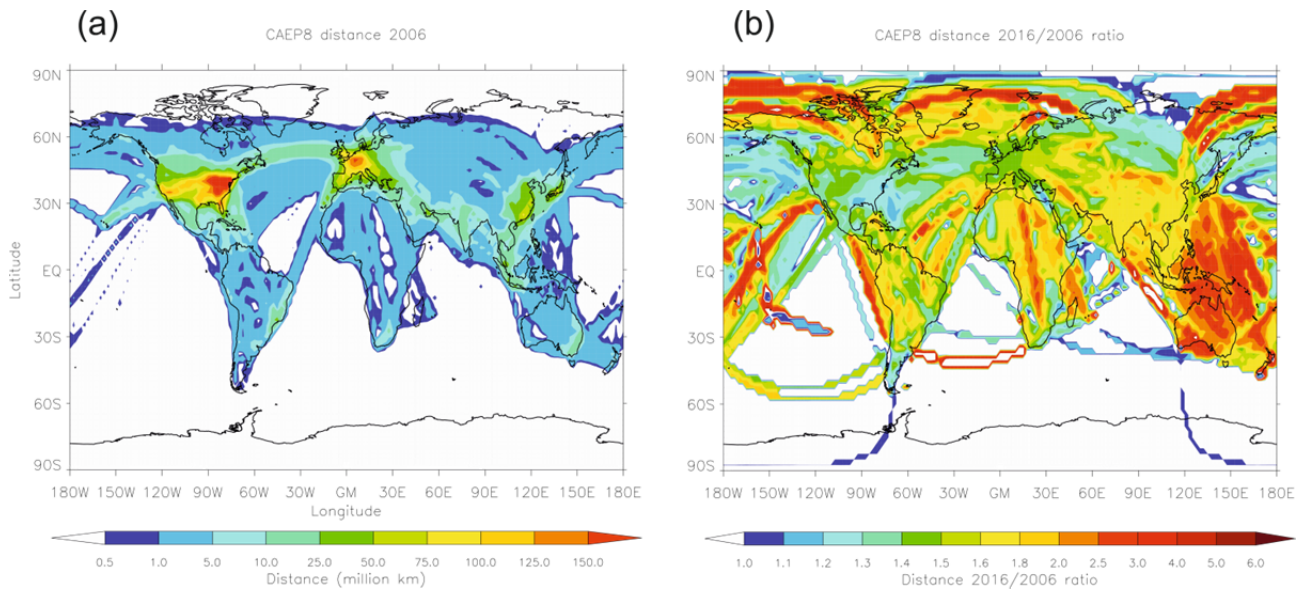
Figure 1(a): Base year 2006 and (b) 2016/2006 ratio for integrated distance travelled for altitudes above 500 hPa

The calculated distance travelled for 2016 is based on CAEP8/MDG aircraft movement central projections (ICAO/CAEP, 2009). By 2016, the global distance is estimated to be 58 billion km, with 87% of these distances occurring above 500 hPa. Figure 1(b) shows the ratio of distance travelled between years 2016 and 2006. It is evident from Figure 1(b) that there are strong regional differences, with the highest growth observed in areas of the developing world and Australasia. Here, growth between 2× to 5× of baseline traffic were observed. For areas of the world with high densities of traffic in 2006, such as Western Europe and North America, the distance is also expected to grow, but with a lower factor of less than 1.5×.

3   POTENTIAL CONTRAIL COVERAGE (BPC)

The ERA-Interim data (ECMWF, 2012) from 2001 to 2011 across four time slices (0, 6, 12 and 18 UTC) were used to represent current meteorology. The potential contrail coverage was calculated by applying the offline methodology described by Sausen et al. (1998) to this meteorology. The propulsion efficiency values for the aircraft fleet for the years 2006 and 2016 were assumed to be 0.36 and 0.4, respectively. Figure 2(a) shows an example of how bpc at 12 UTC in 2006 may look, assuming present day climate. Here, 12 UTC was chosen as an example because out of the four time slices used, this was the one with the greatest amount of global air traffic. The global potential coverage for 2006 was found to be 19.8%, with the largest values in tropical and polar regions.
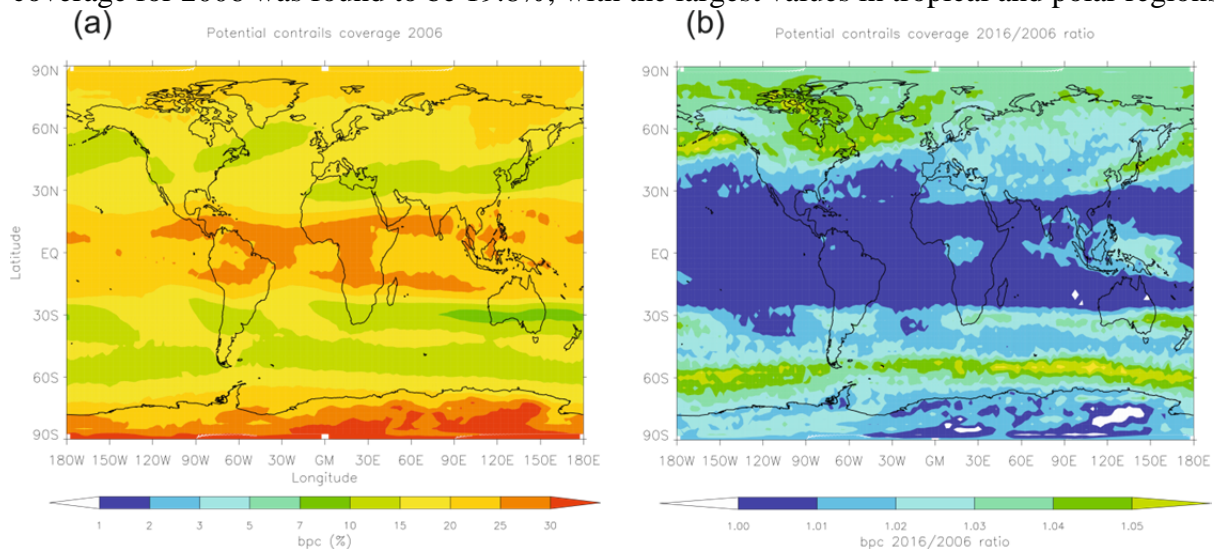
Figure 2(a): Base year 2006 and (b) 2016/2006 ratio for integrated potential contrail coverage at 12 UTC

The global potential contrail coverage is estimated to increase by about 1% between 2006 and 2016. Figure 2(b) shows the 2016 bpc changes with respect to 2006 caused by the change in fleet propulsion efficiency. These results do not account for future changes in temperature and water vapour since present-day meteorology is assumed.

4 CONTRAIL COVERAGE (BCO)

The distance travelled and potential contrail coverage described in Sections 2 and 3 were used to produce the contrail coverage for 2006 and 2016. The results for 2006, depicted in Figure 3(a), produced a global contrail coverage of 0.098%, with the highest values over North America, Western Europe, the Far East and the NAFC. This value is within the 0.07-0.11% range from previous studies, based on different movement inventories and methodologies (Stuber and Forster, 2007; Rap et al., 2010; Burkhardt and Kärcher, 2011; Frömming et al., 2011).
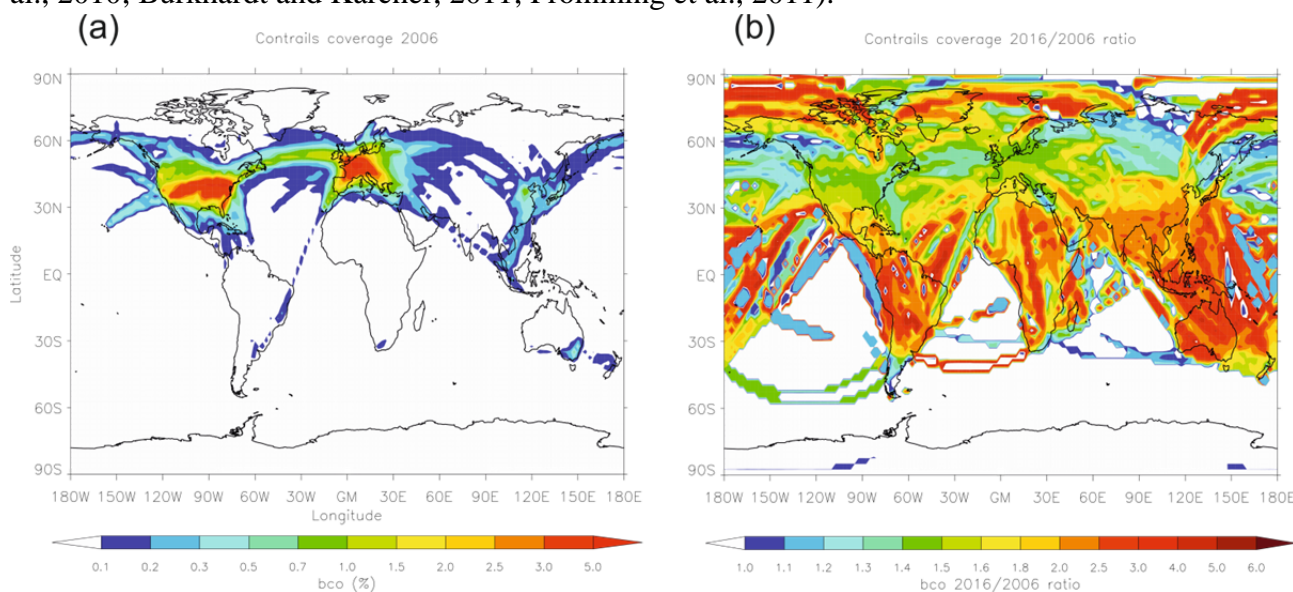
Figure 3(a): Base year 2006 and (b) 2016/2006 ratio for contrail coverage

Figure 3(b) shows the contrail coverage for 2016 traffic and present-day meteorology. The combination of significant growth in air traffic (1.5×) and a small increase in potential contrail coverage (1.01) resulted in a 1.6× increase in global contrail coverage. Regionally, the changes in contrail coverage are mainly linked to traffic growth with a slight enhancement at high latitudes where bpc shows a larger increase.

5 SUMMARY OF FINDINGS AND FURTHER WORK

In this study, assuming present-day meteorology, the global contrail coverage for 2006 was estimated to be 0.098%. This value falls within the range from previous studies, 0.07–0.11% (Stuber and Forster, 2007; Rap et al., 2010; Burkhardt and Kärcher, 2011; Frömming et al., 2011). The 2016 coverage was estimated to be 0.155%, representing a 1.6× increase, which is slightly larger than that of the distance travelled. This is partly as a result of increased potential contrail coverage linked to fleet propulsion efficiency. In the next phase of the study, contrail RF will be calculated offline with the UK Meteorological Office's two-stream radiative transfer model (Edwards and Slingo, 1996) which accounts explicitly for the SW and LW scattering by ice clouds. A sophisticated parameterization of the radiative properties of ice clouds in the model, based on a bimodal ice particle size distribution, allows a temperature-dependent prescription of the size and the mass of the particles in both size modes (De León et al., 2012) and will be used to estimate the impact of future air traffic on contrail RF.

6   ACKNOWLEDGEMENTS

REFERENCES

Burkhardt, U. and B. Kärcher, 2011: Global radiative forcing from contrail cirrus. Nature Climate Change 1, 54-58.

De León, R.R., M. Krämer, D.S. Lee, and J.C. Thelen, 2012: Sensitivity of radiative properties of persistent contrails to the ice water path. Atmos. Chem. Phys. 12, 7893–7901.

Edwards, J.M. and A. Slingo, 1996: Studies with a flexible new radiation code. I: Choosing a configuration for a large-scale model. Q. J. Roy. Meteor. Soc. 122, 689–719, DOI: 10.1002/qj.49712253107.

European Centre for Medium-Range Weather Forecasts (ECMWF). ECMWF ERA-Interim Re-Analysis data, [Internet]. NCAS British Atmospheric Data Centre. 2009-, 10 September 2012. Available from http://badc.nerc.ac.uk/view/badc.nerc.ac.uk__ATOM__dataent_12458543158227759.

Frömming, C., M. Ponater, U. Burkhardt, A. Stenke, S. Pechtl and R. Sausen, 2011: Sensitivity of contrail coverage and contrail radiative forcing to selected key parameters. Atmos. Environ. 45, 1483-1490.

ICAO/CAEP, 2009: Agenda Item 4: Modelling and Databases Task Force (MODTF) Goals Assessment Results, International Civil Aviation Organization (ICAO) / Committee on Aviation Environmental Protection (CAEP) Working Paper, Steering Group Meeting, Salvador, Brazil, 22-26 June 2009.

Lee, D.S., D.W. Fahey, P.M. Forster, P.J. Newton, R.C.N. Wit, L.L. Lim, B. Owen, and R. Sausen, 2009: Aviation and global climate change in the 21st century. Atmos. Environ. 43, 3520–3537.

Owen, B., D.S. Lee, and L.L. Lim, 2010: Flying into the Future: Aviation Emissions Scenarios to 2050. Environ. Sci. Technol. 44, 2255–2260.

Rap, A., P.M. Forster, A. Jones, O. Boucher, J.M. Haywood, N. Bellouin and R.R. De Leon, 2010: Parameterization of contrails in the UK Met Office Climate Model. J. Geophys. Res. 115, 1-15.

Sausen, R., K. Gierens, M. Ponater, and U. Schumann, 1998: A diagnostic study of the global distribution of contrails part I: present day climate. Theor. Appl. Climatol. 61, 127–141.

Stuber, N. and P. Forster, 2007: The impact of diurnal variations of air traffic on contrail radiative forcing. Atmos. Chem. Phys. 7, 3153-3162.

Impact of transportation sectors on global aerosol

M. Righi[*], J. Hendricks, R. Sausen
Deutsches Zentrum für Luft- und Raumfahrt, Institut für Physik der Atmosphäre, Oberpfaffenhofen, Germany

Keywords: aerosol, land transport, shipping, aviation, global modeling.

ABSTRACT: The transportation sector, including land transport, shipping and aviation, is one of the major sources of tropospheric aerosol. Aerosol particles can have a significant impact on climate and can affect air quality, in particular in the urban, densely populated areas, with consequent adverse health effects. Emissions from the transportation sector are expected to grow in the near future, especially in the developing countries. At the same time, various mitigation strategies are being applied in order to reduce air pollution and climate impacts. In this work we use the EMAC-MADE global aerosol model to quantify the impact of transportation on global aerosol. We consider a present-day scenario (2000) and use the CMIP5 emission dataset developed in support of IPCC AR5. The model is evaluated by comparing simulated aerosol concentrations and optical depth to station data, focusing on areas where traffic pollution is expected to play a significant role: Europe (EMEP network data), South-East Asia (EANET) and United States (CASTNET and IMPROVE). An important issue in modeling aerosol from traffic-related sources is to achieve an accurate representation of the size distribution of emitted particles, also due to the relatively coarse spatial resolution of global models, which cannot resolve the fine scales typical for the emission processes (and related chemical and microphysical interactions). To quantify the resulting uncertainties, we perform additional sensitivity studies considering different assumptions on the size distributions of emitted aerosol. First results are presented and future prospects are discussed.

1 INTRODUCTION

Land transportation, shipping, and aviation emit several types of gaseous and aerosol species which can have a significant impact on atmospheric composition, affecting both air quality and climate. According to the IPCC Fourth Assessment Report (Kahn Ribeiro et al., 2007), traffic is one of the most relevant source of CO_2 emissions, with the largest contribution from land transport. Energy use from the transportation sector is growing at a rate of 2 %/yr, with developing countries and growing economies experiencing stronger increases.

The impact of aerosol particles on climate is due to both direct interactions with radiation (scattering and absorption, direct aerosol effect) and modifications of cloud microphysical properties and lifetime (indirect aerosol effect). These effects can modify the Earth's radiation budget and cool or warm the atmosphere at different spatial and temporal scales. Aerosol can also have a negative impact on air quality and human health. Particles with diameter smaller than 2.5 μm (known as $PM_{2.5}$) are particularly harmful, due to their ability to affect the human respiratory system. The regions where the traffic activity is most intense, like urban areas, vicinity of harbors and airports are most exposed to transport-related air pollution.

In this work, we aim at providing a comprehensive model-based analysis of the impact of transport (land transport, shipping and aviation) on global atmospheric aerosol on the global scale. We use the EMAC-MADE global aerosol climate model, combined with an emission inventory designed in support of the IPCC Fifth Assessment Report (Lamarque et al., 2010). We perform a set of sensitivity simulations in order to quantify the uncertainty associated with the assumptions on the size distribution of emitted particles, which is essential to determine their number. We present result

---

[*] *Corresponding author:* Mattia Righi, DLR-Institut für Physik der Atmosphäre, Oberpfaffenhofen, D-82205 Wessling, Germany. Email: mattia.righi@dlr.de

for year 2000 conditions. The impacts of future scenarios, based on the different Representative Concentration Pathways (RCP, Moss et al., 2010), will be the subject of a follow-up study.

2   THE EMAC-MADE GLOBAL AEROSOL MODEL

The ECHAM/MESSy Atmospheric Chemistry (EMAC) model is a numerical chemistry and climate simulation system designed to describe tropospheric and stratospheric processes (Jöckel et al., 2006). It uses the Modular Earth Submodel System (MESSy) to link multi-institutional computer codes. The core atmospheric model is the European Center Hamburg General circulation model (ECHAM5, Roeckner et al., 2006). For this work, the model is run in a T42L19 resolution (2.8° on a Gaussian grid and 19 vertical layers up to 10 hPa). MADE (Lauer et al., 2005, 2007) is the sub-module that simulates aerosol microphysics and describes the aerosol population by means of three log-normal modes (Aitken, accumulation and coarse mode). It includes black carbon (BC), particulate organic matter (POM), aerosol sulfate (SO_4), nitrate (NO_3) and ammonium (NH_4), mineral dust, sea salt and aerosol water.

The effects of transportation are estimated by comparing simulations in which emissions from individual transport sectors are switched off (NOLAND, NOSHIP, NOAIRC) with a reference simulation (REF), which includes all emission sources. All simulations cover a period of 10 years (1996-2005) and are performed in the so-called nudged mode, using ECMWF operational analysis data to constrain model dynamics in order to minimize dynamical differences in the different experiments.

The model has been evaluated in previous studies (Lauer et al., 2005, 2007 and Aquila et al., 2011). Since a new set of emissions is used here (see next section), additional evaluation is performed, by comparing simulated aerosol concentrations and aerosol optical depth with station data from different networks (EMEP, IMPROVE, CASTNET, EANET and AERONET) in different regions (Europe, North America and Asia). This comparison shows a particularly good agreement for PM_{10}, $PM_{2.5}$ and AOD, while discrepancies occur in the case of NO_3, a problem possibly related to the model simplified chemical mechanism adopted for this study (including basic tropospheric background chemistry and the sulphur cycle).

3   EMISSION SETUP AND SIZE DISTRIBUTION OF THE EMITTED PARTICLES

We use the CMIP5 anthropogenic and biomass burning emissions from Lamarque et al. (2010) for the year 2000. We also derive sulfur emission for the aviation sector (not available in the original dataset), by scaling BC emission with the corresponding emission factors. BC emission factors are estimated from the QUANTIFY data (Lee et al. 2005) as the ratio between emission and fuel consumption, while for SO_2 a value of 0.8 $g(SO_2)/kg_{fuel}$ is taken (Lee et al., 2010). An additional sensitivity study for low-sulfur scenario is performed, with a value of 0.0052 $g(SO_2)/kg_{fuel}$ (Petzold et al., 1999).

The emission dataset does not include information about number emissions, which must be derived from mass emissions by assuming typical size distribution of emitted particles. These assumptions are critical, since they determine the number of emitted particles and can have a large impact on the resulting effects, both in terms of concentrations and of climate impacts. Information about size distribution is very uncertain and depends on the emitting source, on the local conditions and on the age of polluted air masses. In order to assess these uncertainties, we perform sensitivity simulations with different assumptions on the size of the particles emitted from the transportation sectors. The parameters are taken as much as possible from measurements close to the relevant area (urban areas, ship plumes, aircraft exhaust plumes).

3.1   *For land transport, we assume:*

-   AEROCOM (REF): based on Dentener et al. (2006, D06) recommendations, in reasonable agreement with measurements in Berlin urban area (Birmili et al., 2009, B09).
-   YOUNG: based on the measurements of B09, including a young Aitken mode and a soot mode.

- AGED: based on the measurements of B09, considering a more aged population, with a soot and an accumulation mode.

3.2 *For shipping:*

- AGED2 (REF): based on measurements in aged plumes by Petzold et al. (2008), which were already applied in Righi et al. (2011, R11).
- AGED1: similar to AGED2, with slightly different values for the parameters.
- AGEDALL: assumes a very aged population, with all particles released in the accumulation mode with parameters from D06

3.3 *For aviation:*

- HIGH-S (REF): based on measurements by Petzold et al. (1999, P99) of engine exhausts.
- LOW-S: uses the same parameters as HIGH-S, but assumes a lower fuel sulfur content (0.0052 vs. 0.8 $g(SO_2)/kg_{fuel}$).
- NUC: assigns sulfur particles to a nucleation mode based on the simulations by Kärcher et al. (2007, K07).

4   RESULTS

The impacts of traffic emissions on tropospheric aerosol mass burden are summarized in Figure 1. Burdens are computed for a relevant domain specific for each sector, that is the lower boundary layer (0-250 m height) for land transport (over continents) and shipping (over ocean), whereas for aviation an altitude range of about 8-13 km is considered, which corresponds to the typical cruise altitudes for the current fleet. The results reveal that land transport impacts are dominated by BC and NO_3, which are related to the large emissions of BC and NO_x for this sector. The latter is also due to relatively low amounts of SO_4 from land transport, which leaves more ammonia available for the formation of ammonium nitrate. The shipping sector impact is also dominated by NO_3, with significant effects also on SO_4. Carbonaceous components are quite low, due to low emissions. However ships are the only direct source of pollution over the ocean, therefore their relative importance might be non-negligible. Aviation effects in the upper troposphere are mostly due to BC and SO_4, while the NO_3 concentration is decreased, since SO_4 emission from aircraft hamper the formation of nitrate at these altitudes.
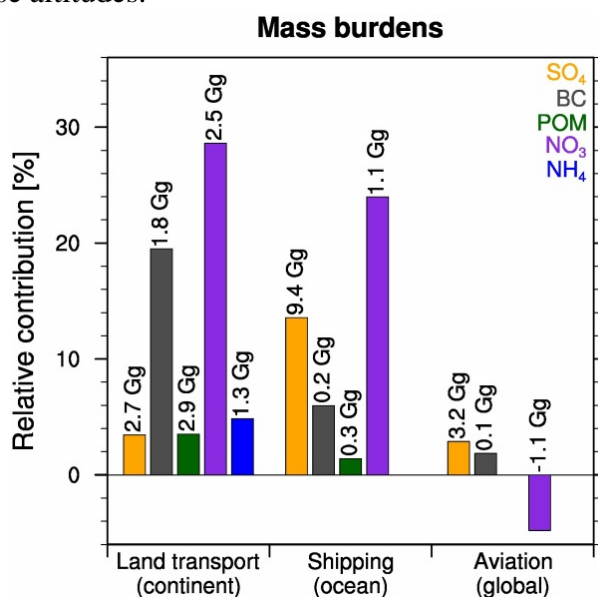
Figure 1: Relative contribution of the traffic sectors to the multi-year average mass burdens in the two lowermost model layers (0-250 m), for land transport (on the continents) and shipping (on the oceans), and between model layers 7 and 9 (8-13 km), for aviation. The value on top of each bar shows the corresponding absolute contribution (in units of Gg).

The geographical distributions of traffic impacts are shown in Figure 2 for the most relevant species. BC surface level changes due to transport (top-left panel) are most evident on the continents. Largest values of about 1 $\mu g/m^3$ are found over Eastern U.S., Europe, India and China and in the vicinity of large metropolitan areas outside these regions. The relative contributions (bottom-left panel) are also significant and can be larger than 50% in several regions. Interestingly, the impact of land transport over China and India is quite low in relative terms, in spite of large absolute changes, due to the presence of other pollution sources (like industry or domestic sources), which dominates over land transport emissions. Shipping (middle panels) largely affects SO_4 concentration over the oceans, with variations above 1 $\mu g/m^3$ (40-60 %) along the most-travelled routes (Northern Pacific and Central Atlantic). These effects can be important also along the coastlines, with significant impacts for air pollution and a potentially large adverse effect on human health for these regions. Aviation effects (right panels) are mostly confined to the Northern Hemisphere mid-latitudes, at around 250 hPa, although some effect can be noticed also close to the surface, due to airport activities.
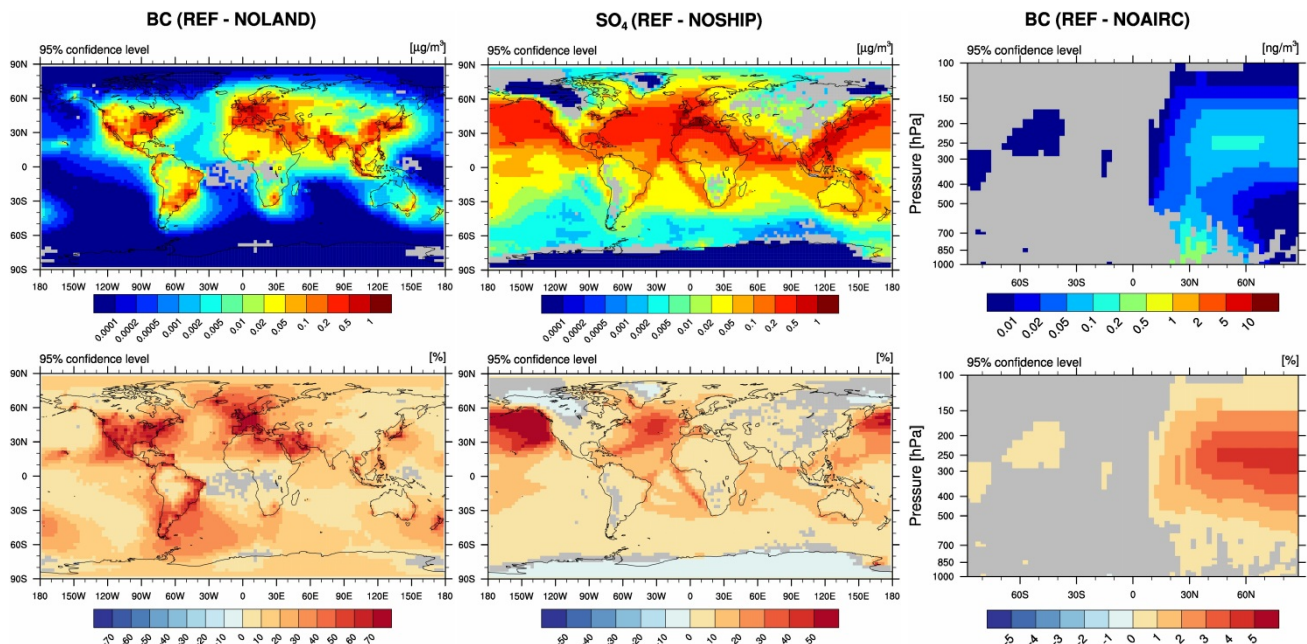
Figure 2: Multi-year average absolute impact (top) and relative contribution (bottom) of land transport on BC surface level concentration (left, with AEROCOM size distribution), of shipping on SO_4 surface level concentration (middle, with AGED2 size distribution) and of aviation on BC zonal mean concentration (right, with HIGH-S size distribution). Non-significant grid points (according to the t-test at 95% confidence level) are masked out in gray.

The impact on particle number (Figure 3, in terms of burdens, similar to Figure 1) suggests a quite strong dependency of the results on the assumed size distribution of the emitted particles. The impact of land transport emissions on number concentration decreases when a more aged size distribution is assumed (AGED), while similar impacts are found for the AEROCOM and YOUNG distributions. For shipping, results are quite similar and confirm the previous study by R11, who assumed the same size distributions with a different emission setup. The simulated aviation effects reveal a very strong change in number concentration, depending on the fuel sulphur content (HIGH_S versus LOW_S), opening interesting perspectives in view of future prospects on the adoption of low-sulfur fuels for aircrafts. The inclusion of a more detailed description of nucleating particles from aircraft (NUC) does not show a critical impact in terms of number.

We plan to extend this study by considering 2030 emissions in different RCPs. We expect important changes, with decreasing impacts of land transport traffic over Europe and U.S. (due to regulations and improved technologies) and increasing effects in South East Asia (due to growing economy). Reduced sulfur content in shipping fuels, in view of recent policy measures, should also produce significant changes with respect to the present day situation. Aviation impacts are projected to grow in all scenarios, due to increasing traffic.
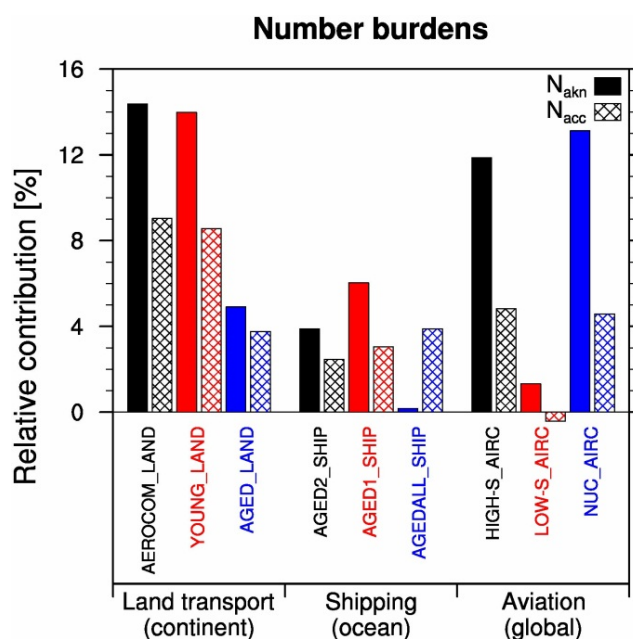
Figure 3: Relative contribution of the traffic sectors to the multi-year average number burdens for the different sensitivity analyses. The Aitken/accumulation modes are marked with the solid/hatched pattern. Values are calculated on the same domains as for mass burdens (Figure 1).

5   CONCLUSION AND OUTLOOK

The main conclusions of this work can be summarized as follows:
- Land transport significantly impacts surface level aerosol (BC and NO_3) concentrations, with highest effect over Eastern U.S., Europe, India and China.
- The shipping impact is mostly due to aerosol sulfate (SO_4) and peaks along the shipping routes of the Northern Pacific and the Central Atlantic. Significant effects are also simulated along the coastlines, with possible important consequences on air pollution and health.
- The effects of aviation are mostly confined to the Northern mid-latitudes upper troposphere and lowermost stratosphere, although some impacts can be noticed at the surface level, related to emissions from airport activities.
- Impacts on number concentration are very sensitive to adopted size distributions for emitted particles.

REFERENCES:

Aquila, V., J. Hendricks, A. Lauer, A., N. Riemer, H. Vogel, D. Baumgardner, A. Minikin, A. Petzold, J. P. Schwarz, J. R. Spackman, B. Weinzierl, M. Righi, and M. Dall'Amico, 2011. MADE-in: a new aerosol microphysics submodel for global model simulation of insoluble particles and their mixing state. Geosci. Model Dev. 4, 325–355.

Birmili, W., B. Alaviippola, D. Hinneburg, O. Knoth, T. Tuch, J. Borken-Kleefeld, and A., Schacht, 2009. Dispersion of traffic-related exhaust particles near the Berlin urban motorway â estimation of fleet emission factors. Atmos. Chem. Phys. 7, 2355–2374.

Dentener, F., S. Kinne, S., T. C. Bond, O. Boucher, J. Cofala, S. Generoso, P. Ginoux, S. L. Gong, J. J. Hoelzemann, A. Ito, L. Marelli, J. E. Penner, J.-P. Putaud, C. Textor, M. Schulz, G.R. van Der Werf}, and J. Wilson, 2006. Emissions of primary aerosol and precursor gases in the years 2000 and 1750 prescribed data-sets for AeroCom. Atmos. Chem. Phys. 6, 4321–4344.

Kärcher, B., O. Möhler, P. J. Demott, S. Pechtl, F. Yu., 2007. Insights into the rols of soot aerosols in cirrus cloud formation. Atmos. Chem. Phys. 7, 4203–4227.

Lamarque, J.-F., T. C. Bond, V. Eyring, C. Granier, A. Heil, Z. Klimont, D. S. Lee, C. Liousse, A. Mieville, B. Owen, M. G. Schultz, D. T. Shindell, S. J. Smith, E. Stehfest, J. A. van Aardenne, O. R. Cooper, M. Kainuma, N. Mahowald, J. R. McConnell, V. Naik, K. Riahi, and D. P. van Vuuren, 2010: Historical (1850-2000) gridded anthropogenic and biomass burning emissions of reactive gases and aerosols: methodology and application. Atmos. Chem. Phys. 10, 7017–7039.

Lauer A., J. Hendricks, I. J. Ackermann, B. Schell, H. Hass, and S. Metzger, 2005. Simulating aerosol microphysics with the ECHAM/MADE GCM – Part I: Model description and comparison with observations. Atmos. Chem. Phys. 5, 3251–3276.

Lauer A., V. Eyring, J. Hendricks, P. Jöckel, and U. Lohmann, 2007. Global model simulations of the impact of ocean-going ships on aerosols, clouds, and the radiation budget. Atmos. Chem. Phys. 7, 5061–5079.

Lee, D. S., B. Owen, A. Graham, C. Fichter, L. L. Lim, and D. Dimitriu, 2005. Allocation of international aviation emissions from scheduled air traffic – Present day and historical (Report 2 o 3). Manchester Metropolitan University, Centre for Air Transport and the Environment.

Lee, D. S., D. W. Fahey, P. M. Forster, P. J. Newton, R. C. N. Wit, L. L. Lim, B. Owen, and R. Sausen, 2010. Transport impact on atmosphere and climate: Aviation. Atmos. Environ. 44, 4678–4734.

Moss, R. H., J. A. Edmonds, K. A. Hibbard, M. R. Manning, S. K. Rose, D. P. van Vuuren, T. R. Carter, S. Emori, M. Kainuma, T. Kram, G. A. Meehl, J. F. B. Mitchell, N. Nakicenovic, K. Riahi, S. J. Smith, R. J. Stouffer, A. M. Thomson, J. P. Weyant, and T. J. Wilbanks, 2010. The next generation of scenarios for climate change research and assessment. Nature 463, 747–756.

Petzold, A., A. Döpelheuer, C. A. Brock, and F. Schröder, 1999. In situ observations and model calculations of black carbon emission by aircraft at cruise altitude. J. Geophys. Res. 104, 22171–22181.

Righi, M., C. Klinger, V. Eyring, J. Hendricks, A. Lauer and A. Petzold, 2011. Climate impact of biofuels in shipping: global model studies of the aerosol indirect effect. Environ. Sci. Tech. 45, 3519–3525.

Roeckner, E., E. Brokopf, M. Esch, M. A. Giorgetta, S. Hagema, and L. Kornblueh, 2006. Sensitivity of simulated climate to horizontal and vertical resolution. J. Clim. 19, 3771–3791.

A 10-Year Irish Observational AVHRR and Radiosonde Contrail Climatology

G. M. Whelan[*], F. Cawkwell
Geography Dept., University College Cork, Ireland

H. Mannstein
DLR Institute for Atmospheric Physics, Germany

P. Minnis
NASA Langley Research Center, USA

Keywords: contrail detection, AVHRR, radiosondes, atmospheric contrail conditions, ice-supersaturation, contrail optical depth

ABSTRACT: Ten years (2001 to 2010) of upper-atmospheric observations from 4x daily dry-bias-corrected radiosonde ascents from Valentia (Ireland) are analyzed via application of the Schmidt-Appleman criterion to characterize the susceptibility of the atmosphere over Ireland to contrail formation and persistence seasonally, diurnally and inter-annually. A 10-yr AVHRR contrail-climatology for Ireland (51-56N and 11-4W) is also compiled using an Automated Contrail Detection Algorithm (CDA) (Mannstein et al., 1999). From analysis of radiosonde observations, an average contrail-layer thickness of 1.1 km, and a ~20% probability of contrail-layer occurrence is found. However, strong seasonal and diurnal variability is observed in contrail-layer thickness and probabilities. The thickest contrail-layers of 1.5 km are found in 00:00 and 06:00 UTC ascents in winter (DJF), corresponding to contrail-layer occurrence probabilities of 27 and 31% respectively – and coinciding with a night-time peak in transatlantic flights crossing Irish airspace at ~04:00 UTC. On average, the thinnest contrail-layers (0.6 km) are found in 12:00 UTC ascents during summer (JJA) months (with a 5% probability of contrail-layer occurrence).

Advanced Very High Resolution Radiometer (AVHRR) imagery from multiple NOAA satellites at 03:30, 06:00, 12:00 and 22:25 UTC from 2001 to 2010 are examined using the CDA in conjunction with an Interactive Contrail Assessment Tool (Minnis et al., 2005). Inconsistencies arise when comparing contrail-coverages and optical depths from multiple satellites, due to slight calibration differences of the thermal channels, which must be corrected to produce a consistent contrail-climatology. Analyses of coincident 12:00 UTC AVHRR imagery from different satellites indicate that, when appropriate bias-correction methods are implemented, consistent contrail-coverage results across multiple NOAA satellites are achievable. The 12:00 UTC contrail-coverage was greatest in DJF (1%) and MAM (1%), less in SON (0.9%) and least in JJA (0.7%) with high inter-annual variability. In general, monthly trends in contrail-coverage are in good general agreement with trends observed in CISSLs and Irish overflights. Optical depth is also retrieved for all imagery and an average value (across all satellites), before bias-correction, of 0.24 is found (with no seasonal trend observed). Optical depth values were slightly lower following manual assessment of imagery but still approximately double the value quoted by Meyer et al., (2002) and in good agreement with the results of Minnis et al. (2011).

1 INTRODUCTION

Aircraft condensation-trails (contrails) produced in the wake of jet aircraft have been found to produce a positive net radiative forcing effect: with strong regional, seasonal and diurnal dependencies. A regional linear-contrail Radiative Forcing (RF) estimate of +0.23 Wm^{-2} was derived for a region

---

[*] *Corresponding author:* Gillian M. Whelan, Geography Dept., University College Cork, College Road, Cork, Ireland. Email: whelan.gillian@umail.ucc.ie

in the UK near a flight corridor (Stuber et al., 2007). However, this value does not include the effect of contrail-induced cirrus cloud, which is estimated by Burkhardt et al., (2011) to be about 9 times that of linear contrails alone. Considering Ireland's location at the entrance to the North Atlantic Flight Corridor, with more than one quarter million overflights annually through Irish space at altitudes above 24,000 ft, contrail climate impacts could be of particular concern to the Irish regional climate.

The susceptibility of the atmosphere over Ireland to contrail formation (and persistence), by this high density of commercial air-traffic, is analyzed by applying the modified Schmidt-Appleman criterion of Schumann (2005) to 10 years of 4x daily radiosonde ascents from Valentia. The radiative impact of contrails is dependent upon the amount of sky-area covered and the contrail optical depth. Both contrail-coverages and optical depths are retrieved from AVHRR satellite imagery. A proposed method of combining results from imagery from multiple AVHRR instruments onboard different satellites is presented which provides reasonably consistent results across different satellites. This will enable a consistent multi-satellite contrail climatology to be compiled over an entire decade to facilitate the assessment of the potential Irish regional climate impact of contrails.

2   RADIOSONDE RESULTS

To determine the atmospheric susceptibility of the Irish atmosphere to contrail formation and persistence, 10 years (2001 to 2010) of atmospheric radiosonde soundings from Valentia (in south-west Ireland), at 4x daily intervals are analyzed.

Contrail critical temperatures ($T_{crit(RH)}$) are calculated based on the modified Schmidt-Appleman criterion (Schumann, 2005). For contrails to form and persist, the atmosphere must be supersaturated with respect to ice, and the ambient temperature must be below the calculated $T_{crit(RH)}$. Standard resolution RS80A (2001 to 2005) and RS92 (2006 to 2010) dry-bias-corrected radiosonde ascent profiles are examined for the presence of Contrail Ice-Supersaturated Layers (CISSLs). CISSLs are found in ~20% of the 13,734 valid ascent profiles evaluated in this study.

The greatest frequency of CISSL occurrence over Ireland, (as shown in Table 1) is found in the 06:00 UTC ascents in winter (DJF). The overall seasonal variability in 18:00 and 06:00 UTC ascents show the strong impact of daylight hours on CISSL occurrence.

Table 1: 10-yr average CISSL percentage frequency of occurrence (left) and thickness in km (right)

CISSL Frequency (%)	00:00 UTC	06:00 UTC	12:00 UTC	18:00 UTC	All Ascents	Average CISSL thickness (km)	00:00 UTC	06:00 UTC	12:00 UTC	18:00 UTC	All Ascents
DJF	27	31	16	28	26	DJF	1.5	1.5	1.0	1.4	1.3
MAM	30	26	10	16	20	MAM	1.2	1.2	1.1	1.0	1.2
JJA	24	16	5	5	12	JJA	0.9	0.8	0.6	0.7	0.7
SON	26	27	10	24	22	SON	1.2	1.2	0.8	1.0	1.0
ANNUAL	27	25	10	18	20	ANNUAL	1.2	1.2	0.9	1.1	1.1

Typically, CISSLs are ~1.1 km thick with strong seasonal and diurnal dependencies. The average winter and summer (JJA) values across all ascents (1.3 and 0.7 km, respectively) are similar to those found in the UK (1.3 and 0.9 km) by Rädel and Shine (2007), with typically lower JJA values in this study. The lower values of CISSL thickness and frequency during summer observed in this study are most likely due to the use of a contrail critical temperature threshold that is specifically calculated throughout each ascent profile, at every pressure level - which is often much lower than the upper limit of -40 ^{o}C critical temperature threshold that was used by Rädel and Shine (2007) to identify 'cold' ice-supersaturated regions (CISSRs). However, imposing a fixed contrail critical temperature does remove some of the dependencies of results on ambient relative humidity, pressure level and particularly aircraft contrail-factor (and some of these associated measurement uncertainties). By doing so, more universally applicable information about the atmosphere is presented, however for the purposes of this study it is preferable to attempt to constrain the CISSL results to the conditions of contrail formation and persistence of the typical commercial jet aircraft flying through the 'real' atmosphere (i.e. as a function of pressure and ambient relative humidity).

The strong seasonal/diurnal influence on CISSL frequency and thickness found in this study is dampened if contrail critical temperature ($T_{crit(RH)}$) is not calculated explicitly as a function of pressure and ambient relative humidity, and may also lead to an overestimation of contrail frequencies (for commercial aircraft) at certain pressure levels. To investigate this further, CISSLs (with $T_{crit(RH)}$ calculated using the modified Schmidt-Appleman criterion of Schumann (2005)) and CISSRs (with $T_{crit(233 K)}$ set fixed at -40 °C (233 K)) were analyzed for the 200, 250, and 300 hPa pressure levels for all Valentia radiosonde ascents over the ten years of interest. At higher pressure levels, the difference between CISSL and CISSR is more apparent. For some months (e.g. November and December), contrail frequency will either slightly increase, or substantially decease, with altitude between 200 and 300 hPa depending on whether $CISSR_{(Tcrit(233 K))}$ or $CISSL_{(Tcrit(RH))}$ is used. In both cases, the 250 hPa pressure level indicates the highest contrail frequency of occurrence for most months.

10yr (2001 to 2010) Average Contrail Formation Frequencies in Valentia Radiosondes Pressure Levels
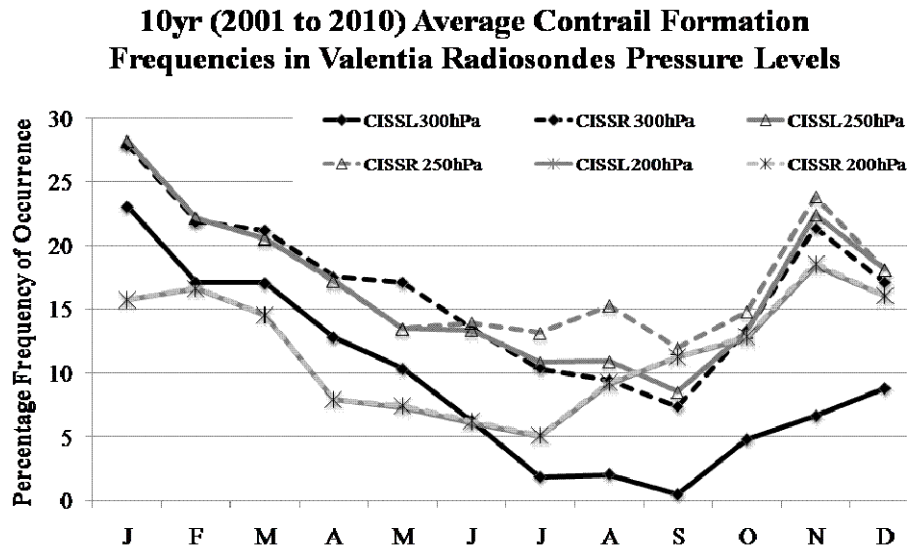
Figure 1: Comparison of 10 yr average CISSL (T_{crit} as calculated using the modified Schmidt-Appleman criterion) [solid lines] and CISSR (T_{crit} held fixed at 233 K) [dashed lines].

At the 250 hPa pressure level, where the mean $T_{crit(RH)}$ is ~222 K, contrail frequency is overestimated in August and September, due to generally warmer ambient summer temperatures. At 200 hPa, the mean $T_{crit(RH)}$ is ~220 K and the ambient temperatures are generally below this value - so there is very little difference between CISSL and CISSR and both will depend mainly on ice-supersaturation conditions. At 300 hPa, where the mean $T_{crit(RH)}$ ~224 K, there is a huge difference between CISSL and CISSR as ambient temperatures typically fall between 224 and 233 K. This is potentially a very important consideration for flight level studies of contrail-susceptible atmospheric conditions and suggests that when planning operational flight rerouting to avoid contrails, whilst minimizing fuel usage and other aircraft emissions, the modified Schmidt-Appleman criterion should be used to calculate $T_{crit(RH)}$ for the aircraft type as a function of pressure, relative humidity and temperature over the proposed route.

Since $T_{crit(RH)}$ varies only by ~0.4 K in the monthly mean values, some experimentation was carried out to calculate CISSR using other set values of T_{crit} as a function of pressure. Using $T_{crit} = 224$ K (and not 233 K), gives results similar to CISSLs in 96% of ascents. The 4% difference between $CISSR_{224K}$ and $CISSL_{Tcrit(RH)}$ is statistically significant, indicating that $T_{crit(RH)}$ should ideally be calculated for each individual case as explained above.

3   SATELLITE CONTRAIL RETRIEVALS

3.1 *Creating a consistent satellite contrail climatology*

Differences in the brightness temperatures of contrails at two specific thermal infrared wavelengths and their characteristic linear shape allow them to be detected by passive satellite remote sensing methods. The automated Contrail Detection Algorithm (CDA) of Mannstein et al., (1999) is applied to ten years of archived AVHRR thermal imagery using the 11 and 12 µm brightness temperatures

obtained from multiple NOAA satellites over Ireland to estimate the percentage contrail-coverage (CC%) of each scene.

Harmonizing data acquired from different satellites can add significant value to the outputs but also poses a number of problems, such as the introduction of a potential inconsistency in the derived data due to slight differences in the calibration of the thermal channels, which must be taken into account. To this end, a sampling of coincident 2007 AVHRR noon imagery from the NOAA-17 (N17) and NOAA-18 (N18) satellites were processed using the CDA in conjunction with the Inter-active Contrail Assessment Tool of Minnis et al., (2005) that allows the user to subjectively add/remove contrails as required. Slight differences in the CDA's detection efficiency (DE) and false-alarm rates (FAR) for each satellite were found and seasonally-dependant CC% correction factors were derived and applied to the imagery.
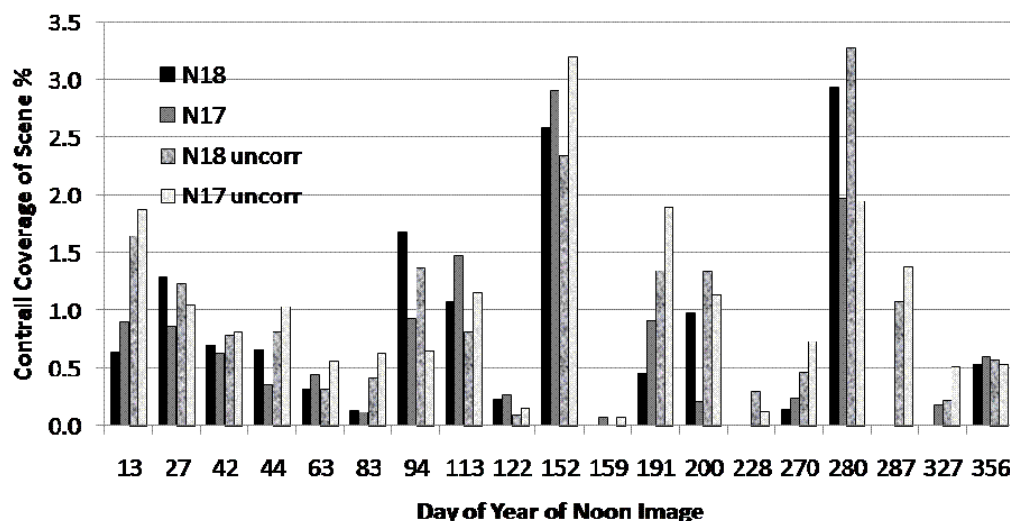
Figure 2: Comparison of coincident N17 and N18 noon contrail-coverage, before ('uncorr') and after manual post-processing.

Comparisons of updated CC% for 2007 indicate that N17 and N18 coincident imagery produce results that are reasonably consistent, i.e. no statistically significant difference between concurrent CC% results, an average CC% difference similar to the FARs for each satellite and a correlation coefficient ~0.9. This suggests that, with appropriate care taken, it is possible to create a reasonably consistent contrail climatology using AVHRR imagery from multiple satellites.

Imagery from other years was examined with the Interactive Contrail Assessment Tool to provide a more robust evaluation of DE, FAR and bias-correction factors (CFs). CFs for winter, spring (MAM), summer, and autumn (SON) for N18 are 1.03, 0.94, 0.89, and 0.98, respectively, and for N17 are 0.88, 0.95, 0.76 and 0.89. N17 and N18 have DEs of 80.8% and 81.8%, with FARs of 0.26 and 0.23, respectively.

For both satellites, minimum CFs occur during JJA indicating that CC% is generally overestimated more during this time of year by the automated method. In general, N17 requires more correction than N18 and only N18 in winter months shows a very slight underestimation of CC%. Overall, the CFs are close to 1 (CF = 1 means no correction required) and little correction to this value is required generally. However, the seasonal variation in CF for each satellite does indicate the need to apply an appropriate bias-correction to CC% in order to obtain a more accurate representation of the seasonal variation in CC%. It should also be noted that very faint contrails are not as yet detectable in satellite imagery and therefore cannot be evaluated in this study (Kärcher et al., 2009). Thus, the reported CC% may still be an underestimation.

3.2 *Seasonally-derived noon contrail-coverages over Ireland*

Following application of the bias-correction factors discussed in the previous section (broken down even further to a monthly correction factor), the monthly mean CC% for Ireland from each satellite is obtained.

Monthly Mean N17 12h00 CC% over Ireland

Monthly Mean N18 12h00 CC% over Ireland
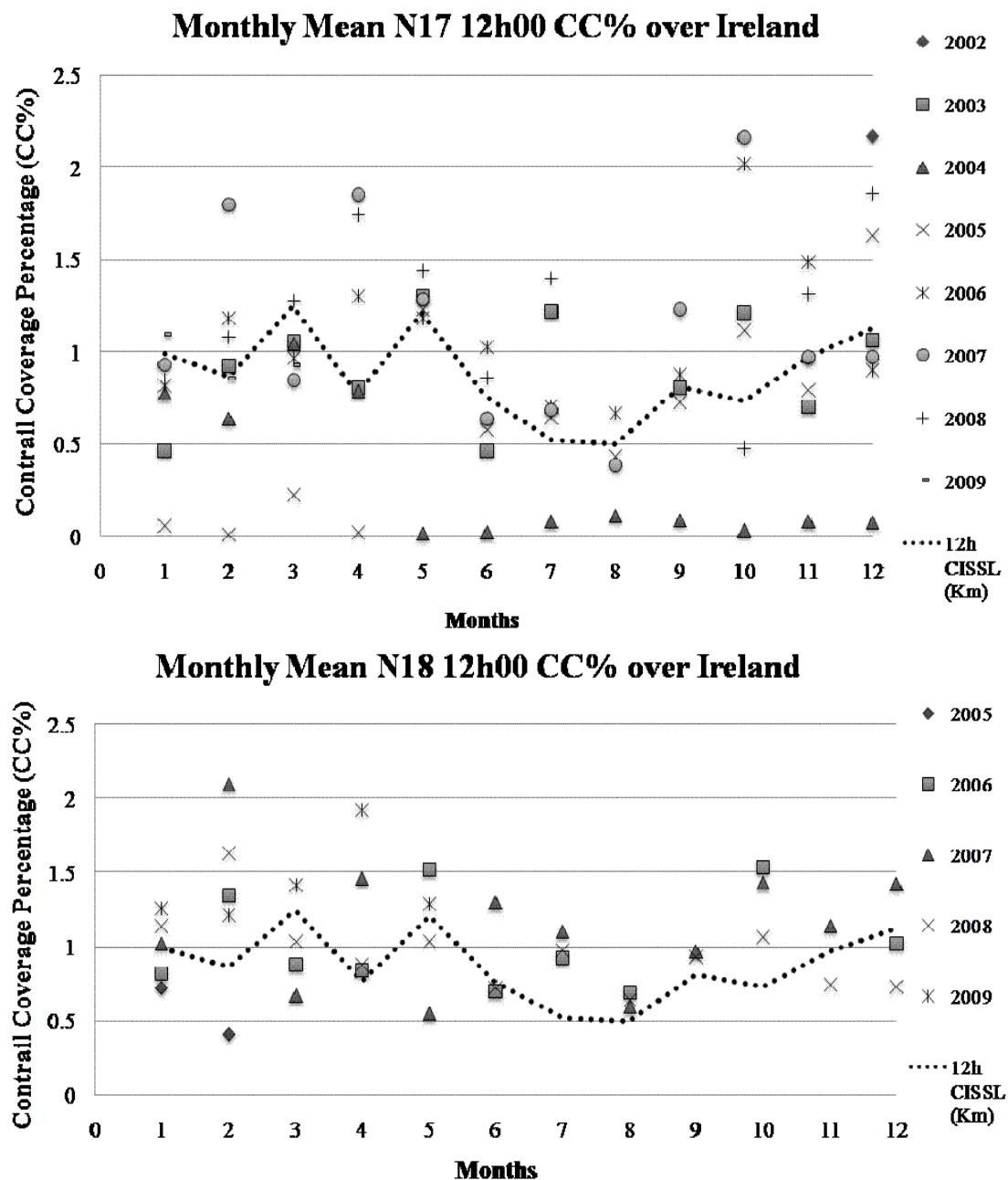
Figure 3: N17 (top) & N18 (bottom) noon monthly mean CC%, with 10 yr average CISSL noon thickness.

2002 – 2008 Average Overflights in Irish Airspace
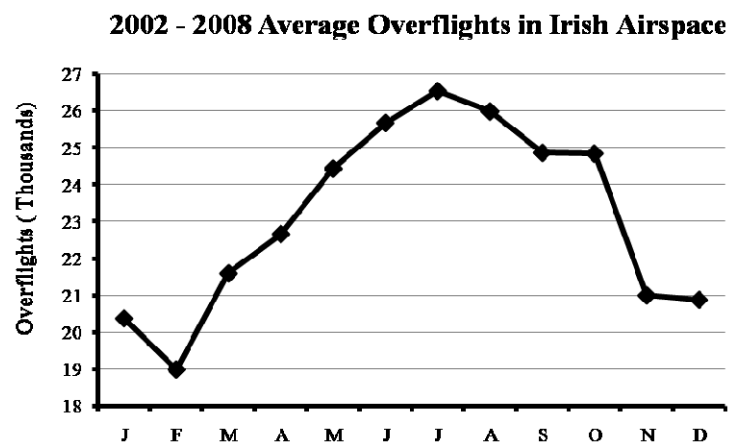
Figure 4: Monthly mean overflights (above 24,000ft) through Irish-airspace from 2002 to 2008.

As shown, the corrected CC% monthly means for all N17 and N18 noon imagery covering Ireland [51-56N and 4-11W] show good agreement across both satellites. The 10 yr average monthly

mean CISSL thickness from Valentia is also presented in these graphs for reference purposes. As both graphs demonstrate, the seasonal trend in CC% is similar to CISSL thickness for most months.

During October (and April), the peak in CC% (observed for both satellites) is likely due to a combination of increased CISSL formation frequency and increased overflights during these months. The February peak in CC% is likely related to maximum in 12:00 UTC CISSL frequency of occurrence. In July, when the 12:00 UTC CISSL thicknesses and frequency are at a minimum, overflights through Irish airspace reach their summer peak - this suggests that contrail events in July, when they do occur, are more likely to be extreme. This might explain a greater average CC% than might otherwise have been expected by CISSL results alone.

3.3 *Irish Contrail Optical Depth*

Using the method of Meyer et al., (2002), contrail optical depth values were derived from each image. The average (uncorrected) value for Ireland from all satellites is ~0.24 and varies from 0.17 (N14) to 0.28 (N18) with no seasonal trend observed. These values are double those found in Central Europe with AHVRR (Meyer et al., 2002), but are in good overall agreement with Minnis et al., (2011) using MODIS imagery.
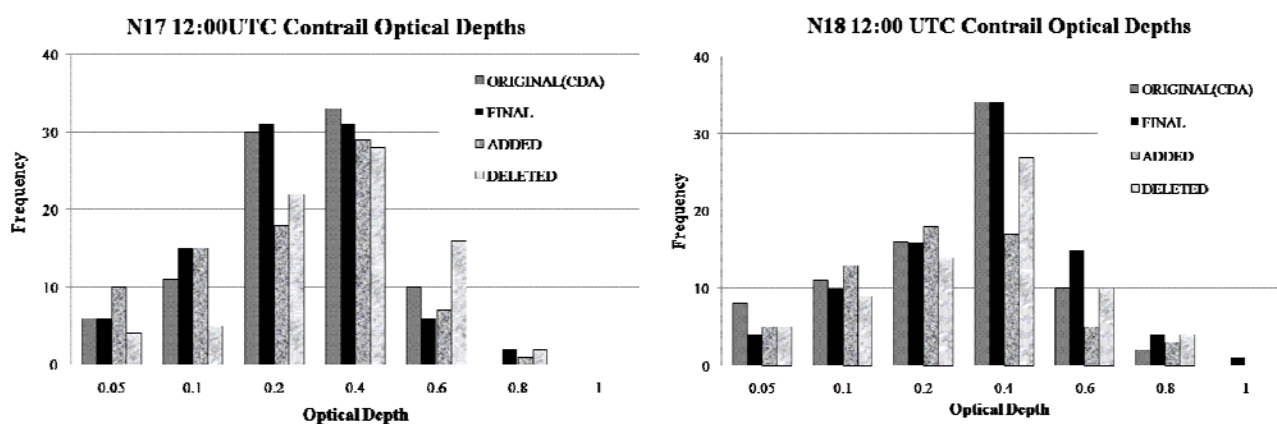
Figure 5: N17 & N18 optical depth of original, added, deleted and final contrails after manual post-processing of imagery.

Optical depth values were lower for both satellites after the manual assessment was performed. When optical depth values were corrected, the mean N17 value went from 0.21 to 0.20 and the mean N18 value dropped from 0.28 to 0.24. For both satellites, the average optical depth of 'deleted' contrails was larger than the average while slightly fainter contrails (with lower than average optical depths) were added. Very faint contrails are not detectable in satellite imagery and cannot be evaluated in this study, thus it is possible that even the updated lower optical depth values may still be a slight overestimation.

4   SUMMARY AND CONCLUSIONS

Based on ten years of 4x daily Valentia radiosonde ascents, contrail susceptible atmospheric conditions occur more often at night in winter and spring. AVHRR imagery from multiple NOAA satellites can be successfully combined to create an observational contrail climatology that is reasonably consistent, when differences in the CDA's DEs and FARs are evaluated and accounted for. Strong inter-annual variability in CC% was found across N17 and N18 noon imagery. Seasonal variations in CC% were observed in response to varying contrail-layer conditions and overflights. Overall, noon CISSL results were in good general agreement with satellite-derived 12:00 UTC contrail-coverages from the two different AVHRR instruments presented.

A 10 yr consistent satellite-derived contrail-coverage, optical depth and long-wave RF climatology for Ireland is currently being compiled and analyzed using AVHRR imagery from multiple NOAA satellites at 12:00, 06:00, 03:30 and 22:25 UTC to investigate the potential regional climate impact of contrails.

5   ACKNOWLEDGEMENTS

REFERENCES

Kärcher, B., U., Burkhardt, S., Unterstrasser and P. Minnis, 2009: Factors controlling contrail cirrus optical depth. Atmos. Chem. Phys, 9, 6229-6254.

Mannstein, H., R., Meyer and P. Wendling, 1999: Operational detection of contrails from NOAA-AVHRR-data. Int. J. Remote Sens. 20, 1641–1660.

Meyer, R., H., Mannstein, R., Meerkoetter, U., Schumann, and P. Wendling, 2002: Regional radiative forcing by line-shaped contrails derived from satellite data, J. Geophys. Res., 107, D10,10.1029/2001JD000426.

Minnis, P., R., Palikonda, B. J., Walter, J. K., Ayers and H. Mannstein, 2005: Contrail properties over the eastern North Pacific from AVHRR data, Meteor. Z., 14, 515–523.

Minnis, P., D. P., Duda, R., Palikinda, K., Kholpenkov, S., Bedka, R., Boeke, T., Chee, J. K., Ayers and K., Bedka, 2011: Contrail Retrievals from MODIS for ACCRI, EMS2011-716, 8, ph28.

Rädel, G., and K. P., Shine, 2007: Evaluation of the use of radiosonde humidity data to predict the occurrence of persistent contrails, Q. J. Roy. Meteor. Soc., 133, 1413–1423.

Schumann, U., 2005: Formation, properties and climatic effects of contrails, C. R. Physique, 6, 549–565.

Stuber, N., and P. Forster, 2007: The impact of diurnal variations of air traffic on contrail radiative forcing, Atmos. Chem. Phys., 7, 3153–3162.

Setting up a Turbojet test cell as a platform for environmental impact assessment

V. Archilla[*], A. Gonzalez, A. Entero, A. Jimenez, D. Mercader, J. Mena
Turbojet Test Center, INTA, Spain

J. Rodriguez Maroto, M. Pujadas, E. Rojas, J.M. Fernzández-Mainez, D. Sanz, J.C. Bezares
Polluting Emission Group, CIEMAT, Spain

1   STATEMENT OF THE SITUATION

Increasing air traffic has forced the EU Institutions to face goals in order to reduce the engine emissions. The gas turbine engine manufacturers are required to increase the engine efficiency, reducing fuel consumption and pollutant emissions. In recent years increased concerns about environmental issues at airports and the surrounding communities as well as the global impact on climate change, have led regulatory agencies to investigate measurement methodologies for limiting particulate matter emitted by aircraft engines.

2   USING CFD AS A TOOL IN ENGINE TESTING

Computational Fluid Dynamics (CFD) is a powerful tool that allows the study of a fluid configuration for a given geometry and working conditions.

The INTA test bed cell is been designed to accommodate the biggest of the civil aircraft engines. It is comprised of an air intake, the main test cell, the augmentor tube where the exhaust gases are discharged, a silencer basket and an exhaust chimney.

---
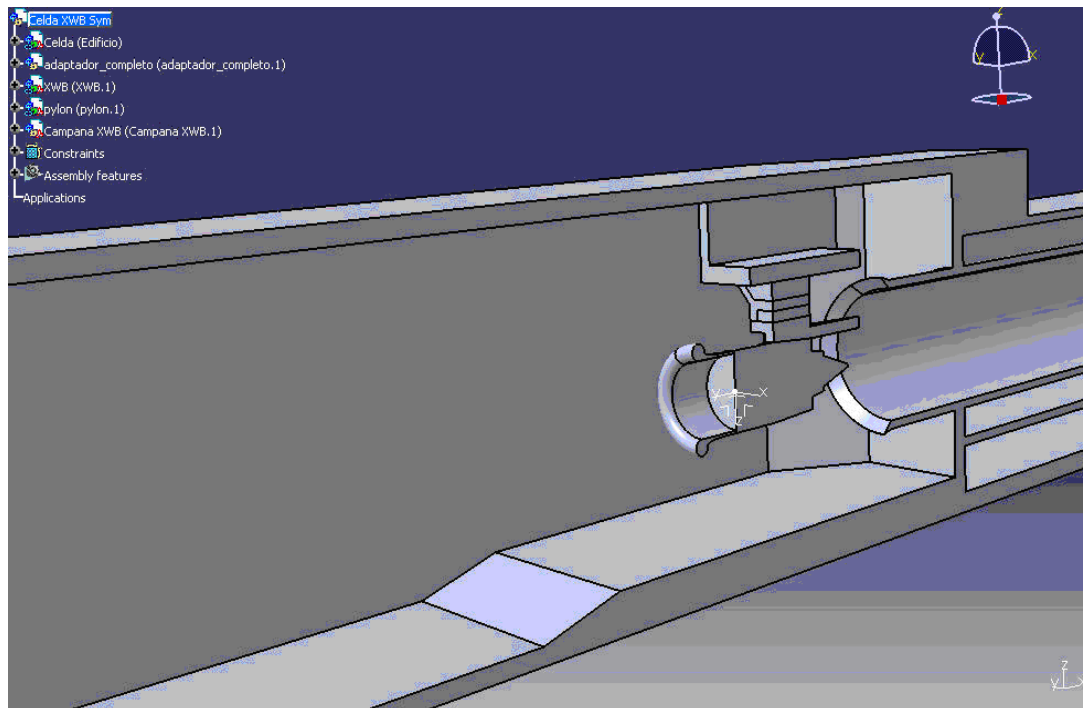
[*] *Corresponding authors:* Turbojet Test Center, INTA, Spain (archillapv@inta.es), Polluting Emission Group, CIEMAT, Spain (manuel.pujadas@ciemat.es)

The purpose of the CFD study can be summarized in these lines:
1) To ascertain the pathlines of the flow since it leaves the engine until it exhausts through the stack.
2) To map the temperatures, pressures and velocities of the stream.
3) To calculate the ratio of air that flows through the cell but does not pass through the engine (dilution ratio).
4) To set the criteria for the installation of a Continuous Emissions Monitoring System (CEMS) in the stack of the Test Facility.
5) To ascertain the criteria for a later study about the dispersion of the weight of the pollutant in the local area in relation with the environmental conditions (wind, temperature and relative humidity).

Using ANSYS Fluent as a CFD tool, ICEM CFD as the mesher and CATIA as the design program, the flow configuration for a high bypass civil aircraft engine in the INTA testing facility has been studied.

Knowing the geometry of the engine, the mass flux that exits the engine, the exhaust temperature of the gasses (both core-primary flux and bypass-secondary flux) and the operating conditions, the simulations performed consist in a 2D simulation for the airflow in the test cell, since the gasses leave the engine until the mixed flow of engine exhaust and the air that enters the test cell hit the drilled basket that lies at the end of the augmentor discharge tube. From this situation, a profile of temperature and mass flow is extracted form the 2D and modified as a boundary condition for a 3D simulation in the chimney. After the calculations in the chimney are done, the physical properties of the flux that exits the facility are known, and a 3D calculation of the flux that surrounds the facility is made for an array of different exterior windspeeds.

2.1 2D simulations:

Taking advantage of the discharge tube's cylindrical geometry, a simplified bidimensional axilsymetric model has been calculated for conditions that vary from low idle to the engine's maximum takeoff condition. The geometry used for the simulation is as follows:

| Grid | Oct 08, 2012 |
| FLUENT 6.3 (axi, pbns, spe, rke) |
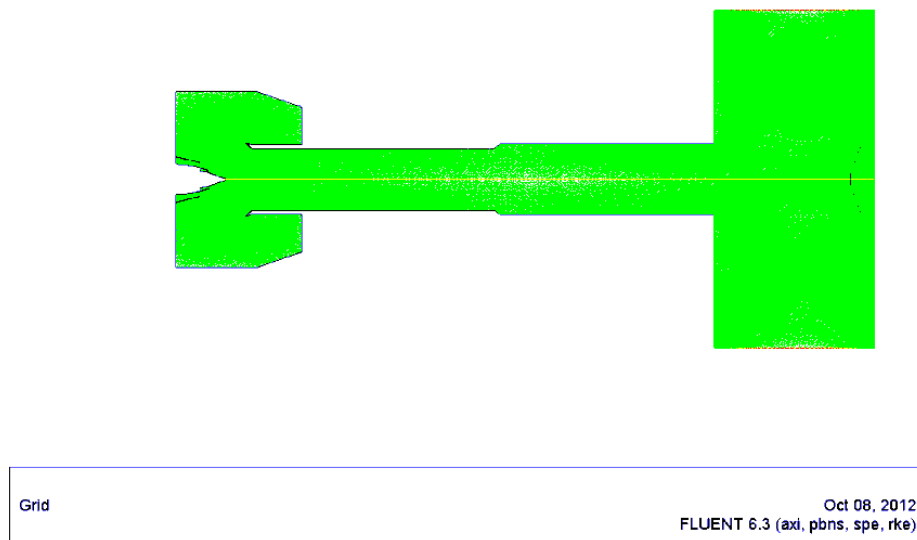
This grid simulates the exhaust of the gasses that go through the engine, the air that flows around the engine and the discharge of the mix into the augmentor tube. These gasses travel along the length of the augmentor, where they mix, until they hit the drilled basket at its end. The basket is simulated as a porous volume, so that a profile can be extracted for the next part of the simulation.

Detail of the basket:
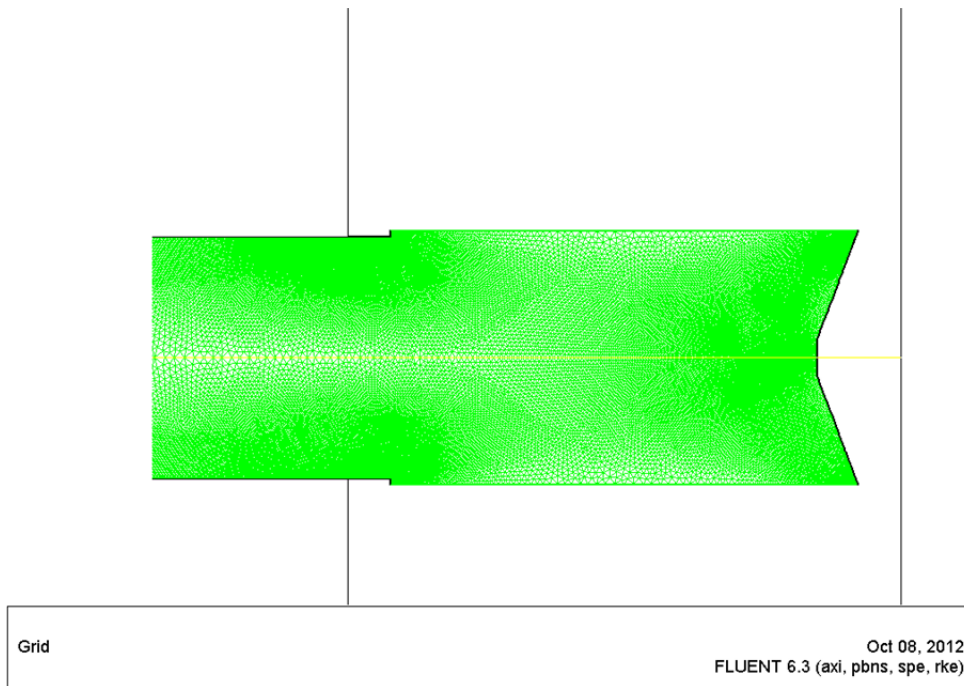
An array of simulations is then performed for different engine workpoints.

Velocity contours for maximum takeoff:
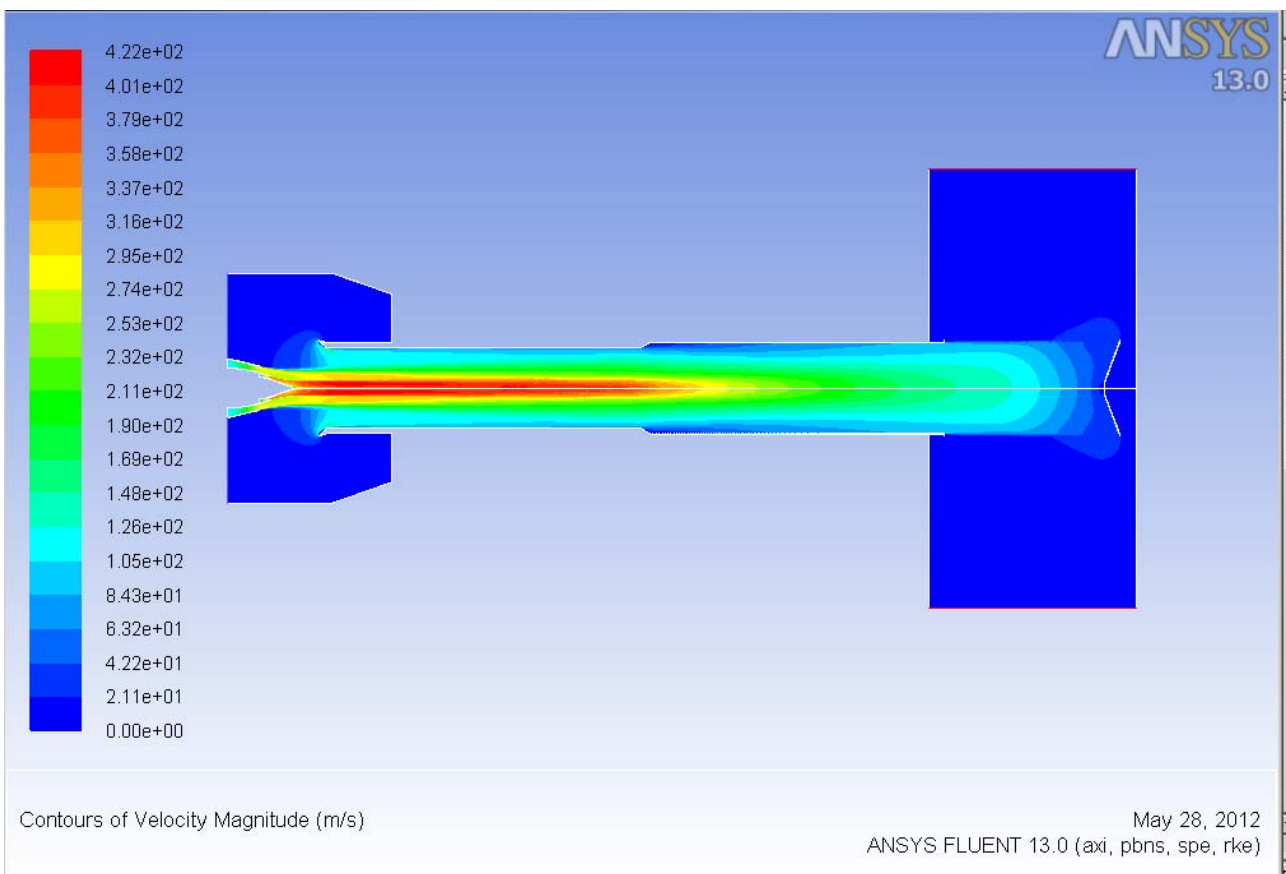
Extrapolating the solution obtained in the bidimensional simulation, a new simulation is run. The profiles obtained at the end of the discharge tube are used as a boundary condition for a 3D simulation of the flux in the inside of the facility's exhaust chimney:
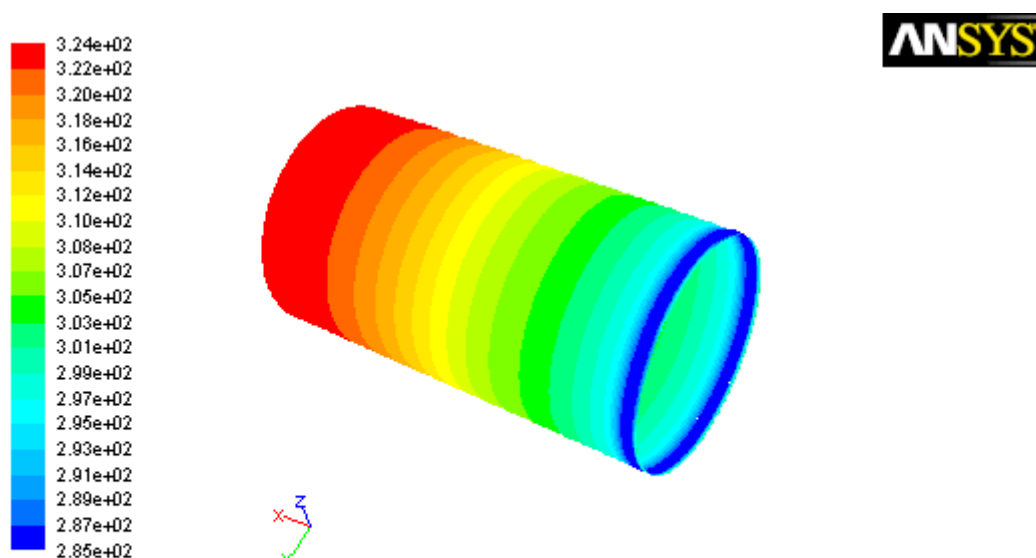
Contours of Static Temperature (k)   Aug 11, 2010
                                             ANSYS FLUENT 12.1 (3d, pbns, spe, rke)

Once simulated, the results are used to calculate pathlines and maps along the chymney:
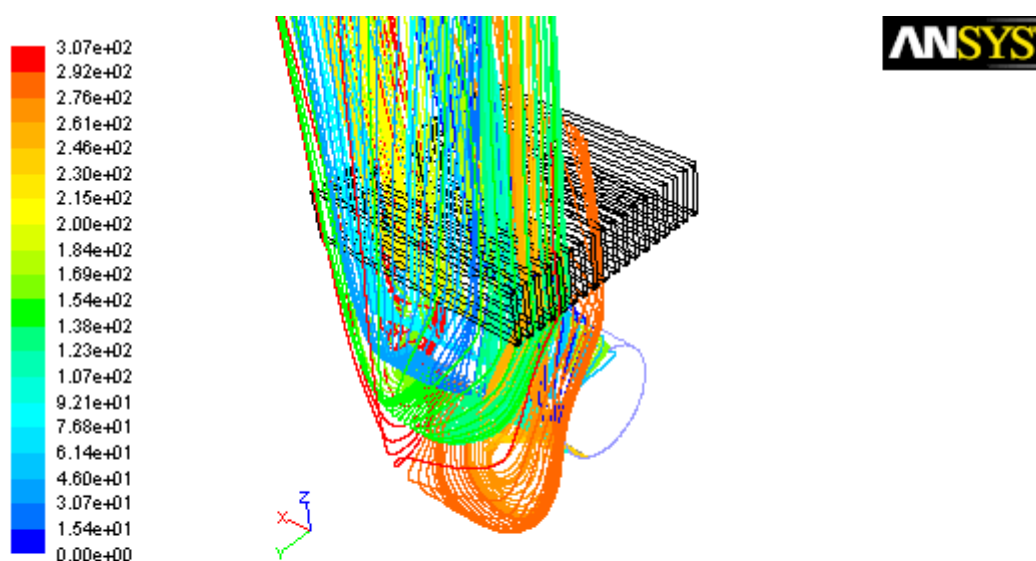
Pathlines Colored by Particle ID   Aug 11, 2010
                                             ANSYS FLUENT 12.1 (3d, pbns, spe, rke)

Thanks to these simulations profiles of temperature, velocity, and chemical species and pathlines are predicted in the flowfield. These profiles at the outlet of the exhaust's chimney can be used to predict the dispersion of the gases once outside of the facility.

Contours of Velocity Magnitude (m/s)   Aug 11, 2010
                                                ANSYS FLUENT 12.1 (3d, pbns, spe, rke)
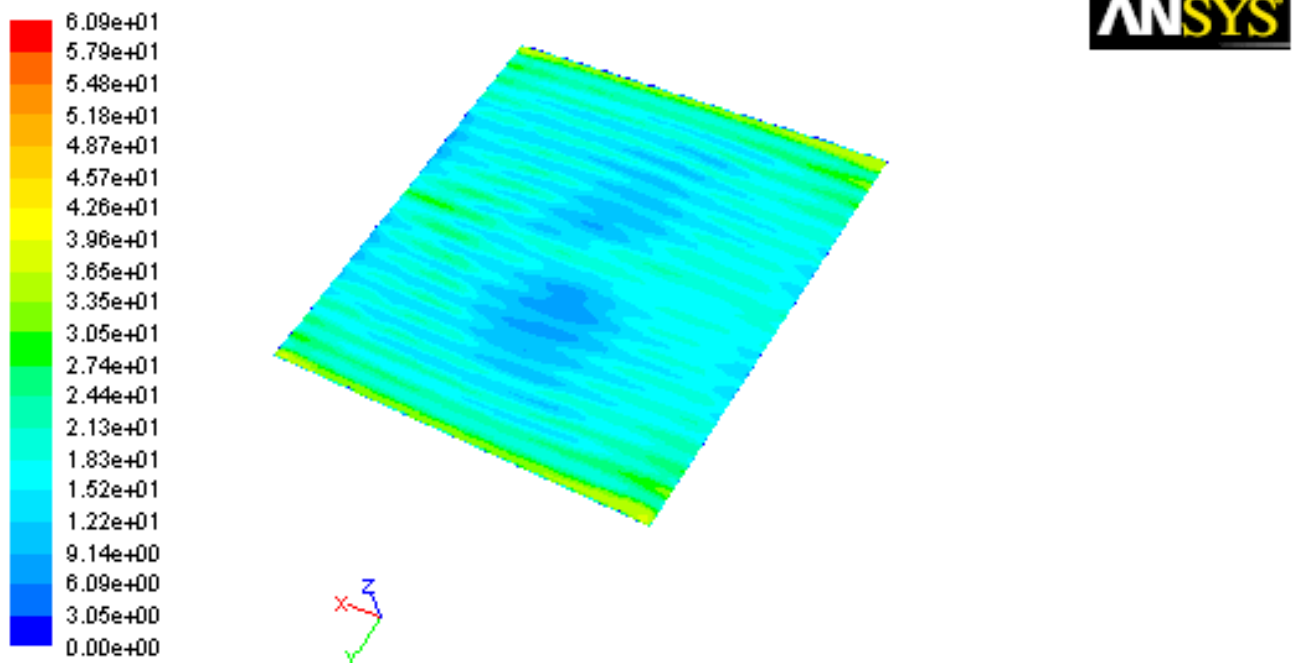
2.2 *Study of pathlines in the exterior:*

For this calculation a 3D simulation of the airflow of the test cell is used. The external conditions are varied for different airspeeds blowing in the direction from the exhaust chimney to the intake.

The simulations have been done using the exhaust profile for the engine at max takeoff conditions.

As can be seen in the next images, results vary dramatically win the external windspeed:

For an external airflow of 5 m/s:

Pathlines Colored by Particle ID   May 09, 2011
                                                ANSYS FLUENT 12.1 (3d, pbns, spe, rke)

For an external airflow of 10 m/s:

Pathlines Colored by Particle ID   May 09, 2011
ANSYS FLUENT 12.1 (3d, pbns, spe, rke)
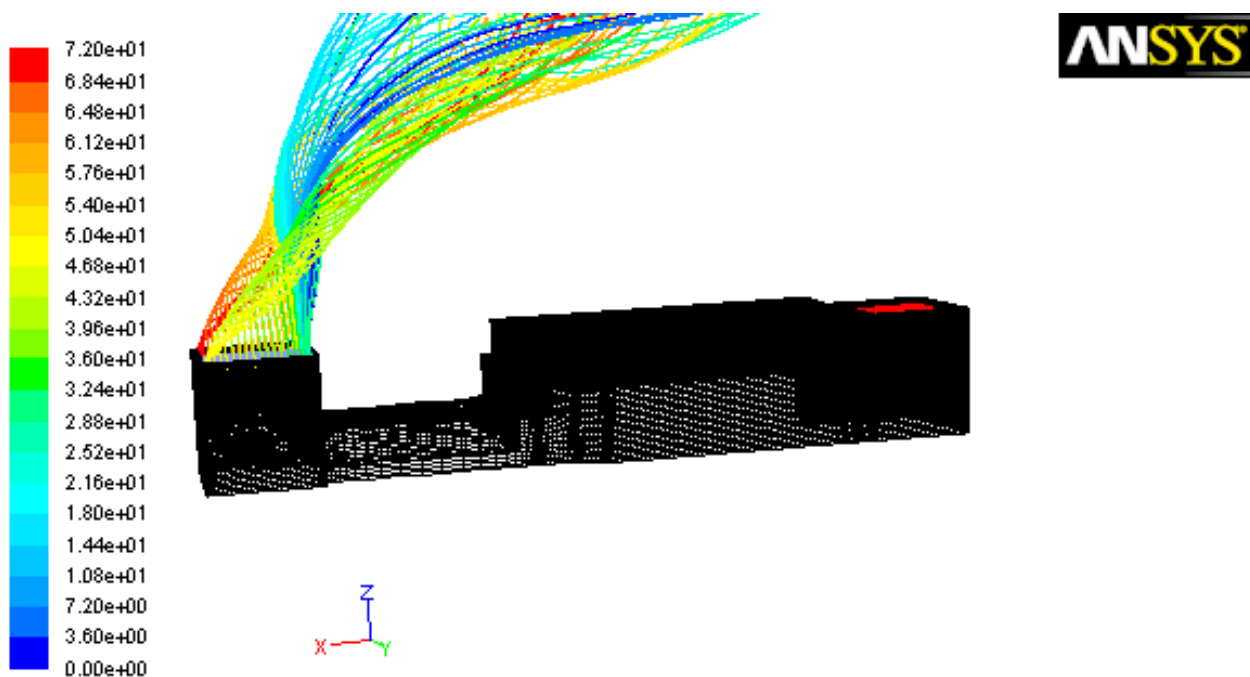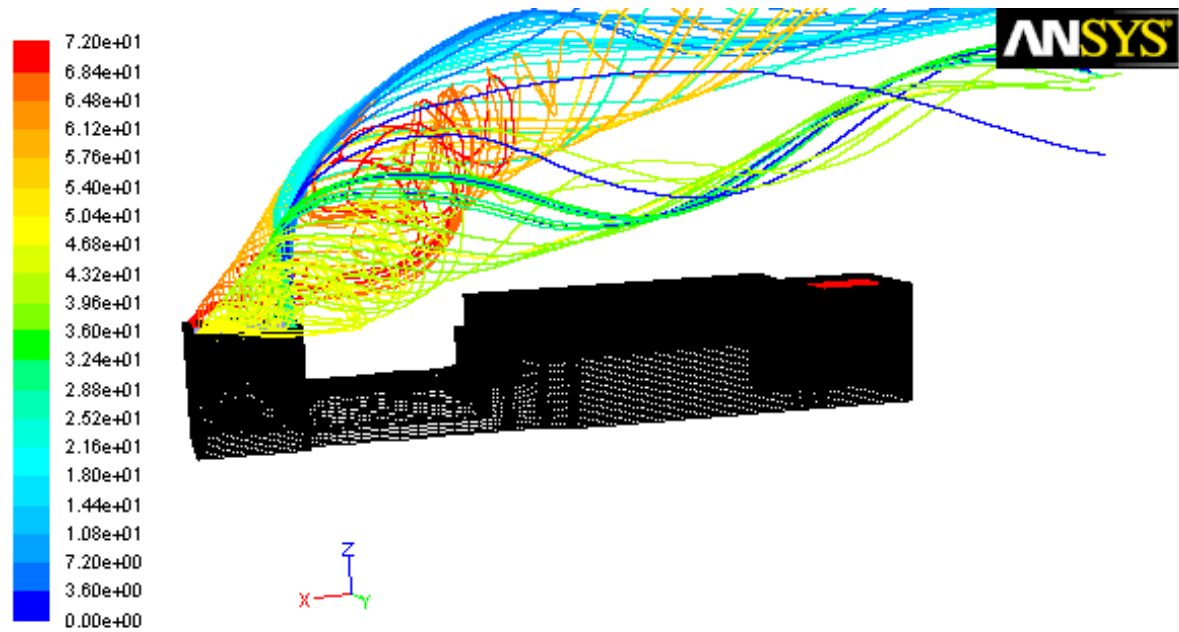
2.3 *Dilution calculation:*

For the sampling of the emissions to be accurate, it is necessary to know the amount of air that goes through the test cell at the different workpoints. The results can be summarized in the next graphic:

	75%HP	80%HP	85%HP	90%HP	95%HP	MTO
Régimen	75	80	85	90	95	97
GPrim (Kg/s)	44,77	63,5	83	106,28	131,09	139,73
GSec (Kg/s)	466,75	625,55	772,03	924,98	1048,55	1081,11
Exterior	1060,29	1425,82	1762,15	2111,29	2399,16	2456,49
Dilution rate	2,0728222	2,0692548	2,0609218	2,0472917	2,0338069	2,012131
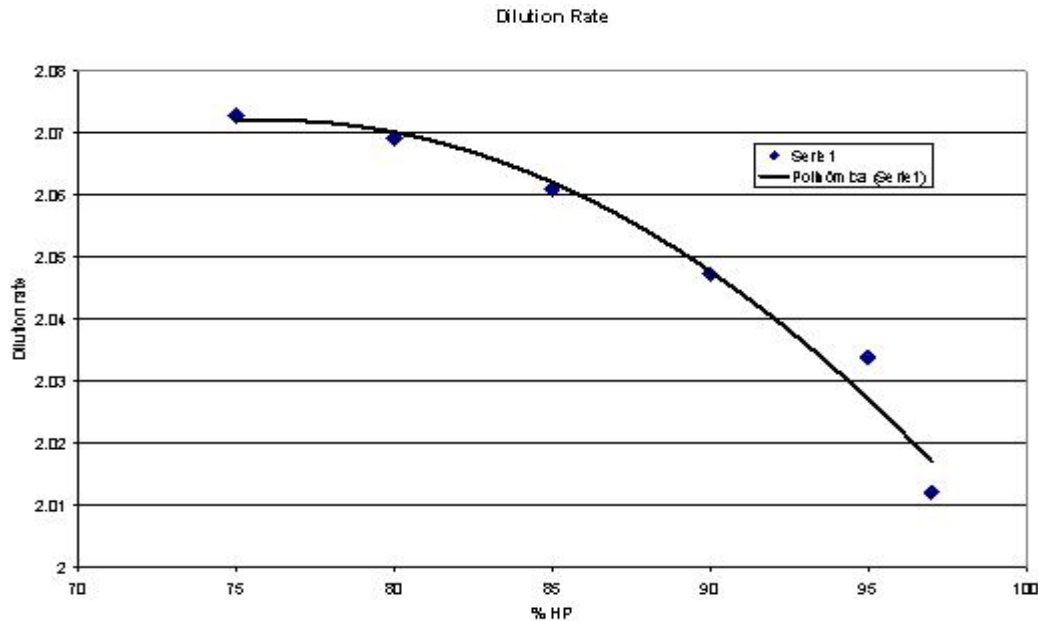
Dilution Rate

It is then observed that at high power the dilution ratio descends almost following a 2nd order polynomial tendency. This has to be taken into account when studying the concentration of pollutants during the engine running.

Performance and production testing are managed in test beds, which are a basic activity in the life cycle of aircraft engines. During these trials, test beds act as stationary sources of air pollutants.

It is envisaged that these facilities can be upgraded to allow characterization of pollutant emissions and increase the knowledge on their impact on local air quality. Thus they would provide a relevant means to assess the atmospheric effects of aircraft emissions. This development will allow test cells to achieve an additional benchmarking capability and other objectives, such as: obtaining exhaust emissions factors, supporting the development of emissions inventories databases and providing trend-analysis and emissions references for international or national air quality regulatory agencies.
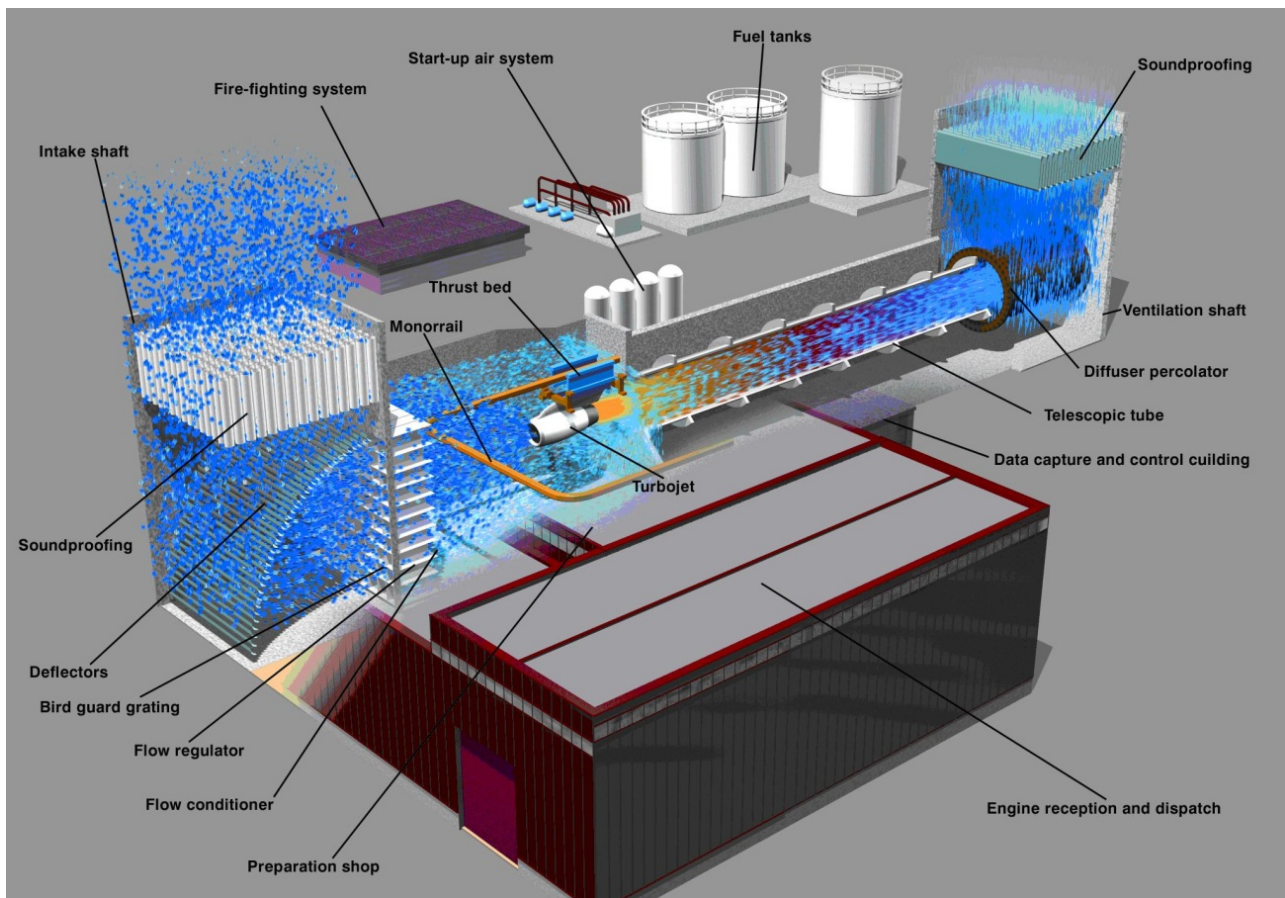
3   WHAT A TURBOJET TESTBED CAN OFFER TO ENVIRONMENTAL RESEARCH GROUPS?

A test facility running an endurance test reflects a ground-level aircraft emissions assessment. It is a good laboratory to establish the degrees of sensitivity, accuracy, repeatability and test operations acceptability for each engine exhaust measurement technique.

Test facilities will be proven to be an ideal setting to carry out pollutant measurement activities without hindering normal airport operations. The operation of the turbofan in a test facility represent the reference emissions Landing and Take-off (LTO) cycle, whose four power modes (idle/taxi, take-off, climb and approach) are represented in the certification or endurance test.
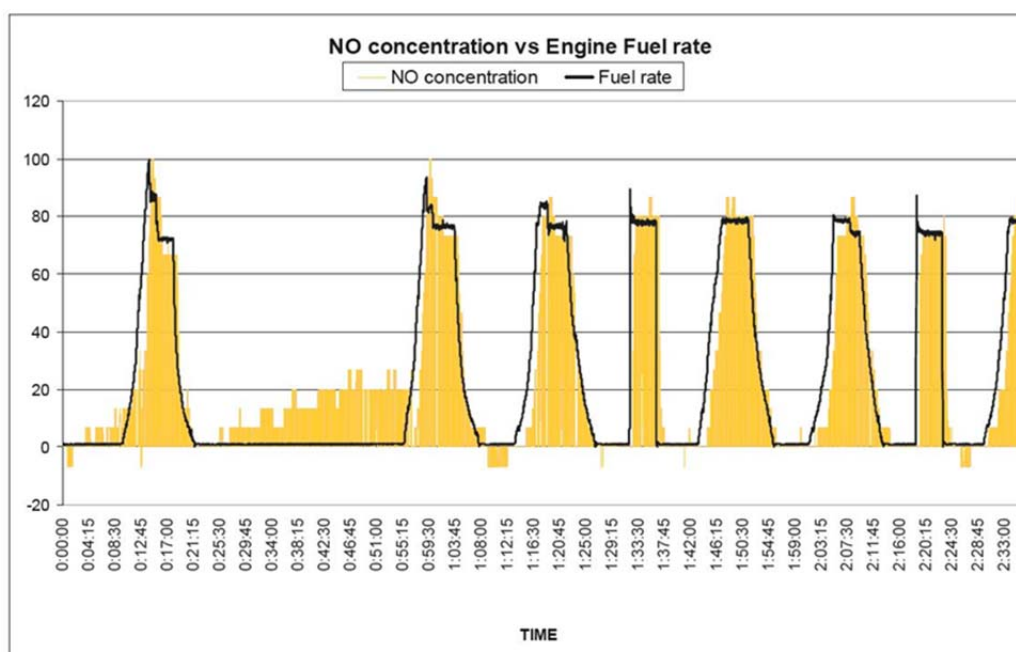
The standard method used to quantify and measure emissions (gases and non-volatile particles, "soot") is typically performed near to the engine nozzle. Due to the fact that hydrocarbon particles are dynamics and they cool down downstream where the temperature are lower and the flow is mixed with air, INTA has developed a new sampling point, inside to the stack, just 30 meter from the engine nozzle. This sampling point allows innovative measurement techniques to be applied to assess both engine and test facilities emissions impact on the environment. Even taking into account the dilution rate inside the test facility, there is no loss of information because we are able to quantify the mass, number, size, nature of the non-volatile particles and the emission indexes (examples are showed on charts).
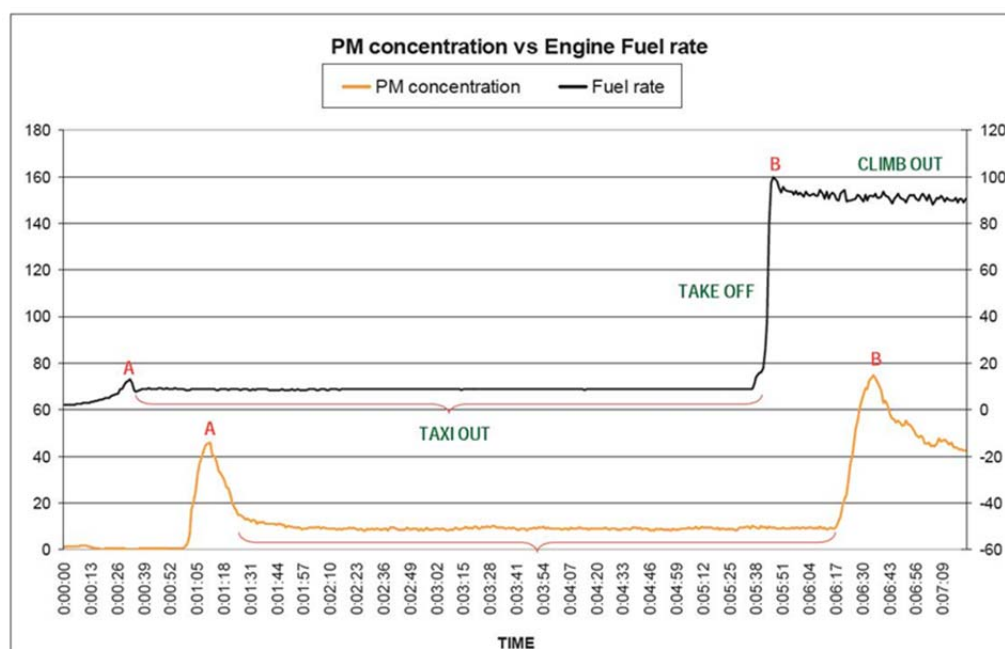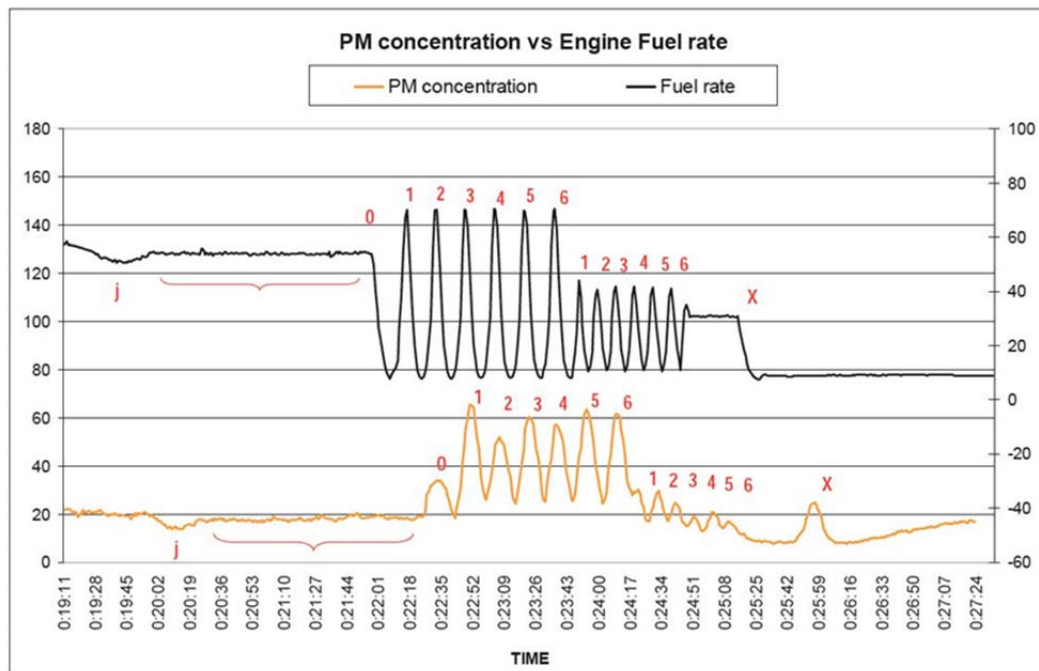
Endurance testing in controlled environments allows pollutant emissions measurement in the different phases on current airport activities: approach, taxi, take off and climb-out. How it is showed in the illustration, the dilution effects do not hinder the detection of the either gaseous or particulate emissions measurements. Both stationary and transitory manoeuvers can be featured using different techniques for environmental test.

Using CEMS along with CFD tools, allows not only get real data of the pollution, but do simulation of the profiles at the outlet of the stack. It allows studying the pollutants evolution in the atmosphere, and concentration profiles together with air pollution dispersion modelling under different environmental conditions for a local or regional area.

This poster was based in a preliminary and experimental test at INTA facility. Future researches will be focus in the following:

a) Particulates emissions measurements:

1) Measurement of particulates concentration

   – In Number, (particulates/Ncm3)
   – In Mass, (g/Nm3)2)

2) Measurement of Size Distribution:
   – In number (dN/dlogDp)
   – In mass (aerodynamic equivalent diameter) (dm/dlogDp)

3) Morphology and elemental chemical composition
4) Chemical composition (heavy metal, PAHs, etc) global and for size.

b) Gaseous emissions measurements:

1) Point concentration measurements:

   – Inorganic gases NO, NO2, SO2, CO
   – VOC (species identification / quantification)

2) Integrated concentration measurements:

   – FTIR open path configuration.

REFERENCES

Jane A. Leggett (Specialist in Energy and Environmental Policy), Bart Elias (Specialist in Aviation Policy), Daniel T. Shedd (Legislative Attorney), 11th June 2012: *Aviation and the European Union's Emission Trading Scheme.*

François Quentin (ACARE Co-Chairman), 12th December 2007 (Brussels): *ACARE: the European Technology Platform for Aeronautics* (Seminar of the Industrial Leaders of European Technology Platforms)

Reducing emissions from the aviation sector (http://ec.europa.eu)

Aircraft Particulate Emissions from Non Engine Sources: Auxiliary Power Units, Abraided Tires, and Brakes

Jonathan P. Franklin[*], Scott C. Herndon, Richard C. Miake-Lye, Edward C. Fortner
Aerodyne Research Inc., Billerica, MA, USA

Prem Lobo, Philip D. Whitefield
Center of Excellence for Aerospace Particulate Emissions Reduction Research, Missouri University of Science and Technology, Rolla, MO, USA

W. Berk Knighton
Montana State University, Bozeman, MT, USA

Raymond J. Hoffelt
City of Chicago, Chicago, IL, USA

ABSTRACT: Exhaust from aircraft engines has been extensively studied, but relatively little has been done to study the matter emissions from other potential aircraft sources at airports including auxiliary power units (APUs), abraided tire from touchdown events, as well as particulate emissions from brakes. A comprehensive suite of particulate instumentation deployed using the Aerodyne Mobile Laboratory characterized the mass-based composition as well as the volume-based composition of three different models of APU on six different aircraft. Using downwind sampling techniques at an active runway, particulate emissions from abraided tires as well as brakes from in-use aircraft as they landed were also measured. Particulate emission indices for APUs are on par with those of the main engines. The fuel flow and run time for the APU is essential in determining the APUs contribution to total particulate emissions at airports and thus depends on the airport practice. A benzothiozole derivative tracer was detected using a Soot Particle High Resolution Aerosol Mass Spectrometer in the abraded tire particulate plume arising from 'touchdown'. This tracer, as well as the volume based composition of tire smoke plumes, were used to place an upper limit for particulate matter burden due to touchdown events. Touchdown events are highly variable, depending on runway conditions (wet vs. dry runway) as well as pilot action (gentle vs hard landing). Despite the variability the total burden to atmospheric particulate matter is minimal compared to a typical landing take off cycle for an aircraft engine. Particulate matter from brake wear was not detected and was also concluded to be a very minor source of particulate matter at an airport.

1   INTRODUCTION

In recent years there have been many studies of emission sources at airports (Webb et al., 2008; Whitefield et al., 2008; Herndon et al., 2012: Kim et al., 2012; Lobo et al., 2007). However, many of these studies have focused on aircraft engine emissions and not some of the smaller, less obvious emission sources commonly found at airports, specifically auxiliary power units (APUs), tires, and brakes (Webb et al., 2008). One recent study has provided estimates for tire and brake emissions (Bennett et al. 2011), by quantifying particles, which were resuspended from the aircraft undercarriage and were commingled between different sources as well as field measurements of staged aircraft landings. The work reported here was carried out as part of an Airport Cooperative Research Program to specifically address and quantify the emissions from these three aircraft sources by measuring the pollutants as emitted into the air near active airport runways.

---

[*] *Corresponding author:* Jonathan P. Franklin, Aerodyne Research Inc. 45 Manning Rd. Billerica, MA 01821. Email: jfranklin@aerodyne.com

1.1 *Auxiliary Power Unit*

An aircraft auxiliary power unit (APU) is a small gas-turbine engine usually mounted in the tail cone of commercial aircraft, behind the rear pressure bulkhead. APU's provide power as well as environmental control to the cabin while taxiing and at the gate. APU's are also responsible for providing bleed air for main engine start and restarting engines mid-flight when needed. During an in depth measurement of PM and gas phase emissions from a Honeywell (formerly Garrett) Model GTCP85-98CK APU, PM emissions were characterized under various load conditions as part of the AAFEX (Alternative Aviation Fuels Experiment) study. That study found that PM number and mass-based emission indices both decreased as APU load was increased (Kinsey et al. 2012). Those measurements also reported that the PM mass-based emissions indices were as much as 10 times higher than the reported emission indices for most engines in the current fleet, which was supported by data from another measurement of the PM and gas phase emissions of a recommissioned Artouste Mk113 APU (Lobo et al., 2012). However both of these APUs are very old technology and not representative of APUs currently in service in the commercial fleet. Thus, the present study aimed to provide more current and relevant APU data.

1.2 *Abraded Tire Particulate Matter*

When compared to road tires, aircraft tires are designed to carry very heavy loads at very high speeds for very short periods of time. While there are large volumes of data on road tire wear and PM emissions, very little data is available for aircraft tires. In lieu of specific aircraft tire data, some expectations of the characteristics of aircraft tire wear PM were inferred from road tire literature in the planning of this study. Wik and Dave (Wik and Dave, 2009) summarize particle emissions from road traffic tire wear ranging from 7.3×10^6 kg (Denmark) to 600×10^6 kg (U.S.A.). However, much of the mass lost from tires stays on the road visible as skidmarks. In fact, some early measurements concluded that less that 5% of the tire wear ends up as airborne particles (Cadle and Williams, 1978; Pierson and Brachazek, 1974) and less than 1% of the abraded rubber is emitted in the gas phase (Cadle and Williams, 1978). Nonetheless, Lukewille et al. (2001) suggest that road traffic tire abrasion PM may be largest source of non-exhaust PM, second only to re-suspended road dust. Benett et al. concluded that while a sizeable amount of tire material is lost during each landing only a very small amount ends up as respireable aerosol and the majority will remain on the runway.

1.3 *Particulate Matter from Braking*

Brake PM emissions originate when the breaks are applied and the friction between brake discs and lining causes wear. There are two main types of aircraft brakes: steel brakes and carbon brakes, and they generally employ three different kinds of friction materials: sintered metal, carbon/carbon (C/C) composites, and organic materials (Tatarzycki and Webb, 1992).

2 EXPERIMENTAL DESCRIPTION

Results described in this work were collected as part of the ACRP 02:17 campaign staged at the O'Hare International Airport just north of Chicago, IL. Particulate matter (PM) emissions from in-service commercial APUs from the fleet of United Air Lines (UAL) were measured on March 8, 2011 from aircraft in the maintenance area as well as the terminal area. Tire and Brake emissions were measured down wind of an active runway from in use landing aircraft on March 9-11, 2011 and August 22-26, 2011.

Figure 1. Aerodyne mobile lab preparing to sample the APU of a Boeing 777 as well as the sample inlet behind the exhaust port of an Airbus A320.

Analytical Instrument Package: The Analytical suite and capabilities of the Aerodyne Mobile Laboratory has been described previously (Herndon et al. 2005, Kolb et al. 2004) and were optimized for this campaign (Herndon et al. 2012, Yu et al. 2012, Herndon et al. 2008). During these measurements, two different sampling schemes were used. APU emissions were extracted through an adjustable height probe positioned in the exhaust core between 1 and 3 meters behind the aircraft (Figure 1). The Probe was connected via a flexible line. The APU exhaust stream does not have any appreciable thrust, and as a consequence was influenced by the ambient wind, which further diluted the sample. A second scheme was used for downwind sampling of tire and brake emissions, which included two separate inlets. The first inlet was used to measure gas phase species, such as CO, NO, NO_2. The second inlet was used for sampling of PM species such as number concentration, mass-based composition, black carbon, and size distribution.

APUs from 6 different aircraft, comprising three different airframes, were sampled. During these tests, the APU was run in three different conditions: idle, cabin packs, and motoring engine 1. The idle condition is when the APU is running with no external load. The cabin packs condition puts the load of powering the cabin of the aircraft, including the lights and air conditioners. Finally, the APU was used to briefly motor Engine 1 of the aircraft as it would if it were actually starting the engine. APUs tested in the gate area were not run in the Engine 1 Motoring condition for safety reasons.

Figure 2. Sampling positions of the Aerodyne Mobile Lab along runway 10-28 at O'Hare International Airport. Arrows represent the upwind sampling vector and approximate locations of sampled emissions origins.

In order to measure PM emissions from tires and brakes as aircraft were landing, the Aerodyne Mobile laboratory was escorted to areas very close to the active runway (Runway 10-28). The pink boxes in Figure 2 represent the positions where the mobile laboratory was parked for in-situ sampling of aircraft PM brake and tire emissions downwind of the active runway. The position of the mobile lab was chosen in order to place the sample inlets down wind of typical landing and braking regions on the runway, which were suggested by Airport Operations. Arrows represent the approximate sampling vector for each sampling position. Sampling distances ranged from 100 m to 1100 m depending on the location of the mobile laboratory and the prevailing wind direction.

3 RESULTS AND DISCUSSION

The auxiliary power unit characterization work was conducted (described above) using a sampling probe. The touchdown event (abraded tire) and braking phase emissions (brake dust) measurements were conducted using downwind measurement techniques. The results of the measurements and analysis for each of these topics are discussed below. Some effort to summarize the findings in the context of the airport emissions burden is also included for each source characterized here.

3.1 *Auxiliary Power Unit Results*

APU Model	Operating Condition	GMD (nm)	GSD	EIn (#/kg fuel)	BC EI (mg/kg fuel)
				Table 1: Summary of APU PM Emissions for each APU Model Studied as a Function of Operating Condition	
GTCP 331-200	Idle	30 ± 4	2.2 ± 0.1	$(8.0 \pm 7.4) \times 10^{14}$	112 ± 23
	Both Packs	29 ± 2	2.1 ± 0.1	$(1.0 \pm 0.3) \times 10^{15}$	103 ± 35
	Motor Engine	33 ± 2	2.1 ± 0.1	$(1.0 \pm 0.3) \times 10^{15}$	196 ± 53
GTCP 331-500	Idle	30 ± 3	2.1 ± 0.0	$(6.4 \pm 2.1) \times 10^{13}$	20 ± 1
	Both Packs	22 ± 1	1.9 ± 0.0	$(3.8 \pm 1.4) \times 10^{14}$	21 ± 2
	Motor Engine	31 ± 3	2.0 ± 0.1	$(7.5 \pm 3.0) \times 10^{13}$	11 ± 2
GTCP 36-300	Idle	17 ± 2	1.8 ± 0.1	$(2.3 \pm 1.0) \times 10^{15}$	39 ± 17
	Both Packs	20 ± 1	1.9 ± 0.1	$(4.5 \pm 0.9) \times 10^{15}$	104 ± 46
	Motor Engine	19 ± 2	1.7 ± 0.1	$(7.7 \pm 1.4) \times 10^{15}$	425 ± 22

Table 1 illustrates that the more modern APU (GTCP331-500) has the lowest number and mass-based emission indices among the three types of APU's tested. This data is significantly different compared to the emissions reported from the GTCP85-98CK APU measured at the AAFEX campaign (Kinsey et al., 2012). The PM mass-based emission indexes for the GTCP85 (AAFEX) APU were approximately 200-600 mg/kg fuel burned, compared to a range of 10-425 mg/kg fuel for this study. For PM number-based emission index, the range of values for the GTCP85 APU was 2 - 6×10^{15} particles/kg fuel while this study reported values of 6×10^{13} - 7×10^{15}.

Emission indices for APUs measured in this campaign can also be compared to main engine EI data. Number-based EI's for main engines measured at 30 meters in the ACRP report 9 (Whitefield et al. 2008) range from $0.1 - 1 \times 10^{16}$ particles / kg fuel. Mass-based EI's from this report range from $40 - 700$ mg / kg fuel. APU emission indices were compared to 30 meter probe data because APU emissions are naturally diluted prior to sampling. When the organic PM component of APU emissions is compared to that of main engines measured at 30 meters, it is found to be approximately 2-4 times higher, but not as high as the highest main engine organic PM emission index, which is typically associated with lubrication oil.

Because APU emission indices are on par with those of main engines, fuel flows and operation times are paramount in determining the overall contributions to airport PM emissions from aircraft auxiliary power units. Therefore, the realistic APU usage scenarios must factor these conditions which will change between different airport types.

3.2 *Touchdown and abraded tire emissions results*

Tire and brake emissions sampling are slightly different from other types of aircraft emission sampling because emission events are not directly connected with combustion. Tire touchdown events can often be seen as a large white smoke plume. Figure 3 shows a time series of the measured PM signals. The OPC shows an increase in larger diameter particles. It was found that the HR-TOF-AMS m/z 211 signal responded specifically to tire touchdown events. This mass to charge ratio corresponds to a benzothiozole derivative, a known component of tires (Kumata et Al., 1997, Kumata et al., 2002). While the SP-AMS detected benzothiozole in the particle phase, nothing was detected in the gas phase by the PTR-MS. This suggests that essentially all the benzothiozole in the tire touchdown plume was in the condensed particle phase. Light absorbing aerosol instruments, except for MAAP black carbon, also responded to the tire touchdown event. CAPS extinction and SP-AMS, but not MAAP, responding to tire smoke illustrates that this PM is different than engine exhaust BC aerosol, which all three instruments will respond to. The response can be somewhat expected because the tire smoke is visibly more of a white smoke, which will scatter light in the CAPS Extinction cell, but not absorb light, which is how the MAAP quantifies black carbon.
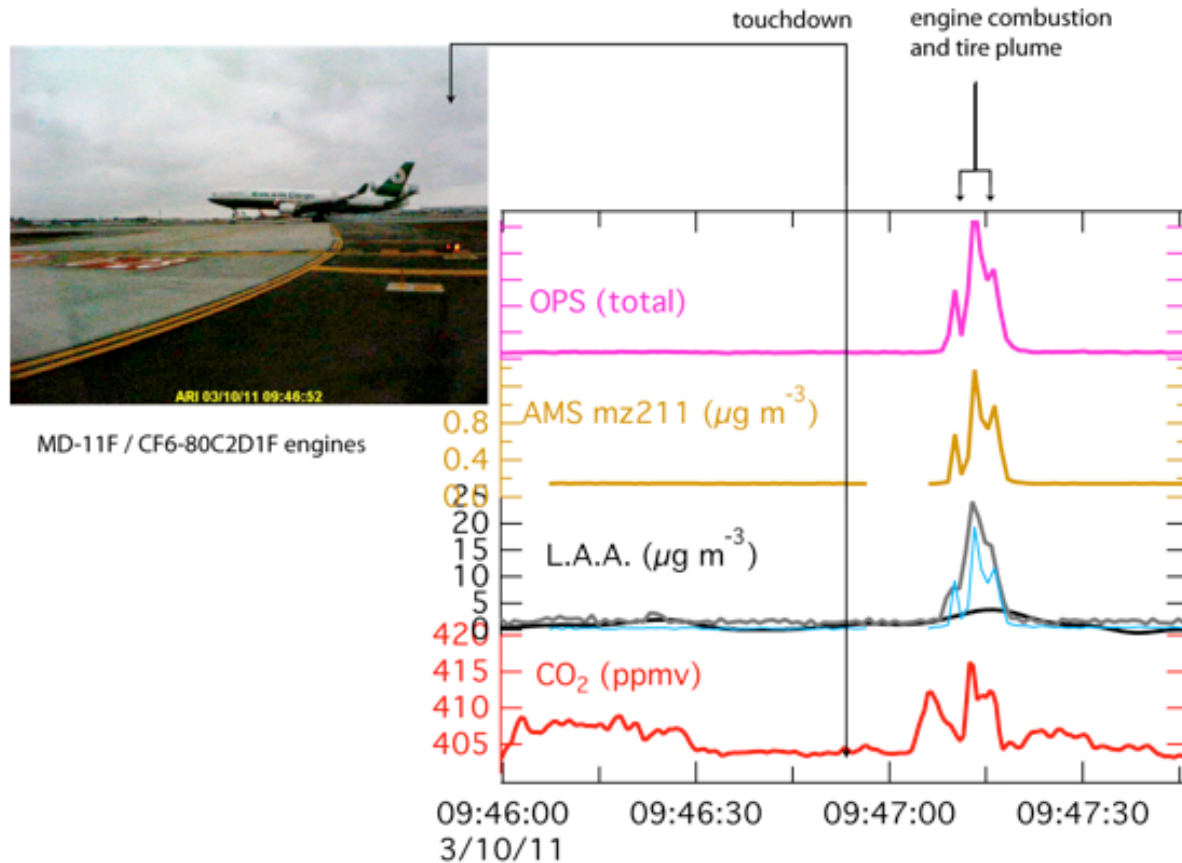
Figure 3. Time Series of PM instrumentation during a touchdown event of a MD-11F.

Two methods were used to approximate mass lost from tires during touchdown events. The first method is a volumetric based approach calculated using equation 1:

$$\text{Total mass} = \text{Peak value } (\mu g/m^3) \times (\Delta t_p + \text{wind speed}/2)^3 \tag{1}$$

The Peak value is the largest mass-concentration measured during the touchdown plume. In the example shown in figure 3 the peak value is 22 $\mu g/m^3$. The Δt_p term refers to the duration of the plume and must be used because the wind speed scales the spatial extent of the plume. This approach assumes a spherical plume of PM upon touchdown.

The second method uses the associated CO_2 emission rate and an estimate of the amount of time in the upwind sampling volume, using equation 2:

$$\text{Total mass} = \text{PM EI (g/kg fuel)} \times \text{Fuel Flow Rate (kg/s)} \times \Delta t_v \text{ (s)} \tag{2}$$

This method is based on the assumption that emissions are generated for a short time during the rotational acceleration of the tire and are then entrained in the trailing vortexes of the aircraft. Assuming the tire emissions are well mixed into the emissions vortex, the mass of lost tire mass can be approximated as an emission index. The drawback to this approach is that it will only work when the PM plume from the tires match the combustion plume, specifically carbon dioxide.

For the touchdown event shown in figure 3, the two methods of calculating lost tire mass yield estimates of 285 and 250 mg per touchdown using the CAPS extinction monitor's peak PM value. The peak PM value can also be approximated using the integration of the size distribution spectrum from the combination of the DMS500 and OPS spectrum. Using an assumed effective density of 1 g / cm^3 in the size distribution spectrum leads to a peak value of at least 8 μg / m^3, which compares well with the peak value of 22 μg / m^3 reported from the CAPS extinction monitor.

Table 2: Selected Winter Dry Touchdown Measurements

Plume Start Time	Airframe	Peak Particle Volume(μg m3)	Approximate Plume Duration (s)	Plume Average Wind (m/s)	Tire Loss Upper limit (mg)
3/10/11 09:47:10	MD11F	127	10	1.3	249
3/10/11 09:57:17	CRJ702ERNG	32	5	1.8	23
3/10/11 10:01:28	AE3007A1	28.7	8	2.5	230
3/10/11 10:04:31	737-832(W)	2.87	5	1.7	2
3/10/11 10:05:52	747-4KZF	123	9	1.75	481
3/10/11 10:08:51	ERJ170-200LR	72	6	2.36	204
3/10/11 10:23:09	AE3007	38	7	1.74	69
3/10/11 10:24:32	777-222ER	42.1	12	2.6	1279
3/10/11 10:26:40	757-222	16.2	5	1.9	14
3/10/11 10:33:24	A320-232	83	6	1.7	88
3/10/11 10:37:48	737-487	134	10	1.7	658
3/10/11 10:39:46	EMB145LR	19	4	2.1	11
3/10/11 10:42:49	A320-232	53	3	1.9	10

Table 3: Selected Summer Dry Touchdown Measurements

Plume Start Time	Airframe	Peak Particle Volume (μg m3)	Duration (s)	Wind (m/s)	Tire Loss Upper Limit (mg)
8/24/11 09:06:51	747	22	9	1.7	9.8
8/24/11 09:58:31	747	13	11	2.48	33.0
8/24/11 10:08:39	747	2	40	2.48	244.0
8/24/11 11:42:26	767	49	37	2.7	6106.6
8/24/11 11:46:14	737	3	15	5.6	701.2
8/24/11 11:48:06	777	17	14	5.5	970.1
8/24/11 11:52:58	ERJ	13	10	5.5	270.4
8/24/11 11:54:35	MD80	2	13	5.5	91.4
8/24/11 12:04:26	ERJ	0	14	5.1	<1
8/24/11 12:05:54	767	0	15	6.1	<1

Tables 2 and 3 show upper limits to tire loss to particulate matter for the winter and summer measurements of this study. While there are a few larger signals in the summer study, the data does not show conclusively that there is more tire mass lost to aerosols in the summer, when the runway is hotter, than in the winter. However, there is a significant reduction in signal when looking at tire plumes when the runway is wet. The measurements from the wet runway indicate very strongly that the PM emissions from tire events are strongly suppressed.

3.3 *Results from the braking phase characterization*

Detection of PM emissions from brake wear is complicated by the lack of visual detection, such as the smoke plume from tire touchdown events as well as the lack of a gas phase tracer. Plume events with clear combustion tracers, such as high NO_x to CO_2 or low CO to CO_2 ratios, or when aircraft visibly used reverse thrust were excluded from analysis to give the best chance at finding PM from brakes only. No distinctly larger size mode was detected in the DMS 500 or OPC data. SP-AMS comparisons of "brake" events to idle or takeoff events produced linear results between the organic and metal signals indicating that the AMS was unable to detect a distinct brake signature.

The data suggests that brake PM emissions either do not reach the sampling inlet because they are so large that they settle out before reaching the inlet, or that the brake emissions are mixed in with the exhaust emissions and are indistinguishable from engine exhaust PM. Either way, the contribution of brakes to overall PM at airports appears to be negligible.

4   ACKNOWLEDGEMENTS

REFERENCES

Bennett, M., Christie, S.M., Graham, A., Thomas, B.S., Vishnayakov, V., Morris, K., Peters, D.M., Jones, R., Ansell, A., 2011: Composition of Smoke Generated by Landing Aircraft. *Environ. Sci. Technol.* 45, 8, 3533–3538.

Cadle S, Williams R 1978: Gas and particle emissions from automobile tires in laboratory and field studies. *Rubber Chemistry and Technology* 52, 146-158.

Herndon, S.C., Jayne, J.T., Zahniser, M.S., Worsnop, D.R., Knighton, B., Alwine, E., Lamb, B.K., Zavala, M., Nelnson, D.D., Mcmanus, J.B., Shorter, J.H., Canagaratna, M.R., Onasch, T.B., Kolb, C.E. 2005: Characterization of urban pollutant emission fluxes and ambient concentration distributions using a mobile laboratory with rapid response instrumentation. *Faraday Discuss.* 130, 327-339.

Herndon, S. C., Jayne, J. T., Lobo, P., Onasch, T., Fleming, G., Hagen, D. E., Whitefield, P. D., and Miake-Lye, R. C. 2008: Commercial Aircraft Engine Emissions Characterization of in-Use Aircraft at Hartsfield-Jackson Atlanta International Airport. *Environmental Science and Technology* 42, 1877-1883.

Herndon, S., Wood, E., Franklin, J., Miake-Lye, R., Knighton, W. B., Babb, M., Nakahara, A., Reynolds, T., Balakrishnan, H. 2012: Measurement of Gaseous HAP Emissions from Idling Aircraft as a Function of Engine and Ambient Conditions. *ACRP Report 63*, Transportation Research Board, Washington, DC 112 pp.

Kim, B., Rachami, J., Robinson, D., Robinette, B., Nakada, K., Arunachalam, S., Davis, N., Haeng Baek, B., Shankar, U., Talgo, K., Yang, D., Hanna, A. F., Wayson, R. F., Noel, G., Cliff, S. S., Zhao, Y., Hopke, P. K., Kumar, P. 2008: Guidance for Quantifying the Contribution of Airport Emissions to Local Air Quality. *ACRP Report 71*, Transportation Research Board, Washington, DC (2008) 78 pp.

Kinsey, J.S., Timko, M.T., Herndon, S.C., Wood, E.C., Yu, Z., Miake-Lye, R.C., Lobo, P., Whitefield, P., Hagen D., Wey, C., Anderson, B.E., Beyersdorf, A.J., Hudgins, C.H., Thornhill, K.L., Winstead, E., Howard, R., Bulzan, D.I., Tacina, K.B., and Knighton, W.B. 2012: Determination of the emissions from an aircraft auxiliary power unit (APU) during the Alternative Aviation Fuel Experiment (AAFEX), *Journal of the Air and Waste Management Association* 62, 4, 420-430.

Kolb, E.E., Herndon, S.C., Mcmanus, J.B., Shorter, J.H., Zanhiser, M.S., Nelson, D.D., Jayne, J.T., Canagaratna, M.R., Worsnop, D.R. 2004: Mobile Laboratory with Rapid Response Instruments for Real-time Measurements of Urban and Regional Trace Gas and Particulate Distributions and Emission Source Characteristics. *Environ. Sci. Technol.* 38, 5694-5703.

Kumata H, Takada H, Ogura N (1997) 2-(4-morpholinyl)benzothiazole as an indicator of tire-wear particles and road dust in the urban environment. In: Eganhouse RP, editor. Molecular Markers in Environmental Geochemistry. pp. 291-305.

Kumata H, Yamada J, Masuda K, Takada H, Sato Y, Sakurai T, Fujiwara K 2002. Benzothiazolamines as tire-derived molecular markers: Sorptive behavior in street runoff and application to source apportioning. Environmental Science & Technology 36: 702-708.

Lobo, P., Whitefield, P.D., Hagen, D.E., Herndon, S.C., Jayne, J.T., Wood, E.C., Knighton, W.B., Northway, M.J., Miake-Lye, R.C., Cocker, D., Sawant, A., Agrawal, H., Miller, J.W., 2007: The Development of Exhaust Speciation Profiles for Commercial Jet Engines. ARB Contract No. 04-344 Report, California Air Resources Board.

Lobo , P., Rye, L., Williams, P. I., Christie, S., Uryga-Bugajska, I., Wilson, C. W., Hagen, D. E., Whitefield, P. D., Blakey, S., Coe, H., Raper, D., and Pourkashanian, M., 2012: "Impact of Alternative Fuels on Emissions Characteristics of a Gas Turbine Engine - Part I: Gaseous and PM Emissions", *Environmental Science and Technology,* in review.

Lukewhile A, Berok I, Amman M, Cofala J, Gyarfas F, Heyes C, Karvosenoja N, MKlimont Z, W S 2001: A framework to estimate the potential and costs for the control of fine particulate emissions in Europe. Laxenburg, Austria, IIASA Interrim Report IR-01-023.

Pierson W, Brachazek W 1974. Airborne particulate debris from rubber tires. Rubber Chemistry and Technology 47: 1275-1299.

Tatarzycki, E.M., Webb, R.T., 1992: Friction and Wear of Aircraft Brakes, *ASM Handbook* 18: (ASM International), 582-587.

Webb, S., Whitefield, P. D., Miake-Lye, R. C., Timko, M. T., Thrasher, T. G., 2008: Research Needs Associated with Particulate Emissions at Airports. ACRP Report 6, Transportation Research Board, Washington, DC (2008) 34 pp.

Whitefield, P. D., Lobo, P., Hagen, D. E., Timko, M. T., Miake-Lye, R. C., Taylor, C., Ratliff, G., Lukachko, S., Sequeria, C., Hileman, J., Waitz, I.,Webb, S., Thrasher, T. G., Ohsfeldt, M. R., Kaing, H. K., Essama, S. C., 2008: Summarizing and Interpreting Aircraft Gaseous and Particulate Emissions Data. ACRP Report 9, Transportation Research Board, Washington, DC 59 pp.

Wik A, Dave G 2009. Occurrence and effects of tire wear particles in the environment - A critical review and an initial risk assessment. Environmental Pollution 157: 1-11.

Yu, Z., Herndon, Scott C., Ziemba, Luke D., Timko, Michael T., Liscinsky, David S., Anderson, Bruce E., Miake-Lye, Richard C., "Identification of Lubrication Oil in the Particulate Matter Emissions from Engine Exhaust of In-Service Commercial Aircraft, Environmental Science and Technology, 2012 46, 9630-9637.

Transmission Electron Tomography: from 2D to 3D microphysical properties of aerosols. Application to aircraft soot emissions

D. Lottin, D. Delhaye
ONERA – The French Aerospace Lab, 29 avenue de la Division Leclerc, F-92322 Châtillon, France

D. Ferry[*]
Aix-Marseille Université, CNRS, CINaM UMR 7325, Campus de Luminy, Case 913, F-13009 Marseille, France

J. Yon
COmplexe de Recherche Interprofessionnel en Aérothermochimie, CORIA-CNRS, Avenue de l'Université, F-76801 Saint-Etienne de Rouvray, France

F.X. Ouf
Aerosol Physics and Metrology Laboratory, IRSN, BP68, F-91192 Gif-sur-Yvette, France

Keywords: Electron Tomography, aerosols, aircraft soot aggregates, microphysical properties

ABSTRACT: The morphology and microphysical properties of aerosols are often characterized by transmission electron microscopy. This technique enables to determine 2D characteristic sizes of aggregates from their projection but the 3D characteristic sizes can be extrapolated by using 2D-3D transposition relationships. In this study we use Transmission Electron Tomography to directly determine the 3D characteristic sizes of aggregates. We present a new analysis tool, named "SootExpert", that is especially developed to enable the process of aggregate's tomogram and measure 3D characteristic sizes. We show the performance of SootExpert and its use on a numerically generated aggregate. Then we use this tool to study an aircraft soot aggregate by conventional transmission electron microscopy and transmission electron tomography. The comparison of the results highlights the major role played by the size of primary particles in the determination of 3D characteristics using 2D-3D transposition relationships.

1 INTRODUCTION

Combustion aerosols emitted by aircrafts are extensively studied due to their potential impact on the atmosphere (Lee et al., 2009) and to their health concerns (Ferry et al., 2011). Their microphysical properties are commonly determined from Transmission Electron Microscopy (TEM) analyses. This experimental technique provides 2D characteristics of aggregates and 3D properties are obtained by using 2D-3D transposition relationships (Baron and Willeke, 2001, and references therein). These relationships originate from numerical studies of aggregates, which are built assuming a fractal dimension of 1.75 and monodisperse primary particles. However, combustion aggregates may have microphysical characteristics that differ from those considered in simulations, like a polydispersion of primary particles (Park et al., 2004, Delhaye et al., 2006) and fractal dimension different from 1.75. One may thus wonder about the general character and the validity of the 2D-3D transposition relationships. Cai et al. (1993) and Köylü et al. (1995b) attempted to validate these 2D-3D transposition relationships on laboratory-flame soot aggregates by combining direct 3D optical measurements with TEM analyses. Nevertheless, no experimental validation of these 2D-3D transposition relationships based on a single technique, which enables to determine both 2D and 3D properties, has been conducted to date. In this context, we present a study that aims at determining

---

[*] *Corresponding author:* Daniel Ferry, Aix-Marseille Université CNRS, CINaM UMR 7325, Campus de Luminy, Case 913, F-13009 Marseille, France. Email: daniel.ferry@univ-amu.fr

both 2D and 3D microphysical characteristics of aircraft soot aggregates from conventional TEM and Transmission Electron Tomography (TET) experiments.

2   CHARACTERIZATION OF SOOT AGGREGATES BY CONVENTIONAL TEM

2.1   *Aircraft soot aggregates sampling*

Aircraft soot aggregates are sampled on TEM grids (Holey carbon films, AGAR Scientific) in the exhaust of a commercial CFM56-5B aircraft turbofan engine during landing/take-off cycles. Details of the sampling procedure are given in Delhaye *et al.* (2006).

2.2   *2D characteristics of soot aggregates from TEM*

A high resolution TEM (Tecnai G2, PHILIPS) with a resolution of 0.24 nm at 200 keV is used to study soot aggregates. It is used to perform both the conventional TEM and TET measurements. Note that the sample holder is tilted from -70 to +70 degrees with respect to the zero position (sample holder perpendicular to the electron beam) during TET experiments. Electron micrographs are analyzed with the "ImageJ" freeware (http://imagej.nih.gov/ij/) in order to measure 2D characteristic sizes of any aggregate (Fig. 1), namely the diameter of its primary particles (d_p), its maximal projected length (L_{2D}) and projected area (A_{2D}).
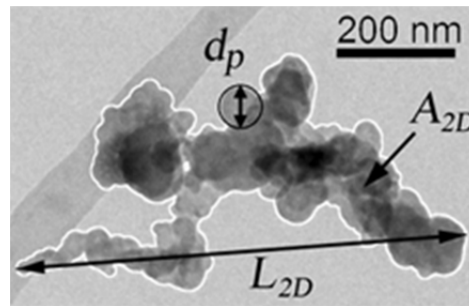
Figure 1: TEM micrograph of an aircraft soot aggregate. 2D characteristic sizes are shown namely the primary particle diameter (d_p), maximal projected length (L_{2D}) and projected area (A_{2D}).

The mean value of $<d_p>$ is determined from measurements performed on more than 5000 primary particles that belong to 317 aggregates. It leads to size distributions that can be fitted with log-normal laws whatever a single aggregate (Fig. 2a) or a set of aggregates (Fig 2b) is considered.
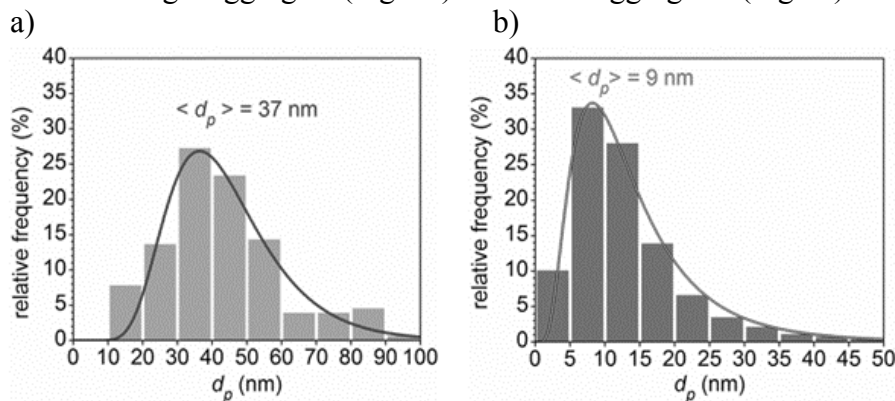
Figure 2: Size distribution of primary particles diameter. a) ca. 100 diameters are measured on the aggregate of Fig.1. The size distribution geometric mean diameter is $<d_p> = 37$ nm. b) ca. 5000 diameters are measured on a collection of 317 aggregates. The size distribution geometric mean diameter is $<d_p> = 9$ nm.

These measurements also allow to determine other aggregates characteristics like the gyration diameter ($d_{g,2D}$), the fractal dimension (Df_{2D}) or the number of primary particles N_p of each aggregate from the following expressions (Baron and Willeke, 2001 and references therein):

$$N_p = k_a \left(\frac{4 A_{2D}}{\pi <d_p>^2} \right)^{\alpha} \qquad (1)$$

where k_a and α are the projected area constant and exponent (Köylü et al, 1995a)

$$A_{2D} = k_L . L_{2D}^{Df_{2D}} \tag{2}$$

where k_L is the fractal prefactor

$$d_{g,2D} = 2\sqrt{\frac{\sum_{i=1}^{A_{2D}}\left((x_i - x_C)^2 + (y_i - y_C)^2\right)}{A_{2D}}}, \tag{3}$$

where (x_i, y_i) are the coordinates of the ith pixel of the aggregate's projection and (x_C, y_C) the coordinates of its center of mass.

2.3 *3D characteristics of soot aggregates from TEM*

The soot aggregates 3D characteristics are extrapolated from 2D measurements by the mean of the following classical 2D-3D transposition relationships (Baron and Willeke, 2001):

$$Df_{3D} = \alpha . Df_{2D} \tag{4}$$

$$d_{g,3D} = \sqrt{\frac{Df_{3D} + 2\alpha}{Df_{3D} + 2}} . d_{g,2D} \tag{5}$$

The volume (V) of an aggregate is also given by the following expression:

$$V = N_p . \frac{\pi d^3}{6} \tag{6}$$

where d corresponds to $<d_p>$ if monodispersed primary particles are assumed or d corresponds to the log-normal size distribution in the case of polydispersed primary particles.

3 3D CHARACTERIZATION OF SOOT AGGREGATES BY TRANSMISSION ELECTRON TOMOGRAPHY

3.1 *Aggregates reconstruction from electron micrographs*

Computing the volume (tomogram) of an aggregate requires three main steps: acquisition of a series of projection (of the aggregate) at different tilt angles, electron micrographs alignment, and aggregate's reconstruction. At this stage the volume of the studied aggregate can be visualized in 3D and measurements can be performed to determine its size characteristics. In our study, a series of projection typically consists of 140 micrographs recorded with a tilt angle that varies from -70 to +70 deg with a step angle of 1 degree. We use "TomoJ" (Messaoudi *et al.*, 2007), a java plugin of the freeware "ImageJ", to align micrographs and reconstruct our aggregates from the tilted series. Note that we use a Simultaneous Iterative Reconstruction Technique (SIRT) algorithm (Tong *et al.* ,2006 and references therein) for the reconstruction step. We also use the "ImageJ 3D Viewer" plugin (Schmid *et al.*, 2010) to 3D visualize the reconstructed aggregates.

3.2 *SootExpert: a new tool for 3D image processing and size measurements*

Although "TomoJ" allows to reconstruct aggregates with various efficient algorithms, it delivers noisy tomograms that prevents the measurement of the 3D aggregates characteristics. A denoising step and a segmentation step are thus required prior to any 3D measurement. For that purpose, we have developed a new "ImageJ" java plugin that we named "SootExpert". It mainly consists of two algorithms. The first one aims at denoising the tomogram and determine the intensity threshold value that allows to determine the reconstructed aggregate's volume as close as possible to the original. The second algorithm is devoted to the determination of the aggregate's 3D characteristics, namely its volume (V), gyration diameter (d_g) and 3D maximal length (L_{3D}). The most important and innovative part of SootExpert lies in a new approach to determine the intensity threshold value leading to the most relevant tomogram. Instead of using the derivative of the aggregate's surface to define the intensity threshold value (Adachi *et al.*, 2007), we propose a new method based on the superim-

position of the original tilted series with another tilted series that is built from the aggregate's tomogram for the same projection angles and for all the intensity values. The value of the threshold intensity is the one that leads to the best match between the initial series and the reconstructed series, insuring that the aggregate's reconstruction is as close as possible to the original studied aggregate.

3.3 *Validation of "SootExpert" on a numerically simulated aggregate*

Performance of SootExpert are validated with numerically generated aggregates, according to a ballistic diffusion algorithm, since their 3D characteristics are perfectly known. We can therefore compare these characteristics to those determined with SootExpert in order to validate its ability to accurately determine the best intensity threshold value of the tomogram and the characteristic sizes of a studied aggregate. In order to illustrate this point, we consider here an aggregate composed of 103 primary particles of size d_p = 30 nm and that has a fractal dimension Df_{3D} = 1.65 (Fig. 3a). We also chose to analyze this numerical aggregate according to the experimental conditions. Thus we use a set of 140 projections of this aggregate for angles that vary from -70 deg. to +70 deg. and a step angle of 1 deg.

a) b)
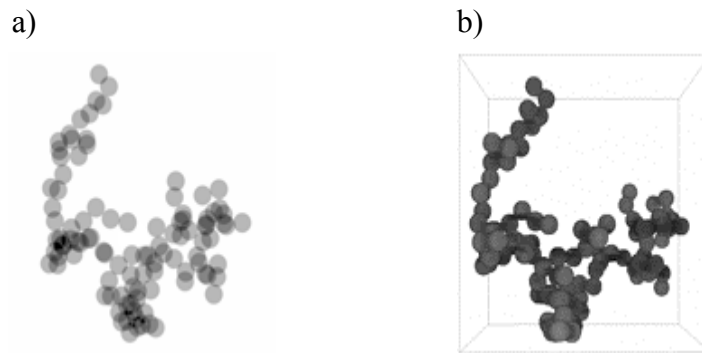
Figure 3: Numerically generated aggregate used to validate "SootExpert". a) One projection of the tilted series. b) 3D visualization of the tomogram processed by "SootExpert".

We use "TomoJ" to build the aggregate's tomogram and "SootExpert" to process it (Fig. 3b) and determine its 3D characteristic sizes. Measured values obtained with "SootExpert" are compared to the real 3D characteristics of this aggregate in Table 1. It clearly shows that SootExpert is an efficient tool to process the tomogram and determine the 3D characteristics of an aggregate.

Table 1: Comparison of the 3D characteristic size values of the numerical aggregate (presented in Fig. 3) and values determined by "SootExpert". V is the volume, d_g the gyration diameter and L_{3D} the maximal length of the aggregate. $\Delta x/x$ is the relative difference between the numerical aggregate's size and the measured one.

	Aggregate	"SootExpert"	$\Delta x/x$
L_{3D} (nm)	456	433	0.05
d_g (nm)	310	295	0.05
V (x 10^6 nm^3)	1.46	1.63	0.12

4 2D AND 3D CHARACTERISTIC SIZES OF AN AIRCRAFT SOOT AGGREGATE

In this section we determine and compare the 2D and 3D characteristic sizes of a single aircraft soot aggregate (see Fig. 1) by analyzing it by both TEM and TET. Electron micrographs of the tilted series are analyzed according to the procedure presented in section 2.2 and values of L_{2D} and $d_{g,2D}$ are given in Table 2 as well as the 3D extrapolated characteristic sizes of this aggregate that are calculated from these 2D measurements (see section 2.3). In parallel, the soot aggregate's tomogram (Fig. 4) is built from the tilted series. SootExpert is used to determine the values of L_{3D}, $d_{g,3D}$ and V that are also presented in Table 2.

Table 2: 2D and 3D characteristic sizes of an aircraft soot aggregate obtained by TEM and SootExpert. 2D values are given for the whole set of micrographs of the tilted series. L_{iD} , $d_{g,iD}$ and V are respectively the maximal length, the gyration diameter and the volume of the aggregate.

	TEM ($i = 2$)	TEM extrapolated ($i = 3$)	SootExpert ($i = 3$)
L_{iD} (nm)	755→785	-	698
$d_{g,iD}$ (nm)	388→423	442→471	404
V (x10^5 nm^3)	-	116→154	122
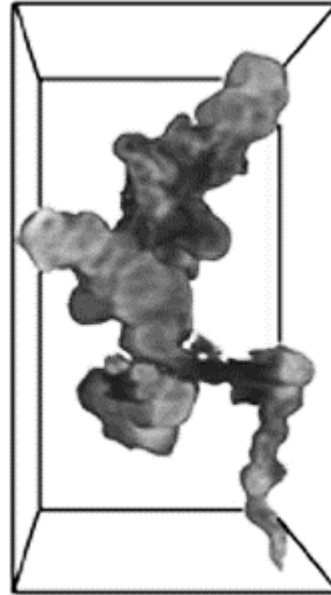
Figure 4: 3D reconstruction of the aircraft soot aggregate presented in Figure 1.

This analysis indicates that whatever the projection angle considered, measurements performed on the aggregate's projections are in a quite good agreement with the 3D measurements performed on the reconstructed aggregate. We have now to investigate about the effect of various parameters (like Df value, primary particles mono or polydispersion) before generalizing this observation as a rule. However, the size of primary particles appears to play a major role in the calculation of d_g and V by 2D-3D transposition. Indeed, the value of d_g extrapolated from TEM is in good correlation with the SootExpert determined value only if the value of $<d_p>$ is determined on the aggregate at stake. It is also important to note that take into account the primary particles size polydispersion is of major importance in the calculation of V .

5   CONCLUSION

We have presented in this paper an approach that allows to determine the 2D and 3D microphysical properties of aggregates based on a single experimental technique, namely TEM. We have developed an ImageJ java plugin named "SootExpert" that efficiently processes electron micrographs and enables to determine aggregates 3D characteristic sizes from a tomogram. We have shown that the size of primary particles is a key parameter when using 2D-3D transposition relationships. We also have shown that a reliable 3D extrapolation of 2D TEM measurements requires to consider the aggregate's primary particles polydispersion. The next step of this study consist of determining the fractal dimension of aggregates from their tomogram and compare them to the values obtained by the classical 2D-3D transposition relationships, in order to explore the validity of the 2D classical fractal TEM analysis on aggregates.

REFERENCES

Adachi, K., S.H. Chung, H. Friedrich, P.R. Buseck, 2007: Fractal parameters of individual soot particles determined using electron tomography: Implications for optical properties. *J. Geophys. Res. 112*, D14202.

Baron, P.A., K. Willeke, (ed.), 2001: *Aerosol measurement. Principles, techniques, and applications. Second edition.* John Wiley & sons, Inc., Hoboken, New Jersey, ISBN 0-471-78492-3, 1131.

Cai, J., N. Lu, C.M. Sorensen, 1993: Comparison of size and morphology of soot aggregates as determined by light scattering and electron microscope analysis. *Langmuir 9*, 2861-2867.

Delhaye, D., E. Ruiz, D. Ferry, B. Demirdjian, J. Suzanne, O. Penanhoat, J. Gouge, 2006: Physico-chemical characterization of soot emitted by a commercial aircraft engine: Morphology, size, structure and elemental composition. *Proceeding of the TAC-Conference, June 26 to 29, Oxford, UK.*

Ferry, D., C. Rolland, D. Delhaye, F. Barlesi, P. Robert, P. Bongrand, J. Vitte, 2011: Jet exhaust particles alter human dendritic cell maturation. *Inflamm. Res. 60*, 255-263.

Köylü, Ü. Ö., G.M. Faeth, T.L. Farias, M.G. Carvalho, 1995a: Fractal and projected structure properties of soot aggregates. *Combustion and Flame 100*, 621-633.

Köylü, Ü. Ö., Y. Xing, D.E. Rosner, 1995b: Fractal morphology analysis of combustion-generated aggregates using angular light scattering and electron microscope images. *Langmuir 11*, 4848-4854.

Lee, D. S., D.W. Fahey, P.M. Forster, P.J. Newton, R.C.N. Wit, L.L. Lim, B. Owen, R. Sausen, 2009: Aviation and global climate change in the 21st century. *Atmos. Environ. 43*, 3520-3537.

Messaoudi, C., T. Boudier, C.O.S. Sorzano, S. Marco, 2007: TomoJ: tomography software for three-dimensional reconstruction in transmission electron microscopy. *BMC Bioinformatics 8*, 288-296.

Park, K., D.B. Kittelson, P.H. McMurry, 2004: Structural properties of diesel exhaust particles measured by Transmission Electron Microscopy (TEM): Relationships to particle mass and mobility. *Aerosol Sci. Tech., 38*, 881-889.

Schmid, B., J. Schindelin, A. Cardona, M. Longair, M. Heisenberg, 2010: A high-level 3D visualization API for Java and ImageJ. *BMC Bioinformatics 11*, 274-280.

Tong, J., I. Arslan, P. Midgley, 2006: A novel dual-axis iterative algorithm for electron tomography. *J. Struct. Biol. 153*, 55-63.

A global model study of sulphate and black carbon aerosol perturbations due to aviation emissions and impact on ozone: a EC-REACT4C study

G. Pitari[*], D. Iachetti, N. De Luca, G. Di Genova
Dipartimento di Scienze Fisiche e Chimiche, Università degli Studi de L'Aquila, Italy

ABSTRACT: The University of L'Aquila climate-chemistry model (ULAQ-CCM) is a global coupled model including troposphere and stratosphere and a rather comprehensive aerosol module. The validation of aerosol products from the ULAQ model has focused on surface aerosol mass density on remote sites, total optical depth on a regional basis, aerosol extinction profiles using SAGE-II and HALOE data and black carbon (BC) vertical profiles using recent aircraft campaign data. Three numerical experiments were performed with the ULAQ model using emission inventories from the collaborative European project EC-REACT4C: no aircraft emissions (EXP1), NO_x and H_2O emissions only (EXP2), and including all gas and particle emissions (EXP3). These experiments have the purpose to study the direct radiative forcing (RF) of sulphate and BC aerosols and to study the indirect impact on the NO_x-HNO_3 balance (and hence on O_3) via heterogeneneous chemistry on the surface of sulphate particles. The ULAQ-CCM calculated changes of sulphuric acid aerosol surface area density reach maximum values of $1.5 \ \mu m^2/cm^3$ at about 10 km altitude in the NH mid-latitudes. Aircraft emissions of BC particles may significantly affect the mass density of carbonaceous aerosols ($0.3 \ ng/m^3$ at the same location). One conclusion is that the impact of aviation SO_2 and freshly emitted ultrafine sulphuric acid aerosols is to reduce the net RF associated to aviation emissions of NO_x (i.e. O_3 and CH_4), H_2O and sulphur from $4.5 \ mW/m^2$ to $3.1 \ mW/m^2$, via changes of heterogeneous chemistry and cooling due to additional or larger sulphate particles.

1 INTRODUCTION

According to the current consensus state of knowledge (Lee et al., 2010), emissions from aviation directly affects atmospheric chemistry and climate in the following ways, in terms of radiative forcing (RF): emissions of CO_2 result in a positive RF (warming); emissions of H_2O result in a positive RF (warming); emissions of sulphate particles arising from sulphur in the fuel result in a negative RF (cooling); emissions of soot particles result in a positive RF (warming); the formation of persistent linear contrails that may form (depending upon atmospheric conditions) in the wake of an aircraft result in both positive and negative RF effects but overall, cause a positive RF effect (warming); the formation of contrail-cirrus cloud from spreading contrails similarly to line shaped-contrails results in both positive and negative RF effects but overall, is considered to cause a positive RF effect (warming).

Aviation emissions indirectly affects atmospheric chemistry and climate in the following ways: (1) emissions of NO_x result in the formation of tropospheric O_3 via atmospheric chemistry, with a positive RF (warming); (2) emissions of NO_x result in destruction or increase of stratospheric O_3 via atmospheric chemistry, depending upon altitude: above about 20 km, models always predict O_3 destruction. Using recent chemical kinetics data, chemistry-transport models (CTM) predict a net O_3 column decrease, larger than in IPCC (1999), with a global negative RF (cooling); (3) emissions of NO_x result in the destruction of ambient methane, also via atmospheric chemistry, with a negative RF (cooling), which is accompanied by a parallel, decadal loss of tropospheric O_3; (4) emissions of

---
[*] *Corresponding author:* Giovanni Pitari, Dipartimento di Scienze Fisiche e Chimiche, Università degli Studi de L'Aquila, Italy. Email: gianni.pitari@aquila.infn.it

H_2O have an indirect (small) negative correction, obtained via O_3 chemistry (through additional formation of HO_x and consequent O_3 destruction); (5) emissions of sulphate particles arising from sulphur in the fuel result in negative RF (cooling): an indirect effect occurs via heterogeneous chemistry. In this case more NO_x is lost towards nitric acid (HNO_3) and the O_3 destruction/increase is decreased in magnitude; in addition, the lower stratospheric O_3 increase due to NO_x emissions may change into destruction due to increasing Cl_x and Br_x (since chlorine and bromine nitrates will decrease): the net effect on O_3 is dependent upon altitude and model transport, as well as the sign of this indirect sulphate-related RF; (6) a sub-component of aviation-induced cirrus is a mechanism whereby soot particles seed cirrus clouds (or 'soot-cirrus'): soot may either increase or decrease the number of ice particles and impact upon both the albedo and the emissivity of cirrus clouds. This effect may result in either positive or negative RF effects (warming/cooling) but is rather uncertain over the sign and proven existence of the effect (Penner et al., 2009).

In this paper we discuss model results relative to point 5 of the above listed indirect effects. The numerical model is first described in section 2 and validated in terms of aerosol predictions (section 3) and then used for photochemical and radiative forcing calculation (section 4).

2 MODEL DESCRIPTION

The University of L'Aquila model used in this study is a global scale climate-chemistry coupled model (ULAQ-CCM) extending from the surface to the mesosphere (0.04 hPa) and operated here in CTM mode. Dynamical data (i.e. velocity stream-function and velocity potential) are provided by the background GCM run in a reference case, with no feedbacks on climate radiation and dynamics of aviation induced changes of CO_2, H_2O, CH_4, O_3, aerosol and ice particles. The ULAQ-CCM has been fully described in Pitari et al. (2002a), Eyring et al. (2006) and Morgenstern et al. (2010) for the SPARC-CCMVal model inter-comparison and validation campaigns. Since then, some important updates have been made in the model: (a) increase of horizontal and vertical resolution, now T21 with 126 log-pressure levels (approximate pressure altitude increment of 568 m); (b) inclusion of a numerical code for the formation of upper tropospheric cirrus cloud ice particles (Karcher and Lohmann, 2002); (c) update of species cross sections using JPL (2011) recommendations and Schumann-Runge bands treated following the parameterization of Minschwaner et al. (1993) based on (fixed-T) ODF formulation; (d) upgrade of the radiative transfer code for calculations of photolysis, solar heating rates and top-of-atmosphere radiative forcing. The oceanic surface temperature is assimilated from the Hadley Centre for Climatic Prediction and Research; the parameterization of periodic natural forcings (solar cycle, QBO) is included on-line. The new radiative transfer module, operating on-line in the ULAQ-CCM, is a two-stream delta-Eddington approximation model (Toon et al., 1989) used for chemical species photolysis rate calculation in UV-visible wavelengths and for solar heating rates and radiative forcing in UV-VIS-NIR bands. The model uses 150 wavelength bins in the UV and visible range and 100 in the NIR, covering the solar spectrum from Lyman-alpha up to 7 μm. Earth orbit eccentricity, solar cycle, sphericity and refraction are taken into account. The ULAQ model calculations of photolysis rates and surface and top-of-atmosphere radiative fluxes have been validated in the framework of SPARC-CCMVal and AEROCOM inter-comparison campaigns (Randles et al., 2012).

The chemistry module is organized with all medium and short-lived species grouped in families: O_x NO_x, NO_y (NO_x + HNO_3), HO_x, CHO_x, Cl_y, Br_y, SO_x, aerosols. Long-lived and surface-flux species included in the model are N_2O, CH_4, H_2O, CO, NMHCs, CFCs, HCFCs, HFCs, halons, OCS, CS_2, DMS, H_2S, SO_2 for a total of 40 transported species (plus 57 aerosol size categories) and 26 species at photochemical equilibrium. The model includes the major components of stratospheric and tropospheric aerosols (sulphate, carbonaceous, soil dust, sea salt), with calculation at each size bin of surface fluxes, removal and transport terms. The size distributions of sulphate (both tropospheric and stratospheric) and PSC aerosols are calculated using a fully interactive and mass conserving microphysical code for aerosol formation and growth, starting from SO_x chemistry and SO_2 emissions. Lower stratospheric denitrification and dehydration are calculated using the predicted size distribution of PSC particles; the most important heterogeneous reactions on sulphate and PSC aerosols are included in the chemistry module. The main features of the ULAQ aerosol module are summarized in Pitari et al. (2002a) and in Textor et al. (2006), the latter in the framework of the

Aerocom project.

The ULAQ model is used here for three numerical experiments, using emission inventories from the collaborative European project EC-REACT4C: no aircraft emissions (EXP1), NO_x and H_2O emissions only (EXP2), and including all gas and particle emissions (EXP3). All three simulations were performed over a period of 15 years (1996-2010) after a 5 years spin-up (1991-1995), with emission inventories for the year 2006 (base case from the EC-REACT4C collaborative project).

3   AEROSOL VALIDATION

Sulphate aerosols dominate the aerosol population and mass distribution in the upper troposphere, i.e. the region directly perturbed by aviation emissions. The particle size distribution is determined by homogeneous and heterogeneous nucleation, condensation/evaporation, water vapour growth, coagulation, dry and wet deposition, sedimentation, large-scale transport. The main removal processes of aerosol particles parameterized in the model are: washout calculated as a function of the precipitation rate (wet deposition), scavenging by direct and turbulent deposition on the surface (dry deposition) and loss caused by gravitational attraction (sedimentation). Aerosol particles are divided in size bins and each one of this size categories is separately transported. Mechanically generated particles (i.e. soil dust and sea salt), as well as carbonaceous aerosols (i.e. organic, OC, and black carbon, BC) are treated with binned emissions and the same removal mechanisms listed above, taking into account that BC particles are largely emitted as hydrophobic (about 80%) and are later aged to hydrophilic. The ULAQ model aerosol predictions have been validated as follows: (1) surface aerosol mass concentration: predictions of annually averaged aerosol mass concentration at the surface are compared with data from the University of Miami Aerosol Network (Prospero et al., 1989) over the past two decades. (2) Total aerosol optical thickness: comparisons between measured and calculated optical depth are made on a regional basis. Remote sensing measurements
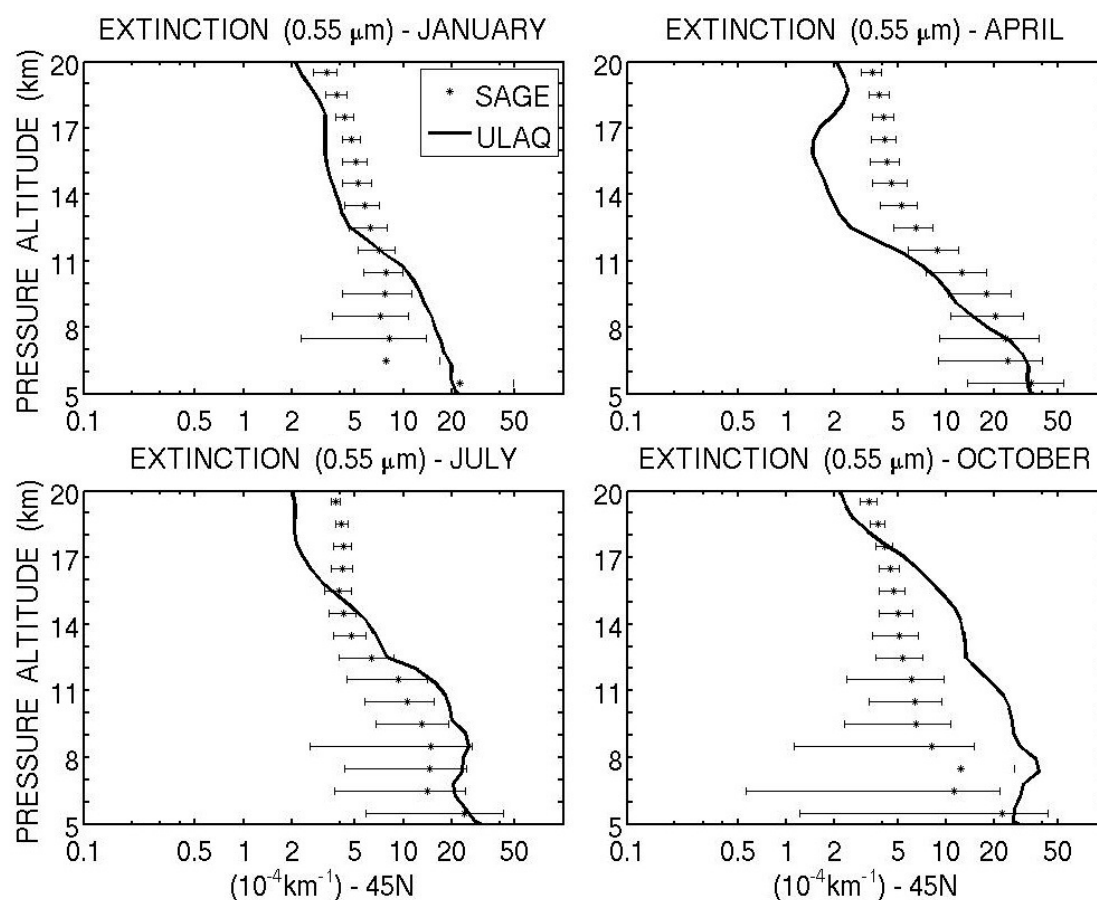
Fig.1: Extinction profiles at 0.55 μm: ULAQ calculations (solid line) and SAGE-II-derived values (asterisks) are shown at 45N for January, April, July and October (volcanically clean conditions).

OPTICAL DEPTH AT 0.55 μm (5.5-20 Km)
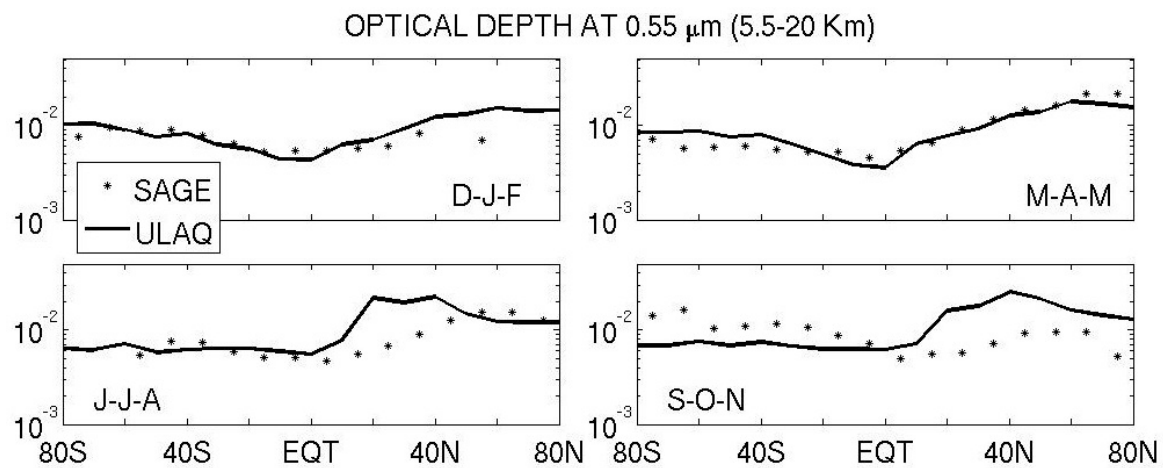
Fig.2: ULAQ calculations (solid line) and SAGE-II-derived values (asterisks) of aerosol optical depth at 0.55 μm, integrated between 5.5 km and 20 km altitude, for winter, spring, summer and autumn months.

BLACK CARBON MASS MIXING RATIO
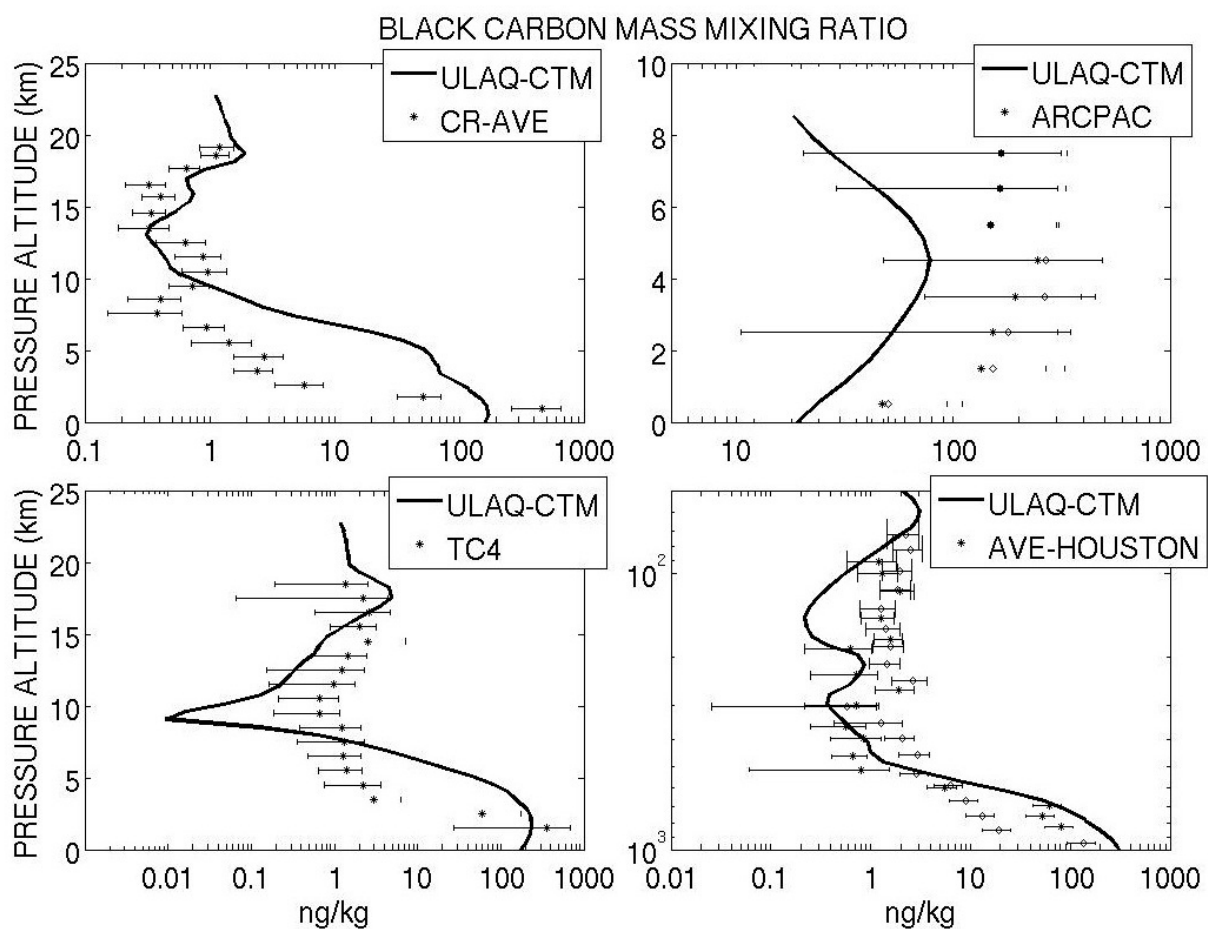
Fig.3: BC model profiles in the vicinity of recent aircraft measurements in order to get a qualitative sense of how the ULAQ model performs in the mid-upper troposphere. The measurements were made with three independent Single Particle Soot absorption Photometers (SP2s) onboard NASA and NOAA research aircraft at tropical, middle latitudes and at high latitudes over North America (Schwarz et al., 2006; Schwarz et al., 2008; Spackman et al., 2010; Spackman et al., 2011).

from space are used to validate the model (AVHRR, MODIS, TOMS). (3) Extinction profiles: SAGE-II data are used to validate the calculated extinction profiles at 0.55 μm and 1.020 μm and optical depth in the upper troposphere and lower stratosphere (UTLS) from 5.5 to 20 km altitude; HALOE extinction profiles at 3.46 and 5.12 μm wavelengths are also used for this purpose. (4) BC vertical profiles of mass mixing ratios are compared with recent aircraft measurements at tropical, mid-latitude and at high latitude locations over North America (Schwarz et al., 2006; Schwarz et al., 2008; Spackman et al., 2010; Spackman et al., 2011). Validation examples are shown in Fig. 1-3, where Fig. 1-2 refer to point (3) above and Fig. 3 to point (4).

4   OZONE PHOTOCHEMISTRY

The ULAQ-CCM photochemistry scheme and radiation transfer code have been validated participating to the SPARC-PhotoComp intercomparison. In this way we expect the model predictions of NO_x and O_3 and their changes due to aviation emissions to be only marginally affected by photochemical biases. The ULAQ-CCM study on the impact of aviation particles focuses in particular on the NO_x-HNO_3 balance (and hence on O_3) via heterogeneous chemistry on the surface of sulphate particles. Fig. 4 shows the calculated aerosol changes (EXP3-EXP1) in terms of sulphate surface and mass densities (panels a,b) and BC mass density (panel c). The calculated changes of sulphuric acid aerosol surface area densities reach maximum values of about 1.5 $\mu m^2/cm^3$ at 10 km altitude in the NH mid-latitudes; in addition, aircraft emissions of BC particles may significantly affect the mass density of carbonaceous particles, with a calculated change of 0.3 ng/m^3 at the same location.
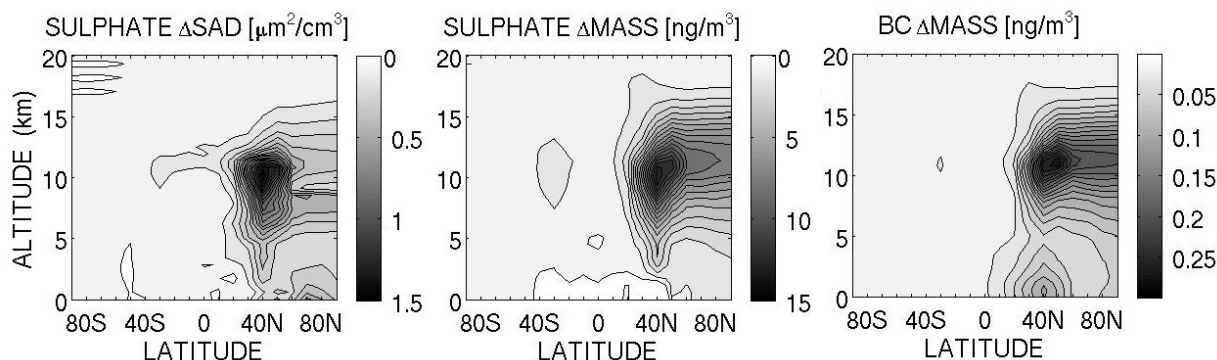
Fig.4: Zonally and annually averaged perturbations due to aviation emissions of sulphate (surface area and mass densities, left and mid panels, respectively) and black carbon aerosols (mass density, right panel).
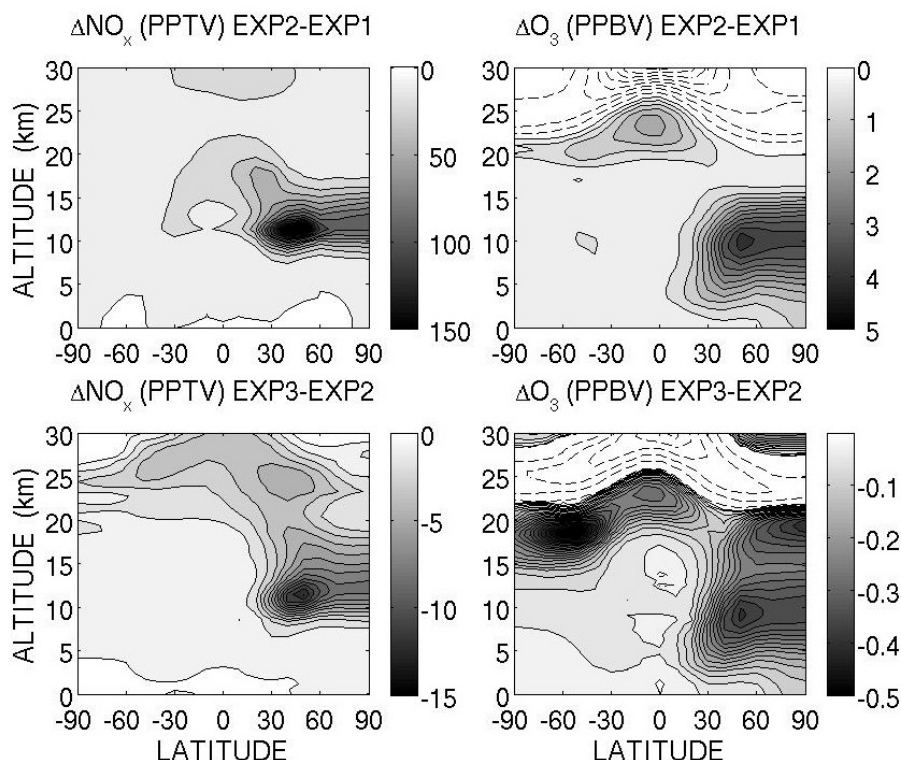
Fig.5. Zonally and annually averaged changes produced by aviation emissions of NO_x (pptv, left) and O_3 (ppbv, right). Top panels are changes from EXP2-EXP1, i.e. non including aerosol emissions from aviation; bottom panels are changes in EXP3 with respect to EXP2, i.e. the net effect of sulphate aerosol emissions. Dashed lines in the O_3 panels are negative/positive and spaced by -0.5 ppbv and 0.25 ppbv in top/bottom panels, respectively.

An indirect impact of emissions of sulphate particles arising from sulphur in the fuel result occurs via heterogeneous chemistry; in this case more NOx is lost towards nitric acid (HNO_3) and the tropospheric O_3 increase is decreased in magnitude (EXP3-EXP1), with respect to the case where no additional aerosols are produced by aircraft emissions (EXP2-EXP1), as shown in Fig. 5. The ULAQ model calculates a 10% reduction of the NO_x accumulation in the NH mid-latitudes at cruise altitudes and a corresponding 10% reduction of the ozone increase in EXP3-EXP1 with respect to EXP2-EXP1. It is interesting to note how the O_3 changes follow the NO_x perturbation with same/opposite sign below/above the lower stratospheric turnover point of O_3 production/loss from the NO_x catalytic cycles. The relatively large O_3 decrease in EXP3 with respect to EXP2 in the polar lower stratosphere is due to the NO_x decrease feedback on reactive chlorine and bromine (both increasing due to the loss of chlorine and bromine nitrates). A summary of top-of-atmosphere radiative forcings from NO_x, H_2O and aerosol emissions from aviation is shown in Table 1. NO_x emissions drive changes of O_3 and OH, thus perturbing the methane lifetime. The small RF change of sulphate in the first column (i.e. EXP2-EXP1) is due to the NO_x forced OH change, which in turn affects SO_x chemistry and SO_4 production. The results shown in Fig. 5 and Table 1 are qualitatively consistent with those discussed in Pitari et al. (2002b).

Chemical species	RF [mW/m²] (EXP2-EXP1)	RF [mW/m²] (EXP3-EXP1)
O_3	13.5	11.8
CH_4	-8.6	-7.4
H_2O	1.1	1.1
Sulphate	-1.5	-4.6
BC	0.0	2.2
TOTAL	4.5	3.1

Table 1. Summary of Top-of-Atmosphere Radiative Forcing mean values for species emitted by the aircraft or formed via chemical reactions, calculated using aircraft emission scenarios for 2006. The O_3 RF follows the above discussed changes in NO_x and particle emissions.

5 CONCLUSIONS

The attempt of this study is to quantify the effects on ozone photochemistry of aerosol perturbations due to aircraft emissions. We have first successfully validated the background model predictions of aerosol products, using satellite, ground based and aircraft measurements. Sulphate aerosols emitted in aircraft plumes have been shown to produce a significant impact on the NO_x accumulation (10% reduction in the NH mid-latitudes at cruise altitudes) and then on O_3 production (-10%). The overall RF due to NO_x, H_2O and aerosol emissions is shown to be smaller by about 1.4 mW/m² with respect to the case where only gas emissions from the aircraft are taken into account (i.e. NO_x and H_2O).

ACKNOWLEDGMENTS

REFERENCES

Eyring, V., et al.: Assessment of temperature, trace species, and ozone in chemistry-climate model simulation of the recent past, *J. Geophys. Res., 111,* D22308, doi:10.1029/2006JD007327, 2006.

JPL: Chemical Kinetics and Photochemical Data for Use in Atmospheric Studies, Evaluation Number 17, *JPL Publication 10-6,* 2011.

Kärcher, B., and U. Lohmann: A parameterization of cirrus cloud formation: homogeneous freezing of supercooled aerosols, *J. Geophys. Res., 107,* 4010, 10.1029/2001JD000470, 2002.

Lee, D., et al.: Transport Impacts on Atmosphere and Climate: Aviation, *Atmos. Env., 44, 4678-4734,* 2010.

Minschwaner, K., R. J. Salawitch, and M. B. McElroy: Absorption of Solar Radiation by O2: Implications for O3 and Lifetimes of N2O, CFCl3, and CF2Cl2, *J. Geophys. Res., 98,* 10,543–10,561, doi:10.1029/93JD00223, 1993.

Morgenstern, O., et al.: A review of CCMVal-2 models and simulations, *J. Geophys. Res., 115,* D00M02, doi:10.1029/2009JD013728, 2010.

Penner, J.E., Y. Chen, M. Wang, X. Liu: Possible influence of anthropogenic aerosols on cirrus clouds and anthropogenic forcing, *Atmos. Chem. Phys. 9,* 879–896, 2009.

Pitari G., E. Mancini, V. Rizi and D. T. Shindell: Impact of Future Climate and Emission Changes on Stratospheric Aerosols and Ozone, *J. Atmos. Sci., 59,* 2002a.

Pitari, G., E. Mancini, and A. Bregman: Climate forcing of subsonic aviation: indirect role of sulfate particles via heterogeneous chemistry. *Geophys. Res. Lett. 29* (22), 2057. doi:10.1029/2002GL015705, 2002b.

Randles, C.A., et al.: Intercomparison of shortwave radiative transfer schemes in global aerosol modeling: Results from the AeroCom Radiative Transfer Code Experiment, *submitted to ACPD*, 2012.

Schwarz, J.P.: Single-Particle measurements of midlatitude black carbon and light-scattering aerosols from the boundary layer to the lower stratosphere, *J. Geophys. Res., 110,* D16207, 2006.

Schwarz, J.P., et al: Coatings and their enhancement of black-carbon light absorption in the tropical atmosphere, *J. Geophys. Res.,* doi:10.1029/2007JD009042, 2008.

Spackman, J.R: Aircraft observations of enhancement and depletion of black carbon mass in the springtime Arctic, *ACP,* 2010.

Spackman, J.R. , R.S. Gao, J.P. Schwarz, L.A. Watts, D.W. Fahey, L. Pfister, and T.P. Bui: Seasonal variability of black carbon mass in the tropical tropopause layer, *Geophys. Res. Lett., 38,* L09803, doi:10.1029/2010GL046343, 2011.

Toon, O. B., C. P. McKay, T. P. Ackerman, and K. Santhanam: Rapid Calculation of Radiative Heating Rates and Photodissociation Rates in Inhomogeneous Multiple Scattering Atmospheres, *J. Geophys. Res., 94,* 16,287–16,301, doi:10.1029/JD094iD13p16287, 1989.

Performance Characteristic of a Multi-fuel Hybrid Engine

Feijia Yin, Dr. Arvind G. Rao[*], Prof. J.P. van Buijtenen
Technische University Delft, Faculty of Aerospace Engineering, 2629HS Delft, the Netherlands

ABSTRACT: Future demands for sustainability indicate that aircraft should be fuel efficient, less noisy and less polluting. However, with the conventional incremental aviation technologies, it seems there is very little chance to meet these requirements. This paper demonstrates a novel hybrid engine concept for future Blended Wing Body (BWB) aircraft. The proposed hybrid engine includes two combustion chambers, providing a possibility to for multi-fuel, like a combination of liquid hydrogen (LH2)/liquid natural gas (LNG) and kerosene/biofuel, enabling the reduction of CO_2 emissions. Firstly, sensitivity analysis of engine design parameters on the engine performance was carried out. Secondly, genetic algorithm was used to optimize design parameters of hybrid engine. Eventually, a comparison was made between hybrid engine and a baseline engine, namely PW4056.

1   INTRODUCTION

Compared to 40 years ago, aircraft has been 20 decibels quieter and 70% more fuel-efficient, reducing carbon monoxide (CO) by 50% and unburned hydrocarbon (UHC) and smoke by 90% [1]. However, it is estimated that air traffic will grow by 5% annually, which results in a growth of aviation CO_2 emission of 2-3% per year [2]. Noise emission cannot be ignored as well. Overall, air transport is highly responsible for environmental impact. Therefore, the ACARE has set an ambitious objective for the year of 2050 to reduce CO_2 emission by 75%, NO_x emission by 90%, and noise emission by 65% in reference to the year of 2000 [3]. To meet all the ACARE requirements, some innovative engine configurations have been investigated.

Because of the increase in air traffic, fuel demand is predicted to rise by 3% every year, whereas, aviation fuel production is predicted to decrease every year since the production peak will be reached [4]. Furthermore, CO_2 emission is the product of chemical reaction of hydrocarbon fuel, which will not be eliminated unless non-carbon fuel is burnt. Consequently, alternative fuels become a candidate.

To summarize, a new engine concept is desired, which should be able to burn alternative fuel, have higher engine efficiency, and be quitter. To fulfil these demands, a novel hybrid engine concept was proposed.

2   THE HYBRID ENGINE CONCEPT

The so-called hybrid engine concept is a turbofan based engine with two combustion chambers, as presented in Figure 2.1

---

[*] *Corresponding author:* Technische University Delft, Faculty of Aerospace Engineering, 2629HS Delft, the Netherlands, A.GangoliRao@tudelft.nl
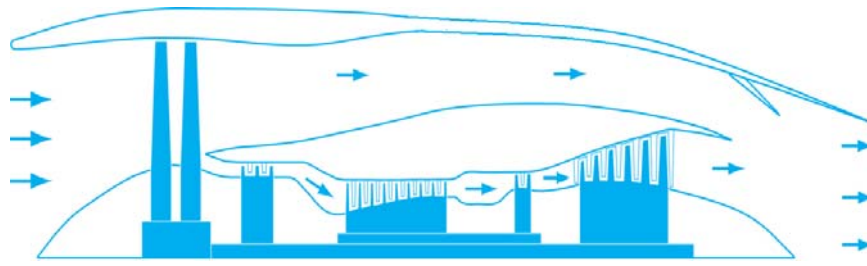
Figure 2.1: The schematic of hybrid engine.

The main features of the hybrid engine are as below:
- Counter rotating fans which is good for BLI and improves the propulsive efficiency of hybrid engine.
- Two combustion chambers, one is main combustion chamber which is burning cryogenic fuels such as LH2/LNG; the other one is an inter-stage turbine burner consuming kerosene/biofuels [5,6].
- The use of flameless combustion technology for the second combustor will reduce emissions of CO, NOx, UHC and soot to a minimum [6].
- The implementation of mixer enables increase of thrust and reduction of engine noise.
- A heat exchanger for exchanging of LH2 and bleed cooling air will lead to reduction of cooling air mass for a given turbine inlet temperature, thus reducing specific fuel consumption simultaneously increasing thrust.

Some benefits can be obtained using cryogenic fuel in the first combustion chamber. First of all, since the flammability limit for H_2 is much wider than for kerosene, the combustion can take place at lean conditions to reduce NOx emission [7]. Moreover, Using LH2 in the first combustion chamber will increase the concentration of water vapour and reduce the concentration of O_2 in the second combustion chamber, thus creating a vitiated environment in which Flameless Combustion can be sustained using kerosene/biofuel [6].

To investigate the feasibility of hybrid engine concept mentioned above, some research has been done by Delft University of Technology (TUDelft) [7,8,9].

3   MODELS AND VALIDATION

There are some gas turbine simulation tools available for performance analysis, for example, GSP® and GASTurb®. GSP was developed by the Dutch National Aerospace Laboratory (NLR) and the TUDelft. It is component-based gas turbine modelling environment [10], where both steady state and transient simulation of any gas turbines can be performed. GASTurb has been widely used in gas turbine performance analysis. It supplies various predefined engine configurations, thus making it easier to start a calculation process immediately [11].

Despite of the advantages of GSP and GASTurb, it is desirable to create an in-house model for hybrid engine optimization. Validation of hybrid engine models is shown in Table 3.1. Net thrust (FN) and specific fuel consumption (SFC) are calculated in GSP, GASTurb and in-house model respectively and compared to the actual engine data. The baseline engine is PW4056 and cruise is the checkpoint.

Table 3.1: Comparison of net thrust and the specific fuel consumption.

	Actual Data	GSP	In-House
FN [kN]	40.037	40.039	40.08
SFC [g/kN.s]	16.617	16.69	16.722

4   DESIGN PARAMETERS SENSITIVITY ANALYSIS

Thermodynamic performance of gas turbines is quite sensitive to the change of design parameters, especially hybrid engine where 7 design parameters were chosen. Hence, sensitivity of hybrid engine parameters was analysed in GSP at cruise, where altitude is 10668 meters and Mach number is

0.8. The layout of model is presented in Figure 4.1. LH2 was implemented in the first combustion chamber, and kerosene was used in inter-stage turbine burner. A mixer module has been included after low pressure turbine. To minimize pressure loss due to mixing process, equality of the static pressure ratio between bypass and core was maintained. Additionally, core flow Mach number of the mixer inlet and component efficiencies were assumed as constant.
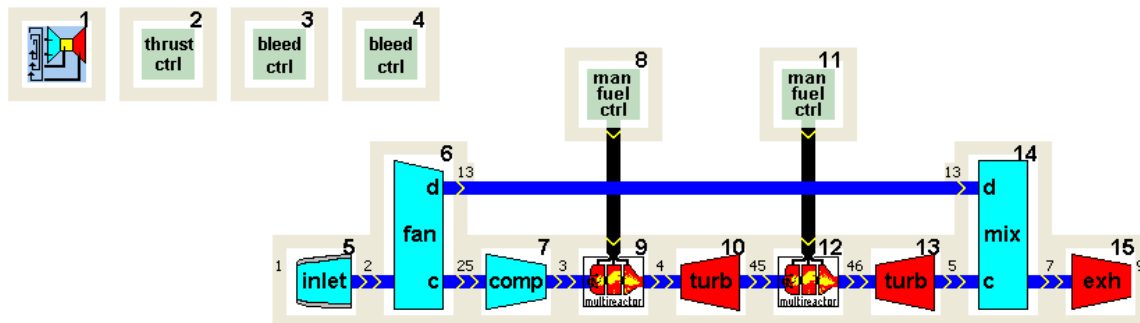

Figure 4.1: The schematic of hybrid engine model in GSP.

Figure 4.2 presents the variation of SFC and net thrust with HPC pressure ratio. It indicates that an optimum HPC pressure exists to obtain lower SFC and higher net thrust. The reason is thermal efficiency of an engine is proportional to engine pressure ratio whereas the maximum propulsive efficiency is reached at some point of pressure ratio such that an optimum total efficiency can be obtained thus the optimal SFC and FN exist.
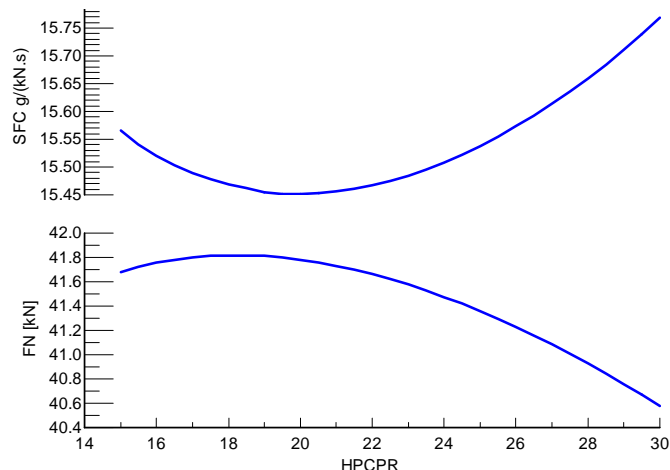
Figure 4.2: Variation of SFC and FN with HPC pressure ratio.

For an engine with mixer, a best combination of fan pressure ratio and bypass ratio has to be selected.

Figure 4.3 presents a typical plot of variation of SFC with fan pressure ratio for various bypass ratio. It indicates that higher bypass ratio is matched with lower fan pressure ratio. Because total mass flow is constant, the core air mass decreases with increasing bypass ratio. For a given turbine inlet temperature, to obtain the same compressor pressure ratio with less air mass, turbine exit temperature is lower as well as exit pressure. Since the pressure ratio of bypass and core has to be constant, the fan pressure ratio needs to be lower.
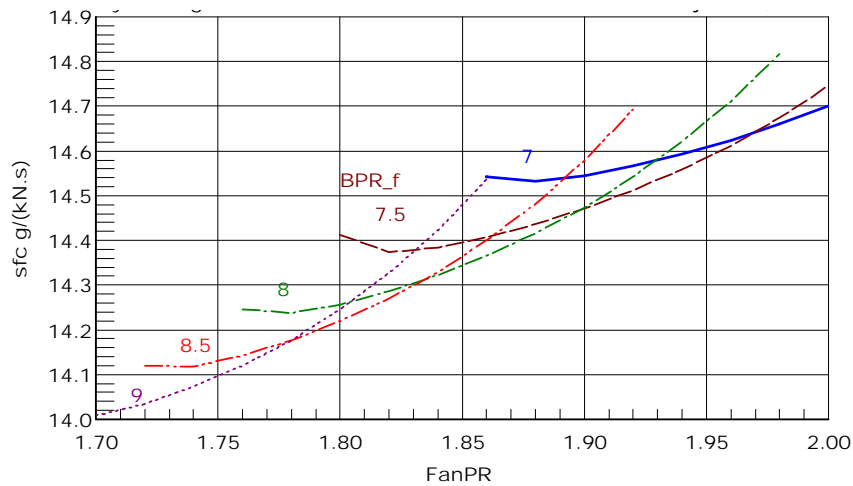
Figure 4.3: Variation of the SFC with FPR for various BPR

Turbine inlet temperature is one of the most important design parameters. Its value mostly affects the thermal cycle of an engine. Figure 4.4 presents variation of SFC and FN with TT4 for various TT46. For a given TT46, SFC decreases with increasing TT4, while FN increases with increasing TT4.
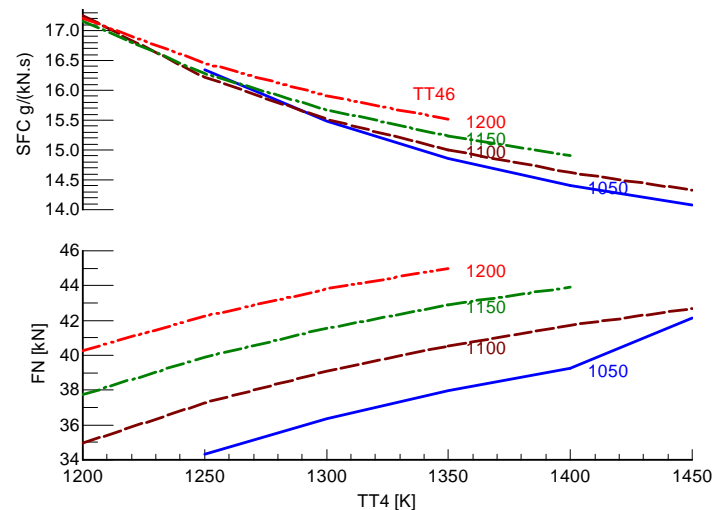
Figure 4.4: Variation of SFC and FN with TT4 for various TT46.

The most common way to store LH2 is using a number of pressurized cylindrical vessels, which is a big challenge for conventional aircraft. Although a larger free space of BWB offers an opportunity, the fuel ratio between LH2 and kerosene needs to be optimized to make a full use of space in BWB. Sensitivity analysis has been processed as presented in Figure 4.5. It shows that there is a minimum SFC region with respect to the suitable ratio of LH2 and kerosene , meanwhile, FN can still be relatively high. However, the optimum ratio still needs to be determined according to the capacity of an aircraft.
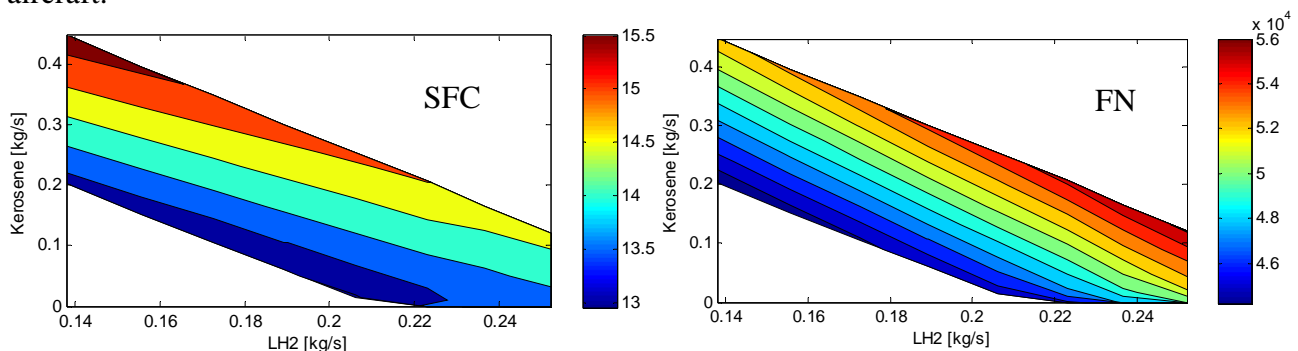
Figure 4.5: The variation of SFC and FN with fuel ratio of LH2 and kerosene

5 CYCLE OPTIMIZATION STUDIES

Optimization is everywhere, from engineering design to computer sciences and from scheduling to economics [12]. There are numerous optimization algorithms existing already. However, most problems are very difficult to find out optimum solutions. As can be seen in the proceeding section, the performance of hybrid engine itself is very nonlinear. To solve this problem, a very powerful optimization method is essential.

5.1 *Methodology*

This paper chose genetic algorithm (GA) for the reason that genetic algorithm has many advantages over traditional methods. Genetic algorithm was developed by Holland [13] and his colleagues in the 1960s and 1970s. In GA, a solution vector is called a chromosome, which is made of genes. A group of chromosomes together is called population. Initially, genes were assumed to be binary by Holland. In later applications, more various gene types have been introduced [14]. GA can deal with a variety of problems whether the objective function is linear or nonlinear, stationary or nonstationary, continuous or discontinuous. Despite the choice of population size, the number of generations, the rate of crossover or mutation, and the selection criteria will all influence the optimization results. These should be carried out very carefully.

5.2 *Implementation of Optimization Program*

A developed in house optimization program using genetic algorithm was implemented. The aim was to search for minimum SFC limited by all the defined bounds and constraints, which are presented in Table 5.1. Proper GA factors were specified. The optimized engine parameters are shown in Table 5.2.

Table 5.1: Bounds and constraints of design parameters

Bounds of design parameters	
FPR	[1.3, 1.8]
LPCPR	[1.0, 1.8]
HPCPR	[15, 25]
Tt4 [K]	[1300, 1500]
Tt46 [K]	[1150, 1400]
BPR	[5, 8.5]
Constraints of design parameters	
Corrected Mass Flow [kg/s]	[700, 800]
OPR	<= 55
FN [kN]	>= 40

Table 5.2: Optimized engine design parameters and performance.

Optimized Design Parameters	
Mass Flow(kg/s)	758.5
BPR	8.3
FPR	1.8
LPCPR	1.6
HPCPR	20.5
Tt4 [K]	1498.5
Tt46 [K]	1174.6
Engine Performance	
SFC [g/kN/s]	13.9382
FN [kN]	47.461

The performance of the optimized hybrid engine has been compared with the baseline engine PW4056. Results are shown in Figure 5.1. It can be concluded that using hydrogen the hybrid engine has potential to reduce CO_2 emissions by more than 80% compared to the baseline engine.

Meanwhile, the higher thrust and lower specific fuel consumption can be obtained for the hybrid engine.
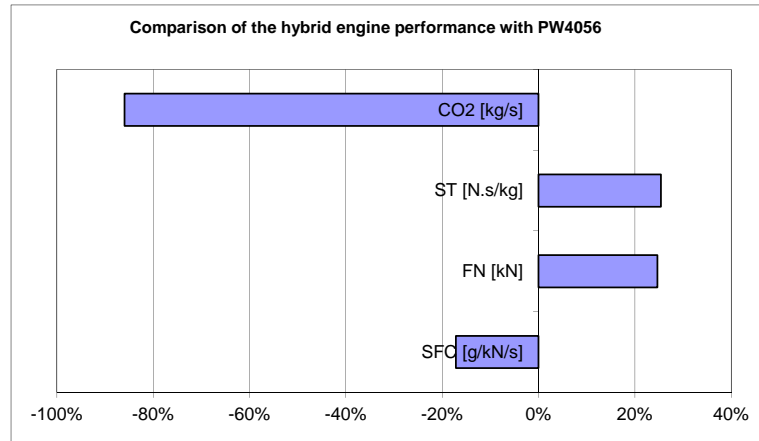

Figure 5.1: Comparison of hybrid engine performance with PW4056

6   CONCLUSIONS

This paper presents a sensitivity analysis process for the hybrid engine, showing a possible design space to meet requirements. Apart from that, a preliminary cycle optimization has been processed using genetic algorithm. Compared to PW4056, the proposed hybrid engine concept reduces CO_2 emission by more than 80%, SFC by around 19% and increase thrust by over 20%. Further work will be carried out later on.

ACKNOWLEDGEMENT

REFERENCE

Air transport action group (ATAG), "the economic & social benefits of air transport", September 2005.

Air transport action group (ATAG), "the economic and social benefits of air transport 2008", April 2008.

Advisory Council for Aeronautics Research in Europe (ACARE), "flightpath 2050 Europe's vision for aviation", Report of the High Level Group on Aviation Research, Publication Office of European Union, ISBN 978 92 79 19724 6, 2011.

J. Brand, et. al, "Potential use of hydrogen in air propulsion", AIAA.

Liu, F., and Sirignano, W.A., "Turbojet and Turbofan Engine Performance increase through Turbine Burners", 38th AIAA Aerospace Sciences Meeting and Exhibit, Reno, Nevada, AIAA-2000-0741, 2000.

Sirignano, W.A, and Liu, F., "Performance Increase for in Gas-Turbine Engines through Combustion inside the Turbine", Journal of Propulsion and Power, Vol. 15(1), pp. 111-118, 1999.

Rao, A.G., Yin, F., and van Buijtenen, J.P., "A Novel Engine Concept for Aircraft Propulsion", ISABE Conference, Gothenburg, Sweden, ISABE-2011-1341, 2011.

Tang, K-G., Rao, A. G., and van Buijtenen, J.P., "Conceptual Study of a Hybrid Engine with Inter Turbine Burner", ASME Turbo Expo 2010, Glasgow, GT2010-22719.

Tang, K-G., "Next Generation Aircraft Propulsion: Concept Study of a Hybrid Turbofan Engine", master thesis, Delft University of Technology.

GSP Development Team, "GSP 11 User Manual - Version 11.1.0", National Aerospace Laboratory NLR, 2010.

http://www.gasturb.de/

Yang, X., "Engineering Optimization-an introduction with metaheuristic application", John Wiley & Sons, Inc., 2010.

J.H. Holland (1975), "Adaptation in Natural and Artificial Systems", University of Michigan Press, Ann Arbor, Michigan; re-issued by MIT Press (1992).

Konak A., Coit David W. and Smith Alice E., "Multi-objective optimization using genetic algorithm: A tutorial", Reliability Engineering and System Safety 91(2006) 992-1007, 2006.

Quantifying the Composition of Volatile Particulate Matter Emissions from Aircraft Engines

Z. Yu[*], H.-W. Wong, J. Peck, S. C. Herndon, R. C. Miake-Lye
Aerodyne Research, Inc., USA

M. Jun, I. A. Waitz
Massachusetts Institute of Technology, USA

D. S. Liscinsky, A. Jennings, B. S. True, M. Colket
United Technologies Research Center, USA

L. D. Ziemba, E. L. Winstead, B. E. Anderson
NASA Langley Research Center, USA

ABSTRACT: A combined theoretical modeling and experimental measurement investigation is pursuing better understanding of how the various volatile particle contributions affect the number, size, and mass of the particulate matter (PM) emissions of aircraft engines and how these properties evolve in the exhaust. The studied contributions come from partially combusted fuel hydrocarbons and engine lubrication oil, and how these organics are mediated by emitted sulfate has been studied using a new microphysical modeling capability.

In this study, an existing microphysical modeling tool was advanced to simulate the microphysical behavior of organic PM emissions from aircraft engines. Through the modeling efforts, the organic species were found to condense on the sulfuric acid-water nuclei and/or on the soot surfaces. The exact composition and partitioning were dependent on several parameters such as species volatility, initial concentration, and mass accommodation coefficients on soot. Well-controlled laboratory experiments were performed to understand the effects of the above key parameters, and provided a means to specify model parameterizations for a variety of volatile organic compounds.

In parallel with the laboratory studies, field measurements were performed on operating engines to understand the role that lubrication oil has in contributing volatile HCs to the particle phase. The obtained results clearly show that nanometer size particles are being vented from engines, and that their composition is the lube oil used in the turbofan engine lubrication system. Form the field measurements on in-service aircrafts, we found that the contribution from lubrication oil to total PM organic ranges from 5% to 100%, depending on engine type, age and maintenance.

1   INTRODUCTION

The hydrophilicity, composition, and size of atmospheric fine particles are critical to understanding their potential environmental, climate, and health impacts. It is believed that particle hydrophilicity is important for cloud formation (Kanakidou et al., 2005) and particle chemical composition affects particle radiative forcing properties (Schwarz et al., 2008). Both particle chemical composition and size were also found to determine their health impact (Seaton et al., 1995; Pope and Dockery, 2006). Aircraft emitted particulate matter (PM) in the atmosphere generally consists of liquid coated soot particles and homogeneous liquid droplets. The volatile (liquid) components of these particles mainly consist of sulfuric acid and condensable organic species. The role of sulfuric acid in the formation and atmospheric evolution of aviation PM has been widely studied (Kärcher, 1998; Wong et al., 2008; Kärcher and Yu, 2009). However, the effects of organic emissions on aviation PM for-

---

[*] *Corresponding author:* Zhenhong Yu, Aerodyne Research, Inc., 45 Manning Road, Billerica, MA 01821, USA. Email: zyu@aerodyne.com

mation and evolution is less understood, even though recent field measurements suggested that they are the most dominant components at low thrust settings due to incomplete combustion (Petzold et al., 2005; Timko et al., 2010a). Clearly, novel experimental and modeling approaches elucidating the role of organic emissions in the atmospheric evolution of hydrophilicity, composition, and size of aircraft emitted aerosols are needed to advance our understanding of the effects of aviation PM emissions on environment and human health.

2   EXPERIMENTAL AND MODELING RESULTS AND DISCUSSIONS

2.1 *Microphysical Modeling*

Nucleation of water-insoluble hydrocarbons was modeled independently from H_2SO_4-H_2O nucleation because water-insoluble hydrocarbons are not expected to participate in forming aqueous clusters via a nucleation process. Nucleation of water-soluble hydrocarbons was examined among possible pathways, including multi-component nucleation extended from binary sulfuric acid-water nucleation, binary hydrocarbon and water nucleation as well as separate unary nucleation. Clusters formed via nucleation can subsequently grow to larger particles via coagulation with other aqueous clusters or hydrocarbon clusters.
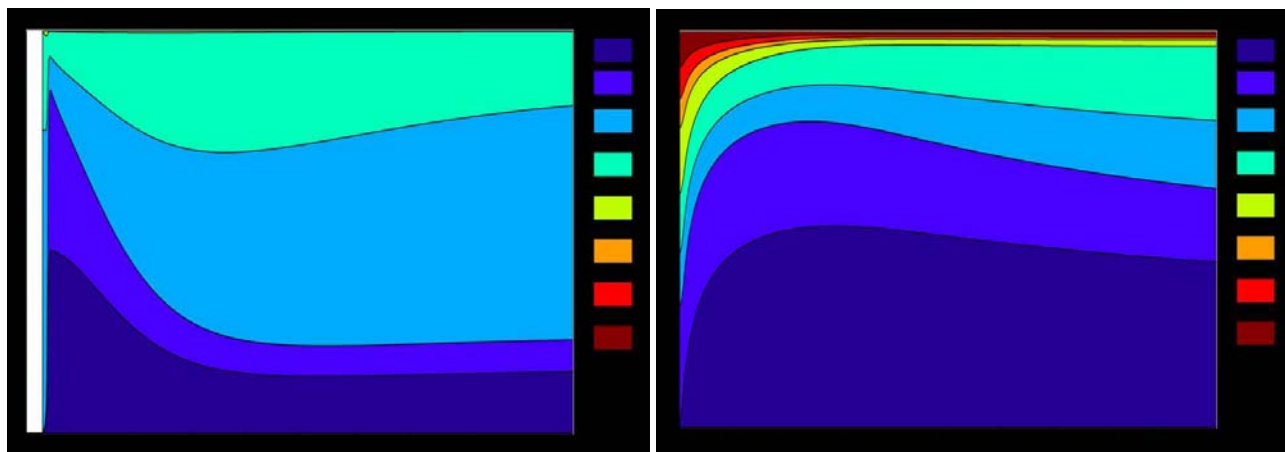
Figure 1 and 2 show evolution of mass compositions of liquid particles and soot coatings predicted from the model, respectively. The predicted mass composition of soot coatings is not significantly different from that of the soot coating without nucleation and coagulation modes; however, the soot particle growth is suppressed significantly as a result of decreasing total soot coating mass. About 80% of the total sulfate mass and about 50% of water-insoluble hydrocarbon mass was found moving to the nucleation mode as compared to results from calculations where only soot mode microphysics were considered. The mass composition of liquid particles, on the other hand, demonstrated that aqueous liquid aerosols in the initial aircraft plume started to have a substantial amount of water-insoluble hydrocarbons as they grew downstream. Smaller liquid particles tend to obtain more hydrocarbon mass fractions, and these particles with small aqueous cores and thick hydrocarbon films could be considered as primarily organic aerosols. This suggests that organics constitute a significant mass fraction in very fine aerosols, where species with low volatility (e.g., $C_{20}H_{12}$ and $C_{24}H_{12}$) could account for a significant amount of organic mass. The contribution of water-soluble hydrocarbons is almost negligible in the nucleation and coagulation processes, but they still can contribute to the growth of soot particles by enhancing the hydrophilic fraction of the soot surfaces and consequently the hygroscopic growth of the soot particles.

For the volatile composition of soot particles, the mass budget for individual species is divided into three modes:

1) soot coatings due to activation and condensation,
2) liquid aerosol droplets and embryos formed via nucleation and coagulation,
3) vapor phase including monomers and gases.

As shown in Figure 3,
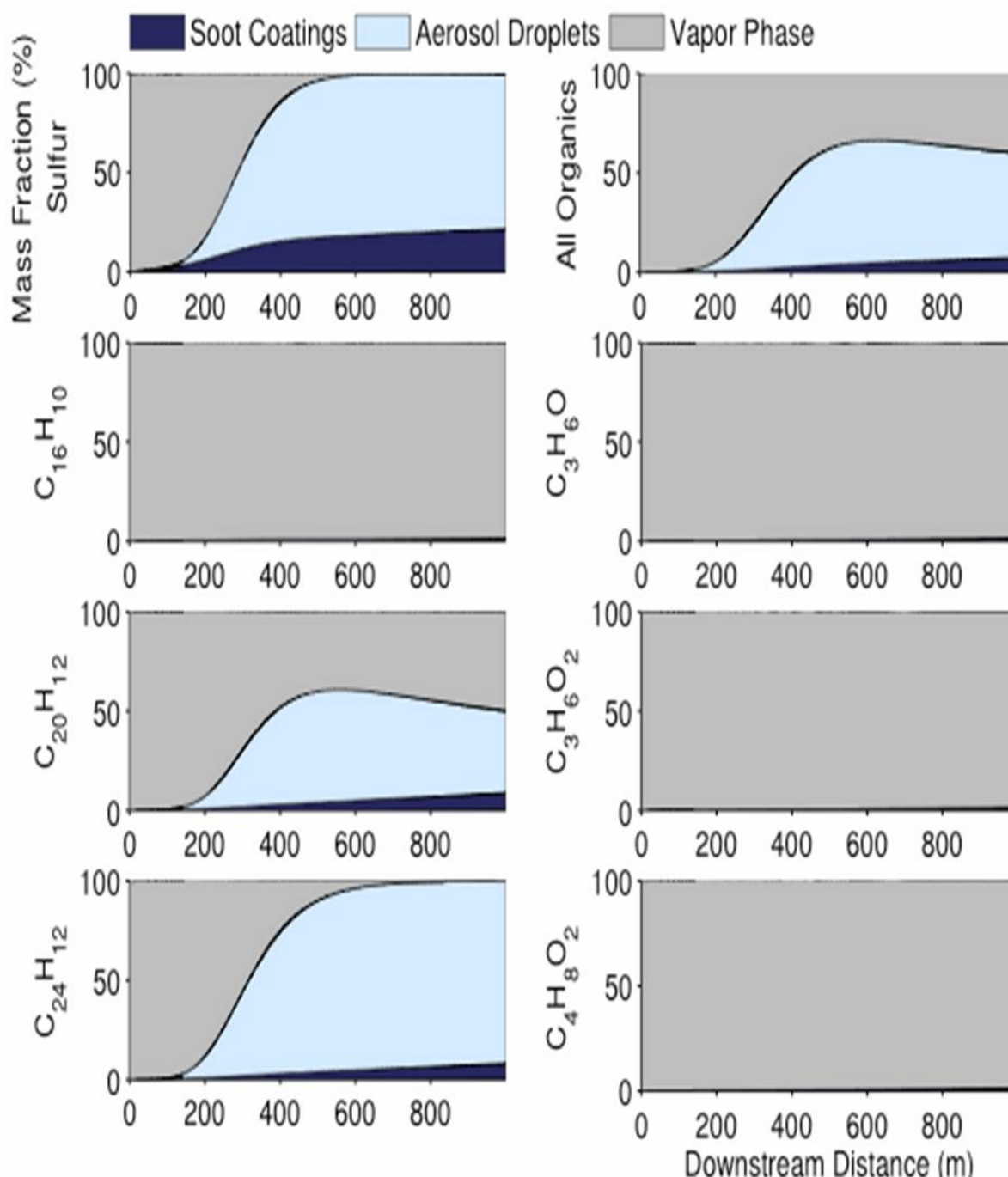
sulfate mass in aerosol droplets and soot coatings increased with downstream distance, and 100% of sulfate mass was transferred from vapor phase to liquid phase at 1 km downstream. Under high ambient relative humidity levels (such as 80% in this case), binary H_2SO_4-H_2O nucleation becomes a dominant process to transfer sulfate mass into aerosol droplets, even at a short distance downstream. This is significantly different than the prediction when the nucleation process is turned off in the simulation where all sulfate mass condensed on soot coatings. Soot particle growth, however, continues after depletion of sulfuric acid gas via scavenging of liquid aerosols on soot particles. For condensable water-insoluble hydrocarbons, similar evolutions were observed: hydrocarbon mass in the vapor phase is transferred relatively quickly into homogeneous liquid aerosols via condensation on or coagulation with homogeneous H_2SO_4-H_2O aerosols; this is followed by gradual coagulation of these particles with soot. Note, however, that benzopyrene ($C_{20}H_{12}$) mass fraction in the liquid droplets initially increases but starts to decrease at about 500 m downstream. Consequently, its mass fraction in the vapor phase increases because evaporation of the hydrocarbon species from smaller droplets occurs due to the Kelvin effect. This result implies that the nucleation mode is likely to be

more sensitive to the volatility of species than the soot mode because much smaller clusters and droplets are involved in the process. Water-soluble hydrocarbons, on the other hand, are not favored to be partitioned into homogeneous liquid particles or soot particles because of their high vapor pressure.

2.2 Laboratory Investigation

The microphysical modeling of gas to particle processing (e.g. condensation) on soot particles requires knowledge of species volatility, initial concentration, and mass accommodation coefficients on soot. The volatility and concentration establish the 'driving force' while the accommodation coefficient represents the efficiency of the gas-particle interaction. To investigate and understand the required parameters and compare to model predictions, controlled experiments were performed at UTRC with the help of ARI.

The combustion soot particles used in this study were produced by a miniCAST (Combustion Aerosol Standard, Model 5200). The geometric mean diameter (GMD) of the generated soot particles was controlled by precisely setting the flame stoichiometry and dilution parameters provided by the designer of the miniCAST. Before mixing with the vaporized VOCs, the soot stream was passed through a thermal denuder (TD) at 150 °C to remove the volatile and semi-volatile components and ensure low organic coating on the soot particles (Huffman et al. 2008). A schematic of experimental setup is show in Figure 4.
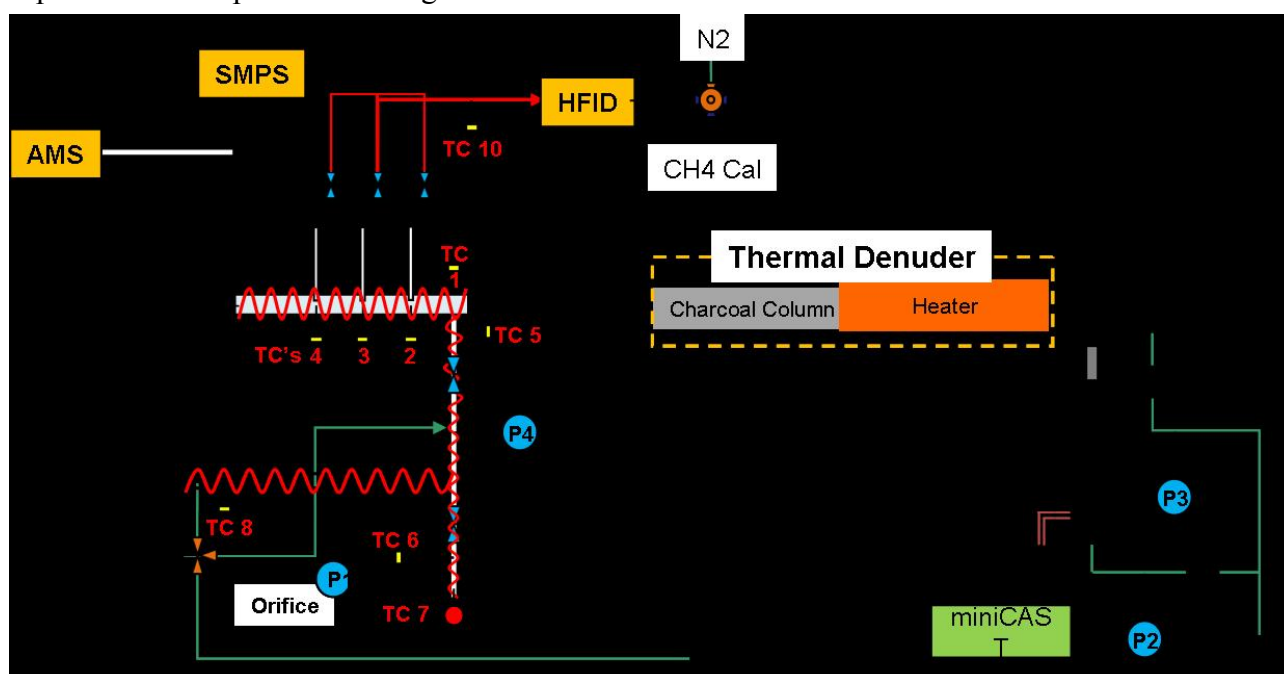
The effective uptake coefficient, γ_{obs}, can be experimentally determined by the measurements on uptake of VOC and collisions with soot per molecule as the following:
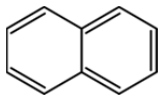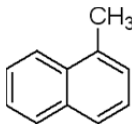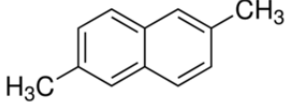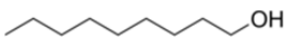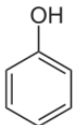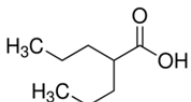
$$\frac{\Delta n}{n} = \gamma_{obs} \frac{cA_d N}{4F_g} \qquad (1)$$

where Δn is the VOC mass coated on soot particles and measured by the CToF-AMS; n is the concentration of the VOC vapor measured by the HFID; c is the mean thermal velocity of VOC vapor, which equals $\sqrt{\dfrac{8RT}{\pi M}}$; N is the total number of soot particles determined from the SMPS measurement; A_d is the surface area of soot particle; and F_g is the system flow rate. The determination of A_d is based on simultaneous SMPS and AMS measures (Cross et al. 2010).

For a variety of volatile organic compounds, the obtained uptake coefficients as well as some critial physical properties were listed in Table 1 for comparison.

Table 1. List of VOC physical properties and uptake coefficients on combustion soot particles determined in this work.

Name	Structural representation	MP (°C)	BP (°C)	VP at 25°C (Pa)	γ	R	Solubility in water (g/L)
Naphthalene		80	218	11.6	$(1.11\pm0.03)\times10^{-5}$	0.95	0.031
1-methyl-naphthalene		-22	240	9.03	$(8.5\pm0.4)\times10^{-5}$	0.99	0.026
2,6-dimethyl-naphthalene		106	264	2.12	$(1.79\pm0.06)\times10^{-4}$	0.80	0.0013
1-nonanol		-6	214	3.03	$(2.4\pm0.5)\times10^{-5}$	0.50	1.0
Phenol		43	182	46.6	$(1.36\pm0.09)\times10^{-5}$	0.96	8.3
Propylene glycol		-59	188	20.0	$(7.4\pm0.9)\times10^{-6}$	0.68	Fully misci-ble

Fresh combustion soot is typically considered as hydrophobic. As shown in Figure 5, the logarithm
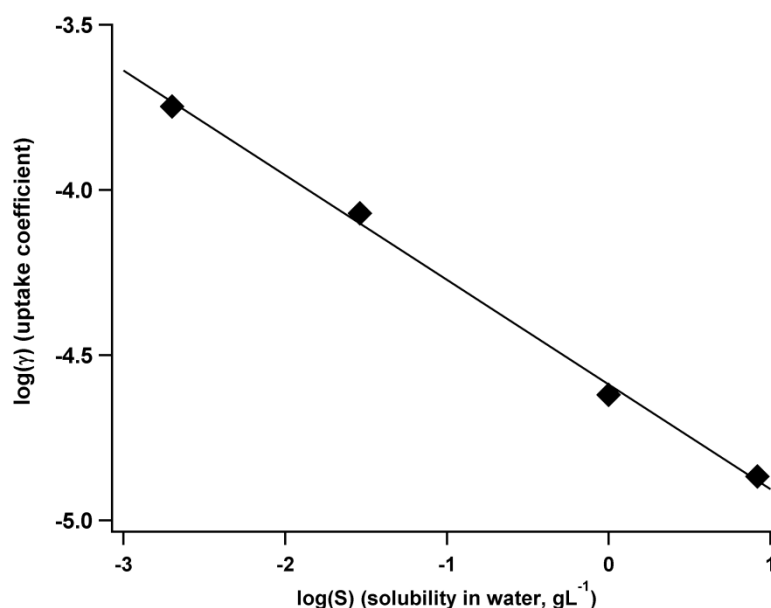
of uptake coefficient seems in a linear inverse correlation with the logarithm of solubility in water, in g L^{-1}. The slope of the linear fit is -0.32±0.01 and the correlation coefficient, R, is 0.999, implying a very strong correlation. This plot suggests that a phenomenological power-law relation exists between uptake coefficient of VOC on denuded combustion soot particle and solubility of VOC in water.

2.3 Field Measurements

The field measurements at Midway International Airport (MDW) and O'Hare International Airport (ORD) in Chicago were performed on February 17-18, 2010 with the help of Southwest Airlines, United Airlines and the City of Chicago. Emission plumes of the aircraft were investigated using a variety of gaseous and particulate measurement instruments located on board the Aerodyne mobile laboratory (Kolb et al. 2004; Herndon et al. 2005). Engine exhaust plumes were sampled through 1-inch outside-diameter stainless tubing in front of the laboratory and drawn into individual instru-

ments. A HR-ToFAMS was deployed to detect semi-volatile organic PM from aircraft engine exhaust.

All of the identified plumes described in this work were due to near-idle engine operation based on CO and NO_x concentrations: the ratio EI-CO/EI-NO_x is significantly larger than unity at idle operation. Tail numbers were recorded and used to verify the visual identification of engine/airframe.

Mass spectrum of semi-volatile composition of PM emissions was used to identify and characterize lubrication oil contribution. Intensity ratio of m/z=85 to m/z=71, I(85)/I(71), was used to quantify the lubrication oil emissions. The obtained results are listed in Table 2.

Table 2. Emission indices of organic PM (EI_m-org) and black carbon (EI_m-BC) due to the observed aircraft engine plume events as well as the determined oil contribution to organic PM. Events 1 – 5 are obtained from MDW while 6 – 12 from ORD.

Event	Engine	EI_m-org (mg kg^{-1})	EI_m-BC (mg kg^{-1})	I(85)/I(71)	Oil Type	Oil contribution
1	CFM56-7B24	-	-	-	-	-
2	BR715C1-30	386±49	200±47	5.9±0.8	ExxonMobil	0.66±0.10
3	CF34-3B1	-	-	-	-	-
4	CFM56-7B24	-	95±54	-	-	-
5	PW150A	-	-	-	-	-
6	PW4077	8±1	39±6	1.1±0.5	ExxonMobil	0.05±0.06
7	V2522-A5	10±2	206±10	3.7±0.7	ExxonMobil	0.38±0.09
8	PW2037	13±2	214±9	3.5±1.0	ExxonMobil	0.36±0.13
9 & 10	PW2037 & CF34-3B1	12±2	141±8	4.1±1.1	BP	1.00±0.35
11	AE3007A1P	-	117±31	-	-	-
12	CF4-8E5G01	46±2	-	2.4±0.4	BP	0.55±0.13

This work has demonstrated that aircraft engine lubrication oil emitted from aircraft deoiling system can be an important emission vector of semi-volatile hydrocarbon mass that does not have to do with the combustion process.

3   CONCLUSIONS

Based on the microphysical modeling, we found that organic coating on soot particles is strongly dependent on initial gaseous concentration and mass accommodation coeffceint. Uninary nucleation of hydrocarbon species is unfavorable; while homogeneous nucleation is driven by binary sulfuric acid-water nucleation and grown through condensation of hydrocarbon vapors.

Our laboratory investigation determined uptake coeffcient for a variety of organic compounds, water-soluble and water-insoluble. a phenomenological power-law relation exists between uptake coefficient of VOC on denuded combustion soot particle and solubility of VOC in water.

We found in this study that Oil from aircraft deoiling system is an important emission that is independent of combustion process. Using the developed Aerosol mass Spectrometer (AMS), lubrication oil emissions from a number of in-service commercial aircrafts were characterized and quantified.

REFERENCES

Cross, E. S., Onasch, T. B., Ahern, A., Wrobel, W., Slowik, J. G., Olfert, J., Lack, D. A., Massoli, P., Cappa, C. D., Schwartz, J. P., Spackman, J. R., Fahey, D. W., Sedlacek, A., Trimborn, A., Jayne, J. T., Freedman, A., Williams, L. R., Ng, N. L., Mazzoleni, C. Dubey, M., Brem, B., Kok, G. L., Subramanian, R., Freitag, S., Clarke, A., Thornhill, D., Marr, L. C., Kolb, C. E., Worsnop, D. R., and Davidovits, P. 2010. Soot Particle Studies - Instrumental Inter-Comparison – Project Overview. *Aerosol Sci. Tech.*, 44, 592-611.

Herndon, S. C.; Jayne, J. T.; Zahniser, M. S.; Worsnop, D. R.; Knighton, B.; Alwine, Lamb, B. K; Zavala, M.; Nelson, D. D.; McManus, J. B.; Shorter, J. H.; Canagaratna, M. R.;Onasch, T. B.; and Kolb, C. E. 2005: Characterization of urban pollutant emission fluxes and ambient concentration distributions using a mobile laboratory with rapid response instrumentation, *Faraday Discuss.*, 130, 327-339.

Kanakidou, M., Seinfeld, J. H., Pandis, S. N., Barnes, I., Dentener, F. J., Facchini, M. C., Dingenen, R. V., Ervens, B., Nenes, A., Nielsen, C. J., Swietlicki, E., Putaud, J. P., Balkanski, Y., Fuzzi, S., Horth, J., Moortgat, G. K., Winterhalter, R., Myhre, C. E. L., Tsigaridis, K., Vignati, E., Stephanou, E. G., and Wilson, J. (2005). Organic Aerosol and Global Climate Modelling: A Review. *Atmos. Chem. Phys.*, 5:1053-1123.

Kärcher, B. (1998). Physicochemistry of Aircraft-Generated Liquid Aerosols, Soot, and Ice Particles. 1. Model Description. *J. Geophys. Res.-Atmospheres*, 103:17111-17128.

Kärcher, B., and Yu, F. (2009). Role of Aircraft Soot Emissions in Contrail Formation. *Geophys. Res. Lett.*, 36:L01804, doi: 10.1029/2008GL036649.

Kolb, C. E.; Herndon, S. C.; McManus, J. B.; Shorter, J. H., Zahniser, M. S.; Nelson, D. D.; Jayne, J. T.; Canagaratha, M. R.; and Worsnop, D. R. 2004: Mobile Laboratory with Rapid response Instruments for Real-Time Measurements of urban and Regional Trace Gas and Particulate Distributions and Emissions Source Characteristics. *Environ. Sci. Technol.*, 38, 5694-5703.

Petzold, A., Gysel, M., Vancassel, X., Hitzenberger, R., Puxbaum, H., Vrochticky, S., Weingartner, E., Baltensperger, U., and Mirabel, P. (2005). On the Effects of Organic Matter and Sulphur-Containing Compounds on the Ccn Activation of Combustion Particles. *Atmos. Chem. Phys.*, 5:3187-3203.

Pope, C. A., and Dockery, D. (2006). Health Effects of Fine Particulate Air Pollution: Lines That Connect. *J. Air & Waste Manage. Assoc.*, 56:709-742.

Schwarz, J. P., Spackman, J. R., Fahey, D. W., Gao, R. S., Lohmann, U., Stier, P., Watts, L. A., Thomson, D. S., Lack, D. A., Pfister, L., Mahoney, M. J., Baumgardner, D., Wilson, J. C., and Reeves, J. M. (2008). Coatings and Their Enhancement of Black Carbon Light Absorption in the Tropical Atmosphere. *J. Geophys. Res.-Atmospheres*, 113:D03203, doi: 10.1029/2007JD009042.

Seaton, A., Godden, D., MacNee, W., and Donaldson, K. (1995). Particulate Air Pollution and Acute Health Effects. *The Lancet*, 345:176-178.

Timko, M. T., Onasch, T. B., Northway, M. J., Jayne, J. T., Canagaratna, M., Herndon, S. C., Wood, E. C., Miake-Lye, R. C., and Knighton, W. B. (2010). Gas Turbine Engine Emissions Part 2. Chemical Properties of Particulate Matter. *ASME J. Eng. Gas Turbines Power*, 132:061505, doi: 10.1115/1.4000132.

Wong, H.-W., and Miake-Lye, R. C. (2010). Parametric Studies of Contrail Ice Particle Formation in Jet Regime Using Microphysical Parcel Modeling. *Atmos. Chem. Phys.*, 10:3261-3272.

Modelling alternative fuels for aircraft: influence on the evolution and behaviour of aerosols

C. Rojo[*], X. Vancassel
Onera – The French Aerospace Lab, F-92322, Châtillon, France

Ponche, Jean-Luc
LMSCP, University of Strasbourg, 67482, France

Keywords: aircraft plumes, biofuels, particle formation and growth, organics, soot particles, condensation trails

ABSTRACT: Aircraft emit important amounts of particulate and gaseous matter in the atmosphere contributing to the increase of the total amount of anthropogenic emissions. Therefore aviation has most likely a significant impact on the atmospheric radiative budget and on climate change. Introducing alternative fuels in aviation can be considered as a viable option to reducing its impact, being economically and environmentally sustainable. There are several alternative fuels that are undergoing tests and evaluations to suit aviation regulations and infrastructure, in order to eventually substitute Jet A1. Recent experimental data indicates general trends in the emissions of these new fuels. Globally, Fischer Tropsch processed fuels are being considered. These tend to have lower aromatic and sulphur contents inducing a simultaneous reduction in sulphuric acid and soot emissions. However modifying the nature and composition of the fuel used can entail unexpected consequences. The main uncertainties concern the impact of airborne particles on the atmosphere. It is therefore essential to study and determine the evolution of aerosols in the aircraft plume. To manage this task, a microphysical trajectory box model is used, which has been previously tested with standard kerosene. It describes the expansion of the jet plume and the evolution of aircraft-produced aerosols. However, modelling aircraft plumes with alternative fuels have entailed a few revisions and adaptations of several microphysical processes. Therefore, homogeneous freezing has been considered in the model and may contribute in ice formation. Background aerosols entrained into the plume have also been taken into account since they now may also play a part in the aerosol evolution in the near field of an aircraft. The assessment of the changes in aerosol behaviour and evolution, depending on the fuel used could help determine the potential benefits for the environment of their introduction in aviation.

1 INTRODUCTION

Aviation has an impact on climate and local air quality. It affects the atmospheric composition by releasing gases such as carbon dioxide, water vapour, nitrogen and sulphur oxides, and particulate matter (soot), (Lee et al., 2009). These emissions are responsible of new particle formation in the plume, including contrails, and may increase cirrus cloudiness and deteriorate local air quality. As air traffic keeps increasing, these environmental issues which enhance climate change become more important. Scientists are working in various areas in order to limit the impact of aviation on the environment.

A viable choice to reduce this impact may be the use of alternative fuels. Not only would their introduction be beneficial for the environment, but it would also help providing an energetic independence towards petrol based fuels. Indeed as the price of the barrel of oil rises, other energetic sources are explored and favoured (IATA).

Introducing new fuels in aviation is likely to alter the composition and evolution of aircraft-produced aerosols, hence alter the impact of aviation on the atmosphere. Indeed, these changes in aerosol composition will have an influence on particle growth and contrail formation, and will have

---

[*] *Corresponding author:* Rojo Carolina, Onera – The French Aerospace Lab, F-92322, Châtillon, France

to be taken into account in the models. Therefore it is necessary to assess the influence of the jet fuels used on the entailed emissions in the near field of an aircraft.

Comprehensive studies have been made on aerosol emissions in aircraft plumes for typical Jet-A1 kerosene (e.g. Kärcher, 1995, 1998; Yu et al., 1998; Yu et al., 1999) but few studies are available for alternative fuels. These are expected to emit a significant amount of organic material, less primary particles and contain reduced sulphur levels (Timko et al., 2010).

The model we use in order to assess the atmospheric impact of these new fuels is a microphysical model developed by (Sorokin et al., 2001; Vancassel et al., 2010). However the model has to be adapted to simulate the combustion of alternative fuels and numerous parameters have to be revised. Our goal is to understand and predict the behaviour of gases and particles emitted and formed in an aircraft plume. Therefore, in this work, we focalize on the analysis of microphysical transformations of particles in aircraft plumes, so that they can be better taken into account in climate models. However, our results can provide first conclusions on the possible benefit of the use of alternative fuels.

2   ALTERNATIVE FUELS FOR AVIATION

Various types of alternative fuels are being investigated and must respect several criteria (Stratton et al., 2010). These criteria concern diverse areas, such as the compatibility with the infrastructure, the properties of the fuel or its elaboration. Alternative fuels which are likely to be used in the near future are the "drop-in" fuels, that is which can be used with the actual infrastructure and engines (DeWitt et al., 2008), and can also be mixed with standard kerosene without altering the fuel's properties. This type of fuel can be considered as a potential replacement of conventional kerosene. That excludes for example alternative alcohol-based fuels (Hileman et al., 2008). Alternative fuels should have similar characteristics as standard kerosene (Jet A1) for safety reasons. For instance, their properties have to be constant within the large temperature and pressure variations commonly encountered during flights (from   -60°C at 150 hPa to around 50°C at ground levels). Other aspects have to be taken into account when elaborating an alternative fuel. For example, some criteria are an efficient usage of land avoiding competition with food production or water resources. Additionally, these new fuels should emit lower lifecycle greenhouse gases in order to be beneficial for the environment (Stratton et al., 2010).

Several alternative fuels respect all these criteria: the fuels elaborated via Fischer-Tropsch (FT) synthesis and the hydrotreated renewable jet (HRJ). Fischer-Tropsch fuels can be produced from various sources such as coal (CtL), gas (GtL), biomass (BtL) and mixed coal and biomass (CBtL). However, BtL fuels are more beneficial for the environment since they induce a reduction of carbon dioxide emissions across their lifecycle. Hydrotreated renewable jets are mostly produced from biomass. Since 2011, many airline companies integrated these new sustainable fuels in their flights after their certification. They generally use blends of 20% to 50% of FT or HRJ fuels (ATAG.). A recent European directive (2009/2/EC) promotes the use of biofuels in the transport sector in order to reach a goal established at 10 % of alternative fuels used by 2020 (IFP).

In the last few years, several campaigns have taken place measuring the emissions of alternative fuels for aircraft such as AAFEX (Anderson, 2009; Anderson et al., 2011) or SWAFEA (Novelli, 2009). These campaigns provide large amounts of data, showing the trends observed when using different types of fuels.

The main differences when using FT fuels or HRJ are the reduction of soot emissions (due to the lower aromatic content of the fuels) and the reduction of the emitted sulphur. Consequently the 50/50 blends combustion exhausts will also present much lower sulphuric acid and aromatic concentrations, and its soot particle number will drop by 50% at intermediate engine power conditions (Timko et al., 2010). Indeed, since aromatics are soot precursors (Richter et al., 2000) and the blend has a diminished aromatic content, the soot emissions are reduced. We have reported the general trends observed in various campaigns in the following table.

Fuel	Standard Kerosene (~Jet A1)	Blend 50% Jet A1, 50% FT	100% alternative fuel (FT)
Soot (#/m³)	8×10^{11}	4×10^{11}	8×10^{10}
Refernces	Schumann et al. 2002	Hileman et al., 2008	Corporan et al., 2007
Sulfur content (ppm)	600	300	~ traces
Refernces	Hileman et al. 2010, PARTNER		
Organic Matter EI (mg.kg^{-1} fuel)	~50	20	10
References	Slemr et al. 2001, Spicer et al. 1994	Timko et al. 2010, Kinsey et al., 2010, AAFEX	

Table 1. Typical emissions measured or estimated for different fuels

These emissions are used to initialize our model. However, several adaptations must be carried out concerning freezing pathways and background aerosols entrainment, which are described in the next section. Indeed with such a reduction in soot emissions and in volatile particles (due to the lower content of fuel sulphur), these mechanisms and aerosols may play a much more important role.

3   MICROPHYSICAL PROCESSES AND MODEL DESCRIPTION

During flight, ambient air is sucked up by the jet engine. As combustion takes place, the aircraft engine emits a great number of gaseous and particulate compounds. In particular, sulphur contained in the fuel leads to the formation of sulphur oxides in the plume, which are partly converted into sulphuric acid (Reiner and Arnold, 1994).

Soot and organic matter (such as hydrocarbons), are mainly due to incomplete combustion of the fuel. These emitted gases and particles are now going to undergo several processes in the changing aircraft plume.

These processes can be simulated using trajectory box models (e.g. Miake-Lye et al., 1991; Kärcher, 1995) characterising aerosol microphysical properties in a parameterized jet plume, diluted isobarically and homogeneously in the atmosphere. This kind of model as illustrated in figure 1, using basic plume description is very convenient to take into account all the main processes of transformation of gaseous and particulate combustion products in a comprehensive manner.
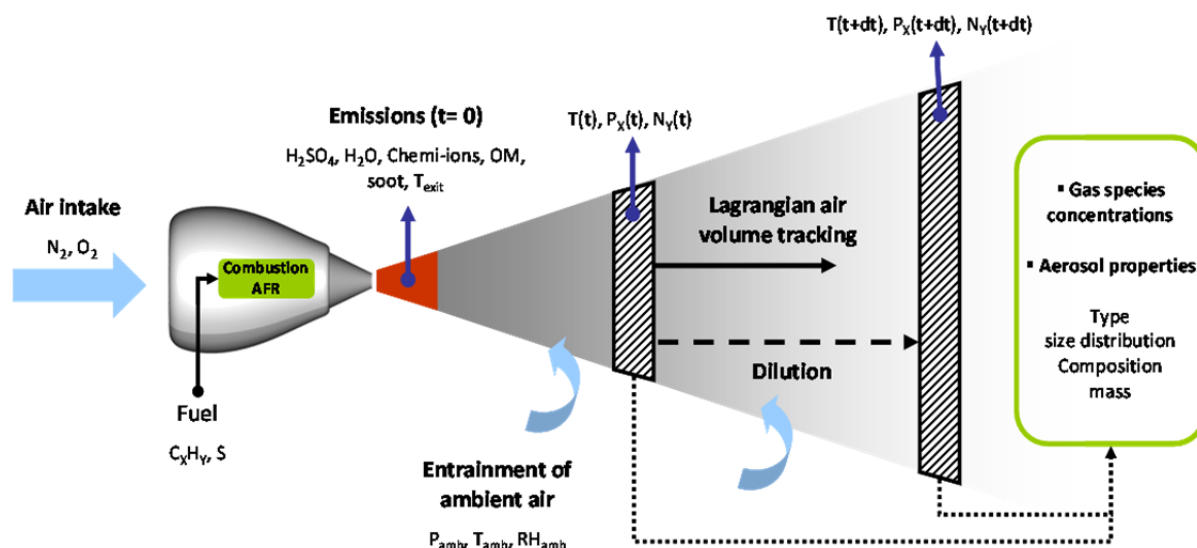
Figure 1. Scheme of the modelling of an aircraft plume

The model we have been developing, based on Kärcher (1998), Yu et al. (1997), Sorokin et al. (2001) and Vancassel et al. (2004), provides 11 types of aerosols (Neutral and Negative Sulphate Clusters, Dry Soot, Activated Soot, Neutral and Positive Organic Clusters, Neutral Positive and Negative Mixed Aerosol, Ice Particles homogeneously and heterogeneously formed), and includes many physical processes.

The model considers an initial mixture of sulphuric acid, water vapour, organics, chemi ions and soot particles.

Chemi ions are typically positive organic clusters and negative sulphate (Arnold et al., 2000). The question of organics, which will become crucial with new fuels, has been handled following Yu et al. (1999).

At the engine nozzles' exit, the temperature is around 580-600K. The plume is then affected by a very fast cooling and dilution. The dilution, i.e. the volume change, due to entrainment of ambient air is associated to the temperature variation.

During the simulation, the Lagrangian model follows the particle in the plume, and the continuity equation for the mixing ratio χ of gaseous or particulate compounds can be separated into mixing processes, chemical reactions and microphysical processes. The last point can be divided into nucleation of volatile particles, condensation of water vapour and sulphuric acid, Brownian coagulation and freezing:

$$\left(\frac{d\chi}{dt}\right)_{micro} = \left(\frac{d\chi}{dt}\right)_{nuc} + \left(\frac{d\chi}{dt}\right)_{cond} + \left(\frac{d\chi}{dt}\right)_{coag} + \left(\frac{d\chi}{dt}\right)_{frz} \qquad (1)$$

These thermodynamic processes are going to influence particle evolution.

Nucleation. The formation of secondary aerosols takes place via the creation of a liquid/vapour interface, requiring an energy supply (e.g. Pruppacher et al., 1997). This energy barrier has to be overcome by the nucleus to homogeneously nucleate. In the case of heterogeneous nucleation, the energy barrier is lowered by the presence of material such as soot which acts as condensation nuclei. Classical nucleation is not suitable to explain new particle formation in aircraft plumes (Yu et al., Turco, 1997). Notably sulphuric acid ion clusters improve cluster particle formation and accelerate subsequent growth by collision mechanisms. Charge-enhanced condensation and coagulation are treated by adjusting the accommodation coefficients appropriately.

Coagulation. Freshly nucleated particles, characterized by Brownian motion, are going to scatter and collide with each other. In our model, which takes into account multiple types and multicomponents aerosols, we have used a complex solution from (Jacobson, 2002).

Water uptake. Aerosols in the aircraft plume may grow by water uptake, which is calculated in two different ways.

When the relative humidity is under 100%, the equilibrium between sulphuric acid and water in the droplet is quasi-instantaneous, i.e., water molecules' uptake is adjusted to the sulphuric acid content of the particle via hydration/evaporation which is typical for atmospheric particles (Steele and Hamill, 1981). In supersaturated conditions (RH above 100%), the water uptake is kinetically controlled. The aerosols' mass and radius variation is determined by solving the classical mass transport equation. The presence of organics tends to modify water uptake as they change the particle composition and therefore the respective components' mole fraction and activity. The question of the hygroscopic behaviour of organics is difficult to address since it requires a choice of the organic species considered and a precise knowledge of its thermodynamic properties. In a first attempt, we have used the assumption that the organic hygroscopicity was lower than sulphuric acid in the way suggested by (Kärcher and Koop, 2005).

Freezing. There are two pathways describing the freezing mechanisms, the heterogeneous freezing and the homogeneous freezing. Generally the latter is neglected in relation to the former, notably when conventional kerosene is used, due to the large amounts of condensation nuclei and due to the acidity of the aqueous mixture.

Heterogeneous freezing consists in water vapour condensing onto activated soot in supersaturated conditions, which then freezes. If the conditions required are met, ice particles are formed and condensation trails can be observed. The corresponding ice nucleation rate is calculated using the classical theory (Fletcher, 1958; Pruppacher and Klett, 1997). The presence of the soot nucleus reduces the free energy of formation of the critical ice. This approach assumes that a liquid coating forms first and freezes subsequently. Due to thermodynamic considerations, a transition between gas and solid, through a supercooled solution is necessary in terms of energy to be provided. Besides, measurements in fresh exhaust plumes indicate the spherical shape of the ice crystals, which confirms that a liquid state was initially reached before freezing.

Homogeneous freezing does not require any solid support or condensation nuclei, which explains the higher energetic barrier to overcome in order to form ice crystals.

4   RESULTS AND DISCUSSION

Homogenous freezing is commonly neglected when simulating aircraft plumes in which conventional fuel is used. Indeed in this case, heterogeneous freezing is the dominant ice nucleation pathway. However, as the soot emissions decrease, the homogeneous freezing is expected to become more significant while heterogeneous freezing diminishes (Kärcher et al., 2007). In order to assess the possible role of each ice nucleation pathway, we have simulated various cases starting with the standard emissions of Jet A1, and then progressively reducing the soot emissions only. As the number of emitted soot increases, ice formation via homogeneous freezing declines rapidly, whilst the surface of ice formed heterogeneously rises. At a 90 % soot emission reduction, characteristic of an alternative fuel, the two pathways are in competition.

However, alternative fuels are characterised not only by a reduction in soot emissions but also by a diminution of sulphuric acid formation, hence a decrease in particle volatile size and number as illustrated in figure 2. Therefore, in the simulations with alternative fuels, little difference is observed when considering homogeneous freezing. Nevertheless, it is imaginable that soot emission reduction will continue further on, and in that case, homogeneous freezing may be the predominant ice formation pathway.
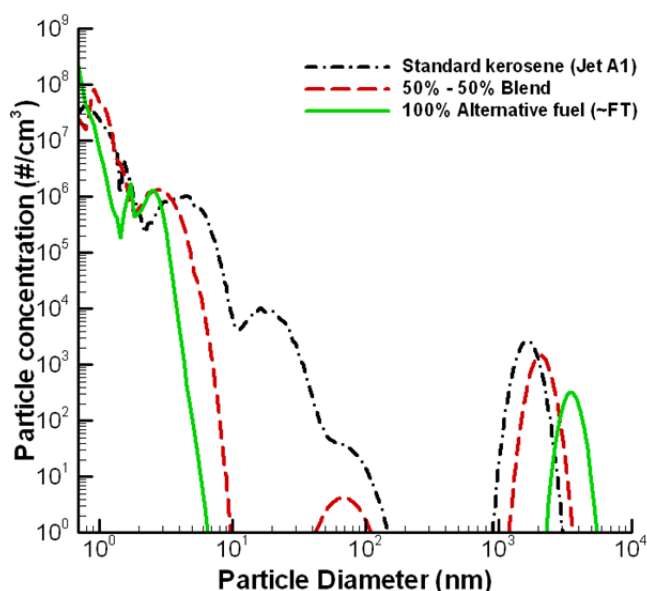
Figure 2. Size distributions of aerosols emitted and formed in aircraft plumes at 125 m behind the engine nozzle, using various fuels. In black dotted a standard kerosene; in red dashed a 50% blended fuel (FT-Jet A1) and in green solid a 100% FT fuel
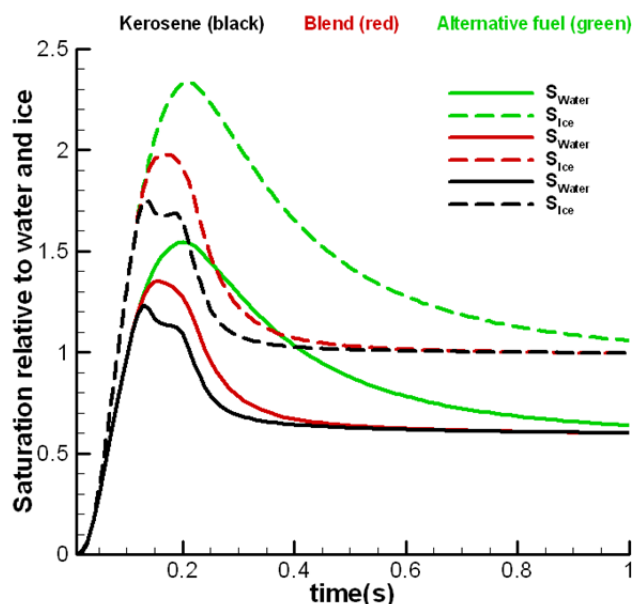
Figure 3. Water and ice saturation ratios in diluting aircraft plumes using various fuels. In black dotted a standard kerosene; in red dashed a 50% blended fuel (FT-Jet A1) and in green solid a 100% FT fuel

In figure 2, simulations of the emissions from three different types of fuels are shown. The black dotted line depicts the size distribution of aerosols from the combustion of kerosene; the red dashed line represents the aerosols from a 50% blended fuel (FT-Jet A1) and the green solid line a 100% FT fuel. A reduction of volatile particles (diameters around 10nm) using an alternative fuel is revealed as expected, along with a reduction of soot (diameters around 100 nm). The consequences on ice formation are a reduction of the number of crystals (about 10 times less) accompanied by an increase of the crystal size (about 3 times bigger). These variations in the crystal properties may have an influence on the optical depth of the formed condensation trail and hence, an impact on the radiative budget of the atmosphere.

Modifying the fuel used in aviation may also have an impact on the water and ice saturation ratios in the plume. Illustrated in figure 3, the water saturation is depicted in solid lines with the same colour code than previously used (black kerosene, red blend, green FT). The ice saturation ratio is

shown in dashed lines. When burning an alternative fuel, supersaturated conditions are encountered during longer times. This phenomenon is explained by the fact that fewer soot particles are present in the plume, therefore bigger amounts of water remain in the gas phase. This may induce the formation of larger but fewer aerosols. In a similar way, the ice crystals formed not only may increase to larger sizes but might be considerably more persistent.

The aerosol number reduction entailed by the introduction of alternative fuels leads to the consideration of other formerly often neglected processes in the near field. For instance, the entrainment of background aerosols could no longer be ignored. Their contribution in the plume is expected to be more important, especially in aircraft corridors. If we consider the ambient soot for example, as illustrated in figure 4, its contribution to the soot in the plume increases when using a blended or a FT fuel.
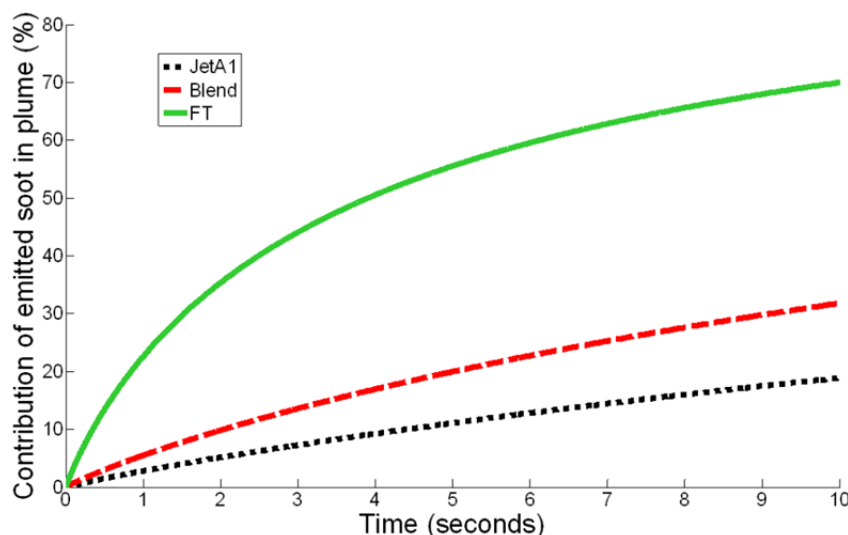
Figure 4. Contribution of background soot particles during the dilution of three aircraft plumes using various fuels. In black dotted a standard kerosene; in red dashed a 50% blended fuel (FT-Jet A1) and in green solid a 100% FT fuel

Not only the contribution of background particles may be more important, but taking them into account may also modify the mean properties of the aerosols in the plume. Indeed, if we consider the entrainment of ambient soot particles, the mean composition of soot might be altered.

5   CONCLUSIONS

As the amounts of alternative fuels used in the aeronautical sector increase, the assessment of their impact on the environment becomes essential. Therefore, this work uses a microphysical model capable to simulate the emissions of various fuels and their evolution in the near field of an aircraft.

The reduction in soot emissions and in formed volatile particles induced by the introduction of these new fuels may affect the behaviour of the aerosols in the aircraft plumes. Indeed, the ice crystals formed might attain larger sizes and their number might decrease, possibly changing the optical properties of the contrails.

However, our findings also point out the necessity of taking into account various processes usually neglected. The background particles might indeed play a larger part during the aerosols' evolution. The possible greater reductions in soot also may point out the importance of mechanisms such as homogeneous freezing.

Conjointly to these considerations, efforts are being made in the speciation and integration of organic matter and its properties in the model.

REFERENCES:

Arnold, F., Kiendler, A., Wiedemer, V., Aberle, S., Stilp, T., Busen, R., 2000. Chemiion concentration measurements in jet engine exhaust at the ground: Implications for ion chemistry and aerosol formation in the wake of a jet aircraft. *Geophys. Res. Lett. 27*, PP. 1723–1726.

Anderson, B.E., 2009. Alternative Aviation Fuel Experiment (AAFEX).

Anderson, B.E., Beyersdorf, A.J., Hudgins, C.H., Plant, J.V., Thornhill, K.L., Winstead, E.L., Ziemba, L.D., Howard, R., Corporan, E., Miake-Lye, R.C., Herndon, S.C., Timko, M., Woods, E., Dodds, W., Lee, B., Santoni, G., Whitefield, P., Hagen, D., Lobo, P., Knighton, W.B., Bulzan, D., Tacina, K., Wey, C., VanderWal, R., Bhargava, A., 2011. Alternative Aviation Fuel Experiment (AAFEX).

ATAG, Aviation Environment. URL www.enviro.aero

DeWitt, M.J., Corporan, E., Graham, J., Minus, D., 2008. Effects of Aromatic Type and Concentration in Fischer−Tropsch Fuel on Emissions Production and Material Compatibility. *Energy Fuels 22*, 2411–2418.

Fletcher, N.H., 1958. Size Effect in Heterogeneous Nucleation. *The Journal of Chemical Physics 29*, 572.

Hileman, J.I., Wong, H.M., Ortiz, D., Brown, N., Maurice, L., Rumizen, M., 2008. The feasibility and potential environmental benefits of alternative fuels for commercial aviation, in: *Proceedings of the 26th International Congress of the Aeronautical Sciences.*

IATA, 2010 Report on Alternative Fuels.

IFP, IFP Energies nouvelles. URL http://www.ifpenergiesnouvelles.com

Jacobson, M.Z., 2002. Analysis of aerosol interactions with numerical techniques for solving coagulation, nucleation, condensation, dissolution, and reversible chemistry among multiple size distributions. *J. Geophys. Res. 107*, 23 PP.

Kärcher, B., 1995. A trajectory box model for aircraft exhaust plumes. *J. Geophys. Res. 100*, 18835–18844.

Kärcher, B., 1998. Physicochemistry of aircraft-generated liquid aerosols, soot, and ice particles 1. Model description. *J. Geophys. Res. 103*, 17,111–17,128.

Kärcher, B., Koop, T., 2005. The role of organic aerosols in homogeneous ice formation. *Atmos. Chem. Phys. 5*, 703–714.

Kärcher, B., Möhler, O., DeMott, P.J., Pechtl, S., Yu, F., 2007. Insights into the role of soot aerosols in cirrus cloud formation. *Atmos. Chem. Phys. 7*, 4203–4227.

Lee, D.S., Fahey, D.W., Forster, P.M., Newton, P.J., Wit, R.C.N., Lim, L.L., Owen, B., Sausen, R., 2009. Aviation and global climate change in the 21st century. *Atmos. Environ. 43*, 3520–3537.

Miake-Lye, R.C., Martinez-Sanchez, M., Brown, R.C., Kolb, C.E., 1991. Plume and wake dynamics, mixing and chemistry behind an HSCT aircraft. *AIAA paper*.

Novelli, P., 2009. Sustainable Way for Alternative Fuels and Energy in Aviation (SWAFEA).

Pruppacher, H.R., Klett, J.D., 1997. *Microphysics of clouds and precipitation.* Springer.

Reiner, T., Arnold, F., 1994. Laboratory investigations of gaseous sulfuric acid formation via SO3+H2O+M→H2SO4+M: Measurement of the rate constant and product identification. *The Journal of Chemical Physics 101*, 7399–7407.

Richter, H., Howard, J.B., 2000. Formation of polycyclic aromatic hydrocarbons and their growth to soot–a review of chemical reaction pathways. *Progress in Energy and Combustion Science 26*, 565–608.

Sorokin, A., Vancassel, X., Mirabel, P., 2001. On volatile particle formation in aircraft exhaust plumes. *Phys. Chem. Earth. (C). 26*, 557–561.

Steele, H.M., Hamill, P., 1981. Effects of temperature and humidity on the growth and optical properties of sulphuric acid—water droplets in the stratosphere. *J. Aerosol Sci. 12*, 517–528.

Stratton, R.W., Wong, H.M., Hileman, J.I., 2010. Life cycle greenhouse gas emissions from alternative jet fuels. Partnership for AiR Transportation Noise and Emissions Reduction. Massachusetts Institute of Technology, Cambridge, MA.

Timko, M.T., Yu, Z., Onasch, T.B., Wong, H.-W., Miake-Lye, R.C., Beyersdorf, A.J., Anderson, B.E., Thornhill, K.L., Winstead, E.L., Corporan, E., DeWitt, M.J., Klingshirn, C.D., Wey, C., Tacina, K., Liscinsky, D.S., Howard, R., Bhargava, A., 2010. Particulate Emissions of Gas Turbine Engine Combustion of a Fischer−Tropsch Synthetic Fuel. *Energy Fuels 24*, 5883–5896.

Vancassel, X.P., Garnier, F.A., Mirabel, P.J., 2010. *In Plume Physics and Chemistry. Encyclopedia of Aerospace Engineering.*

Yu, F., Turco, R.P., 1998. The formation and evolution of aerosols in stratospheric aircraft plumes: Numerical simulations and comparisons with observations. *J. Geophys. Res. 103*, 25,915–25,934.

Yu, F., Turco, R.P., Kärcher, B., 1999. The possible role of organics in the formation and evolution of ultrafine aircraft particles. *J. Geophys. Res. 104*, 4079–4087.

Future Arctic Shipping routes and European air quality in 2025

J. E. Williams[*], P. F. J. van Velthoven
Royal Netherlands Meteorological Institute, De Bilt, The Netherlands

Keywords: Shipping Emissions, Air Quality, Future effects, Europe

ABSTRACT: Future SRES emission projections (A1B) for 2025 estimate that the relative contribution of shipping emissions towards total emissions from the transport sector increases markedly as a result of new shipping routes and a corresponding mitigation of road transport and non-transport emissions by new technologies. Compared to 2000 this shifts transport emissions northwards into a region which is exhibiting rapid changes with respect to sea-ice coverage and temperature. Here we present the results of simulations performed as part of the EU-QUANTIFY project which focus on the impact of these shipping emissions on European air-quality. We find there is a strong seasonality in the changes in near-surface O_3 around the Europe compared to 2003, resulting in a decrease in near-surface O_3 during boreal wintertime around the source regions and increases during boreal summertime. Comparing the impact of regional shipping emissions between 2003 and 2025 shows that, although there are similar effects, the largest increases in near-surface O_3 occur along the new shipping routes to the west of Ireland away from the continent. The enhanced in-situ O_3 production due to increases in shipping NO_X around the coast is mostly negated by the simultaneous mitigation of non-transport and road transport emissions

1 INTRODUCTION

The emission of nitrogen oxides (NO_X) by the shipping sector has been shown to exert a significant impact towards tropospheric ozone (O_3) in the lower troposphere for 2003, (Hoor et al, 2009) especially in the Northern Hemisphere (NH). Estimates in the future SRES A1B emission scenarios (Nakicenovic et al., 2000) project an increase in Shipping NO_X Emissions (SNE) from ~4.8 Tg N yr^{-1} in 2000 to ~6.5 Tg N yr^{-1} in 2025 (Eide et al, 2007). This increase principally occurs along the most dominant global shipping routes such as that from Asia towards Europe and around Africa. However these estimates can be considered as upper bounds as recent studies have shown that decreases in global shipping emissions have occurred during the last few year as a result of the decrease in global trade that has occurred since 2008 (de Ruyter de Winter, 2012), with the global economy now experiencing a prolonged recession. By 2025 the total SNE is predicted to be of an equal magnitude as those from road transport due to the successful mitigation of NO_X emissions from vehicles (Hodnebrog et al, 2011). In combination with the estimated decrease in future non-transport NO_X emissions (Nakicenovic et al., 2000) this means that a larger fraction of anthropogenic NO_X emissions is shifted off-shore and emitted directly into the Marine Boundary Layer (MBL). The regions in which SNE are released is also changing, with the increasing loss of Arctic Sea ice, meaning new shipping routes are expected in the high north. The strong seasonal cycle in the photo-chemical activity in the Arctic region related to the Polar Winter means that the changes imposed on the composition of the lower tropospheric deserve further investigation.

Here we analyse the results of a set of simulations completed as part of the EU-QUANTIFY project for differentiating the effects of future shipping emissions on global composition using the Chemistry Transport Model TM4. Due to the uncertainty associated with estimating anthropogenic future emissions (Smokers et al, 2011) we limit our analysis to the potential effects during 2025. One of the most dramatic changes in shipping is expected to occur in the Arctic Circle therefore we

---

[*] *Corresponding author:* Jason Williams, Chemistry and Climate division, Royal Netherlands Meteorological Institute, De Bilt, The Netherlands. Email: williams@knmi.nl

concentrate on the European Domain in order to assess the impact that the re-distribution of anthropogenic emissions has on regional air quality. We use a model simulation with perturbed shipping emissions to assess the relative impact this transport sector has on tropospheric O_3 in the lower troposphere.
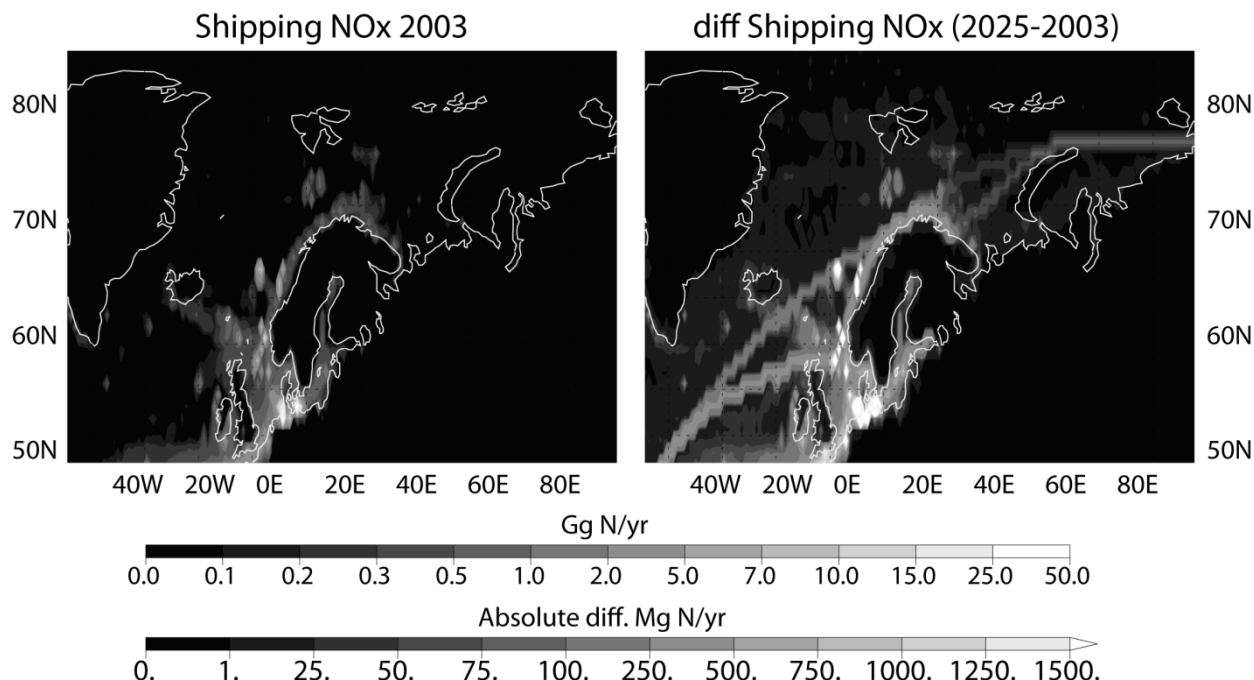
2   THE INCREASE IN EUROPEAN SHIPPING EMISSIONS

Figure 1: The annually integrated distribution of shipping NO_x emissions around Europe as provided in Endresen et al, 2007 (left panel). The associated increase in shipping NO_x emissions in 2025 as provided in Eide et al, 2007 (right panel).

Figure 1 shows the regional distribution in SNE for the year 2000 as an annual total (Endresen et al, 2007), along with the increase in Mg N yr-1 for 2025 using the estimates of Eide et al (2007). As would be expected the highest SNE occurs along the most active shipping routes in the Baltic, the North Sea, and around the Netherlands coast and the Norwegian Coast. Analysing the distribution in the increases in SNE for 2025 reveals that the increased traffic between Canada and Asia is due to shipping routes that cross the Arctic circle as a result of increased accessibility. The largest increases occur at the entrance to the Baltic Sea around Denmark, especially around Bremerhaven, the estuary which connects Hamburg with the Sea and also Rotterdam harbour in the Netherlands and along the shipping routes from Africa (not shown), which pass along the Portuguese Coast, through the Bay of Biscay and into the North Sea. There are also noticeable increases around the oil platforms off the Norwegian Coast. Although we only choose the show differences in the NO_x emissions there are associated differences in emissions of CO, SO_2 and non-methane hydrocarbons.

Due to the reductions in both regional non-transport anthropogenic emissions (from 2.94 Tg N yr^{-1} to 2.17 Tg N yr^{-1}) and those related to road transport, the fraction of anthropogenic NO_x originating from shipping increases from ~12% (2003) to ~23% (2025) in this scenario for the European Domain shown in Fig. 1. Some seasonality exists in the shipping emissions as a result of the Arctic shipping routes only being passable during the boreal summertime when sea-ice coverage is low.

3   MODEL DESCRIPTION

The version of TM4 used here employs a vertical resolution of 34 levels, a horizontal resolution of 3° x 2° and is driven by ECMWF meteorological data fields. It has recently participated in several multi-model studies and performs close to the model ensemble average (Myhre et al., 2011; Hodnebrog et al, 2011). For the chemistry component the modified CBM4 scheme is adopted, which has

recently been updated with the most recent recommendations for the reaction data (Williams and van Noije, 2008). The emission scenarios employed are the SRES estimates for 2000 and follow the A1B scenario for 2025 (Nakicenovic et al., 2000), with shipping emissions being taken from Endresen et al. (2007). Biomass burning and biogenic contributions are fixed throughout for both the present and future simulations in order to focus on the anthropogenic effects. For a complete description of the emissions employed the reader is referred to Hodnebrog et al, (2011). The meteorological data for 2003 is used for all simulations so that the possible effects due to climatic change and changing surface albedo are excluded in this study. It should also be noted that no diurnal cycle is applied to any of the emissions from the transport sector and that sub-grid plume chemistry is also neglected which could moderate the results shown here by altering the in-situ production of tropospheric O_3 (Kim et al., 2009).

We compare the simulations for 2003 and 2025 against the corresponding simulations where there is a 5% perturbation (reduction) in the estimated shipping emissions. Using the same meteorology to drive TM4 allows the differentiation between the effects of the shipping sector on tropospheric composition and air-quality. The methodology behind this approach has been described in the literature by Grewe et al. (2010), where a 5% perturbation in shipping emissions is applied and transformed into a 100% effect using a linear scaling approach.

4   EFFECT OF SHIPPING EMISSIONS ON EUROPEAN NEAR-SURFACE OZONE
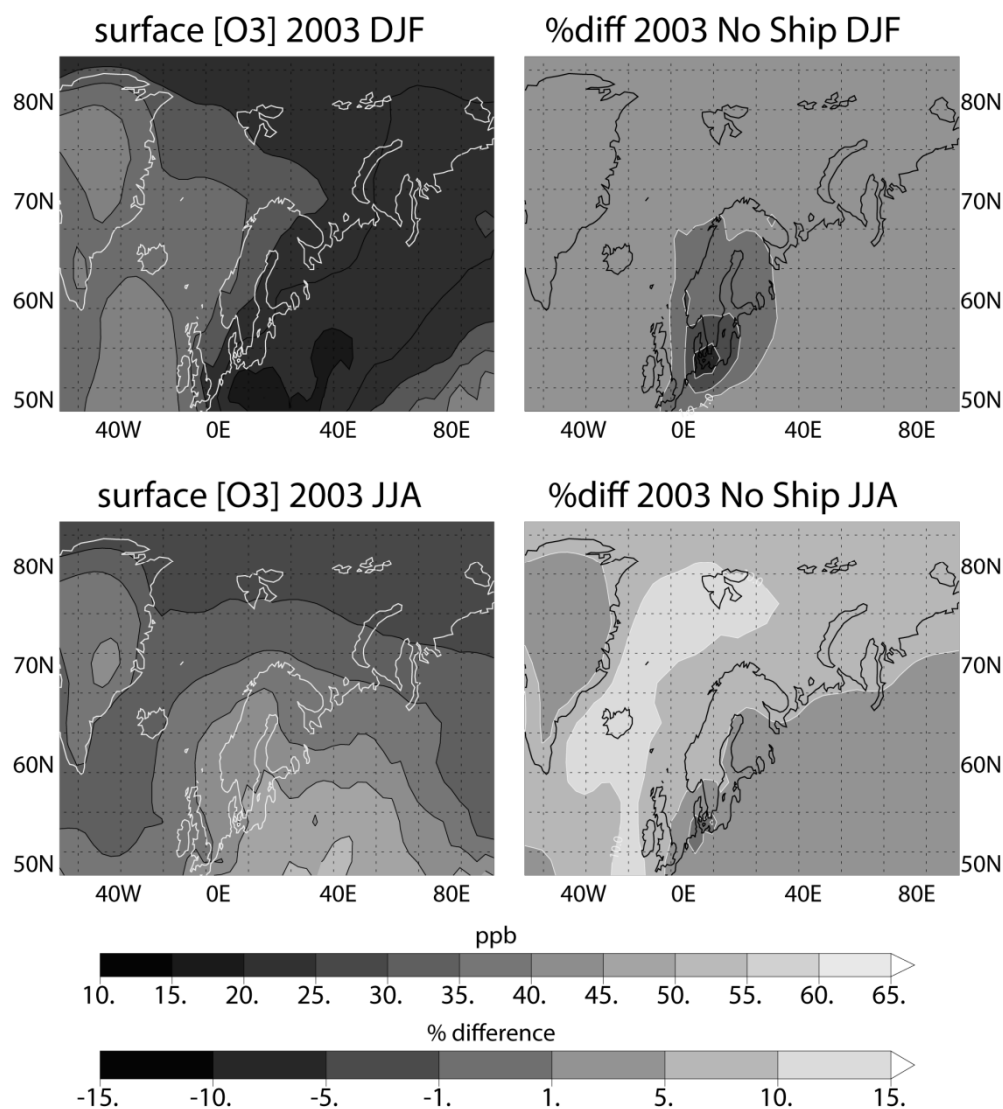
Figure 2: The seasonal distribution in near surface (0-500m) O3 in Europe for seasons DJF (top) and JJA (bottom). The impact of SNE for each season is also shown, where the differences are calculated using (2003-no_ship)/2003.

Figure 2 shows the distribution of near-surface (0-500m) mixing ratios of tropospheric O_3 for the seasons December-January-February (DJF) and June-July-August (JJA) for 2003. Also shown is the influence of SNE on the distribution of near-surface O_3 calculated using the 5% perturbation run. Here the relative differences are calculated using the relationship (2003-NOSHIP/2003).

For DJF the surface mixing ratios of O_3 are relatively low (~20-30 ppb) across the entire European continent. The highest mixing ratios of ~35-45 ppb occur over the Atlantic to the west of Ireland and over Greenland. This is anti-correlated with the seasonal distribution of NO_X, where the highest resident mixing ratios in NO_X occur over the Benelux countries (not shown). When analysing the distribution of the differences imposed by shipping emissions on O_3 mixing ratios, there is a clear reduction in near-surface O_3 of up to 7% around Northern Germany, Denmark and southern Norway. This is due to the low photo-chemical activity which occurs for this season due to the short days (i.e. suppressed NO_X re-cycling between NO and NO_2 and O_3 formation), high NO_X mixing ratios and that NO_X is introduced as NO, which titrates near-surface O_3. Further away from these high SNE locations there are modest increases of between ~2-5%

For JJA the surface mixing ratios are generally higher when compared to DJF (~30-55 ppb), with the maximal values being found towards southern Europe and the Mediterranean which experience high photo-chemical activity. The longer days in this season result in SNE enhancing in-situ O_3 production compared to DJF. Also there are more shipping emissions emitted towards the Arctic for this season. This increases resident mixing ratios in near-surface O_3 by between 5-15% around the UK, Iceland, Norway and the surrounding ocean. The largest increases occur out in the Atlantic close to the location of the SNE, where increases of 10-15% occur that have important implications for the oxidative capacity of the MBL.

5 CHANGES IN NEAR-SURFACE OZONE IN EUROPE DURING 2025
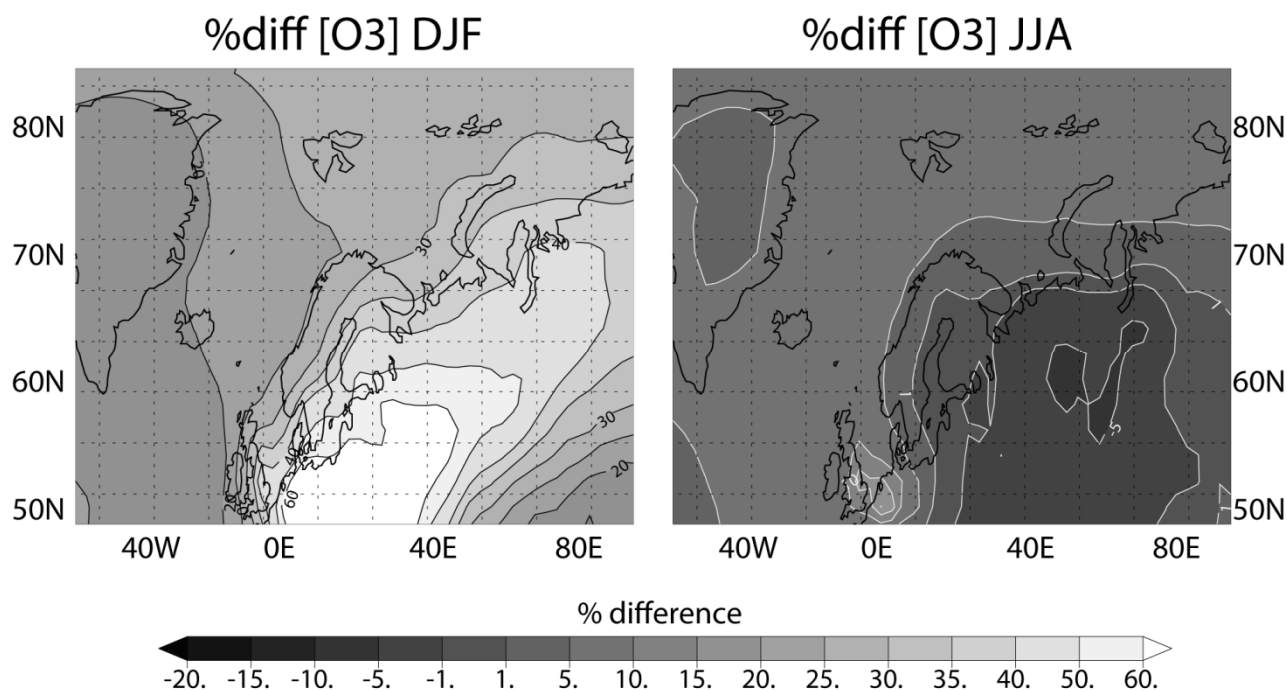
Figure 3: The percentual differences between the seasonal distribution in near surface (0-500m) O_3 between 2003 and 2025. The differences are calculated using the following relationship: (2025-2003)/2003.

Figure 3 shows the percentual differences in the distribution of near-surface O_3 between 2003 and 2025, where differences are calculated using the relationship (2025-2003/2003). It can be seen that there is a strong seasonality in the difference between these years, where both regional increases and decreases occur in the resident mixing ratios. This net change is the result of the cumulative changes in both the transport and non-transport emissions due to anthropogenic activity estimated for the year 2025.

For DJF significant increases in the seasonal resident mixing ratios of near-surface O_3 occur of between ~10-60%, with maximal increases occurring over North-West Europe. This shows that the

largest effect on near-surface O_3 between the different years is due to the mitigation of industrial and road transport NO_x emissions in 2025. For the higher latitudes increases are of the order of 20-30% extending out into the Baring Sea. In general, there is a decrease of between 20-25% in the resident near-surface NO_x available across the entire domain (not shown) resulting in less titration of near-surface O_3. This is in part due to an increase in the amount of NO_x converted into HNO_3 near the emission sources via an enhancement in the efficiency of the reaction of OH with NO_2 (related to the increase in near-surface O_3). Once formed, a fraction of this HNO_3 is deposited to the surface in either precipitation or by surface uptake, which shortens the chain length of the NO_x re-cycling mechanism by removing reactive nitrogen from the troposphere. The regeneration of NO_x via photolytic destruction of HNO_3 is relatively small during DJF. A larger fraction of NO_x is also converted to PAN, the other main reservoir species for reactive nitrogen present in the troposphere, with increases of between ~5-15% in the resident mixing ratios over the entire region (not shown), although the PAN mixing ratios remain small. PAN is lost mainly via a temperature dependent decomposition back to NO_x, partly near the source but mostly once it has been transported away out of the boundary layer or in the continental outflow.

For JJA changes of ±5% occur in near-surface O_3 over the continent (except around the North Sea) and increases of 5-10% are simulated over the ocean related to the significant increase in resident NO_x due to the enhancement in regional shipping activity and the emission of SNE at more northerly latitudes. Therefore, in spite of the reduction in the cumulative regional NO_x emissions, the changes in near-surface O_3 are relatively modest. Examining the regional differences in the seasonal near-surface NO_x mixing ratios shows for JJA (not shown) reveals that the largest increases occur along the shipping routes between Ireland and Greenland and over the top of Norway in the Arctic Circle. Nearer the coast the increase in shipping SNE is essentially negated by less outflow of NO_x from the continent and therefore the impact on resident O_3 mixing ratios is small.

6 EFFECT OF SHIPPING EMISSIONS ON EUROPEAN NEAR-SURFACE OZONE DURING 2025
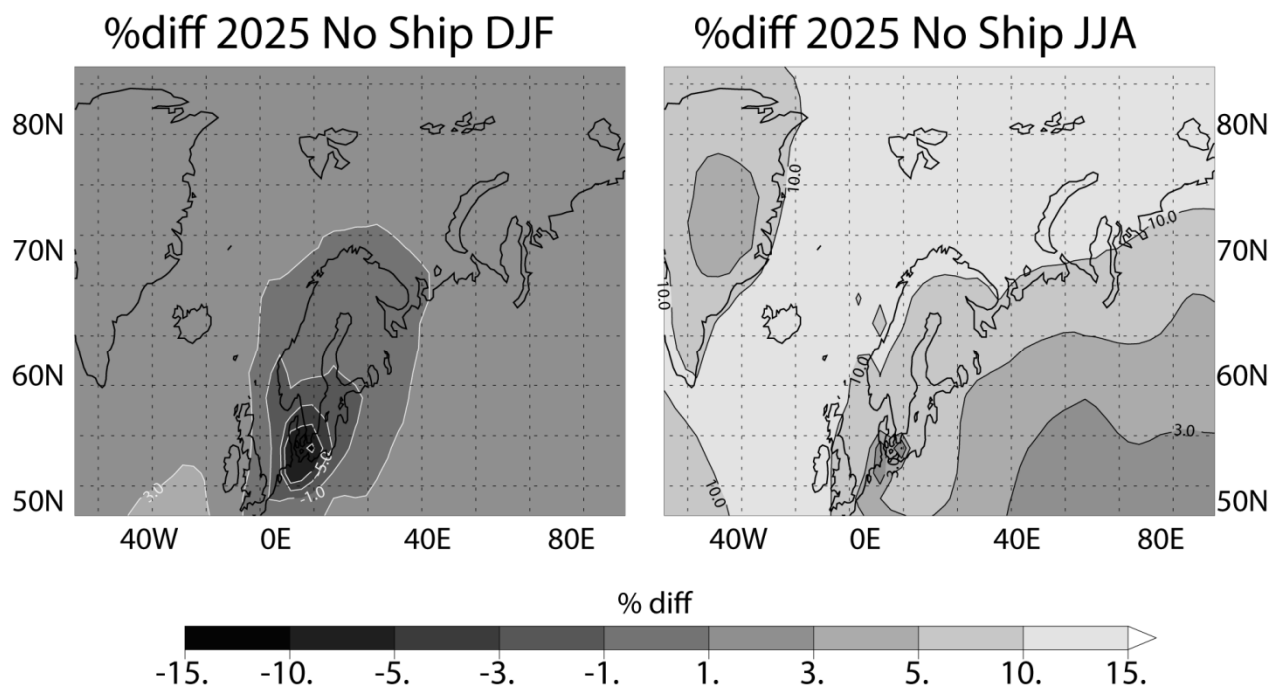
Figure 4: The impact of shipping NO_x emissions on the seasonal distribution of near-surface (0-500m) O_3 during 2025. The differences are calculated using the following relationship: (2025-2025_ls)/2025.

Finally, in Figure 4, we show the influence of SNE on the seasonal distribution of near-surface O_3 during 2025. There is a lot of similarity with the effects shown in the right panels of Fig. 2 for 2003 except that the magnitude of the differences is somewhat larger and covers a more extended area. For instance the impact of SNE along the new shipping routes is typically between 10-15% during JJA, with the impact inland being limited to the order of a few percent. Again there is a titra-

tion effect around Northern Germany and Denmark. Therefore future estimates of European SNE have only a marginal affect on air quality directly over the continent with the largest impact being in the MBL.

7 SUMMARY

In this study we have investigated the influence of future shipping emissions on air quality in the European domain using the global chemistry-transport model TM4. Analysing the differences in shipping emissions estimated for 2003 and 2025 shows that increases occur around the Baltic, Rotterdam harbour and to the West of Ireland where new shipping routes into the Arctic are thought to become more accessible. By performing 3D global simulations using these estimates we find that there is strong seasonality in the simulated effects, where titration of near-surface O_3 occurs during the winter season over land near the main source regions (e.g. Northern Germany) whereas increases of between 5-15% occur during the summer months when there is higher photo-chemical activity. When comparing the influence of shipping emissions between 2003 and 2025 shows that the impact on near-surface (0-500m) O_3 is similar in spite of the increase in the fraction of anthropogenic NO_X emissions from shipping. The exceptions are that there is enhanced O_3 production along the new shipping route, where the strong mitigation of non-transport and road emissions on the continent somewhat negates the increase in shipping NO_X which occurs near the coasts.

REFERENCES

De Ruyter de Wildt, M., H. Eskes and K. F. Boersma, 2012: The global economic cycle and satellite-derived NO2 trends over shipping lanes, Geophys. Res. Letts., 39, L01802, doi:10.1029/2011GL049541.

Eide, M. S., O. Endresen, A. Mjelde, L. E. Mangset and G. Gravir, 2007: Ship emission of the future, Tech. Report No. 2007-1325, Det Norske Veritas, Høvik, Norway.

Endresen, O., E. Sorgard, H. L. Behrens, P. O. Brett and I. S. A. Isaksen, 2007: A historical reconstruction of ships' fuel consumption and emissions, J. Geophys. Res., 112, D12301, doi:10.1029/2006jd007630.

Grewe, V., E. Tsati and P. Hoor, 2010: On the attribution of contributions of atmospheric trace gases to emissions in atmospheric model applications, Geosci. Model. Dev., 3, 487-499, doi:10.5194/gmd-3-487-2010, 2010.

Hodnebrog, Ø., T. K. Berntsen, O. Dessens, M. Gauss, V. Grewe, I. S. A. Isaksen, B. Koffi, G. Myrhe, D. Olivié, M. J. Prather, J. A. Pyle, F. Stordal, S. Szopa, Q. Tang, P. van Velthoven, J. E. Williams, and K. Ødemark, 2011: Future impact of non-land based traffic emissions on atmospheric ozone and OH – an optimistic scenario and a possible mitigation strategy. Atms. Chem. Phys., 11, doi:10.5194/acp-11-11293-2011, 11293-11317.

Hoor, P., J. Borken-Kleefeld, D. Caro, O. Dessens, O. Endresen, M. Gauss, V. Grewe, D. Hauglustaine, I. S. A. Isaksen, P. Jöckel, J. Lelieveld, G. Myrhe, E. Meijer, D. Olivié, M. J. Prather, C. Schnadt Poberaj, K. P. Shine, J. Staehelin, Q. Tang, J van Aardenne, P. van Velthoven, and R. Sausen, 2009: The impact of traffic emissions on atmospheric ozone and OH: results from QUANTIFY, Atms. Chem. Phys., 9, doi;10.5194/acp-9-3113-2009, 3113-3136.

Kim, H. S., C.H. Song, R. S. Park, G. Huey and J. Y. Ryu, 2009: Investigation of ship-plume chemistry using a newly-developed photochemical/dynamic ship-plume model, Atms. Chem. Phys., 9, 7531-7550.

Myhre, G., K. P. Shine, G. Radel, M. Gauss, I. S. A. Isaksen, Q. Tang, M. J. Prather, J. E. Williams, P. van Velthoven, O. Dessens, B. Koffi, S. Szopa, P. Hoor, V. Grewe, J. Borken-Kleefeld, T. K. Berntsen and J. S. Fuglestvedt, 2011: Radiative forcing due to changes in ozone and methane caused by the transport sector, Atmos. Environ., 45, 387-394.

Nakicenovic, N., O. Davidson, G. Davis, A. Grübler, T. Kram, E. L. La Rovere, B. Metz, T. Morita, W. Pepper, H. Pitcher, A. Sankovski, P. Shukla, R. Swart, R. Watson and Z. Dadi, 2000: Special Report on Emissions Scenraios, Cambridge University Press, Cambridge, 599pp.

Smokers, R, I. Skinner, B. Kampman, F. Fraga and N. Hill, 2011: Identification of the major risks/uncertainties associated with the achievability of considered policies and measures, EC publication, www.eutransportghg2050.eu.

Williams, J. E. and T. P. C. van Noije, 2008: On the upgrading of the modified Carbon Bond Mechanism IV for use in global Chemistry Transport Models, KNMI Scientific Report WR 2008-02, De Bilt, The Netherlands, 64 pp.

Ambiguous global warming potentials for aviation nitrogen oxides emissions

A. Skowron[*], D. S. Lee, R. R. De León
Dalton Research Institute, Manchester Metropolitan University, United Kingdom

ABSTRACT: Usage of the Global Warming Potential (GWP) is the established method for comparing the potential impact of emissions of different greenhouse gases on climate under the Kyoto Protocol. However the GWP places emissions of gases with different lifetimes and radiative properties on a common scale. This leads to weaknesses and uncertainties, which are challenging particularly for a short-lived species and their precursors, e.g. the aviation NO_x emissions. IPCC AR4 summarized studies that attempted to define an aviation NO_x GWP. Only three studies were identified, which yielded GWPs for aviation NO_x of: 100, 130 and -3. These few and disparate numbers are the motivation of this study. The state-of-the-art 3D Chemical Transport Model (CTM) - MOZART 3 was applied for this study. The simulations have been conducted for a series of aircraft NO_x pulse experiments. The pulses were applied globally for a period of a year, having aircraft emissions ranging from 0.72 to 10 Tg (N)/yr. The response of the chemical system varies with size of the pulse and in a non-linear way, which results in significant diversity of aviation NO_x GWPs; the difference between calculated GWP values for a 100-year time horizon reaches 130%. This is an important insight into a discussion about usage of aviation NO_x GWP and it sheds a light on understanding the discrepancy between reported numbers.

1 INTRODUCTION

The Global Warming Potential (GWP) is an established tool for comparing the potential impact of emissions of different gases on climate under the Koyto Protocol. GWP places emissions of gases with different lifetimes and radiative properties on a common scale. This is challenging particularly for short-lived species and their precursors, e.g. aviation NO_x emissions (Wit et al., 2005). The NO_x emissions at cruise altitudes result in a short-term and local (Northern Hemisphere, UTLS) enhancement of O_3 and a global long-term destruction of a small amount of ambient CH_4. The additional long-term O_3 destruction also occurs and follows CH_4 lifetime. Nonetheless, the overall radiative forcing induced by current day emissions of aviation NO_x is positive (Lee et al., 2009). The nature of the effects of NO_x emissions on climate, its temporal and spatial variations in magnitude, makes the usage of GWP scientifically contentious.

GWPs for aviation NO_x, based on a pulse emission, have been derived in a very limited number of investigations. IPCC AR4 (Forster et al., 2007) identified only three studies: Wild et al. (2001), Derwent et al. (2001) and Stevenson et al. (2004) which yielded the values 130, 100 and -3, respectively. These few and disparate estimates are the motivation of this study.

2 METHODOLOGY

The Model for Ozone and Related chemical Tracers, version 3 (MOZART-3) was applied for this study. This state-of-the-art 3D Chemical Transport Model (CTM) was extensively evaluated by Kinnison et al. (2007). Model for Atmospheric Transport and Chemistry (MATCH) (Rash et al., 1997) constitute the basis for MOZART-3 and it accounts for advection, shallow and deep convec-

---

[*] *Corresponding author:* Agnieszka Skowron, Dalton Research Institute, Manchester Metropolitan University, John Dalton Building, Chester Street, M1 5GD Manchester, United Kingdom. Email: a.skowron@mmu.ac.uk

tion, boundary layer mixing, wet and dry deposition. MOZART-3 represents a comprehensive tropospheric and stratospheric chemistry with 108 species included within O_x, NO_x, HO_x, ClO_x and BrO_x chemical families, together with CH_4 and its products.

MOZART-3 is driven by meteorological fields from European Centre for Medium Range Weather Forecast (ECMWF), reanalysis ERA-Interim for the year 2005 and 2006 (Simmons et al., 2007). The surface emissions are taken from Lamarque et al. (2010) and POET (Precursors of Ozone and their Effects on Troposphere) project (Granier et al., 2005). The aircraft emissions constitute a REACT4C 2006 dataset, with 0.71 Tg(N)/yr. The horizontal resolution used in this study is T42 (~ 2.8° x 2.8°) and vertical domain extends from surface to 0.1 hPa with 60 hybrid sigma layers. Eleven experiments were performed, one reference (aircraft) and ten perturbation (additional aircraft) simulations. The model's simulations were performed for two years; the first year (2005) constituted the spin-up and the second year (2006) was taken into account for an analysis, for each experimental case. The aircraft NO_x pulses were applied globally for a period of year during 2006, having aircraft emissions ranging from 0.72 to 10 Tg(N)/yr.

The Edwards-Slingo radiation code (Edwards and Slingo, 1996) was used to calculate the short-lived O_3 radiative forcing (RF). This radiative transfer model (RTM) was developed in the UK Meteorological Office. Due to lack of computational time the O_3 RF using RTM was calculated only for three pulse experiments: 0.72, 1.42 and 7.10 Tg(N)/yr. The rest of the O_3 responses were normalized to the results from radiative transfer model. The O_3 responses, for each pulse experiment, are the same in terms of their geographical distribution, just the magnitude of the responses differs. Thus, the normalization in this situation was justified.

The steady-state radiative forcings for a short-lived O_3, CH_4-induced O_3 and CH_4 were derived and Fuglestvedt et al.'s (2010) methodology was adopted for GWP calculations.

3 RESULTS

3.1 *The O_3 non-linearity*

The middle and upper tropospheric NO_x mixing ratios are of 50-200 pptv. At these concentrations the net O_3 production increases almost linearly with additional NO_x (IPCC, 1999). Some evidence of the decline of O_3 production with higher NO_x emissions rates was shown by Rogers et al. (2002). Here, for the first time, the non-linearity of O_3 chemistry on a global scale in UTLS region is presented. It is shown that an experimental design of pulse emissions can lead the O_3 production to the edges of its linear regime. Figure 1 presents that different pulse sizes yield different results, with O_3 saturating at higher NO_x rates.
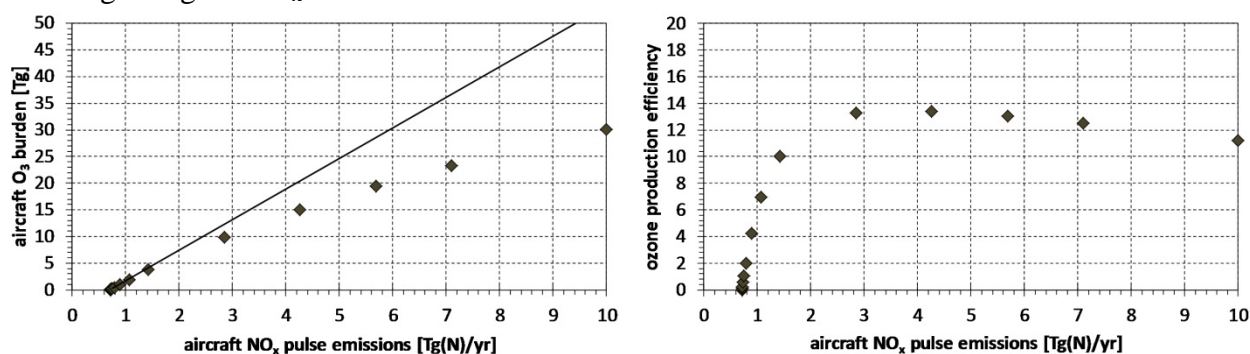

Figure 1. Scatter plots of aircraft O3 burden (left) and O3 production efficiency (right) against series of aircraft NOx rates (dots are individual experiments, line is a linear solution).

The rapid increase of O_3 with additional NO_x occurs for small pulse sizes, till around 2-times NO_x (additional 100% of current aircraft NO_x), which gives 1.42 Tg(N)/yr of total emitted NO_x. The deviation from linear solution varies with size of the pulse and constitute 8% for 2-times (additional 0.71 Tg(N)/yr) NO_x pulse, 19% for 4-times (additional 2.1 Tg(N)/yr) NO_x pulse and 36% for 10-times (additional 6.4 Tg(N)/yr) NO_x pulse emissions.

The ozone production efficiency (OPE, the number of O_3 molecules produced per emitted NO_x molecule) picture shows a significant saturation for emissions higher than 1.5 Tg(N)/yr. Relative decline of OPE occurs for emissions higher than 5.7 Tg(N)/yr.

3.2 *Heterogeneity of GWP*

The chemical and transport schemes within different models are controlling sensitivities of O_3 production. This is one of the reasons of discrepancies found between reported GWP values.

We found that with observed O_3 non-linearities a unique number of aviation NO_x GWP does not exists (Figure 2). This is another reason of diversity among published estimations of GWPs for aviation NO_x emissions.
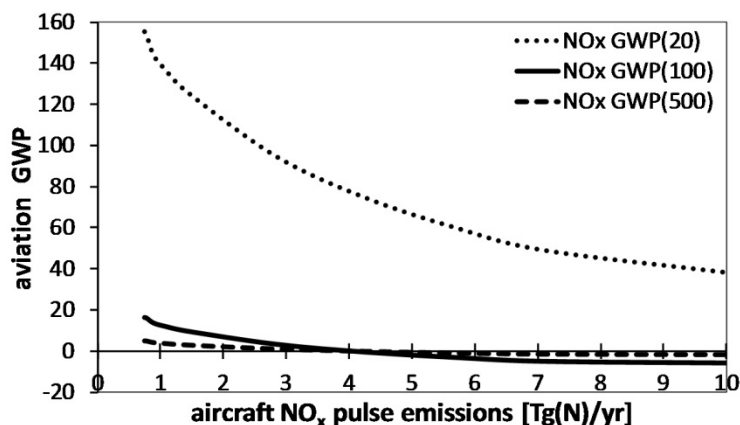
Figure 2. Calculated aviation NOx GWP for a 20-, 100- and 500-year time horizons as a function of different aircraft NOx pulse sizes.

The calculated value of GWP for 100-year time horizon (H=100) varies from 16 for 0.03 Tg(N)/yr of additional NO_x, 10 for 0.71 Tg(N)/yr of additional NO_x to -5 for 6.4 Tg(N)/yr of additional NO_x emissions. Depending on experimental design (size of the aviation NO_x pulse emission) the GWP value changes from positive to negative. The difference in reported numbers for GWP (H=20) reaches 68% and for GWP (H=100 and 500) the difference constitutes 130%.

The time evolution of aviation NO_x GWP presents another dimension of diversity among reported values (Figure 3). While the shape of the response (exponential decay with time) remains similar for each pulse size, the calculated numbers are the source of the misleading information. The GWP for small pulse sizes (not higher than 2.1 Tg(N)/yr of additional NO_x) remains positive for each time horizon. The GWP for pulse emissions of 4.3 Tg(N)/yr (3.5 Tg(N)/yr of additional NO_x) and greater are positive for H=20, but for H=100 and H=500 the sign changes to negative. The difference between 1.05-times and 1.5-times pulse for H=20 is 11% and it rises to 25% for H=100 and H=500. The difference between 1.5-times and 10-times pulse is 64% for H=20 and 141% for H=100 and H=500. These numbers constitute a significant range of uncertainty. This diversity and heterogeneity suggests that the standard formulation of GWP definition does not fully capture complex relations of the NO_x-O_3-CH_4 system.
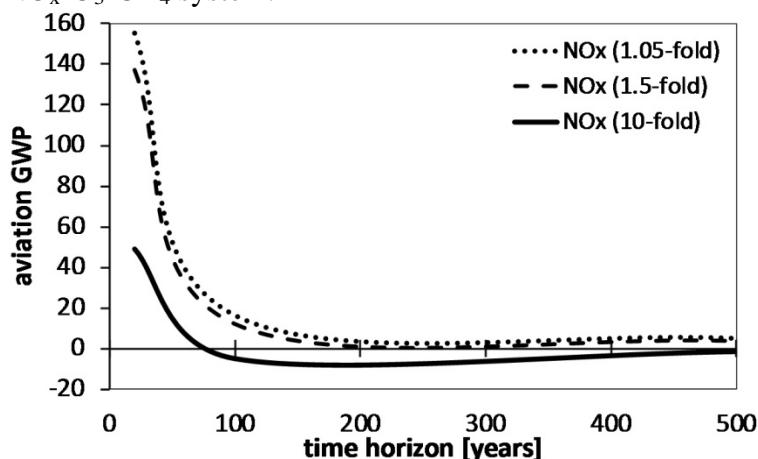
Figure 3. Calculated aviation NOx GWP for different pulse sizes (1.05-times, 1.5-times and 10-times background aircraft NOx emissions) as a function of time horizon.

4 DISCUSSION AND CONCLUSIONS

There are a very limited number of studies which defines GWPs for aviation NO_x emissions. IPCC AR4 (Forster et al., 2007) summarized them and only three numbers of GWP (H=100) were presented: 130 (Wild et al., 2001), 100 (Derwent et al., 2001) and -3 (Stevenson et al., 2004). While the first two values are within the same range, the third number introduces confusion. Recently, the GWPs were re-evaluated by Fuglestvedt et al. (2010) yielding values: 71 for Wild et al. (2001) and -2.1 for Stevenson et al. (2004). The chemical and transport schemes within different models can cause differences; however, it is worth to mention that Stevenson et al. (2004) and Derwent et al. (2001) used the same model. The difference is hidden in the size of a NO_x pulse: signals of ~0.7-times, ~1.5-times and 10-times greater than background aviation NO_x were applied, respectively. Our study presents, that even with one model a wide range of O_3 responses is achievable. By applying a large pulse sizes the linear O_3 response (with additional NO_x) is pushed into saturation regime, which leads to the non-linearity. Thus, caution made by Stevenson et al. (2004) over interpretation of their results is appropriate.

The GWP (H=100) value for the 10-times pulse size derived in our study is -5, which is comparable with Stevenson et al. (2004) work. The numbers of GWP (H=100) for small pulse sizes founded in our study are of 16-14, which are much smaller than Wild et al.'s value, 71. The inter-model differences can play a role here.

One of the solutions for the reported diversity can be the narrowness of the freedom in experimental design of a NO_x pulse emissions. Taking into account only linear regime of O_3 responses (pulse experiments ranging from 0.75 to 1.42 Tg(N)/yr) the range of aviation NO_x GWP values is significantly limited and the difference between reported numbers reaches 12% for H=20 and 26% for H=100 and H=500. The average values of GWP for aviation NO_x emissions are: 148 for H=20, 15 for H=100 and 4 for H=500.

Another way of dealing with these discrepancies is possibly hidden in the steady-state experiments (Fuglestvedt et al., 2010, Myhre et al., 2011). Berntsen et al. (2005) pointed out, that "(…) the introduction of the SGWP metric does not alter the picture dramatically, but introduces a dimension which increases the variation in the results", which, in the light of this study, possibly can bring some kind of consistency.

The response of the chemical system varies with size of the pulse and in a non-linear way, which results in significant diversity of aviation NO_x GWPs. This sheds a light on understanding the discrepancy between numbers reported in literature. The greatest utility of GWP as a metric is its relativity and prevalence among a wide community. The policy requires an approach consistent with Kyoto-type approaches. However, such a wide range of results make it difficult to recommend an aviation NO_x GWP for formulating policy.

The further detailed assessments of coupled NO_x-O_3-CH_4 system, on both global and regional basis, needs to be carried on in order to make the aviation NO_x emissions more accessible in terms of intergovernmental climatic agreements.

REFERENCES

Berntsen, T. K., J. S. Fuglestvedt, M. M. Joshi, K. P. Shine, N. Stuber, M. Ponater, R. Sausen, D. A. Hauglustaine, and L. Li, 2005: Response of climate to regional emissions of ozone precursors: Sensitivities and warming potentials, Tellus, Series B: Chemical and Physical Meteorology 57, 283-304.

Derwent, R. G., W. J. Collins, C. E. Johnson, and D. S. Stevenson, 2001: Transient behaviour of tropospheric ozone precursors in a global 3-D CTM and their indirect greenhouse effects. Climatic Change 49, 463-487.

Edwards, J. M., and A. Slingo, 1996: Studies with a flexible new radiation code. I: Choosing a configuration for a larqe-scale model. Quarterly Journal of the Royal Meteorological Society 122, 689-719.

Forster, P., V. Ramaswamy, P. Artaxo, T. Berntsen, R. Betts, D. W. Fahey, J. Haywood, J. Lean, D. C. Lowe, G. Myhre, J. Nganga, R. Prinn, G. Raga, M. Schulz, and R. Van Dorland, 2007: Changes in Atmospheric Constituents and in Radiative Forcing. In: Climate Change 2007: The Physical Science Basis. Contribution of Working Group I to the Fourth Assessment Report of the Intergovernmental Panel on Climate Change [Solomon, S., D. Qin, M. Manning, Z. Chen, M. Marquis, K. B. Averyt, M. Tignor, H. L. Miller (ed.)]. Cambridge University Press, Cambridge, United Kingdom and New York, NY, USA.

Fuglestvedt, J. S., K. P. Shine, J. Cook, T. Berntsen, D. S. Lee, A. Stenke, R. B. Skeie, G. J. M. Velders, and I. A. Waitz, 2010: Transport impacts on atmosphere and climate: Metrics. Atmospheric Environment 44, 4648–4677.

IPCC, 1999: Aviation and the Global Atmosphere - A Special Report of IPCC Working Groups I and III, [Penner, J. E., D. H. Lister, D. J. Griggs, D. J. Dokken, M. McFarland (ed.)]. Intergovernmental Panel on Climate Change, Cambridge University Press, New York, USA, 365 p.

Granier, C., A. Guenther, J. F. Lamarque, A. Mieville, J. F. Muller, J. Olivier, J. Orlando, G. Peters, G. Petron, G. Tyndall, and S. Wallens, 2005: POET, a database of surface emissions of ozone precursors. (available at http://www.aero.jussieu.fr/projet/ACCENT/POET.php).

Kinnison, D. E., G. P. Brausser, S. Walters, R. R. Garcia, D. R. Marsh, F. Sassi, V. L. Harvey, C. E. Randall, L. Emmons, J. F. Lamarque, P. Hess, J. J. Orlando, X. X. Tie, W. Randel, L. L. Pan, A. Gettelman, C. Granier, T. Diehl, U. Niemeier, and A. J. Simmons, 2007: Sensitivity of chemical tracers to meteorological parameters in the MOZART-3 chemical transport model, Journal of Geophysical Research 112, D20302, doi:10.1029/2006JD007879.

Lamarque, J. F., T. C. Bond, V. Eyring, C. Granier, A. Heil, Z. Klimont, D. Lee, C. Liousse, A. Mieville, B. Owen, M. G. Schultz, D. Shindell, S. J. Smith, E. Stehfest, J. Van Aardenne, O. R. Cooper, M. Kainuma, N. Mahowald, J. R. McConnell, V. Naik, K. Riahi, and D. P. van Vuuren, 2010: Historical (1850–2000) gridded anthropogenic and biomass burning emissions of reactive gases and aerosols: methodology and application. Atmospheric Chemistry and Physics 10, 7017–7039.

Lee, D. S., D. Fahey, P. Forster, P. J. Newton, R. C. N. Wit, L. L. Lim, B. Owen, and R. Sausen, 2009: Aviation and global climate change in the 21st century. Atmospheric Environment 43, 3520–3537.

Myhre, G., K. P. Shine, G. Rädel, M. Gauss, I. S. A. Isaksen, Q. Tang, M. J. Prather, J. E. Williams, P. van Velthoven, O. Dessens, B. Koffi, S. Szopa, P. Hoor, V. Grewe, J. Borken-Kleefeld, T. K. Berntsen, and J. S. Fuglestvedt, 2011: Radiative forcing due to changes in ozone and methane caused by the transport sector. Atmospheric Environment 45, 387–394.

Rasch, P. J., N. M. Mahowald, and B. E. Eaton, 1997: Representations of transport, convection, and the hydrological cycle in chemical transport models: Implications for the modelling of short-lived and soluble species, Journal of Geophysical Research 102, 28,127– 28,138.

Rogers, H.L., D.S. Lee, D.W. Raper, P.M.D. Forster, C.W. Wilson, and P.J. Newton, 2002: The impact of aviation on the atmosphere. Aeronautical Journal 106 (1064), 521–546.

Simmons, A.J., S. Uppala, D. Dee, and S. Kobayashi, 2007: ERA-Interim: New ECMWF reanalysis products from 1989 onwards. ECMWF Newsletter 110.25-35.

Stevenson, D. S., R. M. Doherty, M. G. Sanderson, W. J. Collins, C. E. Johnson, and R. G. Derwent, 2004: Radiative forcing from aircraft NOx emissions: Mechanisms and seasonal dependence. Journal of Geophysical Research 109, D17307.

Wild, O., M. J. Prather, and H. Akimoto, 2001: Indirect long-term global radiative cooling from NOx emissions. Geophysical Research Letters 28, 1719-1722.

Wit, R. C. N., B. H. Boon, A. van Velzen, M. Cames, O. Deuber, and D. S. Lee, 2005: Giving wings to emission trading. Inclusion of aviation under the European emission trading system (ETS): design and impacts. CE-Delft, No. ENC.C.2/ETU/2004/0074r, the Netherlands.

Index of Authors